UNIVERSIDADE DE LISBOA
FACULDADE DE CIÊNCIAS

New sugar-based molecular entities as potential therapeutics against infectious and neurodegenerative diseases

"Documento Definitivo"

Doutoramento em Química
Especialidade em Química Orgânica

Catarina Alexandra dos Santos Dias

Tese orientada por:
Professora Doutora Amélia P. Rauter
Doutora Teresa Alves

Documento especialmente elaborado para a obtenção do grau de doutor

2018

UNIVERSIDADE DE LISBOA
FACULDADE DE CIÊNCIAS

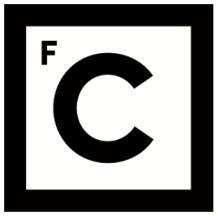

Ciências
ULisboa

New sugar-based molecular entities as potential therapeutics against infectious and neurodegenerative diseases

Doutoramento em Química
Especialidade em Química Orgânica

Catarina Alexandra dos Santos Dias

Tese orientada por:
Professora Doutora Amélia P. Rauter
Doutora Teresa Alves

Júri:

Presidente:

- Doutor Fernando José Vieira dos Santos, Professor Auxiliar e Membro do Conselho Científico da Faculdade de Ciências da Universidade de Lisboa

Vogais:

- Doutora Maria Emília da Silva Pereira de Sousa, Professora Auxiliar da Faculdade de Farmácia da Universidade do Porto
- Doutora Ana Paula Assunção Esteves, Professora Associada da Escola de Ciências da Universidade do Minho
- Doutora Maria Eduarda Machado de Araújo, Professora Auxiliar da Faculdade de Ciências da Universidade de Lisboa
- Doutora Teresa Paulo Tavares da Silva Alves, Diretora CEO da empresa Cipan SA-Companhia Industrial Produtora de Antibióticos
- Doutor Rodrigo Freire Martins de Almeida, na qualidade de individualidade de reconhecida competência na área científica.

Documento especialmente elaborado para a obtenção do grau de doutor

2018

To my family

Acknowledgments

Firstly, I would like to thank my supervisor Prof. Amélia Pilar Rauter, not only for her scientific guidance and support, but for the inspiration and joy she shares with everyone who works with her. Thank you for your will and patience to fight for all of us, so we do not miss any opportunity to grow academically and personally. I would also like to thank my co-supervisor, Dr. Teresa Alves, for all the kindness and support she has always shown for me, and for believing that I could be an asset for the R&D team at CIPAN.

The mysteries surrounding alkyl deoxy glycosides were tackled from a multi-disciplinary approach from the beginning. To the biology team, Dr. Ricardo Dias, Professor Rogerio Tenreiro, and to my colleague João Pais, thank you for all your insights and work regarding the search for the mechanism of action and valuable discussions. To the computational (bio)chemistry team, Dr. Miguel Machuqueiro, Dr. Diogo Vila-Viçosa and Rafael Nunes, thank you so much for the biomolecular simulations with membranes. Thanks are also due to Dr. Ana Pelerito from INSA, for assessing the antimicrobial activity on *B. anthracis*, and Dr. Ana Viana for the AFM images. Finally, I am deeply grateful to Dr. Rodrigo Almeida and his team for having received me in his lab and introducing me to biophysics, the discipline that unravel the antimicrobial mechanism of action in the end. I also thank Dr. Maria Conceição Oliveira, for performing all the HRMS of the synthesized compounds.

I would also like to express my gratitude to Dr. Walter Magnus, for having kindly received me in Eli Lilly medicinal chemistry laboratories, to carry out the synthesis of neuroprotective phenolic glycosides. To Teresa Man, a special thank for having guided me and helped whenever I needed, always with a smile and without hesitating to interrupt her own work. To everyone in the ChemWest labs of Eli Lilly, thank you for making me feel welcome. It was indeed a life changing experience.

The (current and past) members of the Carbohydrate Chemistry Group are also deeply acknowledged. The support and care of many colleagues helped me to overcome the setbacks and to stay focused through these challenging five years. A very special thanks to my dear friends Ana Marta de Matos and Rafael Nunes, for their friendship, emotional support, and companionship in all our adventures. Patricia Serra, Vasco Cachatra and Andreia Almeida, thank you for your effort and perseverance for the synthesis of dodecyl glycosides analogues, and to Alice Martins for her encouragement words, and for the cytotoxicity assessment. María Teresa Sánchez and Nuno M. Xavier are also gratefully acknowledged for all their help and valuable discussions.

I also want to thank everyone at CIPAN, for their support in the last year, either with their smile or words of encouragement, and for making me feel part of the team from the beginning.

Most importantly, none of this would have been possible without the love and patience of my family. I particularly thank to my parents, the cornerstones of my life and my education, and to my beloved sister. I owe them everything I am today. To my nephews Tiago and Tomás, my most inspiring scientists, thank you for filling my life with unconditional love, joy and fun.

A very special thanks to my partner André, for his love and emotional support. Thank you for your patience, your proud eyes, and for always being by my side.

Funding

Fundação para a Ciência e a Tecnologia (FCT) and CIPAN are gratefully acknowledged for my BDE Grant SFRH/BDE/51998/2012. FCT is also acknowledged for the support of the project UID/Multi/0612/2013. The European Union is gratefully acknowledged for the support of the project “Diagnostic and Drug Discovery Initiative for Alzheimer's Disease” (D3i4AD), FP7-PEOPLE-2013-IAPP, GA 612347. The Management Authorities of the European

Regional Development Fund and the National Strategic Reference Framework for the support of the Incentive System – Research &Technological Development Co-Promotion FACIB Project nr. 21457.

Table of Contents

Abstract

The increasing average life expectancy in developed countries led to an escalating concern regarding geriatric infectious diseases. In particular nosocomial infections are known to be more frequent and severe in the elderly, being this susceptibility often related to neurodegenerative disorders.

Alkyl 2-deoxy/2,6-dideoxy-*arabino*-hexopyranosides have been studied by the Carbohydrate Chemistry Group, revealing potent antimicrobial activity over Gram-positive bacteria, namely *Bacillus* species. Additionally, promising results arising from NMR interaction studies of 2,6-dideoxyglycosides with cystatin B amyloid fibrils demonstrated their potential for amyloid diseases. These findings were the driving force to explore the chemistry and bioactivity of 2-deoxy sugars against infection and neurodegenerative disorders. Thus, new alkyl 2-deoxy-*O*-/and -*S*-glycosides, and alkyl 3-deoxy, 4-deoxy and 6-deoxy-*O*-glycoside analogues were synthesized, and the importance of the deoxygenation pattern was evaluated. Dodecyl 4,6-dideoxy-α-D-*xylo*-hexopyranoside was the most promising compound for further developments, presenting a MIC below 25 μM for *Bacillus species* and *E. faecalis,* and low toxicity.

More importantly, the action of one of the lead compounds on the thermotropic behaviour of phosphatidylethanolamine-enriched membranes was investigated. The reorganization of the lipid matrix into a hexagonal phase causing bacteria cell lysis is the proposed mechanism for the antimicrobial action of this family of compounds. This is the first report of this unprecedented mode of action of glycosides responsible for specific carbohydrate-phospholipid interactions, triggering innovation on membrane-targeting antibiotics.

Moreover, a deep literature investigation showed that carbohydrates also play a role toward neurodegenerative disease prevention. Thus, 2-deoxyglycosides embodying neuroprotective polyphenols were prepared, envisioning activity and bioavailability improvement of such molecules. In fact, certain resveratrol glycosides were more effective at protecting the neuronal cells from peroxide-induced cytotoxicity than resveratrol itself, while showing coefficient partition measurements typical of central nervous system drugs and ideal for blood-brain-barrier penetration.

This work clearly demonstrates the uniqueness and versatility of carbohydrates as exceptional scaffolds for medicinal chemistry applications.

Keywords:

Infection ● Alzheimer's disease ● Alkyl deoxyglycosides ● Phosphatidylethanolamine ● Hexagonal phase

Resumo

O aumento da esperança média de vida nos países desenvolvidos conduziu a uma preocupação generalizada no que diz respeito a doenças infeciosas na população idosa, levando a que um dos desafios deste século seja o de proporcionar cuidados especializados a uma população maioritariamente envelhecida. O envelhecimento conduz a uma maior suscetibilidade a infeções diversas, pelo que os episódios infeciosos na população idosa são, não só mais frequentes, como também mais severos. Este aumento da suscetibilidade é devido à imunossenescência, a alterações a nível fisiológico que ocorrem naturalmente no processo de envelhecimento e a malnutrição. Neste contexto, a incidência de doenças neurodegenerativas, e em particular da doença de Alzheimer, é um importante fator agravante, uma vez que estes pacientes se tornam dependentes de terceiros, perdem o apetite e, eventualmente, a capacidade de comunicar.

Compostos análogos a 2,6-didesoxi-*arabino*-hexopiranósidos de alquilo têm vindo a ser estudados no laboratório de Química dos Glúcidos (onde decorreu a maioria da investigação reportada na presente Tese), revelando potentes atividades antimicrobianas contra bactérias Gram-positivas, em particular em espécies de *Bacillus*. Além disso, estudos realizados no âmbito da minha tese de mestrado revelaram que alguns destes 2,6-didesoxiglicósidos de dodecilo interagem com a cistatina B em solução, uma proteína amiloidogénica usada como modelo da proteína β-amilóide, mostrando assim que estas entidades moleculares merecem ser estudadas mais profundamente no que se refere também à sua aplicação a doenças neurodegenerativas. Estes resultados foram, pois, a força motriz para explorar 2-desoxi açúcares enquanto novas moléculas com atividades antimicrobianas e/ou neuroprotetoras.

Em primeiro lugar, visando a otimização da atividade antimicrobiana, desenvolveu-se neste trabalho um conjunto de glicósidos, na sua maioria glicósidos surfactantes, estruturalmente dividida em duas unidades: unidade sacarídica ou glícona (cabeça hidrofílica) e a glícona (cauda hidrofóbica). Como consequência das suas propriedades anfifílicas, estes compostos têm o potencial de interagir com a camada bilipídica da membrana celular e, consequentemente, de exercer atividade biológica. A essencialidade da membrana celular, juntamente com a sua estrutura altamente conservada, tornam-na um alvo muito apelativo e promissor no que diz respeito a novos antibióticos, uma vez que dificultam a aquisição de resistência por parte das bactérias. No entanto, este mecanismo tem sido pouco explorado, e quimiotipos cujo mecanismo passa por perturbar a membrana bacteriana são frequentemente desconsideradas devido aos riscos relacionados com a falta de seletividade. No entanto, as diferenças na composição das membranas eucarióticas e procarióticas são bem conhecidas e têm a possibilidade de ser exploradas, tal como é refletido no capítulo 1.1 desta tese. De facto, acreditamos que a luta contra bactérias resistentes reside, a médio prazo, em estratégias altamente inovadoras.

Relativamente às metodologias de síntese usadas, os 2-desoxiglicósidos foram obtidos pela reação de álcoois de cadeia longa com glicais, catalisada por brometo de trifenilfosfónio. Este método, desenvolvido nos anos 80, foi no âmbito desta tese perscrutado e submetido à série de livros "Proven synthetic methods in carbohydrate chemistry", um conjunto de publicações onde cada protocolo é repetido por um verificador independente, de forma a tentar combater a irreprodutibilidade de protocolos de síntese, lacunas na caracterização de intermediários, e rendimentos inflacionados (Capítulo 2).

Outros análogos sintetizados variaram na configuração e átomo da ligação glicosídica (O- e S-), para os quais outras técnicas de síntese tiveram de ser concebidas e executadas, descritas no capítulo 3. Os glicósidos de dodecilo testados em *B. anthracis e B. subtilis*

revelaram atividades semelhantes às já demonstradas pelo *lead* 2,6-didesoxi-L-*arabino*-hexopiranósido de dodecilo (25 μM), sendo que algumas delas possuem ainda uma atividade contra *E. faecalis*, uma bactéria particularmente temida em ambientes hospitalares. O composto *lead* provoca a morte celular das bactérias em menos de 10 minutos, e provoca a ruptura do envelope celular, visível por espectroscopia de força atómica (AFM).

O passo seguinte passou pela descoberta do mecanismo de ação destes compostos em *Bacillus*, e o motivo da seletividade outrora observada. Simulações biomoleculares revelaram um comportamento diferente do habitualmente observado em glicósidos surfactantes, i.e., sem tendência para a formação de poros. Após a exclusão da existência de um alvo intracelular, o estudo da influência que estes compostos têm em bicamadas lipídicas demonstrou ser crucial para desvendar o seu mecanismo de ação. O facto da composição da membrana citoplasmática das espécies de *Bacillus* ser anormalmente rica em fosfolípidos contendo fosfatidiletanolmina (PE), quando comparada com outras bactérias Gram-positivas, constituiu uma pista importante. Uma das características biofísicas destes fosfolípidos é a sua capacidade de adotar uma fase hexagonal inversa (H_{II}). Estas estruturas não lamelares desempenham papéis importantes em processos membranares tais como contacto e fusão, cisão, formação de poros, e eventualmente, perda de integridade celular. Para compreender o papel do PE, dois glicósidos de alquilo com atividade superficial semelhante, mas atividade biológica distinta, foram selecionados e avaliada a sua ação em lipossomas ricos em PE. A formação de fases hexagonais foi investigada através da medição da anisotropia de fluorescência ao longo da temperatura, revelando que, ao contrário do glicósido inativo, o glicósido antibacteriano provoca o desordenamento dos lípidos da membrana, promovendo a transição da fase lamelar para a fase hexagonal. Estes fenómenos constituem, muito provavelmente, a base do mecanismo de ação desta família de compostos. Esta nova descoberta é surpreendente na medida em que, ao passo que as interações carbohidrato/proteína e sua relevância biológica estão bem estabelecidas, esta

é a primeira vez na qual glicósidos são responsáveis por interações especificas carbohidrato-fosfolípido, causando alterações do comportamento termotrópico dos lípidos.

Por último, tentou-se ainda compreender a importância do padrão de desoxigenação para a atividade e toxicidade desta família de compostos. Para tal, foram desenvolvidas metodologias alternativas de forma a obter glicósidos desoxigenados nas posições 3, 4, 4 e 6, 2 e 3, e ainda 3 e 4. Como é apanágio dos agentes antimicrobianos que têm como alvo a membrana fosfolipídica, a relação estrutura-actividade não foi facilmente atribuível, devida à falta de linearidade entre a posição de desoxigenação e/ou o número de grupos hidroxilo removidos, e a actividade antimicrobiana. No entanto, é de destacar o 4,6-didesoxi-α-D-*xylo*-hexopiranósido de dodecilo (**11**, capítulo 4), que apresentou uma MIC inferior a 25 μM para todas as estirpes de *Bacillus* testadas e *E. faecalis*, e uma toxicidade 2 vezes superior à MIC em células intestinais, e 4 vezes superior em células hepáticas.

Não esquecendo a dicotomia infeção/envelhecimento já mencionada, assim como o potencial dos 2-desoxiglicósidos em doenças neuroprotectoras, foi levada a cabo uma extensa investigação da literatura de modo a compreender qual o papel da unidade sacarídica em glicósidos com ação neuroprotetora conhecida, em particular polifenóis (Capítulos 1.2 e 1.3). Curiosamente, os açúcares têm ainda o potencial de melhorar as propriedades fisico-químicas de polifenóis (solubilidade, coeficiente de partição), prevenir oxidação pelo "bloqueio" de grupos fenol, favorecer o acesso ao cérebro, via transportadores de hexoses (GLUTs) na barreira hematoencefálica, e retardar a formação de fibras amilóide pela estabilização do estado nativo dos péptidos através de solvatação preferencial. Estes dados inspiraram a síntese de 2-desoxiglicósidos de entidades moleculares neuroprotetoras, tais como o resveratrol, visando a melhoria desta atividade e das suas propriedades físico-químicas, o que foi realizado com sucesso. A metodologia usada para a síntese de 2- e 2,6-didesoxiglicósidos de resveratrol foi a mesma descrita inicialmente para 2-desoxiglicósidos de dodecilo, i.e., pela reação de um álcool

(neste caso, de um fenol) com um glical, catalisada por TPHB, embora ligeiramente adaptada. Foi ainda sintetizado um glicósido de um derivado do ácido cafeico. Com efeito, alguns dos glicósidos de resveratrol sintetizados revelaram-se mais eficientes a proteger células neuronais da toxicidade induzida por peróxido de hidrogénio, do que o próprio resveratrol. Também o glicósido derivado de um éster de ácido cafeico se revelou bastante promissor. Os dois compostos mais promissores não são tóxicos para neuroblastomas, células intestinais e hepáticas em todas as concentrações testadas. Os coeficientes de partição (LogD) medidos para estes compostos demonstram uma lipofilia moderada, típica de fármacos usados para sistema nervoso central e para a penetração na barreira hematoencefálica. O ensaio PAMPA que avalia a permeação passiva revelou que 2,6-didesoxi-L-*arabino*-piranósidos de resveratrol são mais eficazes que os seus análogos 2-desoxi-D-*arabino*-piranósidos, apesar de não serem mais eficientes que o resveratrol.

Este trabalho demonstra claramente a singularidade e versatilidade dos carbo-hidratos enquanto entidades moleculares excecionais em química medicinal.

Palavras-chave:

Infeção ● Alzheimer ● Desoxiglicósidos de alquilo ● Fosfatidiletanolamina ● Fase hexagonal

Abbreviations and Symbols

AAG	Amphiphilic aminoglycosides
ACh	Acetylcholine
AChE	Acetylcholinesterase
ACN	Acetonitrile
AD	Alzheimer's disease
AFM	Atomic force microscopy
AMP(s)	Antimicrobial peptide(s)
AMPs	Antimicrobial peptides
APP	Amyloid-β precursor protein
Aβ	Amyloid-β peptide
BACE-1	Beta-secretase 1
BAIB	Bis(acetoxy)iodobenzene
BBB	Blood-Brain barrier
BChE	Butyrylcholinesterase
BTEAB	Benzyltriethylammonium bromide
CC	Column Chromatography
CGTase	Cyclodextrin glucanotransferase
CL	Cardiolipin
CLSI	Clinical and Laboratory Standards Institute
CMC	Critical Micellar concentration
CP	Cromatographic purity
DAG	Diacetoneglucose
DCC	Dicyclohexyl carbodiimide
DCM	Dichloromethane
DFT	Density Functional Theory
DG	Dodecyl β-D-glucopyranoside
DMAP	4-Dimethylaminopyridine
DMEM	Dulbecco's Modified Eagle Medium
DMPC	1,2-dimyristoyl-*sn-glycero*-3-phosphocholine
DNA	Deoxyribonucleic acid
DSC	Differential scanning calorimetry
EDTA	Ethylenediaminetetraacetic acid
Equiv.	Equivalent
EtCN	Ethyl nitrite
FDA	Food and Drug Administration
FIA	Flow injection analysis
GAGs	Glycosaminoglycans
GLUTs	Hexose transporters
GS	Gramicidin S
GSK-3	Glycogen synthase kinase-3
GT	Glucosyltransferase
HBA	Hydrogen bond acceptor
HBD	Hydrogen bond donor
Hex	Hex
HII	Hexagonal phase
HRMS	High resolution mass spectrometry
HS	Heparan sulfate
J	Coupling constant

KEGG	Kyoto Encyclopedia of Genes and Genomes
LC-MS	Liquid chromatography–mass spectrometry
LMW	Low molecular weight
LPS	Lipopolysaccharides
LTA	Lipoteichoic acids
LUVs	Large unilamellar vesicles
M.p	Melting point
MBC	Minimal bactericidal concentration
MBIC	Minimal biofilm inhibitory concentration
m-CPBA	*meta*-Chloroperoxybenzoic acid
MD	Molecular dynamics
MIC	Minimal vinhibitory concentration
MLVs	Multilamellar vesicles
MRI	Magnetic Resonance imaging
MRSE	Methicillin-resistant *Staphylococcus epidermidis*
MRSA	Methicillin-resistant *Staphylococcus aureus*
MSSA	Methicillin-sensitive *Staphylococcus aureus*
MTT	3-(4,5-dimethylthiazol-2-yl)-2,5-diphenyltetrazolium bromide
MW	Molecular weight
NBD-DPPE	1,2-dipalmitoyl-*sn*-glycero-3-phosphoethanolamine-N-(7-nitro-2-1,3-benzoxadiazol-4-yl)
NFTs	Neurofribrillary tangles
NMR	Nuclear Magnetic Resonance
Nys	Nystatin
OG	Octyl β-D-glucopyranoside
PA	Phosphatidic acid
PAINs	Pan Assay Interference compounds
PAMPA	Parallel artificial membrane permeability
PC	Phosphatidylcholine
PDE	Phosphodiesterase
PE	Phosphatidylethanolamine
PET	Positron emission tomography
Petrol. ether	Petroleum ether
Phe	Phenylalanine
PI	Phosphatidylinositol
POPC	1-palmitoyl-2-oleoyl phosphatidylcholine
POPE	1-palmitoyl-2-oleoyl phosphatidylethanolamine
POPG	1-palmitoyl-2-oleoyl phosphatidylserine
PPARγ	Peroxisome proliferator–activated receptor-γ
Pro	Proline
PS	Phosphatidylserine
PTS	Phosphotransferases
Pyr	Pyridine
RCT	Randomized clinical trial
Rh-PE	1,2-dimyristoyl-*sn-glycero*-3-phosphoethanolamine-N-(Lissamine rhodamine B sulfonyl)
RNA	Ribonucleic acid
ROS	Reactive oxygen species
SAMP(s)	Small antimicrobial peptide(s)
STZ	Streptozotocin
TBAB	Tetra-*n*-butylammonium bromide

TBAF	Tetra-*n*-butylammonium fluoride
TBDPS	*tert*-Butyldiphenylsilyl
TBMDS	*tert*-Butyldimethylsilyl
TEMPO	2,2,6,6-Tetramethylpiperidine 1-oxyl
T_H	Lamellar-to-hexagonal phase transition temperature
THF	Tetrahydrofuran
TLC	Thin layer chromatography
TMA-DPH	1-(4-trimethylammonium phenyl)-6-phenyl-1,3,5-hexatriene p-toluenesulfonate.
TMS	Tetramethylsilane
TMSOTf	Trimethylsilyl trifluoromethanesulfonate
Tol	Toluene
TPHB	Triphenylphosphane hydrobromide
TTN	Thallium(III) trinitrate
TtSPP	*Thermoanaerobacterium thermosaccharolyticum*
UDP	Uridine diphosphate
UPLC	Ultra-Performance Liquid Chromatography
VRE	Vancomycin-resistant *Enterococcus*

Preface

"…[carbohydrates] are a collection of molecules upon which all plant and animal life depend"
R. W. Binkley

Carbohydrates represent a unique family of polyfunctional compounds particularly important in life processes. A classic example are nucleic acids, the basis of genetic information, which are in fact carbohydrate-containing polymers. Carbohydrates' presence is essential in all cell walls, from microbes to mammals.

It was Emil Fisher (1852-1919) who set the foundations for carbohydrate chemistry by establishing the stereochemical and isomeric nature of sugars, but the great advent of the field took place in the 1970s, when more sophisticated techniques rise.[a] This led to a deeper understanding of biochemical processes at a molecular level, and consequently, the realization of the role of complex oligosaccharides in biological molecular recognition processes. Concurrently, the synthetic challenge towards new biologically active molecules with a specific stereochemistry was becoming appealing for many organic chemists.

Until today, glycosciences based on glycochemistry and glycobiology continue to fascinate scientists worldwide. It is now known that carbohydrates are key code molecules in

[a] Fairbanks, A. J. and Davis, B. *Carbohydrate Chemistry*. Oxford Chemistry Primers. Vol. 99. **2002**. Oxford University Press.

biological events such as conception (fecundation), microbial infection, inflammation and cancer growth. Besides their importance in life processes, carbohydrates have the potential to be chemically manipulated in a multitude of ways, being converted in compounds of interest in food, clothing, pharmaceutical and agrochemical industries. Research in chemistry, biochemistry and biology of carbohydrates have hugely contributed to all these fields and, ultimately, to medicine.

Ageing and infection are the two major societal challenges of the 21st century, on one hand due to the increase in the life expectancy, and on the other due to the emergence of antibiotic resistance. Indeed, infections in elderly populations are known to be more frequent and severe.[b] Immunosenescence, malnutrition and diverse age-associated physiological and anatomical alterations are amongst the reasons for this increased susceptibility to infection. Of these, malnutrition is one of the major causes of immune function decline: not only malnutrition may be the cause of infection, but also infection leads to further malnutrition.[5] In this context, the incidence of a neurodegenerative disorder such as dementia, and more specifically Alzheimer's disease is an important aggravation factor, since these patients become dependent on others, often losing the ability to communicate, their appetite and eventually the ability to swallow.

It has been suggested that not only ageing may be the cause of infection, but infection can also be the cause of ageing.[b] One of the major challenges before nowadays society is, undoubtedly, to provide care for this ageing population.

[b] Gavazzi, G. and Krause, K.-H. Ageing and infection. *The Lancet Infectious Diseases*, **2002**. 2(11): 659-666.; Cotterell, C. Holmes and D. Role of infection in the pathogenesis of Alzheimer's disease. *CNS Drugs*, **2009**. 23(12): 993-1002

Alkyl 2-deoxy/2,6-dideoxy-*arabino*-hexopyranosides have been studied by the Carbohydrate Chemistry group, revealing potent antimicrobial activity against Gram-positive bacteria, in particular *Bacillus* species. Additionally, in the context of my Master degree dissertation, promising results arising from NMR interaction studies of 2,6-dideoxyglycosides with cystatin B amyloid fibrils, show their potential for neurodegenerative diseases. These results inspired this thesis endeavour, comprising the research on carbohydrate-based molecules with antimicrobial activity and anti-neurodegenerative potential. It questions whether the antimicrobial activity of such alkyl deoxyglycosides can be optimized, and how they act. It also queries the ability of the sugar moiety to improve the bioactivity and/or bioavailability of natural products with neuroprotection properties.

In the introduction, the literature portfolio of bioactive products acting on ageing events or infection is unveiled, where the information is divided in three sub-chapters, two of which were book chapters published in international book series. The first section reviews the most recent developments on membrane-targeting antibiotics. Given the further exploratory nature of the application of 2-deoxyglycosides in neurodegeneration, the subchapters 1.2 and 1.3 are both dedicated to this theme. On one hand, the significance of carbohydrates and glycomimetics in Alzheimer's disease is discussed, and on the other hand, the role of coupling sugars to phenolic biomolecular entities is evaluated.

The results obtained, as well as their discussion and the applied methodologies, are disclosed from Chapters 2 to 5. Firstly, the synthesis of 2-deoxyglycosides from glycals catalysed by TPHB is presented as a proven method. This methodology was scrutinized by us and submitted to the book series "Proven synthetic methods in carbohydrate chemistry". This book series, where an independent checker verifies the protocol, aims at opposing the irreproducibility of synthetic protocols and inflated yields reported in chemical communications. In chapter 3, this same method is applied to the synthesis of a series of new

alkyl 2-deoxyglycosides analogues, including *S*-glycosides. More importantly, it describes the search and discovery of the unprecedent mode of action of the lead compound, submitted for publication in the journal Nature Communications. Chapter 4 is dedicated to the assessment of the deoxygenation pattern of alkyl deoxyglycosides, towards their selectivity optimization.

Finally, the research on 2-deoxyglycosides embodying neuroprotective natural products is described in chapter 5, where the bioactivity of such molecular entities is evaluated on peroxide-compromised neuroblastoma cells, and their bioavailability is examined.

The chapters herein transcribed that were published (or submitted) in R&D books and peer-reviewed journals are clearly marked as such. They were written, or mostly written, by the author of this thesis, and the contributions of the remaining authors are fully disclosed in the end of each chapter.

Lisbon, April 2018

Catarina Dias

Chapter 1

Introduction

1.1 Membrane Targeting Antibiotics: Recent Developments Outside the Peptide Space [a]

The inadequate use of antibiotics over the past decades, allied to natural resilience mechanisms of bacteria, led to the rise of antimicrobial resistant strains to a point where antibiotic resistance is becoming a major society challenge of the 21st century. Antibiotics used currently in the clinic target biosynthetic processes, such as protein biosynthesis, RNA, DNA, peptidoglycan and folic acid, which lack efficiency against persistent infections in which bacteria are quiescent, i.e., slow growing or dormant.[1] These phenomena require unconventional strategies, making research on antimicrobial chemotherapy with alternative mechanisms of action of extreme importance.

Antimicrobial peptides (AMPs) are natural antibiotics that have been part of the innate immune system of a number of microorganisms, including humans, for hundreds of millions of years as a host defense mechanism.[2-3] Isolated for the first time in late 1930s, this class of antibiotics acts mainly by disrupting membrane integrity (via interaction with negatively charged cell membrane) and present surprisingly little resistance. A number of interaction models have been proposed to explain their mechanism of action, such as carpet-like, membrane thinning, toroidal pores and barrel-stove.[4] Moreover, recent studies on AMPs' mode of action revealed that they do not only affect membrane permeabilization, and some of them

[a] This chapter was submitted as it is for publication in Future Medicinal Chemistry, and accepted after minor revisions (C. Dias and A. P Rauter, *Future Med. Chem.* **2019**)

are also intracellularly active, inhibiting proteases, DNA and protein synthesis.[2,4] These amazing natural peptides, which activity and mechanism of action have been extensively reviewed,[4-5] have encouraged the scientific community to investigate smaller and more druggable molecules also able to modulate bacterial membranes, even though the collective knowledge on the optimization of this chemical space is scarce. This review will display the most recent findings on membrane targeting antibiotics, focusing on small molecules outside the antimicrobial peptide molecular space.

1.1.1 LIPID DIVERSITY: THE KEY TOWARDS SELECTIVITY

Throughout all living organisms, a small hydrophobic layer defines the borders between a cell's life and death. Although lipid diversity is on the same order of magnitude as that of proteins, and despite their clear importance and essential functions, lipids have not been as well studied as proteins,[6] in particular as drug targets. However, regarding antibiotics, there is one aspect that makes targeting bacteria cell membrane so appealing: its essentiality. The bacterial membrane is essential independently of the metabolic status of the cell, as it is not only vital for homeostasis and metabolic energy transduction, but it also houses one third of cell proteins, which regulate a number of crucial roles. Thus, cell envelope ultra-structures cannot easily change without substantial loss of function, and the development of resistance becomes incredibly difficult, as observed for AMPs.[1]

The major structural lipid in eukaryotic membranes is phosphatidylcholine (PC), accounting for more than 50% of all glycerophospholipids. Due to its geometry, it organizes spontaneously in a planar bilayer (see box 1). Other phospholipids are also present, such as phosphatidylethanolamine (PE), phosphatidylserine (PS), phosphatidylinositol (PI) and phosphatidic acid (PA). The inclusion of the conical shaped PE in bilayers adds curvature, which is crucial to a number of roles, such as budding, fission and fusion.[7] These phospholipids

gather almost exclusively in the inner surface of the bilayer, constituting about 30% of the cell membrane.[8] Conversely, prokaryotic cells have a rather different membrane composition, being mostly composed of PE and PG (phosphatidylglycerol), and devoid of PC. While Gram-negative bacteria can have up to 80% in PE (p.e. *E. coli*), Gram-positive bacteria present diverse membranes with various proportions of PE, PG and CL (cardiolipin).[9]

It is easily observed that mammalian and bacterial membrane phospholipids diverge in nature and relative proportion, and consequently, in biophysical and physical-chemical properties. For instance, while PC and PE are zwitterionic, PG and CL are anionic, resulting in bacterial membranes more negatively charged than their mammalian counterparts. This lipid diversity opens a door towards selectivity. Indeed, a recent *in silico* study shows that the entry of an amphiphilic antimicrobial lipopeptide is more favorable in a POPE:POPG model membrane than in a membrane composed of POPC, enhancing the thermodynamic and kinetic selectivity for bacterial versus mammalian model membranes.[10] Moreover, lipids can adopt different liquid crystalline structures upon hydration. The predominant structures assumed by isolated species of membrane lipids in excess aqueous buffer are the lamellar phase (bilayer) and the inverted hexagonal phase (H_{II}) structure (Figure 1.1.1).[11] Lipid polymorphism is strongly dependent on the molecular shape of lipids: while cone-like molecules (e.g. phosphatidylethanolamine) tend to pack into structures with high radii of curvature, cylindrical molecules (e.g. phosphatidylcholine, PC) organize into flat bilayers.[11-12] Although in biological membranes lipids adopt a bilayer structure, non-lamellar structures, such as inverted hexagonal phase play an important role in membrane processes, specifically membrane fusion, vesicle stability, trans-bilayer transport and pore formation.[13-14] This lipid diversity has the potential to be explored towards selectivity, where differential interaction of amphiphilic drug and bacterial cell vs. host cell can play a key role.

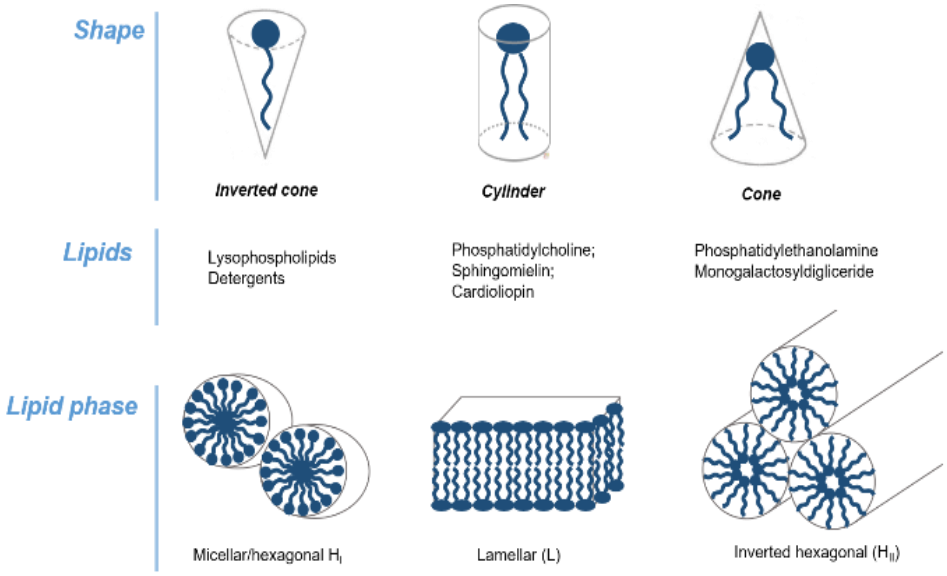

Figure 1.1.1 Lipid shape and polymorphism

1.1.2 PEPTIDES AND ANALOGUES

1.1.2.1 Antimicrobial peptides

Antibacterial peptides were the first membrane targeting antibiotics to be approved by FDA. Most AMPs contain a net excess of positively charged residues and a size ranging from 12 to 50 amino acid residues, of which approximately 50% are hydrophobic in nature.[15] The potency of these peptides is generally in the micromolar range, which is characteristic of nonspecific mode of action. As already discussed, AMPs' mechanism of action relies mainly upon interaction with the bacterial membrane, although other phenomena have been identified, such as interaction with DNA, stimulation of the innate immunity system by promoting the release of natural defence peptides, and stimulating phagocytic cells.[16] The majority of antimicrobial peptides adopt amphiphilic secondary structures in which cationic amino acid side chains (i.e., arginine, lysine, and histidine) are oriented on one face of the molecule while hydrophobic side chains are on the opposing face. This morphology has been termed "facially

amphiphilic".[17] They bind preferentially to negatively charged and zwitterionic phospholipids, exposed in bacterial membranes, giving them the necessary selectivity.

The main limitation of AMPs is their toxicity, guilty of many serious adverse effects, as well as their low *in vivo* stability due to degradation by proteases, extensive serum binding and loss of antimicrobial activity in the presence of physiological concentration of salts. For these reasons, the discovery process for non-cytotoxic antimicrobial peptides required several rounds of optimization to find derivatives with the suitable physicochemical properties.[18-19] Furthermore, their complex design results in high production costs. However, the positive remarks on antimicrobial peptides, such as lack of resistance, made them reach the market. The lipopeptides daptomycin (**1**) and televacin (**2**) (Figure 1.1.2) were the first antibiotics targeting the membrane approved by the FDA that are clinically used.

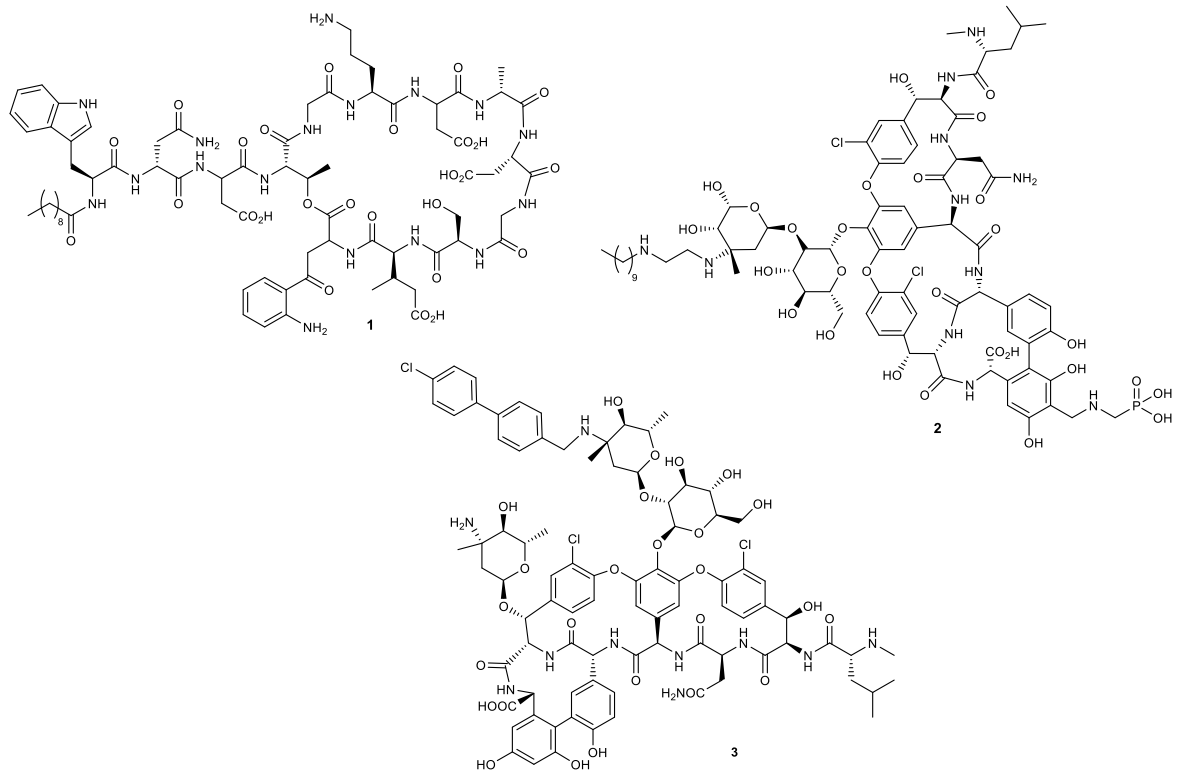

Figure 1.1.2. Antimicrobial peptides daptomycin (**1**), televacin (**2**) and oritavancin (**3**).

In 2014, oritavancin (**3**, Figure 1.1.2), a semi-synthetic glycopeptide similar to vancomycin, a protein biosynthesis inhibitor, was approved by FDA for the treatment of skin infections. Oritavancin, which is active on many resistant Gram-positive organisms including methicillin-resistant or vancomycin-resistant *S. aureus*, also acts by inhibiting peptidoglycan biosynthesis. However, its rapid bactericidal activity against biofilm mediated infections has been attributed to its ability to depolarize and permeate bacterial membranes.[20] Indeed, vancomycin is inactive against staphylococcal biofilms.

Despite their clear importance in the fight against resistant Gram-positive infections, peptides **1**-**3** have to be administrated intravenously. These peptides have inspired new avenues of investigation, which have been pursued in order to find more selective and smaller molecules, with the same antibacterial potential. Some of these lines of investigation will be disclosed in the fore coming sections.

1.1.2.2 Gramicidin S and synthetic analogues

Gramicidin S (GS, **4,** Figure 1.1.3) is a cationic cyclic decapeptide secreted by *Bacillus brevis,* discovered in the early 1940s, with potent antimicrobial activity against Gram-positive and Gram-negative bacteria, as well as pathogenic fungi.[21-22] The high haemolytic activity of this antibiotic restricts its use to topical applications, although it saved many lives in the battle fronts of World War II, where it was used to treat infected wounds.[23] Only later it was discovered that this antibiotic compromises the phospholipid bilayer barrier via a wide variety of transient, differently sized defects.[24] Some attempts to synthesize less toxic analogues of gramicidin S have been described in the literature. Earlier efforts include the use of arylated sugar amino acids as a replacement of one of the two D-Phe-Pro turn regions (**5**, Figure 1.1.3), which was not successful.[25] Later, the synthesis of asymmetric gramicidin S analogues, where

the D-Phe was modified to contain an exposed amide, provided one analogue with a comparable antimicrobial activity as GS, and a slightly reduced hemolytic activity.[26] More recently, Legrand and co-workers presented the synthesis of a new analogue in which the D-Phe-Pro turn was replaced by a γ-amino acid with a thiazole ring (**6**, Figure 1.1.3). This derivative was able to maintain an antimicrobial activity very close to that of gramicidin S, while leading to a remarkably lower hemolysis, reducing it from 80% to 14%.[27] Transition of these analogues into clinic is yet to be reported.

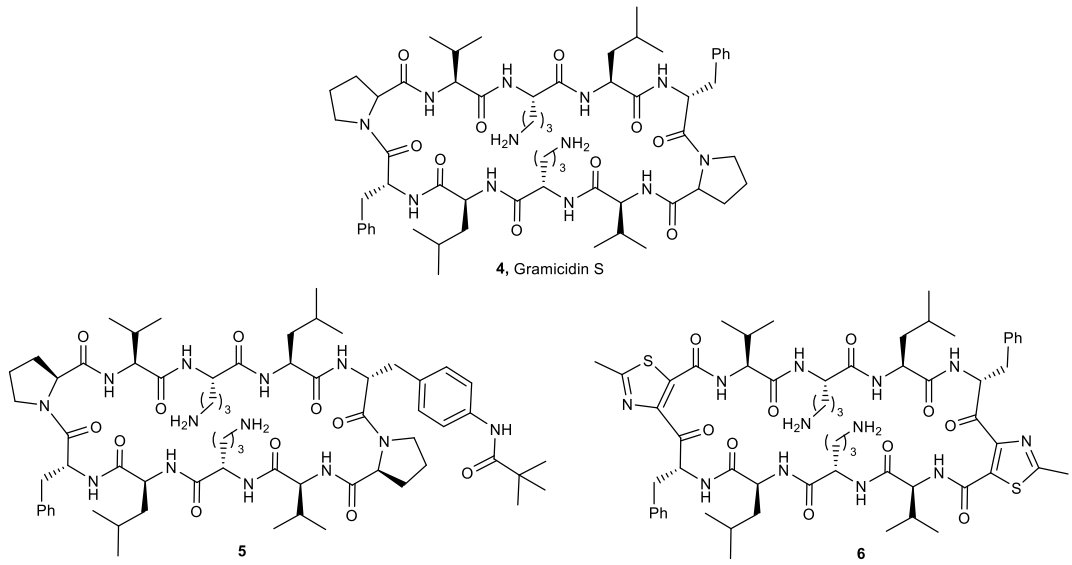

Figure 1.1.3. Structure of Gramicidin S and analogues.

1.1.2.3 Synthetic antimicrobial peptidomimetics (SAMPs)

One approach to overcome AMPs limitations was to develop smaller antibacterial peptides. The preparation of a series of small peptides (2-5 amino acids) and peptide esters with the key features of an AMP – cationic charge and bulky hydrophobic residues – allowed to understand that the pharmacophore was unpredictably small. For antistaphylococcal activity, a net charge of +2 and the presence of at least two bulky/lipophilic moieties are the only structural key features required. For instance, compound **7** is active against *S. aureus*, MRSA

and MRSE at 15, 15 and 10 μg/mL, respectively.[15] The resulting antimicrobial peptides, later called synthetic antimicrobial peptidomimetics (SAMPs) mimic the antibacterial properties of AMPs, while having improved pharmacokinetic properties.[28] More recently, a large *tert*-butyl substituted tryptophan was also synthesized. Ltx5 (**8**, Figure 1.1.4), permeabilizes both the membrane of *E. coli*, and quickly eradicates *S. aureus*, while keeping a high *in vitro* stability in human blood plasma, as well as low toxicity.[28] Later, it was shown that Ltx5, as well as other less active analogues, were able to eliminate metabolic activity in the *S. epidermidis* and *S. haemolyticus* biofilms, although that was only verified at a concentration 10 times higher than the MIC value.[29]

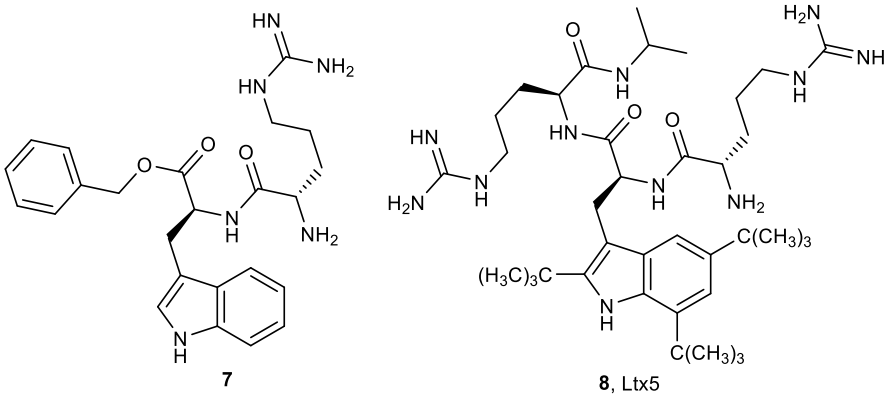

Figure 1.1.4. Structure of two synthetic antimicrobial peptidomimetics.

1.1.3. OUTSIDE THE PEPTIDE MOLECULAR SPACE

1.1.3.1 Ceragenins

Ceragenins are cholic acid derivatives that mimic the activity of endogenous antimicrobial peptides.[9,17] Ceragenins effectively reproduce AMPs facial amphiphilicity while being resistant to proteolysis and more suitable to large-scale synthesis. Many of these structures are polycationic and possess a lipophilic moiety, thus being capable of partitioning into membranes.[9] Their overall positive charge allows them to have selectivity against

microbes with exposed anionic and zwitterionic lipids. Although some forms of ceragenins are effective against both Gram-negative and Gram-positive bacteria, they are generally more potent against Gram-positive organisms. The most potent ceragenin to date is CSA-13 (**9**, Figure 1.1.5), considered a broad-spectrum antimicrobial, being mostly active against Gram positive bacteria, such as *S. aureus* (0.4 μg/mL), *S. pyogenes* (0.5 μg/mL), *B. subtilis* (0.5 μg/mL) and *B. anthracis* (2.5 μg/mL), but also considerably active on the Gram negative *E. coli* (3 μg/mL) and *P. aeruginosa* (2 μg/mL).[9] CSA-13 has also shown potent activity against bacterial biofilms.[30] The antimicrobial activity of ceragenins correlates well with a membrane composition containing a high concentration of phosphatidylethanolamine or uncharged lipids. It was demonstrated that ceragenins caused membrane depolarization, which is sufficient to cause lethality and can be seen as an indicator of potency.[17] While membrane depolarization is pointed as the primary mode of action of ceragenins, an intracellular target is yet to be excluded to influence antimicrobial activity. Remarkably, a recent study supports that *in vivo* activity of CSA-13 may additively and/or synergistically interact with host antibacterial molecules, helping the innate immune system to act on peritoneal *P. aeruginosa* infections.[31] The toxicity concern associated with amphiphilic molecules is also an issue with ceragenins. This was recently tackled by immobilizing CSA-13 on magnetic nanoparticles' surface, significantly decreasing the hemolytic activity while maintaining its strong antibacterial activity. This is possible due to an imine link between the ceragenin and the nanoparticle that hydrolyses in acidic environments, such as infection and inflammation sites.[32] In another approach, CSA-13 was combined with pluronic F-127, a nonionic surfactant used as thermoreversible drug release system. In the presence of pluronic F-127, CSA-13 antibacterial activity was only slightly decreased, but its haemolytic activity was significantly inhibited. This study also pointed out that, as CSA-13's antibacterial activity is reduced in blood plasma, CSA-13 application has greater potential to prevent or treat topical bacterial infection.[33]

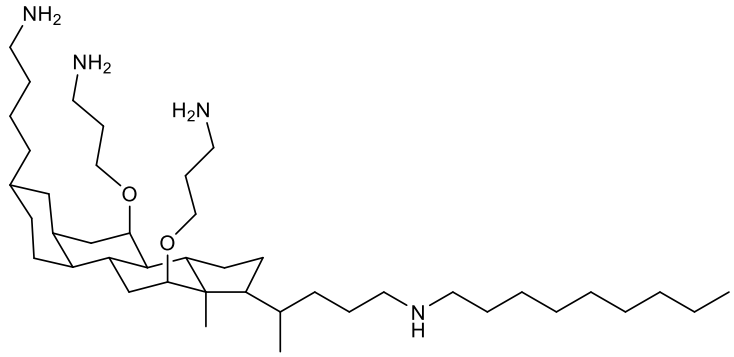

9, CSA-13

Figure 1.1.5. Structure of ceragenin CSA-13.

1.1.3.2 Reutericyclin and derivatives

Reutericyclin (**10**, Figure 1.1.6) is a naturally occurring tetramic acid antibiotic produced by sourdough isolates of *Lactobacillus reuteri*,[34-36] active against Gram-positive bacteria, including pathogens such as methicillin-resistant *Staphylococcus aureus*, *Streptococcus sp*. and *Clostridium difficile*.[34] It is a highly hydrophobic and negatively charged molecule, thus being able to partition into the cytoplasmic membrane, although it does not form pores. Rather, it acts by translocating protons across the cytoplasmic membrane and consequently dissipating the transmembrane ΔpH, resembling the action of weak organic acid (acetic acid and sorbic acid).[35] The structure of reutericyclin is still under development stage, particularly due to its chemically instability and consequent challenging synthesis. To overcome this, Hurdle and co-workers proposed a series of easily synthesizable reutericyclin derivatives, such as **11** (Figure 1.1.6), that were able to eradicate staphylococcal biofilms much more effectively than the original compound, unlike the standard topical antibiotic mupirocin, which is not able to eradicate biofilms.[36] Reutericyclines were then proposed to de developed as new topical antibiotics. However, attempts to further optimize the structure towards a more potent antibacterial activity also increased cytotoxicity in kidney cells.[34] These development challenges are expected during membrane targeting antibiotic molecules and are in line with

the discovery of non-toxic AMPs, as discussed previously. Further investigation on reutericyclin derivatives is required before clinical studies.

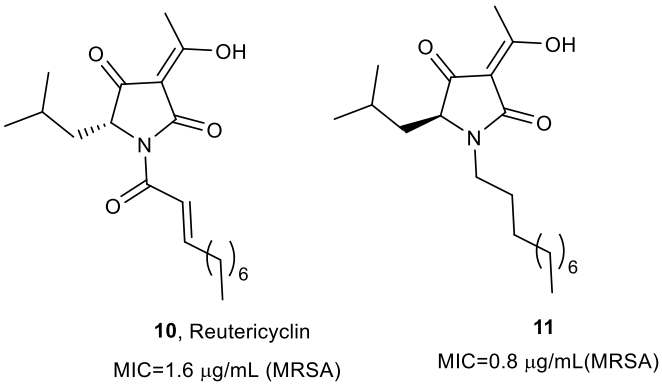

Figure 1.1.6. Reutericyclin and structure of its analogue **11**.

1.1.3.3 Carbohydrate based amphiphiles

Aminoglycosides

Aminoglycosides are a group of antibiotics used as last resource treatment of serious systemic Gram-negative infections, that inhibit protein biosynthesis by binding to the 16s ribosomal RNA. Like other classic antibiotics, their widespread use led to the emergence of bacterial resistance, which, in association with the serious side effects they cause, contributed to their clinical decline.[37] In recent years, aminoglycosides have been revisited, and several groups have tried to incorporate hydrophobic units in these oligosaccharide structures to obtain membrane disrupting antimicrobial agents.[38-39] These so called amphiphilic aminoglycosides (AAG) can result from introduction of one or several lipophilic groups on the AG amino and/or hydroxy groups (Figure 1.1.7). Parent aminoglycosides coupled with lipophilic moieties include neomycin B (**12**), neamine (**13**), tobramycin (**14**) and paromycin. Simply by benzylating neomycin B hydroxy groups (compound **15**, Figure 1.1.7), antibiotic activity against Gram-positive bacteria was improved.[40] Schweizer and co-workers also reported that

decoration of neomycin B with a palmitoyl moiety (compound **16**, Figure 1.1.7), followed by conversion of the free amines into guanidines resulted in a compound 32 times more potent than neomycin B against MRSA, with only 13% of hemolysis.[41]

Successful alterations to neamine include its *O*-alkylation with naphtylpropyl groups (compound **17**, Figure 1.1.7). Such compounds presented an activity on Gram-positive bacteria of 2-16 μg/mL, and in vitro affinity to LPS comparable to that of polymyxin B.[42] One of the most active compounds also showed a low toxicity in eukaryotic cells at 10 μM.

Fridman and his team have been trying to find the structural parameters essential to antimicrobial activity and membrane selectivity of Tobramycin derived amphiphilic aminoglycosides.[40, 43] They established that linear aliphatic chains are better than aryl based ones and, by altering the number, length, bond and position of said aliphatic chains, they were able to generate AAGs with potent antimicrobial activity against a broad spectrum of bacteria, in some cases, 32-fold more potent than tobramycin. The C14 aliphatic chain analogues were the most potent antimicrobial agents when compared to the corresponding C12 and C16 chain analogues. Unfortunately, they could not establish a linear correlation between the antimicrobial potency and the hemolytic activity of tobramycin analogues, as all parameters affected differently both biological outcomes. However, amide bound C12 analogue (compound **18**, Figure 1.1.7) was significantly more potent than tobramycin against a number of staphylococcal strains and caused little measurable heamolysis in rats. The analogue AAG with the chain linked to tobramycin via a triazole was highly hemolytic. Some of the tobramycin derivatives, including compound **18**, also inhibited biofilm growth of *S. mutans* and *S. epidermidis* (MBIC 4-64 μg/mL).[43] Although these parameters only do apply to tobramycin, the optimized hydrophobicity/hydrophilicity ratio could be translated to paromycin derivatives. Coupling this aminoglycoside with two C7 aliphatic chains resulted in

a potent antimicrobial activity (MIC 2-16 μg/mL) against several staphylococcal strains, including MRSA, while presenting negligible hemolysis at 32 μg/mL.[40]

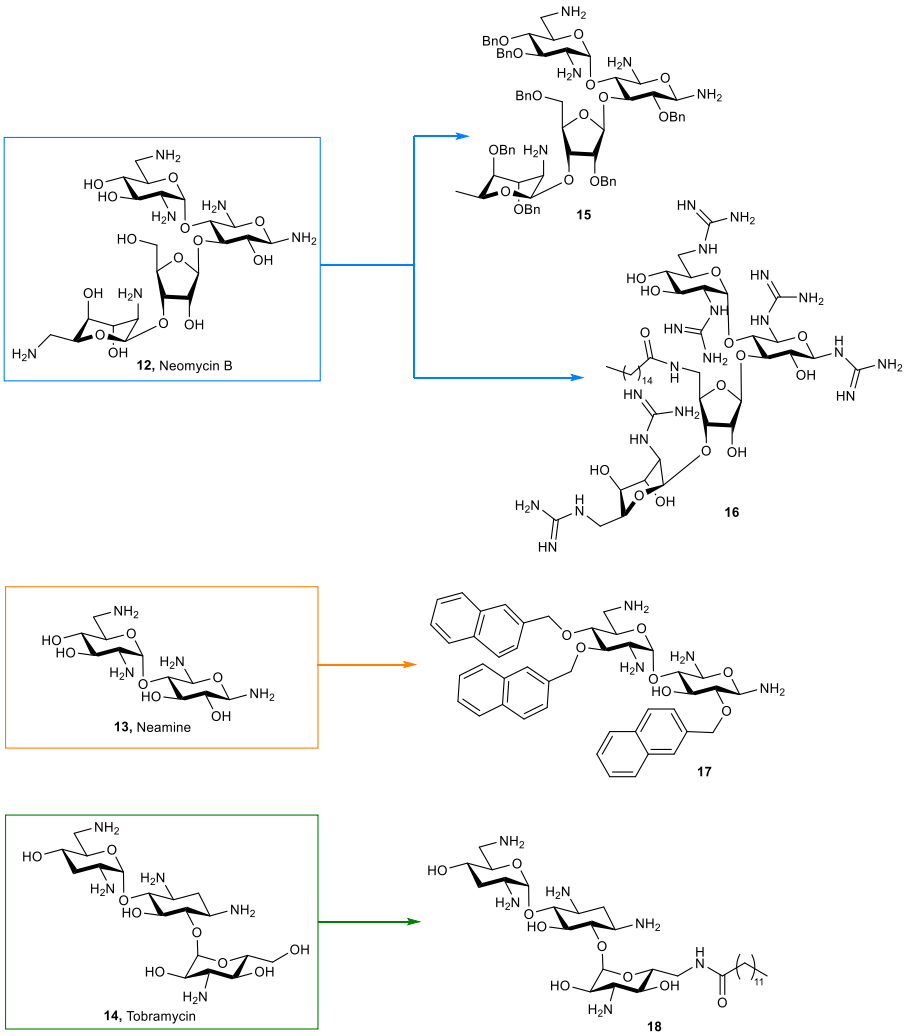

Figure 1.1.7. Structure of amphiphilic aminoglycosides **12** to **18**.

The mode of action of these new aminoglycosides has not yet been disclosed, although its amphiphilic nature and their LPS affinity *in vitro* point to a membrane related mechanism. Nevertheless, it would be interesting to deeply understand how compounds **15** to **18** interact with bacteria membranes.

Polyene Macrolides

Polyene macrolides are potent antifungal agents used to treat both superficial and invasive fungal infections. These amphipathic molecules, structurally characterized by a large lactone ring with multiple double bounds, target the membrane of sensitive organisms and form small diameter channels (~ 0.6 nm) that ultimately lead to cell death. Examples include and amphotericin B (**19**), approved for the treatment of invasive mycoses in humans, and nystatin (**20**), which use is limited to topical infections due to its high toxicity, despite its higher antifungal activity (Figure 1.1.8).[44-45]

The toxicity and severe side effects caused by polyene macrolides is easily explained by the fact that they target membranes containing sterols (ergosterol and cholesterol), common to both fungal and mammalian cells. Interestingly, a very recent work showed that the ability of nystatin to form and stabilize pores is not dependent on the presence of such sterols, but rather on the presence of highly ordered membrane domains.[45] In addition, the authors also showed that pore formation is accompanied by strong Nys-induced membrane reorganization, highlighting that, although ergosterol might be essential to Nys antifungal activity, other biophysical membrane properties need to be addressed to further understand the mechanism of action and toxicity of such molecules.[45]

Alterations in the structure of polyene macrolides towards less toxic analogues have been attempted. Worth mentioning is the biosynthetic engineering of *Streptomyces noursei* that resulted in a series of nystatin analogues with changes in the polyol region and exocyclic carboxyl group. It was found that replacement of the C-16 carboxyl with a methyl group and hydroxylation of C-9 (**21**, Figure 1.1.8) increased the antifungal activity while reducing the hemolytic activity, increasing in 2-fold the selectivity (relative to amphotericin B).[46]

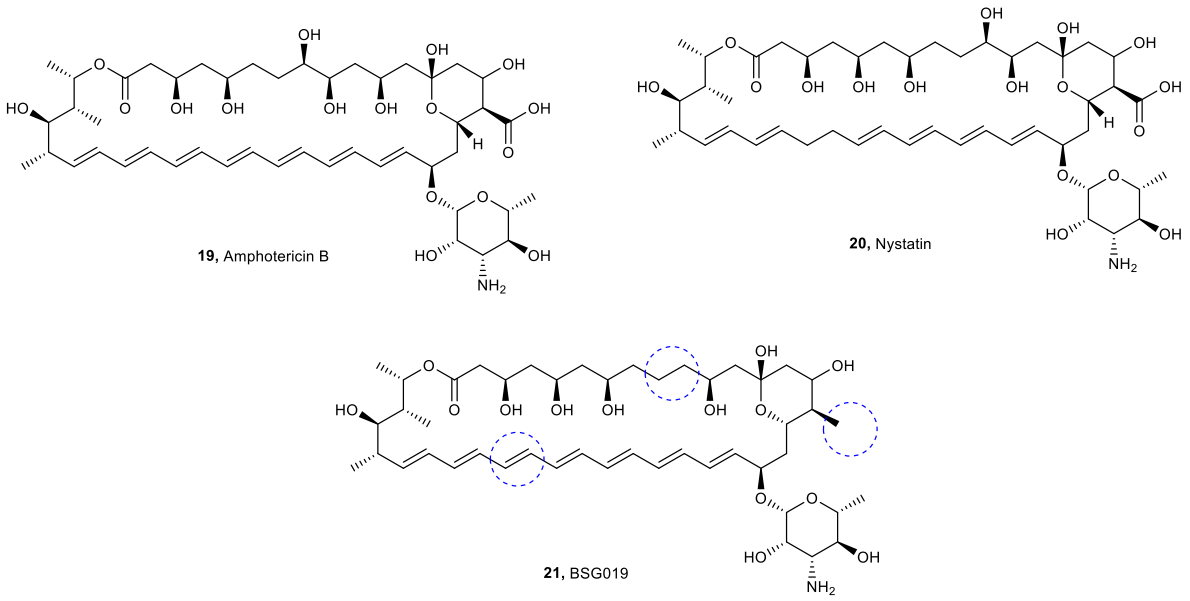

Figure 1.1.8. Polyene macrolides amphotericin B (**19**), nystatin (**20**) and BSG019 (**21**).

1.1.3.4 Other structures

Xanthone derivatives

Recently, two xanthone derivatives symmetrically decorated with isoprenyl and arginine moieties (**22** and **23**, Figure 1.1.9), have shown potent antimicrobial activity against Gram-positive bacteria, in particular MRSA (0.78-3.13 μg/mL) and VRE (1.56-6.25 μg/mL).[47] Given their amphiphilic and cationic character, their ability to disrupt bacterial membranes leading to the leakage of intracellular components comes with no surprise. These molecules are, however, surprisingly selective towards bacteria, causing 50% blood cell haemolysis (HC_{50}) only above 750 μg/ mL and 2000 μg/ mL. This is allegedly due to electrostatic preference of negatively charged bacterial membranes over the zwitterionic eurkaryotic cells. As already discussed, membrane-targeting antibiotics present little resistance, since it is difficult for bacteria to remodel their membranes. The optimized xanthone derivatives were no exception, presenting no significant change in the MIC after bacterial exposure. In addition, compound **22** was successfully tested in an animal model of cornea infection.[47]

Porphyrin derivative (XF73)

The dicationic porphyrin XF73 (**25**, Figure 1.1.9) is a fairly recent antistaphylococcal compound, developed by Destiny Pharma Ltd. With a MIC comparable to that of daptomycin, tetracycline and vancomycin (1 μg/mL), it acts by compromising the cytoplasmic membrane, inducing >90% reduction of membrane potential at 4xMIC, loss of intracellular cations and reduction of cell viability.[48] XF-73 is currently in clinical development, and successfully passed phase I clinical trials.[49]

Quinolone derivative (HT61)

HT61 (**24**, Figure 1.1.9) is a quinoline-derived antimicrobial exhibiting bactericidal activity against both multiplying and quiescent *S. aureus*. It also kills mupirocin resistant MRSA. HT61 is able to kill bacteria in 2 hours by depolarizing the cell membrane.[50] It was recently shown that depolarization of the membrane and release of intercellular constituents occurs at concentrations both above and below the MIC, and that HT61 selectively binds to anionic lipids.[51] This quinolone derivative was also explored as enhancer of the antimicrobial activity of topical applications of neomycin, gentamicin, mupirocin and chlorhexidine, against both MSSA and MRSA.[52] Phase II clinical trial on the use of HT61 in anterior nares of subjects with nasal carriage of *S. aureus* was recently completed, but the results are not available.[53]

Benzophenone derivatives

In 2009 a set of benzophenone-based antibiotics were presented, exhibiting MICs of 0.68 μM to 1.36 μM against the Gram-positive bacteria MRSA and VRSA (**26** and **27**, Figure 1.1.9).[54] At the time, preliminary studies showed that **26** (SV1) and **27** (SV7) disrupted the

membrane potential. Later, additional studies confirmed this mechanism of action, and showed that this was a consequence of potassium ions release from the bacteria cell.[55] Interestingly, these compounds have also good affinities for polyanionic components of the cell wall, such as lipoteichoic acids (LTA), present in Gram-positive membranes, and lipopolysaccharides (LPS) which are part of Gram-negative membranes. These benzophenone derived compounds display no hemolytic activity up to a concentration that is 100 times the MIC values.

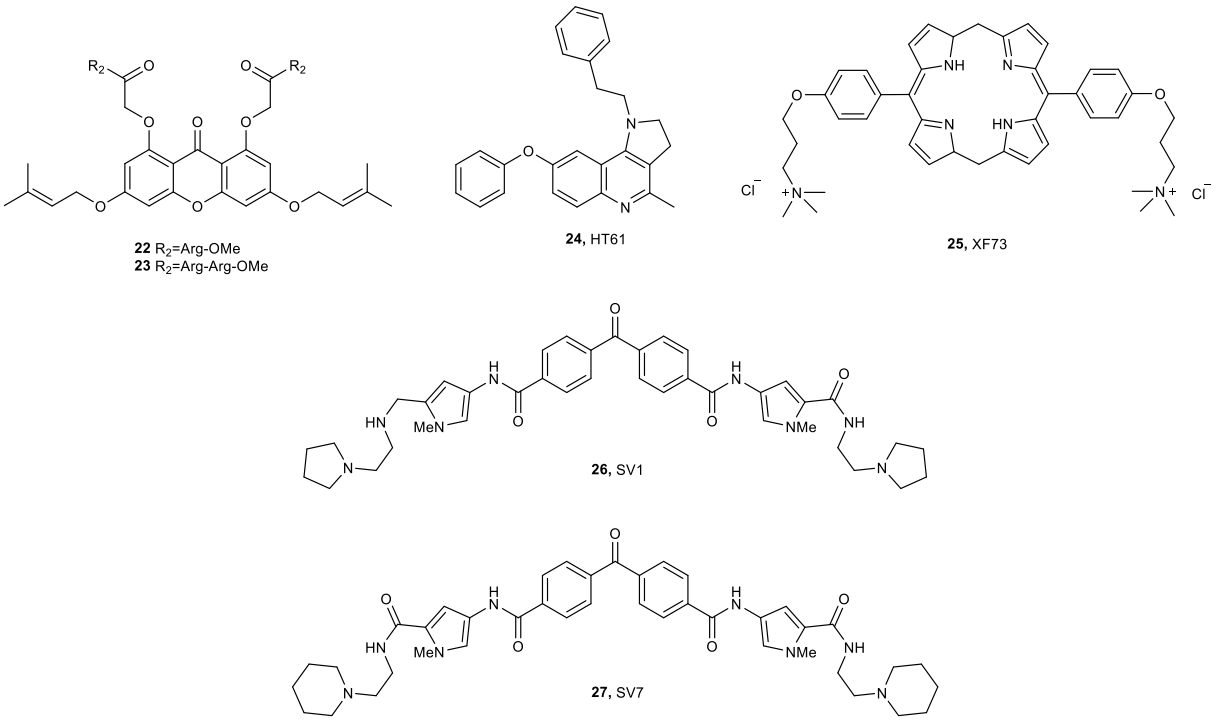

Figure 1.1.9. Membrane targeting antimicrobials **22-27.**

1.1.4. CONCLUSION

The essentiality of cell membrane, adding to its highly conservative structure, makes it a promising target for new antibiotics, and adds difficulty to drug resistance. The fact that bacterial membrane is essential independently of the metabolic status of the cell may be particularly relevant for persistent and biofilm mediated infections.[1] In addition, molecules that target the cell membrane or cell walls have also the potential to synergize with conventional

antibiotics or antiseptics by weakening the cell envelope and increasing cellular permeability.[53] However, this mechanism has been underexploited, and chemotypes with bacterial membrane disruption properties are often avoided and disregarded due to concerns over selectivity. In fact, most research on this field shows that the optimization towards membrane selectivity is highly variable and pattern identification has not been easy. The well-known differences between eukaryotic and prokaryotic cell membrane composition should be further explored, as demonstrated in this report. Most antibacterials here disclosed act by selectively binding to anionic lipids of bacteria or polyanionic components of the cell wall, such as lipoteichoic acid and lipopolysaccharides. The success of this strategy has been demonstrated for AMPs, the only membrane targeting antibiotics to this date to reach clinic. The pursue of more druggable molecules led to the discovery that the pharmacophore of AMPs is smaller than anticipated, which led to the disclosure of the so called small antimicrobial peptides (SAMPs). On the other hand, research outside the peptide space has been prolific, with several promising classes of membrane targeting antimicrobials, such as ceragenins, reutericyclines, carbohydrate amphiphiles, among others. The repertoire here presented is structurally quite diverse, although they all have in common the presence of an amine and a large lipophilic moiety(ies), which can be (but not limited to) an alkyl chain. Most of the compounds cited still need further optimization regarding membrane selectivity, but the results are promising, especially in an era where the fight against antibiotic resistance requires out-of the box strategies.

REFERENCES

[1] J. G. Hurdle; A. J. O'Neill; I. Chopra; R. E. Lee, Targeting bacterial membrane function: an underexploited mechanism for treating persistent infections. *Nature Reviews. Microbiology* **2011,** *9* (1), 62-75.

[2] L. W. Hamoen; M. Wenzel, Editorial: Antimicrobial Peptides - Interaction with Membrane Lipids and Proteins. *Frontiers in Cell and Developmental Biology* **2017,** *5*, 4.

[3] J. Overhage; A. Campisano; M. Bains; E. C. Torfs; B. H. Rehm; R. E. Hancock, Human host defense peptide LL-37 prevents bacterial biofilm formation. *Infection and Immunity* **2008,** *76* (9), 4176-82.

[4] A. A. Bahar; D. Ren, Antimicrobial peptides. *Pharmaceuticals* **2013,** *6* (12), 1543-75.

[5] S. Omardien; S. Brul; S. A. Zaat, Antimicrobial Activity of Cationic Antimicrobial Peptides against Gram-Positives: Current Progress Made in Understanding the Mode of Action and the Response of Bacteria. *Frontiers in Cell and Developmental Biology* **2016,** *4*, 111.

[6] E. Muro; G. E. Atilla-Gokcumen; U. S. Eggert, Lipids in cell biology: how can we understand them better? *Molecular Biology of the Cell* **2014,** *25* (12), 1819-23.

[7] G. van Meer; D. R. Voelker; G. W. Feigenson, Membrane lipids: where they are and how they behave. *Nature reviews. Molecular cell biology* **2008,** *9* (2), 112-24.

[8] R. F. Epand; M. A. Schmitt; S. H. Gellman; R. M. Epand, Role of membrane lipids in the mechanism of bacterial species selective toxicity by two alpha/beta-antimicrobial peptides. *Biochimica et Biophysica Acta* **2006,** *1758* (9), 1343-50.

[9] R. F. Epand; P. B. Savage; R. M. Epand, Bacterial lipid composition and the antimicrobial efficacy of cationic steroid compounds (Ceragenins). *Biochimica et Biophysica Acta* **2007,** *1768* (10), 2500-9.

[10] D. Lin; A. Grossfield, Thermodynamics of Micelle Formation and Membrane Fusion Modulate Antimicrobial Lipopeptide Activity. *Biophysical Journal* **2015,** *109* (4), 750-9.

[11] P. R. Cullis; M. J. Hope, Chapter 1 Physical properties and functional roles of lipids in membranes. In *New Comprehensive Biochemistry*, D. E. Vance; J. E. Vance, Eds. Elsevier: 1991; Vol. 20, pp 1-41.

[12] D. D. Lasic, Novel applications of liposomes. *Trends in Biotechnology* **1998,** *16* (7), 307-21.

[13] G. Basanez; J. L. Nieva; E. Rivas; A. Alonso; F. M. Goni, Diacylglycerol and the promotion of lamellar-hexagonal and lamellar-isotropic phase transitions in lipids: implications for membrane fusion. *Biophysical Journal* **1996,** *70* (5), 2299-306.

[14] A. Ortiz; J. A. Killian; A. J. Verkleij; J. Wilschut, Membrane fusion and the lamellar-to-inverted-hexagonal phase transition in cardiolipin vesicle systems induced by divalent cations. *Biophysical journal* **1999,** *77* (4), 2003-14.

[15] M. B. Strøm; B. E. Haug; M. L. Skar; W. Stensen; T. Stiberg; J. S. Svendsen, The Pharmacophore of Short Cationic Antibacterial Peptides. *Journal of Medicinal Chemistry* **2003,** *46* (9), 1567-1570.

[16] R. M. Epand; R. F. Epand, Bacterial membrane lipids in the action of antimicrobial agents. *Journal of Peptide Science* **2011,** *17* (5), 298-305.

[17] R. F. Epand; J. E. Pollard; J. O. Wright; P. B. Savage; R. M. Epand, Depolarization, Bacterial Membrane Composition, and the Antimicrobial Action of Ceragenins. *Antimicrobial Agents and Chemotherapy* **2010,** *54* (9), 3708-3713.

[18] D. Takahashi; S. K. Shukla; O. Prakash; G. Zhang, Structural determinants of host defense peptides for antimicrobial activity and target cell selectivity. *Biochimie* **2010,** *92* (9), 1236-41.

[19] C. D. Fjell; J. A. Hiss; R. E. Hancock; G. Schneider, Designing antimicrobial peptides: form follows function. *Nature Reviews Drug Discovery* **2011,** *11* (1), 37-51.

[20] K. D. Brade; J. M. Rybak; M. J. Rybak, Oritavancin: A New Lipoglycopeptide Antibiotic in the Treatment of Gram-Positive Infections. *Infectious Diseases and Therapy* **2016,** *5* (1), 1-15.

[21] G. F. Gause; M. G. Brazhnikova, Gramicidin S and its use in the Treatment of Infected Wounds. *Nature* **1944,** *154*, 703.

[22] N. Izumiya; T. Kato; H. Aoyagi; M. Waki; M. Kondo, *Synthetic aspects of biologically active cyclic peptides—gramicidin S and tyrocidines*. John Wiley (Halsted): New York, 1979; p 166.

[23] M. Ashrafuzzaman; O. S. Andersen; R. N. McElhaney, The antimicrobial peptide gramicidin S permeabilizes phospholipid bilayer membranes without forming discrete ion channels. *Biochimica et Biophysica Acta - Biomembranes* **2008,** *1778* (12), 2814-2822.

[24] D. A. Kelkar; A. Chattopadhyay, The gramicidin ion channel: A model membrane protein. *Biochimica et Biophysica Acta - Biomembranes* **2007,** *1768* (9), 2011-2025.

[25] G. M. Grotenbreg; A. E. Buizert; A. L. Llamas-Saiz; E. Spalburg; P. A. van Hooft; A. J. de Neeling; D. Noort; M. J. van Raaij; G. A. van der Marel; H. S. Overkleeft; M. Overhand, Beta-turn modified gramicidin S analogues containing arylated sugar amino acids display antimicrobial and hemolytic activity comparable to the natural product. *Journal of the American Chemical Society* **2006,** *128* (23), 7559-65.

[26] M. van der Knaap; E. Engels; H. J. Busscher; J. M. Otero; A. L. Llamas-Saiz; M. J. van Raaij; R. H. Mars-Groenendijk; D. Noort; G. A. van der Marel; H. S. Overkleeft; M. Overhand, Synthesis and biological evaluation of asymmetric gramicidin S analogues containing modified d-phenylalanine residues. *Bioorganic & Medicinal Chemistry* **2009,** *17* (17), 6318-6328.

[27] B. Legrand; L. Mathieu; A. Lebrun; S. Andriamanarivo; V. Lisowski; N. Masurier; S. Zirah; Y. K. Kang; J. Martinez; L. T. Maillard, Thiazole-Based γ-Building Blocks as Reverse-Turn Mimetic to Design a Gramicidin S Analogue: Conformational and Biological Evaluation. *Chemistry – A European Journal* **2014,** *20* (22), 6713-6720.

[28] B. E. Haug; W. Stensen; M. Kalaaji; Ø. Rekdal; J. S. Svendsen, Synthetic Antimicrobial Peptidomimetics with Therapeutic Potential. *Journal of Medicinal Chemistry* **2008,** *51* (14), 4306-4314.

[29] K. Flemming; C. Klingenberg; J. P. Cavanagh; M. Sletteng; W. Stensen; J. S. Svendsen; T. Flaegstad, High in vitro antimicrobial activity of synthetic antimicrobial peptidomimetics against staphylococcal biofilms. *Journal of Antimicrobial Chemotherapy* **2009,** *63* (1), 136-45.

[30] C. Nagant; B. Pitts; P. S. Stewart; Y. Feng; P. B. Savage; J. P. Dehaye, Study of the effect of antimicrobial peptide mimic, CSA-13, on an established biofilm formed by Pseudomonas aeruginosa. *Microbiology Open* **2013,** *2* (2), 318-25.

[31] R. Bucki; K. Niemirowicz; U. Wnorowska; F. J. Byfield; E. Piktel; M. Watek; P. A. Janmey; P. B. Savage, Bactericidal Activity of Ceragenin CSA-13 in Cell Culture and in an Animal Model of Peritoneal Infection. *Antimicrobial Agents and Chemotherapy* **2015,** *59* (10), 6274-82.

[32] K. Niemirowicz; U. Surel; A. Z. Wilczewska; J. Mystkowska; E. Piktel; X. Gu; Z. Namiot; A. Kulakowska; P. B. Savage; R. Bucki, Bactericidal activity and biocompatibility of ceragenin-coated magnetic nanoparticles. *Journal of Nanobiotechnology* **2015,** *13*, 32.

[33] K. Leszczynska; A. Namiot; K. Cruz; F. J. Byfield; E. Won; G. Mendez; W. Sokolowski; P. B. Savage; R. Bucki; P. A. Janmey, Potential of ceragenin CSA-13 and its mixture with pluronic F-127 as treatment of topical bacterial infections. *Journal of Applied Microbiology* **2011,** *110* (1), 229-38.

[34] P. T. Cherian; X. Wu; M. M. Maddox; A. P. Singh; R. E. Lee; J. G. Hurdle, Chemical modulation of the biological activity of reutericyclin: a membrane-active antibiotic from Lactobacillus reuteri. *Scientific Reports* **2014,** *4*, 4721.

[35] M. G. Ganzle, Reutericyclin: biological activity, mode of action, and potential applications. *Applied Microbiology and Biotechnology* **2004,** *64* (3), 326-32.

[36] J. G. Hurdle; R. Yendapally; D. Sun; R. E. Lee, Evaluation of analogs of reutericyclin as prospective candidates for treatment of staphylococcal skin infections. *Antimicrobial Agents and Chemotherapy* **2009,** *53* (9), 4028-31.

[37] M. P. Mingeot-Leclercq; Y. Glupczynski; P. M. Tulkens, Aminoglycosides: activity and resistance. *Antimicrobial Agents and Chemotherapy* **1999,** *43* (4), 727-37.

[38] I. M. Herzog; M. Fridman, Design and synthesis of membrane-targeting antibiotics: from peptides- to aminosugar-based antimicrobial cationic amphiphiles. *MedChemComm* **2014,** *5* (8), 1014-1026.

[39] M.-P. Mingeot-Leclercq; J.-L. Decout, Bacterial lipid membranes as promising targets to fight antimicrobial resistance, molecular foundations and illustration through the renewal of aminoglycoside antibiotics and emergence of amphiphilic aminoglycosides. *MedChemComm* **2016,** *7* (4), 586-611.

[40] Y. Berkov-Zrihen; I. M. Herzog; M. Feldman; A. Sonn-Segev; Y. Roichman; M. Fridman, Di-alkylated paromomycin derivatives: Targeting the membranes of Gram positive pathogens that cause skin infections. *Bioorganic & Medicinal Chemistry* **2013,** *21* (12), 3624-3631.

[41] S. Bera; G. G. Zhanel; F. Schweizer, Antibacterial activity of guanidinylated neomycin B- and kanamycin A-derived amphiphilic lipid conjugates. *The Journal of Antimicrobial Chemotherapy* **2010,** *65* (6), 1224-7.

[42] L. Zimmermann; A. Bussière; M. Ouberai; I. Baussanne; C. Jolivalt; M.-P. Mingeot-Leclercq; J.-L. Décout, Tuning the Antibacterial Activity of Amphiphilic Neamine Derivatives and

Comparison to Paromamine Homologues. *Journal of Medicinal Chemistry* **2013,** *56* (19), 7691-7705.

[43] I. M. Herzog; M. Feldman; A. Eldar-Boock; R. Satchi-Fainaro; M. Fridman, Design of membrane targeting tobramycin-based cationic amphiphiles with reduced hemolytic activity. *MedChemComm* **2013,** *4* (1), 120-124.

[44] S. B. Zotchev, Polyene macrolide antibiotics and their applications in human therapy. *Current Medicinal Chemistry* **2003,** *10* (3), 211-23.

[45] A. G. dos Santos; J. T. Marques; A. C. Carreira; I. R. Castro; A. S. Viana; M. P. Mingeot-Leclercq; R. F. M. de Almeida; L. C. Silva, The molecular mechanism of Nystatin action is dependent on the membrane biophysical properties and lipid composition. *Physical Chemistry Chemical Physics* **2017,** *19* (44), 30078-30088.

[46] T. Brautaset; H. Sletta; K. F. Degnes; O. N. Sekurova; I. Bakke; O. Volokhan; T. Andreassen; T. E. Ellingsen; S. B. Zotchev, New Nystatin-Related Antifungal Polyene Macrolides with Altered Polyol Region Generated via Biosynthetic Engineering of Streptomyces noursei. *Applied and Environmental Microbiology* **2011,** *77* (18), 6636-6643.

[47] S. Lin; J. J. Koh; T. T. Aung; F. Lim; J. Li; H. Zou; L. Wang; R. Lakshminarayanan; C. Verma; Y. Wang; D. T. Tan; D. Cao; R. W. Beuerman; L. Ren; S. Liu, Symmetrically Substituted Xanthone Amphiphiles Combat Gram-Positive Bacterial Resistance with Enhanced Membrane Selectivity. *Journal of Medicinal Chemistry* **2017,** *60* (4), 1362-1378.

[48] N. Ooi; K. Miller; J. Hobbs; W. Rhys-Williams; W. Love; I. Chopra, XF-73, a novel antistaphylococcal membrane-active agent with rapid bactericidal activity. *Journal of Antimicrobial Chemotherapy* **2009,** *64* (4), 735-40.

[49] G. Bussi; D. Donadio; M. Parrinello, Canonical sampling through velocity rescaling. *The Journal of Chemical Physics* **2007,** *126* (1), 014101.

[50] Y. Hu; A. Shamaei-Tousi; Y. Liu; A. Coates, A new approach for the discovery of antibiotics by targeting non-multiplying bacteria: a novel topical antibiotic for staphylococcal infections. *PloS one* **2010,** *5* (7), e11818.

[51] A. T. Hubbard; R. Barker; R. Rehal; K. A. Vandera; R. D. Harvey; A. R. Coates, Mechanism of Action of a Membrane-Active Quinoline-Based Antimicrobial on Natural and Model Bacterial Membranes. *Biochemistry* **2017,** *56* (8), 1163-1174.

[52] Y. Hu; A. R. Coates, Enhancement by novel anti-methicillin-resistant Staphylococcus aureus compound HT61 of the activity of neomycin, gentamicin, mupirocin and chlorhexidine: in vitro and in vivo studies. *The Journal of Antimicrobial Chemotherapy* **2013,** *68* (2), 374-84.

[53] L. S. Vermeer; B. L. de Groot; V. Reat; A. Milon; J. Czaplicki, Acyl chain order parameter profiles in phospholipid bilayers: computation from molecular dynamics simulations and comparison with 2H NMR experiments. *European Biophysics Journal* **2007,** *36* (8), 919-31.

[54] S. K. Vooturi; C. M. Cheung; M. J. Rybak; S. M. Firestine, Design, Synthesis, and Structure−Activity Relationships of Benzophenone-Based Tetraamides as Novel Antibacterial Agents. *Journal of Medicinal Chemistry* **2009,** *52* (16), 5020-5031.

[55] S. K. Vooturi; M. B. Dewal; S. M. Firestine, Examination of a synthetic benzophenone membrane-targeted antibiotic. *Organic & Biomolecular Chemistry* **2011,** *9* (18), 6367-6372.

1.2 Carbohydrates and Glycomimetics in Alzheimer's Disease Therapeutics and Diagnosis[a]

1.2.1 ALZHEIMER'S DISEASE

The increasing average life expectancy in developed countries led to an escalating concern associated with the emergence of age related diseases. Amongst them, Alzheimer's disease (AD) is the most prevalent form of late-life dementia, affecting about 35 million individuals worldwide.[1-3] The disease is particularly noteworthy due to its devastating nature, unsuccessful treatment and high socio-economic impact. Alzheimer's disease is multifaceted, characterized by a global decline in cognitive function and its pathogenesis is not yet fully understood. The main hallmark changes of AD brains include the deposition of senile plaques containing Aβ aggregates, the deposition of neurofribrillary tangles (NFTs) containing hyperphosphorylated tau protein, the loss of synaptic function, inflammation and neuronal death.[1]

The events involved in the cholinergic system are illustrated in Figure 1.2.1. The neurotransmitter acetylcholine is produced in the presynaptic neuron by choline acetyltransferase and released in the synaptic cleft, where it binds to the acetylcholine receptor on the postsynaptic membrane. Synaptic transmission is terminated by acetylcholinesterase,

[a] Dias, C.; Rauter, A. P., Chapter 8 Carbohydrates and Glycomimetics in Alzheimer's Disease Therapeutics and Diagnosis. In *Carbohydrates in Drug Design and Discovery*, The Royal Society of Chemistry: 2015; pp 180-208.

that hydrolyses acetylcholine into acetate and choline. The profound loss of cholinergic function in the brain comprises an impressive decrease in the cholineacetyltransferase level, choline uptake, and ACh level in the neocortex and hippocampus.[4] It is well established that enhancing cholinergic transmission by blocking the activity of acetylcholinesterase (AChE) slows down the AD-associated decline in behaviour and cognition. Indeed, currently prescribed drugs for the treatment of mild to moderate AD are AChE inhibitors, namely tacrine, donepezil, and rivastigmine.[4] Nevertheless, these drugs have limited use because they only lead to a temporary symptomatic relief.[2, 4]

Not only acetylcholinesterase, but also butyrylcholinesterase (BChE) is able to hydrolyze ACh. Although about 80% of the cholinergic activity inside the healthy human brain is caused by AChE,[5] AChE levels decrease in late stages of AD, while those of BChE increase.[6] The ratio of BChE/AChE changes from 0.5 in the normal brain to 11 in the AD brain, and it is postulated that BChE may replace AChE in hydrolyzing brain acetylcholine at advanced stages of the AD.[6] In fact, selective BChE inhibitors improve the cognitive performance of aged rats[7] and, more recently, the genesis of fibrils by β-amyloid plaques was shown to be closely related to the increased activity of butyrylcholinesterase.[8] The influence of BChE on AD pathology is still not completely unveiled, encouraging researchers to develop BChE inhibitors aiming to recognize enzyme's role in AD progression, envisioning therapeutic application in late stages of AD.

Although cholinesterase inhibitors are certainly essential in improving the quality of life of patients with mild to moderately severe Alzheimer's disease, these drugs do not represent a cure for the disease. However, investigation towards disease-modifying therapies has grown incredibly in the last decade, predominantly on anti-amyloid strategies, currently the most active area of investigation.[2, 9]

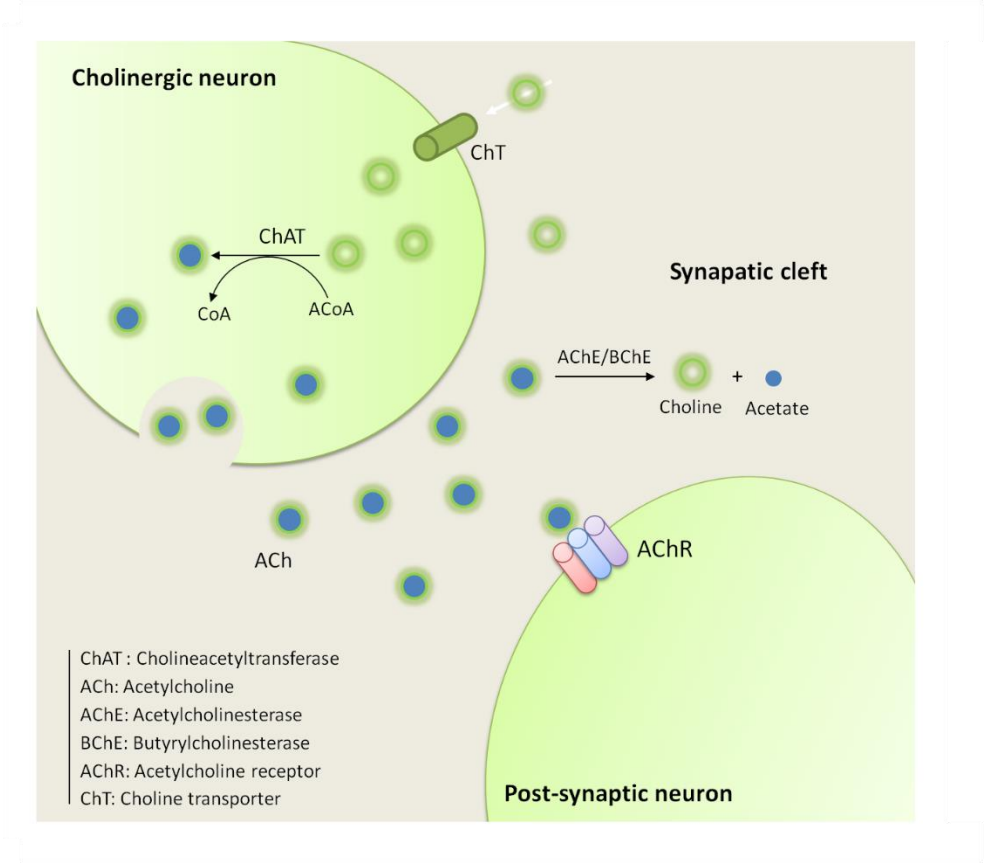

Figure 1.2.1. Cholinergic hypothesis of Alzheimer's disease.

The amyloid hypothesis advocates that the gradual and progressive loss of neuronal tissue or neurons in Alzheimer's disease is caused by the deposition of extracellular senile plaques composed of amyloid-β peptide (Aβ).[2, 10] The amyloid cascade hypothesis has been designed and modified over the last decade to account for the vast number of observed events in AD brains and possible mechanisms underlying the disease (figure 1.2.2). The cascade starts with the proteolytic cleavage of amyloid-β precursor protein (APP), a transmembrane protein with a large extracellular domain, into Aβ.[1, 10] The initial steps of APP digestion consist of APP cleavage by either β-secretase (amyloidogenic pathway) or α-secretase (non-amyloidogenic pathway). When the latter product is further cleaved by γ-secretase the nontoxic P3 peptide is produced. Alternatively, cleavage of the β-secretase product by γ-secretase results in either the toxic Aβ1-42 or Aβ1-40. While Aβ1-40 is the most frequent form of Aβ, Aβ1-42 has a higher

tendency to aggregate. Although the cause-effect phenomena associated with Aβ and the progression of the disease is not well understood, it is established that accumulation of Aβ1-42 is a key initiator of cellular damage in Alzheimer's disease. Its aggregation results in soluble toxic oligomers and/or insoluble amyloid fibrils, which exact molecular composition remains elusive due to their dynamic nature.[10] The smaller soluble forms of multimeric Aβ have been proposed as the most neurotoxic forms. However, it was recently proposed that Aβ oligomers possess distinct conformational polymorphisms and the unique combination of size, hydrophobicity, and conformation determine both its toxicity and that of the final oligomers aggregation state, thus contributing to AD pathology via different mechanisms.[11]

The term "aggregate stress" has been used to describe the events arising from Aβ aggregation and leading to cell apoptosis, including inflammatory response, microglial and astrocytic activation, altered neuronal ionic homeostasis (increased calcium influx), oxidative injury and mitochondrial dysfunction.[2, 10] Kinase and phosphatase activities are also altered, leading to hyperphosphorylation of tau protein, which results in the aggregation of tau into paired helical filaments and, ultimately, neurofibrillary tangles.[10] Although the precise temporal and mechanistic relationship between amyloid depositions and tau pathology is yet to be fully understood, scientists believe that the above mentioned filaments of tau trigger a process of widespread neuronal/neuritic dysfunction and cell death, finally leading to neuronal loss and dementia.[10]

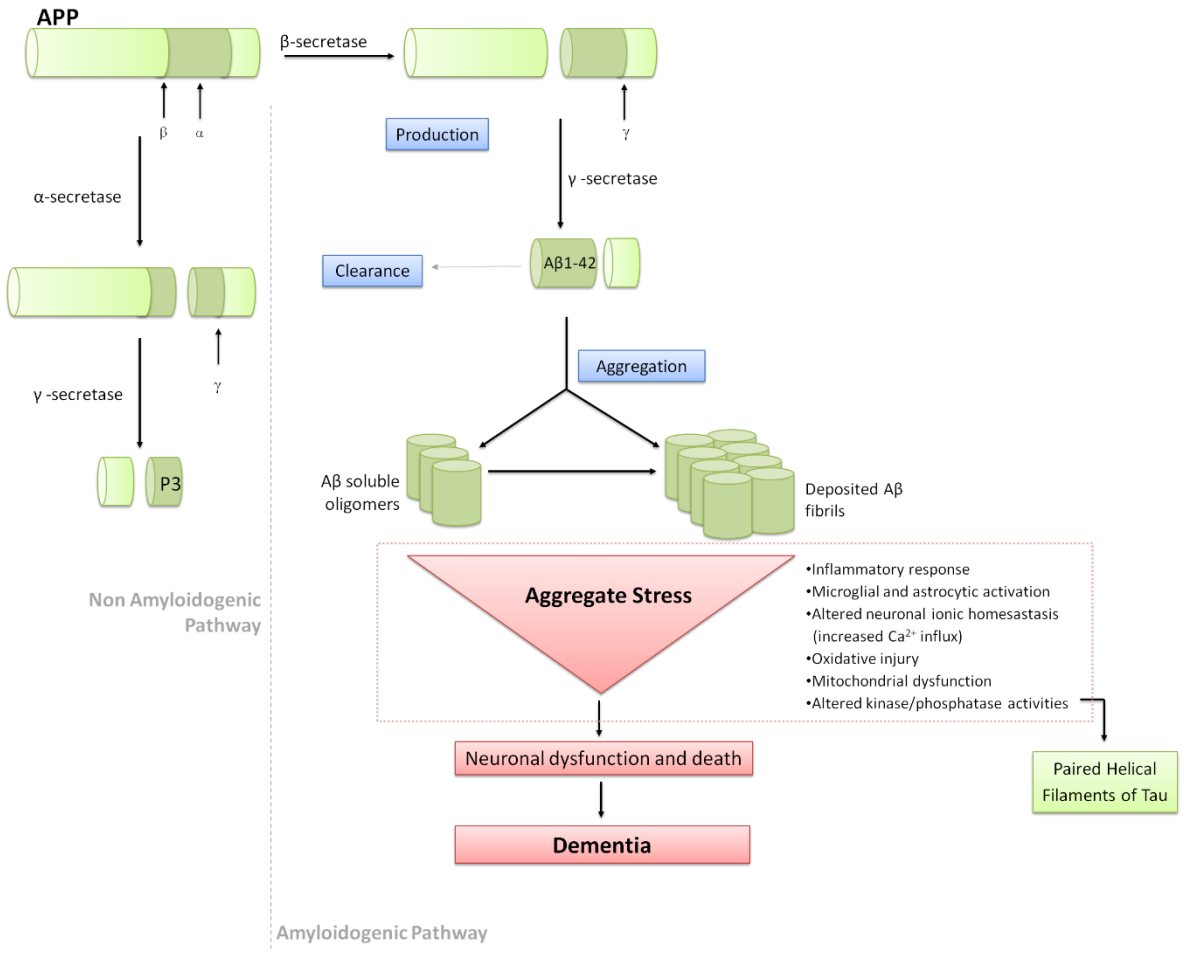

Figure 1.2.2. Amyloid Cascade Hypothesis of Alzheimer's Disease

There are two therapeutic approaches targeting tau pathology: 1) inhibition of tau-phosphorylating kinases such as GSK-3, and 2) inhibition of tau aggregation and/or promotion of aggregate disassembly. Nevertheless, the few compounds targeting tau that reached clinical trials were disappointing regarding cognition.[9] Thus, since formation of tau NFTs is likely a cytological response to the gradual accumulation of Aβ, targeting amyloid seems to be the most sensible approach, and has gained strength as a modifying-disease strategy. For the treatment of amyloidosis, there are three main strategies: 1) Reducing the production of Aβ (β and γ-secretase inhibitors); 2) Enhancing amyloid clearance and 3) Interfering with amyloid aggregation.[12]

The relevance of carbohydrates in drug discovery arises not only from their importance in life processes, but also because these stereochemically rich and polyfunctional molecules have the potential to be chemically manipulated in a multitude of ways. Moreover, as the brain requires a significant amount of glucose, there is a density of hexose transporters (GLUTs) at the blood brain barrier (BBB), favouring carbohydrate based drugs' access to the brain.[13] Thus, in addition to inherently bioactive carbohydrates, these molecules can also be linked to bioactive compounds envisioning new derivatives and/or pro-drugs to improve targeting and pharmacological properties, such as water solubility and minimization of toxicity. Furthermore, carbohydrate-binding receptors expressed by microglia, resident immune cells of the central nervous system with the capacity to eliminate extracellular aggregates, are strongly involved in repair function during neurodegenerative or neuroinflammatory processes. Thus, carbohydrate-based drugs pursuing selective stimulation or inhibition of these receptors can contribute to a neural repair promoting microenvironment.[14]

Carbohydrate-based molecules have been extensively used over the last decade to meet the necessity of new neuroprotective compounds. Their structural diversity is overwhelming, including free and protected sugars, cyclitols, nucleosides, peptidomimetics and glycosaminoglycans. Nature has proven particularly resourceful in providing biologically active glycosides. Glycosylated terpenoids, flavonoids, iridoids, chromones and caffeoyl derivatives are amongst the vast number of secondary metabolites found in the literature addressing at least one of the abovementioned strategies for AD treatment. Chemists have also been inspired in natural products to develop innovative structures with high pharmaceutical potential. Herein we will discuss the importance of carbohydrates and carbomimetic structures, addressing different aspects of neuroprotection currently under investigation, namely targeting amyloid and cholinergic hypotheses. The potential of carbohydrates in diagnosis will also be

highlighted, focusing on both metabolic signatures of mitochondrial stress found in AD patients, as well as imaging of amyloid aggregates with glyconanoparticles.

1.2.2 CARBOHYDRATE-BASED MOLECULES AND GLYCOMIMETICS IN AMYLOID-β EVENTS

1.2.2.1. Terpene glycosides

1.2.2.1.1 Ginsenosides

As previously stated, the plant kingdom has been highly important in drug discovery. The recognised nootropic and anti-aging effects of the well-known plant *Panax ginseng*, widely used in chinese traditional medicine, have been attributed to ginsenosides, which are dammarane-type triterpene glycosides (see Figure 1.2.3). Although the neuroprotective activities of ginsenosides have been extensively studied and recently reviewed,[15-17] the investigation of their neuroprotective properties continues incredibly active, with a variety of recent studies concerning their potential for neurodegenerative diseases and their mechanism of action, in particular focusing on AD. Amongst the most recent findings lies the ability of ginsenoside Rg1 (Figure 1.2.3) to reduce Aβ production by inhibiting γ-secretase,[18] and β-secretase, via stimulation of peroxisome proliferator–activated receptor-γ (PPARγ),[19-20] thus improving neuropathological and behavioural changes in mice overexpressing APP.[18] This ginsenoside also promotes non-amyloidogenic cleavage of APP by enhancing α-secretase activity,[21] while ginsenoside Rb1 is able to inhibit β-secretase *in vitro*, and protects cells from toxicity induced by Aβ25-35,[17] the shortest peptide sequence retaining toxicity comparable with that of full-length Aβ1-42 and commonly used as an AD model. Along with Rb1, ginsenosides Rg1, Rd, Re, Rg3, Rg5 and Rh2 (Figure 1.2.3) are also reported to exert neuroprotective effects against Aβ-induced toxicity and inflammation.[16-17, 22] For instance, Rg1 has a protective effect against Aβ1–40 induced neuronal injury and apoptosis in neuroblastoma

cells, likely by inhibiting inflammatory cytokines production and by intervening in the apoptotic cascade.[23-24] Consistently, similar results were obtained in a comparable study using endothelial cells and Aβ25-35.[25] Rg1 also protects against Aβ-induced mitochondrial dysfunction, namely by increasing mitochondrial membrane potential, ATP levels and cytochrome C oxidase activity, rescuing neurons from oxidative stress.[26] Rg3 promotes Aβ clearance by microglial uptake, internalization and digestion and by increasing the gene expression of neprilysin, a rate-limiting enzyme in APP degradation into Aβ.[17] Treatment with this ginsenoside improved the LPS-induced cognitive impairments of rats, by inhibiting the expression of pro-inflammatory mediators.[27] This effect was also registered *in vitro* for Rg5, which additionally suppresses the production of ROS and pro-inflammatory cytokines in microglia.[28] Modulation of amyloid-induced neuroinflammatory responses in cultured microglia or stimulated brain by Rh2 was also investigated.[17] Finally, Rg1,[22, 29-30] Rb1[31] and Rd[22, 32] are all reportedly able to attenuate tau hyperphosphorylation, namely by regulating glycogen synthase kinase-3β (GSK-3β)0.[29-30, 32]

In summary, the advances in the research for ginsenosides' effects and mechanisms of action show that these naturally occurring glycosides intervene in a number of ladders of the amyloid cascade and ameliorate amyloid pathology in several animal models. Moreover, they act on the regulation of synaptic plasticity and neurotransmitter release, as described in section 1.2.3.1.1. More importantly, a single ginsenoside, namely Rg1, is able to act on multiple sites of action, and can be considered a candidate for development of a multi-target drug. These drugs are mostly pertinent in age-related neurodiseases, where multiple etiological and pathological targets are involved. Ginseng extracts have been studied in clinical trials, but the results are ambiguous and of difficult interpretation, due to the use of different extraction methods and different ginseng species.[16] Thus, given all the neuroprotective properties of these

glycosides, allied with their lack of toxicity, randomised clinical trials to evaluate cognition improvement in AD patients are mandatory.

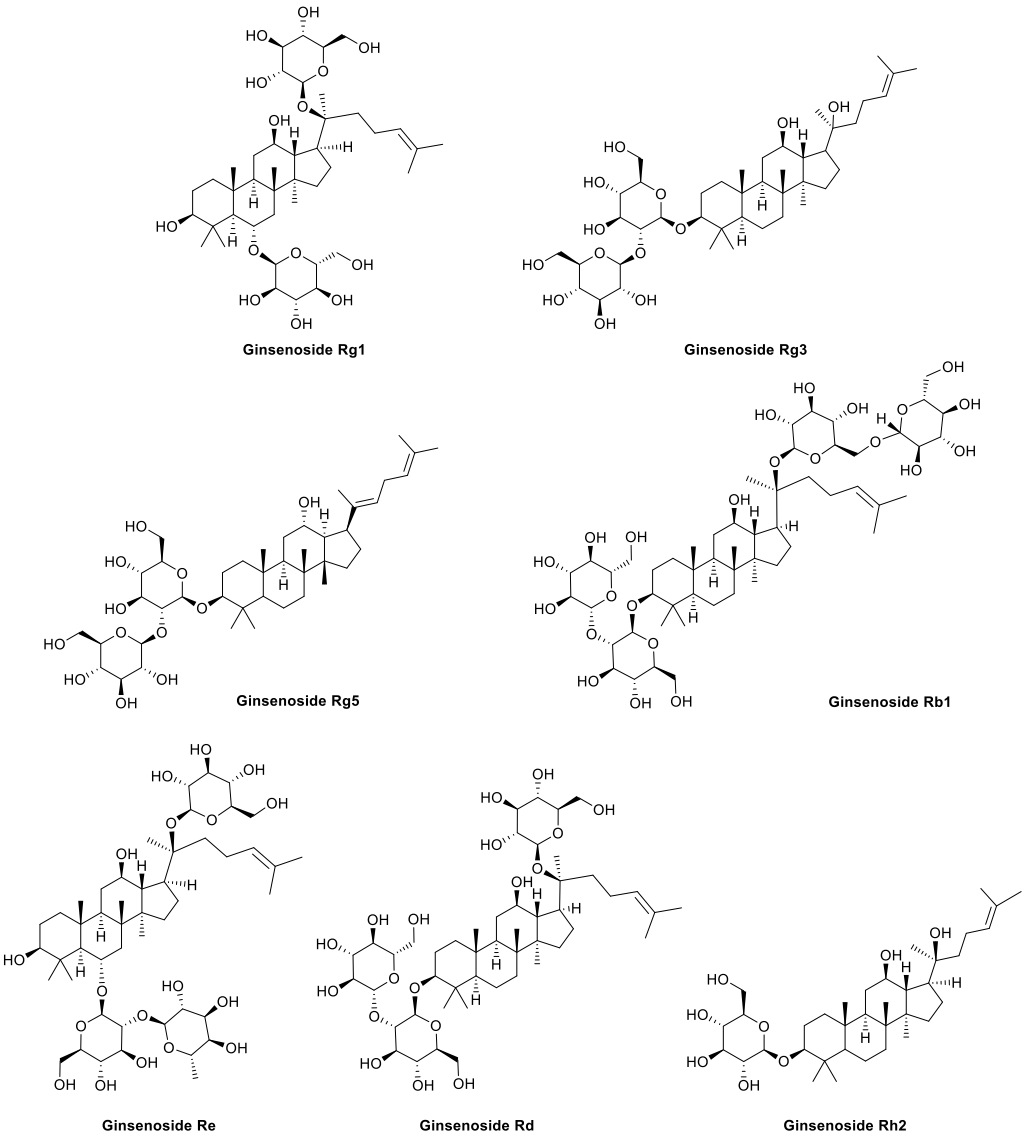

Figure 1.2.3. Ginsenosides with anti-amyloid properties

1.2.2.1.2 Other terpene glycosides

Other triterpene saponins along with monoterpene glycosides have also been described as neuroprotective, improving cognitive function in animal models. Asperosaponins A, B and C (Figure1.2.4) are triterpene saponins isolated from *Dipsacus asper* that protect PC12 cells from Aβ25-35 induced cytotoxicity.[33] Also the triterpene glycoside hederacolchiside-E (Figure

1.2.4) protects against Aβ1–42-induced toxicity in SK-N-SH cells and enhances the cognitive function in mice with memory impairments.[34] In addition, a triterpene monoglycoside (Figure 1.2.4) identified in *Actaea racemosa* reduces the production of Aβ1-42 with an IC_{50} of 0.1 μM in cultured cells overexpressing APP, by modulation of γ-secretase.[35]

Paeoniflorin, a monoterpene glycoside isolated from *Radix Paeoniae alba*, has demonstrated to attenuate Aβ1-42 induced neurotoxicity by regulating calcium homeostasis and ameliorating oxidative stress in hippocampus of rats,[36] and consequently reversed Aβ1-42-induced spatial learning and memory deficit.[37]

A number of O-glycosylated iridoids, monoterpenes embodying a cyclopentane ring fused to a six-membered oxygen heterocycle, have also been reported as neuroprotectors against amyloid-induced toxicity. For instance, geniposide (Figure 1.2.4) protects neuroblastoma cells from stress induced by formaldehyde, which promotes misfolding and aggregation of tau and Aβ proteins, through modulation of the apoptotic cascade.[38] Catalpol (Figure 1.2.4), an iridoid isolated from the roots of *Rehmannia glutinosa*, protects neuronal cells from Aβ1–42 triggered neurotoxicity to neurons, and also inhibits the glia-mediated inflammation process.[39]

1.2.2.2 Phenolic Glycosides

Natural occurring phenolic compounds are known for their beneficial health-promoting effects in chronic and degenerative diseases. The inhibition of amyloid fibril formation exerted by these antioxidants has been proposed to be associated with their ability to "break" β-sheets, as a consequence of structural constraints and specific aromatic interactions, with the phenolic rings being capable of disrupting peptide aromatic π-π stacking and the hydroxy groups forming competitive hydrogen bonding.[40] Given the biocompatible properties of carbohydrates, glycosylated phenolic compounds become highly significant in the quest for new drug candidates.

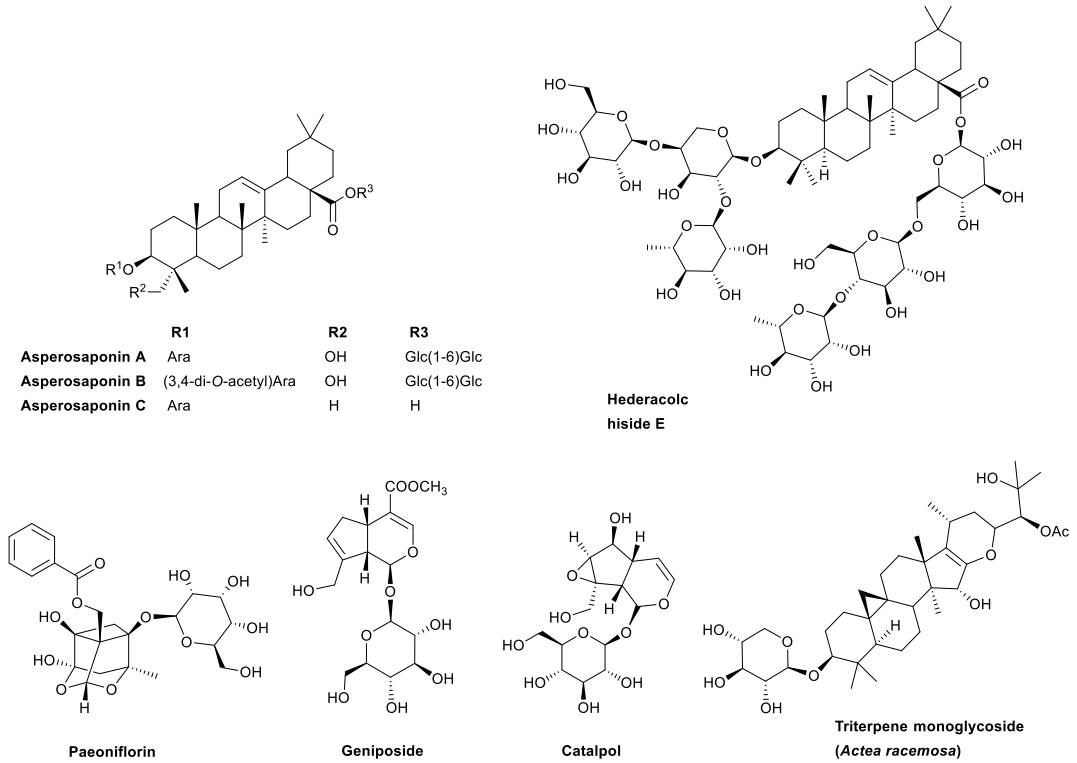

Figure 1.2.4. Other terpene glycosides able to modulate fibrillogenesis.

Acteoside (Figure 1.2.5), a phenylethanoid glycoside from *Orobanche minor*, strongly inhibits the aggregation of Aβ1-42, with an IC_{50} of 8.9 μM[41] and protects against Aβ-induced cell injury by attenuation of reactive oxygen species production, by modulation apoptotic signal pathway through Bcl-2 family[42] and by upregulation of heme oxygenase-1.[43] Both the flavonol glucuronide hibifolin and the flavone glycoside linarin (Figure 1.2.5) protect cells against Aβ25–35-induced apoptosis.[44-45] While the former protects primary cortical neurons by several mechanisms, namely by abolishing Ca^{2+} mobilization, inhibiting caspase activation and suppressing DNA fragmentation,[44] the latter prevents neurotoxicity by acting on the apoptotic cascade through inhibition of GSK-3β and up-regulation of the anti-apoptotic protein Bcl-2.[45] 3-*O*-[β-D-xylopyranosyl-(1→2)-β-D-galactopyranosyl]quercetin (Figure 1.2.5), isolated from *Panax notoginseng*, prevents Aβ-induced cell death by inhibiting Aβ aggregation, reducing brain damage in scopolamine-treated rats.[46] Interestingly, the aglycone itself did not show a

comparable effect in amyloid aggregation, suggesting that the neuroprotective properties of this compound are strongly related to the presence of the sugar moiety.

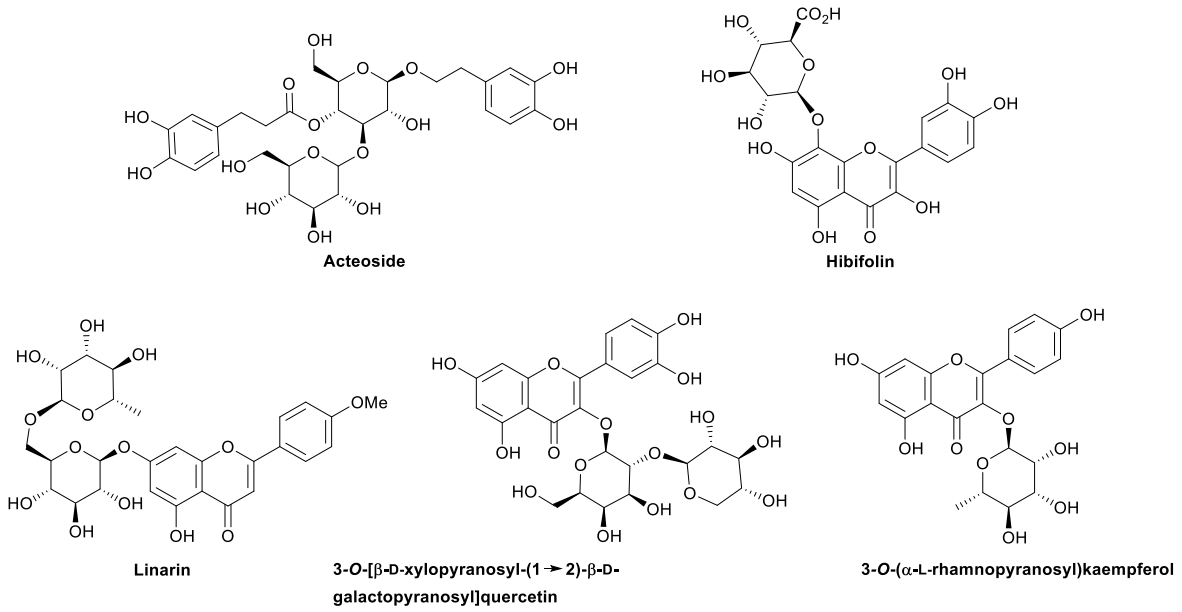

Figure 1.2.5. Phenolic glycosides intervening in amyloid events.

A recent study showed how polyphenol glycosides and respective aglycons use different pathways to remodel and inactivate amyloid-β oligomers.[47] Using the pairs phloretin/2'-*O*-(β-D-glucopyranosyl)phloretin, resveratrol/piceid, naringenin/naringin, apigenin/7-*O*-(β-D-glucopyranosyl)apigenin, quercetin/rutin and quercetin/3-*O*-(β-D-glucopyranosyl)quercetin (figure 1.2.6), the authors showed that aglycons convert Aβ oligomers into large, off-pathway aggregates, while the respective glycosides rapidly dissociated Aβ oligomers into soluble, disaggregated peptide. Surprisingly, these polyphenol glycosides selectively target toxic Aβ conformers relative to non-toxic ones. Their disaggregation activity is believed to rely on the presence of both polyphenol and sugar in the same molecule, in which the aglycon initiates the remodeling process by disrupting intermolecular contacts between Aβ peptide through π-stacking interactions. The so-called CH-π stacking interactions driven by association of the CH sugar bonds with π-electron cloud of the aromatic rings were suggested to cause interaction of sugars with the newly exposed

aromatic rings of the Aβ residues, preventing their association. Interestingly, combinations of free polyphenols and sugars failed to disaggregate Aβ oligomers, highlighting the importance of polyphenol glycosides for the prevention of Aβ toxicity.[47] Coherently, a different study shows that 3-*O*-(α-L-rhamnosyl)kaempferol (Figure 1.2.5) protects cells against Aβ-induced toxicity, and morphological assays showed that this flavonol glycoside inhibits fibrillogenesis of Aβ1-42 leading to the formation of smaller, soluble and non-toxic aggregates, and destabilizes pre-formed fibrils into non-toxic aggregates.[48]

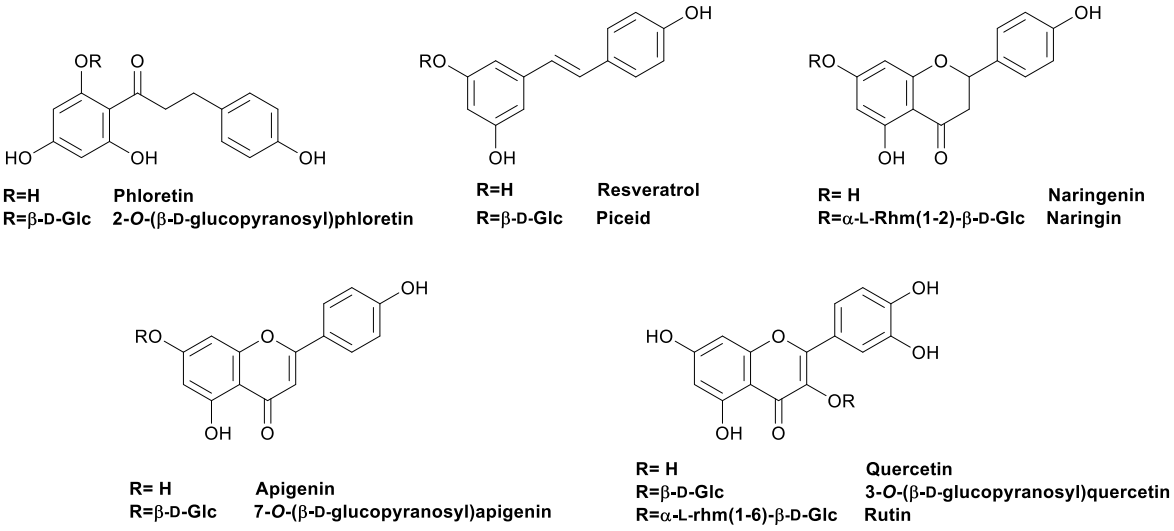

Figure 1.2.6. Polyphenol glycoside/aglycon pairs used in the study conducted by Ladiwala *et al.*[47]

Inspired in nature and taking advantage of synthetic tools, Raja and co-workers generated a clicked galactose-curcumin conjugate (see Figure 1.2.7) that is able to inhibit not only Aβ but also tau peptide aggregation at concentrations as low as 8 nM and 0.1 nM, respectively.[49] Curcumin is a polyphenol known for its multiple neuroprotective mechanisms including inhibition of inflammation, disruption of amyloid-β and tau peptide aggregation, among others. However, its pharmaceutical use is restricted due to its poor water and plasma solubility and consequent low bioavailability. This non-toxic galactose-curcumin conjugate

possessing a triazole-based linker is ca. 1000 times more soluble than curcumin in water, and exhibits enhanced ability to inhibit both amyloid-β and tau aggregation.[49]

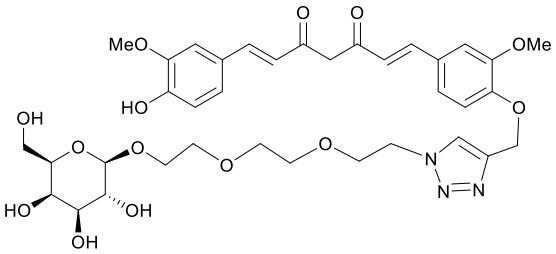

Figure 1.2.7. Sugar-curcumin conjugate.

1.2.2.3 Other glycosides and C-glycosyl compounds

Although terpene and phenolic glycosides have particular expression in the structural diversity of compounds that intervene in amyloid related events, other O- and C-glycosylated structures have been described with similar properties.

Amongst the C-glycosyl compounds, the chromones aloeresin D and C-2'-decoumaroyl-aloeresin G (Figure 1.2.8), both isolated from *Aloe vera*, inhibit β-secretase activity, with IC_{50} values of 39.0 and 20.5 μM, respectively.[50] The presence of a phenol group linked to the chromone scaffold at position 3 also resulted in a potential candidate for the treatment of AD, namely puerarin (Figure 1.2.8), a glucosyl isoflavone isolated from *Pueraria lobata*. It exhibits beneficial effects on various medicinal purposes due to its wide spectrum of pharmacological properties. These include neuroprotection, antioxidant, anti-inflammation, inhibition of alcohol intake, among others, as recently reviewed.[51] In particular, puerarin prevents Aβ-induced neurotoxicity through inhibiting neuronal apoptosis,[52-53] and attenuates Aβ25-35-induced lipid peroxidation and the overproduction of reactive oxygen species (ROS), mainly by interrupting GSK-3β signalling, resulting in an increase of cell survival.[54-55] Administration of puerarin also reversed the Aβ1-42 induced impairment in spatial memory.[56]

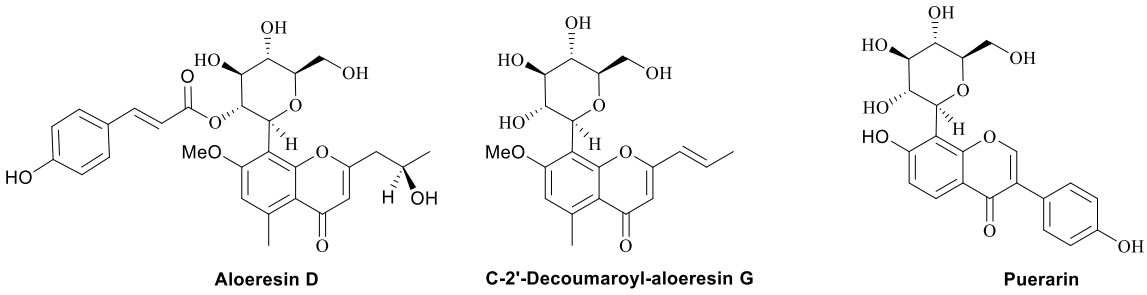

Figure 1.2.8. Examples of C-glycosyl compounds with anti-amyloid properties.

The glycosides embodying two short hydrophobic dipeptide units (Ala-Val and Val-Leu) (figure 1.2.9) are peptidomimetics that intervene in amyloid-β aggregation, in which the D-glucopyranosyloxy moiety is linked to the peptide via aminoalkyl (C1) and carboxyethyl (C6) groups. These peptidomimetis are inhibitors of Aβ1-40 amyloid fibril formation, at the ratio of 0.1:1 (peptidomimetics/Aβ). While the central sugar moiety may perturb the regular interstrand hydrogen-bond network and destabilize β-sheet formation locally, the dipeptide units have the potential to interact with the hydrophobic regions of Aβ.[57] Hence, hydrophobic recognition and hydrophilic β-breakage strategies are combined in this innovative structure generated through glycochemistry approaches.

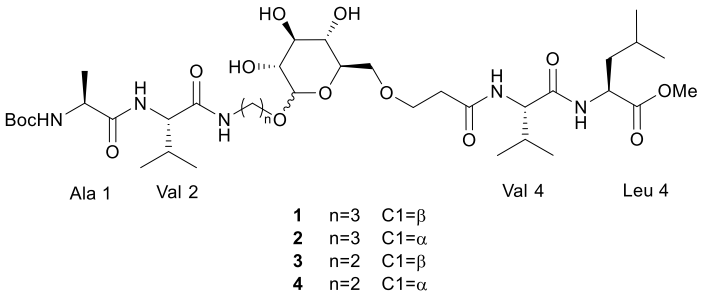

Figure 1.2.9. Peptidomimetics that inhibit amyloid-β aggregation.

Other important characteristic of AD patients′ brains with therapeutical implications is the high concentrations of Cu, Fe and Zn in amyloid plaques, and it is well established that

interaction of Aβ with metal ions *in vitro* leads to its aggregation, particularly with Zn^{2+}.[58] In this context, two glycosides incorporating metal-ion chelators, namely *N*,*N*′-bis{[5-(β-D-glucopyranosyloxy)-2-hydroxy]benzyl}-*N*,*N*′-dimethylethane-1,2-diamine (H_2GL^1) and *N*,*N*′-bis{[3-*tert*-butyl-5-(β-D-glucopyranosyloxy)-2-hydroxy]benzyl}-*N*,*N*′-dimethylethane-1,2-diamine (H_2GL^2) have been reported (Figure 1.2.10). Both compounds have moderate affinity for Cu^{2+} and Zn^{2+}, and were able to reduce Zn^{2+}-induced and Cu^{2+}-induced Aβ aggregation by approximately 50%,[57] thus acting as a starting point for the generation of new leads for metal-ion chelation therapy.

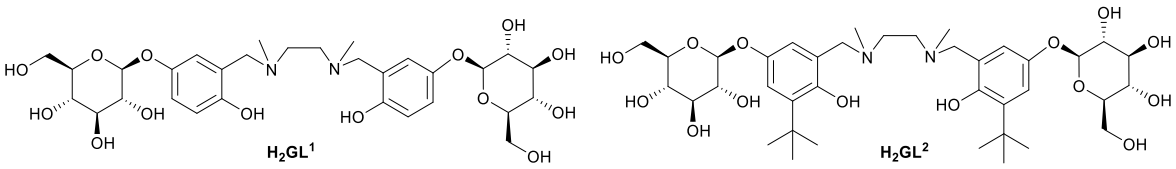

Figure 1.2.10. Carbohydrate-containing metal-ion chelators.

1.2.2.4 Sugars and Cyclitols

1.2.2.4.1 Free and Protected sugars

As previously shown, a diversity of glycosides and C-glycosyl compounds intervene in amyloid related events and the sugar moiety is highly involved in this interaction. However, free and protected sugars have also been reported to act on amyloid fibril formation.

The mechanism for retardation of amyloid fibril formation by free sugars was recently investigated using polypeptide chains in 3Hmut Wil protein as a model. The results showed that trehalose, sucrose and glucose (figure 1.2.11) retarded the amyloid fibril formation of this protein, not by direct interaction, but by stabilizing the native state through preferential hydration.[59] Interestingly, it was shown that trehalose inhibits formation of Aβ1-40 fibrils and oligomers and reduces Aβ1-40-induced toxicity in SH-SY5Y cells, although these effects are not verified with Aβ1-42.[60]

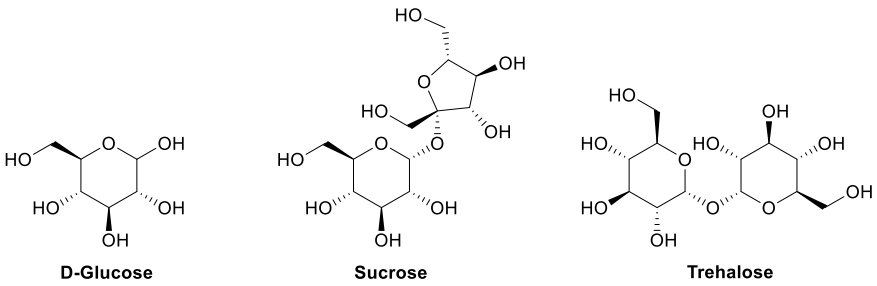

Figure 1.2.11. Free sugars able to retard amyloid fibril formation of 3HMut Will protein.

The protected sugar 1,2,3,4,6-penta-*O*-galloyl-β-D-glucopyranose (PGG, Figure 1.2.12), a natural product isolated from *Paeonia suffruticosa* that incorporates acylated phenol groups as sugar substituents, inhibits Aβ fibril formation, destabilizes pre-formed Aβ fibrils *in vitro* and *in vivo* and protects neuronal cells (SK-N-SH) from Aβ-induced toxicity, restoring cell survival by 30%. Also treatment with *Paeonia suffruticosa* extract improved long-term memory of transgenic mice over-expressing APP,[61] but the effect of PGG alone in the memory deficit of transgenic mice was not tested.

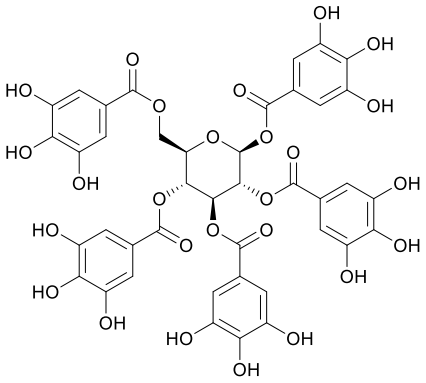

Figure 1.2.12. 1,2,3,4,6-Penta-*O*-galloyl-β-D-glucopyranoside.

1.2.2.4.2 Cyclitols

Not only carbohydrates, but also carbohydrate mimetics have drawn the attention of researchers towards new compounds with anti-amyloidogenic properties. Amongst them, inositol stereoisomers (figure 1.2.13) play an important role as Aβ aggregation inhibitors,

leading to off-pathway high-molecular-weight oligomers in mice brain. Their formation resulted in improvement of the cognitive function, synaptic physiology changes and prevention of accelerated mortality of mice.[62] The most promising stereoisomer was, until recently, *scyllo*-inositol, which passes the blood-brain-barrier using inositol transporters and is able to bind to Aβ, modulate its folding, inhibit its aggregation and dissociate pre-formed aggregates, with therapeutic effect on animals.[9] However, *scyllo*-inositol failed phase II randomized clinical trial (RCT).[63] Diverse *scyllo*-inositol derivatives were recently generated with deoxy, fluoro, chloro and methoxy substitution. Amongst them, 1,4-di-*O*-methyl-*scyllo*-inositol (figure 1.2.13) was the most effective one for the prevention of Aβ1-42 aggregation, although it was not more effective than *scyllo*-inositol.[64] Nonetheless, given the serious adverse effects registered by the administration of *scyllo*-inositol in high doses in the phase 2 RCT,[9, 63] the search for new derivatives maintaining the same activity but possibly safer is highly significant.

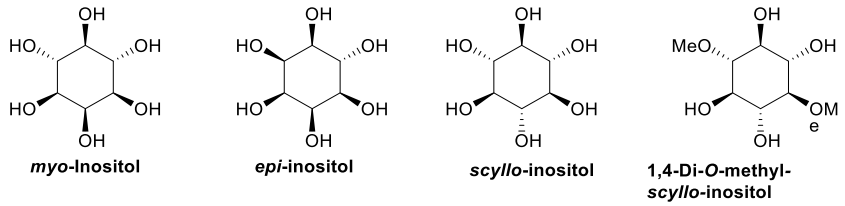

Figure 1.2.13. Inositol stereoisomers and the *scyllo*-inositol methylated derivative.

1.2.2.5 Glycosaminoglycans

Glycosaminoglycans (GAGs) are basic building blocks of the extracellular matrix and are an important component of the cell membrane glycocalyx covering.[65] The association between GAGs and amyloid deposits and their possible involvement in the amyloidogenic pathway has been long studied and reviewed.[65-69] Several proteoglycans with GAG chains are known to co-localize with Aβ in senile plaques and to accumulate in the AD brain, such as dextran, heparan, keratin, deramatan and chondroitin sulfates.[69] The binding of proteoglycans and heparin to Aβ peptides is known to enhance both amyloid aggregation and fibril formation.

It is also postulated that GAGs may protect aggregated Aβ from proteolytic degradation.[66] Moreover, proteoglycans or GAGs have been implicated in a number of other amyloid related neurodegenerative diseases, namely Prion diseases and Parkinson's disease.[69]

The possible therapeutic implications of these facts and the possibility of a unique binding site mediating Aβ-GAG interaction appealed scientists to search for a GAG-specific therapeutic intervention. Indeed, many efforts have been made to find compounds able to interfere with the interaction between endogenous GAGs and Aβ in such a way that it would prevent the formation of senile plaques or neurofibrillary tangles. There are two main approaches focused on the therapeutic potential of GAGs: one involving low molecular weight (LMW) GAGs and analogues inhibiting amyloid aggregation by competitive binding to Aβ, and a second one focusing on heparan sulfate (HS) biosynthesis inhibitors.

1.2.2.5.1 Low Molecular Weight Glycosaminoglycans and Polysaccharides

Low-molecular weight enoxaparin and dalteparin, obtained from depolimerization of heparin and already marketed as anticoagulants, are two examples of LMW heparins that inhibited amyloidogenesis in a AA amyloid mouse model.[70] In particular, enoxaparin can cross BBB and attenuates Aβ accumulation and deposition in the brain. Also, neuroparin (C3), a LMW glycosaminoglycan derived from heparin composed by 4–10 oligosaccharides, was shown to have a positive effect in animal models with characteristic AD lesions, namely by reducing tau 2 immunoreactivity in the rat hippocampus, stimulated by injection of Aβ25–35.[68] Indeed, C3, which is also known to cross the BBB, has reached human phase III trial. Also heparin itself can attenuate the neurotoxicity and proinflamatory effects of Aβ.[65]

Additionally, a novel acidic oligosaccharide rich in mannuronate blocks (MW ~ 1300 Da), extracted from the brown algae *Echlonia Kurome Okam*, inhibited Aβ-induced toxicity

and apoptosis in cells, by blocking Aβ aggregation.[71] A 30-day administration of this oligosaccharide to rats also attenuates memory impairment by scopolamine.[72]

Other example of oligomeric/polymeric structures studied in the context are those with a chitosan backbone conjugated with sialic acid analogues, such as keto-deoxynonulosonic acid (KDN) or tetrahydropyran-2-carboxylic acid (figure 1.2.14).[73] These polysaccharides were developed previewing their potential to interact with cell surface glycoproteins and gangliosides. These structures, conjugated via EDC chemistry, are able to attenuate amyloid-β induced toxicity in neuronal cells. The endocyclic oxygen and the multi –OH tail present in the sialic acid structure seemed to be essential for the neuroprotective effect.[73]

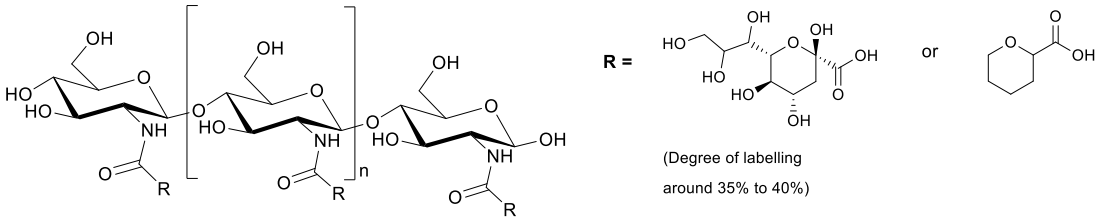

Figure 1.2.14. Polysaccharides with a chitosan backbone conjugated with KDN or tetrahydropyran-2-carboxylic acid.

1.2.2.5.2 Heparan Sulfate Biosynthesis Inhibition

Due to the important role of heparan sulfate (HS) biosynthesis in organ and cell function, its targeting should be carefully considered, because it may result in undesirable side effects. However, two 4-deoxy glucose derivatives, namely 2-acetamido-1,3,6-tri-*O*-acetyl-2,4-dideoxy-α- and β-D-*xylo*-hexopyranoses (Figure 1.2.15) were reported to inhibit HS biosynthesis and, consequently, inhibited splenic AA amyloid deposition in mice (by 65 to 70%), at 0.1 mM, with no toxicity associated.[74] Thus, despite of the possible side effects and the concerns it entails, inhibition of HS biosynthesis or modification of HS structure could be

a worth exploring research avenue for new lead compounds with therapeutic application in amyloidosis.

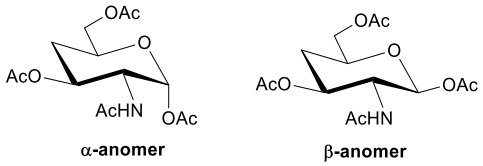

Figure 1.2.15. 2-Acetamido-1,3,6-tri-*O*-acetyl-2,4-dideoxy-α- and β-D-*xylo*-hexopyranose.

1.2.3 CARBOHYDRATE-BASED MOLECULES TARGETING THE CHOLINERGIC SYSTEM

1.2.3.1 AChE inhibitors

1.2.3.1.1 Saponins and other terpene glycosides including ginsenosides

As previously discussed, nature has played an important role in drug discovery, and AChE inhibitors are not an exception. The significant role of terpene and terpenoid glycosides in the cholinergic hypothesis is highlighted with triterpene, terponoid and monoterpene glycosides.

The extensively studied anti-amyloidogenic properties of ginsenosides were already considered. However, the neuroprotective properties of these triterpene saponins can also be attributed to their effects in the cholinergic system. Rg1 and Rb1 (Figure 1.2.3) were found to increase the density of central muscarinic cholinergic receptors, and the level of ACh in the central nervous system, which might result from choline acetyltransferase activity increase and acetylcholinesterase activity inhibition.[15, 17] Moreover, both compounds increase neural plasticity and Rg1 also increases proliferation and differentiation of neural progenitor cells. This ginsenoside significantly improved memory deficits in aged rats, ovarioctomized rats, and cerebral ischemia-reperfusion rats.[17]

Timosaponin AIII (Figure 1.2.16), a saponin from *Anemarrhena asphodeloides*, inhibited AChE *in vitro* (IC_{50}=5.4 μM) and in scopolamine-treated mouse brain, with a comparable effect to that of tacrine.[74] These effects were reflected in an overall improvement of the scopolamine-induced learning and memory deficits in rats.[75]

The terpenoid glycosides cynatroside A and cynatroside B (Figure 1.2.16), from C*ynanchum atratum*, presented AChE inhibition with IC_{50} of 6.4 and 3.6 μM, respectively.[76] The latter compound inhibits AChE in a reversible and non-competitive manner, with a positive effect in both short term and long term memory in scopolamine-treated mice.[77]

A number of monoterpene glycosides were also described as AChE inhibitors. Paeoniflorin (Figure 1.2.4), which anti-amyloidogenic properties were already discussed, upregulated the activity of choline acetyltrasferase and down-regulated the activity of AChE in the hippocampus of Aβ1–42-treated rats.[37] Nuciferoside (Figure 1.2.16), a β-cyclogeraniol diglycoside identified in the extract of *Nelumbo nucifera*, showed a significant non-competitive inhibition against AChE with IC_{50} value of 3.20 μM.[78] In addition, the iridoid glycosides loganin, E-harpagoside, 8-*O*-[(*E)-p*-methoxycinnamoyl]harpagide and catalpol are all reported to inhibit AChE. Loganin, found in *Flos lonicerae, Fruit cornus* and *Strychonos nux vomica*, inhibits AChE activity in the hippocampus and frontal cortex of mice, resulting in a significant improve of the scopolamine-induced memory impairments.[79] (*E*)-harpagoside and 8-*O*-[(2*E*)-3-(4-hydroxyphenyl)acryloyl]harpagide (Figure 1.2.16), found in *Scrophularia buergeriana*, improve cholinergic function by decreasing the activity of AChE in the brain of senescent mice.[80] Both iridoid glycosides also have significant protective effects against glutamate-induced neurodegeneration in primary cultures of rat cortical neurons.[81] Catalpol (figure 1.2.4) also registered anti-AChE activity in mice brain and increased choline acetyltransferase in positive neurons.[82]

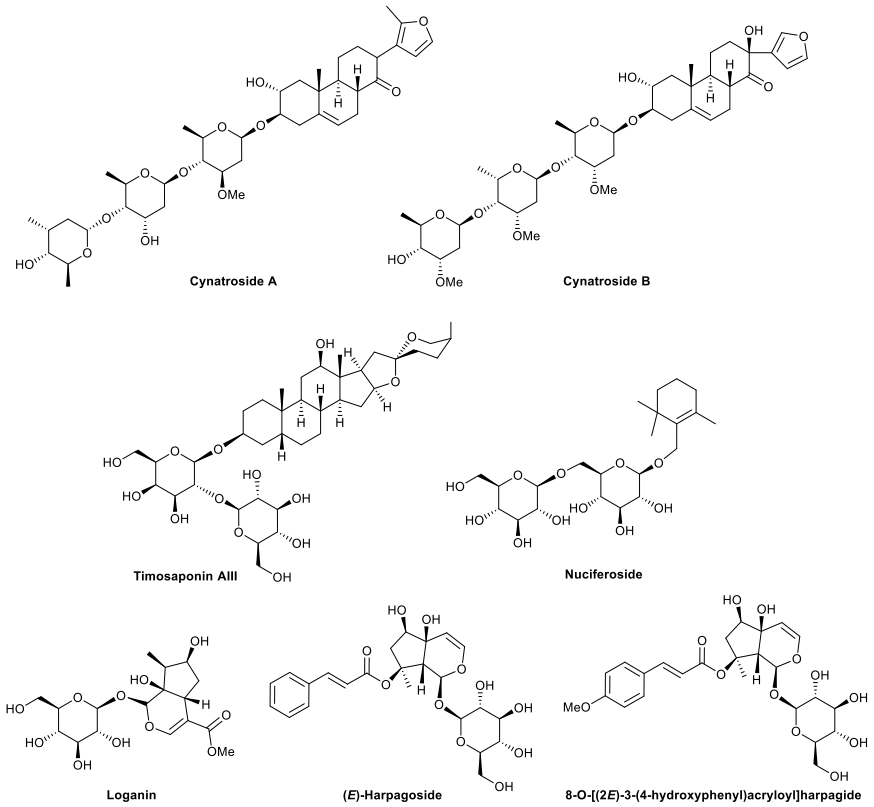

Figure 1.2.16. Terpene glycosides able to modulate cholinergic function.

1.2.3.1.3 Flavonoid glycosides

Countless flavonoids can be found in the literature with anti-AChE activity. Amongst them, flavonoid glycosides assume a main role. In fact, screening 17 flavonoids by the TLC bioautographic assay pointed the 7-glycosides tilianin[83] and linarin[83-84] (Figure 1.2.17) as the two most active compounds inhibiting AChE. This same study showed that the presence of a 4'-OMe group and a 7-*O*-glycosyl moiety were important for the AChE inhibition.[83] Recently, icariin (Figure 1.2.17), also bearing the same structural features, improved the cognitive impairments in senescence-accelerated-prone mice (SAMP) by significantly inhibiting AChE activity in the brain through monoamine levels increase and oxidative damage inhibition.[85] This natural glycoside also decreased hippocampal levels of ACh, AChE and choline acetyltransferase in a rat model of chronic cerebral hypoperfusion.[86] In addition, the flavonol 3-glycosides tiliroside and quercitrin (Figure 1.2.17) from *Agrimonia pilosa*,[87] and the

myricetin glycosides from *Cleistocalyx operlatus*,[88] also demonstrated AChE inhibitory activity. Tiliroside and quercitrin displayed IC_{50} values of 25.5 μM and 66.9 μM,[86] respectively, while 3-(β-D-galactopyranosyl)-3'-methylmyricetin and 3-(β-D-galactopyranosyl)-3',5'-dimethylmyricetin presented IC_{50} values of 19.9 μM and 37.8 μM.[87] 3-({6-*O*-[(2*E*)-3-(4-hydroxyphenyl)acryloyl]-β-D-glucopyranosyl}(1→2)-α-L-rhamnopyranosyl)quercetin (Q-ag) and 3-({6-*O*-[(2*E*)-3-(4-hydroxyphenyl)acryloyl]-β-D-glucopyranosyl}(1→2)-α-L-rhamnopyranosyl)kaempferol (K-ag) (Figure 1.2.17) from *Ginkgo biloba* standardized extract EGb-761®, increase extracellular levels of acetylcholine in rat brain by 151% compared to controls, at a dose of 10 mg/kg.[89]

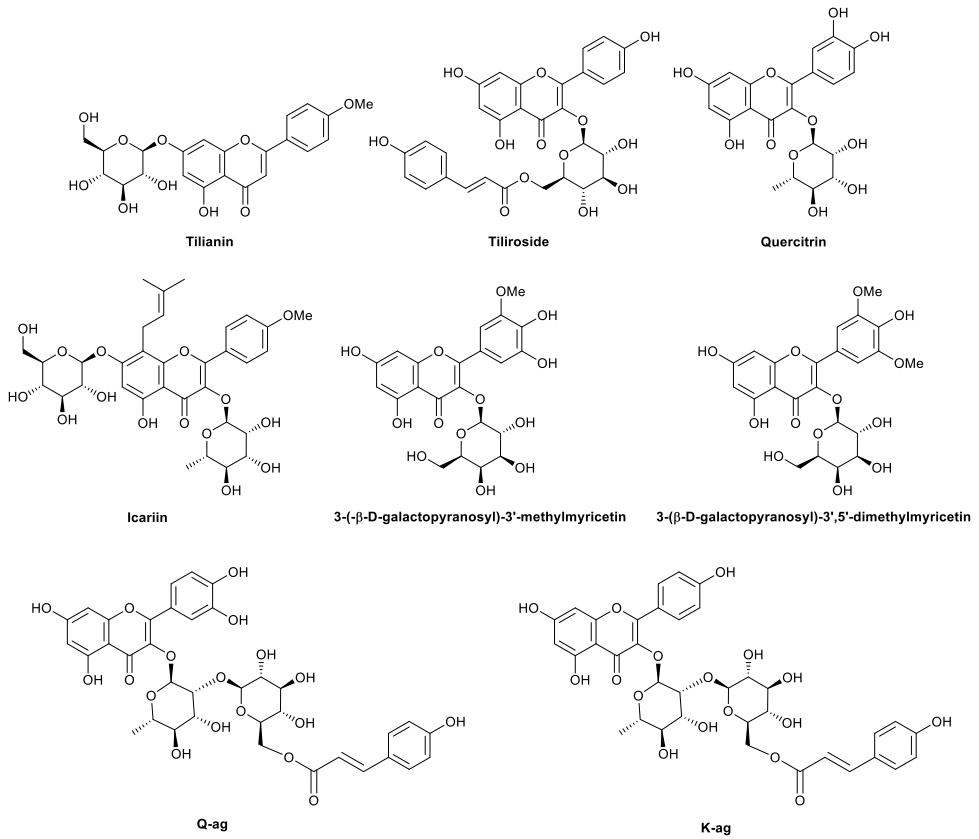

Figure 1.2.17. Flavonoid glycosides with anti-AChE activity.

1.2.3.1.4 Phenylethanoid glycosides and other substituted phenyl glycosides

Several phenylethanoid glycosides and other substituted phenyl glycosides embodying phenolic group(s) were also reported as AChE inhibitors *in vitro*. Vanilloside (Figure 1.2.18),

isolated from *Nelumbo nucifera*, inhibits AChE in a non-competitive manner, with an IC_{50} value of 4.55 μM.[78] The phenylpropanoid diglycosides rosavin and rosavin analogues (*E*)-3-phenylprop-2-en-1-yl β-D-xylopyranosyl-(1→6)-β-D-glucopyranoside, (*E*)-3-(4-methoxyphenyl)prop-2-en-1-yl α-L-arabinopyranosyl-(1→6)-β-D-glucopyranoside and (*E*)-3-phenylprop-2-en-1-yl α-L-rhamnopyranosyl-(1→6)-β-D-glucopyranoside (Figure 1.2.18), from *Rhodiola rosea L.* displayed anti-AChE activity, with IC_{50} of 1.72, 3.71, 4.23, 2.05 μM, respectively.[90] Indeed, rosavin displayed the most potent AChE inhibition out of the natural compounds described so far. Inspired by these results, a small library of phenylpropanoid glycosides was attained, with analogues incorporating substituted phenyl groups, with F, Cl and Br, and varying the methoxy and hydroxy substitution patterns. However, none of the synthesized derivatives was as active as the natural diglycosides shown in figure 1.2.18.[90]

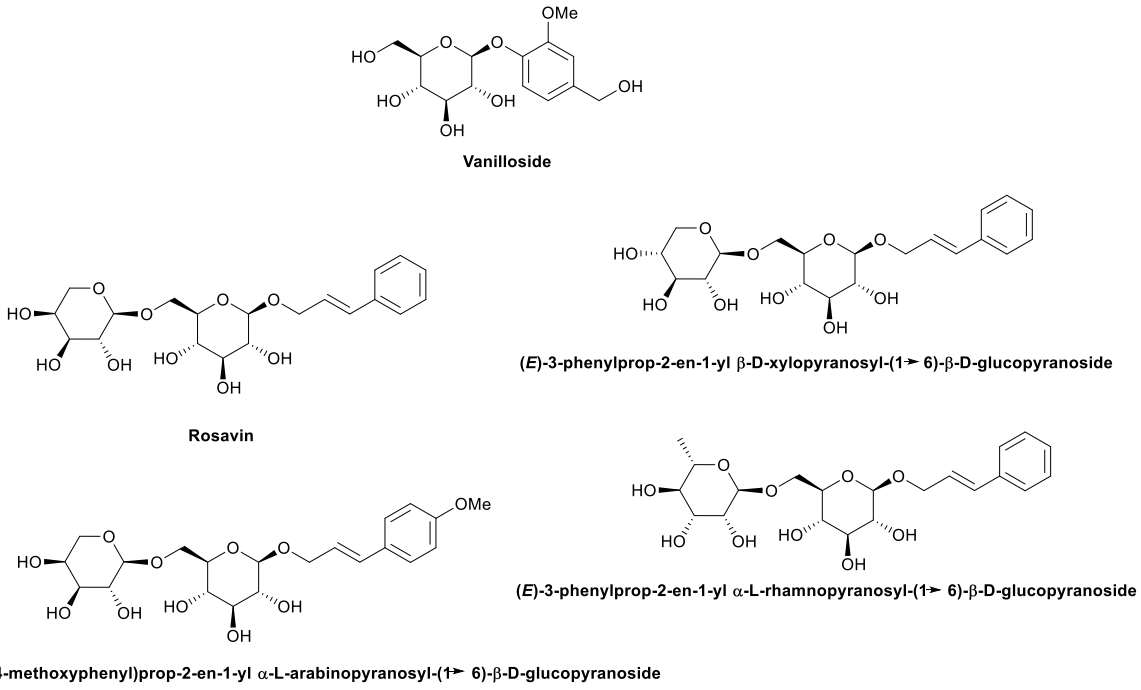

Figure 1.2.18. Vanilloside, rosavin and rosavin analogues.

Derivatives of the natural antidepressant helicid were synthesized starting from 4-hydroxybenzaldehyde, followed by glycosylation, deprotection and condensation with amines.[91] These transformations afforded noteworthy AChE inhibitors with IC_{50} under 10 μM,

three of them under 0.55 μM (Figure 1.2.19). Interestingly, while helicid was not active up to 500 μM, its epimer at C-3 presented an IC_{50} of 0.45 μM. However, the most potent inhibitor, the 4-formylphenyl β-D-ribopyranoside, exhibits the same configuration of carbons 2, 3 and 4 as helicid and its hydroxymethyl group is replaced by a hydrogen atom, presenting an IC_{50} value of 0.20 μM on electric eel AChE, twice more active than galantamine.[91]

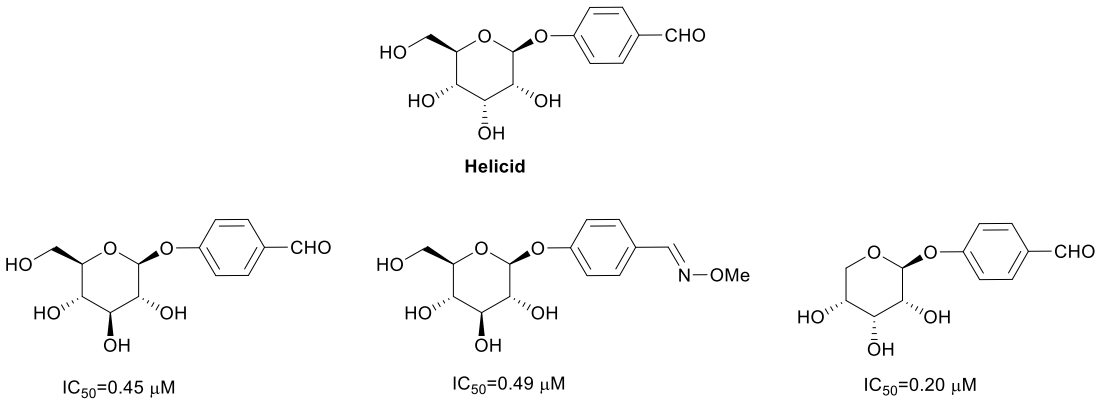

Figure 1.2.19. Helicid and helicid analogues with anti-AChE activity.

1.2.3.2 Butyrylcholinesterase inhibitors

1.2.3.2.1 Nucleosides

As already discussed, the recent association between BChE and maturation of senile plaques in AD brains has encouraged researchers to develop BChE inhibitors envisioning therapeutic application in late stages of AD. Recently, a series of N^7 and β-linked 2-acetamido-6-chloropurine nucleosides with a benzyl protected sugar bicyclic moiety were developed by Rauter and co-workers, exhibiting a highly and selective BChE inhibition.[92] One of these N^7 nucleosides (figure 1.2.20, A) displayed an IC_{50} value of 0.14 μM, of the same order of magnitude as that of rivastigmine.[92] Further studies on the impact of the sugar and purine structures in the activity led to a new and more effective structure, a N^7 linked 2-acetamido-6-chloro-α-D-mannosylpurine (figure 1.2.20, B). This nucleoside exhibit an inhibitory constant (*K*i) of 50 nm and a selectivity factor of 340-fold for BChE over AChE.[93] Interestingly, the

glucuronamide-based purine nucleosides bearing a six-membered ring protected with acetyl groups (figure 1.2.21, A) were selective inhibitors of AChE. Also those nucleosides linked to furanosyl moieties (figure 1.2.21, B) showed the same trend.[94] The selectivity toward BChE inhibition observed can be tentatively explained by the hindrance experienced by the inhibitor when accessing the active site of AChE, which has several bulky residues that hinder access to enzyme pocket, while the catalytic site of BChE is large enough for the inhibitor to adopt its preferred conformation and form stable enzyme–inhibitor complexes, as observed for the selective BChE inhibitor octyl 2-deoxy-D-*arabino*-hexopyranoside (figure 1.2.20, C).[95] This compound, which did not inhibit AChE, caused 100% inhibition of BChE at a concentration of 100 μM. [95]

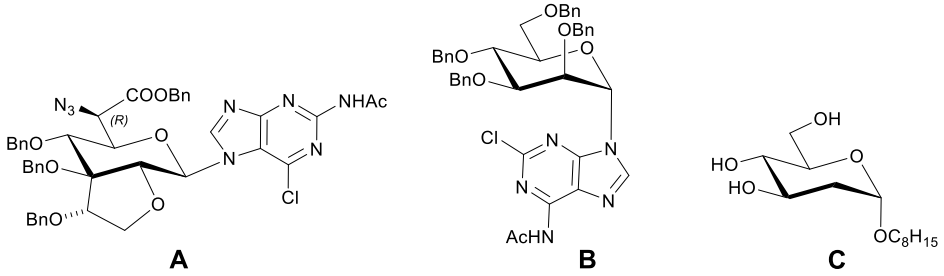

Figure 1.2.20. N^7 nucleosides (A and B) and octyl 2-deoxy-D-*arabino*-hexopyranoside (C) with selective BChE inhibitory activity.

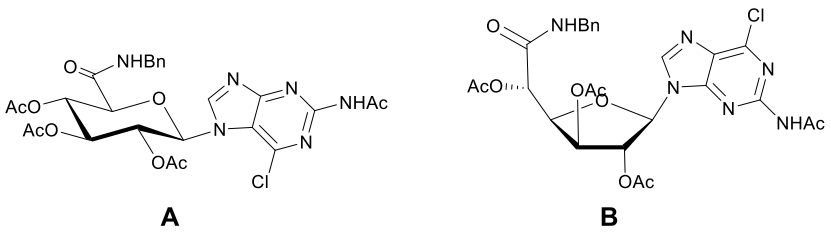

Figure 1.2.21. Nucleosides with selective AChE inhibitory activity.

1.2.3.2.2 Natural BChE Inhibitors

Also in the plant kingdom there are examples of selective BChE inhibitors, namely forsythoside B (figure 1.2.22), a phenylethanoid glycoside isolated from *Verbascum*

xanthophoeniceum,[96] and symcososide (figure 1.2.22), a component of *Symplocos racemosa*.[97] Forsythoside B was able to inhibit 98% of BChE activity at a concentration of 100 μM, with only mild activity against AChE.[96] On the other hand, symcososide proved to be more selective towards BChE, displaying an IC_{50} of 21.1 μM for this enzyme, but no activity towards AChE.[97]

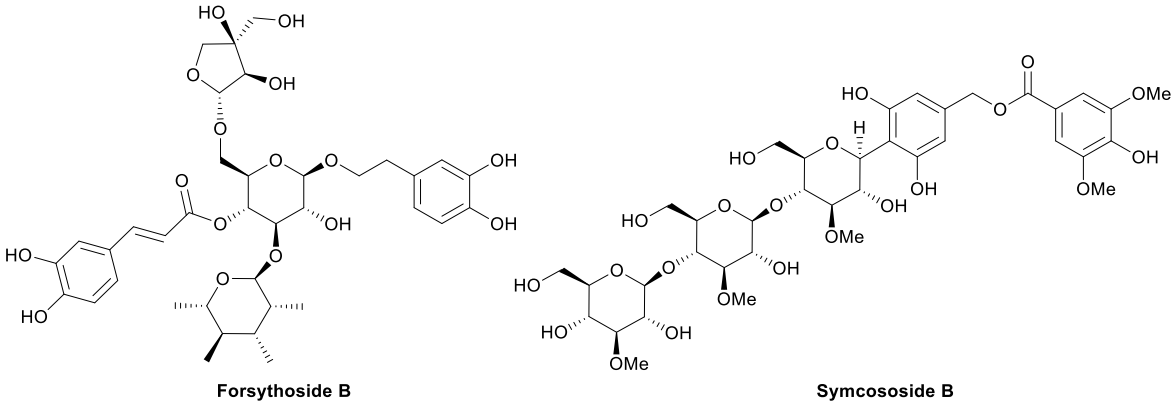

Figure 1.1.22. BChE inhibitors of natural origin.

Although there is still plenty to learn about the role of BChE in human brain and how selective BChE inhibitors can act on AD patients, a recent study showing that selective BChE inhibitors improve the cognitive performance of aged rats[6] supports that this is a valuable line of investigation.

1.2.4 DIAGNOSIS

In clinical practice, diagnosis of «possible» or «probable» AD is currently obtained mainly by mental status testing, since it is not yet available a neuroimaging technique able to visually differentiate between normal aging process and dementia. Definitive diagnosis is generally confirmed at post-mortem by the presence of intra- and extracellular protein aggregates in brain tissue.[98] Efforts have been done in order to find metabolic biomarkers for diagnosis of AD. Metabolic pathway analysis of familial AD mouse models revealed

significant alterations in the levels of metabolites involved in energy metabolism including nucleotide metabolism, mitochondrial Krebs cycle, carbohydrate, and amino acid metabolic pathways.[99] Metabonomic profiling of transgenic AD mice also revealed that that are significant differences in both brain and plasma levels of different sugar metabolites, namely in D-fructose (brain) and in D-glucose, D-galactose, and D-gluconic acid (plasma), when compared to healthy mice.[100] Carbohydrate metabolic pathway alteration in this model suggests the potential of carbohydrate structures for diagnosis. However, these biomarkers are yet to be investigated for their use in diagnosis.

Aβ *in vivo* imaging has been actively pursued over the last years, mainly regarding non-invasive techniques including positron emission tomography (PET), magnetic resonance imaging (MRI) and near IR fluorescence imaging. Based on the fact that gangliosides and glycosaminoglycans bind to Aβ and may play significant roles in initiation of amyloid aggregation, Kouyoumdjian and co-workers developed superparamagnetic iron oxide glyconanoparticles which magnetic cores are coated with sialic acid units (figure 1.2.23) to detect β-amyloid.[101] Indeed, these non-toxic glyconanoparticles could selectively bind to Aβ. The superparamagnetic nature of the glyconanoparticles allowed detection of Aβ by MRI both *in vitro* and *ex vivo* on mouse brains. Authors suggest that other carbohydrates and carbohydrate-containing compounds, such as glycosaminoglycans and ganglioside GM1, can be utilized to further enhance Aβ binding selectivity and specificity.[101] Nevertheless, these studies were conducted *ex vivo*, and diagnosis was performed post-mortem. For future imaging *in vivo*, it will be crucial to know whether these glyconanoparticles can access the plaques in the brain, passing the blood brain barrier.

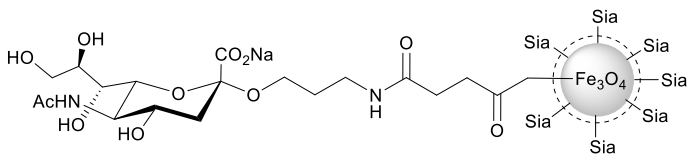

Figure 1.2.23 Glyconanoparticle coated with sialic acid units.

1.2.5 CONCLUSIONS

Investigation towards effective therapeutic drugs for AD has proven challenging. Pursuing the understanding of the mechanisms underlying the disease was the key issue to identify new therapeutic possibilities. A diversity of glycostructures has shown potential for neuroprotection, as shown in figure 1.2.24 summarizing the carbohydrate-based families of compounds acting on amyloidosis, cholinergic function and diagnosis. From natural to synthetic origin, from carbohydrates to carbomimetics, from small molecules to polysaccharides, many structures have been identified as potential future drugs for the prevention, treatment or diagnosis of this devastating disease. Amongst them, only the carbomimetic *scyllo*-inositol and the oligosaccharide neuroparin reached clinical trials. While the former did not meet the endpoints, results of neuroparin are yet to be known. The complex and multifactor aspects of AD may explain why drugs that address only one cause (one drug/one target strategy) afford disappointing results in clinical trials. Many authors have discussed how a multi-target therapy based on a compound with poly-pharmacology is more likely to be efficient. Many of the compounds discussed in this review address more than one target, namely the ginsenosides Rg1 and Rb1, as well as the monoterpene glycoside paeoniflorin, which can act in both amyloid plaques and in the cholinergic system, with effects in the cognition of animals. Moreover, the use of carbohydrates linked to other bioactive molecules to favour their access to brain through the hexose transporters in the BBB, or to improve their pharmacological properties, e.g. a sugar-curcumin conjugate, highlights the importance of carbohydrate-containing drugs.

Also in diagnosis, the potential of carbohydrates is noticeable, either by the use of endogenous sugar metabolites as disease biomarkers or by the use of carbohydrate-based

structures with high affinity to amyloid-β plaques. These findings strongly encourage further investigation in this area.

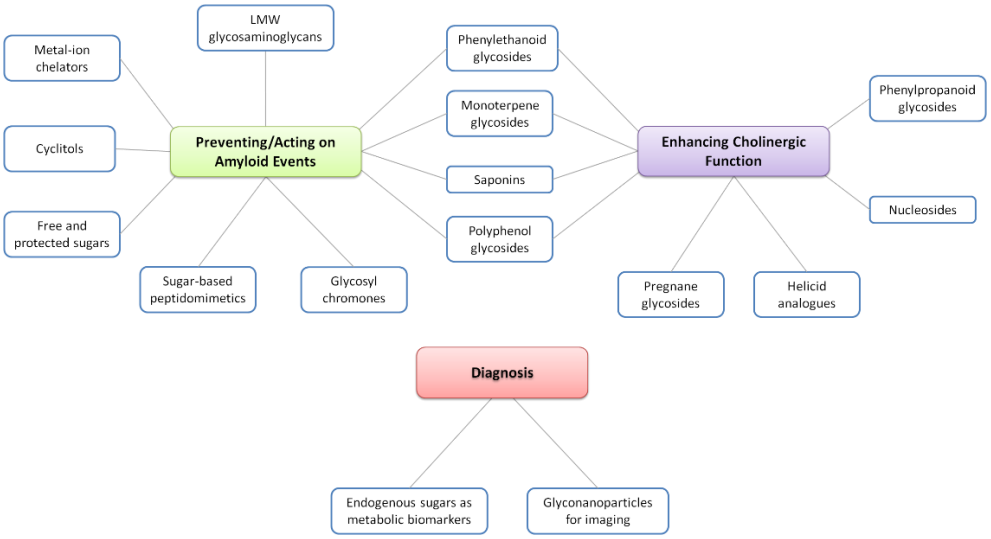

Figure 1.2.24. Carbohydrates in Alzheimer's disease therapeutics and diagnosis.

REFERENCES

[1] D. J. Selkoe, Alzheimer's disease: genes, proteins, and therapy. *Physiological Reviews* **2001,** *81* (2), 741-66.

[2] M. Citron, Strategies for disease modification in Alzheimer's disease. *Nature Reviews Neuroscience* **2004,** *5* (9), 677-85.

[3] R. W. Jones, Chapter 3 - Preventing Alzheimer's Disease A2 - Bairu, Menghis. In *Global Clinical Trials for Alzheimer's Disease*, M. W. Weiner, Ed. Academic Press: San Diego, 2014; pp 33-46.

[4] H. S. Won; S. S. Kenneth; S. Yoo-Hun, Therapeutic Agents for Alzheimers Disease. *Current Medicinal Chemistry - Central Nervous System Agents* **2005,** *5* (4), 259-269.

[5] R. J. Barrnett, Morphological and biochemical correlates of neural activity. *Archives of Neurology* **1965,** *13* (2), 220-220.

[6] E. Giacobini, Cholinergic function and Alzheimer's disease. *International Journal of Geriatric Psychiatry* **2003,** *18* (S1), S1-S5.

[7] N. H. Greig; T. Utsuki; D. K. Ingram; Y. Wang; G. Pepeu; C. Scali; Q. S. Yu; J. Mamczarz; H. W. Holloway; T. Giordano; D. Chen; K. Furukawa; K. Sambamurti; A. Brossi; D. K. Lahiri, Selective butyrylcholinesterase inhibition elevates brain acetylcholine, augments learning and lowers Alzheimer beta-amyloid peptide in rodent. *Proceedings of the National Academy of Sciences USA* **2005,** *102* (47), 17213-8.

[8] S. Darvesh; M. K. Cash; G. A. Reid; E. Martin; A. Mitnitski; C. Geula, Butyrylcholinesterase is Associated with β-Amyloid Plaques in the Transgenic APP(SWE)/PSEN1dE9 Mouse Model of Alzheimer Disease. *Journal of Neuropathology and Experimental Neurology* **2012,** *71* (1), 2-14.

[9] F. Mangialasche; A. Solomon; B. Winblad; P. Mecocci; M. Kivipelto, Alzheimer's disease: clinical trials and drug development. *The Lancet Neurology* **2010,** *9* (7), 702-16.

[10] E. Karran; M. Mercken; B. De Strooper, The amyloid cascade hypothesis for Alzheimer's disease: an appraisal for the development of therapeutics. *Nature Reviews Drug Discovery* **2011,** *10* (9), 698-712.

[11] R. Kayed; C. A. Lasagna-Reeves, Molecular mechanisms of amyloid oligomers toxicity. *Journal of Alzheimer's disease* **2013,** *33 Suppl 1*, S67-78.

[12] G. M. Hirschfield; P. N. Hawkins, Amyloidosis: new strategies for treatment. *The International Journal of Biochemistry & Cell Biology* **2003,** *35* (12), 1608-13.

[13] A. A. Qutub; C. A. Hunt, Glucose transport to the brain: a systems model. *Brain Research Reviews* **2005,** *49* (3), 595-617.

[14] B. Linnartz; L. G. Bodea; H. Neumann, Microglial carbohydrate-binding receptors for neural repair. *Cell and Tissue Research* **2012,** *349* (1), 215-27.

[15] Y. Cheng; L. H. Shen; J. T. Zhang, Anti-amnestic and anti-aging effects of ginsenoside Rg1 and Rb1 and its mechanism of action. *Acta Pharmacologica Sinica* **2005,** *26* (2), 143-9.

[16] K. Y. Yoo; S. Y. Park, Terpenoids as potential anti-Alzheimer's disease therapeutics. *Molecules* **2012,** *17* (3), 3524-38.

[17] H. J. Kim; P. Kim; C. Y. Shin, A comprehensive review of the therapeutic and pharmacological effects of ginseng and ginsenosides in central nervous system. *Journal of Ginseng Research* **2013,** *37* (1), 8-29.

[18] F. Fang; X. Chen; T. Huang; L. F. Lue; J. S. Luddy; S. S. Yan, Multi-faced neuroprotective effects of Ginsenoside Rg1 in an Alzheimer mouse model. *Biochimica et Biophysica Acta* **2012,** *1822* (2), 286-92.

[19] Q. Quan; J. Wang; X. Li; Y. Wang, Ginsenoside Rg1 decreases Abeta(1-42) level by upregulating PPARgamma and IDE expression in the hippocampus of a rat model of Alzheimer's disease. *PLoS One* **2013,** *8* (3), e59155.

[20] L.-M. Chen; Z.-Y. Lin; Y.-G. Zhu; N. Lin; J. Zhang; X.-D. Pan; X.-C. Chen, Ginsenoside Rg1 attenuates β-amyloid generation via suppressing PPARγ-regulated BACE1 activity in N2a-APP695 cells. *European Journal of Pharmacology* **2012,** *675* (1-3), 15-21.

[21] C. Shi; D.-d. Zheng; L. Fang; F. Wu; W. H. Kwong; J. Xu, Ginsenoside Rg1 promotes nonamyloidgenic cleavage of APP via estrogen receptor signaling to MAPK/ERK and PI3K/Akt. *Biochimica et Biophysica Acta - General Subjects* **2012,** *1820* (4), 453-460.

[22] J. Liu; X. Yan; L. Li; Y. Zhu; K. Qin; L. Zhou; D. Sun; X. Zhang; R. Ye; G. Zhao, Ginsennoside Rd Attenuates Cognitive Dysfunction in a Rat Model of Alzheimer's Disease. *Neurochemical Research* **2012,** *37* (12), 2738-2747.

[23] W. Li; Y. Chu; L. Zhang; L. Yin; L. Li, Ginsenoside Rg1 prevents SK-N-SH neuroblastoma cell apoptosis induced by supernatant from Abeta1-40-stimulated THP-1 monocytes. *Brain Research Bulletin* **2012,** *88* (5), 501-6.

[24] W. Li; Y. Chu; L. Zhang; L. Yin; L. Li, Ginsenoside Rg1 attenuates tau phosphorylation in SK-N-SH induced by Abeta-stimulated THP-1 supernatant and the involvement of p38 pathway activation. *Life Sciences* **2012,** *91* (15-16), 809-15.

[25] J. Yan; Q. Liu; Y. Dou; Y. Hsieh; Y. Liu; R. Tao; D. Zhu; Y. Lou, Activating glucocorticoid receptor-ERK signaling pathway contributes to ginsenoside Rg1 protection against beta-amyloid peptide-induced human endothelial cells apoptosis. *Journal of Ethnopharmacology* **2013,** *147* (2), 456-66.

[26] T. Huang; F. Fang; L. Chen; Y. Zhu; J. Zhang; X. Chen; S. S. Yan, Ginsenoside Rg1 Attenuates Oligomeric Aβ(1-42)-Induced Mitochondrial Dysfunction. *Current Alzheimer Research* **2012,** *9* (3), 388-395.

[27] B. Lee; B. Sur; J. Park; S.-H. Kim; S. Kwon; M. Yeom; I. Shim; H. Lee; D.-H. Hahm, Ginsenoside Rg3 Alleviates Lipopolysaccharide-Induced Learning and Memory Impairments by Anti-Inflammatory Activity in Rats. *Biomolecules & Therapeutics* **2013,** *21* (5), 381-390.

[28] Y. Y. Lee; J. S. Park; J. S. Jung; D. H. Kim; H. S. Kim, Anti-inflammatory effect of ginsenoside Rg5 in lipopolysaccharide-stimulated BV2 microglial cells. *International Journal of Molecular Sciences* **2013,** *14* (5), 9820-33.

[29] X. Li; M. Li; Y. Li; Q. Quan; J. Wang, Cellular and molecular mechanisms underlying the action of ginsenoside Rg1 against Alzheimer's disease. *Neural Regeneration Research* **2012,** *7* (36), 2860-6.

[30] X. Y. Song; J. F. Hu; S. F. Chu; Z. Zhang; S. Xu; Y. H. Yuan; N. Han; Y. Liu; F. Niu; X. He; N. H. Chen, Ginsenoside Rg1 attenuates okadaic acid induced spatial memory impairment by the GSK3beta/tau signaling pathway and the Abeta formation prevention in rats. *European Journal of Pharmacology* **2013,** *710* (1-3), 29-38.

[31] H.-h. Zhao; J. Di; W.-s. Liu; H.-l. Liu; H. Lai; Y.-l. Lü, Involvement of GSK3 and PP2A in ginsenoside Rb1's attenuation of aluminum-induced tau hyperphosphorylation. *Behavioural Brain Research* **2013,** *241*, 228-234.

[32] L. Li; Z. Liu; J. Liu; X. Tai; X. Hu; X. Liu; Z. Wu; G. Zhang; M. Shi; G. Zhao, Ginsenoside Rd attenuates beta-amyloid-induced tau phosphorylation by altering the functional balance of glycogen synthase kinase 3beta and protein phosphatase 2A. *Neurobiology of Disease* **2013,** *54*, 320-328.

[33] D. Ji; Y. Wu; B. Zhang; C. F. Zhang; Z. L. Yang, Triterpene saponins from the roots of Dipsacus asper and their protective effects against the Abeta(25-35) induced cytotoxicity in PC12 cells. *Fitoterapia* **2012,** *83* (5), 843-8.

[34] C. K. Han; W. R. Choi; K. B. Oh, Cognition-enhancing and neuroprotective effects of hederacolchiside-E from Pulsatilla koreana. *Planta Medica* **2007,** *73* (7), 665-9.

[35] M. A. Findeis; F. Schroeder; T. D. McKee; D. Yager; P. C. Fraering; S. P. Creaser; W. F. Austin; J. Clardy; R. Wang; D. Selkoe; C. B. Eckman, Discovery of a Novel Pharmacological and Structural Class of Gamma Secretase Modulators Derived from the Extract of Actaea racemosa. *ACS Chemical Neuroscience* **2012,** *3* (11), 941-951.

[36] S. Z. Zhong; Q. H. Ge; Q. Li; R. Qu; S. P. Ma, Peoniflorin attentuates Abeta((1-42))-mediated neurotoxicity by regulating calcium homeostasis and ameliorating oxidative stress in hippocampus of rats. *Journal of the Neurological Sciences* **2009,** *280* (1-2), 71-8.

[37] Z. Lan; L. Chen; Q. Fu; W. Ji; S. Wang; Z. Liang; R. Qu; L. Kong; S. Ma, Paeoniflorin attenuates amyloid-beta peptide-induced neurotoxicity by ameliorating oxidative stress and regulating the NGF-mediated signaling in rats. *Brain Research* **2013,** *1498*, 9-19.

[38] P. Sun; J.-y. Chen; J. Li; M.-r. Sun; W.-c. Mo; K.-l. Liu; Y.-y. Meng; Y. Liu; F. Wang; R.-q. He; Q. Hua, The protective effect of geniposide on human neuroblastoma cells in the presence of formaldehyde. *BMC Complementary and Alternative Medicine* **2013,** *13*, 152-152.

[39] B. Jiang; J. Du; J. H. Liu; Y. M. Bao; L. J. An, Catalpol attenuates the neurotoxicity induced by beta-amyloid(1-42) in cortical neuron-glia cultures. *Brain Research* **2008,** *1188*, 139-47.

[40] Y. Porat; A. Abramowitz; E. Gazit, Inhibition of amyloid fibril formation by polyphenols: structural similarity and aromatic interactions as a common inhibition mechanism. *Chemical Biology & Drug Design* **2006,** *67* (1), 27-37.

[41] M. Kurisu; Y. Miyamae; K. Murakami; J. Han; H. Isoda; K. Irie; H. Shigemori, Inhibition of amyloid beta aggregation by acteoside, a phenylethanoid glycoside. *Bioscience, Biotechnology and Biochemistry* **2013,** *77* (6), 1329-32.

[42] H. Wang; Y. Xu; J. Yan; X. Zhao; X. Sun; Y. Zhang; J. Guo; C. Zhu, Acteoside protects human neuroblastoma SH-SY5Y cells against beta-amyloid-induced cell injury. *Brain Research* **2009,** *1283*, 139-47.

[43] H. Q. Wang; Y. X. Xu; C. Q. Zhu, Upregulation of heme oxygenase-1 by acteoside through ERK and PI3 K/Akt pathway confer neuroprotection against beta-amyloid-induced neurotoxicity. *Neurotoxicity research* **2012,** *21* (4), 368-78.

[44] J. T. T. Zhu; R. C. Y. Choi; H. Q. Xie; K. Y. Z. Zheng; A. J. Y. Guo; C. W. C. Bi; D. T. W. Lau; J. Li; T. T. X. Dong; B. W. C. Lau; J. J. Chen; K. W. K. Tsim, Hibifolin, a flavonol glycoside, prevents β-amyloid-induced neurotoxicity in cultured cortical neurons. *Neuroscience Letters* **2009,** *461* (2), 172-176.

[45] H. Lou; P. Fan; R. G. Perez; H. Lou, Neuroprotective effects of linarin through activation of the PI3K/Akt pathway in amyloid-β-induced neuronal cell death. *Bioorganic & Medicinal Chemistry* **2011,** *19* (13), 4021-4027.

[46] R. C. Choi; J. T. Zhu; K. W. Leung; G. K. Chu; H. Q. Xie; V. P. Chen; K. Y. Zheng; D. T. Lau; T. T. Dong; P. C. Chow; Y. F. Han; Z. T. Wang; K. W. Tsim, A flavonol glycoside, isolated from roots of Panax notoginseng, reduces amyloid-beta-induced neurotoxicity in cultured neurons: signaling transduction and drug development for Alzheimer's disease. *Journal of Alzheimer's disease* **2010,** *19* (3), 795-811.

[47] A. R. Ladiwala; J. C. Lin; S. S. Bale; A. M. Marcelino-Cruz; M. Bhattacharya; J. S. Dordick; P. M. Tessier, Resveratrol selectively remodels soluble oligomers and fibrils of amyloid Abeta into off-pathway conformers. *The Journal of Biological Chemistry* **2010,** *285* (31), 24228-37.

[48] M. G. Sharoar; A. Thapa; M. Shahnawaz; V. S. Ramasamy; E.-R. Woo; S. Y. Shin; I.-S. Park, Keampferol-3-O-rhamnoside abrogates amyloid beta toxicity by modulating monomers and remodeling oligomers and fibrils to non-toxic aggregates. *Journal of Biomedical Science* **2012,** *19* (1), 104-104.

[49] S. Dolai; W. Shi; C. Corbo; C. Sun; S. Averick; D. Obeysekera; M. Farid; A. Alonso; P. Banerjee; K. Raja, "Clicked" Sugar–Curcumin Conjugate: Modulator of Amyloid-β and Tau Peptide Aggregation at Ultralow Concentrations. *ACS Chemical Neuroscience* **2011,** *2* (12), 694-699.

[50] L. Lv; Q. Y. Yang; Y. Zhao; C. S. Yao; Y. Sun; E. J. Yang; K. S. Song; I. Mook-Jung; W. S. Fang, BACE1 (beta-secretase) inhibitory chromone glycosides from Aloe vera and Aloe nobilis. *Planta Medica* **2008,** *74* (5), 540-5.

[51] Y.-X. Zhou; H. Zhang; C. Peng, Puerarin: A Review of Pharmacological Effects. *Phytotherapy Research* **2014,** *28* (7), 961-975.

[52] G. Xing; M. Dong; X. Li; Y. Zou; L. Fan; X. Wang; D. Cai; C. Li; L. Zhou; J. Liu; Y. Niu, Neuroprotective effects of puerarin against beta-amyloid-induced neurotoxicity in PC12 cells via a PI3K-dependent signaling pathway. *Brain Research Bulletin* **2011,** *85* (3-4), 212-8.

[53] H. Y. Zhang; Y. H. Liu; H. Q. Wang; J. H. Xu; H. T. Hu, Puerarin protects PC12 cells against beta-amyloid-induced cell injury. *Cell Biology International* **2008,** *32* (10), 1230-7.

[54] F. Lin; B. Xie; F. Cai; G. Wu, Protective Effect of Puerarin on β-Amyloid-Induced Neurotoxicity in Rat Hippocampal Neurons. *Arzneimittelforschung* **2012,** *62* (04), 187-193.

[55] Y. Zou; B. Hong; L. Fan; L. Zhou; Y. Liu; Q. Wu; X. Zhang; M. Dong, Protective effect of puerarin against beta-amyloid-induced oxidative stress in neuronal cultures from rat hippocampus: involvement of the GSK-3β/Nrf2 signaling pathway. *Free Radical Research* **2013,** *47* (1), 55-63.

[56] J. Li; G. Wang; J. Liu; L. Zhou; M. Dong; R. Wang; X. Li; X. Li; C. Lin; Y. Niu, Puerarin attenuates amyloid-beta-induced cognitive impairment through suppression of apoptosis in rat hippocampus in vivo. *European Journal of Pharmacology* **2010,** *649* (1-3), 195-201.

[57] B. Dorgeret; L. Khemtémourian; I. Correia; J.-L. Soulier; O. Lequin; S. Ongeri, Sugar-based peptidomimetics inhibit amyloid β-peptide aggregation. *European Journal of Medicinal Chemistry* **2011,** *46* (12), 5959-5969.

[58] T. Storr; M. Merkel; G. X. Song-Zhao; L. E. Scott; D. E. Green; M. L. Bowen; K. H. Thompson; B. O. Patrick; H. J. Schugar; C. Orvig, Synthesis, characterization, and metal coordinating ability of multifunctional carbohydrate-containing compounds for Alzheimer's therapy. *Journal of the American Chemical Society* **2007,** *129* (23), 7453-63.

[59] M. Abe; Y. Abe; T. Ohkuri; T. Mishima; A. Monji; S. Kanba; T. Ueda, Mechanism for retardation of amyloid fibril formation by sugars in Vlambda6 protein. *Protein Science* **2013,** *22* (4), 467-74.

[60] R. Liu; H. Barkhordarian; S. Emadi; C. B. Park; M. R. Sierks, Trehalose differentially inhibits aggregation and neurotoxicity of beta-amyloid 40 and 42. *Neurobiology of Disease* **2005,** *20* (1), 74-81.

[61] H. Fujiwara; M. Tabuchi; T. Yamaguchi; K. Iwasaki; K. Furukawa; K. Sekiguchi; Y. Ikarashi; Y. Kudo; M. Higuchi; T. C. Saido; S. Maeda; A. Takashima; M. Hara; N. Yaegashi; Y. Kase; H. Arai, A traditional medicinal herb Paeonia suffruticosa and its active constituent 1,2,3,4,6-penta-O-galloyl-beta-D-glucopyranose have potent anti-aggregation effects on Alzheimer's amyloid beta proteins in vitro and in vivo. *Journal of Neurochemistry* **2009,** *109* (6), 1648-57.

[62] J. McLaurin; M. E. Kierstead; M. E. Brown; C. A. Hawkes; M. H. L. Lambermon; A. L. Phinney; A. A. Darabie; J. E. Cousins; J. E. French; M. F. Lan; F. Chen; S. S. N. Wong; H. T. J. Mount; P. E. Fraser; D. Westaway; P. S. George-Hyslop, Cyclohexhexol inhibitors of Aβ aggregation prevent and reverse Alzheimer phenotype in a mouse model. *Nature Medicine* **2006,** *12*, 801.

[63] L. Hughes; S. Guthrie, Chapter 10 - Operationalization of Global Alzheimer's Disease Trials A2 - Bairu, Menghis. In *Global Clinical Trials for Alzheimer's Disease*, M. W. Weiner, Ed. Academic Press: San Diego, 2014; pp 159-177.

[64] Y. Sun; G. Zhang; C. A. Hawkes; J. E. Shaw; J. McLaurin; M. Nitz, Synthesis of scyllo-inositol derivatives and their effects on amyloid beta peptide aggregation. *Bioorganic & Medicinal Chemistry* **2008,** *16* (15), 7177-84.

[65] B. Dudas; K. Semeniken, Glycosaminoglycans and neuroprotection. In *Handbook of Experimental Pharmacology*, 2012/05/09 ed.; 2012; pp 325-43.

[66] J. McLaurin; T. Franklin; X. Zhang; J. Deng; P. E. Fraser, Interactions of Alzheimer amyloid-beta peptides with glycosaminoglycans effects on fibril nucleation and growth. *European Journal of Biochemistry* **1999,** *266* (3), 1101-10.

[67] D. A. Dewitt; R. J. Castellani; G. Perry; M. A. Smith, Involvement of complex carbohydrate chemistry in Alzheimer's disease. *Medical Hypotheses and Research* **2005,** *2*, 393-400.

[68] B. Dudas; M. Rose; U. Cornelli; A. Pavlovich; I. Hanin, Neuroprotective Properties of Glycosaminoglycans: Potential Treatment for Neurodegenerative Disorders. *Neurodegenerative Diseases* **2008,** *5* (3-4), 200-205.

[69] T. Ariga; T. Miyatake; R. K. Yu, Role of proteoglycans and glycosaminoglycans in the pathogenesis of Alzheimer's disease and related disorders: amyloidogenesis and therapeutic strategies-a review. *Journal of Neuroscience Research* **2010,** *88* (11), 2303-15.

[70] H. Zhu; J. Yu; M. S. Kindy, Inhibition of amyloidosis using low-molecular-weight heparins. *Molecular Medicine* **2001,** *7* (8), 517-22.

[71] J. Hu; M. Geng; J. Li; X. Xin; J. Wang; M. Tang; J. Zhang; X. Zhang; J. Ding, Acidic oligosaccharide sugar chain, a marine-derived acidic oligosaccharide, inhibits the cytotoxicity and aggregation of amyloid beta protein. *Journal of Pharmacological Sciences* **2004,** *95* (2), 248-55.

[72] Y. Fan; J. Hu; J. Li; Z. Yang; X. Xin; J. Wang; J. Ding; M. Geng, Effect of acidic oligosaccharide sugar chain on scopolamine-induced memory impairment in rats and its related mechanisms. *Neuroscience Letters* **2005,** *374* (3), 222-6.

[73] D. Dhavale; J. E. Henry, Evaluation of sialic acid-analogs for the attenuation of amyloid-beta toxicity. *Biochimica et Biophysica Acta* **2012,** *1820* (10), 1475-80.

[74] R. Kisilevsky; W. A. Szarek; J. B. Ancsin; E. Elimova; S. Marone; S. Bhat; A. Berkin, Inhibition of amyloid A amyloidogenesis in vivo and in tissue culture by 4-deoxy analogues of peracetylated 2-acetamido-2-deoxy-alpha- and beta-d-glucose: implications for the treatment of various amyloidoses. *The American Journal of Pathology* **2004,** *164* (6), 2127-37.

[75] B. Lee; K. Jung; D. H. Kim, Timosaponin AIII, a saponin isolated from Anemarrhena asphodeloides, ameliorates learning and memory deficits in mice. *Pharmacology, Biochemistry, and Behavior* **2009,** *93* (2), 121-7.

[76] K. Y. Lee; S. H. Sung; Y. C. Kim, New Acetylcholinesterase-Inhibitory Pregnane Glycosides of Cynanchum atratum Roots. *Helvetica Chimica Acta* **2003,** *86* (2), 474-483.

[77] K. Y. Lee; J. S. Yoon; E. S. Kim; S. Y. Kang; Y. C. Kim, Anti-acetylcholinesterase and anti-amnesic activities of a pregnane glycoside, cynatroside B, from Cynanchum atratum. *Planta Medica* **2005,** *71* (1), 7-11.

[78] H. A. Jung; Y. J. Jung; S. K. Hyun; B. S. Min; D. W. Kim; J. H. Jung; J. S. Choi, Selective cholinesterase inhibitory activities of a new monoterpene diglycoside and other constituents from Nelumbo nucifera stamens. *Biological & Pharmaceutical bulletin* **2010,** *33* (2), 267-72.

[79] S. H. Kwon; H. C. Kim; S. Y. Lee; C. G. Jang, Loganin improves learning and memory impairments induced by scopolamine in mice. *European Journal of Pharmacology* **2009,** *619* (1-3), 44-9.

[80] E. J. Jeong; K. Y. Lee; S. H. Kim; S. H. Sung; Y. C. Kim, Cognitive-enhancing and antioxidant activities of iridoid glycosides from Scrophularia buergeriana in scopolamine-treated mice. *European Journal of Pharmacology* **2008,** *588* (1), 78-84.

[81] S. R. Kim; K. Y. Lee; K. A. Koo; S. H. Sung; N. G. Lee; J. Kim; Y. C. Kim, Four new neuroprotective iridoid glycosides from Scrophularia buergeriana roots. *Journal of Natural Products* **2002,** *65* (11), 1696-9.

[82] X. Zhang; C. Jin; Y. Li; S. Guan; F. Han; S. Zhang, Catalpol improves cholinergic function and reduces inflammatory cytokines in the senescent mice induced by D-galactose. *Food and Chemical Toxicology* **2013,** *58*, 50-5.

[83] P. Fan; A.-E. Hay; A. Marston; K. Hostettmann, Acetylcholinesterase-Inhibitory Activity of Linarin from Buddleja davidii, Structure-Activity Relationships of Related Flavonoids, and Chemical Investigation of Buddleja nitida. *Pharmaceutical Biology* **2008,** *46* (9), 596-601.

[84] P. P. Oinonen; J. K. Jokela; A. I. Hatakka; P. M. Vuorela, Linarin, a selective acetylcholinesterase inhibitor from Mentha arvensis. *Fitoterapia* **2006,** *77* (6), 429-434.

[85] X. L. He; W. Q. Zhou; M. G. Bi; G. H. Du, Neuroprotective effects of icariin on memory impairment and neurochemical deficits in senescence-accelerated mouse prone 8 (SAMP8) mice. *Brain Research* **2010,** *1334*, 73-83.

[86] R. X. Xu; Q. Wu; Y. Luo; Q. H. Gong; L. M. Yu; X. N. Huang; A. S. Sun; J. S. Shi, Protective effects of icariin on cognitive deficits induced by chronic cerebral hypoperfusion in rats. *Clinical and Experimental Pharmacology & Physiology* **2009,** *36* (8), 810-5.

[87] M. Jung; M. Park, Acetylcholinesterase Inhibition by Flavonoids from Agrimonia pilosa. *Molecules* **2007,** *12* (9), 2130-2139.

[88] B. S. Min; T. D. Cuong; J. S. Lee; B. S. Shin; M. H. Woo; T. M. Hung, Cholinesterase inhibitors from Cleistocalyx operculatus buds. *Archives of Pharmacal Research* **2010,** *33* (10), 1665-70.

[89] J. Kehr; S. Yoshitake; S. Ijiri; E. Koch; M. Nöldner; T. Yoshitake, Ginkgo biloba leaf extract (EGb 761®) and its specific acylated flavonol constituents increase dopamine and acetylcholine levels in the rat medial prefrontal cortex: possible implications for the cognitive enhancing properties of EGb 761®. *International Psychogeriatrics* **2012,** *24* (S1), S25-S34.

[90] X. D. Li; S. T. Kang; G. Y. Li; X. Li; J. H. Wang, Synthesis of some phenylpropanoid glycosides (PPGs) and their acetylcholinesterase/xanthine oxidase inhibitory activities. *Molecules* **2011,** *16* (5), 3580-96.

[91] H. Wen; C. Lin; L. Que; H. Ge; L. Ma; R. Cao; Y. Wan; W. Peng; Z. Wang; H. Song, Synthesis and biological evaluation of helicid analogues as novel acetylcholinesterase inhibitors. *European Journal of Medicinal Chemistry* **2008,** *43* (1), 166-173.

[92] F. Marcelo; F. V. M. Silva; M. Goulart; J. Justino; P. Sinaÿ; Y. Blériot; A. P. Rauter, Synthesis of novel purine nucleosides towards a selective inhibition of human butyrylcholinesterase. *Bioorganic & Medicinal Chemistry* **2009,** *17* (14), 5106-5116.

[93] S. Schwarz; R. Csuk; A. P. Rauter, Microwave-assisted synthesis of novel purine nucleosides as selective cholinesterase inhibitors. *Organic & Biomolecular Chemistry* **2014,** *12* (15), 2446-2456.

[94] N. M. Xavier; S. Schwarz; P. D. Vaz; R. Csuk; A. P. Rauter, Synthesis of Purine Nucleosides from D-Glucuronic Acid Derivatives and Evaluation of Their Cholinesterase-Inhibitory Activities. *European Journal of Organic Chemistry* **2014,** *2014* (13), 2770-2779.

[95] A. Martins; M. S. Santos; C. Dias; P. Serra; V. Cachatra; J. Pais; J. Caio; V. H. Teixeira; M. Machuqueiro; M. S. Silva; A. Pelerito; J. Justino; M. Goulart; F. V. Silva; A. P. Rauter, Tuning the Bioactivity of Tensioactive Deoxy Glycosides to Structure: Antibacterial Activity Versus Selective Cholinesterase Inhibition Rationalized by Molecular Docking. *European Journal of Organic Chemistry* **2013,** *2013* (8), 1448-1459.

[96] M. Georgiev; K. Alipieva; I. Orhan; R. Abrashev; P. Denev; M. Angelova, Antioxidant and cholinesterases inhibitory activities of Verbascum xanthophoeniceum Griseb. and its phenylethanoid glycosides. *Food Chemistry* **2011,** *128* (1), 100-5.

[97] V. Ahmad; A. Rashid, *Butyrylcholinesterase inhibitory C-glycoside from Symplocos racemosa*. 2006; Vol. 80.

[98] R. Barone; L. Sturiale; A. Palmigiano; M. Zappia; D. Garozzo, Glycomics of pediatric and adulthood diseases of the central nervous system. *Journal of Proteomics* **2012,** *75* (17), 5123-39.

[99] E. Trushina; E. Nemutlu; S. Zhang; T. Christensen; J. Camp; J. Mesa; A. Siddiqui; Y. Tamura; H. Sesaki; T. M. Wengenack; P. P. Dzeja; J. F. Poduslo, Defects in Mitochondrial Dynamics and Metabolomic Signatures of Evolving Energetic Stress in Mouse Models of Familial Alzheimer's Disease. *PLos ONE* **2012,** *7* (2), e32737.

[100] Z. P. Hu; E. R. Browne; T. Liu; T. E. Angel; P. C. Ho; E. C. Chan, Metabonomic profiling of TASTPM transgenic Alzheimer's disease mouse model. *Journal of Proteome Research* **2012,** *11* (12), 5903-13.

[101] H. Kouyoumdjian; D. C. Zhu; M. H. El-Dakdouki; K. Lorenz; J. Chen; W. Li; X. Huang, Glyconanoparticle Aided Detection of β-Amyloid by Magnetic Resonance Imaging and Attenuation of β-Amyloid Induced Cytotoxicity. *ACS Chemical Neuroscience* **2013,** *4* (4), 575-584.

1.3 Chemical approaches toward neurodegenerative disease prevention: the role of coupling sugars to phenolic biomolecular entities[a]

Polyphenols are plant secondary metabolites present in the common human diet and known to play important roles in human health. They are poorly absorbed, resulting in a very low concentration in the circulatory streams.[1] The modification of their physicochemical properties such as solubility and partition coefficient by glycosylation seems to exert a positive influence on the entry of polyphenols into enterocytes.[1] The low solubility of most of the polyphenol aglycones may also result from their tendency to form aggregates via hydrophobic interactions with aromatic rings, and hydrogen bonding by the hydroxy groups.[1] In nature, polyphenols occur often as glycosylated derivatives. The sugar moiety of polyphenol glycosides plays a major role in their absorption[1] but polyphenol glycosylation may also exert other benefits by improving bioavailability or preventing oxidation by masking phenolic groups. In this chapter synthetic strategies via chemical or enzymatic methodologies to access biologically active glycosyl polyphenols are illustrated, covering flavonoids, stilbenes, phenylpropanoids and phenylethanoids. Natural occurrence and compound bioactivities are also reviewed for the promising polyphenol molecular entities described that exhibit neuroprotective activities.

[a] Dias, C.; Matos, A. M.; Rauter, A. P., Chemical Approaches Towards Neurodegenerative Disease Prevention: The Role of Coupling Sugars to Phenolic Biomolecular Entities. In *Coupling and Decoupling of Diverse Molecular Units in Glycosciences*, Witczak, Z. J.; Bielski, R., Eds. Springer International Publishing: Cham, 2018; pp 167-194.

1.3.1 GLYCOSYLATED FLAVONOIDS

Flavonoids are polyphenolic secondary metabolites in the plant kingdom whose structural feature is based on derivatives of a phenyl-substituted 1-phenylpropane possessing a C_{15} skeleton. In this chapter the given examples focus particularly on flavones, whose structure is that of a 1-benzopyran (chromene), in which the aromatic ring is designated as ring A and the pyran as ring C, along with the (substituted) phenyl group (ring B) on ring C at position 2 (flavone) or position 3 (isoflavone). Thousands of different scaffolds have been isolated and structurally identified over the past decades, and many have been reported due to their wide-range bioactive profiles often associated with very potent antioxidant and anti-inflammatory effects.[2] They may occur as aglycones or as the corresponding glycosylated forms, either as *O*-glycosides or *C*-glycosyl derivatives; yet, the advantages of glycosyl flavones over the corresponding aglycones have been highlighted in the context of Alzheimer's disease with respect to their ability to remodel and inactivate neurotoxic amyloid β (Aβ) aggregates,[3] again reinforcing the importance of the sugar moiety for optimized anti-neurodegenerative activity.

The growing interest in the therapeutic potential of glycosyl flavonoids has motivated organic and medicinal chemists to develop efficient synthetic and bio-enzymatic routes involving a diverse collection of sugar coupling reactions. By describing the synthesis of some of the most promising molecular entities with neuroprotective activities, we will provide an overview on the most useful methodologies for the generation of flavones bearing in their structure O-linked or C-linked sugars, covering both chemical and enzymatic synthesis reported in the literature.

1.3.1.1 Flavone Glycosides

The 7-*O*-β-glucuronide of baicalein, baicalin (**1**), is one of the most abundant compounds in *Scutellaria baicalensis Georgi*, a plant extensively used in traditional Chinese medicine for the

treatment of inflammatory disorders, bacterial infections, among others.[4] Baicalin (**1**) itself was recently found to improve Aβ-induced learning and memory deficits in rats by attenuating hippocampal injury and neuron apoptosis.[5] Its anti-inflammatory activity has actually been proposed as a paramount mechanism underlying these neuroprotective effects,[4] namely by inhibiting microglial activation and inflammatory cytokine secretion.[6] Moreover, baicalin (**1**) could also upregulate antioxidant enzymes such as superoxide dismutase, catalase and glutathione peroxidase, thus contributing to decreased oxidative injury in the brain of diseased animals.[5]

Based on its promising therapeutic potential, Li and co-workers described an efficient route for baicalin (Scheme 1.3.1) starting from the selectively acetylated aglycone **3**, which was accessed after a series of simple protection-deprotection reactions,[7] and using the first type of sugar donor ever applied in the synthesis of flavonoid glycosides: a glycosyl bromide.[8] In this method, 6-OTBDPS protected bromide **2** was coupled to the aglycone in an Ag_2O-promoted reaction that afforded only the β-glucoside in 92% yield due to acyl neighboring group participation, thus overpowering the otherwise dominant anomeric effect that would have given the α-anomer as the major product. After deprotection with TBAF, position 6" was then submitted to Widlanski oxidation using TEMPO and BAIB to give the glucuronic acid derivative **4**, followed by a deacylation reaction that led to the desired product, baicalin (**1**).

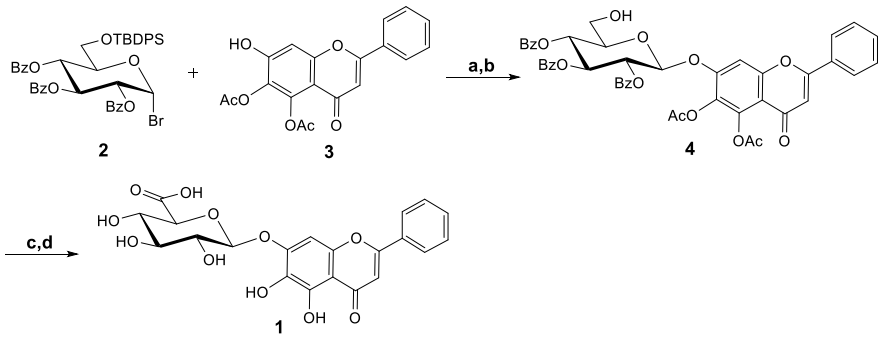

Scheme 1.3.1. Reagents and conditions: a) Ag_2O, 4ÅMS, quinoline, r.t. (92%); **b)** TBAF, AcOH, THF, 4h (86%); **c)** TEMPO, BAIB, DCM/H_2O, r.t. (87%), **d)** $Mg(OMe)_2$, MeOH, r.t. (85%) (Li et al.2015).

The 4'-hydroxy analogue of baicalin (**1**), scutellarin (**5**), is the major component of *the Erigeron breviscapus* Hand-Mazz flavonoid extract, also used in traditional Chinese medicine for the treatment of cerebral infarction and other cardiovascular diseases.[9] Similarly, this compound was found to attenuate neuroinflammation through the suppression of microglial activation,[10] and was indeed associated with major improvements in neuronal injury and behavior of rats with cerebral ischemia.[11-12] Moreover, it is able to inhibit Aβ aggregation *in vitro*, while preventing Aβ-mediated neuronal cell death. [13]

Nonetheless, pharmacokinetic studies have revealed that scutellarin (**5**) displays a rather poor bioavailability due to the action of endogenous β-glucuronidase enzymes that readily hydrolyze the glycosidic bond.[14-16] To surpass this problem, Li and co-workers designed and synthesized the scutellarin β-*O*-glucosyl analogue **6** with improved physicochemical properties and an even more pronounced attenuation of H_2O_2-induced neuronal damage when compared to scutellarin (**5**).[17] Using scutellarin itself as the aglycone source, the authors coupled compound **7** to the glucosyl bromide **8** with Ag_2O and $CuSO_4$ as promotors; yet, the β-*O*-glucoside **6** was achieved in only moderate yield (40%) (Scheme 1.3.2).

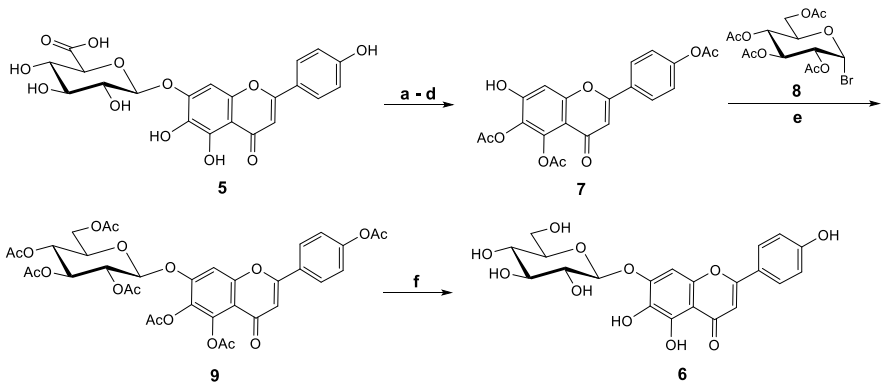

Scheme 1.3.2. Reagents and conditions: a) 6N HCl, EtOH, 120 ºC (17%); **b)** pyridine, Ac_2O, DMAP, 25 ºC (79%); **c)** BnBr, K_2CO_3, KI, acetone, reflux (70%); **d)** Pd/C, H_2, DCM/EtOH, 25 ºC (95%); **e)** $CuSO_4$, AgO, quinoline, 25 ºC (40%); **f)** NaOH, $CHCl_3$, 0 ºC (41%).[17]

Among the most promising *O*-glucosyl flavonoid leads against neurodegenerative diseases is quercetin 3-β-*O*- glucoside (**10**) (trivial name: isoquercetin), which has been isolated from a variety of sources, including mangos or medicinal plants such *Serjanis erecta Radlk* (Sapindaceae) or *Psidium guajava* L.[18-20] In addition to its antioxidant and anti-inflammatory activities, this compound is able to prevent hippocampal neuronal apoptosis after cerebral ischemia and reperfusion injury,[21-22] and displays protective effects against Aβ-induced cytotoxicity. Importantly, it was also found to inhibit both BACE-1 and AChE with IC_{50} values of 41.2 μM and 66.9 μM, respectively.[23-24] Furthermore, a comparative study between polyphenolic glycosides and their respective aglycones has shown that whilst quercetin (**11**) acts by remodeling Aβ toxic oligomers into large aggregates, isoquercetin (**10**) rapidly disaggregates the amyloid structures into soluble polypeptides as a result of a synergistic action between the sugar and the aglycone.[3]

Isoquercetin (**10**) can be obtained from quercetin (**11**) by the action of UGT78D1, a flavonoid-specific uridine diphosphate glycosyltransferase (Scheme 1.3.3) that catalyzes the *in vitro* regioselective transfer of a glucose or a rhamnose unit from UDP-glucose or UDP-rhamnose, respectively, to flavonoid glycosyl acceptors containing a hydroxyl group in position 3, as reported by Ren and co-workers.[25] This study was able to clarify the substrate specificity of this enzyme in detail, showing that only flavones hydroxylated in both rings A and B are recognized by UGT78D1, highlighting 2'-OH flavones as exceptions to this rule.

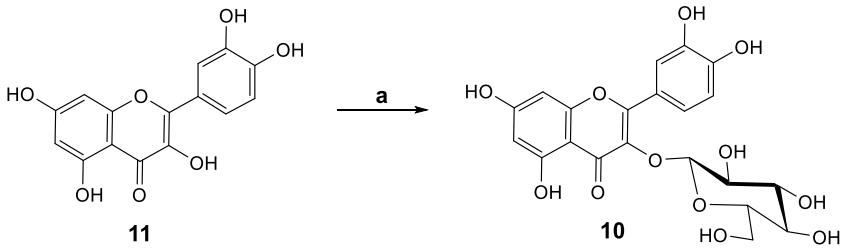

11 **10**

Scheme 1.3.3. Reagents and conditions: a) Recombinant UGT78D1, 50 mM Tris-HCl pH 7.2, UDP-Glucose, 30 ºC.[25]

Tiliroside (**12**) is a kaempferol 3-β-*O*-glycoside that can be found in *Agrimonia pilosa* or *Potentilla chinesis* for instance, and displayed stronger AChE inhibitory activity when compared to

isoquercetin (**10**), with an IC_{50} value of 25.5 μM.[24, 26] It was also found to inhibit neuroinflammation in activated microglial cells by modulating pro-inflammatory intracellular pathways, which was at least in part attributed to its antioxidant properties.[27]

The synthesis of tiliroside (**12**) was described in 1981 by Vermes and co-workers (Scheme 1.3.4).[28] In the first step of this route, glucosyl bromide **13** and 4',7-*O*-dibenzyl kaempferol (**14**) were coupled in a reaction promoted by Ag_2CO_3 to afford the β-anomer in 54% yield. After debenzylation followed by acetylation and selective removal of the 6''-*O*-chloroacetyl protecting group, intermediate **15** was generated and subsequently esterified by *p*-coumaroyl chloride in pyridine. Further deprotection directly afforded tiliroside (**12**) in good yield. Many other phenylpropanoid glycosides with neuroprotective activities such as this one will be presented, and their synthetic routes described in detail in section **1.3.3**.

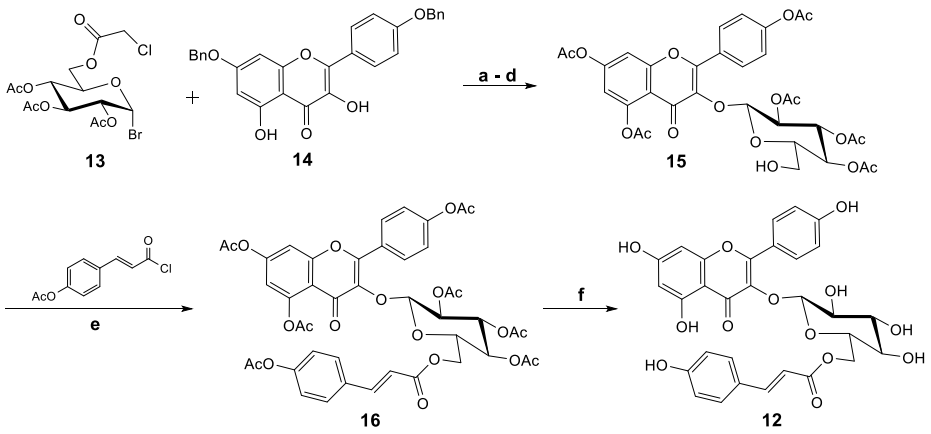

Scheme 1.3.4. Reagents and conditions: a) Ag_2CO_3, pyridine, drierite, 0 °C (54%); **b)** H_2, Pd/C, EtOH, r.t. (90%); **c)** Ac_2O, pyridine, r.t. (88%); **d)** MeOH, thiourea, r.t. (90%); **e)** DCM, pyridine (62%); **f)** $CHCl_3$, NaOMe, MeOH (67%).[28]

1.3.1.2 C-Glycosyl Flavones and Isoflavones

Despite the remarkable neuroprotective effects associated with the flavone O-glycosides described above, *C*-glycosyl flavonoids have been receiving growing attention for their insusceptibility to *in vivo* hydrolysis by glucosidases, allowing them to remain intact in the blood circulation following oral administration.[29] Even though the synthesis of the C–C bond usually

requires stronger conditions when compared to the formation of the C-O bond in O-glycosides, a variety of methods have been reported in the literature over the past few decades, offering a wide range of options for regio- and stereoselective reactions using different glycosyl donors and acceptors when the time comes to design a synthetic route for the target compound.[30]

Vitexin (**17**) and isovitexin (**18**), the 8-β-*C*- and 6-β-*C*-glucosyl derivatives of apigenin, respectively, are good examples of the potential of natural *C*-glycosyl flavonoid derivatives against neurodegenerative disorders. These compounds can be found in *Serjanis erecta Radlk* (Sapindaceae)[19] or the flour from the *Prosopis alba* seed,[31] for instance, and both were able to inhibit AChE and BChE with IC_{50} values ranging from 6.2 μM to 12.2 μM, although vitexin was substantially more effective as a BACE-1 inhibitor than isovitexin (IC_{50} = 51.1 μM vs. >100 μM), thus indicating a preference for the sugar moiety to be in position 8 for improved affinity towards the enzyme.[32] Vitexin (**17**) has also been described to exert neuroprotective effects in cerebral ischemia and reperfusion injury by positively and negatively modulating cell proliferation and apoptosis pathways, respectively.[33] In addition, vitexin (**17**) was found to have a more pronounced impact in reversing Aβ-induced cytotoxicity not only when compared to isovitexin (**18**), but also when put alongside with the earlier presented isoquercetin (**10**).[19]

Back in 1995, Mahling and co-workers developed a synthetic route for both vitexin (**17**) and isovitexin (**18**) by taking advantage of the Fries-type rearrangement, described to occur in *O*-aryl glycosides with high regio- and stereoselectivity to afford the corresponding *ortho*-hydroxy *C*-glycosyl phenolic derivative.[30, 34-35] Hence, in the first step of this synthesis (Scheme 1.3.5), the reaction of the glycosyl trichloroacetimidate **19** with the silyl-protected acetophenone **20** was catalysed by TMSOTf at – 30 ^{0}C and afforded the α-*O*-glycoside **21** in 85% yield. After cleavage of the remaining TBS group followed by regioselective benzylation in position 4, a Fries-type rearrangement took place in another TMSOTf-catalysed reaction, this time at room temperature, to afford the corresponding β-*C*-glycosyl derivative in 57% yield. Subsequent acylation converted this

derivative into intermediate **17** and, at this point, the Baker-Venkataraman rearrangement was carried out and resulted in a mixture of compounds **23** and **24**, which were both cyclized and further deprotected after separation to give vitexin (**17**) and isovitexin (**18**).

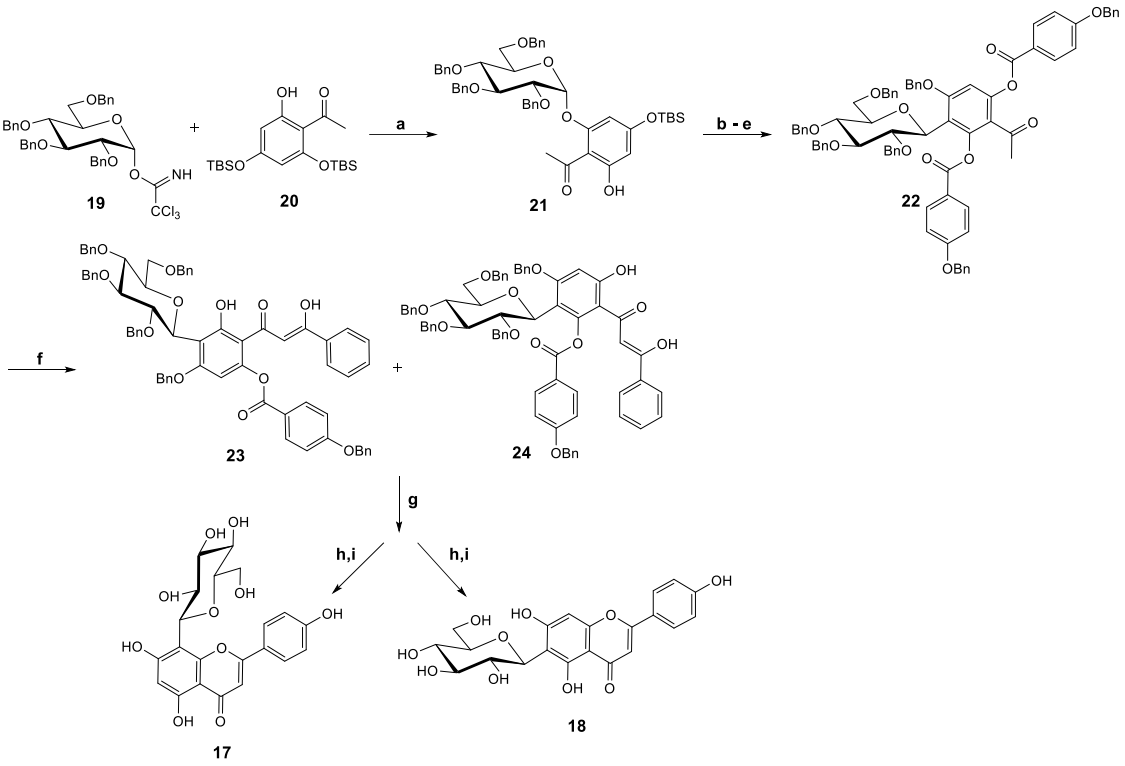

Scheme 1.3.5. Reagents and conditions: a) TMSOTf, DCM, -30 ºC (85%); **b)** TBAF, THF (86%); **c)** BnBr, NaH, DMF (89%); **d)** TMSOTf, DCM, r.t. (57%); **e)** WSC, DMAP, 4-(benzyloxy)benzoic acid, DCM (81%); **f)** TBA·HSO_4, K_2CO_3, H_2O/Benzene, 60 ºC (39%); **g)** TMSOTf, DCM, r.t. (17%); **h)** NaOMe, MeOH, 50 ^{0}C (62% and 100%, respectively); **i)** H_2, Pd/C, EtOAc/MeOH (88% and 89%, respectively).[34]

Vitexin (**17**) and isovitexin (**18**) were also obtained as protected intermediates in a more recent and concise synthesis developed by Furuta and co-workers[36] with the ultimate goal of accessing compound **25**, an anti-inflammatory glycosyl flavone isolated from oolong tea extract.[37] In this route (Scheme 1.3.6), trichloroacetimidate **19** was directly coupled with the monobenzyl-protected acetophenone **26** to afford the desired β-*C*-glucosyl derivative in 69% yield, which was further acylated to give intermediate **27**. In contrast with the previous work by Mahling *et al.*, this procedure involves the initial formation of a glycoside at low temperature, which then undergoes, by warming up, the *O* → *C* Fries-type rearrangement *in situ*.[30]

In another one-pot reaction using potassium carbonate in pyridine under reflux, intermediate **27** was converted into both protected isovitexin (**28**) and protected vitexin (**29**); yet, to accomplish the synthesis of the target compound, only **28** proceeded in this route. After debenzylation, it was submitted to an intramolecular Mitsunobu reaction using modified experimental conditions in which inversion of the configuration of carbon 2'' led to the transformation of the *gluco* derivative into the desired *manno* derivative in tandem with the formation of a fused tetracyclic system with the aglycone. Further deprotection afforded the target compound **25**, but it is still interesting to note that this was the major product of Mitsunobu reaction regardless of the presence of a primary alcohol and another phenolic group in its precursor, thus highlighting reaction regiospecificity.

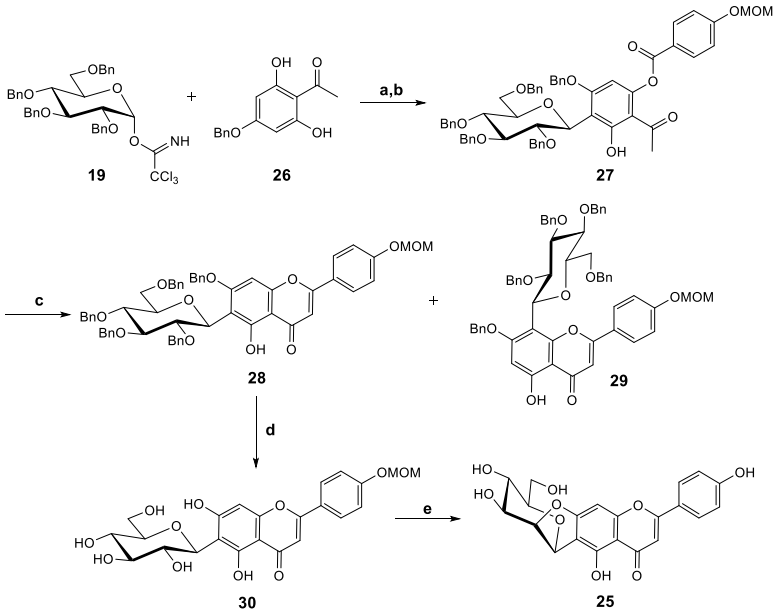

Scheme 1.3.6. Reagents and conditions: a) TMSOTf, DCM, 0ºC → r.t. (69%); **b)** 4-(methoxymethoxy)benzoic acid, DCC, DMAP, DCM, r.t. (82%); **c)** K_2CO_3, pyridine, reflux (17% and 15%, respectively); **d)** $Pd(OH)_2$, H_2, EtOH, 35 ºC (95%); **e)** 1,1'-azobis(*N*,*N*-dimethylformamide), Bu_3P, THF, 50 ºC; then HCl-dioxane, MeOH, r.t. (32%).[36]

Orientin (**31**) and isoorientin (**32**) are another pair of *C*-glucosyl flavonoid derivatives extensively studied for their potential against neurodegenerative processes and can both be found, for instance, in buckwheat bran,[38] *Glochidion hypoleucum* (Miq.) Boerl leaves, or *Stellaria holostea*.[39]

Orientin (**31**) was able to alleviate cognitive deficits in mice with Alzheimer's disease, while attenuating mitochondrial dysfunction induced by Aβ.[40] Moreover, it exerted neuroprotective effects by inhibiting the activity of three members of the caspase family, including caspase 3, which is directly involved in synaptic loss and cognitive dysfunction in Alzheimer's disease.[41-42] Both orientin (**31**) and isoorientin (**32**) are BACE-1 inhibitors with IC_{50} values of 16.0 μM and 20.9 μM, respectively, showing that the presence of the additional hydroxy group in position 3' when compared to vitexin (**17**) and isovitexin (**18**) positively affects the affinity towards the enzyme, especially in the case of 6-β-*C*-glucosyl derivatives. Furthermore, they are also AChE and BChE inhibitors, and seem to be slightly selective towards the later, with similar IC_{50} values of roughly 11 μM.[32]

In contrast to the described synthetic approaches for vitexin (**17**) and isovitexin (**18**), each of these luteolin *C*-glucosyl derivatives have been accessed individually in more effective, regioselective routes. Kumazawa and co-workers reported, on the one hand, the synthesis of orientin (Scheme 1.3.7) in which the glucosyl fluoride **33** was coupled with acetophenone **34** in a $BF_3 \cdot Et_2O$-promoted reaction to afford the β-*C*-glucosyl derivative **35** in 96% yield.[43] Subsequently, an aldol condensation led to chalcone **37** which, after cyclization and deprotection, gave orientin (**31**) in very good yield.

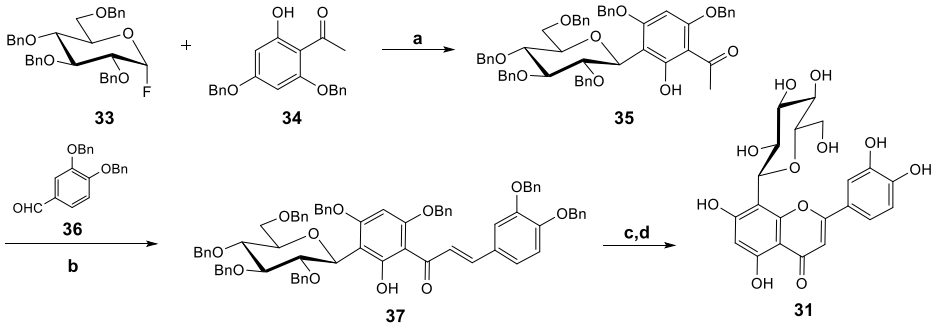

Scheme 1.3.7. Reagents and conditions: a) $BF_3 \cdot Et_2O$, MS4Å, DCM, -78 ºC → r.t. (96%); **b)** 1,4-dioxane, aq. NaOH 50%, r.t. (84%); **c)** I_2, DMSO, reflux (84%); **d)** Pd/C, H_2, EtOH, r.t. (quantitative yield).[43]

On the other hand, these authors were able to develop a synthetic path towards isoorientin (Scheme 1.3.8) using the same coupling methodology but taking advantage of differences in hydrogenolysis rates between benzyl and 2-methylbenzyl protecting groups.[44] Indeed, after a series

of protection-deprotection reactions, the free hydroxy group was *para* to the sugar moiety in intermediate **40**, and after aldol condensation, cyclization and deprotection, isoorientin (**32**) was successfully generated. It is noteworthy that, in this route, the C-glycosylation step was significantly less effective (75% yield) than the one described in the synthesis of orientin (**31**, 95% yield), even though the coupling method applied was the same in both cases. Given that the only difference between the two glycosyl acceptors was the 2-methylbenzyl group in compound **39**, this result highlights the impact of protecting groups on the efficiency of this type of coupling reactions.

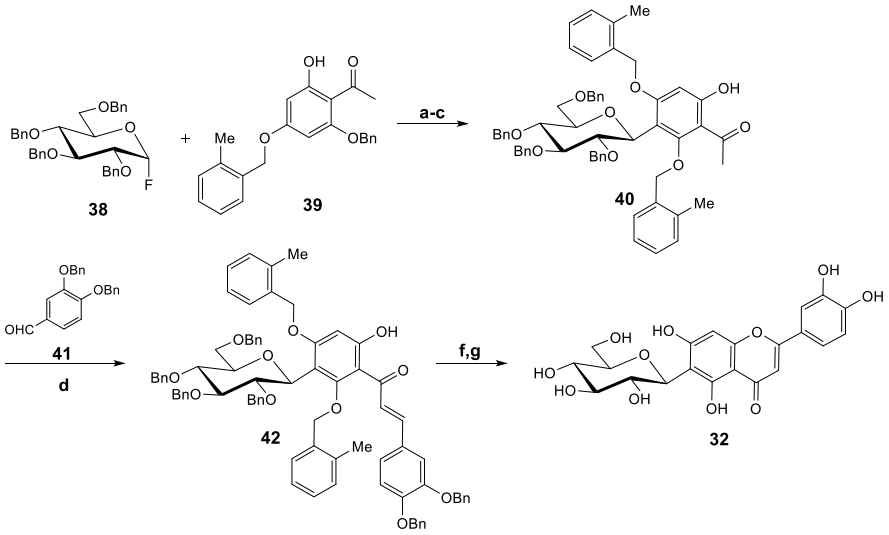

Scheme 1.3.8. Reagents and conditions: a) $BF_3{\cdot}Et_2O$, MS 4Å, DCM, -78 ºC → r.t. (75%); **b)** anhydrous K_2CO_3, 2-methylbenzyl chloride, DMF, 80 ºC (quantitative yield); **c)** Pd/C, H_2, EtOAc, r.t. (40%); **d)** 1,4-dioxane, aq. NaOH 50%, r.t. (91%); **f)** I_2, DMSO, 200 ºC (76%); **g)** Pd/C, H_2, EtOAc/EtOH, r.t. (quantitative yield).[44]

More recently, the biosynthesis of vitexin (**17**), isovitexin (**18**), orientin (**31**) and isoorientin (**32**) was accomplished by Hao and co-workers *using Desmodium incanum* root proteins, starting from the corresponding 2-hydroxyflavanones, the required substrates of *C*-glycosyltransferases existent in *Desmodium spp*.[45-46] As clarified in a previous report,[47] Wessely-Moser isomerization is responsible for the interconversion between the corresponding 8-β-*C*- (**45** and **46**) and 6-β-*C*-glucosyl derivatives (**49** and **50**), as 2-hydroxyflavanones may exist in solution in either open chain or cyclized

structures (Scheme 1.3.9). Despite the consequent lack of regioselectivity, these intermediates afforded the respective flavones in overall excellent yields after acid-promoted chemical dehydration.

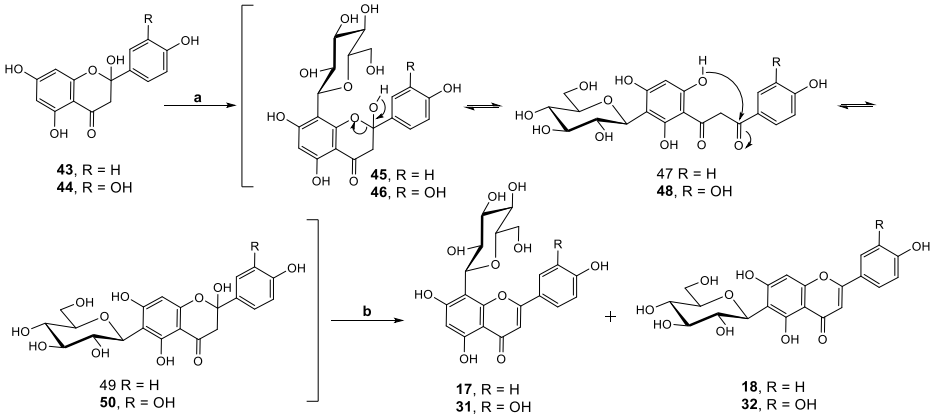

Scheme 1.3.9. Reagents and conditions: a) *D. Incanum* root protein, 100 mM HEPES, 2mM DTT, pH 7.5, UDP-Glucose, 30 °C; **b)** 1M HCl (vitexin, **17**, 44% and isovitexin, **18**, 53%; orientin, **31**, 43% and isoorientin, **32**, 56%).[45, 47]

Puerarin (**51**), the major component of *Puerariae Lobatae Radix*,[48] is another *C*-glucosyl flavonoid with potential against neurodegenerative disorders (Chapter 1.2) and has received particular attention in regard to its ability to act against diabetes-induced cognitive dysfunction, complementing its known antidiabetic.[48-50] This is of particular importance due to the well-established relationship between type 2 diabetes and Alzheimer's disease[51] and, in fact, puerarin (**51**) was found to have neuroprotective activity in STZ-induced diabetic rodents with learning and memory deficits by exerting antioxidant, anti-inflammatory and anti-apoptotic effects.[52-53] As already mentioned, this *C*-glucosyl isoflavone was able to attenuate Aβ-induced oxidative stress, cell injury and resulting cognitive impairment,[54-58] and could also improve learning and memory functions in rats with vascular dementia by activating cellular antioxidant defense mechanisms.[59]

The total synthesis of puerarin (**51**) was firstly reported by Lee and co-workers in 2003 (Scheme 1.3.10).[60] In this approach, the benzyl protected glycopyranolactone **52** was coupled to the lithiated glycosyl acceptor **53** at low temperature, followed by reduction with triethylsilane and

$BF_3 \cdot Et_2O$ to give the β-anomer in 56%. After a couple of protection-deprotection reactions, a Friedel-Crafts reaction catalyzed by $AlCl_3$ and subsequent deacetylation gave intermediate **55**, which then underwent aldol condensation with *p*-methoxybenzaldehyde (**56**) to afford chalcone **57**. After acetylation, TTN-promoted oxidative rearrangement of ring B followed by closure of ring C and demethylation gave puerarin (**51**) in moderate overall yield.

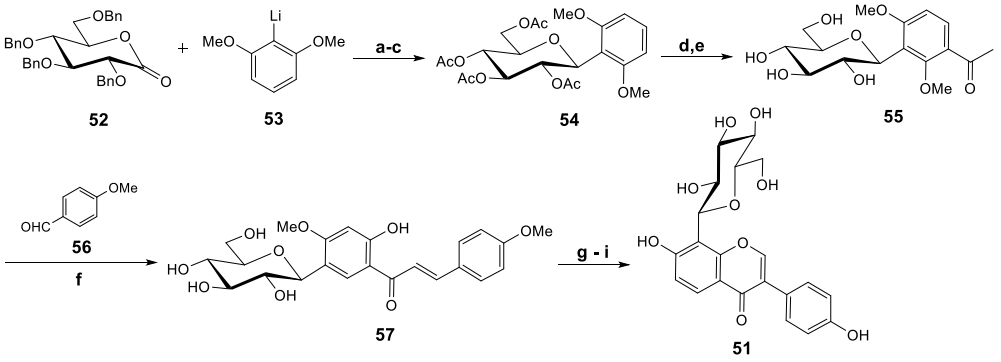

Scheme 1.3.10. Reagents and conditions: a) THF, -78 ºC → -10 ºC; then TESH, $BF_3 \cdot Et_2O$, DCM, -78 ºC → r.t. (56%); **b)** Pd/C, H_2, MeOH, r.t. (quantitative yield); **c)** pyridine, Ac_2O, r.t. (96%); **d)** $AlCl_3$, AcCl, Et_2O, r.t. (69%); **e)** 1: Na, MeOH; 2: Dowex 50WX8-200 (97%); **f)** NaOH, EtOH, r.t. (92%); **g)** pyridine, Ac_2O, r.t. (85%); **h)** 1: $Tl(NO_3)_3$, $MeOH/CH(OCH_3)_3$; 2: 10% HCl, MeOH, reflux (84%); **i)** TMSI, ACN (35%).[60]

The trihydroxyisoflavone analogue of puerarin (**51**) is the 8-β-D-glucosylgenistein (**58**), the main component of the EtOAc extract of *Genista tenera*, a plant found in Madeira island and used in folk medicine to treat diabetes.[61] In addition to its potent antidiabetic activity, 8-β-D-glucosylgenistein (**58**) was found to interact with $A\beta_{1\text{-}42}$ polypeptides, suggesting potential neuroprotective effects as well. In this study, the binding epitope of 8-β-D-glucosylgenistein (**58**) with Aβ was disclosed, confirming the already expected key role of both aromatic rings in the resulting interaction, and reinforcing the importance of the sugar moiety in the anti-amyloidogenic activity of this compound.

The synthesis of 8-β-D-glucosylgenistein (**58**) (Scheme 1.3.11) was accomplished by coupling the commercially available glucopyranoside **59** and acetophenone **60** catalysed by TMSOTf, to give the desired C-glycosylation product in 56% yield, which was selectively benzylated to afford

intermediate **61**.[61] Then, aldol condensation with *p*-benzyloxybenzaldehyde followed by acetylation led to the formation of chalcone **63** and subsequent TTN-promoted oxidative rearrangement, ring closure and deprotection afforded the target compound, **58**.

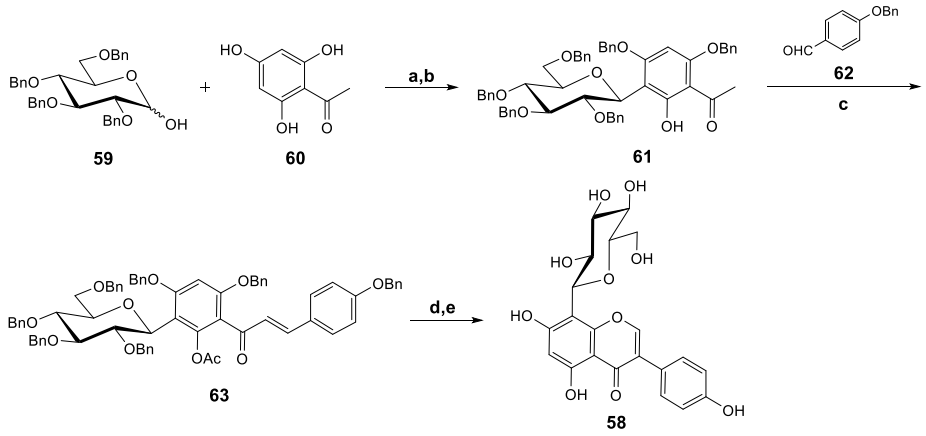

Scheme 1.3.11. Reagents and conditions: a) 1. TMSOTf, DCM/ACN, drierite, -40 °C → r.t. (56%); **b)** BnBr, K_2CO_3, r.t. (74%), **c)** 1: 1,4-dioxane, aq. NaOH 50%, reflux; 2: pyridine, Ac_2O, DMAP, r.t. (60%); **d)** 1: $Tl(NO_3)_3$, MeOH/$CH(OCH_3)_3$, 40 °C; 2: THF/MeOH, aq. NaOH 50%, r.t. (63%); **e)** Pd/C, H_2, EtOAc/MeOH, r.t. (96%).[61]

In a nutshell, the coupling of sugars with polyphenols to generate bioactive glycosyl flavonoids may involve a variety of different strategies and experimental conditions which primarily depend upon the available starting materials, reaction promotors or catalysts, and the nature of the pursued C-C or C-O bond. Regio- and stereoselectivity can be achieved with the use of the appropriate sugar protecting groups and glycosyl acceptor, while temperature is a key factor in the formation of either *O*- or *C*-glycosyl derivatives, particularly when a Fries-type rearrangement is involved in the reaction mechanism. Also, by covering the synthesis of structurally complex compounds such as the presented bioactive glycosyl flavones and isoflavones, this section enclosed a number of useful protection-deprotection strategies, interesting rearrangement reactions and cyclization approaches, which may be convenient in the synthesis of new nature-inspired glycosylated molecules towards neurodegenerative disease prevention.

1.3.2. STILBENOID GLYCOSIDES

Stilbenoids are natural compounds occurring in a number of plant families, particularly in grapevine.[62] Amongst them, the most well-known is resveratrol (*E*)-3,4',5-trihydroxystilbene, **64**), possessing anti-inflammatory, anti-oxidant and chemopreventive activities. This powerful compound is present in wine and has been speculated to be responsible for so called French paradox, where the saturated fat rich French diet correlates with a low mortality from coronary heart disease.[63-64] Resveratrol also occurs ubiquitously in nature as resveratrol 3-β-glucoside (piceid, **67**) (Figure 1.3.1). Other stilbenes include pterostilbene (*E*)-4'-hydroxy-3,5-dimethoxystilbene, **65**), piceantannol (*E*)-3,3',4',5-tetrahydroxystilbene, **66**) and astringine (**68**) which biological activities have been reviewed.[65]

Much attention has also been paid to stilbenes potential ability to protect from neurodegeneration. In fact, research points resveratrol as neuroprotective, not only due to the already mentioned antioxidant and anti-inflamatory activities, but also due to its ability to inhibit Aβ oligomeric cytotoxicity and to reduce neuronal cell death.[66] In a comparative study, the inhibitory activity of a series of stilbenes against Aβ(25-35) fibril formation was assessed. Both resveratrol **64** and piceid **67** effectively and dose dependently inhibited Aβ more extensively than curcumin.[67]

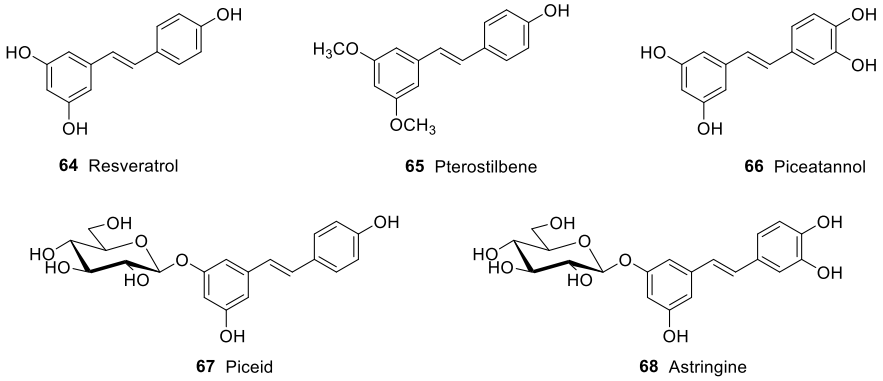

Figure 1.3.1. Structure of natural stilbenes and stilbene glycosides.

Despite the promising activities of resveratrol and its glycoside piceid, their bioavailability on humans is quite poor.[63, 68] Indeed, the oral bioavailability of resveratrol is less than 1% as a

consequence of quick and extensive metabolism, mainly through glucuronidation and sulfation, although it is not known whether resveratrol metabolites have a positive biological impact. The water-insolubility of stilbenes such as resveratrol, pterostilbene, and piceatannol limits their further pharmacological exploitation. Literature shows several efforts to develop new stilbene analogues with higher solubility and bioavailability, and glycochemistry has definitely played a very relevant role. Glycosylation allows water-insoluble and unstable organic compounds to be converted into the corresponding water-soluble and stable compounds.

The synthesis of piceid itself was first described by Orsini and co-workers, in an attempt to obtain this natural product more efficiently (Scheme 1.3.12).[69] The synthetic strategy aimed at building the stilbene skeleton first, by Wittig reaction of the aldehyde **69** and phosphonium ylide **70**, followed by desylilation. Methyl protected intermediary **71** was then glycosylated in aqueous base under the phase transfer catalyst benzyltriethylammonium bromide (BTEAB) which afforded glucoside **73** in 32%. The diglucoside was also formed and isolated in 13% yield. Further deprotection (2 steps) afforded piceid (**67**) in 60% yield (13% overall yield).[69] This methodology was also employed to the synthesis of other stilbene glycosides such as combrestatin analogues.

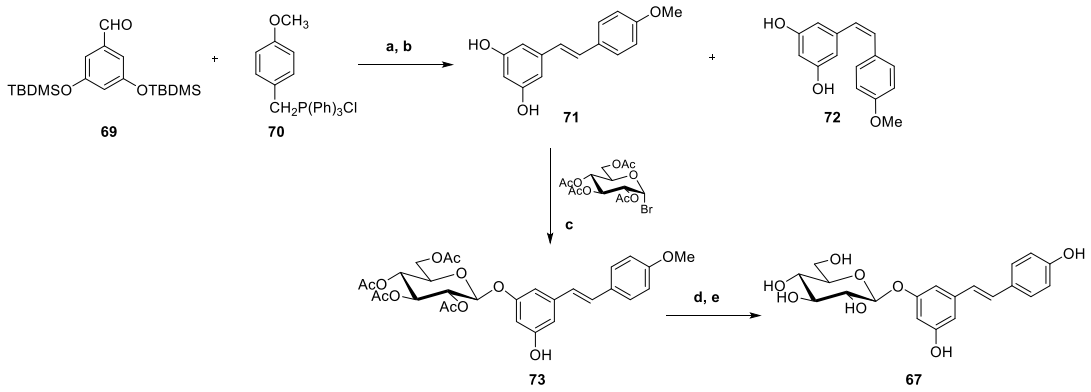

Scheme 1.3.12. Reagents and conditions: a) BuLi, THF, -20 ºC (98%, Z/E 2.3:1); b) TBAF, THF, quant.; c) BTEAB, NaOH, $CHCl_3$, 60 ºC, 32%; d) MeONa, MeOH, 25 ºC, quant.; e) EtSNa, DMF (60%).[69]

More recent efforts towards glycosylation of resveratrol take advantage of biotransformation for a simpler and more efficient synthesis. Glucosyltransferase *Pa*GT3 from *Phytolacca americana*

expressed in *Bacillus subtilis* was used to convert resveratrol into its 3- and 4′-β-glucosides (**67** and **74**), as well as pterostilbene and piceatannol into their 4′-β-glucosides **75** and **76** respectively (Scheme 1.3.13). Glucosylation reactions were performed at 37°C, in potassium phosphate buffer supplemented with UDP-glucose and enzyme. Although the procedure was not very effective towards piceid (12% yield), it afforded the 4′-β-glucosides in yields ranging from 50-76%.[70]

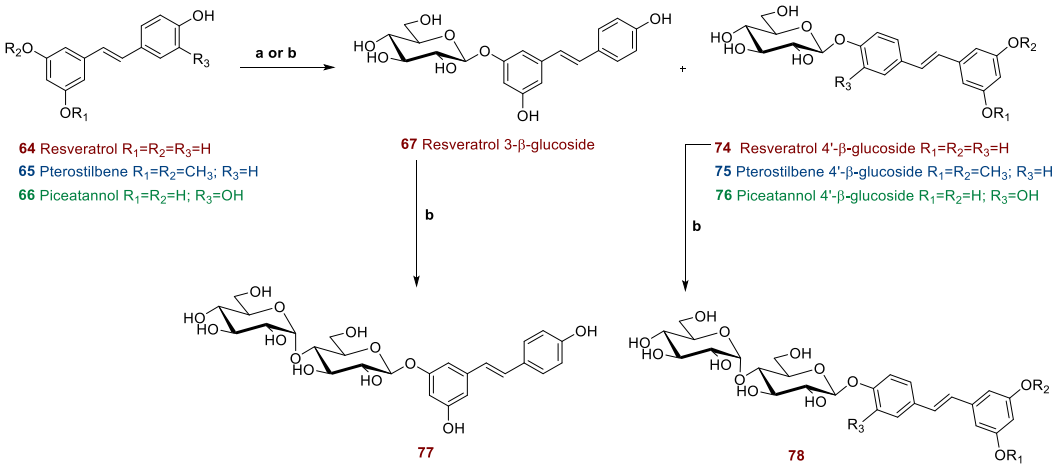

Scheme 1.3.13. Glycosylation of stilbenes resveratrol, pterostilbene and piceantannol. Reagents and conditions: a) *Pa*GT3, potassium phosphate buffer (pH 7.2), UDP-glucose. b) cyclodextrin glucanotransferase (CGTase).[70-71]

Glycosylation of stilbenes was also performed using cultured cells from *P. Americana* and glucosyltransferase (*Pa*GT). This biocatalytic glycosylation using cultured cells, in opposition to the direct use of the extracted enzyme, afforded resveratrol glucosides **67** and **74** in 35% and 22% yield, respectively,[71] favoring the formation of piceid, and 77% of piceatannol glucoside **76**, which proved to be the best substrate for this enzyme. Pterostilbene was only slightly converted into **75**. In addition, resveratrol 3- and 4'-β-glucosides were further glycosylated using cyclodextrin glucanotransferase (CGTase) to afford resveratrol 3- and 4'-β-maltosides (**77** and **78**), respectively, with yields of 17% and 27%. The phosphodiesterase (PDE) inhibitory activity or resveratrol and pterostilbene was

enhanced by glycosylation, since resveratrol 3- and 4'-β-glucosides, resveratrol 4'-β-maltoside and pterostilbene 4′-β-glucoside were better PDE inhibitors than their corresponding aglycone. This is particularly relevant as PDE inhibitors could be used in the treatment of neurodegenerative disorders such as Alzheimer's disease as they show potential to exert a neuroprotective role. Interestingly, piceatannol 4′-β-glucoside revealed also potent histamine release inhibitory activity (anti-allergic activity).[70-71]

Enzymatic synthesis has also been employed in further glycosylation of the natural piceid, generating more soluble piceid glycosides such as **79**, which was obtained after incubation of piceid with maltosyltransferase from *Caldicellulosiruptor bescii* and maltotriose at 70 ºC, in 18% yield. The water solubility of maltosyl piceid **79** is 8540 and 1860 times greater than that of resveratrol and piceid, respectively.[72] Since the α-1,4-glycosidic linkages present in **79** can be easily hydrolyzed *in vivo* by α-glucosidase, this piceid glycoside could potentially be a resveratrol prodrug, with increased bioavailability and delayed metabolism (Scheme 1.3.14).[72] Several piceid glucosides have also been obtained using cyclodextrin glucanotransferase from *Bacillus macerans*.[73]

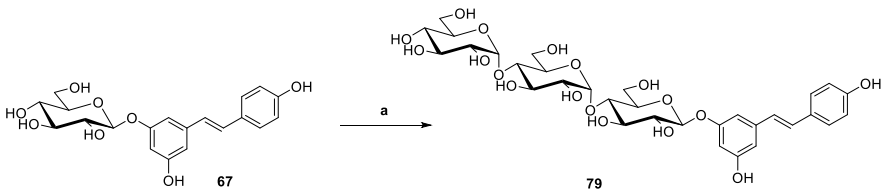

Scheme 1.3.14. Enzymatic synthesis of maltosyl piceid. a) Maltosyltransferase (MTase), maltotriose.[72]

More recently, a sucrose phosphorylate from *Thermoanaerobacterium thermosaccharolyticum* (TtSPP) was engineered envisioning quantitative glycosylation of resveratrol in aqueous media (Scheme 1.3.15). Desmet and co-workers were able to identify a residue particularly important in the active site of TtSPP, which normally does not have a pocket deep enough for the biding resveratrol. Such residue, R134, was replaced by a smaller residue aiming at leaving an opening in the enzyme's closed conformation, enabling the accommodation of larger substrates. Indeed, the variant R134A,

where arginine 134 was replaced by alanine, proved to have a reasonable affinity for resveratrol and to be very effective in the glycosylation of resveratrol at gram scale, allowing the quantitative production of resveratrol 3-α-glucoside in an aqueous system, using sucrose as a cheap glycosyl donor.[74]

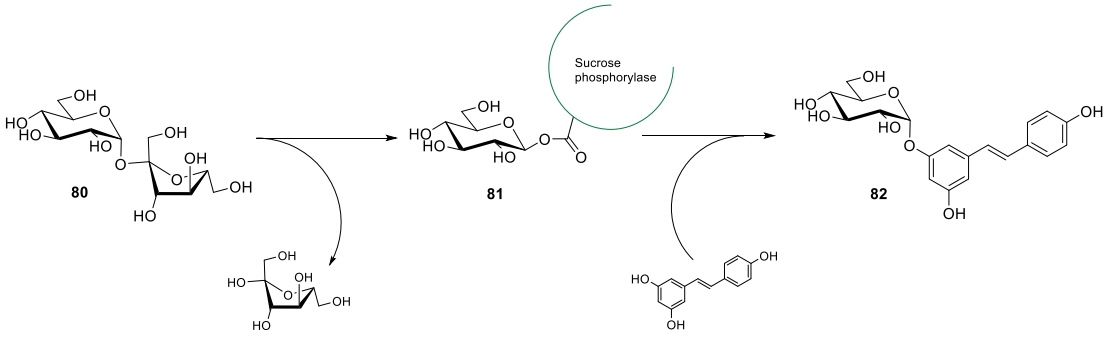

Scheme 1.3.15. Synthesis of resveratrol 3-α-glucoside with R134A variant of sucrose phosphorylase.[74]

Cyclodextrin glucanotransferase was also used to convert resveratrol and starch to α-glucosylated resveratrol products at 3-OH, at 4'-OH and at both 3-OH and 4'-OH, with increased water solubility when compared to that of resveratrol.[1] Interestingly, while the water solubility of piceid is 0.37 g/L, its alfa anomer presented a solubility higher than 2 g/L.[1] Nevertheless, it would be interesting to compare the bioactivity of **82** with its anomer piceid, as configuration may play an important role in bioactivity and bioavailability, as demonstrated for the solubility. To the best of our knowledge, no bioactivity studies were conducted on resveratrol 3-α-glucoside so far.

Keeping in mind the challenge of resveratrol low water solubility, a new resveratrol analogue was developed, where glucosyl units were added to a resveratrol core with a succinate linker. It was speculated that the presence of glycosyl groups may also improve bioavailability by influencing phenomena taking place upstream of entry into erythrocytes, as occurs for quercetin 3-*O*-glucoside. For the construction of the resveratrol analogue, a succinyl linker was firstly attached to the 3-hydroxy group of diacetoneglucose (**83**) (Scheme 1.3.16). The resulting succinyl ester (**85**) was used for the transesterification with resveratrol hydroxy groups using EDC. Hydrolysis of the isopropylidene protecting groups afforded the resveratrol derivative **87** in a 57% overall yield. This

compound is relatively stable in acidic conditions but can be converted into resveratrol by blood esterases. Pharmacokinetics parameters were also improved, as its administration resulted in a blood concentration versus time curve shifted to longer times in comparison to resveratrol. This chemical transformation is particularly attractive as it may be employed in other bioactive polyphenols with poor water solubility. In addition, coating the hydroxy groups with sugar moieties can even make them more palatable.[75] Thus, it would be interesting to study this kind of modification in other polyphenols and, in addition to pharmacokinetics properties, study its influence in their organoleptic characteristics.

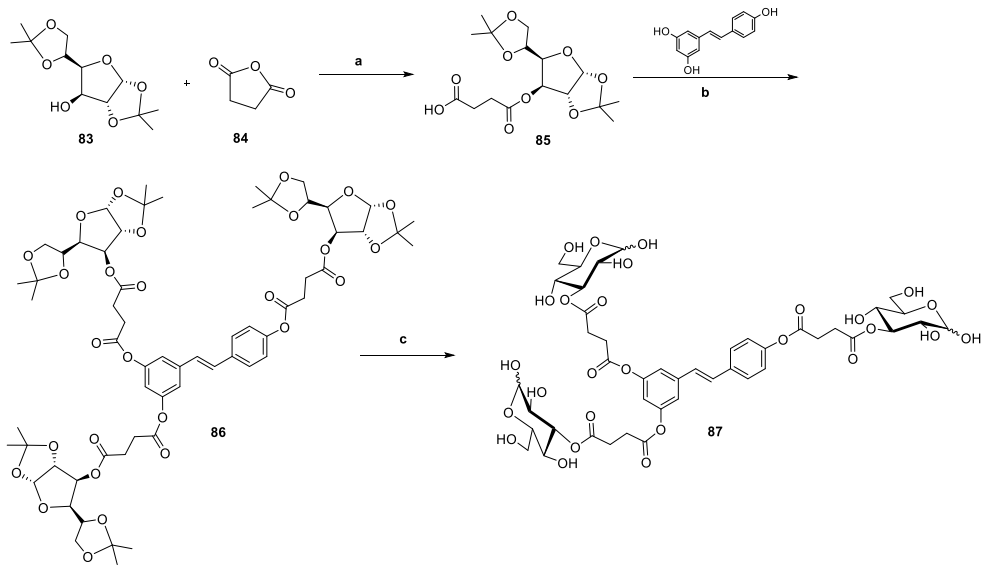

Scheme 1.3.16. Reagents and conditions: a) Pyr. DMAP, rt (78%); b) Pyr, DMAP, EDC, rt. (74%); c) TFA, rt (98%).[75]

1.3.3. Phenylethanoid and Phenylpropanoid Glycosides

Many phenylethanoid and phenylpropanoid glycosides, either of natural or synthetic origin, have been described to possess neuroprotective activities, tackling both the amyloid cascade and the cholinergic system.

Acteoside (**95**) is a natural phenylpropanoid glycoside, also known as verbascoside, first isolated from the plant *Verbascum sinuatum* in the 60s.[76] Meanwhile, a number of relevant

bioactivities have been described, including its neuroprotective properties (chapter 1.2). However, even before the mechanisms of neuroprotection were unraveled, the unsatisfactory extraction of this natural product from plant sources, prompted Sakuno and co-workers to develop the total synthesis of acteoside.[76] The synthetic strategy involves reaction of glucosyl chloride **88** (which was prepared from the per-acetylated corresponding sugar) with the phenyletyl derivative **89** by the Koenigs-Knorr method in the presence of silver carbonate (Scheme 1.3.17). The presence of an acetyl group at position 2 directs to the formation of the 1,2-*trans* glycosidic bond through a neighboring group participation mechanism.[76]

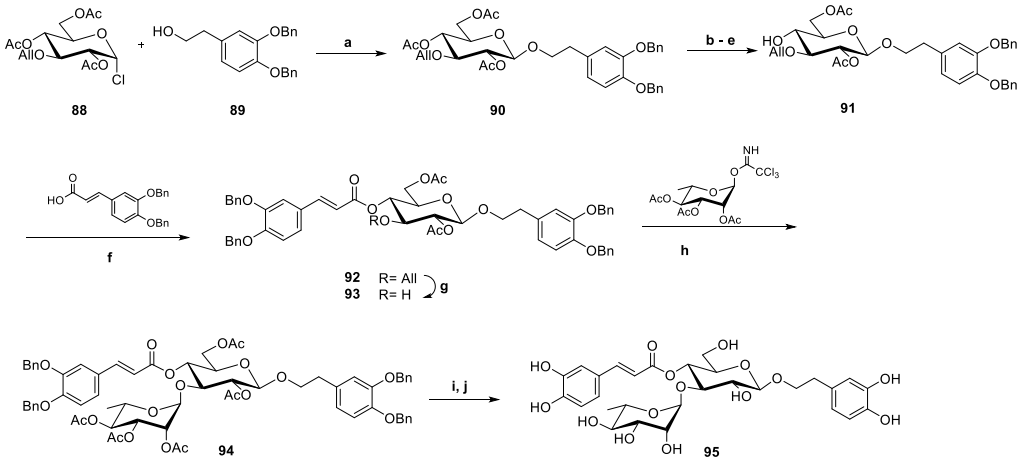

Scheme 1.3.17. Synthesis of acteoside by Kawada *et al*. Reagents and conditions: a) Ag_2CO_3, DCE (72%); b) NaOMe, MeOH (94%); c) TrCl, C_5H_5N (86%); d) Ac_2O, C_5H_5N (92%); e) AcOH, dioxane (79%); f) DCC, DMAP, DMAP·HCl, DCM (79%); g) SeO_2, AcOH-dioxane (66%); h) $BF_3{\cdot}Et_2O$, DCM (73%); i) $MeNH_2$, MeOH-DCM (49%); j) 1,4-ciclohexadiene, 5% Pd/C, DMF-EtOH (44%).[76]

A series of protection and deprotection steps to afford glycoside **91** is followed by introduction of the caffeoyl moiety by esterification. Oxidative cleavage of the 3-*O*-allyl group and rhamnosylation, performed with 2,3,4-tri-*O*-acetyl-α-L-rhamnopyranosyl trichloroacetimidate in the presence of boron trifluoride diethyl etherate gives the expected α-rhamnoside **94** in 73% yield. Finally, two considerable challenges lie on both the selective deacetylation over the cleavage of caffoeyl ester, and the selective removal of benzyl groups while keeping the double bond. Acetyl cleavage was consummate with methylamine in methanol ($MeNH_2$-MeOH), after which catalytic

transfer hydrogenation of benzyl ethers using 1,4-cyclohexadiene as a hydrogen source afforded acteoside (**95**) successfully, in an overall yield of 3.5%.[76]

More recently, an alternative and more efficient route towards phenylethanoid glycosides, such as acteoside, has been described,[77] using a low substrate concentration and *N*-formylmorpholine modulated glycosylation for the construction of β- and α-glycosidic bonds. Interestingly, contrary to what was reported by Kawada and co-workers, the coupling of the β-glucoside **98** with the protected caffeic acid furnished not only the (*E*)-isomer of **99**, but also trace amounts of the (*Z*)-isomer. Nevertheless, acteoside was obtained in an overall yield of 10.8% (*E/Z* 12:1) (Scheme 1.3.18).[77]

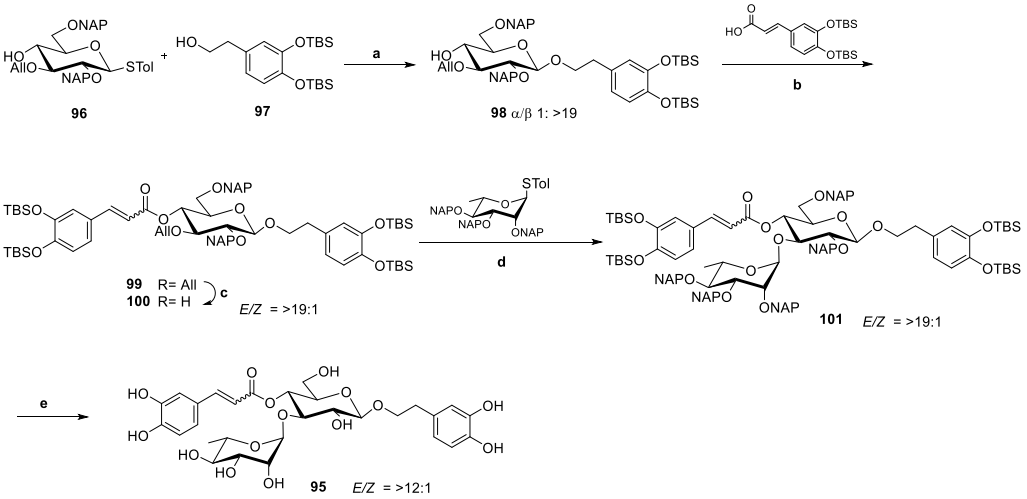

Scheme 1.3.18. Synthesis of acteoside by Mulani et al. a) TMSOTf, -60 ºC, 1:2:1 DCM-ACN-EtCN (63%); b) NIS, TMSOTf, -40 ºC, 1:2:1 DCM-ACN-EtCN (60%); c) $PdCl_2$, NaOAc, AcOH, acetone (70%); d) i. NFM; ii. NIS, TMSOTf, DCM (60%); e) i. DDQ, 3:1 MeOH, CH2Cl2; ii. TREAT-HF, ET_3N, pyr. (two steps 68%).[77]

It is well established that enhancing cholinergic transmission by blocking the activity of acetylcholinesterase (AChE) slows down the AD-associated decline in behavior and cognition. The natural phenylpropanoid diglycoside rosavin (**107**) and its analogues (*E*)-3-phenylprop-2-en-1-yl β-D-xylopyranosyl-(1→6)-β-D-glucopyranoside (**115**), (*E*)-3-(4-methoxyphenyl)prop-2-en-1-yl-α-L-arabinopyranosyl-(1→6)-β-D-glucopyranoside (**116**) and (*E*)-3-phenylprop-2-en-1-yl-α-L-rhamnopyranosyl-(1→6)-β-D-glucopyranoside (**117**) (Scheme 1.3.20) displayed a remarkable anti-AChE with IC_{50} values of 1.72, 3.71, 4.23, 2.05 μM, respectively, as explained previously (chapter

1.2).[78] This natural product was firstly synthesized as shown in Scheme 1.3.18. The dissacharide **104** was first constructed by reaction of the glycosyl bromide **102** with the isopropylidene protected glucose **103**. After cleavage of the isopropylidene groups, acetylation, and introduction of the anomeric sulfanyl group, the glycosyl donor **105** was obtained. Activated by iodine, this donor reacted with the cinnamyl alcohol to affordd the acetylated precursor **106**, which further deprotection gave rosavin (**107**).

Rosavin, along with its natural analogues **115** to **117**, was also synthesized by an alternative methodology, where the phenylpropanoid monoglycosides **113a** and **113b** were firstly synthesized, and then coupled with the appropriate glycosyl trichloroacetimidate (**118**, **119** or **120**), promoted by TMSOTf. Further deprotection afforded the natural rosavin analogues (Scheme 1.3.20). The same procedure was employed for the synthesis of a small library of phenylpropanoid glycosides, with derivatives incorporating substituted phenyl groups with F, Cl and Br, and varying the methoxy and hydroxy substitution patterns. However, none of the synthesized derivatives was as active as the natural diglycosides **107**, **115-117**.[78] Other methodologies for the synthesis of rosavin and its counterparts can be found in the literature, including the use of Mizoroki-Heck type reaction, involving the coupling of phenylboronic acid and allyl glycosides.[79]

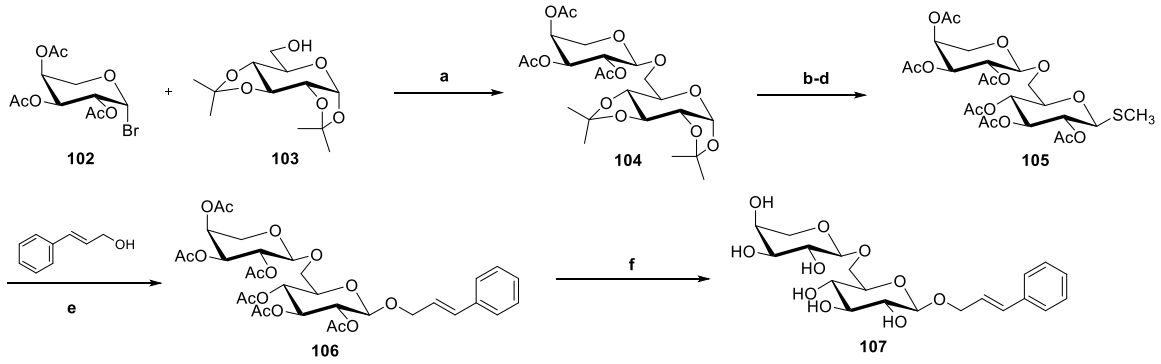

Scheme 1.3.19. a) $AgClO_4$, $CaCO_3$, acetone (18%); b) AcOH, 60 ºC; c) Ac_2O, $HClO_4$; d) $HSCH_3$, BF_3-Et_2O, $CHCl_3$ (64%); e) I_2, $CHCl_3$ (30%); f) MeONa, MeOH (95%).[78]

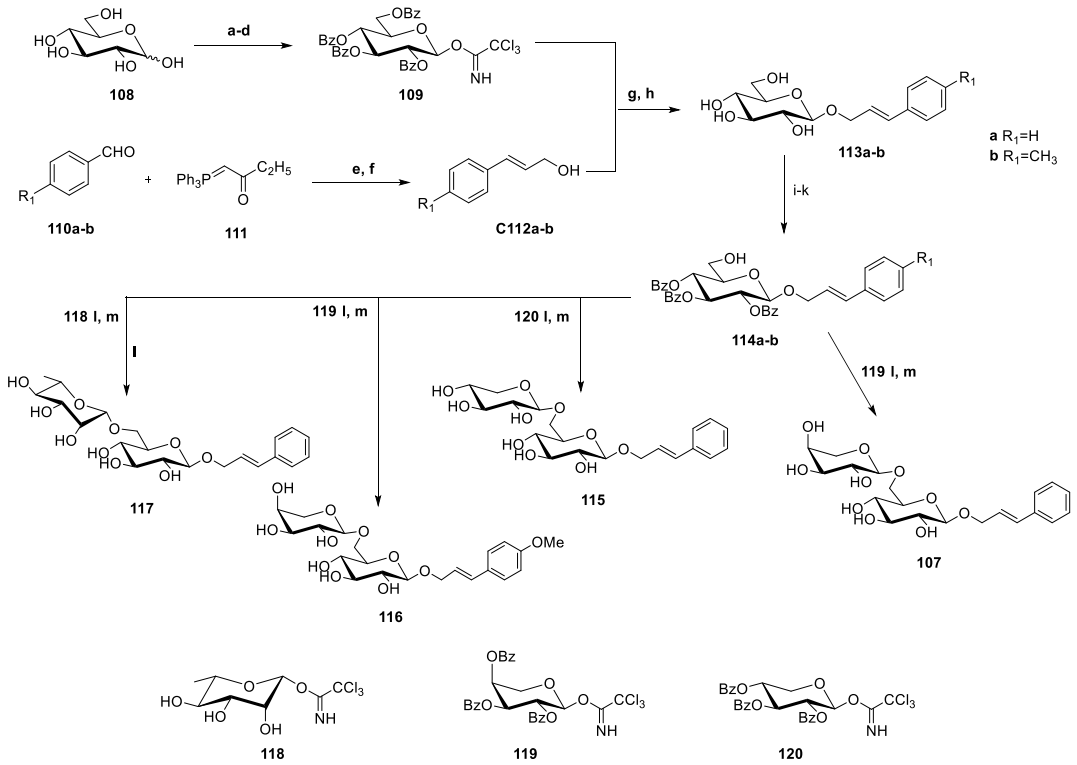

Scheme 1.3.20. Reagents and conditions: a) BzCl/Py, rt; b) HBr-AcOH/Ac_2O, rt; c) NaI/H_2O/acetone, 30 °C (85% three steps); d) DBU/CCl_3CN, rt (80%); e) PhMe 80 °C; f) DIBAlH, PhMe, -20 °C; g) TMSOTf, DCM, -20 °C; h) $NaOCH_3$, MeOH, 0 °C (41%, 61%, two steps); i) TrCl, DMAP, TEA, DMF, MS 4 Å (56%, 64%); j) BzCl, Py (87%, 90%); k) 90% TFA, DCM (84%, 86%); l) TMSOTf, DCM, −20 °C; m) NaOMe, MeOH (78% to 83%, two steps). (Yields in parentheses separated by comma are given for compounds type a and b, respectively).[78]

Other examples of powerful anti-AChE glycosides are the derivatives of the natural antidepressant helicid, which activities have been presented on chapter 1.2. These were synthesized starting from 4-hydroxybenzaldehyde, followed by glycosylation, deprotection and condensation with amines, as depicted in Scheme 1.3.21.[80] These transformations afforded noteworthy AChE inhibitors with IC_{50} under 10 µM, three of them even under 0.55 µM. The synthetic approach was based on reaction of glycosyl bromides with 4-hydroxybenzaldehyde in the presence of TBAB to afford the corresponding protected phenyl glycosides. Subsequent Zemplén deacetylation yielded the sugar-linked helicid analogues **122** and **124**. Schiff base derivative **127** was synthesized by reaction of **126** with methoxyamine (Scheme 1.3.21).[80] Although an extensive library of helicid derivatives

was obtained by this method, only the most active ones are depicted in Scheme 20. Interestingly, while helicid was not active up to 500 µM, its epimer at C-3 (**122**) presented an IC_{50} of 0.45 µM. However, the most potent inhibitor is the 4-formylphenyl β-D-ribopyranoside (**124**). It exhibits the same configuration of carbons 2, 3 and 4 as helicid but its hydroxymethyl group is replaced by a hydrogen atom, presenting an IC_{50} value of 0.20 µM on electric eel AChE, twice more active than galantamine. Also, the Shiff base **127** has an IC_{50} value of 0.49 µM. These results highlight the close correlation of the bioactivity with the sugar structure.[80]

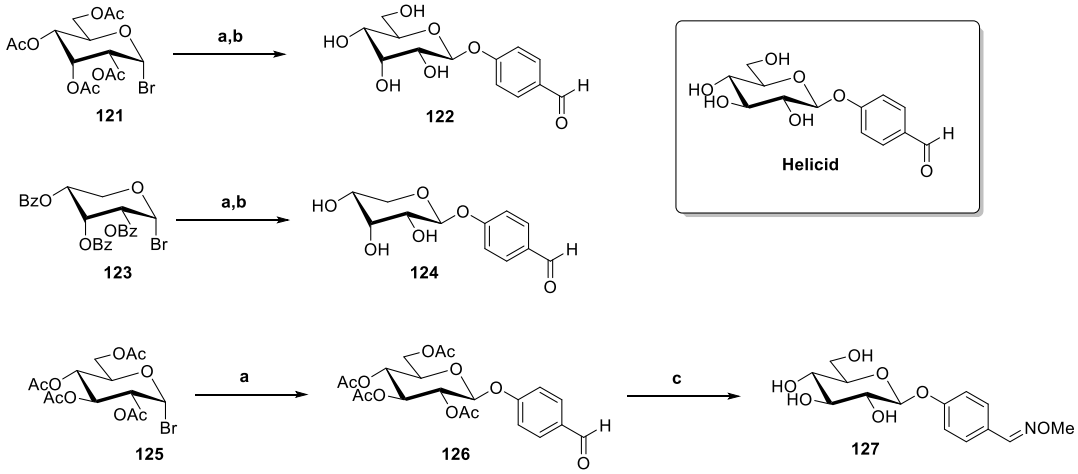

Scheme 1.3.21. Preparation of helicid derivatives. Reagents and conditions: a) Preparation of helicid derivatives TBAB, NaOH, $CHCl_3$/H2O, 45 ºC. b) NaOMe, rt, 3h; c) amine, EtOH, reflux or 45 ºC, 2-6h.[80]

Structurally similar to the compounds discussed so far is also salidroside (**132**) (Scheme 1.3.22), a phenylpropanoid glycoside isolated from *Rhodiola* species that is one of the active principles responsible for plant antidepressant and anxiolytic activities. The low content of salidroside in *Rhodiola sachalinensis*, the unsustainable overexploitation of this species, and the need to fully exploit its potential clinical applications, have encouraged chemists to the develop a synthetic approach towards 2-(4-hydroxyphenyl)ethyl β-glucopyranoside. Various examples in the literature show the preference for the silver carbonate promoted glycosylation of tyrosol (**128**), which aromatic hydroxy group can be protected or unprotected, using peracetylated glucosyl bromide as a glycosyl donor.[81-82] In 2011, a multi-kilogram scale-up of salidroside was reported, featuring the selective

acetylation of tyrosol aromatic hydroxy group in aqueous media, and affording the target natural glycoside in 72% yield (Scheme 1.3.22).[82]

Outstandingly, this natural glucoside protects neurons from glutamate-induced oxidative stress and apoptosis and was shown to be therapeutically effective against cognitive decline during ageing. Salidroside also intervenes in the amyloid cascade events, as it protects against Aβ25–35-induced oxidative stress. In fact, pretreatment with salidroside noticeably attenuated Aβ25–35-induced loss of cell viability and apoptosis in a dose-dependent manner.[49] A fairly recent study also supports these findings and further attests the activity of this tyrosol glycoside by showing that it protects four different Drosophila models of AD against Aβ-induced neurotoxicity. The study also reveals that salidroside decreased Aβ levels and Aβ deposition in the fly's brain and ameliorated toxicity in Aβ-treated primary neuronal culture.[83]

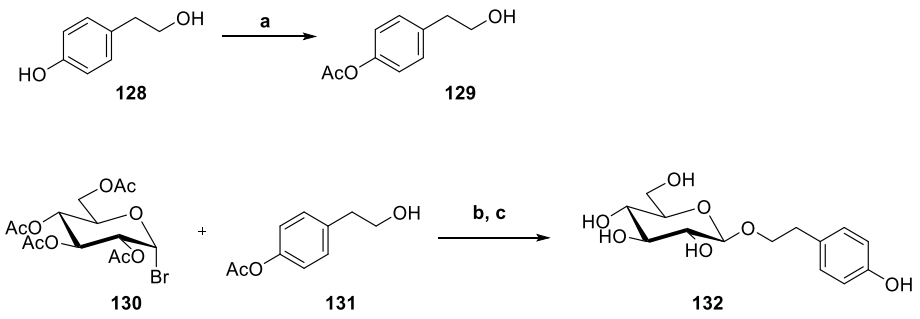

Scheme 1.3.22. Synthesis of salidroside. Reagents and conditions: a) Ac_2O, NaOH, H2O (90%); b) Ag_2CO_3, DCM, molecular sieves (4Å); c) NaOMe, MeOH (80%, two steps).[82]

However, perhaps one of the most well-known phenylpropanoid derivatives with well documented neuroprotective activities is curcumin (**133**, Scheme 1.3.23), an active ingredient in the spice turmeric consisting of two cinnamoyl units linked by a methylene group. Curcumin has been reported to act on several biochemical pathways associated with the onset and progression of AD. It disrupts amyloid-β and tau peptide aggregation, inhibits inflammation and protects against oxidative stress.[84-85] However, its pharmaceutical use is restricted due to its poor water and plasma solubility and consequent low bioavailability.[85-86] Considering that the addition of a sugar moiety

would significantly increase the water/plasma solubility of the molecule while retaining all the characteristics of the curcumin pharmacophore, the clicked galactose-curcumin conjugate (already mentioned in chapter 1.2) was developed using click-chemistry,[87] as depicted in Scheme 1.3.23. The curcumin monoalkyne **134** was coupled with an acetyl-protected galactoside bearing an azide and, after removal of acetyl groups, a galactose-curcumin conjugate possessing a triazole-based linker was obtained. This non-toxic curcumin derivative is ca. 1000 times more soluble than curcumin in water, and exhibits enhanced ability to inhibit both amyloid-β and tau aggregation, at concentrations as low as 8 nM and 0.1 nM, respectively.[87]

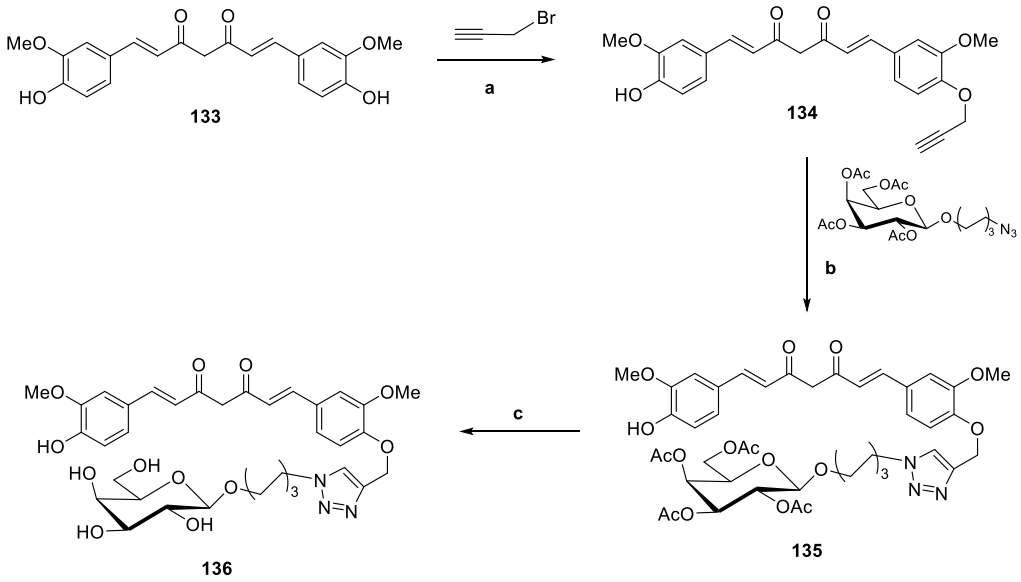

Scheme 1.3.23. a) K_2CO_3, DMF, r.t; b) i. $CuSO_4.5H_2O$, sodium ascorbate, *t*-BuOH/THF/H_2O, r.t (76%); c) NaOMe, MeOH, r.t (70%).[87]

1.3.4. CONCLUSION

This sub-chapter is devoted to highlight the biological importance of linking sugars to polyphenols and to the methodologies described for this purpose. Examples of polyphenol glycosides that exhibit an increased neurodegenerative protective effect when compared to their aglycones, are given in this chapter. The role of sugar binding to improve polyphenol solubility and ameliorating its

bioavailability is also clearly illustrated with examples. Chemical and enzymatic approaches to glycoside synthesis are described for various families of polyphenols, namely stilbenoids that include the well-known resveratrol, phenylethanoids and propanoids covering also the "dimeric analogue" curcumin and the flavonoids, covering only flavone glycosides. To flavone and isoflavone C-glycosylation is given a particular attention, given the relevance of the C-C bond, that is not hydrolytically cleaved, allowing *C*-glycosyl flavonoids to remain intact in the blood circulation following oral administration.

This body of knowledge should encourage chemists and biochemists to further investigate the role of sugar binding to polyphenols, not only to diversify and optimize coupling conditions but also to discover new biomolecular entities to effectively prevent neurodegenerative impairments with clinical applications.

REFERENCES

[1] P. Torres; A. Poveda; J. Jimenez-Barbero; J. L. Parra; F. Comelles; A. O. Ballesteros; F. J. Plou, Enzymatic Synthesis of α-Glucosides of Resveratrol with Surfactant Activity. *Advanced Synthesis & Catalysis* **2011,** *353* (7), 1077-1086.

[2] I. Uriarte-Pueyo; M. I. Calvo, Flavonoids as acetylcholinesterase inhibitors. *Current Medicinal Chemistry* **2011,** *18* (34), 5289-302.

[3] A. R. Ladiwala; M. Mora-Pale; J. C. Lin; S. S. Bale; Z. S. Fishman; J. S. Dordick; P. M. Tessier, Polyphenolic glycosides and aglycones utilize opposing pathways to selectively remodel and inactivate toxic oligomers of amyloid beta. *Chembiochem: a European Journal of Chemical Biology* **2011,** *12* (11), 1749-58.

[4] C. Chen; X. Li; P. Gao; Y. Tu; M. Zhao; J. Li; S. Zhang; H.-Q. Liang, Baicalin attenuates Alzheimer-like pathological changes and memory deficits induced by amyloid β1–42 protein. *Metabolic Brain Disease* **2015,** *30* (2), 537-544.

[5] H. Ding; H. Wang; Y. Zhao; D. Sun; X. Zhai, Protective Effects of Baicalin on Aβ1–42-Induced Learning and Memory Deficit, Oxidative Stress, and Apoptosis in Rat. *Cellular and Molecular Neurobiology* **2015,** *35* (5), 623-632.

[6] J. Xiong; C. Wang; H. Chen; Y. Hu; L. Tian; J. Pan; M. Geng, Abeta-induced microglial cell activation is inhibited by baicalin through the JAK2/STAT3 signaling pathway. *The International Journal of Neuroscience* **2014,** *124* (8), 609-20.

[7] Y.-F. Li; B. Yu; J.-S. Sun; R.-X. Wang, Efficient synthesis of baicalin and its analogs. *Tetrahedron Letters* **2015,** *56* (24), 3816-3819.

[8] A. Robertson; R. Robinson, CCXXV.-Experiments on the synthesis of anthocyanins. Part I. *Journal of the Chemical Society* **1926,** *129* (0), 1713-1720.

[9] Z. Pan; T. Feng; L. Shan; B. Cai; W. Chu; H. Niu; Y. Lu; B. Yang, Scutellarin-induced endothelium-independent relaxation in rat aorta. *Phytotherapy Research* **2008,** *22* (11), 1428-33.

[10] M. Fang; Y. Yuan; P. Rangarajan; J. Lu; Y. Wu; H. Wang; C. Wu; E.-A. Ling, Scutellarin regulates microglia-mediated TNC1 astrocytic reaction and astrogliosis in cerebral ischemia in the adult rats. *BMC Neuroscience* **2015,** *16* (1), 84.

[11] M. Fang; Y. Yuan; J. Lu; H. E. Li; M. Zhao; E.-A. Ling; C.-Y. Wu, Scutellarin promotes microglia-mediated astrogliosis coupled with improved behavioral function in cerebral ischemia. *Neurochemistry International* **2016,** *97*, 154-171.

[12] H. Tang; Y. Tang; N. Li; Q. Shi; J. Guo; E. Shang; J. A. Duan, Neuroprotective effects of scutellarin and scutellarein on repeatedly cerebral ischemia-reperfusion in rats. *Pharmacology, Biochemistry, and Behavior* **2014,** *118*, 51-9.

[13] J. T. Zhu; R. C. Choi; J. Li; H. Q. Xie; C. W. Bi; A. W. Cheung; T. T. Dong; Z. Y. Jiang; J. J. Chen; K. W. Tsim, Estrogenic and neuroprotective properties of scutellarin from Erigeron breviscapus: a drug against postmenopausal symptoms and Alzheimer's disease. *Planta Medica* **2009,** *75* (14), 1489-93.

[14] J. M. Huang; W. Y. Weng; X. B. Huang; Y. H. Ji; E. Chen, Pharmacokinetics of scutellarin and its aglycone conjugated metabolites in rats. *European Journal of Drug Metabolism and Pharmacokinetics* **2005,** *30* (3), 165-170.

[15] C. Gao; H. Zhang; Z. Guo; T. You; X. Chen; D. Zhong, Mechanistic Studies on the Absorption and Disposition of Scutellarin in Humans: Selective OATP2B1-Mediated Hepatic Uptake Is a Likely Key Determinant for Its Unique Pharmacokinetic Characteristics. *Drug Metabolism & Disposition* **2012,** *40* (10), 2009-2020.

[16] X. Chen; L. Cui; X. Duan; B. Ma; D. Zhong, Pharmacokinetics and metabolism of the flavonoid scutellarin in humans after a single oral administration. *Drug Metabolism & Disposition* **2006,** *34* (8), 1345-1352.

[17] N. G. Li; M. Z. Shen; Z. J. Wang; Y. P. Tang; Z. H. Shi; Y. F. Fu; Q. P. Shi; H. Tang; J. A. Duan, Design, synthesis and biological evaluation of glucose-containing scutellarein derivatives as neuroprotective agents based on metabolic mechanism of scutellarin in vivo. *Bioorganic & Medicinal Chemistry Letters* **2013,** *23* (1), 102-6.

[18] M. Masibo; Q. He, Major Mango Polyphenols and Their Potential Significance to Human Health. *Comprehensive Reviews in Food Science and Food Safety* **2008,** *7* (4), 309-319.

[19] C. Carla Guimarães; D. Dias Oliveira; M. Valdevite; A. Fachin; S. Pereira; S. França; A. Pereira; P. Pereira. The glycosylated flavonoids vitexin, isovitexin, and quercetrin isolated from Serjania erecta Radlk (Sapindaceae) leaves protect PC12 cells against amyloid-β25-35 peptide-induced toxicity *Food and Chemical Toxicology* [Online], **2015,** *86*, 88-94.

[20] X. Lozoya; M. Meckes; M. Abou-Zaid; J. Tortoriello; C. Nozzolillo; J. T. Arnason, Quercetin glycosides in Psidium guajava L. leaves and determination of a spasmolytic principle. *Archives of Medical Research* **1994,** *25* (1), 11-5.

[21] C. P. Wang; J. L. Li; L. Z. Zhang; X. C. Zhang; S. Yu; X. M. Liang; F. Ding; Z. W. Wang, Isoquercetin protects cortical neurons from oxygen-glucose deprivation-reperfusion induced injury via suppression of TLR4-NF-small ka, CyrillicB signal pathway. *Neurochemistry International* **2013,** *63* (8), 741-9.

[22] C. P. Wang; Y. W. Shi; M. Tang; X. C. Zhang; Y. Gu; X. M. Liang; Z. W. Wang; F. Ding, Isoquercetin Ameliorates Cerebral Impairment in Focal Ischemia Through Anti-Oxidative, Anti-Inflammatory, and Anti-Apoptotic Effects in Primary Culture of Rat Hippocampal Neurons and Hippocampal CA1 Region of Rats. *Molecular Neurobiology* **2017,** *54* (3), 2126-2142.

[23] H. A. Jung; S. Karki; J. H. Kim; J. S. Choi, BACE1 and cholinesterase inhibitory activities of Nelumbo nucifera embryos. *Archives of Pharmacal Research* **2015,** *38* (6), 1178-1187.

[24] M. Jung; M. Park, Acetylcholinesterase Inhibition by Flavonoids from Agrimonia pilosa. *Molecules* **2007,** *12*, 2130-2139.

[25] G. Ren; J. Hou; Q. Fang; H. Sun; X. Liu; L. Zhang; P. G. Wang, Synthesis of flavonol 3-O-glycoside by UGT78D1. *Glycoconjugate Journal* **2012,** *29* (5-6), 425-32.

[26] W. Qiao; C. Zhao; N. Qin; H. Y. Zhai; H. Q. Duan, Identification of trans-tiliroside as active principle with anti-hyperglycemic, anti-hyperlipidemic and antioxidant effects from Potentilla chinesis. *Journal of Ethnopharmacology* **2011,** *135* (2), 515-21.

[27] R. Velagapudi; M. Aderogba; O. A. Olajide, Tiliroside, a dietary glycosidic flavonoid, inhibits TRAF-6/NF-kappaB/p38-mediated neuroinflammation in activated BV2 microglia. *Biochimica et Biophysica Acta* **2014,** *1840* (12), 3311-9.

[28] B. Vermes; V. M. Chari; H. Wagner, Structure Elucidation and Synthesis of Flavonol Acylglycosides. III.. The synthesis of tiliroside. *Helvetica Chimica Acta* **1981,** *64* (6), 1964-1967.

[29] F. L. Courts; G. Williamson, The Occurrence, Fate and Biological Activities of C-glycosyl Flavonoids in the Human Diet. *Critical Reviews in Food Science and Nutrition* **2015,** *55* (10), 1352-1367.

[30] R. G. dos Santos; A. R. Jesus; J. M. Caio; A. P. Rauter, Fries-type Reactions for the C-Glycosylation of Phenols. *Current Organic Chemistry* **2011,** *15* (1), 128-148.

[31] F. Cattaneo; M. S. Costamagna; I. C. Zampini; J. Sayago; M. R. Alberto; V. Chamorro; A. Pazos; S. Thomas-Valdés; G. Schmeda-Hirschmann; M. I. Isla, Flour from Prosopis alba cotyledons: A natural source of nutrient and bioactive phytochemicals. *Food Chemistry* **2016,** *208*, 89-96.

[32] J. S. Choi; M. N. Islam; M. Y. Ali; Y. M. Kim; H. J. Park; H. S. Sohn; H. A. Jung, The effects of C-glycosylation of luteolin on its antioxidant, anti-Alzheimer's disease, anti-diabetic, and anti-inflammatory activities. *Archives of Pharmacal Research* **2014,** *37* (10), 1354-1363.

[33] Y. Wang; Y. Zhen; X. Wu; Q. Jiang; X. Li; Z. Chen; G. Zhang; L. Dong, Vitexin protects brain against ischemia/reperfusion injury via modulating mitogen-activated protein kinase and apoptosis signaling in mice. *Phytomedicine* **2015,** *22* (3), 379-84.

[34] J.-A. Mahling; K.-H. Jung; R. R. Schmidt, Glycosyl imidates, 69. Synthesis of flavone C-glycosides vitexin, isovitexin, and isoembigenin. *Liebigs Annalen* **1995,** *1995* (3), 461-466.

[35] T. Kometani; H. Kondo; Y. Fujimori, Boron Trifluoride-Catalyzed Rearrangement of 2-Aryloxytetrahydropyrans: A New Entry to C-Arylglycosidation. *Synthesis* **1988,** *12*, 1005-1007.

[36] T. Furuta; T. Kimura; S. Kondo; H. Mihara; T. Wakimoto; H. Nukaya; K. Tsuji; K. Tanaka, Concise total synthesis of flavone C-glycoside having potent anti-inflammatory activity. *Tetrahedron* **2004,** *60* (42), 9375-9379.

[37] I. Yoshiyuki; T. Kuniro; N. Haruo, Novel derivative of flavone c-glycoside and composition containing the same. EP 1533313 A1, 2003/07/03 Application date, 2003.

[38] M. Zmijewski; A. Sokol-Letowska; E. Pejcz; D. Orzel, Antioxidant activity of rye bread enriched with milled buckwheat groats fractions. *Roczniki Panstwowego Zakladu Higieny* **2015,** *66* (2), 115-21.

[39] E. Ancheeva; G. Daletos; R. Muharini; W. H. Lin; L. Teslov; P. Proksch, Flavonoids from Stellaria nemorum and Stellaria holostea. *Natural Product Communications* **2015,** *10* (3), 437-40.

[40] L. Yu; S. Wang; X. Chen; H. Yang; X. Li; Y. Xu; X. Zhu, Orientin alleviates cognitive deficits and oxidative stress in Abeta1-42-induced mouse model of Alzheimer's disease. *Life Sciences* **2015,** *121*, 104-9.

[41] B. N. Law; A. P. Ling; R. Y. Koh; S. M. Chye; Y. P. Wong, Neuroprotective effects of orientin on hydrogen peroxideinduced apoptosis in SHSY5Y cells. *Molecular Medicine Reports* **2014,** *9* (3), 947-54.

[42] M. D'Amelio; V. Cavallucci; S. Middei; C. Marchetti; S. Pacioni; A. Ferri; A. Diamantini; D. Zio; P. Carrara; L. Battistini; S. Moreno; A. Bacci; M. Ammassari-Teule; H. Marie; F. Cecconi, Caspase-3 triggers early synaptic dysfunction in a mouse model of Alzheimer's Disease. *Nature Neuroscience* **2011,** *14* (1), 69-76.

[43] T. Kumazawa; T. Kimura; S. Matsuba; S. Sato; J. Onodera, Synthesis of 8-C-glucosylflavones. *Carbohydrate Research* **2001,** *334* (3), 183-93.

[44] T. Kumazawa; T. Minatogawa; S. Matsuba; S. Sato; J. Onodera, An effective synthesis of isoorientin: the regioselective synthesis of a 6-C-glucosylflavone. *Carbohydrate Research* **2000,** *329* (3), 507-13.

[45] B. Hao; J. C. Caulfield; M. L. Hamilton; J. A. Pickett; C. A. O. Midega; Z. R. Khan; J. Wang; A. M. Hooper, Biosynthesis of natural and novel C-glycosylflavones utilising recombinant Oryza sativa C-glycosyltransferase (OsCGT) and Desmodium incanum root proteins. *Phytochemistry* **2016,** *125*, 73-87.

[46] M. L. Hamilton; J. C. Caulfield; J. A. Pickett; A. M. Hooper, C-Glucosylflavonoid biosynthesis from 2-hydroxynaringenin by Desmodium uncinatum (Jacq.) (Fabaceae). *Tetrahedron Letters* **2009,** *50* (40), 5656-5659.

[47] F. Kerscher; G. Franz, Biosynthesis of Vitexin and Isovitexin: Enzymatic Synthesis of the C-Glucosylflavones Vitexin and Isovitexin with an Enzyme Preparation from Fagopyrum esculentum M. Seedlings. In *Zeitschrift für Naturforschung C*, 1987; Vol. 42, p 519.

[48] K. Wu; T. Liang; X. Duan; L. Xu; K. Zhang; R. Li, Anti-diabetic effects of puerarin, isolated from Pueraria lobata (Willd.), on streptozotocin-diabetogenic mice through promoting insulin expression and ameliorating metabolic function. *Food and Chemical Toxicology* **2013,** *60*, 341-7.

[49] L. Zhang; H. Yu; X. Zhao; X. Lin; C. Tan; G. Cao; Z. Wang, Neuroprotective effects of salidroside against beta-amyloid-induced oxidative stress in SH-SY5Y human neuroblastoma cells. *Neurochemistry International* **2010,** *57* (5), 547-55.

[50] Z. Li; Z. Shangguan; Y. Liu; J. Wang; X. Li; S. Yang; S. Liu, Puerarin protects pancreatic beta-cell survival via PI3K/Akt signaling pathway. *Journal of Molecular Endocrinology* **2014,** *53* (1), 71-9.

[51] P. S. Koekkoek; L. J. Kappelle; E. van den Berg; G. E. H. M. Rutten; G. J. Biessels, Cognitive function in patients with diabetes mellitus: guidance for daily care. *The Lancet Neurology* **2015,** *14* (3), 329-340.

[52] X. Liu; Y. Mo; J. Gong; Z. Li; H. Peng; J. Chen; Q. Wang; Z. Ke; J. Xie, Puerarin ameliorates cognitive deficits in streptozotocin-induced diabetic rats. *Metabolic Brain Disease* **2016,** *31* (2), 417-423.

[53] S. S. Zhao; W. N. Yang; H. Jin; K. G. Ma; G. F. Feng, Puerarin attenuates learning and memory impairments and inhibits oxidative stress in STZ-induced SAD mice. *Neurotoxicology* **2015,** *51*, 166-71.

[54] J. Li; G. Wang; J. Liu; L. Zhou; M. Dong; R. Wang; X. Li; X. Li; C. Lin; Y. Niu, Puerarin attenuates amyloid-beta-induced cognitive impairment through suppression of apoptosis in rat hippocampus in vivo. *European Journal of Pharmacology* **2010,** *649* (1-3), 195-201.

[55] F. Lin; B. Xie; F. Cai; G. Wu, Protective effect of Puerarin on beta-amyloid-induced neurotoxicity in rat hippocampal neurons. *Arzneimittel-Forschung* **2012,** *62* (4), 187-93.

[56] C. Wang; N. Xie; H. Zhang; Y. Li; Y. Wang, Puerarin protects against beta-amyloid-induced microglia apoptosis via a PI3K-dependent signaling pathway. *Neurochemical Research* **2014,** *39* (11), 2189-96.

[57] H. Y. Zhang; Y. H. Liu; H. Q. Wang; J. H. Xu; H. T. Hu, Puerarin protects PC12 cells against beta-amyloid-induced cell injury. *Cell Biology International* **2008,** *32* (10), 1230-7.

[58] Y. Zhou; N. Xie; L. Li; Y. Zou; X. Zhang; M. Dong, Puerarin alleviates cognitive impairment and oxidative stress in APP/PS1 transgenic mice. *International Journal of Neuropsychopharmacology* **2014,** *17* (4), 635-644.

[59] J. Zhang; W. Guo; B. Tian; M. Sun; H. Li; L. Zhou; X. Liu, Puerarin attenuates cognitive dysfunction and oxidative stress in vascular dementia rats induced by chronic ischemia. *International Journal of Clinical and Experimental Pathology* **2015,** *8* (5), 4695-704.

[60] D. Y. W. Lee; W.-Y. Zhang; V. V. R. Karnati, Total synthesis of puerarin, an isoflavone C-glycoside. *Tetrahedron Letters* **2003,** *44* (36), 6857-6859.

[61] A. R. Jesus; C. Dias; A. M. Matos; R. F. M. de Almeida; A. S. Viana; F. Marcelo; R. T. Ribeiro; M. P. Macedo; C. Airoldi; F. Nicotra; A. Martins; E. J. Cabrita; J. Jiménez-Barbero; A. P. Rauter, Exploiting the Therapeutic Potential of 8-β-d-Glucopyranosylgenistein: Synthesis, Antidiabetic Activity, and Molecular Interaction with Islet Amyloid Polypeptide and Amyloid β-Peptide (1–42). *Journal of Medicinal Chemistry* **2014,** *57* (22), 9463-9472.

[62] L. Bavaresco; C. Fregoni; E. Cantù; M. Trevisan, *Stilbene compounds: From the grapevine to wine*. 1999; Vol. 25, p 57-63.

[63] E. Wenzel; V. Somoza, Metabolism and bioavailability of trans-resveratrol. *Molecular Nutrition & Food Research* **2005,** *49* (5), 472-81.

[64] S. Renaud; M. de Lorgeril, Wine, alcohol, platelets, and the French paradox for coronary heart disease. *Lancet (London, England)* **1992,** *339* (8808), 1523-6.

[65] K. A. Roupe; C. M. Remsberg; J. A. Yanez; N. M. Davies, Pharmacometrics of stilbenes: seguing towards the clinic. *Current Clinical Pharmacology* **2006,** *1* (1), 81-101.

[66] S. D. Rege; T. Geetha; G. D. Griffin; T. L. Broderick; J. R. Babu, Neuroprotective effects of resveratrol in Alzheimer disease pathology. *Frontiers in Aging Neuroscience* **2014,** *6*, 218.

[67] C. Riviere; T. Richard; L. Quentin; S. Krisa; J. M. Merillon; J. P. Monti, Inhibitory activity of stilbenes on Alzheimer's beta-amyloid fibrils in vitro. *Bioorganic & Medicinal Chemistry* **2007,** *15* (2), 1160-7.

[68] T. Walle, Bioavailability of resveratrol. *Annals of the New York Academy of Sciences* **2011,** *1215*, 9-15.

[69] F. Orsini; F. Pelizzoni; B. Bellini; G. Miglierini, Synthesis of biologically active polyphenolic glycosides (combretastatin and resveratrol series). *Carbohydrate Research* **1997,** *301* (3-4), 95-109.

[70] H. Hamada; K. Shimoda; N. Shimizu; Y. Shimizu; M. Akagi, Synthesis of Glycosides of Resveratrol, Pterostilbene, and Piceatannol by Glucosyltransferase from Phytolacca americana Expressed in Bacillus subtilis and their Chemopreventive Activity Against Cancer, Allergic, and Alzheimer’s Diseases. *Glycobiology Insights* **2014,** *4* (4216-GBI-Synthesis-of-Glycosides-of-Resveratrol,-Pterostilbene,-and-Piceatannol.pdf), 1-6.

[71] D. Sato; N. Shimizu; Y. Shimizu; M. Akagi; Y. Eshita; S. Ozaki; N. Nakajima; K. Ishihara; N. Masuoka; H. Hamada; K. Shimoda; N. Kubota, Synthesis of glycosides of resveratrol, pterostilbene, and piceatannol, and their anti-oxidant, anti-allergic, and neuroprotective activities. *Bioscience, Biotechnology, and Biochemistry* **2014,** *78* (7), 1123-8.

[72] H. Park; J. Kim; K. H. Choi; S. Hwang; S. J. Yang; N. I. Baek; J. Cha, Enzymatic synthesis of piceid glucosides using maltosyltransferase from Caldicellulosiruptor bescii DSM 6725. *Journal of Agricultural and Food Chemistry* **2012,** *60* (33), 8183-9.

[73] S. Mathew; M. Hedström; P. Adlercreutz, Enzymatic synthesis of piceid glycosides by cyclodextrin glucanotransferase. *Process Biochemistry* **2012,** *47* (3), 528-532.

[74] M. E. Dirks-Hofmeister; T. Verhaeghe; K. De Winter; T. Desmet, Creating Space for Large Acceptors: Rational Biocatalyst Design for Resveratrol Glycosylation in an Aqueous System. *Angewandte Chemie International Edition* **2015,** *54* (32), 9289-9292.

[75] L. Biasutto; E. Marotta; A. Bradaschia; M. Fallica; A. Mattarei; S. Garbisa; M. Zoratti; C. Paradisi, Soluble polyphenols: Synthesis and bioavailability of 3,4′,5-tri(α-d-glucose-3-O-succinyl) resveratrol. *Bioorganic & Medicinal Chemistry Letters* **2009,** *19* (23), 6721-6724.

[76] T. Kawada; R. Asano; S. Hayashida; T. Sakuno, Total Synthesis of the Phenylpropanoid Glycoside, Acteoside. *The Journal of Organic Chemistry* **1999,** *64* (25), 9268-9271.

[77] S. K. Mulani; J. H. Guh; K. K. Mong, A general synthetic strategy and the anti-proliferation properties on prostate cancer cell lines for natural phenylethanoid glycosides. *Organic & Biomolecular Chemistry* **2014,** *12* (18), 2926-37.

[78] X. D. Li; S. T. Kang; G. Y. Li; X. Li; J. H. Wang, Synthesis of some phenylpropanoid glycosides (PPGs) and their acetylcholinesterase/xanthine oxidase inhibitory activities. *Molecules* **2011,** *16* (5), 3580-96.

[79] M. Kishida; H. Akita, Synthesis of Rosavin and its analogues based on a Mizoroki-Heck type reaction. *Tetrahedron: Asymmetry* **2005,** *16* (15), 2625-2630.

[80] H. Wen; C. Lin; L. Que; H. Ge; L. Ma; R. Cao; Y. Wan; W. Peng; Z. Wang; H. Song, Synthesis and biological evaluation of helicid analogues as novel acetylcholinesterase inhibitors. *European Journal of Medicinal Chemistry* **2008,** *43* (1), 166-173.

[81] Y. Guo; Y. Zhao; C. Zheng; Y. Meng; Y. Yang, Synthesis, biological activity of salidroside and its analogues. *Chemical & Pharmaceutical Bulletin* **2010,** *58* (12), 1627-9.

[82] T. Shi; H. Chen; L. Jing; X. Liu; X. Sun; R. Jiang, Development of a Kilogram-Scale Synthesis of Salidroside and Its Analogs. *Synthetic Communications* **2011,** *41* (17), 2594-2600.

[83] B. Zhang; Y. Wang; H. Li; R. Xiong; Z. Zhao; X. Chu; Q. Li; S. Sun; S. Chen, Neuroprotective effects of salidroside through PI3K/Akt pathway activation in Alzheimer's disease models. *Drug Design, Development and Therapy* **2016,** *10*, 1335-43.

[84] A. Noorafshan; S. Ashkani-Esfahani, A review of therapeutic effects of curcumin. *Current Pharmaceutical Design* **2013,** *19* (11), 2032-46.

[85] S. Mishra; K. Palanivelu, The effect of curcumin (turmeric) on Alzheimer's disease: An overview. *Annals of Indian Academy of Neurology* **2008,** *11* (1), 13-19.

[86] S. Prasad; A. K. Tyagi; B. B. Aggarwal, Recent developments in delivery, bioavailability, absorption and metabolism of curcumin: the golden pigment from golden spice. *Cancer Research and Treatment* **2014,** *46* (1), 2-18.

[87] S. Dolai; W. Shi; C. Corbo; C. Sun; S. Averick; D. Obeysekera; M. Farid; A. Alonso; P. Banerjee; K. Raja, "Clicked" Sugar–Curcumin Conjugate: Modulator of Amyloid-β and Tau Peptide Aggregation at Ultralow Concentrations. *ACS Chemical Neuroscience* **2011,** *2*, 694-9.

Chapter 2

Glycal transformation into 2-deoxy glycosides[a]

[a] Dias, C.; Santos, M.S.; Rauter, A. P.; Malik, M.; Glycal transformation into 2-deoxy glycosides. In: *Carbohydrate Chemistry - Proven Synthetic Methods (Vol. 3)*, Roy, R.; Vidal, S., Eds., CRC Press - Taylor & Francis: Boca Raton, Florida, 2015; pp 57-72.

In this chapter, we illustrate the synthesis of 2-deoxy glycosides via reaction of glycals with alcohols in the presence of triphenylphosphane hydrobromide (TPHB). A special emphasis is given to the reaction of glycals with long-chain alcohols, which leads to materials with a variety of potential applications, in particular as antimicrobial agents.[1-3] The reaction is easy to perform, stereoselective, and when long-chain alcohols are used as synthons, the bioactivity of the formed 2-deoxy glycosides can be tuned by small changes in the glycal starting material structure, e.g. 6-deoxygenation, and configuration.[2] The acid catalyzed addition of an alcohol to an acetylated glycal occurs usually with concomitant Ferrier allylic rearrangement, giving the 2,3-unsaturated derivative as major reaction product. However, when TPHB is used, as first described by Bolitt et al.[4] to prepare 2-deoxy glycosides from glycals, formation of 2,3-unsaturated glycosides is minimal. Amongst the variety of glycals of D- and L-series we have already transformed in this way,[1-3] we exemplify now the TPHB-mediated glycosylation of octan-1-ol and of dodecan-1-ol, which occurs with α-stereoselectivity, resulting from the anomeric effect. Glycosides **2–5** were obtained by reaction of 3,4,6-tri-*O*-acetyl-1,5-anhydro-2-deoxy-D-*arabino*-hex-1-enitol (**1**) in dichloromethane, using 2 equivalents of alcohol at room temperature for 12 h. The 2-deoxy α-anomers were isolated in 69% yield (**2**) and 83% yield (**4**), and the 2-deoxy β-glycosides were isolated in 15% (**3**) and 12% yield (**5**). The α-anomer of the octyl or dodecyl 2,3-unsaturated glycosides (**6** and **7**, respectively) was isolated in 2 % yield, when the reaction was run at room temperature and in 6% (**6**) and 4 % (**7**) when the reaction was run under reflux. In order to simplify glycoside and nucleophile separation, the reaction was carried out with 1.05 equiv. alcohol at room temperature. Reaction time increased to 24 h, no Ferrier products were detected, and selectivity for the α-anomer was also improved as shown by the reaction yields obtained for compounds

2, 3, 4 and **5,** isolated in 71%, 5%, 77% and 7%, respectively. Zemplén deprotection of compounds **2-5** gave glycosides **8-11** in high yield.

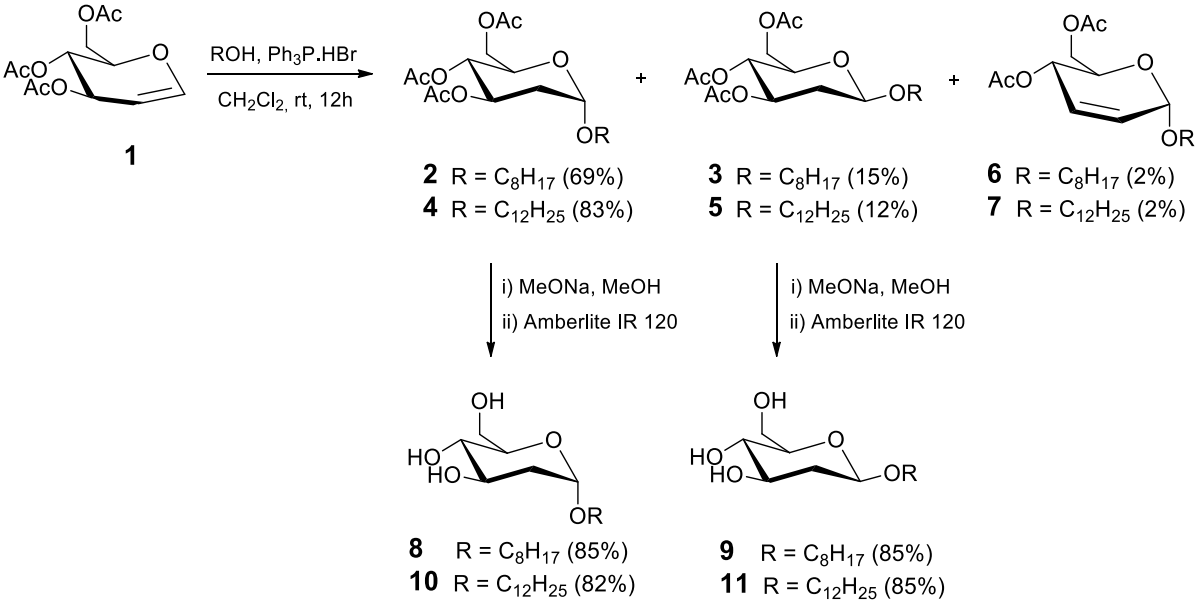

Scheme 1. Synthesis of octyl and dodecyl 2-deoxy-D-*arabino*-hexopyranosides.

Experimental

General Methods. Starting materials and reagents were purchased from Sigma-Aldrich, Fluka, and Acros. Solvents were dried prior to use with molecular sieves 4 Å, with the exception of methanol, dried over 3 Å molecular sieves. TLC was carried out on aluminum sheets (20x20 cm) coated with silica gel 60 F-254, 0.2 mm thick (Merck) with detection by charring with 10% H_2SO_4 in ethanol. Column chromatography (CC) was performed using silica gel 230-400 mesh (Merck). Melting points were measured by differential scanning calorimetry, using a Setaram TG-DSC111 apparatus. Temperature was calibrated with LGC standard reference materials (Hg, In, Sn, Pb), and energy calibrated by both Joule effect and standard reference material (Sapphire NIST SRM 720). Samples of compounds **8**–**11** were weighed into aluminium crucibles which were sealed under air, without protective atmosphere, and DSC scans were performed at a rate of 1 ºC/min, from room temperature to 140 ºC. The stability of

the samples and accuracy of the determinations were ensured performing successive heating and cooling scans which showed pronounced thermal hysteresis, giving reproducible results on successive heating and cooling cycles. No pretransitions or 'double melting points' were observed demonstrating the absence of solvent loss or formation of liquid crystalline phases. Melting point of compounds **8**–**11** was also measured with a SMP3 Melting Point Apparatus, Stuart Scientific, Bibby. Elemental analyses were performed at the Service of Microanalyses of Instituto Superior Técnico, Universidade Técnica de Lisboa. Optical rotations were measured with a Perkin Elmer 343 polarimeter. NMR experiments were recorded on a Bruker Avance 400 spectrometer at 298 K, operating at 100.62 MHz for ^{13}C and at 400.13 MHz for ^{1}H for solutions in $CDCl_3$ containing 0.03% TMS or in CD_3OD (Sigma-Aldrich).

General procedure for the glycosylation reaction. The nucleophile (36.5 mmol) and a solution of Ph_3P•HBr (686 mg, 2.0 mmol) in dry dichloromethane (16.0 mL) were added to a solution of 3,4,6-tri-*O*-acetyl-1,5-anhydro-2-deoxy-D-*arabino*-hex-1-enitol (**1**, 5.04 g, 18.5 mmol) in the same solvent (16.0 mL). The mixture was stirred at room temperature for 12 h, washed with a satd. $NaHCO_3$ (30 mL), the organic phase was concentrated, and column chromatography (1:10 EtOAc–cyclohex) afforded the α-anomer of the corresponding 2-deoxy glycosides as major product with both the β-anomer and the Ferrier compound isolated as minor products. Isolated compounds are listed in the order of elution.

Octyl 3,4,6-tri-*O*-acetyl-2-deoxy-α-D-*arabino*-hexopyranoside (2), octyl 3,4,6-tri-*O*-acetyl-2-deoxy-β-D-*arabino*-hexopyranoside (3), and octyl 4,6-di-*O*-acetyl-2,3-dideoxy-α-D-*erythro*-hex-2-enopyranoside (6). Reaction of glycal **1** with octan-1-ol (3.9 mL, 36.5 mmol) gave compounds **2, 3** and **6**.

Compound **2**: Syrup (5.11 g,69%); $[\alpha]_D^{20}$= +77 (*c* 1, CH_2Cl_2); R_f (1:3 EtOAc–PE) = 0.42; IR (neat): 1748 cm^{-1} (C=O); ^{1}H NMR ($CDCl_3$) δ 5.33 (ddd, 1H, $J_{2ax,3}$=12 Hz, $J_{2eq,3}$=6 Hz, $J_{3,4}$=10 Hz, H-3), 4.99 (t, 1H, $J_{4,5}$=10 Hz, H-4), 4.94 (d, 1H, $J_{1,2a}$=3 Hz, H-1), 4.31 (dd, 1H, $J_{5,6a}$=5 Hz, H-6a), 4.05 (dd, 1H, $J_{6b,6a}$=12 Hz, H-6b), 3.96 (ddd, 1H, $J_{5,6b}$=2 Hz, H-5), 3.62 (dt, 1H, $J_{1'a,1'b}$=14 Hz, $J_{1'a,2'}$=7 Hz, H-1'a), 3.38 (dt, 1H, H-1'b), 2.23 (dd, 1H, $J_{2e,2a}$=12 Hz, $J_{2e,3}$=5.6 Hz, H-2eq), 2.09 (s, 3H, CH_3-Ac), 2.04 (s, 3H, CH_3-Ac), 2.01 (s, 3H, CH_3-Ac), 1.82 (td, 1H, $J_{2a,3}$=12 Hz, H-2ax), 1.63-1.53 (m, 2H, H-2'a,b), 1.39-1.21 (m, 10H, H-3' to H-7'), 0.89 (t, 3H, $J_{7',8'}$=7 Hz, H-8'); ^{13}C NMR ($CDCl_3$) δ 170.6 (C=O), 170.1 (C=O), 169.9 (C=O), 96.8 (C-1), 69.4 (C-4), 69.1 (C-3), 67.8 (C-1'), 67.7 (C-5), 62.4 (C-6), 35.0 (C-2), 31.8, 29.3, 29.2, 29.1, 26.1, 22.6 (C2'-C-7'), 20.9, 20.7 (CH_3-Ac), 14.0 (C-8'). Calcd for $C_{20}H_{34}O_8$: C, 59.68; H, 8.51. Found: C, 59.70; H, 8.80.

Compound **3**: Syrup (1.11 g, 15%); $[\alpha]_D^{20}$= -18 (*c* 1, CH_2Cl_2); R_f(1:3 EtOAc-PE)=0.40; IR (neat): 1749 cm^{-1} (C=O); ^{1}H NMR ($CDCl_3$) δ 5.07-4.95 (m, 2H, H-3, H-4), 4.56 (dd, 1H, $J_{1,2a}$ =10 Hz, $J_{1,2e}$=2 Hz, H-1), 4.30 (dd, 1H, $J_{6a,5}$=5 Hz, $J_{6a,6b}$=12 Hz, H-6a), 4.11 (dd, 1H, $J_{6b,5}$=2 Hz, H-6b), 3.87 (dt, 1H, $J_{1'a,1'b}$=9 Hz, $J_{1'a,2'a,b}$=7 Hz, H-1'a), 3.60 (ddd, 1H, $J_{5,4}$=9 Hz, H-5), 3.46 (dt, 1H, H-1'b), 2.32 (ddd, 1H, $J_{2eq,3}$=5 Hz, $J_{2eq,2ax}$=13 Hz, H-2eq), 2.09 (s, 3H, CH_3-Ac), 2.04 (s, 3H, CH_3-Ac), 2.03 (s, 3H, CH_3-Ac), 1.75 (ddd, 1H, $J_{2ax,3}$=12 Hz, H-2ax), 1.66-1.52 (m, 2H, H-2'a,b), 1.38-1.18 (m, 10H, H-3' to H-7'), 0.88 (t, 3H, $J_{7',8'}$=7 Hz, H-8'); ^{13}C NMR ($CDCl_3$) δ 170.9 (C=O), 170.4 (C=O), 169.8 (C=O), 99.6 (C-1), 71.9 (C-5), 70.8 (C-4), 70.0 (C-1'), 69.1 (C-3), 62.5 (C-6), 36.2 (C-2), 31.8, 29.7, 29.5, 29.3, 29.2, 26.0, 22.7 (C-2' to C-7'), 20.9, 20.8, 20.7 (CH_3-Ac), 14.0 (C-8'). Calcd for $C_{20}H_{34}O_8$: C, 59.68; H, 8.51. Found: C, 59.60; H, 8.70.

Compound **6:** Syrup (0.11 g, 2 %); $[\alpha]_D^{20}$= +38 (*c* 1, CH_2Cl_2); R_f(1:3 EtOAc/Petrol. ether)=0.67; IR (neat): 1757 cm^{-1} (C=O); ^{1}H NMR ($CDCl_3$) δ 5.92–5.81 (m, 2H, H-2, H-3), 5.32 (br d, 1H, $J_{4,5}$= 10 Hz, H-4), 5.03 (br s, 1H, H-1), 4.28, 4.27, 4.25, 4.24 (Part AX of ABX system, 1H, $J_{6a,6b}$ = 12 Hz, $J_{6a,5}$ = 5 Hz, H-6a), 4.19, 4.16 (Part B of ABX system, 1H, H-6b), 4.11 (ddd,

1H, $J_{5,6b}$=2 Hz, H-5), 3.77 (dq, 1H, $J_{1'a,1'b}$=9 Hz, $J_{1'a,2'a,b}$=7 Hz, H-1'a), 3.50 (dq, 1H, $J_{1'b,2'a,b}$ = 7 Hz, H-1'b), 2.11 (s, 3H, CH_3-Ac), 2.09 (s, 3H, CH_3-Ac), 1.66–1.53 (m, 2H, H-2'a,b), 1.41–1.20 (m, 10H, H-3' to H-7'), 0.88 (t, 3H, $J_{7',8'}$= 7.0 Hz, H-8'); ^{13}C NMR ($CDCl_3$) δ 171.1 (C=O), 170.6 (C=O), 129.1, 128.1 (C-2, C-3), 94.5 (C-1), 69.1 (C-1'), 67.0 (C-5), 65.4 (C-4), 63.1 (C-6), 29.8 (C-2'), 31.9, 29.5, 29.4, 26.4, 22.8 (C-3'-C-7'), 21.1, 20.9 (CH_3-Ac), 14.2 (C-8'). Calcd for $C_{18}H_{30}O_6$: C, 63.14; H, 8.83. Found: C, 62.90; H, 9.10.

Dodecyl 3,4,6-tri-*O*-acetyl-2-deoxy-α-D-*arabino*-hexopyranoside (4), dodecyl 3,4,6-tri-*O*-acetyl-2-deoxy-β-D-*arabino*-hexopyranoside (5) and Dodecyl 4,6-di-*O*-acetyl-2,3-dideoxy-α-D-*erythro*-hex-2-enopyranoside (7). Reaction of **1** with dodecan-1-ol (5.6 mL, 36.5 mmol) gave compounds **4**, **5** and **7**.

Compound **4**: Syrup (7.05g, 83%); $[\alpha]_D^{20}$= +66 (*c* 1, CH_2Cl_2); R_f (1:3 EtOAc/PE)=0.48; IR (neat): 1748 cm^{-1} (C=O); ^{1}H NMR ($CDCl_3$) δ 5.33 (ddd, 1H, $J_{3,2a}$ =12 Hz, $J_{3,2e}$=6 Hz, $J_{3,4}$=10 Hz, H-3), 5.00 (t, 1H, $J_{4,5}$=10 Hz, H-4), 4.94 (d, 1H, $J_{1,2a}$=3 Hz, H-1), 4.32 (dd, 1H, $J_{6a,5}$=5 Hz, $J_{6a,6b}$ =12 Hz, H-6a), 4.06 (dd, 1H, $J_{6b,5}$=2 Hz, H-6b), 3.97 (ddd, 1H, $J_{5,4}$=10 Hz, H-5), 3.62 (dt, 1H, $J_{1'a,1'b}$=9 Hz, $J_{1'a,2'}$=6 Hz, H-1'a), 3.38 (dt, 1H, $J_{1'b,2'}$=6 Hz, H-1'b), 2.24 (dd, 1H, $J_{2eq,2ax}$=13 Hz, $J_{2e,3}$=6 Hz, H-2eq), 2.10 (s, 3H, CH_3-Ac), 2.05 (s, 3H, CH_3-Ac), 2.02 (s, 3H, CH_3-Ac), 1.83 (td, 1H, H-2ax), 1.63-1.53 (m, 2H, H- 2'a,b), 1.37-1.22 (m, 18H, H-3'to H-11'), 0.89 (t, 3H, $J_{12',11'}$=7 Hz, H-12'); ^{13}C NMR ($CDCl^3$) δ 170.8 (C=O), 170.2 (C=O), 170.0 (C=O), 96.9 (C-1), 69.5 (C-4), 69.2 (C-3), 67.9 (C-1'), 67.7 (C-5), 62.4 (C-6), 35.1 (C-2), 31.9, 29.7, 29.6, 29.5, 29.4, 29.3 26.2, 22.7 (C-3'-C-11'), 21.0, 20.8, 20.7 (CH_3-Ac), 14.1 (C-12'). Calcd for $C_{24}H_{42}O_8$: C, 62.86; H, 9.23. Found: C, 63.20; H, 9.50.

Compound **5**: Syrup (1.01g, 12%); $[\alpha]_D^{20}$= -19 (*c* 1, CH_2Cl_2); Rf (1:3 EtOAc/Petrol. ether)=0.42; IR (neat): 1748 cm^{-1} (C=O); ^{1}H NMR ($CDCl_3$) δ 5.03-4.99 (m, 2H, H-3, H-4), 4.56 (dd, 1H, $J_{1,2a}$=10 Hz, $J_{1,2eq}$=2 Hz, H-1), 4.30 (dd, 1H, $J_{6a,6b}$=12 Hz, $J_{5,6a}$=5 Hz, H-6a), 4.11 (dd, 1H,

$J_{6b,5}$=3 Hz, H-6b), 3.87 (td, 1H, $J_{1'a,1'b}$=10 Hz, $J_{1'a,2'}$=6 Hz, H-1'a), 3.60 (ddd, 1H, $J_{4,5}$=9 Hz, H-5), 3.46 (ddd, 1H, H-1'b), 2.32 (ddd, 1H, $J_{2eq,3}$=4 Hz, $J_{2ax,2eq}$=12 Hz, H-2eq), 2.10 (s, 3H, CH_3-Ac), 2.05 (s, 3H,CH_3-Ac), 2.02 (s, 3H, CH_3-Ac), 1.75 (ddd, 1H, $J_{2ax,3}$=10 Hz, H-2ax), 1.63-1.53 (m, 2H, H-2'a,b), 1.33-1.22 (m, 18H, H-3'to H-11'), 0.84 (t, 3H, $J_{11',12'}$ =6 Hz, H-12'); ^{13}C NMR ($CDCl_3$) δ 99.6 (C-1), 71.9 (C-5), 71.0 (C-3), 70.8 (C-1'), 70.0 (C-4), 62.5 (C-6), 36.3 (C-2), 31.9, 29.7, 29.6, 29.5, 29.4, 26.0, 22.7 (C-3'to C-11'), 20.9, 20.8 (CH_3-Ac), 14.1 (C-12'). Calcd for $C_{24}H_{42}O_8$: C, 62.86; H, 9.23. Found: C, 63.20; H, 9.40.

Compound **7:** Syrup (0.13 g, 2%); $[\alpha]_D^{20}$= +48 (*c* 1, CH_2Cl_2); R_f (1:3 EtOAc/Petrol. ether)=0.61; IR (neat): 1757 cm^{-1} (C=O); ^{1}H NMR ($CDCl_3$) δ 5.90-5.79 (m, 2H, H-2, H-3), 5.30 (br d, 1H, $J_{4,5}$= 10 Hz, H-4), 4.95 (br s, 1H, H-1), 4.28, 4.27, 4.25, 4.24 (Part AX of ABX system, 1H, $J_{6a,6b}$ = 12 Hz, $J_{6a,5}$=5 Hz, H-6a), 4.19, 4.16 (Part B of ABX system, 1H, $J_{5,6b}$ = 2 Hz, H-6b), 4.11 (ddd, 1H, H-5), 3.77 (dq, 1H, $J_{1'a,1'b}$ = 9 Hz, $J_{1'a,2'a,b}$=7 Hz, H-1'a), 3.50 (dq, 1H, $J_{1'b,2'}$= 7 Hz, H-1'b), 2.10 (s, 3H, CH_3-Ac), 2.09 (s, 3H, CH_3-Ac), 1.66–1.54 (m, 2H, H-2'a,b), 1.35–1.24 (m, 18H, H-3' to H-11'), 0.88 (t, 3H, $J_{11',12'}$= 7 Hz, H-12'); ^{13}C NMR ($CDCl_3$) δ 170.7 (C=O), 170.2 (C=O), 128.9, 127.9 (C-2, C-3), 94.3 (C-1), 68.9 (C-1'), 66.8 (C-5), 65.2 (C-4), 63.0 (C-6), 29.7 (C-20), 31.8, 29.6, 29.6, 29.5, 29.4, 29.3, 26.2, 22.6 (C-3´-C-11'), 20.9, 20.7 (CH_3-Ac), 14.1 (C-12'). Calcd for $C_{22}H_{38}O_6$: C, 66.30; H, 9.61. Found: C, 66.00; H, 9.90.

General procedure for the Zemplén deacetylation. To a solution of a substrate (1 mmol) in dry methanol (10 mL) was added a solution of sodium methoxide in methanol (0.25 mL, *ca*. 1 M, prepared by dissolving sodium in dry methanol directly before use). The reaction mixture was stirred for 1.5h and then neutralized with Amberlite (IR-120, H^+ form). The mixture was concentrated and filtered through silica gel (5 g, 230-400 mesh, eluted with EtOAc).

Octyl 2-deoxy-α-D-*arabino*-hexopyranoside (8). Deacetylation of **2** gave **8** (0.49 g, 85 %); mp. 107.8-109.6 (EtOAc/*n*-hex); mp. by DSC:108.7 ºC; $[\alpha]_D^{20}$= +68 (*c* 1, MeOH); R_f

(EtOAc)=0.56; IR (neat): 3371 cm^{-1} (C-OH); ^{1}H NMR (CD_3OD) δ 4.90 (br d, 1H, $J_{1,2a}$=2.7 Hz, H-1), 3.90-3.81 (m, 2H, H-6a, H-3), 3.74-3.67 (m, 2H, H-6b, H-1'a), 3.54 (ddd, 1H, H-5), 3.38 (dt, 1H, $J_{1'a,1'b}$ =10 Hz, $J_{1'a,2'a}$= $J_{1'a,2'b}$ 6 Hz, H-1'b), 3.26 (t, 1H, $J_{3,4}$=$J_{4,5}$= 9 Hz, H-4), 2.07 (dd, 1H, $J_{2eq,3}$=5 Hz, $J_{2eq,2ax}$=13 Hz, H-2eq), 1.67-1.56 (m, 3H, H-2ax, H-2'a, H-2'b), 1.46-1.26 (m, 10H, H-3'to H-7'), 0.93 (t, 3H, $J_{7',8'}$=6.4 Hz, H-8'); ^{13}C NMR (CD_3OD) δ 99.4 (C-1), 74.8 (C-5), 74.2 (C-4), 70.8 (C-3), 69.1 (C-1'), 63.7 (C-6), 39.8 (C-2), 33.9, 31.5, 31.4, 31.3, 28.3, 24.6 (C-2'-C-7'), 15.3 (C-8'). Calcd for $C_{14}H_{28}O_5$: C, 60.84; H, 10.21. Found: C, 60.50; H, 10.50.

Octyl 2-deoxy-β-D-*arabino*-hexopyranoside (9). Deacetylation of **3** gave **9** (0.50 g, 85 %); mp. 83.5 – 85.1 ºC (EtOAc/*n*-hex), mp. by DSC =84.3 ºC; $[\alpha]_D^{20}$= -13 (*c* 1, MeOH); R_f(EtOAc)=0.54; IR (neat): 3465 cm^{-1} (C-OH); ^{1}H NMR (CD_3OD) δ 4.48 (d, 1H, $J_{1,2ax}$ =10 Hz, H-1), 3.89-3.77 (m, 2H, H-6a, H-1'a), 3.63 (dd, 1H, $J_{6b,5}$=5 Hz, $J_{6b,6a}$=12 Hz, H-6b), 3.49 (ddd, 1H, $J_{3,2eq}$=4 Hz, $J_{3,2ax}$=12 Hz, $J_{3,4}$=12 Hz, H-3), 3.42 (dt, 1H, $J_{1'b,2'a}$=$J_{1'b,2'b}$=7 Hz; $J_{1'b,1'a}$=14 Hz, H-1'b), 3.18-3.07 (m, 2H, H-4, H-5), 2.04 (dd, 1H, $J_{2eq,2ax}$=12 Hz, $J_{2eq,3}$=4 Hz, H-2e), 1.58-1.47 (m, 2H, H-2'a,b), 1.42 (q, 1H, $J_{2ax,2eq}$ = $J_{2ax,3}$ = $J_{2ax,1}$ 11.67 Hz, H-2ax), 1.35-1.16 (m, 10H, H-3' to H-7'), 0.85 (t, 3H, $J_{8',7'}$=7 Hz, H-8'); ^{13}C NMR (CD_3OD) δ 101.9 (C-1), 78.8 (C-4), 73.9 (C-5), 73.3 (C-3), 71.1 (C-1'), 63.7 (C-6), 41.2 (C-2), 33.8, 31.5, 31.3, 31.2, 27.9, 24.5 (C-2'-C-7'), 15.2 (C-8'). Calcd for $C_{14}H_{28}O_5$: C, 60.84; H, 10.21. Found: C, 60.60; H, 10.40.

Dodecyl 2-deoxy-α-D-*arabino*-hexopyranoside (10). Deacetylation of **4** gave **10** (0.57g, 82%); mp 113.9-115.5 ºC (EtOAc/*n*-hex); mp by DSC 114.8 ºC; $[\alpha]_D^{20}$= +64 (*c* 1, MeOH); R_f(EtOAc)=0.48; IR (neat): 3354 cm^{-1} (C-OH); ^{1}H NMR (CD_3OD) δ 4.90 (d, 1H, $J_{1,2ax}$=3 Hz, H-1), 3.90-3.81 (m, 2H, H-3, H-6a), 3.75-3.67 (m, 2H, H-6b, H-1'a), 3.55 (ddd, 1H, $J_{5,4}$ =9 Hz, $J_{5,6a}$ =2 Hz, $J_{5,6b}$ =5 Hz, H-5), 3.38 (dt, 1H, $J_{1'b,2'a}$ = $J_{1'b,2'b}$ =6 Hz, $J_{1'b,1'a}$=10 Hz, H-1'b), 3.26 (t, 1H, $J_{4,3}$= $J_{4,5}$=9 Hz, H-4), 2.07 (dd, 1H, $J_{2eq,2ax}$=13 Hz, $J_{2eq,3}$=5 Hz, H-2eq), 1.67–1.54 (m, 3H, H-2ax, H-2'a, H-2'b), 1.45–1.26 (m, 18H, H-3'to H-11'), 0.93 (t, 3H, $J_{11',12'}$=7 Hz, H-12');

^{13}C NMR (CD_3OD) δ 99.4 (C-1), 74.8 (C-4), 74.2 (C-5), 70.9 (C-3), 69.1 (C-1'), 63.7 (C-6), 39.8 (C-2), 34.0, 31.7, 31.6, 31.6, 31.5, 31.4, 28.3, 24.6 (C-2'-C-11'), 15.3 (C-12') Calcd for $C_{14}H_{36}O_5$: C, 65.03; H, 10.91. Found: C, 65.10; H, 11.20.

Dodecyl 2-deoxy-β-D-*arabino*-hexopyranoside (11). Deacetylation of **5** gave **11** (0.59 g (85%); m.p. 101.9-104.9 ºC (EtOAc/*n*-hex); m.p. by DSC 103.4 ºC; $[\alpha]_D^{20}$= -1.6 (*c* 1, MeOH); Rf 0.45 (EtOAc); IR (neat): 3466 cm^{-1} (C-OH); ^{1}H NMR (CD_3OD) δ 4.56 (dd, 1H, $J_{1,2eq}$=2 Hz, $J_{1,2ax}$=10 Hz, H-1), 3.97-3.87 (m, 2H, H-1'a, H-6a), 3.72 (dd, 1H, $J_{6b,5}$=5 Hz, $J_{6b,6a}$=12 Hz, H-6b), 3.58 (ddd, 1H, $J_{3,2eq}$=5 Hz, $J_{3,2ax}$ 12 Hz, $J_{3,4}$=12 Hz, H-3), 3.50 (dt, 1H, $J_{1'b,2'a}$=$J_{1'b,2'b}$=7 Hz, $J_{1'b,1'a}$ =10 Hz, H-1'b), 3.25-3.16 (m, 2H, H-5, H-4), 2.13 (ddd, 1H, $J_{2eq,2ax}$ =12 Hz, H-2eq), 1.65-1.58 (m, 2H, H-2'a, H-2'b), 1.51 (dd, 1H, $J_{2ax,3}$ = $J_{2ax,2eq}$= $J_{2ax,1}$ 12 Hz, H-2ax) 1.44-1.26 (m, 18H, H-3'to H11'), 0.93 (t, 3H, $J_{11',12'}$=7 Hz, H-12'); ^{13}C NMR (CD_3OD) δ 102.0 (C-1), 78.9 (C-4), 74.0 (C-5), 73.4 (C-3), 71.2 (C-1'), 63.8 (C-6), 41.3 (C-2), 33.9, 31.7, 31.6, 31.6, 31.4, 31.3, 28.1, 24.6 (C-2'-C-11'), 15.3 (C-12'). Calcd for $C_{14}H_{36}O_5$: C, 65.03; H, 10.91. Found: C, 65.30; H, 11.10.

Acknowledgments

The authors thank QREN – COMPETE program for the support of FACIB project (QREN – SI I&DT Co-Promotion Project nr. 21547). Fundação para a Ciência e a Tecnologia is gratefully acknowledged for the research grant SFRH/BDE/51998/2012 and for financial support of CQB Strategic Project PEst-OE/QUI/UI0612/2013.

REFERENCES

[1] F.V. M. Silva; M. Goulart; J. Justino; A. Neves; F. Santos; J. Caio; S. Lucas; A. Newton; D. Sacoto; E. Barbosa; M. S. Santos; A. P. Rauter. Alkyl deoxy-arabino-hexopyranosides:

Synthesis, surface properties, and biological activities. *Bioorganic Medicinal Chemistry* **2008**, *16*, 4083–4092.

[2] A. Martins; M.S. Santos; C. Dias; P. Serra; V. Cachatra; J. Pais; J. Caio; V. H. Teixeira; M. Machuqueiro; M. S. Silva; A. Pelerito; J. Justino; M. Goulart; F. V. Silva; A. P. Rauter. Tuning the Bioactivity of Tensioactive Deoxy Glycosides to Structure: Antibacterial Activity Versus Selective Cholinesterase Inhibition Rationalized by Molecular Docking *European Journal of Organic Chemistry*, **2013**, *8*, 1458–1459.

[3] A. P. Rauter; S. Lucas; T. Almeida; D. Sacoto; V. Ribeiro; J. Justino; A. Neves; F. V. M. Silva; M. C. Oliveira; M. J. Ferreira; M. S. Santos; E. Barbosa. Synthesis, surface active and antimicrobial properties of new alkyl 2,6-dideoxy-L-*arabino*-hexopyranosides, *Carbohydrate Research* **2005,** *340*, 191–201

[4] V. Bolitt; C. Mioskowski; S.-G. Lee; J. R. Falck. Direct preparation of 2-deoxy-D-glucopyranosides from glucals without Ferrier rearrangement. *Journal of Organic Chemistry*, **1990**, *55*, 5812–5813.

Chapter 3

The first sugar-based bactericides targeting phosphatidylethanolamine-enriched membranes[a]

[a] C. Dias, J. P. Pais, R. Nunes, A. F. Almeida, P. Serra, N. M. Xavier, D. Vila-Viçosa, M. Machuqueiro, Ana S. Viana, A. Martins, M. S. Santos, A. Pelerito, R. Dias, R. Tenreiro, M. C. Oliveira, M. Contino, N. Colabufo, R. F. M. de Almeida, A. P. Rauter. This chapter was submited to *Nature communications* and later accepted after revisions (*Nat. Commun.***9**, 4857, **2018**). My contributions to this paper were the syntheses of dodecyl glycosides 1-3, 6, 12, 13, 15 and 16 (and their intermediates), the determination of the mechanism of action by performing the fluorescence studies on PE-enriched membranes, as well as the development of a suitable method to determine T_H transition. I took an extremely active part on writing the paper.

Anthrax is an infectious disease caused by *Bacillus anthracis,* a Gram-positive bacterium affecting livestock and humans who handle infected farm animals. In addition, this species is a serious bioterrorism threat.[1-2] All types of anthrax have the potential, if untreated, to spread throughout the body causing severe illness and death. Regrettably, therapeutic options for anthrax are insufficient, relying on long-term, intravenous, combined antibiotic treatment with quinolones and tetracyclines[2]. However, the ease of *B. anthracis* to develop resistance to the antibiotics of choice, namely ciprofloxacin, is well documented and examples of new antibacterial molecules against *B. anthracis* are scarce.[3-6]

Our preliminary puzzling results on two dodecyl deoxy glycosides, differing only in the presence of glycone OH-6, both with tensioactive properties of the same order of magnitude, but only one of them acting as a potent and selective antimicrobial over *Bacillus* spp.,[6] encouraged us to explore this family of compounds and face the challenge of unravelling their mechanism of action. The observed selectivity does not fit the behaviour of glucoside surfactants,[7] also reported as permeability enhancers at concentrations over 190 μM on human cell lines, allowing significant cell recovery due to negligible membrane disruption.[8]

Aiming to understand our unexpected findings, we generated a small library of deoxy glycosides and analogues for structure-activity relationships and conducted mechanistic studies on *B. cereus* for its genetic similarity to *B. anthracis,* and highly studied genome.[9] Structural features, namely atom linking the dodecyl chain to the sugar (C-O vs. C-S vs. C-C bond), deoxygenation pattern (2,6-dideoxy, 6-deoxy, 2-deoxy), sugar configuration (*arabino*, *threo*, *lyxo* and *manno*) and hexopyranoside vs. pentopyranoside structure, were investigated.

The antibacterial profiling and the bioactivity on *B. cereus* spore germination were both evaluated. Target assessment and genetic studies were carried out, as well as computational studies aiming to rationalize the behaviour of these sugar-based surfactants. Since *Bacillus* spp. bacterial membranes are rich in phosphatidylethanolamine (PE), studies on the polymorphic phase behaviour of PE-rich liposomes were conducted, allowing a deeper understanding of the mechanism of action.

RESULTS AND DISCUSSION

Synthesis

A small library of dodecyl deoxy glycosides differing by atom (O, S, C) linking the alkyl chain to the glycone, in deoxygenation pattern, configuration (*arabino*, *threo*, *lyxo* and *manno*) and bearing a hexoside/pentoside glycone structure has been generated by synthesis. Dodecyl 2-deoxy *O*- and *S*-glycosides **1**-**4**, **6**, **8**-**13** (Figure 1A) were accessed by the proven method using glycals,[10] triphenylphosphane hydrobromide catalysis and dodecan-1-ol or dodecane-1-thiol, followed by deprotection (Scheme S1, page 136). Noteworthy, pentopyranoside **9** adopted, in $CDCl_3$, the unusual $^4C_1$ conformation, as suggested by NMR and rationalized by DFT calculations (Figures S1 and S2, table S1).

In order to disclose the biological impact of 2-deoxygenation, 6-deoxy-*manno* enantiomers **4** and **6** (Figure 1B) were prepared starting from L-rhamnose and D-mannose, respectively, in good overall yields (Scheme S2, page 149).

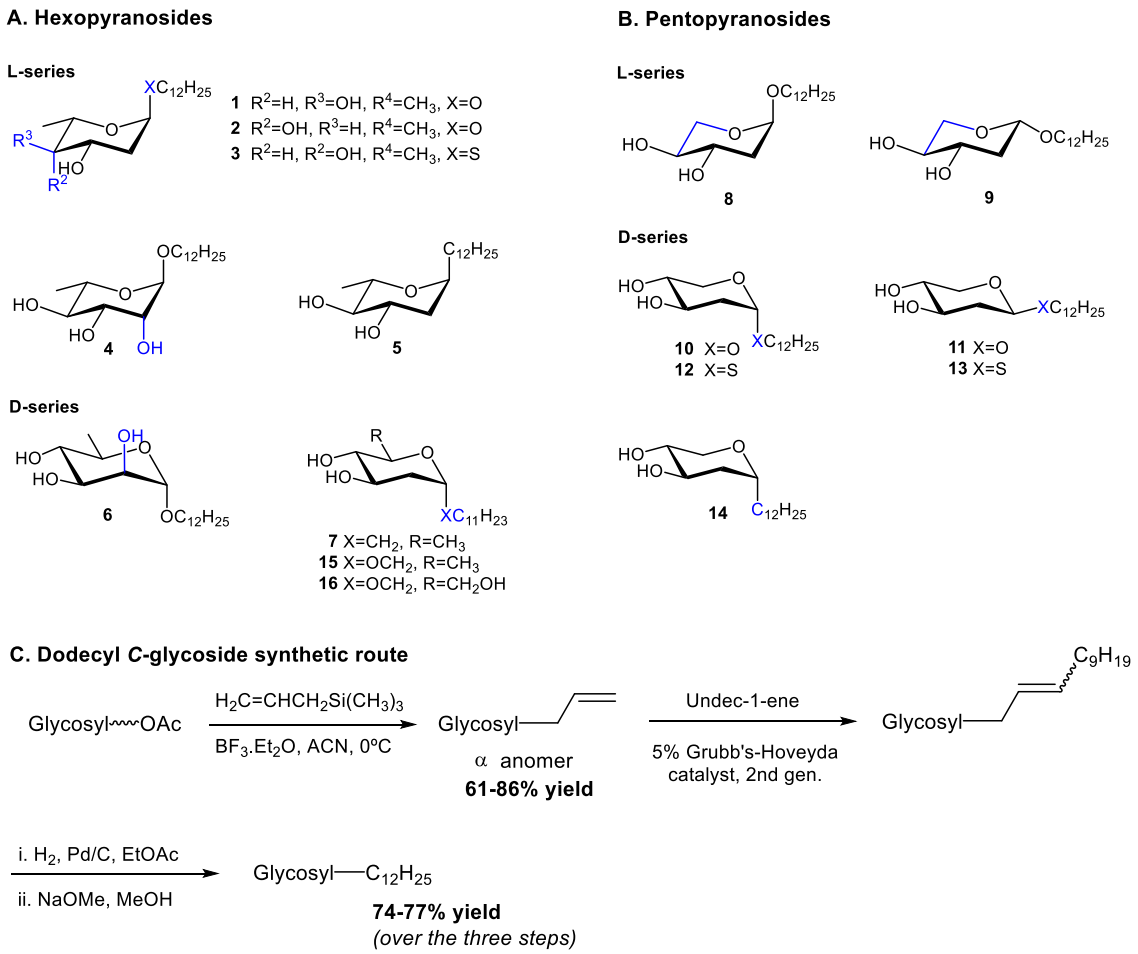

Figure 1. Lead series generated by design and synthesis (see SI). **A)** Hexopyranosides; **B)** Pentopyranosides; **C)** Synthetic approach to *C*-Glycosides.

Dodecyl *C*-glycosides **5**, **7** and **14** were accessed by a novel approach (Figure 1C), whose key step is the metathesis reaction of allyl α-*C*-glycosides with undec-1-ene in the presence of the 2nd generation Grubbs-Hoveyda catalyst (5 mol%) (Scheme S3, page 156). The anomeric allylation of peracetate 2-deoxy sugar precursors afforded allyl α-*C*-glycosides in good yields (Figure 1C), in agreement with previous reports,[11] a reaction herein employed on deoxy sugars for the first time. Double bond hydrogenation and Zemplén deacetylation gave the target molecules in high yield over the three steps (Figure 1C). This efficient methodology opens the way to a diversity of *C*-glycosides, whose synthesis involves often drastic reaction conditions.

Susceptibility against B. anthracis *and cytotoxicity*

Reports about the mesomorphic behaviour of alkyl 2-deoxy-α-D-*arabino*-hexopyranosides and 6-deoxy-β-D-glucopyranosides[12-13] encouraged us to unravel the impact of deoxy glycosides at the biological level. Their bactericide activity over *B. anthracis* sterne, pathogenic, and ovine, *B. cereus*, and *E. faecalis* was evaluated (Table 1). All compounds were active over the tested *B. anthracis* strains, 56% of them being more active over the pathogenic strain. C-C linkage seems to benefit D-series bioactivity, while the relative configuration at C-3 and C-4 has no impact. 2-Hydroxyglycosides **4** and **6** maintain the activity over *B. anthracis* sterne and pathogenic strains, thus inferring that in hexopyranosides C-6 deoxygenation is required for activity. MIC values over *E. faecalis* were mostly above 48 μM.

Compound cytotoxicity was also assessed by evaluating the effect on Caco-2 cell viability by the MTT assay (Table 1, Figure S3) revealing *C*-glycosides **5**, **7** and **14**, dodecyl α-L- (**8**) and α-D-pentopyranosides (**10**) as the less toxic compounds.

Bactericidal activity and antimicrobial resistance

Time-kill studies of *B. cereus* ATCC 14579 were performed to assess glycoside **1** bacteriostatic or bactericidal activity, in parallel to the generation of its analogue library of compounds. The broth microdilution method according to CLSI guidelines[14] was chosen for the simultaneous data assessment by varying multiple experimental conditions, but the MIC values obtained were 2-fold higher than those obtained for the agar dilution method. The time-kill assay was accomplished with a temporal resolution of 10 min, the minimal time required for sampling, at the concentrations of 4-32 μg/mL (Figure S4, Table S2). Although the resolution is far superior to the traditional method collecting results hourly, at 10^6 starting cell concentration the kinetics of bacterial cell death could not be detected at 16 μg/mL compound concentration or

higher, due to complete cell death, observed at the first temporal point. Still, a 1000-fold reduction ($T_{99.9}$) was reached within 60 min for initial bacterial load of 10^7 and 10^8 CFU/mL. No significant bacterial cell death was observed at 4 and 8 µg/mL in comparison to controls. In all performed assays, MIC equal to MBC values indicated bactericidal activity (Table S3). The extremely fast bacterial death is also pointing towards a biophysical action at the cellular envelope.

Table 1. Antibacterial activity expressed in MICs[a], and cytotoxicity over Caco-2 cells expressed in IC_{50} (MTT assay).

Compound	MIC (µM)					Cytotoxicity IC_{50} (µM)	
	B. anthracis			*E. faecalis*	*B. cereus*	24h	48h
	Sterne	Pathogenic	Ovine				
Hexopyranosides							
1	25	25	25	>50	25	100	>50
2	25	25	25	>50	25	100	50
3	24	48	48	>48	48	>50	>50
4	24	24	48	48	n.d.	n.d.	n.d.
5	27	54	54	>54	27	>100	100
6	24	24	>48	>48	48	n.d.	n.d.
7	27	27	27	>54	27	>100	>100
15	50	50	50	50	25	100	50
16	n.d.[b]	n.d.[b]	n.d.[b]	n.a.[b]	n.d.[b]	100	>50
Pentopyranosides							
8	26	52	52	52	n.d	>100	100
9	26	26	52	52	n.d.	n.d.	n.d.
10	26	52	52	>52	52	>100	>100
11	26	26	52	52	52	>100	>50
12	50	25	50	50	25	n.d.	n.d.
13	25	50	50	>50	50	n.d.	n.d.
14	28	28	28	56	28	>100	100

a) Müller-Hinton agar dilution method following CLSI guidelines; b) Not tested since **16** is not active over *B.* spp.[6]

The effect of compound **1** on *B. cereus* cells was monitored by *ex-situ* atomic force microscopy (AFM) (Figure 2). 3D-topographic images clearly show the typical rod-shape

expected for *B. cereus* and the complete loss of cellular integrity at MIC value. At sub-inhibitory concentrations, cellular damage by the presence of cracks and discontinuities at the cellular envelope is detected, in line with the bactericidal action of glycoside **1** by direct interaction with the cell envelope of *B. cereus*.

Resistance development, through natural mutagenesis, was assessed by submitting *B. cereus* to serial passage on gradient concentration of compound **1**. No alteration of MIC and MBC values was observed after 15 daily serial passages. Moreover, compound **1** antibacterial activity remains the same over *B. cereus* strains resistant to the main classes of known antibiotics (Table S4), demonstrating that its mechanism of action is not related to that of those drugs, and the mechanisms of resistance do not compromise compound activity. These findings show that this type of structures does not face the earlier emergence of bacterial resistance.

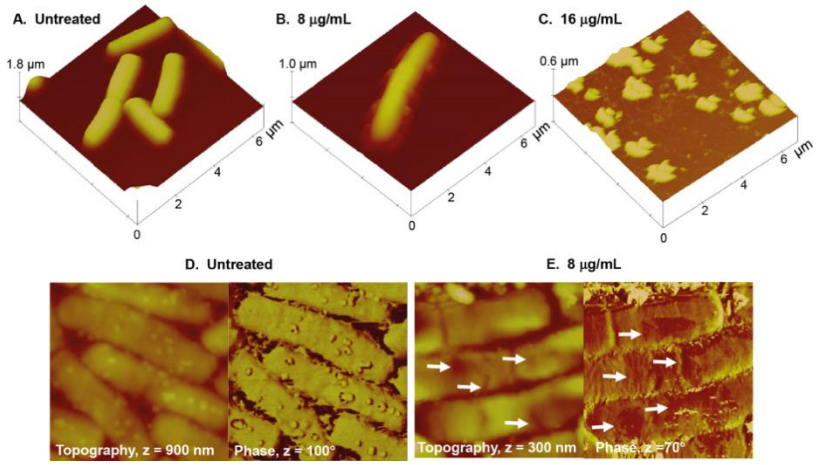

Figure 2. Tapping™ mode AFM imaging of *B. cereus* deposited on mica surface, before (A and D) and after exposure to compound **1** (B, C and E). A-C are 3D-representations of topographic images, while D and E are detailed topographic and phase contrast images (3.5×3.5 µm^2) of untreated cells and upon interaction with glycoside **1** (8 µg/mL), respectively. The arrows indicate lesions in the cellular envelope.

The search for the mechanism of action

Differential metabolomics analysis was carried out for detection of eventual interaction of compound **1** with cellular subsystems. By using Phenotype MicroArray-based approach, the differential analysis of *B. cereus* ATCC 14579 metabolism showed selective inhibition to several carbon sources. The associated metabolic pathways were identified according to the KEGG (Kyoto Encyclopedia of Genes and Genomes) database, and hierarchical mapped (Figure S5). Several clusters were identified, yielding as main targets the environmental information processing systems, namely ABC transport systems and phosphotransferases (PTS). Given the surfactant properties of these glycosides, differentiation between specific vs. non-specific mode of action can only be done by exclusion, since the surfactant effect is present. Hence, a genetic dissection for protein target assessment was carried out. A mutant library was created by random transposition, using *B. cereus* ATCC 14579 as isogenic system and its susceptibility to compound **1** was evaluated. MIC values remained unchanged when compared with the parental strain, indicating the absence of any resistance to the test compound, although a high number of mutants was obtained. In parallel, a library of specific knockout mutants for the several ABC and PTS systems previously identified as putative targets were challenged with compound **1** (Table S5). Again, no difference between MIC values was observed in comparison with parental strain. These results suggest the absence of proteins as specific targets.

Aiming to understand the role of cellular envelope ultrastructure, protoplasts of *B. cereus*, *Staphylococcus aureus,* and spheroplasts of *Escherichia coli* K12 were submitted to the action of compound **1** (Figure 3). The external cell wall of Gram-positive bacteria is not relevant since MIC values for bacteria and protoplasts are the same. *E. coli* spheroblast and *B. cereus protoplast,* containing 85% and 43% phosphatidylethanolamine (PE), respectively,[15] have high susceptibility to **1** (Figure 3, Table S6) while no activity was found over *S. aureus* (PE ca. 0%), indicating that cytoplasmic membrane composition is crucial for activity. *E. faecalis*, showing

minor susceptibility, contains other zwitterionic lipids and unusual uncharged lipids in the cytoplasmic membrane, with biophysical properties different from those of the anionic lipids. In the presence of cationic bactericides, *E. faecalis* behaved similarly to Gram-positive bacteria with high PE content, but the mechanism of action was unknown.[15]

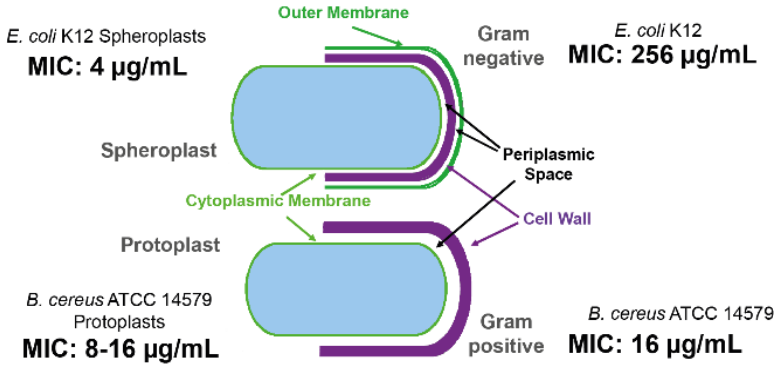

Figure 3. Effect of **1** in Gram-positive bacteria/protoplasts, and in Gram-negative bacteria/spheroplasts.

Compound effect on spore germination was also evaluated. When spore coat was cracked and bacterial cell membrane became accessible, bactericidal effect occurred (Table S7, Figure S6), and the spore became unavailable for future germination. So far, results point to a mechanism of action driven by interactions with bacterial cytoplasmic membrane.

In silico *studies on membrane destabilization*

Given the key role of cell membrane on bactericidal action, *in silico* studies on membrane destabilization by molecular dynamics (MD) simulations were carried out with a 1,2-dimyristoyl-*sn-glycero*-3-phosphocholine (DMPC) bilayer. Even though PC lipids are only common in eukaryotes and virtually absent in *Bacillus* membranes, they are the most reliable model system for biomolecular simulations of lipid bilayers.[16] In the context of surface-active drugs, a widespread mode of action is based on transmembrane pore formation.[17] Pore

morphological complexity and size, and formation kinetics make it challenging to characterize such systems by conventional MD simulations.[18-21] Herein, an approach based on the effect of compound **1** on the stability of pre-formed membrane pores was devised. Systems featuring a large pore size and different number of glycoside molecules (0%, ~20 mol% or ~50 mol% of compound **1**) in the two-component bilayer were obtained following an equilibration procedure. The stability of the pre-formed pores was evaluated by monitoring the size of the transmembrane water cavity throughout the simulations (Figures 4 and S7), and pore closure was observed after a few tens of nanoseconds. Interestingly, by increasing the molar ratio of compound **1**, pore closure occurs in shorter time-scales, indicating that this compound does not stabilize pre-formed transmembrane pores in PC bilayers, in contrast to other membrane-active drugs.

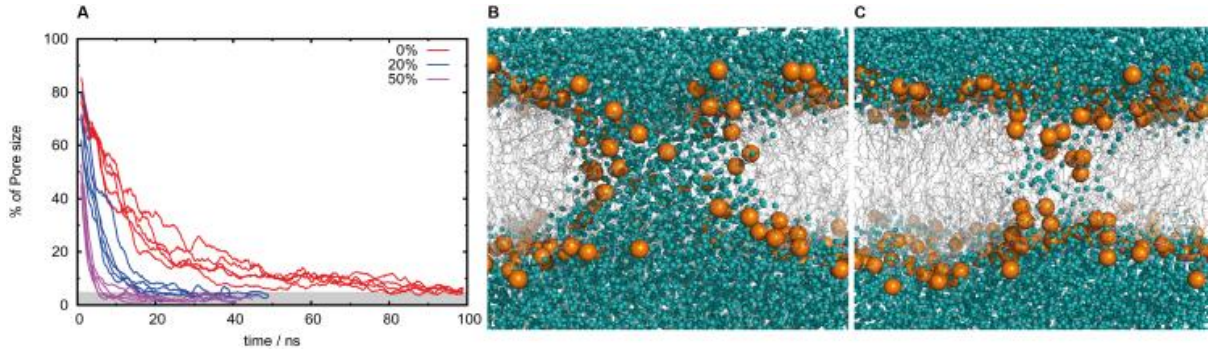

Figure 4. Estimated size of pre-formed membrane pores over time (A). The five replicates of each system, namely, pure DMPC (control, red) and mixtures containing ~20% (blue) or 50% (pink) of compound 1 are presented. A full pore (B) corresponds to a region with ~1800 water molecules between leaflets. The gray region represents very small pore sizes (C) and, in many cases, complete closure of the pore. Pore size was estimated using the number of water molecules in the interior of the transmembrane cavity.

Deoxy glycoside impact on membrane structural properties was investigated by simulations of a series of glycoside-DMPC binary mixtures in a hydrated bilayer environment

(glycosides **1**, **4** and **8**), as well as octyl β-D-glucopyranoside (OG) and dodecyl β-D-glucopyranoside (DG), both exhibiting detergent properties[22-23] and whose effect on model phosphatidylcholine membrane systems has been previously studied experimentally (Figures S8-S14).[24] To evaluate their effect on phospholipid acyl chain ordering, we computed the deuterium order parameters $|S_{CD}|$ (Figures S9-S11). Glycosides **1**, **4** and **8** promote an ordering of phospholipid acyl chains, this effect being slightly more pronounced for glycosides featuring less hydrophilic headgroups, while binary mixtures with OG or DG show a different behaviour, e.g. addition of DG to the bilayer has only a negligible effect on DMPC acyl chains. Furthermore, increasing OG molar fractions promotes a decrease in DMPC acyl chain ordering, in reasonable agreement with the literature.[24] Therefore, the results clearly show a different behaviour for the deoxy glycosides when compared to alkyl glucoside detergents and highlight that sugar deoxygenation modulates the effect of these molecules over a lipid bilayer mimicking human cell membrane, thus giving molecular insights into the low toxicity observed in Caco-2 cells.

Interaction of selected alkyl deoxy glycosides with PE bilayers

In the quest for deoxy glycoside mode of action, the crucial findings rely on the selectivity for *Bacillus* spp., cytoplasmic membrane composition, and the absence of specific protein targets, converging into a phospholipid molecular target, as cell membranes with exposed PE showed the highest susceptibility. A unique biophysical feature of PE is its propensity to adopt an inverted hexagonal (H_{II}) phase while PC lipids form the most stable bilayer (lamellar) phases, namely the fluid L_α phase. Progressive increase of stress in membrane curvature resulting from L_α to H_{II} phase transition can induce structural defects in membrane morphology, increased permeability and, eventually, loss of integrity. *In vivo*, these processes can lead to cell death.[25] To understand the key role of PE, compound **1** and the

inactive glycoside **16** (Table 1), both with similar surface activity,[6] were investigated. Interaction with PE bilayers was first detected by monitoring turbidity changes at 450 nm induced by these glycosides in PE large unilamellar vesicles (LUVs). Both compounds induced a concentration-dependent turbidity increase, reflecting that significant membrane interaction with the compounds can be easily detected in the range of concentrations where the most promising agents are active. The two compounds studied show completely different trends, pointing to different interaction modes (Figure S15). PE lamellar to hexagonal phase transition was then examined by a well-established method, the temperature dependence of the steady-state fluorescence anisotropy of an appropriate probe incorporated in PE liposomes.[26-27] This method was chosen among other major techniques to study lipid polymorphism because it allows to carry out the experiment in conditions close to physiological,[28] using compound:lipid ratios and absolute compound concentration that can be directly related to those that correspond to the biological studies described above in this study.

In order to select an appropriate probe, controls were performed with multilamellar vesicles composed exclusively of POPE. Three probes already reported in the literature as detectors of phase transition were tested: 1,2-dipalmitoyl-*sn*-glycero-3-phosphoethanolamine-N-(7-nitro-2-1,3-benzoxadiazol-4-yl) (NBD-DPPE),[29] 1,2-dimyristoyl-*sn*-glycero-3-phosphoethanolamine-N-(Lissamine rhodamine B sulfonyl) (Rh-PE),[29] and 1-(4-trimethylammoniumphenyl)-6-phenyl-1,3,5-hexatriene p-toluenesulfonate (TMA-DPH).[27] Rh-PE and TMA-DPH detected the lamellar to hexagonal phase transition at 71 ºC, in agreement with T_H values reported in the literature.[29-31] In both cases, the T_H was observed as a minimum on the thermotropic dependence of fluorescence anisotropy curve where, in the first place, anisotropy decreases reflecting the increase of the motional freedom of the probe in the lamellar phase, abruptly increasing after the transition to H_{II}.[29] TMA-DPH was selected for subsequent studies as it yielded better defined curves and more precise T_H values (Figures S16

and S17). Moreover, the fluorescence anisotropy of TMA-DPH also reports on the PE order at the level of the ester/first acyl chain methyl groups, giving precious information on the effects of the compounds on the organization of the bilayer in the Lα phase and thus a deeper understanding on the biophysical mechanism behind their action.

Using multilamellar vesicles (MLVs) composed of POPE/SoyPE 3:1 mol:mol, the fluorescence anisotropy of the TMA-DPH probe over a temperature range of 24-44 ºC demonstrated a parabolic profile with a well-defined minimum at 35.3±0.6 ºC (Figure 4), corresponding to the lamellar to hexagonal phase transition temperature (T_H). Identical MLVs suspensions containing compound **1** or **16** (50 μM) were also tested and compared (Figure 5). For temperatures preceding T_H, the presence of compound **1** leads to a decrease in fluorescence anisotropy values when compared to those observed for both control and compound **16**, reflecting a decrease in the order of the lipid matrix, as opposed to compound effect on bilayers of the human cell abundant PC, a phospholipid without tendency to form hexagonal phases. On the other hand, compound **16** seems to induce order in the vesicles, when compared to the control. Moreover, while this compound does not affect T_H of the PE binary mixture (T_H=35.2±1.1°C), compound **1** clearly decreases T_H (T_H= 32.2±0.8 ºC), increasing the propensity of PE mixture to reorganize into a hexagonal phase. This observation also corroborates the different trends of turbidity and distinct mechanisms underlying membrane interactions with each compound.

Although cell membranes are more complex than liposomes, these results point to structural tendencies of lipids while interacting with glycoside **1** and support the distinct behaviour of compounds **1** and **16** against *Bacillus* spp. The bioactivity relates to PE reorganization thereby promoting lamellar to hexagonal phase transition, which emerges as the mechanism underlying membrane disruption and bactericidal activity of compound **1** over *Bacillus* species. Worth mentioning, PE constitutes only 23% of mammalian plasma membrane

phospholipids, and is present on the inner monolayer,[32] therefore not directly accessible to the antimicrobial agent, highlighting the importance of this mode of action with therapeutic potential. This new family of bactericides bares no charge, unlike highly toxic antimicrobial peptides (AMPs) which are, in general, cationic, showing strong preference for bacterial anionic lipids, such as phosphatidylglycerol or cardiolipin.[33]

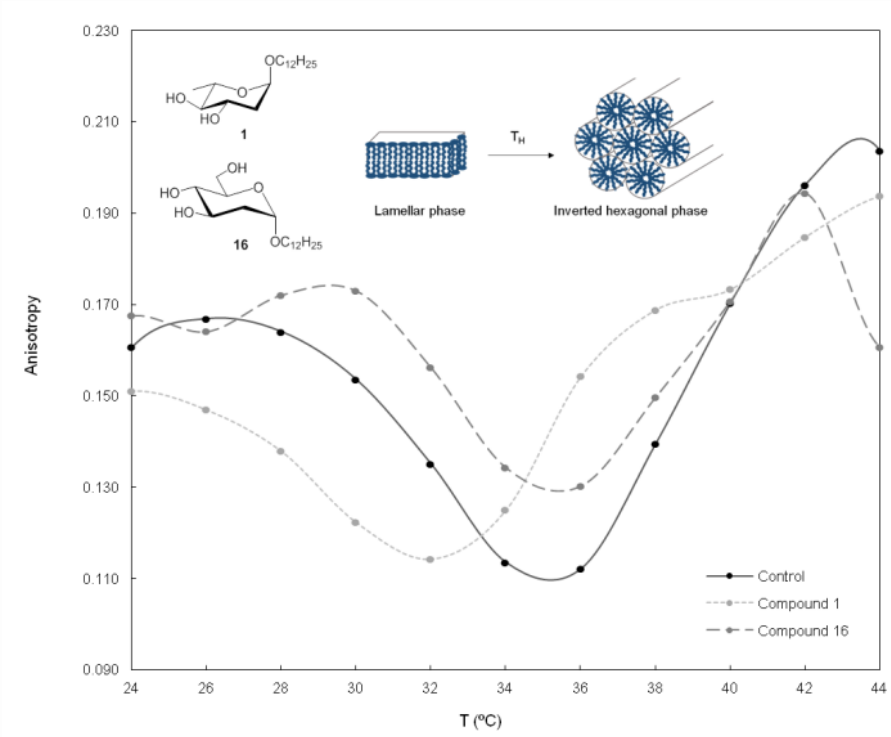

Figure 5. Steady-state fluorescence anisotropy of TMA-DPH in binary mixtures of POPE/Soy:PE 3:1 in the presence or absence of compounds **1** and **16** (50 μM). Each dot represents the mean of at least three independent replicates.

CONCLUSION

One aspect that makes targeting cell membrane so appealing is its essentiality, which does not depend on the metabolic state of the cell. Unfortunately, chemotypes with bacterial membrane disruption properties are often disregarded due to concerns over selectivity. In our view, and others,[34] membrane-targeting antibiotics have been underexploited. The well-known

differences between eukaryotic and prokaryotic cell membrane composition, encouraged us to search for new leads selectively interacting with prokaryotic cell membranes, succeeding with the development of the present family of dodecyl deoxy glycosides. The glycone conducting to the highest bactericide activity over the three *B. anthracis* strains and the lowest toxicity is that of dodecyl deoxy *C*-glycosides of D-series with α-configuration. Indeed, deoxygenation is the key modulator conducting to the unprecedented mode of action, underlying glycoside efficacy, low toxicity and selectivity. By playing a determinant role in PE-rich membrane interaction, bacteria resistance to these bactericides is avoided since cell envelope ultrastructures cannot easily change without substantial loss of function. In summary, we set forth a creative approach relying on a multidisciplinary strategy and covering chemistry, biology and biophysics, led to the discovery of new deoxy glycoside antimicrobials with a new mechanism of action, against anthrax.

EXPERIMENTAL SECTION

Chemical synthesis. Reactions were conducted under nitrogen using dried solvents, unless otherwise stated, and monitored by thin-layer chromatography carried out on silica-coated aluminium foil plates (visualized by UV or 10% H_2SO_4 in MeOH). Compounds were purified by column chromatography and their structural characterization was accessed by NMR and high-resolution mass spectrometry (HRMS) analyses. Detailed procedures and full characterization of all compounds are available in Supplementary Information.

Antimicrobial assays and bacterial strains. For results presented in table 1, the broth microdilution method on Müller-Hinton medium was employed to determine the MICs, according to the Clinical and Laboratory Standards Institute (CLSI) guidelines.[14] Three strains

of the *B. anthracis* (INSA private collection), *B. cereus* (ATCC 11778) and *E. faecalis* (ATCC 29212) were used. Compounds were incubated with bacteria for 16 h at 37 °C prior to determining the MIC, which is defined as the lowest concentration of the tested compounds at which no bacterial growth was observed. For all biological studies described below, the strains used were *B. cereus* ATCC 14579 and/or S. *aureus* ATCC 25923, unless otherwise stated. For determination of bactericidal activity, MICs were determined by a modified microdilution method also according to CLSI.[14] The minimum bactericidal concentration (MBC) was determined in Müller-Hinton Agar, and bacterial growth was assessed at 17 h. MBC was considered the lowest concentration of compound where no bacterial growth was observed (average of at least 3 independent experiments). A very similar protocol was used for the time-kill assay, where the incubation was performed with the desired starting bacterial population (10^6, 10^7, and 10^8 cells/mL). Then, at desired incubation times, aliquots were retrieved, serial diluted and transferred to MHA, where the number of colony forming units (CFU) was determined (experimental details for MIC, MBC and time-killing curves are available in SI).

Resistance development: Resistant mutants to the major families of antibiotics were created using a variant of the gradient plate methodology,[35] for the following antibiotics of diverse classes: erythromycin (macrolide), penicillin, vancomycin (glycopeptide), ciprofloxacin (quinolone), tetracycline (Sigma-Aldrich). The plates were inoculated with 100 µL of 0.5 McFarland bacterial suspension of *B. cereus* ATCC 14579 strain, carefully dispersed on the agar surface using spreading spheres. The plates were incubated at 30 ºC for 24 h. After, the colony closest to the higher concentration in the gradient was collected, re-suspended and re-inoculated in new fresh gradient plates. This procedure was repeated for 15 days.

Cytotoxicity. Caco-2 cell culture and viability assays were performed using a pre-established methodology.[36] Caco-2 cells were grown in DMEM high glucose supplemented with 10% foetal bovine serum, 2 mM glutamine, 100 U/mL penicillin, and 100 μg/mL streptomycin, in a humidified incubator at 37 °C with a 5 % CO_2 atmosphere. The cells were trypsinized twice a week with trypsin/EDTA (0.05%/0.02%) and the medium was also changed twice a week. Determination of cell growth was performed using the MTT (3-[4,5-dimethylthiazol-2-yl]-2,5-diphenyltetrazolium bromide) assay. On day 1, 20,000 cells/well were seeded into 96-well plates in a volume of 100 μL. On day 2, the different drugs concentration (0.1–100 μM) were added to the plate. In all the experiments, the various drug-solvents (EtOH, DMSO) were added in each control to evaluate a possible solvent cytotoxicity. After the established incubation time with drugs, MTT (0.5 mg/mL) was added to each well, and after 3-4 h incubation at 37 °C, the supernatant was removed. The formazan crystals were solubilized using 100 μL of DMSO/EtOH (1:1) and the absorbance values at 570 nm and 630 nm were determined on the microplate reader Victor3 from Perkin Elmer Life Sciences.

Preparation of protoplasts and spheroplasts. Bacterial spheroplasts and protoplasts [LPS and peptidoglycan-free bacteria] were prepared by harvesting bacterial cells by centrifugation (10,000 g for 10 min at 4 ºC) and washing with 10 mM Tris-HCl (pH 8) at 4 ºC. Cells were resuspended, supplemented with sucrose (0.6 M) at room temperature. Lysozyme (0.5 mg/mL) (Sigma Aldrich) was added, very slowly aiming to decrease the aggregation of plasts, after 30 min of incubation. The plasts (used at the same concentration as in the biological activity assay) were incubated with the desired compound and with polymyxin B as a positive control, at various concentrations.

Morphologic evaluation by atomic force microscopy. Samples containing *B. cereus* ATCC 14579 (10^6 CFU/mL) in MH medium were incubated with compound **1** at various concentrations (0, 8 and 16 μg/mL) and after 2 h aliquots were taken. A drop (40 μL) containing the bacteria was deposited onto freshly cleaved mica surfaces for 30 min, gently washed with Milli-Q water and dried under mild nitrogen flux. The surface was examined ex-situ, at ambient temperature (21 ºC), using Nanoscope IIIa multimode atomic force microscope (Digital Instruments, Veeco, Santa Barbara, CA) and etched silicon tips (TESP-V2, Bruker) with a resonance frequency of ca. 300 kHz. Images were acquired with scan rates between 1.2 and1.5 Hz. It is worth to note that washing and drying steps, as wells as tip repetitive scanning did not influence the results presented in this work.

Differential metabolomics analysis. Bacterial metabolic response to **1** was evaluated using Phenotype MicroArrays (Biolog), assessing the metabolism of 95 different carbon sources by *B. cereus*. PM1 microplates were prepared with PM inoculating fluid (100 μL), sealed, shielded from light and incubated at 35 ºC with orbital shaking. Compound **1 (**at the final concentration of 16, 8, 4 and 0 μg/mL) was added at 1h of incubation. Bacterial growth was monitored by OD_{590nm} at time 0', at 30', at 60' after incubation, then hourly for 27 h.

Susceptibility of Bacillus spores. Production of spores from *B. cereus* ATCC 14579 was carried out by incubation at 37 ºC in sporulation medium (CCY – *Bacillus* t Sporulation media:[37] 1g/L acid casein hydrolysate, 1 g/L bacto casitone (pancreatic casein hydrolysate), 0.4 g/L yeast extract, 20 mg/L L-glutamine, 0.06% (v/v) glycerol, 1.77 g/L KH_2PO_4, 4.53 g/L K_2HPO_4, 0.5mM $MgCl_2.{}_6H_2O$, 0.01mM $MnCl_2.{}_4H_2O$, 0.05 mM $ZnCl_2$, 0.2 mM $CaCl_2.{}_6H_2O$, 0.05 mM $FeCl_3.{}_6H_20$.)[37] for 96 h. Purification of the spores was achieved by centrifugation at 4 ºC, 15000 g and washing 10 times with Milli RO water. For preparation to the susceptibility assays, the

spores were suspended in 1 mM PBS and 0.01 % Tween 20, then submitted to heat treatment at 70 ºC for 30 min. Germination was achieved in AGFK buffer (30 mM L-asparagine, 5,6 mM D-Glucose, 5,6 mM D-Fructose, 20 mM KCl and 50 mM Tris-HCl, pH 8,4) at 37 ºC. Susceptibility to compound **1** was assessed at all the preparation steps, 20 min and 2 h after the germination process.

Computational Methods. DFT calculations were performed with Gaussian09.[38] All geometry optimizations and subsequent frequency calculations were carried out with PBE0[39]/6-311G**[40]. Solvent effects were accounted by the integral equation formalism of the polarizable continuum model (IEFPCM) [41] on the electronic density (SMD)[42]. MM/MD simulations were performed using GROMACS version 4.0.7.[43-44] The GROMOS 54A7 force field,[45] which already includes phosphatidylcholine corrections,[46] was employed, along with the GROMOS 56A$_{CARBO}$ force field[47] to model carbohydrates. All systems were solvated with adequate number of SPC[48] water molecules in periodic tetragonal boxes. The simulations were performed in an NPT ensemble with temperature and pressure being kept at 308 K and 1 bar, respectively. Initial configurations for the membrane pore and glycoside/phospholipid bilayer simulations were pre-equilibrated and energy minimized/initialized following stepwise procedures as described in SI. Errors were computed as the correlation-corrected standard deviation in the mean following standard methods.[49]

Steady state fluorescence anisotropy. 1-palmitoyl-2-oleoyl-*sn*-glycero-3-phosphoethanolamine (POPE) and 1,2-Diacyl-*sn*-glycero-3-phosphoethanolamine from soybean (SoyPE) were purchased from Avanti Polar Lipids (Alabaster, AL, USA) and Sigma-Aldrich (St. Louis, MO, USA) respectively. TMA-DPH was purchased from Molecular Probes, Inc. (Eugene, OR, USA). HEPES buffer contains 10 mM HEPES, 150 mM NaCl, 1 mM EDTA

(pH 7.4). LUVs were extruded with Whatman® nuclepore polycarbonate filters (Sigma-Aldrich, St. Louis, USA) in a mini-extruder (Avanti Polar Lipids, Alabaster, USA). Turbidity was measured in a spectrophotometer (Beckam Instruments Inc., Fullerton, USA), while steady-state fluorescence anisotropy measurements were made using a Horiba Jobin Yvon Spex Fluorolog 3-22/Tau 3 spectrofluorometer (Kyoto, Japan). MLVs containing 0.4 mol % TMA-DPH were obtained by co-dissolving the lipids (POPE:soyPE 3:1), probe and glycoside in chloroform, followed by solvent evaporation under nitrogen stream and high vacuum desiccation. Dried lipid films were then hydrated with 10 mM HEPES buffer (pH 7.4) to the desired final concentration (0.5 mM lipid, and 0/50 μM glycoside). Lipid suspensions were subjected to 5 cycles of freezing and thawing at 25 ºC Anisotropy was measured exciting samples at 360 nm and collecting emission at 430 nm, using 2.7 nm slit width. Temperature was maintained with an isothermal bath and was monitored with a thermistor, inserted into the sample chamber.

Vesicle aggregation: MLVs composed exclusively of 2 mM POPE were prepared as above, and then converted into LUVs by 17 passages through two stacked 0.1 μm polycarbonate filters in a mini-extruder, at 30 ºC. LUVs were titrated with the compounds **1** or **19** in ethanol, or ethanol (control) and, after 5 min, turbidity was measured at 450 nm, at 35 ºC. Zero absorbance was set with LUVs, prior to addition of glycoside.

Acknowledgments: The European Union is gratefully acknowledged for the support of the project “Diagnostic and Drug Discovery Initiative for Alzheimer's Disease” (D3i4AD), FP7-PEOPLE-2013-IAPP, GA 612347. The authors thank the Management Authorities of the European Regional Development Fund and the National Strategic Reference Framework for the support of the Incentive System – Research &Technological Development Co-Promotion FACIB Project nr. 21457. Fundação para a Ciência e a Tecnologia is also acknowledged for the

support of project UID/Multi/0612/2013, and for the Ph.D. grants co-sponsored by CIPAN SFRH/BDE/51998/2012 (CD) and SFRH/BDE/51957/2012 (JPP).

Author contributions (detailed): A. P. Rauter designed the project and most of the experiments, and coordinated the work carried out by all contributors, supervising also the synthetic work. C. Dias, R. Nunes, A. F. Almeida, N. M. Xavier and P. Serra were involved in the synthesis of alkyl deoxy glycosides and their *C*-glycosyl analogs. The role of A. Martins and A. Pelerito is related to the antimicrobial activity assays over *B. anthracis*, while toxicity was assessed by J. Pais and M. Contino, supervised by N. Colabufo. Biology experiments were performed by J. Pais supervised by R. Dias and R. Tenreiro. J. Pais, M.S. Santos and A. Viana were involved in bacteria morphological assessment and the AFM images were obtained by J. Pais and A. Viana. Computational studies were carried out by R. Nunes and D. Vila-Viçosa, supervised by M. Machuqueiro. R. F. M. Almeida has conceived the biophysical approach and experiments realized by C. Dias. M. C. Oliveira performed the HRMS experiments for the characterization of compounds. C. Dias, R. Nunes and A. P. Rauter took an active part in writing the paper.

3.1 Supporting Information for "The First Sugar-Based Bactericides Targeting Phosphatidylethanolamine-Enriched Membranes"

Table of contents **Page**

1 | Materials and Methods – Additional information

Chemical synthesis

Starting materials and reagents were purchased from Sigma–Aldrich, Fluka and Acros. The solvents were dried prior to use with 4 or 3 Å (methanol) molecular sieves. TLC was carried out on aluminum sheets (20 cm x 20 cm) coated with 0.2 mm silica gel 60 F-254

(Merck) and detection was accomplished by spraying the plates with a solution of H_2SO_4 in ethanol (10%) followed by heating at 120 °C. The compounds were purified by column chromatography (CC) using silica gel 60*G* (0.040–0.063 mm, Merck) or silica gel 60*G* (0.015–0.040 mm, Merck). Melting points were obtained with a SMP3 Melting Point Apparatus, Stuart Scientific, Bibby. Optical rotations were measured with a Perkin–Elmer 343 polarimeter. NMR spectra were recorded with a Bruker Avance 400 spectrometer at 298 K operating at 100.62 MHz for ^{13}C NMR and at 400.13 MHz for ^{1}H NMR. The solvents used were $CDCl_3$ with 0.03% TMS and CD_3OD (Sigma–Aldrich). The chemical shifts are reported as δ (ppm) and the coupling constants (*J*) are given in Hz. *C*-glycosides are named systematically but glycone NMR data is given with primed locants, while primed locants are given for the dodecyl chain of *O*-/ and *S*-glycosides.

High resolution mass spectra of new compounds were acquired on a Bruker Daltonics HR QqTOF Impact II mass spectrometer (Billerica, MA, USA). The nebulizer gas (N_2) pressure was set to 1.4 bar, and the drying gas (N_2) flow rate was set to 4.0 L/minute at a temperature of 200 °C. The capillary voltage was set to 4500 V and the charging voltage was set to 2000 V.

Starting materials and intermediate compounds that are not cited in the main text are here numbered in increasing order of appearance and preceded with S. In one-pot procedures covering several steps, the intermediates were isolated for characterization purposes and data is given for new compounds.

A. Synthesis of dodecyl 2-deoxyglycosides and dodecyl 2-deoxy-1-thioglycosides

The one-pot approach covering glycosylation and deacylation gave pure glycosides **1**, **1b** and **10**-**13**. Isolation of protected compounds **S6-S13** was required to access the pure unprotected anomers, whose resolution via the one-pot procedure was not achieved.

Deprotection was accomplished by effective removal of the acetyl groups via Zemplén reaction, and benzyl groups by catalytic hydrogenation, affording the target glycosides in almost quantitative yields (Scheme S1). Glycal starting materials were synthesized as described below.

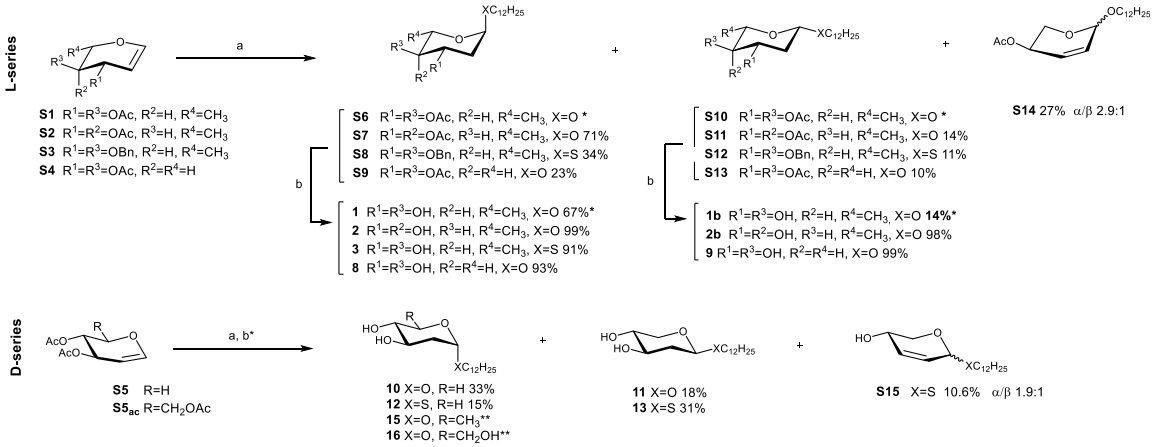

Scheme S1. Synthesis of dodecyl 2-deoxy glycosides. Reagents and conditions: a) $C_{12}H_{25}XH$, TPHB, DCM; b) NaOMe/MeOH (for compounds **1**,**1b**, **2**, **2b**, **8**-**13**) or H_2, Pd/C, MeOH (for compound 3); *one-pot procedure; **Synthesized starting from **S5**$_{ac}$ as described.[6]

A.1 Glycal synthesis (S1, S2, S4 and S5)

General procedure. To a solution of the free sugar (12.0 mmol) in pyridine (10 mL/g), acetic anhydride (2 equiv./OH) and DMAP (0.3 mmol) were added. Reaction mixture was left to stir at room temperature for 2 h. Then, the solution was diluted with dichloromethane and washed 3 times with HCl 2M and then with water. Organic phase was dried with anhydrous $MgSO_4$, filtered and concentrated under vacuum, affording the peracetylated sugar as a colourless oil. The resulting product was then dissolved in glacial acetic acid (10 mL/g) to which methanol (18 mmol, 0.7 mL, 1.5 equiv.) and acetyl bromide (2.7 mL, 36 mmol, 3 equiv.) were added. Reaction mixture was kept stirring at room temperature protected from light and under nitrogen. After 3h, reaction mixture was diluted with dichloromethane and washed 3

times with saturated $NaHCO_3$ and with brine. Organic phase was dried with anhydrous $MgSO_4$, filtered and concentrated under vacuum, affording the corresponding glycosyl bromide.

To a solution of glycosyl bromide in acetone (5 mL/mmol), sodium dihydrogen phosphate (0.26 mol, 41.21 g, 22 equiv.) and zinc (0.18 mol, 11.77g, 15 equiv.) were added and stirred vigorously, at room temperature. After 10 min, water (0.5 mL/mmol) was also added and kept stirring for 1h30. Reaction mixture was extracted with EtOAc, and washed twice with saturated $NaHCO_3$ and then brine. Organic phase was dried with anhydrous $MgSO_4$, filtered and concentrated under vacuum. The resulting residue was purified with column chromatography with hex/EtOAc, affording the corresponding glycal.

3,4-Di-*O*-acetyl-1,5-anhydro-2,6-dideoxy-L-*arabino*-hex-1-enitol (S1). Obtained from L-rhamnose (8.0 g, 48.7 mmol) as a colourless oil, in 67% yield (7.0 g, 32.7 mmol). R_f =0.7 (EtOAc/ Pet. Et. 1:2). **^{1}H RMN** ($CDCl_3$) δ 6.38 (br d, 1H, $J_{1,2}$ = 6.1 Hz, H-1), 5.35 (m, 1H, H-3), 5.03 (dd, 1H, $J_{3,4}$=6.4 Hz, $J_{4,5}$=7.0 Hz, H-4), 4.79 (dd, 1H, $J_{2,3}$= 3.0 Hz, H-2), 4.11 (quint, 1H, $J_{4,5}$= $J_{5,6}$=7.0 Hz, H-5), 2.09 (s,, 3H, -OAc), 2.05 (s, 3H, -OAc), 1.31 (d, 3H, H-6). ^{13}C RMN ($CDCl_3$) δ 170.7, 169.9 (C=O, OAc), 145.0 (C-1), 98.80 (C-2), 72.5 (C-5), 71.8 (C-4), 68.3 (C-3), 21.1 (-CH_3, OAc), 20.7 (-CH_3, OAc), 17.1 (C-6). Spectroscopic data is in full agreement with the literature.[50]

3,4-Di-*O*-acetyl-1,5-anhydro-2,6-dideoxy-L-*lyxo*-hex-1-enitol (S2). Obtained from L-fucose (1.7 g, 10.4 mmol) as an hygroscopic white solid, in 36% yield (0.794 g, 3.7 mmol). R_f = 0.66 (EtOAc/hex 1:5); $[\alpha]_D^{20}$= +8 º (c1.0, $CHCl_3$); **^{1}H RMN** ($CDCl_3$) δ 6.47 (br d, 1H, $J_{1,2}$ = 6.3 Hz, H-1), 5.58 (m, 1H, H-3), 5.29 (dd, 1H, $J_{3,4}$=1.1 Hz, $J_{4,5}$ = 3.1 Hz, H-4), 4.64 (dd, 1H, $J_{2,3}$=1.3 Hz, H-2), 4.06 (q, 1H, $J_{5,6}$=6.5 Hz, H-5), 2.16 (s, 3H, -OAc), 2.02 (s, 3H, -OAc), 1.28 (d, 3H, H-6). ^{13}C RMN ($CDCl_3$) δ 170.6 (C=O, -OAc), 170.3 (C=O, -OAc), 146.0 (C-1), 98.1 (C-2), 71.4 (C-5), 66.1 (C-4), 64.9 (C-3), 21.1 (-CH_3, OAc), 20.7 (-CH_3, OAc), 20.6 (-CH_3, OAc), 16.4 (C-6). Spectroscopic data is in full agreement with the literature.[51]

3,4-Di-*O*-acetyl-1,5-anhydro-2-deoxy-L-*threo*-pent-1-enitol (S4). Obtained from L-xylose (0.9 g, 6.0 mmol) as a colourless liquid, in 66% yield (0.80 g, 4.0 mmol). R_f = 0.76 (Pet. Et./EtOAc 3:1); **^{1}H NMR** ($CDCl_3$) δ 6.61 (d, 1H, $J_{1,2}$ = 5.6 Hz, H-1), 5.00-4.95 (m, 3H, H-2, H-3, H-4), 4.20 (br d, 1H, $J_{5a,5b}$ = 12.3 Hz, H-5a), 3.98 (br d, H-5b), 2.10 (s, 3H, -OAc), 2.07 (s, 3H, -OAc). **^{13}C NMR** ($CDCl_3$) δ 169.9 (C=O, -OAc), 169.8 (C=O, -OAc), 148.0 (C-1), 97.4 (C-2), 67.2 (C-4), 63.6 (C-5), 63.4 (C-3), 21.1 (-CH_3, OAc), 21.0 (-CH_3, OAc).

3,4-Di-*O*-acetyl-1,5-anhydro-2-deoxy-D-*threo*-pent-1-enitol (S5). Obtained from D-xylose (10.0 g, 66.61 mmol) as a hygroscopic white solid, in 65% yield (8.658 g, 43.29 mmol). R_f = 0.34 (EtOAc/Petrol. ether 1:6); NMR data was in full agreement with that described above for its enantiomer (compound S**4**) and with the literature.[50]

***A1.1. Synthesis of glycal S3*.**

3,4-Di-*O*-benzyl-1,5-anhydro-2,6-dideoxy-L-*arabino*-hex-1-enitol (S3). To a solution of glycal **S1** (2.197g, 10.26 mmol) in THF (70 mL), powdered NaOH (4.24 g, 102.60 mmol, 10 equiv.) and TBAI (1.895g, 5.13 mmol, 0.5 equiv.) were added. After 10 min stirring at room temperature, benzyl bromide (3.7 mL, 30.78 mmol, 6 equiv.) was added and the mixture was stirred for 3h. Reaction mixture was then poured in water (150 mL) and extracted with dichloromethane (3x100 mL). Organic phase was washed with water, dried with anhydrous $MgSO_4$, filtered and concentrated under vacuum. The resulting residue was purified by column chromatography with hex/EtOAc 60:1, affording title compound (0.134 g) as a colourless oil in 80% yield. R_f = 0.71 (hex/EtOAc 6:1); $[\alpha]_D^{20}$= +16 º (c1.0, $CHCl_3$); **^{1}H RMN** ($CDCl_3$) δ 7.38-7.26 (m, 10H, -Ph) 6.36 (d, 1H, $J_{1,2}$ = 6.0 Hz, H-1), 4.90-4.84 (m, 2H, H-2, CH_2Ph), 4.71-4.64 (m, 2H, CH_2Ph), 4.57 (d, 1H, CH_2Ph), 4.21 (br d, 1H, $J_{2,3}$ = 6.2 Hz, H-3), 3.95 (qd, 1H, $J_{5,6}$=6.7 Hz, H-5), 3.48 (dd, 1H, $J_{3,4}$= 8.7 Hz, H-4), 1.36 (d, 3H, H-6). **^{13}C RMN** ($CDCl_3$) δ

144.7 (C-1), 138.4, 138.2, 128.4, 127.9, 127.7, 127.6 (Ph, -OBn), 100.1 (C-2), 79.5 (C-4), 76.4 (C-3), 74.0 (C-5) 73.9 ($\underline{C}H_2$, -OBn), 70.5 ($\underline{C}H_2$, -OBn), 17.5 (C-6). Spectroscopic data is in full agreement with the literature.[52]

A.2. Synthesis of dodecyl 2-deoxyglycosides 1/1b, 10-13 (one-pot procedure)

General one-pot procedure. Glycal (**S1** or **S5,** 5.0 mmol) was dissolved in dichloromethane (10 mL/g), followed by the addition of TPHB (0.1 equiv or 0.3 equiv. for reaction with dodecan-1-ol or dodecan-1-thiol, respectively), and dodecan-1-ol (1.5 equiv. for **S1** and 1.2 equiv. for **S5**) or dodecan-1-thiol (2 equiv). The reaction was stirred at room temperature for 1 h (**1**, **1b**), 2 h (**10, 11**) or overnight (**12**, **13**). Reaction mixture was either directly neutralized with a free base resin (e.g. IRA-400 for **1**, **1b** or Amberlyst A21 for **10**, **11**) and concentrated under vacuum, or diluted with dichloromethane, washed with saturated $NaHCO_3$, and water, and the organic phase was dried with magnesium sulfate and concentrated in vacuum (**12**, **13**). In all cases, the resulting residue was dissolved in methanol (0.1mL/mg) and a freshly prepared solution of 1% NaOMe in MeOH (0.1 mL/100mg residue) was added. The mixture was stirred at room temperature for 1 h. Neutralization with Amberlite (IR-120) was followed by filtration and evaporation of the solvent. The residue was purified by column chromatography (CC).

Dodecyl 2,6-dideoxy-α-L-*arabino*-hexopyranoside (1). Obtained from glycal **S1** in 67% isolated yield after CC eluted with EtOAc. Physical and spectroscopic data in full agreement with the literature.[6]

Dodecyl 2,6-dideoxy-β-L-*arabino*-hexopyranoside (1b). Obtained from glycal **S1** in 14% isolated yield after CC eluted with EtOAc. Physical and spectroscopic data in full agreement with the literature.[6]

Dodecyl 2-deoxy-α-D-*threo*-pentopyranoside (**10).** Obtained from glycal **S5** in 33% isolated yield after CC eluted with hex/EtOAc 5:1; m.p. 53.6-54.4 ºC; $[\alpha]^{20}_{D}$ = +81º (*c* 1; MeOH); R_f = 0.24 (hex/EtOAc 2:1); **^{1}H-RMN** (400 MHz, $CDCl_3$) (δ/ppm; J/Hz): δ 4.84 (br dd, 1H, $J_{1,2e}$ = 1.7 Hz, $J_{1,2a}$= 3.3 Hz, H-1), 3.92 (td, 1H, $J_{3,2a}$ = 5.5, $J_{3,4}$= 12.0 Hz, H-3), 3.68 (dd, 1H, $J_{5e,5a}$= 9.7, $J_{4,5e}$= 4.1 Hz, H-5e), 3.66-3.60 (m, 1H, H-1'b), 3.59-3.46 (m, 2H, H-4, H-5a), 3.37-3.31 (m, 1H, H-1a'), 2.44 (s, 1H, OH-4), 2.35 (s, 1H, OH-3), 2.12 (ddd, 1H, $J_{2e,2a}$= 12.9 Hz, H-2a), 1.62 (ddd, 1H, $J_{3,2e}$= 2.0 Hz, H-2e), 1.60-1.53 (m, 2H, H-2'), 1.38-1.19 (m, 19H, H-3' to H-11'), 0.86 (t, 3H, *J*= 6.7 Hz, H-12'). **^{13}C-RMN** (100.6 MHz, $CDCl_3$) (δ/ ppm): δ 97.6 (C-1), 72.1 (C-4), 69.7 (C-3), 67.6 (C-1'), 62.1 (C-5), 37.3 (C-2), 31.9, 29.7, 29.7, 29.6, 29.6, 29.6, 29.5, 29.4, 26.2, 22.7 (C-2' – C-11'), 14.3 (C-12'). **HRMS:** Calcd for $[M+Na]^+$ 325.2349; Found: 325.2338 (error 3.5 ppm).

Dodecyl 2-deoxy-β-D-*threo*-pentopyranoside (**11**). Obtained from glycal S5 in 18% isolated yield after CC eluted with hex/EtOAc 5:1; M.p. 68.1-68.7 ºC; $[\alpha]^{20}_{D}$ = −72 (*c* 1; MeOH); R_f = 0.19 (hex/EtOAc 2:1) **^{1}H-RMN** (400 MHz, $CDCl_3$) (δ/ppm; J/Hz): δ 4.78 (br t, 1H, $J_{1,2a}$ =$J_{1,2e}$= 3.1 Hz, H-1), 4.14 (dd, 1H, $J_{5a,5e}$= 12.5 Hz; $J_{4,5a}$= 2.3 Hz, H-5a), δ 3.78-3.71 (m, 2H, H-3, H-1a), 3.64 (s, 1H, OH-4), 3.48-3.37 (m, 3H, H-4, H-1b, OH-3), 2.24-2.15 (m, 2H, H-2e), 1.78 (dt, 1H, $J_{3,2a}$= 8.1 Hz, $J_{2e,2a}$= 14.3 Hz, H-2a), 1.64-1.56 (m, 3H, H-2'),1.39-1.19 (m, 19H, H-2' a H-11'), 0.89 (t, 3H, *J*= 6.6 Hz, H-12). **^{13}C-RMN** (100.6 MHz, $CDCl_3$) (δ/ ppm): δ 98.1 (C-1), 69.3 (C-4), 68.6 (C-1'), 67.9 (C-3), 60.8 (C-5), 37.3 (C-2), 31.9, 29.7, 29.6, 29.6, 29.6, 29.5, 29.4, 29.4, 26.2, 22.7 (C-2' to C-11'), 14.3 (C-12'). **HRMS:** Calcd for $[M+Na]^+$ 325.2349; Found: 325.2336 (error 4.1 ppm).

Dodecyl 2-deoxy-1-thio-α-D-*threo*-pentopyranoside (**12**). Obtained from **S5** in 15% isolated yield after CC eluted with toluene/EtOAc 3:2 as an oil; R_f = 0.38 (EtOAc/tol. 3:2); m.p. 75.9-78.9 ºC; $[\alpha]^{20}_{D}$= +130º (c1.0, $CHCl_3$); **^{1}H RMN** (MeOD) δ 5.22 (t, 1H, $J_{1,2}$=4.0 Hz, H-1), 3.80 (dd, 1H, $J_{4,5ax}$=8.9 Hz, $J_{5ax,5eq}$=11.5 Hz, H-5ax), 3.73 (ddd, 1H, $J_{3,4}$=8.0 Hz, $J_{2a,3}$=9

Hz, H-3), 3.65 (dd, $J_{4,5eq}$= 4.7 Hz, H-5eq), 3.37 (ddd, H-4), 2.60 (dt, 1H, $J_{1'a,1'b}$=12.5 Hz, $J_{1'a,2'}$= 7.0 Hz, H-1'a), 2.54 (dt, 1H, $J_{1'b,2'}$= 7.0 Hz, H-1'b), 2.10 (dt, 1H, $J_{1,2eq}$=3.9 Hz $J_{2ax,2eq}$=13.5 Hz, H-2eq), 1.88 (ddd, $J_{1,2a}$=4.5 Hz, 1H, H-2ax),1.66-1.55 (m, 2H, H-2'), 1.44-1.22 (m, 18H, H-3' to H-11'), 0.90 (t, 3H, $J_{11,12}$= 7.1 Hz, H-12'), **^{13}C RMN** (MeOD) δ 81.8 (C-1), 72.2 (C-4), 70.1 (C-3), 64.7 (C-5), 38.5 (C-2), 33.1 (C-1'), 31.7, 30.8, 30.7, 30.5, 30.3, 29.9 (C-2' a C-10'), 23.8 (C-11'), 14.5 (C-12'). **HRMS:** Calcd for $[M+Na]^+$ 341.2121; Found: 341.2112.

Dodecyl 2-deoxy-1-thio-β-D-*threo*-pentopyranoside (**13).** Obtained from **S5** in 31% isolated yield after CC eluted with toluene/EtOAc 3:2 as an oil; R_f = 0.26 (EtOAc); m.p. 84.9-86.5; $[\alpha]_D^{20}$= −54º (c1.0, $CHCl_3$); **^{1}H RMN** (MeOD) δ 4.61 (dd, 1H, $J_{1,2a}$=11.3 Hz, $J_{1,2e}$=1.8 Hz, H-1), 3.93 (dd, 1H, $J_{4,5eq}$=5.0 Hz, $J_{5ax,5eq}$=11.4 Hz, H-5eq), 3.52 (br ddd, 1H, $J_{3,4}$=10.0 Hz, $J_{2a,3}$=5 Hz, $J_{2e,3}$=3.9 Hz, H-3), 3.38 (ddd, $J_{4,5ax}$= 11.4 Hz, H-4), 3.18 (t, $J_{4,5ax}$=$J_{4,5eq}$=11.4 Hz, H-5ax), 2.69 (dt, 1H, $J_{1'a,1'b}$=13.0 Hz, $J_{1'a,2'}$= 7.2 Hz, H-1'a), 2.61 (dt, 1H, $J_{1'b,2'}$= 7.4 Hz, H-1'b), 2.15 (ddd, 1H, $J_{1,2ax}$=$J_{1,2eq}$=1.9 Hz, $J_{2ax,2eq}$=12.8 Hz, H-2eq), 1.66-1.55 (m, H-2'), 1.55-1.49 (ddd, 1H, $J_{1,2a}$=4.5 Hz, H-2ax), 1.43-1.22 (m, 18H, H-3' a H-11'), 0.90 (t, 3H, $J_{11,12}$= 6.5 Hz, H-12'), **^{13}C RMN** (MeOD) δ 82.2 (C-1), 73.3 (C-3), 72.3 (C-4), 70.5 (C-5), 40.2 (C-2), 33.1 (C-1'), 31.7, 31.0 30.8, 30.7, 30.5, 30.3, 29.9 (C-2' a C-10'), 23.8 (C-11'), 14.5 (C-12'). **HRMS:** Calcd for $[M+Na]^+$ 341.2121; Found: 341.2113.

Dodecyl 2,3-dideoxy-1-thio-α-D-*glycero*-pent-2-enopyranoside (S15α). Obtained from glycal **S5** as an anomeric mixture (1.9:1 α/β) in 10.6% isolated yield, after CC eluted with toluene. R_f = 0.88 (Toluene/EtOAc 3:2). **^{1}H RMN** (Acetone-d_6) δ 5.95 (br dd, $J_{2,3}$=10 Hz, H-3α), 5.88 (dd, $J_{1,2}$=3 Hz, $J_{2,3}$=10 Hz, H-2α), 5.78-5.65 (m, H-2β and H-3β), 4.48 (br s, H-1α), 4.44 (d, $J_{1,2}$=7.53 Hz, H-1β) , 4.18 (dd $J_{4,5eq}$=2.4 Hz, $J_{5ax,5eq}$=12 Hz, H-5eq α), 4.17 (H-4β, under H-5eq α signal), 4.03 (br s, OH α), 3.80 (br s, H-4α), 3.64 (d, H-5ax α), 3.55-3-39 (m, H-5β), 2.72-2.55 (m, H-1'αβ), 1.68-1.53 (m, H-2'αβ), 1.44-1.35 (m, H-3'αβ), 1.34-1.20 (m, H-4' to H-11'αβ), 0.88 (t, $J_{11,12}$=7 Hz, H-12'αβ).**^{13}C RMN** (Acetone-d_6) δ 133.1 (C-3β), 130.0 (C-

2β), 129.9 (C-2 α), 129.1 (C-3α) 80.20 (C-1α), 72.9 (C-4β), 67.6 (C-5β), 65.5 (C-5α), 62.1 (C-4α), 51.3 (C-1β), 32.7 (C-1'αβ), 31.9 (C-2'α), 31.6 (C-2'β), 30.9 – 29.6 (C-3' to C10', under acetone-d_6 signαl), 32.4 (C-11'αβ), 14.4 (C-12'αβ); **HRMS:** Calcd for $[M+H]^+$ 301.2196; Found: 301.2196 (error 0.0 ppm).

A.3. Synthesis of dodecyl glycosides 2/2b, 3, 8 and 9 (two step procedure - glycosylation and deprotection)

A.3.1. General glycosylation procedure. Glycal **(S2, S3** or S**4,** 5.0 mmol**)** was dissolved in dichloromethane (10 mL/g), followed by the addition of TPHB (0.1 equiv or 0.3 equiv. for reaction with dodecan-1-ol or dodecan-1-thiol, respectively), and dodecan-1-ol or dodecan-1-thiol (2 equiv). The reaction was stirred at room temperature for 3h (**S7/S11**) or overnight (**S9**/**S13** and **S8**/**S12**)**.** Reaction mixture was diluted with dichloromethane, washed with saturated $NaHCO_3$ and water, and the organic phase was dried with magnesium sulfate and concentrated in vacuum. The residue was purified by column chromatography.

Dodecyl 2,6-dideoxy-3,4-di-*O*-acetyl-α-L-*lyxo*-hexopyranoside (S7). Obtained from glycal **S2** in 71% isolated yield, after CC eluted with hex/EtOAc 17:1. R_f = 0.43 (hex/EtOAc 5:1); $[\alpha]_D^{20}$ = -104º (*c*1.0, $CHCl_3$); m.p. 40.9-41.7 ºC, **^{1}H RMN** ($CDCl_3$) δ 5.26 (br dd, 1H, $J_{2ax,3}$= 12.8 Hz, $J_{2eq,3}$=5.4 Hz, H-3), 5.16 (br s, 1H, H-4), 4.92 (d, 1H, $J_{1,2ax}$=2.6 Hz, H-1), 4.03 (q, 1H, $J_{5,6}$=6.5 Hz, H-5), 3.60 (td, 1H, H-1'a), 3.34 (td, 1H, H-1'b), 2.13 (s, 3H, -OAc), 2.02 (td, 1H, $J_{2ax,2eq}$ $J_{2a,3}$=12.8 Hz, H-2ax), 1.96 (s, 3H, -OAc), 1.82 (dd, 1H, H-2eq), 1.53 (m, 2H, H-2'), 1.34-1.19 (m, 18H, H-3' to H-11'), 1.11 (d, 3H, H-6), 0.85 (t, 3H, $J_{11,12}$= 6.6 Hz, H-12'). **^{13}C RMN** ($CDCl_3$) δ 170.8, 170.2 (C=O, OAc), 97.3 (C-1), 69.9 (C-4), 67.5 (C-1'), 66.9 (C-3), 64.4 (C-5), 31.9 (C-2), 30.0, 29.7, 29.6, 29.5, 29.4, 29.3, 29.2, 22.7 (C-2' to C-11'), 21.0, 20.8 (CH_3,

OAc), 16.5 (C-6), 14.3 (C-12'). **HRMS:** Calcd for $[M+H]^+$ 401.2898; Found: 401.2888 (error 2.4 ppm).

Dodecyl 2,6-dideoxy-3,4-di-*O*-acetyl-β-L-*lyxo*-hexopyranoside (S11). Obtained from glycal **S2** in 14% isolated yield, after CC eluted with hex/EtOAc 17:1. R_f =0.43 (hex/EtOAc 5:1); $[\alpha]_D^{20}$=+8º (c1.0, $CHCl_3$) **^{1}H RMN ($CDCl_3$)** δ 5.09 (br d, 1H, $J_{3,4}$ = 2.5 Hz, H-4), 4.97 (ddd, 1H, $J_{2ax,3}$= 13.2 Hz, $J_{2eq,3}$=5.6, H-3), 4.50 (dd, 1H, $J_{1,2ax}$=9.3 Hz, $J_{1,2eq}$=2.2 Hz, H-1), 3.91 (qd, 1H, H-1'a), 3.65 (q, 1H, $J_{5,6}$=6.5, H-5), 3.44 (qd, 1H, H-1'b), 2.15 (s, 3H, -OAc), 1.99 (s, 3H, -OAc), 1.97-1.85 (m, H-2ax and H2eq), 1.64-1.50 (m, 2H, H-2'), 1.35-1.17 (m, 16H, H-3' to H-11' and H-6), 0.87 (t, 3H, $J_{11,12}$= 6.5 Hz, H-12'). **^{13}C RMN** ($CDCl_3$) δ 170.9, 170.2 (C=O, OAc), 99.8 (C-1), 69.8 (C-1'), 69.2, 69.1 (C-3 and C-5), 68.7 (C-3), 31.9 (C-2), 31.8, 29.7, 29.6, 29.6, 29.5, 29.4, 29.3, 26.0, 22.7 (C-2' to C-11'), 20.9, 20.8 (CH_3, -OAc), 16.5 (C-6), 14.1 (C-12'). **HRMS:** Calcd for $[M+Na]^+$ 423.2717; Found: 423.2709 (error 1.8 ppm).

Dodecyl 3,4-di-*O*-benzyl-2,6-dideoxy-1-thio-α-L-*arabino*-hexopyranoside (S8) and **dodecyl 3,4-di-*O*-benzyl-2,6-dideoxy-1-thio-β-L-*arabino*-hexopyranoside (S12).** Obtained from glycal **S3** in 45% yield as an anomeric mixture (α/β ratio 3:1) after CC eluted with hex/EtOAc 30:1.**^{1}H RMN** ($CDCl_3$) *δ* 7.34-7-24 (Ph, -OBn) 5.30-5.28 (m, $J_{1,2}$=6.2 Hz, H-1α), 5.00-4.94 (m, C$\underline{H}_2$Ph, αβ), 4.70-4.57 (m, C$\underline{H}_2$Ph, αβ), 4.46 (t, 1H, $J_{1,2}$=11 Hz, H-1β), 4.13-4.04 (m, H-5α and H-5β), 3.87 (ddd, $J_{2e,3}$=4.2 Hz, $J_{3,4}$=8.9 Hz, $J_{2a,3}$=7.1 Hz, H-3α), 3.69-3.61 (m, H-3β), 3.15-3.07 (m, H-4αβ), 2.71-2.61 (m, H'1β), 2.59-2.43 (m, H1'α), 2.35 (dd, $J_{2ax,2eq}$=13.2 Hz, H-2_{eq}β), 2.28 (dd, $J_{2ax,2eq}$=13.3 Hz, H-2_{eq}α), 2.00-1.98 (m, H-2_{ax}α), 1.99 (q, $J_{2a,3}$=11.8 Hz, H-2_{ax}β), 1.61-1.51 (m, 2H, H-2'αβ), 1.37-1.18 (m, 2H, H-3'-H11' αβ, H-6αβ), 0.87 (t, $J_{11,12}$=6.5 Hz, H-12'α, H-12'β). **^{13}C RMN** ($CDCl_3$) *δ* 128.5, 128.4, 128.1, 128.0, 127.7, 127.6 (CH_2-$\underline{Ph}$), 84.6 (C-1α), 83.6 (C-1β), 80.5 (-$\underline{C}H_2$Ph β), 80.4 (-$\underline{C}H_2$Ph α), 79.6 (-$\underline{C}H_2$Ph β), 77.9 (-$\underline{C}H_2$Ph α), 75.6 (C-4β), 75.4 (C-3β), 75.2 (C-4 α), 71.8 (C-3α), 67.5 (C-5α), 60.4

(C5-β), 37.3 (C-2'β), 36.3 (C-2'α), 31.90 (C-1'α, C-1'β), 31.10, 30.8, 29.9, 29.7, 29.7,29.7, 29.6, 29.6, 29.4, 29.2, 28.9, 22.7 (C-2' to C-11' α and β), 18.4 (C-6β), 18.1 (C-6α), 14.2 (C-12'β), 14.1 (C-12'α). Further purification by column chromatography allowed the isolation of a fraction of the alfa anomer **S8**, which was submitted to hydrogenation to remove benzyl protecting groups to afford compound **3** (see below).

Dodecyl 3,4-di-*O*-acetyl-2-deoxy-α-L-*threo*-pentopyranoside (S9). Obtained from glycal **S4** in 23% isolated yield, after CC eluted with hex/EtOAc 95:5. R_f = 0.55 (hex/EtOAc 6:1); $[\alpha]_D^{20}$= −58º (*c* 1.0, $CHCl_3$); **^{1}H NMR** ($CDCl_3$) δ 5.27 (br ddd, 1H, $J_{3,4}$ = 8.5 Hz, $J_{2ax,3}$ = 10.1 Hz, $J_{2eq,3}$ = 4.8 Hz, H-3), 4.86 (br ddd, 1H, $J_{3,4}$ = 8.5 Hz, $J_{4,5ax}$ = 9.2 Hz, $J_{4,5eq}$ = 5.0 Hz, H-4), 4.82 (br t, 1H, $J_{1,2ax}$ = 3.2 Hz, $J_{1,2eq}$ = 2.8 Hz, H-1), 3.77 (dd, 1H, $J_{5ax,5eq}$ = 11.1 Hz, $J_{4,5eq}$ = 5.0 Hz, H-5eq), 3.69-3.62 (m, 2H, H-5ax, H-1'a), 3.35 (dt, 1H, $J_{1'a,1'b}$ = 9.3 Hz, $J_{1'b,2'}$ = 6.7 Hz, H-1'b), 2.18 (br ddd, 1H, $J_{2ax,2eq}$ = 13.0 Hz, $J_{2eq,3}$ = 4.8 Hz, $J_{1,2eq}$ = 2.8 Hz, H-2eq), 2.05 (s, 3H, -OAc), 2.04 (s, 3H, -OAc), 1.76 (br ddd, 1H, $J_{2ax,2eq}$ = 13.0 Hz, $J_{2ax,3}$ = 10.1 Hz, $J_{2ax,1}$= 3.2 Hz, H-2ax), 1.61-1.54 (m, 2H, H-2'), 1.36-1.23 (m, 18H, H-3' to H-11'), 0.88 (t, 3H, $J_{11',12'}$ = 6.8 Hz, H-12'). **^{13}C NMR** ($CDCl_3$) δ 170.2 (C=O, OAc), 170.1 (C=O, OAc), 97.0 (C-1), 69.6 (C-4), 68.6 (C-3), 68.0 (C-1'), 59.8 (C-5), 34.6 (C-2), 31.9, 29.7, 29.6, 29.6, 29.6, 29.5, 29.5, 29.4, 26.2, 22.7 (C-2’ to C-11'), 21.1 (CH_3, -OAc), 20.9 (CH_3, -OAc), 14.1 (C-12'). **HRMS:** Calcd for $[M+Na]^+$ 409.2561; Found: 409.2568 (error 1.7 ppm).

Dodecyl 3,4-di-*O*-acetyl-2-deoxy-β-L-*threo*-pentopyranoside (S13). Obtained from glycal **S4** in 10% isolated yield, after CC eluted with hex/EtOAc 95:5. R_f = 0.48 (hex/EtOAc 6:1); $[\alpha]_D^{20}$= +52º (*c* 1.0, $CHCl_3$); **^{1}H NMR** ($CDCl_3$) δ 4.94 (br ddd, 1H, $J_{3,4}$ = 6.5 Hz, $J_{2ax,3}$ = 8.7 Hz, $J_{2eq,3}$ = 4.6 Hz, H-3), 4.84 (br ddd, 1H, $J_{3,4}$ = 6.5 Hz, $J_{4,5ax}$ = 7.3 Hz, $J_{4,5eq}$ = 3.9 Hz, H-4), 4.62 (br dd, 1H, $J_{1,2ax}$ = 6.3 Hz, $J_{1,2eq}$ = 2.7 Hz, H-1), 4.12 (dd, 1H, $J_{5ax,5eq}$ = 12.1 Hz, $J_{4,5eq}$ = 3.9 Hz, H-5eq), 3.76 (dt, 1H, $J_{1'a,1'b}$ = 9.2 Hz, $J_{1'a,2'}$ = 6.8 Hz, H-1'a), 3.43-3.35 (m, 2H, H-

5ax, H-1'b), 2.23 (br ddd, 1H, $J_{2ax,2eq}$ = 13.3 Hz, $J_{2eq,3}$ = 4.6 Hz, $J_{1,2eq}$ = 2.7 Hz, H-2eq), 2.07 (s, 3H, -OAc), 2.06 (s, 3H, -OAc), 1.79 (br ddd, 1H, $J_{2ax,2eq}$ = 13.3 Hz, $J_{2ax,3}$ = 8.7 Hz, $J_{1,2ax}$ = 6.3 Hz, H-2ax), 1.61-1.53 (m, 2H, H-2'), 1.35-1.21 (m, 18H, H-3' to H-11', 0.88 (t, 3H, $J_{11',12'}$= 6.5 Hz, H-12'). **^{13}C NMR** ($CDCl_3$) δ 170.2 (C=O, OAc), 170.1 (C=O, OAc), 98.2 (C-1), 69.1 (C-4), 68.9 (C-1'), 68.6 (C-3), 60.9 (C-5), 33.3 (C-2), 31.9, 29.7, 29.7, 29.6, 29.6, 29.6, 29.4, 29.4, 26.1, 22.7 (C-2' to C-11'), 21.1 (CH_3, -OAc), 21.0 (CH_3, -OAc), 14.1 (C-12'). **HRMS:** Calcd for $[M+Na]^+$ 409.2561; Found: 409.2565 (error 1.0 ppm).

Dodecyl 4-*O*-acetyl-2,3-dideoxy-α-L-*glycero*-pent-2-enopyranoside (S14α). Obtained from glycal **S4,** in 20% isolated yield, after CC eluted with hex/EtOAc 95:5. R_f = 0.71 (hex/EtOAc 6:1); m.p. = 40.4−41.1 ºC; $[\alpha]_D^{20}$= −96 º (*c* 1.0, $CHCl_3$); **^{1}H NMR** ($CDCl_3$) δ 6.07-6.04 (m, 2H, H-3, H-2), 4.99 (s, 1H, H-1), 4.95 (br s, 1H, H-4), 4.17 (dd, 1H, $J_{5a,5b}$ = 13.0 Hz, $J_{4,5a}$ = 2.0 Hz, H-5a), 3.83 (d, 1H, $J_{5a,5b}$ = 13.0 Hz, H-5b), 3.77 (dt, 1H, $J_{1'a,1'b}$ = 9.4 Hz, $J_{1'a,2'}$ = 6.7 Hz, H-1'a), 3.48 (dt, 1H, $J_{1'a,1'b}$ = 9.4 Hz, $J_{1'b,2'}$ = 6.7 Hz, H-1'b), 2.10 (s, 3H, -OAc), 1.63-1.55 (m, 2H, H-2'), 1.37-1.23 (m, 18H, H-3' to H-11'), 0.88 (t, 3H, $J_{11',12'}$ = 6.8 Hz, H-12'). **^{13}C NMR** ($CDCl_3$) δ 170.7 (C=O, OAc), 131.1, 124.9 (C-3, C-2), 93.0 (C-1), 68.7 (C-1'), 63.4 (C-4), 61.2 (C-5), 31.9, 29.7, 29.7, 29.6, 29.6, 29.6, 29.4, 29.4, 26.2, 22.7 (C-2' to C-11'), 21.1 (CH_3, -OAc), 14.1 (C-12'); **HRMS:** Calcd for $[M+Na]^+$ 349.2349; Found: 349.2335 (error 4.2 ppm).

Dodecyl 4-*O*-acetyl-2,3-dideoxy-β-L-*glycero*-pent-2-enopyranoside (S14β). Obtained from glycal **S4,** in 7% isolated yield, after CC eluted with hex/EtOAc 95:5. R_f = 0.78 (hex/EtOAc 6:1); $[\alpha]_D^{20}$= −51 º (*c* 1.1, $CHCl_3$). **^{1}H NMR** ($CDCl_3$) δ 5.94 (br d, 1H, $J_{2,3}$ = 10.3 Hz, H-3), 5.87 (br d, 1H, $J_{2,3}$ = 10.3 Hz, H-2), 5.28 (br s, 1H, H-4), 4.93 (s, 1H, H-1), 3.88-3.74 (m, 3H, H-1'a, H-5a,b), 4.47 (dt, 1H, $J_{1'a,1'b}$ = 9.3 Hz, $J_{1'b,2'}$ = 6.7 Hz, H-1'b), 2.07 (s, 3H, -OAc), 1.65-1.56 (m, 2H, H-2'), 1.39-1.21 (m, 18H, H-3' to H-11'), 0.88 (t, 3H, $J_{11',12'}$ = 6.7 Hz, H-12'). **^{13}C NMR** ($CDCl_3$) δ 170.6 (C=O, OAc), 129.4 (C-2), 128.7 (C-3), 94.3 (C-1), 68.9 (C-1'), 65.0

(C-4), 60.2 (C-5), 31.9, 29.8, 29.7, 29.7, 29.6, 29.6, 29.4, 29.4, 26.2, 22.7 (C-' - C-11'), 21.0 (CH_3, -OAc), 14.1 (C-12'); **HRMS:** Calcd for $[M+Na]^+$ 349.2349; Found: 349.2338 (error 3.3 ppm).

A.3.2. Synthesis of dodecyl 2,6-dideoxy-1-thio-α-L-*arabino*-hexopyranoside (3). Dodecyl 3,4-di-*O*-benzyl-2,6-dideoxy-1-thio-α-L-*arabino*-hexopyranoside (**S8,** 0.16 mmol) was dissolved in dried methanol (1mL/100mg) and 10% Pd/C (20mg) was carefully added. After air purge with N_2, reaction was kept under H_2 for 48h. Reaction mixture was filtered over Celite, and the solvent was evaporated under reduced pressure. Title compound was isolated in 91% yield after CC eluted with hex/EtOAc 1:1 to afford the title compound as a white solid (0.048 g, 0.146 mmol) in 91% yield. R_f =0.35 (2:3 Petrol. ether/EtOAc); $[\alpha]_D^{20}$= -165º (c1.0, $CHCl_3$) m.p. 54.4-55.4 ºC; **^{1}H RMN** (MeOD) δ 5.31 (d, 1H, $J_{1,2a}$=5,80 Hz, H-1), 4.01 (dq, 1H, $J_{4,5}$=9.0, $J_{5,6}$= 6.3 Hz, H-5), 3.88 (ddd, 1H, $J_{2ax,3}$=12.4 Hz, $J_{3,4}$=9.0 Hz, $J_{3,2eq}$=4.6 Hz, H-3), 3.10 (t, 1H, $J_{3,4}$=$J_{4,5}$=9.0 Hz, H-4), 2.60-2.48 (m, 2H, H-1'), 2.18 (dd, 1H, $J_{2ax,2eq}$=13.0 Hz, H-2eq), 2.03 (ddd, $J_{2ax,2eq}$=13.0, $J_{2ax,3}$=12.4, $J_{1,2a}$=5.80 Hz, 1H, H-2ax), 1.62-1.55 (m, 2H, H-2'), 1.38-1.31 (m, 2H, H-3'), 1.30 (d, 3H, $J_{5,6}$= 6.3 Hz, H-6), 1.27-1.22 (m, 16H, H-4' to H-11'), 0.87 (t, 3H, $J_{11,12}$=6.5 Hz, H-12'). **^{13}C RMN** (MeOD) δ 80.4 (C-1), 78.5 (C-4), 69.9 (C-3), 67.6 (C-5), 38.1 (C-2), 31.9 (C-1'), 31.1, 29.8, 29.7, 29.6, 29.6, 29.51, 29.3, 29.2, 28.9, 22.7 (C-2' to C-11'), 17.6 (C-6), 14.1 (C-12'). **HRMS:** Calcd for $[M+Na]^+$ 355.2277; Found: 355.2264 (error -3.6 ppm).

A.3.3. General deacetylation procedure. Acetylated glycoside (**S7, S9, S11** or **S13,** 0.6 mmol) was dissolved in dried methanol (6 mL), and a 1M NaOMe solution in MeOH was added (0.1 mL/100mg) and stirred at room temperature for 2h (**2**/**2b**) or 1h15 (**8/9**). The

reaction was neutralized with Amberlite (IR-120), followed by filtration and evaporation of the solvent. The residue was purified by column chromatography.

Dodecyl 2,6-dideoxy-α-L-*lyxo*-hexopyranoside (2). Obtained from **S7** in 99% yield after CC eluted with hex/EtOAc 1:1. R_f = 0.56 (EtOAc); m.p. 54.4-56.9 ºC; $[\alpha]_D^{20}$= −86º (c1.0, $CHCl_3$); **^{1}H RMN** (MeOD) δ 4.83 (br d, 1H, $J_{1,2ax}$=3.8 Hz, H-1)*, 3.92 (ddd, 1H, $J_{2ax,3}$= 11.8 Hz, $J_{2eq,3}$=5.1, H-3), 3.85 (q, 1H, $J_{5,6}$=6.6 Hz, H-5), 3.60 (qd, 1H, H-1'a), 3.53 (br s, 1H, H-4), 3.36 (qd, 1H, H-1'b), 1.90 (ddd, $J_{2ax,2eq}$ $J_{2ax,3}$=12.5 Hz, $J_{1,2ax}$=3.8 Hz, 1H, H-2ax), 1.74 (dd, 1H, $J_{1,2ax}$=5.1 Hz, H-2eq), 1.61-1.51 (m, 2H, H-2'), 1.40-1.23 (m, 18H, H-3' to H-11'), 1.22 (d, 3H, H-6), 0.90 (t, 3H, $J_{11,12}$= 7 Hz, H-12'), **^{13}C RMN** (MeOD) δ 99.0 (C-1), 72.3 (C-4), 68.4 (C-1'), 67.5 (C-3), 67.0 (C-5), 33.4 (C-2), 33.1, 30.8, 30.7, 30.7, 30.6, 30.5, 27.4, 23.7 (C-2' to C-11'), 17.2 (C-6), 14.4 (C-12'). *partially under H_2O peak. **HRMS:** Calcd for $[M+Na]^+$ 339.2506; Found: 339.2489 (error -4.9 ppm).

Dodecyl 2,6-dideoxy-β-L-*lyxo*-hexopyranoside (2b). Obtained from **S11** in 98% yield after CC eluted with hex/EtOAc 1:1. R_f = 0.56 (EtOAc); m.p. 64.4-66.7 ºC; $[\alpha]_D^{20}$= +17º (*c*1.0, $CHCl_3$); **^{1}H RMN** (MeOD) δ 4.45 (dd, 1H, $J_{1,2ax}$=9.9 Hz, $J_{1,2eq}$=1.7 Hz, H-1), 3.85 (br q, 1H, $J_{1',2'}$=9 Hz, H-1'a), 3.68 (ddd, 1H, $J_{2ax,3}$= 11.9 Hz, $J_{2eq,3}$=4.6, Hz, H-3), 3.51-3.42 (m, 3H, H-4, H-5 and H-1'b), 1.81 (ddd, $J_{2ax,2eq}$=11.9 Hz, 1H, H-2eq), 1.69 (br q, 1H, $J_{2ax,3}$ $J_{1,2ax}$ $J_{2ax,2eq}$ =11.9 Hz, H-2ax), 1.60-1.53 (m, 2H, H-2'), 1.36-1.28 (m, 18H, H-3' a H-11'), 1.27 (d, 3H, $J_{5,6}$= 6.5 Hz, H-6), 0.90 (t, 3H, $J_{11,12}$= 6.8 Hz, H-12'), **^{13}C RMN** (MeOD) δ 101.6 (C-1), 71.9 (C-4), 71.4 (C-5), 70.1, 70.1 (C-3 and C-1'), 35.4 (C-2), 33.1, 30.8, 30.8, 30.8, 30.7, 30.6, 30.5, 27.2, 23.8 (C-2' to C-11'), 17.1 (C-6), 14.5 (C-12'). **HRMS:** Calcd for $[M+Na]^+$ 339.2506; Found: 339.2491 (error -4.2 ppm).

Dodecyl 2-deoxy-α-L-*threo*-pentopyranoside (8). Obtained from **S9** in 93% isolated yield after CC eluted with hex/EtOAc 1:4 EtOAc, R_f =0.43 (EtOAc/hex 3:1); m.p. = 52.8−54.2

ºC; $[\alpha]_D^{20}$= −62º (*c* 1.0, $CHCl_3$); **^{1}H NMR** (MeOD) δ 4.80 (br dd, 1H, $J_{1,2ax}$ = 3.5 Hz, $J_{1,2eq}$ = 1.7 Hz, H-1), 3.76 (br ddd, 1H, $J_{2ax,3}$ = 10.8 Hz, $J_{3,4}$ = 8.1 Hz, $J_{2eq,3}$ = 4.9 Hz, H-3), 3.63 (dt, 1H, $J_{1'a,1'b}$ = 9.3 Hz, $J_{1'a,2'}$ = 6.7 Hz, H-1'a), 3.59 (dd, 1H, $J_{5ax,5eq}$=10.1 Hz, $J_{4,5eq}$=4.5 Hz, H-5eq), 3.44 (t, 1H, $J_{5ax,5eq}$=$J_{5ax,4}$=10.1 Hz, H-5ax), 3.42-3.32 (m, 2H, H-4, H-1'b), 2.02 (br ddd, 1H, $J_{2ax,2eq}$=12.9 Hz, $J_{2eq,3}$=4.9 Hz, $J_{1,2eq}$=1.7 Hz, H-2eq), 1.62-1.52 (m, 3H, H-2ax, H-2'), 1.41-1.24 (m, 18H, H-3' to H-11'), 0.90 (t, 3H, $J_{11',12'}$ = 6.7 Hz, H-12'). **^{13}C NMR** (MeOD) δ 99.0 (C-1), 72.5 (C-4), 69.9 (C-3), 68.4 (C-1'), 63.6 (C-5), 38.5 (C-2), 34.1, 30.8, 30.7, 30.7, 30.7, 30.7, 30.6, 30.5, 27.4, 23.7 (C-2' to C-11'), 14.4 (C-12'). **^{1}H NMR** ($CDCl_3$) δ 4.84 (br dd, 1H, $J_{1,2ax}$=3.3 Hz, $J_{1,2eq}$=1.7 Hz, H-1), 3.96-3.88 (m, 1H, H-3), 3.69 (dd, 1H, $J_{5ax,5eq}$=9.9 Hz, $J_{4,5eq}$=4.1 Hz, H-5eq), 3.63 (dt, 1H, $J_{1'a,1'b}$=9.3 Hz, $J_{1'a,2'}$=6.8 Hz, H-1'a), 3.59-3.46 (m, 2H, H-4, H-5ax), 3.34 (dt, 1H, $J_{1'a,1'b}$=9.3 Hz, $J_{1'b,2'}$=6.8 Hz, H-1'b), 2.51 (br s, 1H, OH), 2.11 (br ddd, 1H, $J_{2ax,2eq}$=12.8 Hz, $J_{2eq,3}$=4.1 Hz, $J_{1,2eq}$=1.7 Hz, H-2eq), 1.72 (br s, 1H, OH), 1.64 (br ddd, 1H, $J_{2ax,2eq}$=12.8 Hz, $J_{2ax,3}$=10.9 Hz, $J_{1,2ax}$=3.3 Hz, H-2ax), 1.60-1.52 (m, 2H, H-2'), 1.38-1.21 (m, 18H, H-3' to H-11'), 0.88 (t, 3H, $J_{11',12'}$ = 6.7 Hz, H-12'). **^{13}C NMR** ($CDCl_3$) δ 97.6 (C-1), 72.1 (C-4), 69.6 (C-3), 67.6 (C-1'), 62.1 (C-5), 37.3 (C-2), 31.9, 29.7, 29.6, 29.6, 29.6, 29.6, 29.5, 29.4, 26.2, 22.7 (C-2' to C-11'), 14.1 (C-12'). **HRMS:** Calcd. $[M+Na]^+$ 325.2349; Found: 325.2336 (error 4.1 ppm).

Dodecyl 2-deoxy-β-L-*threo*-pentopyranoside (9). Obtained from **S13** in 99% isolated yield after CC eluted with hex/EtOAc 1:4→ EtOAc. R_f = 0.43 (EtOAc/hex 3:1); m.p. = 68.3-68.8 ºC; $[\alpha]_D^{20}$= +72º (*c* 1.0, $CHCl_3$); **^{1}H NMR** (MeOD) δ 4.53 (dd, 1H, $J_{1,2ax}$ = 8.4 Hz, $J_{1,2eq}$=1.9 Hz, H-1), 3.90 (dd, 1H, $J_{5ax,5eq}$=11.5 Hz, $J_{4,5eq}$=4.7 Hz, H-5eq), 3.78 (dt, 1H, $J_{1'a,1'b}$=9.4 Hz, $J_{1'a,2}$= 6.7 Hz, H-1'a), 3.52 (br ddd, 1H, $J_{2ax,3}$=10.2 Hz, $J_{3,4}$=8.1 Hz, $J_{2eq,3}$ = 4.8 Hz, H-3), 3.44 (dt, 1H, H-1'b), 3.38 (ddd, 1H, $J_{4,5ax}$=9.0 Hz, $J_{3,4}$=8.1 Hz, $J_{4,5eq}$ = 4.7 Hz, H-4), 3.17 (dd, 1H, $J_{5ax,5eq}$=11.5 Hz, $J_{4,5ax}$=9.0 Hz, H-5ax), 2.11 (br ddd, 1H, $J_{2ax,2eq}$ = 12.8 Hz, $J_{2eq,3}$ = 4.8 Hz, $J_{1,2eq}$ = 1.9 Hz, H-2eq), 1.60-1.53 (m, 2H, H-2'), 1.48 (ddd, 1H, $J_{2ax,2eq}$ = 12.8 Hz, $J_{2ax,3}$ = 10.2 Hz,

$J_{1,2ax}$ = 8.4 Hz, H-2ax), 1.37-1.25 (m, 18H, H-3' to H-11'), 0.90 (t, 3H, $J_{11',12'}$ = 6.7 Hz, H-12'). **^{13}C NMR** (MeOD) δ 101.5 (C-1), 72.1 (C-4), 71.7 (C-3), 70.1 (C-1'), 66.1 (C-5), 38.8 (C-2), 33.1, 30.8, 30.8, 30.8, 30.7, 30.7, 30.5, 30.5, 27.2, 23.8 (C-2' to C-11'), 14.5 (C-12'). **^{1}H NMR** ($CDCl_3$) δ 4.80 (br t, 1H, $J_{1,2ax}$ = $J_{1,2eq}$ = 3.5 Hz, H-1), 4.15 (br dd, 1H, $J_{5ax,5eq}$ = 12.5 Hz, $J_{4,5eq}$ = 1.7 Hz, H-5eq), 3.80-3.72 (m, 2H, H-3, H-1'a), 3.68-3.63 (m, 1H, H-4), 3.50-3.36 (m, 3H, H-5ax, OH, H-1'b), 2.21 (br dt, 1H, $J_{2eq,2ax}$=14.2 Hz, $J_{1,2eq}$=$J_{2eq,3}$=3.5 Hz, H-2eq), 2.11-2.03 (m, 1H, OH), 1.78 (br dt, 1H, $J_{2ax,2eq}$=14.2 Hz, $J_{1,2ax}$=$J_{2ax,3}$=3.5 Hz, H-2ax), 1.63-1.56 (m, 2H, H-2'), 1.37-1.22 (m, 18H, H-3' to H-11'), 0.88 (t, 3H, $J_{11',12'}$ = 6.7 Hz, H-12'). **^{13}C NMR** ($CDCl_3$) δ 98.1 (C-1), 69.1 (C-4), 68.6 (C-1'), 67.9 (C-3), 60.8 (C-5), 32.3 (C-2), 31.9, 29.7, 29.6, 29.6, 29.6, 29.5, 29.4, 29.4, 26.2, 22.7 (C-2' to C-11'), 14.1 (C-12'). **HRMS:** Calcd. $[M+Na]^+$ 325.2349; Found: 325.2338 (error 3.5 ppm).

B. Synthesis of dodecyl 6-deoxymannopyranosides

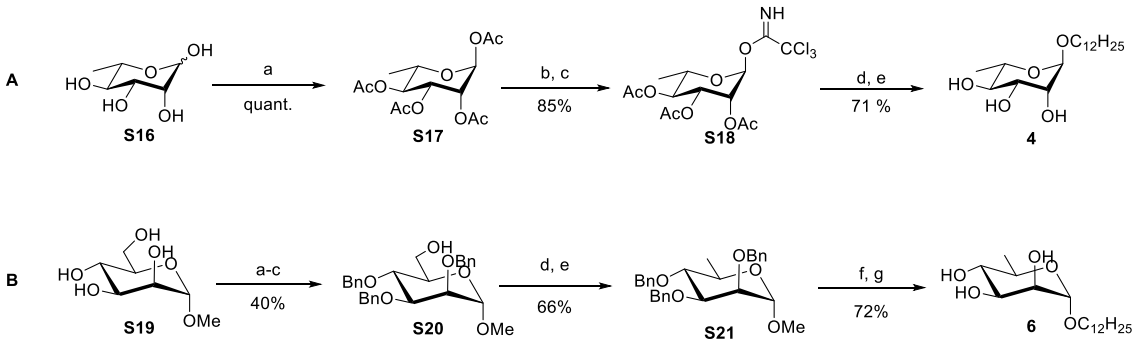

Scheme S2. A: **Synthesis of dodecyl 6-deoxy-α-L-mannopyranoside**. Reagents and conditions: a) Ac_2O, pyr., DMAP; b) NH_2NH_2.AcOH, DMF; c) Cl_3CCN, DBU, DCM; d) $C_{12}H_{25}OH$, TMSOTf, DCM, 4Å MS, 0 ºC; e) NaOMe, MeOH. **B: Synthesis of dodecyl 6-deoxy-α-D-mannopyranoside**. Reagents and conditions: a) TrCl, DMAP, py; b) BnBr, NaH, DMF (71% over two steps); c) I_2, MeOH (57%); d) I_2/Ph_3P/Imidazole, toluene; e) $LiAlH_4$, THF (66% over two steps); f) $C_{12}H_{25}OH$, A-15, Reflux, 10h; g) H_2, Pd/C.

1,2,3,4-Tetra-*O*-acetyl-6-deoxy-α-L-mannopyranose (S17). Commercial L-(+)-rhamnose monohydrate (1.0 g, 5.5 mmol) was dissolved in pyridine (10 mL) and acetic anhydride (6.9 mL, 73.1 mmol, 13 equiv.) was added dropwise at 0 ºC, followed by a catalytic amount of 4-(dimethylamino)pyridine. The reaction reached room temperature and stirred overnight. Dichloromethane was then added, and the solution was washed with 2M HCl aq. solution and brine. The combined organic layers were dried ($MgSO_4$), filtered and concentrated under reduced pressure to yield a very viscous colourless oil of compound **S17**, in quantitative yield and without further purification. R_f = 0.42 (hex/EtOAc 2:1); $[\alpha]_D^{20} = -55^o$ (*c* 1.0, $CHCl_3$); **^{1}H NMR** ($CDCl_3$) δ 6.02 (br d, 1H, $J_{1,2}$ = 1.1 Hz, H-1), 5.30 (dd, 1H, $J_{2,3}$ = 2.9 Hz, $J_{3,4}$ = 9.9 Hz, H-3), 5.25 (br dd, 1H, $J_{1,2}$ = 1.1 Hz, $J_{2,3}$ = 2.9 Hz, H-2), 5.13 (t, 1H, $J_{3,4}$ $J_{4,5}$ = 9.9 Hz, H-4), 3.94 (dq, 1H, $J_{4,5}$ = 9.9 Hz, $J_{5,6}$ = 6.2 Hz, H-5), 2.17 (s, 3H, -OAc), 2.16 (s, 3H, -OAc), 2.07 (s, 3H, -OAc), 2.01 (s, 3H, -OAc), 1.24 (d, 3H, $J_{5,6}$ = 6.2 Hz, H-6). **^{13}C NMR** ($CDCl_3$) δ 170.1(C=O, OAc), 169.9 (C=O, OAc), 169.8 (C=O, OAc), 168.4 (C=O, OAc), 90.6 (C-1), 70.4 (C-4), 68.8 (C-3), 68.7 (C-5), 68.6 (C-2), 20.9 (CH_3, -OAc), 20.8 (CH_3, -OAc), 20.8 (CH_3, -OAc), 20.7 (CH_3, -OAc), 17.4 (C-6).

2,3,4-Tri-*O*-acetyl-6-deoxy-α-L-mannopyranosyl trichloroacetimidate (S18). To a solution of L-rhamnose peracetate **S17** (5.5 mmol) in DMF (20 mL) was added hydrazine acetate (1.77 g, 19.2 mmol, 3.5 equiv.) at room temperature. The reaction was stirred until complete consumption of the starting material (c.a. 96 h) and quenched by adding EtOAc. The solution was washed with brine and water, dried ($MgSO_4$), filtered and concentrated under reduced pressure to afford 2,3,4-tri-*O*-acetyl-6-deoxy-L-mannopyranose (1.36 g, 85%) as a white powder, after recrystallization from EtOAc/hex. **R_f** = 0.21 (hex/EtOAc 2:1). The resulting product (100 mg, 0.35 mmol) and trichloroacetonitrile (104 μL, 1.04 mmol) were dissolved in dichloromethane (1 mL) at 0 ºC. Then, 1,8-diazabicyclo[5.4.0]undec-7-ene (16

μL, 0.11 mmol) was added and the reaction was allowed to reach room temperature. After 2 h, the solution was concentrated under reduced pressure and the residue was purified by flash column chromatography on silica gel (hex/EtOAc 3:1 to 2:1) to give glycosyl trichloroacetimidate **S18** (133 mg, 89%) as yellowish foam. $\mathbf{R_f}$ **=** 0.59 (hex/EtOAc 2:1) = 0.59; **^{1}H NMR** ($CDCl_3$) δ 8.74 (s, 1H, NH), 6.20 (br 1H, d, $J_{1,2}$ = 1.6 Hz, H-1), 5.46 (br dd, 1H, $J_{1,2}$ = 1.6 Hz, $J_{2,3}$ = 3.2 Hz, H-2), 5.37 (dd, 1H, $J_{2,3}$ = 3.2 Hz, $J_{3,4}$ = 10.1 Hz, H-3), 5.18 (t, 1H, $J_{3,4}$ $J_{4,5}$ = 10.1 Hz, H-4), 4.09 (dq, 1H, $J_{4,5}$ = 10.1 Hz, $J_{5,6}$ = 6.2 Hz, H-5), 2.19 (s, 3H, -OAc), 2.08 (s, 3H, -OAc), 2.01 (s, 3H, -OAc), 1.27 (d,3H, $J_{5,6}$ = 6.2 Hz, H-6). **^{13}C NMR** ($CDCl_3$) δ 169.9 (C=O, OAc), 169.9 (C=O, OAc), 169.8 (C=O, OAc), 159.9 (C-1'), 94.6 (C-1), 90.6 (C-2'), 70.3 (C-4), 69.3 (C-5), 68.8 (C-3), 68.4 (C-2), 20.8 (CH_3, -OAc), 20.8 (CH_3, -OAc), 20.7 (CH_3, -OAc), 17.5 (C-6). Spectroscopic characterization is in full agreement with the literature.[53]

Dodecyl 6-deoxy-α-L-mannopyranoside (4). A solution of glycosyl trichloroacetimidate **S18** (68 mg, 0.16 mmol) and dodecan-1-ol (40 μL, 0.18 mmol, 1.1 equiv.) in dichloromethane (2 mL) was stirred in the presence of pre-activated 4 Å molecular sieves (c.a. 100 mg) at room temperature for 30 min. The mixture was then cooled to 0 ºC and trimethylsilyl triflate (3 μL, 0.02 mmol, 0.1 equiv.) was added dropwise. After 2 h at 0 ºC, the reaction was quenched through addition of triethylamine until neutral pH and the solution was concentrated under vacuum to afford a residue containing dodecyl 2,3,4-tri-*O*-acetyl-6-deoxy-α-L-mannopyranoside as major product, as indicated by NMR. $\mathbf{R_f}$ = 0.72 (hex/EtOAc 3:2). The crude residue was then dissolved in dried methanol (0.5 mL), and a 1M NaOMe solution in MeOH (160 μL) was slowly added under vigorous stirring. The reaction proceeded at room temperature overnight, and was quenched with Amberlite (IR-120), followed by filtration and evaporation of the solvent. Purification by flash column chromatography on silica gel eluted with EtOAc afforded glycoside **4** (37 mg, 71%) as white powder. R_f = 0.49 (EtOAc); m.p. =

48.8−49.7 ºC; = −52º (*c* 1.0, $CHCl_3$); **HRMS**: Calcd. [M+Na] 355.2455; Exp. 355.2442 (error 3.6 ppm); NMR data was in full agreement with that described below for its enantiomer (compound **6**).

Methyl 2,3,4-tri-*O*-benzyl-α-D-mannopyranoside (S20). To a solution of methyl-α-D-mannopyranoside (**S19**, 5 g, 25.7 mmol) in pyridine (175 mL), trytil chloride (12.9 g, 46.3 mmol, 1.8 equiv.) and DMAP (256 mg, 0.2 mmol, 0.08 equiv.) were added and kept stirring at room temperature under nitrogen atmosphere for 5h. Reaction mixture was washed with a saturated solution of $NaHCO_3$ (250 mL) and water (250 mL), being the aqueous phases extracted with EtOAC (3x250 mL). Organic phases were combined and dried with anhydrous $MgSO_4$. After evaporation of the solvent, methyl 6-*O*-trytil-α-D-glucopyranoside was obtained virtually pure as a yellow oil; R_f = 0.5 (EtOAc). The residue was then dissolved in DMF (350 mL) and kept at 0 ºC while NaH 60% (3.699 g, 154 mmol, 6 equiv.) was added. After a few min, benzyl bromide (18.3 mL, 154 mmol, 6 equiv.) was added dropwise. Reaction was stirred at room temperature overnight, under nitrogen. Iced water (200 mL) was poured into the reaction mixture and extracted with diethyl ether (3×100 mL). Organic layers were combined, washed with brine and dried with $MgSO_4$. Residue was purified by column chromatography (hex/EtOAc 20:1) affording methyl 2,3,4-tri-*O*-benzyl-6-*O*-trityl-α-D-mannopyranoside as a white powder, in 71% yield. R_f = 0.73 (hex/EtOAc 3:1); m.p. 97.5-98.6 ºC; $[\alpha]_D^{20}$=+10º (c1.0, $CHCl_3$); **^{1}H NMR** ($CDCl_3$) δ 7.53-7.15 (m, 30H, -Ph), 4.84 (m, 2H, -C$\underline{H}_2$Ph, H-1), 4.73 (m, 2H, -C$\underline{H}_2$Ph), 4.64 (s, 2H, -C$\underline{H}_2$Ph), 4.27 (d, 2H, *J*=8.0 Hz, -$\underline{C}H_2$Ph), 4.03 (t, 1H, $J_{3,4}$ = $J_{4,5}$= 8.8 Hz, H-4), 3.88 (dd, 1H, $J_{2,3}$ = 3.1 Hz, H-3), 3.82 (br s, 1H, H-2), 3.77 (dd, 1H, $J_{5,6}$ = 4.0 Hz, H-5), 3.52 (br d, 1H, $J_{6a,6b}$ = 9.7 Hz, H-6a), 3.37 (s, 3H, -OMe), 3.27 (dd, 1H, H-6b). **^{13}C NMR** ($CDCl_3$) δ 146.8, 144.1 (Cq, -OTr), 138.6, 138.6, 138.2 (Cq, -OBn), 128.8, 128.3, 128.3, 128.1, 127.9, 127.7,127.6, 127.5, 127.4, 127.4, 127.1, 126.8 (-Ph), 98.6 (C-1), 86.3 (C-

2), 80.2 (C-3), 75.4 (-$\underline{C}H_2Ph$), 75.0 (C-4), 72.7 (-$\underline{C}H_2Ph$), 71.7 (C-5), 63.0 (C-6), 54.5 (-OCH_3). **HRMS:** Calcd for $[M+Na]^+$ 729.3187; Found: 729.3184 (error 0.4 ppm). 2,3,4-tri-*O*-benzyl-6-*O*-trityl-α-D-mannopyranoside (2.5 g) was dissolved in a solution of I_2 in methanol (0.500g/50 mL). The solution was stirred at 60 ºC for 3h. After evaporation of the solvent, the resulting residue was dissolved in EtOAc (50 mL), washed with a saturated solution of sodium thiosulfate (50 mL), followed by water (50 mL). Organic phase was dried with $MgSO_4$, followed by filtration and evaporation of the solvent. Purification of the residue with column chromatography (hex/EtOAc 3:1) gave compound **S21** (1.13g) in 57% yield as a colourless oil. R_f= 0.40 (hex/EtOAc 3:2); $[\alpha]_D^{20}$= +20º (c1.0, $CHCl_3$); **^{1}H NMR** ($CDCl_3$) δ 7.38-7.24 (m, 15H, -Ph), 4.94 (d, 1H, *J*= 11 Hz, -C$\underline{H}_2$Ph), 4.77 (d, 1H, *J*= 12 Hz, -C$\underline{H}_2$Ph), 4.70 (m, 5H, -C$\underline{H}_2$Ph, H-1), 3.97 (t, 1H, $J_{3,4} = J_{4,5}$= 9.6 Hz, H-4), 3.90 (dd, 1H, $J_{5,6a}$ = 2.7 Hz, $J_{6a,6b}$ = 9.7 Hz, H-6a), 3.84 (br dd, 1H, H-6b), 3.81-3.74 (m, 2H, H-2, H-3), 3.62 (m, 1H, H-5), 3.29 (s, 3H, -OMe), 2.2 (br s, 1H, -OH). **^{13}C NMR** ($CDCl_3$) δ 138.4, 138.4, 138.2 (Cq, -OBn), 128.4, 128.4, 128.4, 128.0, 127.8, 127.7,127.6 (-Ph), 99.3 (C-1), 80.2 (C-2), 74.8 (C-3), 74.6 (-$\underline{C}H_2$Ph), 72.9 (C-4), 72.2 (-$\underline{C}H_2$Ph), 72.0 (C-5), 62.4 (C-6), 54.8 (-OCH_3). **HRMS:** Calcd for $[M+H]^+$ 465.2272; Found: 465.2252 (error 4.3 ppm).

Methyl 2,3,4-Tri-*O*-benzyl-6-deoxy-α-D-mannopyranoside (S21). To a solution of compound **S20** (0.710 g, 1.53 mmol) in toluene (10 mL), triphenylphosphane, (0.603 g, 2.30 mmol, 1.5 equiv.), imidazole (0.208 g, 3.06 mmol, 2 equiv.) and I_2 (, 0.584 g, 2.30 mmol, 1.5 equiv.), were added and the reaction was stirred at 65 ºC for 2h, under nitrogen. Reaction mixture was cooled to room temperature, diluted with EtOAc (20 mL) and washed with saturated sodium thiosulfate solution (20 mL) and water (20 mL). The organic phase was dried with anhydrous $MgSO_4$, filtered and concentrated under vacuum. Column chromatography (hex/EtOAc 20:1) gave methyl 2,3,4-tri-*O*-benzyl-6-deoxy-6-iodo-α-D-mannopyranoside

(0.770 g, 88%) as a colourless oil. R_f = 0.53 (hex/EtOAc 3:1); $[\alpha]_D^{20}$= +27º (c1.0, $CHCl_3$); **^{1}H NMR** ($CDCl_3$) δ 7.39-7.23 (m, 15H, -Ph), 4.98 (d, 1H, *J*= 11 Hz, -C<u>H</u>$_2$Ph), 4.77-4.63 (m, 4H, -C<u>H</u>$_2$Ph, H-1), 4.60 (br s, 2H, -C<u>H</u>$_2$Ph), 3.89 (dd, 1H, $J_{2,3}$ = 8.7 Hz, $J_{3,4}$ = 2.4 Hz, H-3), 3.79-3.74 (m, 2H, H-2, H-5), 3.58-3.48 (m, 2H, H-4, H-6a), 3.36 (s, 3H, -OMe), 3.31 (m, 1H, H-6b). **^{13}C NMR** ($CDCl_3$) δ 138.2, 138.2, 138.2, 128.4, 128.4, 128.3, 128.0, 127.8, 127.6, 127.6 (-Ph), 99.0 (C-1), 79.9 (C-3), 78.6 (C-2), 75.4 (-<u>C</u>H$_2$Ph), 74.6 (C-5), 72.7 (-<u>C</u>H$_2$Ph), 71.4 (C-4), 55.0 (-OMe), 7.0 (C-6). **HRMS:** Calcd for $[M+Na]^+$ 597.1108; Found: 597.1107 (error -0.4 ppm). Methyl 2,3,4-tri-*O*-benzyl-6-deoxy-6-iodo-α-D-mannopyranoside (0.514 g, 0.89 mmol) was then dissolved in THF (20 mL), a 2M solution of $LiAlH_4$ in THF was added (7.2 mL; 14.3 mmol, 16 equiv.) and the reaction was kept under reflux for 1h. Reaction mixture was cooled down to 0 ºC, 0.3 mL of distilled water were added, followed by 0.3 mL of aqueous NaOH 15% and 0.9 mL of distilled water. This solution was stirred at room temperature for 15 min to allow the precipitation of aluminium and lithium salt. Anhydrous $MgSO_4$ was then added, salts were filtered off, solvent was evaporated and the residue was purified with column chromatography eluted with hex/EtOAc 10:1, affording compound **S21** (0.300g, 75%) as a colourless oil. R_f = 0.35 (hex/EtOAc 5:1); $[\alpha]_D^{20}$= +24º (c1.0, $CHCl_3$); **^{1}H NMR** ($CDCl_3$) δ 7.38-7.24 (m, 15H, -Ph), 4.95 (d, 1H, *J*= 11 Hz, -C<u>H</u>$_2$Ph), 4.78-4.70 (m, 2H, -C<u>H</u>$_2$Ph), 4.65-4.60 (m, 4H, -C<u>H</u>$_2$Ph, H-1), 3.83 (dd, 1H, $J_{2,3}$ = 8.8 Hz, $J_{3,4}$ = 2.6 Hz, H-3), 3.78 (m, 1H, H-2), 3.70-3.59 (m, 2H, H-4, H-5), 3.29 (s, 3H, -OMe), 1.34 (d, 3H, $J_{5,6}$ = 5.7 Hz, H-6). **^{13}C NMR** ($CDCl_3$) δ 138.6, 138.6, 138.3, 128.3, 128.4, 128.0, 127.9, 127.6, 127.6, 127.6, 127.5 (-Ph), 99.0 (C-1), 80.4 (C-4), 80.1 (C-2) 75.4 (-<u>C</u>H$_2$Ph), 74.6 (C-3) 72.8 (-<u>C</u>H$_2$Ph), 72.1 (-<u>C</u>H$_2$Ph), 67.8 (C-5), 54.6 (-OMe), 18.0 (C.6). **HRMS:** Calcd for $[M+H]^+$ 449.2323; Found: 449.2323 (error 0.2 ppm).

Dodecyl 6-deoxy-α-D-mannopyranoside (6). To a solution of compound **S22** (0.230 g, 0.513 mmol) in dodecan-1-ol (2 mL), Amberlyst A15 beeds (0.038 g) were added and the reaction was stirred at 100 ºC for 8h. Reaction mixture was diluted with dichloromethane, the resin was filtered off, and was concentrated again under vacuum. Column chromatography eluted with hex/EtOAc 20:1 afforded dodecyl 2,3,4-tri-*O*-benzyl-6-deoxy-α-D-mannopyranoside (0.239 g, η=77%) as a colourless oil. R_f =0.75 (hex/EtOAc 5:1); **^{1}H NMR** ($CDCl_3$) δ 7.38-7.26 (m, 15H, -Ph), 4.94 (d, 1H, *J*= 10 Hz, -C$\underline{H}_2$Ph), 4.78-4.70 (m, 3H, -C$\underline{H}_2$Ph, H-1), 4.65-4.63 (m, 3H, -C$\underline{H}_2$Ph), 3.86 (dd, 1H, $J_{2,3}$ = 9.0 Hz, $J_{3,4}$ = 2.8 Hz, H-3), 3.77 (br s, 1H, H-2), 3.73-3.56 (m, 3H, H-1'a, H-4, H-5), 3.34-3.28 (m, 1H, H-1'b), 1.53-1.44 (m, 2H, H-2'), 1.33 (d, 3H, $J_{5,6}$ = 6.1 Hz, H-6), 1.30-1.18 (m, 18H, H-3' to H-11'), 0.88 (br t, 3H, $J_{11',12'}$=6.5 Hz). **^{13}C NMR** ($CDCl_3$) δ 138.6, 138.6, 138.4, 128.3, 128.3, 128.0, 127.8, 127.5, 127.4 (-Ph), 97.9 (C-1), 80.5 (C-4), 80.2 (C-2) 75.4 (-$\underline{C}H_2$Ph), 75.0 (C-3) 72.7 (-$\underline{C}H_2$Ph), 72.1 (-$\underline{C}H_2$Ph), 67.9 (C-5),67.5 (C-1'), 31.9 (C-2'), 29.6, 29.6, 29.4, 29.3 (C-3' to C-9'), 26.1 (C-10'), 22.7 (C11'), 18.0 (C.6), 14.1 (C-1'). Dodecyl 2,3,4-tri-*O*-benzyl-6-deoxy-α-D-mannopyranoside (0.175 g, 0.29 mmol) was dissolved in MeOH and 2 spatula tips of 10% Pd/C were added, which was stirred at room temperature for 2 h under hydrogen atmosphere. Catalyst was filtered off under Celite and washed with MeOH. The filtrate was concentrated and purified by column chromatography hex/EtOAc 1:2) to afford compound **6** in 94% (0.090 g) as a white solid. R_f = 0.49 (hex/EtOAc 1:2); M.p. 48.7-50.0 ºC; $[\alpha]_D^{20}$ = +49º (c1.0, $CHCl_3$); **^{1}H NMR** (MeOD) δ 4.94 (br s, 1H, H-1), 3.77 (br s, 1H, H-2), 3.67-3.60 (m, 2H, H-3, H-1'a), 3.55 (qd, 1H, $J_{4,5}$ = 2.8 Hz, $J_{5,6}$ = 5.7 Hz, H-5), 3.40-3.33 (m, 2H, H-1'b, H-4), 1.60-1.52 (m, 2H, H-2'), 1.37-1.23 (m, 23H, H-3' a H-11', H-6), 0.88 (br t, 3H, $J_{11',12'}$=6.0 Hz). **^{13}C NMR** (MeOD) δ 101.5 (C-1), 73.9 (C-4), 72.4 (C-3), 72.3 (C-2), 69.7 (C-5), 68.5 (C-1'), 33.1 (C-2'), 30.8, 30.8, 30.8, 30.7, 30.6, 30.5, 30.4 (C-3' to C-9'), 27.4 (C-10'), 23.8 (C11'), 18.0 (C.6), 14.5 (C-12'). **HRMS:** Calcd for

$[M+Na]^+$ 355.2455; Found: 355.2441 (error 4.1 ppm). NMR data is in full agreement with that described above for its enantiomer (compound **4**).

C. Synthesis of *C*-glycosides

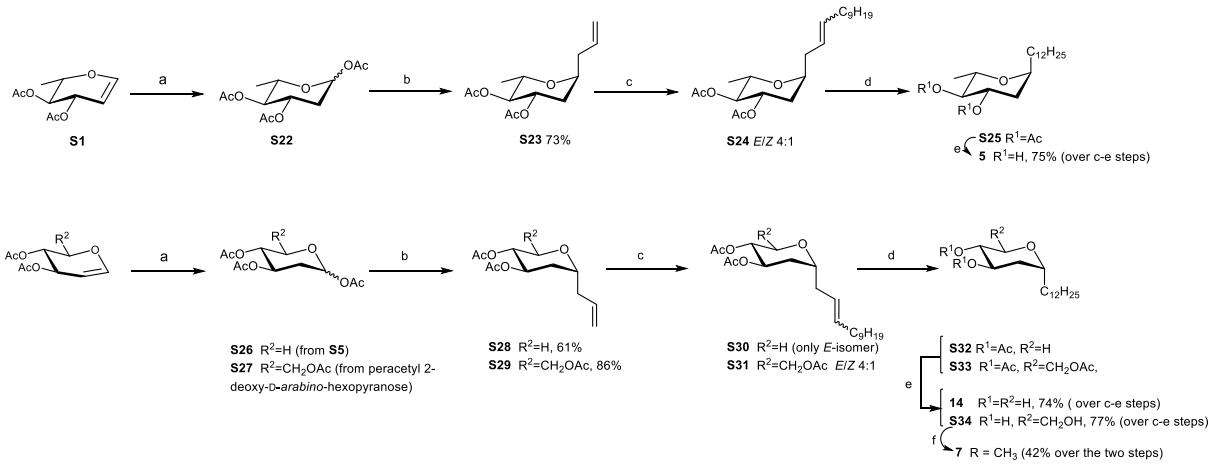

Scheme S3. Synthetic pathway for C-glycosides. Reagents and conditions: a) PPh_3•HBr, AcOH, DCM; b) $H_2C{=}CHCH_2Si(CH_3)_3$, BF_3•Et_2O, ACN, 0ºC; c) undec-1-ene, 2nd generation Grubbs-Hoveyda catalyst (5%), d) H_2, Pd/C, EtOAc; e) NaOMe, MeOH; f) i. TsCl, Pyr; ii: $LiAlH_4$, THF.

1,3,4-Tri-*O*-acetyl-2,6-dideoxy-L-*arabino*-hexopyranose (S22). Triphenylphosphane hydrobromide (0.10 mmol) and acetic acid (2.78 mmol) were added in sequence to a stirred solution of 3,4-di-*O*-acetyl-1,5-anhydro-2,6-dideoxy-L-*arabino*-hex-1-enitol (504 mg, 2.35 mmol) in dichloromethane (18.0 mL) at room temperature. The reaction mixture was stirred for 5 h at room temperature and then washed with a saturated solution of $NaHCO_3$, extracted with dichloromethane and dried with anhydrous sodium sulfate. After filtration, the organic phase was evaporated under reduced pressure to give a residue that was purified by column chromatographic eluted with EtOAc/hex (1:4), affording compound **S22** as colourless oil (213

mg, 33%). α/β= 8.3:1, R_f = 0.36 (EtOAc/hex 1:2). **^{1}H-RMN** ($CDCl_3$) δ 6.19 (d, 1H, $J_{1\alpha,2\alpha}$= 2.08, H1α), 5.77 (dd, 1H, $J_{1\beta,2eq\beta}$= 1.8, $J_{1\beta,2ax\beta}$= 9.9, H-1β), 5.28 (ddd, 1H, $J_{3\alpha,2eq\alpha}$= 5.5, $J_{3\alpha,2ax\alpha}$= 11.29, H-3α), 5.07 – 4.99 (m, 1H, H-3β), 4.81 (t, 1H, $J_{4\alpha,3\alpha}$= $J_{4\alpha,5\alpha}$ =9.7, H-4α), 4.77 (t, 1H, $J_{4\beta,5\beta}$=$J_{4\beta,3\beta}$= 9.6, H-4β), 3.98-3.91 (m, 1H, H-5α), 3.65-3.59 (m, 1H, H-5β), 2.26 (dd, 1H, $J_{2ax\alpha,3\alpha}$= 5.1, $J_{2ax\alpha,2eq\alpha}$= 13.5, H-2axα), 2.34 (ddd, 1H, $J_{2ax\beta,3\beta}$= 5.0, $J_{2ax\beta,2eq\beta}$= 7.0, H-2axβ), 2.12 (s, 3H, CH_3, -OAcα), 2.11 (s, 3H, CH_3, -OAcβ), 2.07 (s, 3H, CH_3, -OAcα), 2.06 (s, 3H, CH_3, -OAcβ), 2.03 (s, 3H, CH_3, -OAcα), 2.02 (s, 3H, CH_3, -OAcβ), 1.93 (td, 1H, H-2eqα), 1.83 (td, 1H, H-2eqβ), 1.24 (d, 3H, $J_{5,6}$= 6.2, H-6β), 1.20 (d, 3H, $J_{5,6}$= 6.2 Hz, H-6α). **^{13}C-RMN** ($CDCl_3$) δ 170.4 (C=O, OAc α), 170.2 (C=O, OAc β), 170.1 (C=O, OAc α and β), 169.3 (C=O, OAc α), 168.9 (C=O, OAc β), 90.9 (C-1β), 90.8 (C-1α), 74.1 (C-4α), 73.6 (C-4β), 70.9 (C-5β), 70.2 (C-3β), 68.4 (C-5α), 68.2 (C-3α), 35.1 (C-2β), 34.1 (C-2α), 22.0 (CH_3, -OAcα), 21.1 (CH_3, -OAcα), 20.9 (CH_3, -OAcβ), 20.8 (CH_3,-OAcα e CH_3, -OAcβ), 17.6 (C-6α), 17.5 (C-6β).

1,3,4-Tri-*O*-acetyl-2-deoxy-D-*threo*-pentopyranose (S26). Triphenylphosphane hydrobromide (0.10 mmol) and acetic acid (2.78 mmol) were added in sequence to a stirred solution of 1,5-anidro-3,4-di-*O*-acetyl-2-deoxy-D-*treo*-pent-1-enitol (473 mg, 2.36 mmol) in dichloromethane (18.0 mL) at room temperature. The reaction mixture was stirred for 5 h at room temperature. The reaction was then washed with a saturated solution of $NaHCO_3$, extracted with dichloromethane and dried with anhydrous sodium sulfate. After filtration, the organic phase was evaporated, and the resulting residue was purified by column chromatography eluted with EtOAc/hex (1:4) to afford **S26** as colourless oil (172 mg, 28%). α/β= 2.4:1, R_f= 0.39 (EtOAc/hex 1:2). **^{1}H-RMN** ($CDCl_3$) δ 6.13 (brs, 1H, $J_{1\alpha,2\alpha}$= 2.6, H-1α), 5.97 (t, 1H, $J_{1\beta,2\beta}$= 3.8, H-1β), 5.3 (ddd, 1H, $J_{3\alpha,2eq\alpha}$= 5.1, $J_{3\alpha,2ax\alpha}$= 9.2, $J_{3\alpha,4\alpha}$= 13.7, H-3α), 5.00 – 4.90 (m, 2H, H-4α e H-3β), 4.85 (dd, 1H, $J_{4\beta,5\beta}$= 4.7, $J_{4\beta,3\beta}$= 7.5, H-4β), 4.18 (ddd, 1H, $J_{5eq\beta,4\beta}$= 2.5, $J_{5ax\beta,5eq\beta}$= 12.5, H-5eqβ), 3.94 (dd, 1H, $J_{5eq\alpha,4\alpha}$= 4.9, $J_{5ax\alpha,5eq\alpha}$= 11.6, H-5eqα), 3.73 (dd, 1H,

$J_{5ax\alpha,4\alpha}$= 9.19, H-5axα), 3.64 (dd, 1H, $J_{5a\beta,4\beta}$= 4.73, H-5axβ), 2.31 – 2.21 (m, 2H, H-2axα e H-2axβ), 2.13 (s, 3H, CH_3, -OAcα), 2.10 (s, 9H, CH_3, -OAcα e CH_3, -OAcβ), 2.07 (s, 6H, CH_3, -OAcα e CH_3, -OAcβ), 1.98-1.87 (m, 2H, H-2eqα and H-2eqβ). **^{13}C-RMN** ($CDCl_3$) δ 170.1 (C=O, OAc α), 170.0 (C=O, OAc α and β), 169.8 (C=O, OAc β), 169.3 (C=O, OAc α and β), 90.8 (C-1α), 90.5 (C1β), 68.7 (C4α), 67.9 (C-3α), 67.6 (C-4β), 66.7 (C-3β), 61.8 (C-5α), 61.0 (C-5β), 33.2 (C-2α), 30.3 (C-2β), 21.1 (CH_3, -OAcβ), 21.0 (CH_3, -OAcα e CH_3, -OAcβ), 20.9 (CH_3, -OAcα).

1,3,4,6-Tetra-*O*-acetyl-2-deoxy-β-D-*arabino*-hexopyranose (S27). 2-deoxy-D-*arabino*-hexopyranose (502 mg, 3.06 mmol) was dissolved in pyridine (5 mL), and acetic anhydride (1.4 mL, 14.68 mmol) and DMAP (catalytic) were added. The reaction mixture was stirred at room temperature for 1h. After completion, the reaction was washed with a solution of 2M HCl. The organic phase was extracted with dichloromethane and dried with anhydrous sodium sulfate. After filtration, the organic phase was evaporated under reduced pressure, resulting in a residue that was purified by column chromatography eluted with EtOAc/hex (1:2), affording compound **S27** as colourless oil (1.0 g, 100%). R_f= 0.43 (EtOAc/hex 1:2). **^{1}H-RMN** ($CDCl_3$) δ 5.80 (d, 1H, $J_{1,2}$= 9.1, H-1), 5.11 – 5.01 (m, 2H, H-3 e H-4), 4.33 (dd, 1H, $J_{6a,5}$= 4.5, $J_{6a,6b}$= 12.3, H-6a), 4.10 – 4.07 (m, 1H, H-6b), 3.76 (s, 1H, H-5), 2.37 – 2.34 (m, 1H, H-2ax), 2.12 (s, 3H, CH_3, -OAc), 2.09 (s, 3H, CH_3, -OAc), 2.05 (s, 6H, CH_3, -OAc), 1.91 (m, 1H, H-2eq). **^{13}C-RMN** ($CDCl_3$) δ 170.7 (C=O, OAc), 170.1 (C=O, OAc), 169.8 (C=O, OAc), 168.8 (C=O, OAc), 91.1 (C1), 72.8 (C5), 70.2 (C4), 68.2 (C3), 62.0 (C6), 34.7 (C2), 21.0 (CH_3, -OAc), 20.9 (CH_3, -OAc), 20.8 (CH_3, -OAc), 20.7 (CH_3, -OAc).

General procedure for the allylation reaction: Allyltrimethylsilane (0.61 mL, 3.84 mmol) and boron trifluoride etherate (0.95 mL, 7.68 mmol) were added successively to a solution of the appropriate *O*-acetyl 2-deoxy sugar (**S22, S26** or **S27**, 500 mg) in dry acetonitrile (3.0 mL) under nitrogen atmosphere at 0 ºC. The reaction mixture was stirred for 15 min at 0 ºC. The reaction mixture was washed with a saturated solution of $NaHCO_3$, and the organic phase was extracted with dichloromethane and dried with anhydrous sodium sulfate. After filtration, the organic phase was evaporated under reduced pressure to give a residue that was purified by chromatographic column.

3-(3,4-Di-*O*-acetyl-2,6-dideoxy-α-L-*arabino*-hexopyranosyl)prop-1-ene (S23). By applying the above mentioned procedure to **S22**, compound **S23** was obtained as a colourless oil (409 mg, 73%). R_f= 0.61 (EtOAc/hex 1:2). **^{1}H-RMN** ($CDCl_3$) δ 5.84 – 5.73 (m, 1H, H-2), 5.16 – 5.09 (m, 3H, H-1b, H-1a and H-3'), 4.69 (t, 1H, $J_{4',3'}$=$J_{4',5'}$= 7.6, H-4'), 4.04 – 3.98 (m, 1H, H-1'), 3.80 (quint, 1H, $J_{5',6'a}$= 6.53, $J_{5',6'b}$= 13.3, H5'), 2.52 (Part A of the system ABX: quint, 1H, $J_{3a,2}$= 7.9, $J_{3a,3b}$= 14.5, H-3a), 2.30 (Part B of the system ABX, 1H, $J_{3b,2}$= 6.8, H-3b), 2.07 (s, 3H, CH_3, -OAc), 2.05 (s, 3H, CH_3, -OAc), 1.99 (td, 1H, $J_{2'ax,2'eq}$= 13.9, $J_{2'ax,3'}$= 9.3, H-2'ax), 1.87 – 1.80 (m, 1H, H-2'eq), 1.23 (d, 3H, H-6'). **^{13}C-RMN** ($CDCl_3$) δ 170.3 (C=O, OAc), δ 170.1 (C=O, OAc), 134.2 (C-2), 117.5 (C-1), 73.6 (C-4'), 69.7 (C-1'), 69.1 (C-3'), 68.2 (C-5'), 36.7 (C-3), 32.4 (C-2'), 21.1 (CH_3, -OAc), 21.0 (CH_3, -OAc), 17.5 (C-6').

3-(3,4-Di-*O*-acetyl-2-deoxy-α-D-*threo*-pentopyranosyl)prop-1-ene (S28). By applying the abovementioned procedure to compound **S26**, product **S28** was obtained as a colourless oil (284 mg, 61%). R_f= 0.54 (EtOAc/hex 1:2). **^{1}H-RMN** ($CDCl_3$) δ 5.84 - 5.73 (m, 1H, H-2), 5.14 – 5.07 (m, 2H, H-1b, H-1a), 5.01 - 4.87 (m, 2H, H-3' and H-4'), 4.08 (dd, 1H, $J_{5'e,4'}$=5.3, $J_{5'e,5'a}$= 11.2, H-5'e), 3.48 (quint, 1H, $J_{1',3a}$= 7.7, $J_{1',3b}$= 12.8, $J_{1',2'ax}$= 6.3, $J_{1',2'eq}$= 1.7, H-1'), 3.22 (t, 1H, $J_{5'a,4}$= 10.4, H-5'a), 2.37 – 2.30 (m, 1H, H-3a), 2.27 – 2.20 (m, 1H, H-3b), 2.15 (dd, 1H, $J_{2'eq,3}$= 4.9, H-2'eq), 2.05 (s, 3H, CH_3, -OAc), 2.04 (s, 3H, CH_3, -OAc), 1.46 (quart, 1H, $J_{2'eq,3}$= 11.4,

$J_{2'eq,2'ax}$= 6.8, H-2'ax). **^{13}C-RMN** ($CDCl_3$) δ 170.5 (C=O, OAc), δ 170.2 (C=O, OAc), 133.7 (C-2), 117.7 (C-1), 75.4 (C-1'), 71.8 (C-3'), 70.0 (C-4'), 67.1 (C-5'), 39.7 (C-3), 35.8 (C-2'), 21.1 (CH_3, -OAc), 20.9 (CH_3, -OAc).

3-(3,4,6-Tri-*O*-acetyl-2-deoxy-α-D-*arabino*-hexopyranosyl)prop-1-ene (S29). By applying the abovementioned procedure to compound **S27**, product **S29** was obtained as a colourless oil (407 mg, 86%). R_f= 0.22 (EtOAc/Hex 1:2). **^{1}H-RMN** ($CDCl_3$) δ 5.81 – 5.73 (m, 1H, H-2), 5.16 – 5.07 (m, 3H, H1b, H-1a to H3'), 4.85 (t, 1H, $J_{4,3}$=$J_{4,5}$= 6.8, H-4'), 4.39 (dd, 1H, $J_{6b,5}$= 5.9, $J_{6b,6a}$= 11.4, H-6b'), 4.07 (m, 2H, H-1' and H-6a'), 3.92 (br s, 1H, H-5'), 2.55 – 2.48 (m, 1H, H-3a), 2.31 – 2.28 (m, 1H, H-3b), 2.06 (s, 3H, CH_3, -OAc), 2.06 (s, 6H, CH_3, -OAc), 2.01 – 1.97 (m, 1H, H-2'ax), 1.86 – 1.84 (m, 1H, H-2'eq). **^{13}C-RMN** ($CDCl_3$) δ 170.3 (C=O, OAc), δ 169.6 (C=O, OAc), δ 169.5 (C=O, OAc), 133.8 (C-2), 117.3 (C-1), 70.5 (C-5'), 69.5 (C-1'), 68.4 (C-3' e C-4'), 61.8 (C-6'), 36.5 (C-3), 31.8 (C-2'), 20.7 (CH_3, -OAc), 20.5(4) (CH_3, -OAc), 20.5(0) (CH_3, -OAc).

General procedure for the metathesis reaction: The 2nd generation Grubbs-Hoveyda catalyst (5%, 1.86 mmol) was added to a solution of allyl glycoside (3.5 mmol) and 1-undecene (3.97 mL, 19.30 mmol, 5.5 equiv.) in dichloromethane (18 mL). The reaction was refluxed under nitrogen for 24h. After the reaction was complete (TLC), the solvent was evaporated and the residue directly purified by column chromatography to afford the product.

(2*E*)-/(2*Z*)-1-(3,4-Di-*O*-acetyl-2,6-dideoxy-α-L-*arabino*-hexopyranosyl)dodec-2-ene (S24). By applying the above mentioned procedure to compound **S23**, the unseparable (2*E*)/(2*Z*) mixture in a 4/1 ratio **S24** was isolated as a colourless oil (766 mg, 75%). R_f = 0.50 (EtOAc/hex 1:5). (*E*)-Isomer: **^{1}H-RMN** ($CDCl_3$) δ 5.54, 5.50 (part AXY of ABXY system, each t, 1H, $J_{1a,2}$= $J_{1b,2}$= 6.5 Hz, $J_{2,3}$= 15.2 Hz, H-2); 5.37, 5.33 (part BXY of ABXY system,

each t, 1H, $J_{3,4a}$= $J_{3,4b}$= 7.1 Hz, H-3),5.11 (td, 1H, $J_{3',2eq'}$= 4.7, $J_{3',2ax'}$= 13.0, H-3'), 4.68 (t, 1H, $J_{3',4'}$= $J_{4',5'}$= 7.8, H-4'), 3.97 – 3.91 (m, 1H, H-1'), 3.81 – 3.75 (m, 1H, H-5'), 2.48 – 2.40 (m, 1H, H-1a), 2.27-2.20 (m, 1H, H-1b), 2.06 (s, 3H, CH_3, -OAc), 2.04 (s, 3H, CH_3,-OAc), 2.01 – 1.95 (m, 3H, H-4a, H-4b and H-2ax'), 1.87-1.77 (m, 1H, H-2eq'), 1.26 (br s, 14H, H-5 to H-11), 1.21 (quart, 3H, $J_{5a',6'}$= 5.3, $J_{6a',6b'}$= 11.5, H-6'), 0.88 (t, 3H, $J_{11,12}$= 6.4, H-12**). ^{13}C-RMN** ($CDCl_3$) δ 170.2 (C=O, OAc), 170.1 (C=O, OAc), 133.8 (C-2), 125.2 (C-3), 74.0 (C-4'), 70.5 (C-1'), 69.2 (C-3'), 68.0 (C-5'), 35.4 (C-1), 32.6 (C-4), 32.4 (C-2'), 31.9, 29.6, 29.4, 29.3, 29.2, 22.7 (C-5 to C-11), 21.1 (CH_3, -OAc), 20.9 (CH_3, -OAc), 17.6 (C6'), 14.1 (C-12). **HRMS:** Calcd. for $[M+Na]^+$ 405.2611; Found: 405.2621 (error: -2.3 ppm).

(2*E*)-1-(3,4-Di-*O*-acetyl-2-deoxy-α-D-*threo*-pentopyranosyl)dodec-2-ene (S30). By applying the above-mentioned procedure to **S28**, compound **S30** was obtained as a colourless oil (780 mg, 74%). R_f = 0.51 (EtOAc/hex 1:5). **^{1}H-RMN** ($CDCl_3$) δ 5.50, 5.46 (part AXY of ABXY system, each t, 1H, $J_{1a,2}$= $J_{1b,2}$= 6.3 Hz, $J_{2,3}$= 15.3 Hz, H-2); 5.37, 5.33 (part BXY of ABXY system, each t, 1H, $J_{3,4a}$= $J_{3,4b}$= 7.4 Hz, H-3), 5.00 – 4.86 (m, 2H, H-3' and H-4'), 4.07 (dd, 1H, $J_{5'e,4}$= 5.4 Hz, H-5'e), 3.44-3.36 (m, 1H, H-1'), 3.21 (t, 1H, $J_{5'a,4}$=$J_{5'a,5'e}$= 10.6, H-5'a), 2.31 – 2.24 (m, 1H, H-1a), 2.19 – 2.10 (m, 2H, H-1b and H-2ax'), 2.04 (s, 3H, CH_3, -OAc), 2.03 (s, 3H, CH_3, -OAc), 2.01 – 1.96 (m, 2H, H-4a, H-4b), 1.47 – 1.38 (m, 1H, H-2eq'), 1.26 (br s, 14H, H-5 to H-11), 0.88 (t, 3H, $J_{11,12}$= 6.4, H-12). **^{13}C-RMN** ($CDCl_3$) δ 170.5 (C=O, OAc), 170.2 (C=O, OAc), 134.1 (C-2), 124.7 (C-3), 76.0 (C-1'), 72.0 (C-3'), 70.1 (C-4'), 67.1 (C-5'), 35.4 (C-1), 32.6 (C-4), 32.0 (C-2'), 31.9, 29.6, 29.5, 29.3, 29.2, 22.7 (C-5 to C-11), 21.1 (CH_3, -OAc), 20.9 (CH_3, -OAc), 14.1 (C-12). **HRMS:** Calcd. for $[M+H]^+$ 369.2636; Found: 369.2621 (error: 4 ppm).

(2*E*)-/(2*Z*)-1-(3,4,6-Tri-*O*-acetyl-2-deoxy-α-D-*arabino*-hexopyranosyl)dodec-2-ene (S31). By applying the abovementioned procedure to **S29**, compound **S31** was obtained as colourless oil (407 mg, 77%). R_f = 0.26 (EtOAc/hex 1:4), *E*/*Z* 4:1 (2*E*)-isomer: **^{1}H-RMN**

($CDCl_3$) δ 5.55, 5.51 (part AXY of ABXY system, each t, 1H, $J_{1a,2}$= $J_{1b,2}$= 6.4 Hz, $J_{2,3}$= 15.5 Hz, H-2); 5.37, 5.33 (part BXY of ABXY system, each t, 1H, $J_{3,4a}$= $J_{3,4b}$= 7.2 Hz, H-3), 5.17 – 5.11 (m, 1H, H-3'), 4.88 (t, 1H, $J_{3',4'}$= $J_{4',5'}$= 7.7, H-4'), 4.37 (dd, 1H, $J_{6a',5'}$= 6.0, $J_{6a',6b'}$= 12.0, H-6'a), 4.11 – 4.04 (m, 1H, H-6'b), 4.03 – 3.97 (m, 1H, H-1'), 3.91 – 3.87 (m, 1H, H-5'), 2.44 (quint, 1H, $J_{1a,2}$= 7.6, $J_{1a,1b}$= 14.6, H-1a), 2.27 – 2.20 (m, 1H, H-1b), 2.09 (s, 3H, CH_3, -OAc), 2.06 (s, 3H, CH_3, -OAc), 2.05 (s, 3H, CH_3, -OAc), 2.02 – 1.97 (m, 3H, H-4a, H-4b and H-2ax'), 1.91 – 1.80 (m, 1H, H-2'eq), 1.26 (brs, 14H, H-5 to H-11), 0.88 (t, 3H, $J_{11,12}$= 6.4, H-12). **^{13}C-RMN** ($CDCl_3$) δ 170.8 (C=O, OAc), 170.1 (C=O, OAc), 169.8 (C=O, OAc), 134.0 (C-2), 124.8 (C-3), 70.6 (C-1'), 70.5 (C-5'), 68.9 (C-3' e C-4'), 62.4 (C-6'), 35.4 (C-1), 32.6 (C-4), 31.7 (C-2'), 29.6, 29.4, 29.3, 29.2, 22.7 (C-5 to C-11), 21.0 (CH_3, OAc), 20.8(3) (CH_3, OAc), 20.8(0) (CH_3, OAc), 14.1 (C-12). **HRMS:** Calcd. for $[M+H]^+$ 441.2847; Found: 441.2830 (error: 3.8 ppm).

General procedure for the hydrogenation and deacetylation reactions: A solution containing the alkene (**S24**, **S30** or **S31**, 2.0 mmol) and 10% Pd/C (10-20% w/w) in EtOAc (6 mL) was stirred under hydrogen atmosphere for 3h, at room temperature. After completion of the starting material, the mixture was filtered through Celite and the solvent was removed under reduced pressure. After dissolution of the residue in MeOH (10 mL/g), a solution of 1% NaOMe in MeOH (1 mL/g) was added. The mixture was stirred at room temperature for 1 h. Neutralization with Amberlite (IR-120) was followed by filtration and evaporation of the solvent to give a residue, which was submitted to column chromatography to afford the respective glycosyl dodecane. The intermediate acetylated products (**S25**, **S32** and **S33)** were purified on a short chromatography column for intermediate product characterization.

1-(3,4-Di-*O*-acetyl-2,6-dideoxy-α-L-*arabino*-hexopyranosyl)dodecane (S25). Colourless oil, quantitative yield (769 mg). R_f= 0.70 (EtOAc/hex 1:5); **^{1}H-RMN** ($CDCl_3$) δ 5.10 (td, 1H, $J_{2ax',3'}$= 9.36, $J_{2eq',3'}$= 5.1, H-3'), 4.67 (t, 1H, $J_{3',4'}$= $J_{4',5'}$= 7.8, H-4'), 3.92 (td, 1H,

$J_{1',1a}$= 14.0, $J_{1',1b}$= 9.1, $J_{1',2'}$= 4.9, H-1'), 3.74 (quint, 1H, $J_{5',6a'}$= 6.5, $J_{5',6b'}$= 13.1, H-5'), 2.06 (s, 3H, CH_3, -OAc), 2.03 (s, 3H, CH_3, -OAc), 1.95 (dt, 1H, $J_{2ax',2eq'}$=13.3, H-2'a), 1.88 – 1.77 (m, 2H, H-2'eq, H-1a), 1.47 – 1.42 (m, 1H, H-1b), 1.26 (br s, 20H, H-2 to H-11), 1.21 (d, 3H, H-6'), 0.88 (t, 3H, $J_{12,11}$= 6.4, H-12). **^{13}C-RMN** ($CDCl_3$) δ 170.3 (C=O. OAc), 170.1 (C=O, OAc), 74.2 (C-4'), 70.6 (C-1'), 69.5 (C-3'), 67.6 (C-5'), 33.4 (C-2'), 31.9, 31.7, 29.6(8), 29.6(5), 29.6(0), 29.5(7), 29.4(0), 29.3(6), 26.0, 22.7 (C-1 to C-11), 17.7 (C-6'), 14.1 (C-12). **HRMS:** Calcd. for $[M+H]^+$ 385.2949; Found: 385.2938 (error: 2.7 ppm).

1-(2,6-Dideoxy-α-L-*arabino*-hexopyranosyl)dodecane (5). White solid, quantitative yield (840 mg). R_f= 0.37 (EtOAc/hex 1:1); m.p.=68.6-69.9 ºC; **^{1}H-RMN** ($CDCl_3$) δ 3.91 – 3.88 (m, 1H, H-1'), 3.71 (ddd, 1H, $J_{2a',3'}$= 11.4, $J_{2e',3'}$= 5.0, H-3'), 3.51 – 3.44 (m, 1H, H-5'), 2.94 (t, 1H, $J_{3',4'}$= $J_{4',5'}$= 8.7, H-4'), 1.90 (ddd, 1H, $J_{2eq',1'}$= 1.4, $J_{2ax',2eq'}$= 11.2, H-2'e), 1.83 (t, 1H, $J_{1a,1'}$= $J_{1a,1b}$= 9.0, H-1a), 1.73 (td, 1H, $J_{2ax',1'}$= 5.9, H-2'ax), 1.33 (br s, 2H, H-1b, H-2 to H-11), 1.26 (d, 3H, $J_{5',6'}$= 6.3, H-6'), 0.93 (t, 3H, $J_{12,11}$= 6.5, H-12). **^{13}C-RMN** ($CDCl_3$) δ 77.8 (C-4'), 72.4 (C-1'), 68.9 (C-5'), 68.7 (C-3'), 36.2 (C-2'), 31.7 (C-2 to C-11), 30.6 (C-1), 29.4(0), 29.3(6), 29.3, 29.1, 25.9, 22.3 (C-2 to C-11), 17.3 (C-6'), 13.1 (C-12). **HRMS:** Calcd. for $[M+H]^+$ 301.2737; Found: 301.2736 (error: -0.4 ppm).

1-(3,4-Di-*O*-acetyl-2-deoxy-α-D-*threo*-pentopyranosyl)dodecane (S32). Colourless oil, quantitative yield (770 mg). R_f= 0. 62 (EtOAc/hex 1:2). **^{1}H-RMN** ($CDCl_3$): 5.01 – 4.87 (m, 2H, H-3' and H4'), 4.07 (dd, 1H, $J_{5e',4'}$= 5.35, $J_{5a',5e'}$= 11.2, H-5'e), 3.40 – 3.35 (m, 1H, H-1'), 3.21 (t, 1H, $J_{5e',5a'}$=$J_{5a',4'}$= 10.8, H-5'a), 2.13 (ddd, 1H, $J_{1',2ax}$ = 1.49, $J_{2ax',2eq'}$= 12.58, $J_{2ax',3'}$= 6.4, H2'ax), 2.05 (s, 3H, CH_3,-OAc), 2.04 (s, 3H, CH_3, OAc), 1.59 – 1.50 (m, 1H, H-1b), 1.47 – 1.39 (m, 2H, H-2'eq and H-1ax), 1.26 (br s, 20H, H-2 to H-11), 0.89 (t, 3H, $J_{12,11}$= 6.4, H-12). **^{13}C-RMN** ($CDCl_3$): 170.5 (C=O, OAc), 170.1 (C=O, OAc), 76.1 (C-1'), 72.0 (C-3'), 70.2 (C-4'), 67.0 (C-5'), 36.3 (C-2'), 35.3 (C-1), 31.9, 29.6(4), 29.6(2), 29.5(3), 29.4(9), 29.3, 25.4, 22.7 (C-

2 to C-11), 21.1 (CH_3, OAc), 20.8 (CH_3, OAc), 14.1 (C-12). **HRMS:** Calcd. for $[M+Na]^+$ 393.2611; Found: 93.2602 (error: 2.4 ppm).

1-(2-Deoxy-α-D-*threo*-pentopyranosyl)dodecane (14). White solid, quantitative yield (570 mg). m.p. 69.8-70.7 ºC, R_f= 0. 24 (EtOAc/hex 1:1). **^{1}H-RMN** ($CDCl_3$) δ 3.88 (dd, 1H, $J_{5e',4'}$= 5.2, H-5'e), 3.50 – 3.44 (m, 1H, H-1'), 3.37 – 3.31 (m, 2H, H-3', H-4'), 3.08 (t, 1H, $J_{5e',5a'}$=$J_{5a',4'}$= 10.7, H-5'a), 1.97 (ddd, 1H, $J_{1',2ax'}$= 1.5, $J_{2ax',2eq'}$= 12.9, $J_{2ax',3'}$= 6.5, H-2'ax), 1.56 – 1.44 (m, 2H, H-1a, H-1b), 1.32 (br s, 20H, H-2 to H-11), 1.28 – 1.22 (m, 1H, H-2'eq), 0.93 (t, 3H, $J_{12,11}$= 6.8, H-12). **^{13}C-RMN** ($CDCl_3$) δ 76.5 (C-4'), 72.6 (C-1'), 71.7 (C-'), 69.7 (C-5'), 39.1 (C-2'), 35.3 (C-1), 31.7, 29.3(8), 29.3(5), 29.3(1), 29.2(9), 25.3, 22.3 (C-2 to C-11), 13.0 (C-12). **HRMS:** Calcd. for $[M+Na]^+$ 309.2400; Found: 309.2400 (error: 0.0 ppm).

1-(3,4,6-Tri-*O*-acetyl-2-deoxy-α-D-*arabino*-hexopyranosyl)dodecane (S33). Colourless oil, quantitative yield (768 mg). R_f= 0.35 (EtOAc/hex 1:2). **^{1}H-RMN** ($CDCl_3$) δ 5.14 (td, 1H, $J_{2ax',3'}$= 12.8, $J_{2eq',3'}$= 4.9, H-3'), 4.87 (t, 1H, $J_{3',4'}$= $J_{4',5'}$= 7.71, H-4'), 4.37 (dd, 1H, $J_{6a',5'}$= 5.9, $J_{6a',6b'}$= 12.0, H-6'a), 4.08 (dd, 1H, $J_{6e',5'}$= 3.3, H-6'e), 3.99 (td, 1H, $J_{1',1}$= 9.4, $J_{1',2'}$= 4.6, H-1'), 3.88 – 3.83 (m, 1H, H-5'), 2.09 (s, 3H, CH_3, -OAc), 2.06 (s, 3H, CH_3, -OAc), 2.05 (s, 3H, CH_3, -OAc), 1.96 (dt, 1H, $J_{2ax',2eq'}$= 13.6, $J_{2ax',3'}$= 9.1, H-2'a), 1.90 – 1.83 (m, 1H, H-2'e), 1.81 – 1.74 (m, 1H, H-1a), 1.45 – 1.39 (m, 1H, H-1b), 1.26 (brs, 20H, H-2 to H-11), 0.88 (t, 3H, $J_{12,11}$= 6.6, H-12). **^{13}C-RMN** ($CDCl_3$) δ 170.8 (C=O, OAc), 170.2 (C=O, OAc), 169.8 (C=O, OAc), 70.8 (C-1'), 70.2 (C-5'), 69.1 (C-3'), 69.0 (C-4'), 62.4 (C-6'), 33.0 (C-2'), 31.9, 31.7, 29.6(4), 29.5(9), 29.3, 25.7, 22.7 (C-1 to C-11), 21.1 (CH_3, OAc), 20.8(3) (CH_3, OAc), 20.8(0) (CH_3, OAc), 14.1 (C-12). **HRMS:** Calcd. $[M+Na]^+$ 465.2823; Found: 465.2803 (error: 4.3 ppm).

1-(2-Deoxy-α-D-*arabino*-hexopyranosyl)dodecane (S34). White solid, quantitative yield (808 mg). m.p. 91.1-91.7 ºC, R_f= 0.27 (EtOAc). **^{1}H-RMN** ($CDCl_3$) δ 3.97 – 3.95 (m, 1H,

H-1'), 3.81 (dd, 1H, $J_{6a',5'}$= 2.6, $J_{6a',6b'}$= 11.7, H-6'a), 3.78 – 3.73 (m, 1H, H-3'), 3.70 (dd, 1H, $J_{6b',5'}$= 5.7, H-6'b), 3.42 (ddd, 1H, $J_{5',4'}$= 8.7, H-5'), 3.22 (t, 1H, $J_{3',4'}$= $J_{4',5'}$= 8.7, H-4'), 1.90 (ddd, 1H, $J_{2ax',2eq'}$= 11.3, $J_{2eq',3'}$= 4.8, $J_{2eq',1'}$= 2.0, H-2'eq), 1.83 (t, 1H, $J_{1ax,1'}$= $J_{1a,1b}$= 9.0, H-1a), 1.73 (td, 1H, $J_{2ax',1'}$= 5.8, H-2'ax), 1.46 (brs, 1H, H-1b), 1.32 (br s, 20H, H-2 to H-11), 0.93 (t, 3H, $J_{12,11}$= 6.4, H-12). **^{13}C-RMN** ($CDCl_3$) δ 73.8 (C-5'), 72.3 (C-1'), 72.2 (C-4'), 68.9 (C-3'), 61.8 (C-6'), 35.9 (C-2'), 30.6 (C-1), 31.7, 29.4, 29.3, 29.2, 29.1, 25.8, 22.3 (C-2 to C-11), 13.0 (C-12). **HRMS:** Calcd. $[M+Na]^+$ 339.2506; Found: 339.2504 (error: -0.7 ppm).

1-(2,6-Dideoxy-α-D-*arabino*-hexopyranosyl)dodecane (7). TsCl (602 mg, 3.16 mmol) in pyridine (2 mL) was added to a solution of the alkyl-2'-deoxy-glycoside **S34** (500 mg, 1.56 mmol) in pyridine (4.0 mL) at 0 ºC and the reaction mixture was stirred at room temperature for 4 h. The solvent was co-evaporated with toluene under reduced pressure, and the resulting residue was dissolved in dry THF (23.0 mL), and $LiAlH_4$ (2M in THF, 8.5 mL) was added. The reaction was stirred under reflux for 2 h. When the reaction was complete, the solution was cooled to 0 ºC and water (0.5 mL) was added dropwise, followed by aqueous NaOH 15% (1.0 mL). The solution was stirred for 15 min at room temperature and then dried with anhydrous sodium sulfate. After filtration and evaporation of the solvent, the resulting residue was purified by column chromatography eluted with EtOAc/hex 1:2, yielding product **7** as a white solid (198 mg, 42%). m.p. 62.1-63.3 ºC, R_f= 0.58 (EtOAc). **^{1}H-RMN** ($CDCl_3$) δ 3.93 – 3.90 (m, 1H, H-1'), 3.78 (ddd, 1H, $J_{2ax',3'}$= 9.0, $J_{2eq',3'}$= 5.1, H-3'), 3.47 (td, 1H, $J_{5',6a'}$= 5.9, $J_{5',6b'}$= 12.4, H-5'), 3.06 (t, 1H, $J_{3',4'}$= $J_{4',5'}$= 9.1, H-4'), 2.61 (br s, 1H, OH), 1.91 (dd, 1H, $J_{2ax',1'}$= 4.8, $J_{2ax',2eq'}$= 12.5, H-2'ax), 1.83 – 1.75 (m, 2H, H-2'eq and H-1a), 1.43 – 1.37 (m, 2H, H-1b and H-2ax), 1.26 (br s, 22H, H-6, H-2b to H-11), 0.88 (t, 3H, $J_{12,11}$= 6.3, H-12). **^{13}C-RMN** ($CDCl_3$) δ 78.8 (C-4'), 72.8 (C-1'), 69.9 (C-3'), 68.3 (C-5'), 36.3 (C-2'), 31.9 (C-2 to C-11), 31.0 (C-1), 29.7, 29.6, 29.4, 26.2, 22.7 (C-2 to C-11), 18.3 (C-6'), 14.1 (C-12). **HRMS:** Calcd. $[M+H]^+$ 301.2737; Found: 301.2730 (error: 1.3 ppm)

Biological Studies

Bactericidal activity: Strains of *Bacillus cereus* ATCC 14579, *Staphylococcus aureus* ATCC 25923, were obtained from the American Type Culture Collection (Rockville, MD). The bacterial cultures were maintained at lyophilized state or stored at -80ºC in Müller-Hinton broth (MH) supplemented with 20% glycerol (Sigma Aldrich). Overnight cultures of bacteria were grown in 50 mL Erlenmeyer flasks, with orbital shake at 200 rpm at 30 ºC. MIC determination was made by a modified micro-dilution method according to CLSI guidelines.[14] Briefly, overnight culture (17 h) of all bacterial strains were diluted to 0.5 McFarland units in Müller-Hinton broth. In sterile 96-well plates (Sarstedt), 150 μL of culture media were added and then supplemented with the compound in study by serial dilution. Finally, the desired wells were inoculated with 10 μL of a 1/10 dilution of the 0.5 McFarland bacterial suspension. Microplates were incubated at 35 °C, with orbital shaking, taking absorbance readings in all wells at intervals of 10 min, for up to 24 h (Anthos Zenith 3100 Microplate Multimode Detector). The lowest concentration at which no bacterial growth was observed is considered the minimal inhibitory concentration (MIC). Aliquots of 5 μL from every well were transferred to Müller-Hinton Agar (MHA) for determination of minimum bactericidal concentration (MBC). Bacterial growth was assessed at 17 h, and MBC was considered the lowest concentration of compound where no bacterial growth was observed. All measurements are the average of a minimum of 3 independent experiments.

In vitro Time-Killing curves: The compounds were added to an exponential phase culture of *B. cereus* in Müller-Hinton containing about 10^6, 10^7, and 10^8 cells/mL. Bacteria were then incubated at 35 ºC, and 5 μL aliquots were withdrawn at different intervals and where diluted in a previously premade microplate. The samples were serial diluted in 1/10 of the previous

concentration, and then, a 10 μL droplet was transferred to MHA and bacterial growth was evaluated. The number of surviving bacteria, expressed as the number of colony forming units (CFU), were counted after an overnight incubation at 30 ºC.

For all the experiments, sample homogeneity and methodology validation was performed by OD_{600nm}, as a measure of cellular density, for all sixteen replicates.

Differential metabolomics analysis: The study of bacterial metabolic response to compound **1**, was performed using Phenotype MicroArrays (Biolog). The impact of compound **1** was assessed in the metabolism of 95 different carbon sources by *B. cereus* ATCC 14579 strain. All the solutions used were supplied by the manufacturer. The PM solutions B-F where sterilized in autoclave at 121 ºC during 15 min, and afterwards stored at 4 ºC until use. The PM additive solution was prepared by mixing these solutions (10 mL of solutions B, C, E and F and 30 mL of solution D and water). The bacterial growth media was used according to instructions provided by the manufacturer. The bacterial suspension, for PM Inoculating Fluid, was prepared by centrifuging the overnight pre-inoculum (at 3000 g, 4 ºC for 5 min) collecting and resuspending the cells in IF-0a, and finally adjusting the bacterial suspension to 0.5 McFarland units. Finally, 100 μL of the PM inoculating fluid, was added to each well of 4 PM1 microplates (Compound **1** at the final concentrations of 16, 8, 4 and 0 μg/mL). The microplates were sealed with parafilm, shielded from light and incubated at 35 ºC with orbital shaking. The compound was added at 1 h of incubation, in order to stabilize and allow bacterial cells to adapt to the new media. The reduction of tetrazolium violet associated to NADH produced by the consumption of each tested carbon source, was monitored by OD_{590nm} at time 0', at 30', at 60' after incubation, and then, hourly for 27 h. (Anthos Zenith 3100 Microplate Multimode Detector). The time-dependent series for each tested carbon source was classified by the

acquisition periods, corresponding to: 1) initial phase of response to the compound **1** (from 0 to 5 h of incubation); 2) late phase of response (from 16 h to 27 h of incubation). After data normalization, results were divided into five categories depending on the effect shown: 1) highly inhibitory effect, when the difference between the effect of the compound **1** and control was higher than 5σ (OD_{590nm}>5σ); 2) inhibitory effect, when the difference observed was between 5σ and 2σ (5σ>OD_{590nm}>2σ); 3) no effect, when bacterial growth was observed in the absence of compound (OD_{590nm}>2σ) and the difference between absence and presence of compound was less than 2σ; 4) no growth, when value with and without the presence of compound was less than 2σ (OD_{590nm}<2σ); 5) potentiation effect, when value without the compound was less than 2σ (OD_{590nm}<2σ) and the difference of value between the presence and absence of compound was superior to σ. The hits classified as category 1, 2 or 5, were correlated to the biological pathways described at "Kyoto Encyclopedia of Genes and Genomes" (KEGG) database.[54] The biological pathways were then ordered by the number of inhibitory hits per pathway. The metabolic reconstruction was performed using graph theory for hierarchical superimposition of the pathways based at the nonparametric Spearman's rank association coefficients (edges) between hits (nodes – according to KO classification system). The SPSS (SPSS Statistics for Windows, SPSS Inc.) software was used for data normalization and determination of nonparametric association coefficients and Cytoscape (Cytoscape, U.S. NIGMS) for the hierarchical representation (Figure S5).

Mutant libraries:

Preparation of electro-competent cells: B. cereus ATCC 14579 cells were grown in an Erlenmeyer flask containing tryptic soy broth (TSB, Difco Laboratories), and placed in an incubator at 37ºC and 200 rpm, until the bacterial suspension reaches a maximum OD of 0.45

– 0.46 measured at 600 nm. The suspension was then incubated during 1 h in 5% glycine or DL-threonine and 250 mM sucrose at 37 °C at 200 rpm. Cells were washed five times in electroporation buffer (250 mM sucrose, 1 mM Hepes, 1 mM $MgCl_2$, 10% glycerol, pH 7.0) and concentrated 150-fold.

Electroporation: Electroporation was performed at 25 μF using a Bio-Rad Gene Pulser X-cell apparatus (Bio-Rad laboratories, U.S.). Electroporation was carried out in 1 mm electroporation cuvettes, at 4 ºC, with 50 μL cells combined with 500 ng of plasmid, in order to respect cells/DNA proportions. It was used voltage of $20kV/cm^{-1}$ with 200 ohms of resistance. After electroporation, cell suspensions were immediately diluted with 1 mL of TSB supplemented with 250 mM sucrose, 5 mM $MgCl_2$, 5 mM $MgSO_4$ and incubated for 2 h at 37 °C, 200 rpm to allow expression of antibiotic resistance markers. Aliquots were spread onto tryptic soy agar (TSA, Difco Laboratories) supplemented with appropriate antibiotic. Transformants harbouring antibiotic resistance were counted following overnight incubation.

Constrution of in vivo *mutant library by random insertion of transposon Tn917 in B. cereus ATCC 14579:* Transposon mutagenesis was performed by obtaining a stationary-phase culture of modified *B. cereus* (pLTV1) cultured overnight at 28 °C in Lysogeny broth (LB) containing tetracycline (50 μg/mL), erythromycin (1 μg/mL), and chloramphenicol (10 μg/mL) (Sigma-Aldrich). This culture was diluted 1:800 in prewarmed (43 °C) LB broth that contained erythromycin (1 μg/mL) and chloramphenicol (5 μg/mL). Then, it was incubated at 43 °C for 24 h with shaking at 200 rpm. The above procedure was repeated one more time. Transposon mutants were subsequently selected on LB agar containing erythromycin (1 μg/mL) and chloramphenicol (5 μg/mL) and incubated at 37°C, resulting in two libraries of 10^6 mutants each.

Southern Blotting: The validation of insertion site of Tn917 carried by plasmid pLVT1 was performed in the two pools of mutants. Briefly, chromosomal DNA from both *B. cereus* ATCC 14579 wild and modified strains, as well as from both generated mutant libraries, were isolated using the CTAB method.[55] After digestion with *Eco*RI the DNA of the mutant libraries and control strains were resolved in an agarose gel 0.8 %. The DNA transfer proceeded overnight, and hybridization was performed at 40 ºC with DNA probe (5.1 kb *Eco*RI restriction fragment of Tn917), labelled with digoxigenin-dUTP, at a concentration of 25 ng/mL. The membrane was revealed with NBT-BCIP.

*Transporter systems knockout mutant library***:** Twenty-eight knockout mutants based in the isogenic system *B. subtilis* 168 on main ABC and PTS systems were purchased from National BioResource Project (NIG, Japan): *Bacillus subtilis*. Table S5 identifies the individual mutants and respective MIC and MBC values obtained for compound **1**.

Computational Methods

DFT calculations: DFT calculations were performed with Gaussian 09 software.[38] The Perdew– Burke–Ernzerhof functional (PBE0), which uses 25% exchange and 75% correlation weighting, was used in all calculations.[39] Geometries were optimized without symmetry constraints and obtained using the 6-311G** basis set for all atoms.[40] Frequency calculations were performed to assess the nature of optimized geometries, and zero imaginary frequency was obtained for all minima. All geometries were optimized in the corresponding media, using the integral equation formalism of the polarizable continuum solvation model (IEFPCM)[41] on the electronic density (SMD).[42] Dielectric constants (bulk relative permittivities) of ε=4.711 (for chloroform) and ε=32.613 (methanol) were used for solvent specification.

General MM/MD Settings: All molecular mechanics/molecular dynamics (MM/MD) simulations were performed using the GROMACS software package (version 4.0.7).[43-44] The GROMOS 54A7 force field[45] was used, which already includes the corrections to phosphatidylcholine parametrization originally implemented in the GROMOS 53A6 force field.[46] For carbohydrates, the GROMOS $56A_{CARBO}$ force field[47] was used. The modelled glycoside and phospholipid (DMPC) molecules were built using PyMOL.[56] All simulations were started from pre-equilibrated systems solvated with adequate number (see below) of explicit SPC water molecules.[48] A tetragonal simulation box was used, applying periodic boundary conditions in all three dimensions with the minimum image convention, and ensuring that the membrane pore or lipid bilayer system could not see the respective periodic image along the membrane normal. Each simulation replicate was started by applying different sets of initial velocities taken from a Maxwellian distribution at 308K. The equations of motion were numerically integrated with a time step of 2 fs, with conformations being saved every 10 ps for analysis purposes. Non-bonded interactions were treated using a twin-range method with cutoffs of 8 Å and 14 Å, updating the neighbor pair list every step and every 5 steps, respectively. A reaction field was used to treat electrostatic interactions larger than 14 Å, using a relative dielectric constant of 54.0.[57] All simulations were performed in the isothermal-isobaric (NPT) ensemble. Solute and solvent were separately coupled to external heat baths using the v-rescale algorithm[58] at 308 K with a $\tau_p = 0.1$ ps. Pressure was kept constant at 1 bar using a Berendsen's semi-isotropic coupling,[59] with isothermal compressibility of 4.5×10^{-5} bar^{-1} and a $\tau_p = 5.0$ ps (unless stated otherwise). All glycoside and/or phospholipid bond lengths were constrained using the parallel version of the linear constraint solver algorithm (P-LINCS),[60] while the SETTLE algorithm[61] was used for constraining water molecules.

Membrane Pore Simulations: Initial configurations for the membrane pore stability studies were built starting from pre-equilibrated systems and by removing several molecules

to form a large enough cavity for the next steps. In these pore stability studies, we only used compound **1**. The final systems consisted of 234 DMPC, 52 glycoside (GL) in 196 DMPC (~20 %), or 124 GL in 124 DMPC (50 %) solvated with ~12000 water molecules. A three-step simulation procedure was then performed to force water molecules to fill the cavity and subsequently allow glycosides and/or phospholipids to equilibrate and stabilize the pore. First, a 60 ps simulation was done at constant volume, with the solvent temperature increased up to 500.0 K and position restraints on all glycoside atoms with force constants of 1000 kJ nm^{-2} mol^{-1} in the two directions perpendicular do the membrane normal and 10 kJ nm^{-2} mol^{-1} in the other. Phospholipid atoms' positions were restrained using a force constant of 1000 kJ nm^{-2} mol^{-1} in all three directions. The second simulation, performed at constant pressure for ~3 ns, was carried out without position restraints to enable free motion of the lipids, the solvent was cooled down to 308 K and the pressure was kept constant at 1 bar in the bilayer plane direction and at 100 bar in the bilayer normal direction (τ_p = 0.5 ps), to force the water molecules to stay inside the cavity. The conformations used in the final simulations were selected as the largest pore sizes allowed, before the lipid bilayer sees its periodic image over direction of the membrane normal. This last step, consisted in 30 ns simulations at constant area, 308 K and 1 bar (τ_p = 2.0 ps, in the direction of the membrane normal), to allow for the lipid positions and pore size equilibrations. The final conformations exhibited pore sizes with ~1800 water molecules. A water molecule is considered inside the pore when the *zz* coordinate of its oxygen atom is between the average *zz* positions, per monolayer, of the 4^{th} methylene of the DMPC tails. Five NPT production replicates were performed (308 K and 1 bar with τ_p = 2.0 ps), starting from different conformations extracted from the last equilibrated nanoseconds of the constant area simulation.

Glycoside/Phospholipid Bilayer Simulations: Bilayer systems consisting of GL/DMPC binary mixtures were constructed starting from a pre-equilibrated lipid bilayer containing 256

DMPC molecules and 8821 water molecules, from which a variable number of phospholipids (n = 2, 10, 30, 60 or 128) was randomly removed and replaced by equal number of glycoside molecules (GL = compounds **1**, **8**, **4**, DG or OG). Equilibrium configurations of each two-component bilayer system at different molar fractions (GL/DMPC = 0.8%, 3.9%, 11.7%, 23.4% or 50.0%; 75.0% was also tested for OG simulations) were subsequently simulated in triplicate, 100 ns long each. A 100% DMPC bilayer was also simulated, with a production time of 300 ns (single replicate), as a control for analysis purposes. In all simulations, the last 80 ns of production were used for analysis.

All systems were energy minimized prior to the MM/MD production simulations according to the following three-step procedure: (i) ~ 10^4 steps with the steepest descent algorithm (without constraints) followed by (ii) ~ 10^4 steps using the limited-memory Broyden–Fletcher–Goldfarb–Shanno (*l*-BFGS) algorithm (also unconstrained) and (iii) a final minimization using the steepest descent algorithm again, but with all bond lengths constrained. MM/MD simulations were subsequently initialized in three-steps. First, a 50 ps simulation, which was carried out with the positions of all atoms restrained using a force constant of 10^3 kJ nm^{-2} mol^{-1}. In the second step, a 300 ps simulation was performed with all atoms again position-restrained, but using a force constant of 10^2 kJ nm^{-2} mol^{-1} instead. Finally, only the sugar ring and phosphorus atoms were restrained with force constants of 10^2 kJ nm^{-2} mol^{-1} and 10^3 kJ nm^{-2} mol^{-1}, respectively, for further 100 ps. The equilibrated conformations obtained as described above were used as starting systems for the several production simulations performed.

Data Analysis: All analyzes were performed using tools available from the GROMACS software package[43-44]or others developed in-house. Plotted data was averaged over at least three replicates, depending on the system. Ensemble averages were calculated considering only the contribution of equilibrated segments of the trajectories. The total bilayer area was determined

from the dimensions of the simulation box along the bilayer plane, averaging over time from all simulations. The degree of phospholipid acyl chain ordering was assessed by calculating the deuterium order parameters, $|S_{CD}|$, defined as:

$$|S_{CD}| = \frac{1}{2}\langle 3\cos^2\theta - 1\rangle$$

where θ is the angle between the vector along the C-D bond and the bilayer normal, and the angular brackets denote an average over time for the entire ensemble. This property can be determined experimentally by ^{2}H-NMR spectroscopy and provides a measure of the orientational anisotropy of each C-D bond with respect to a reference axis.[62] The bilayer thickness, often expressed as the headgroup spacing (i.e. the average distance between phospholipid headgroup phosphates), D_{HH}, was computed as twice the average distance between the positions (component parallel to the membrane normal) of all phosphorus atoms and the center of mass of the bilayer, averaging over the entire trajectory. Errors were computed as the correlation-corrected standard deviation in the mean using standard methods based on the time-dependent autocorrelation function of the given property, which was used to estimate the number of independent blocks in the simulations.[49] The correlation time was taken as the value at which the autocorrelation function becomes lower than 0.1.

2 | Supplementary Text

Conformational analysis of *threo*-pentopyranosides

NMR structure elucidation of the β-L-anomer **9** suggested the adoption of an unusual conformation when the sample was solved in chloroform-*d*. Its anomeric proton signal appeared as a broad triplet with coupling constants $^3J_{1,2e} = {}^3J_{1,2a} = 3.5$ Hz, with an order of magnitude common to that of α-anomers. Both stereoisomers **8** and **9** presented similar H-1

and C-1 resonances, with H-1 chemical shifts of δ=4.84 ppm for **8** and δ=4.80 ppm for **9** and those of C-1 appearing at δ=97.6 ppm and δ=98.1 ppm, respectively. In addition, the anomeric proton of the α-glycoside was observed as a broad double doublet with coupling constants $^{3}J_{1,2a}$ = 3.3 Hz, $^{3}J_{1,2e}$ = 1.7 Hz. Altogether, these results are not in agreement with the expected equatorial orientation of the anomeric substituent for the β-L-glycoside, that usually adopts a $^{1}C_{4}$ conformation. Instead, they suggest an unusual $^{4}C_{1}$ conformation, featuring all substituents of the pentopyranosyl ring in axial orientation, in chloroform-*d*. As anticipated, NMR spectra of the two stereoisomers acquired in methanol-d_4 followed the expected pattern and the typical $^{1}C_{4}$ conformation could be unambiguously assigned. While ^{1}H-NMR data obtained for the α-anomer **8** in chloroform-*d* and methanol-d_4 were very similar, the H-1 signal of the β-anomer **9** was now visible at δ = 4.53 ppm as a double doublet, with $^{3}J_{1,2e}$ = 1.7 Hz and the expected *trans*-diaxial coupling constant of H-1 with H-2a ($^{3}J_{1,2a}$ = 8.4 Hz). Moreover, the chemical shift of C-1 in methanol-d_4 was now found at 101.5 ppm, also supporting the β-configuration in a $^{1}C_{4}$ conformation (figure S1). In the case of enantiomers **10** and **11**, opposing conformational preferences were observed under similar conditions, accordingly.

These results provide evidence that the solvent environment modulates conformer populations of β-L-glycoside **9** in solution. The proposed conformational preferences were further analyzed by DFT calculations (PBE0/6-311G**).[39-40] The geometries of the two chair conformers ($^{4}C_{1}$ and $^{1}C_{4}$) of glycosides **8** and **9** were optimized in both chloroform and methanol (IEFPCM/SMD),[41-42] and the relative Gibbs free energies obtained are provided in Table S1.

In agreement with experimental data, the considerable energy differences obtained for the α-glycoside **8** support a clear preference for the $^{1}C_{4}$ conformer in solution, regardless of the solvent. In contrast, in the case of β-glycoside **9**, the energy of the $^{1}C_{4}$ conformer is higher by 1.0 kcal mol^{-1} in chloroform, pinpointing to a greater stability for the $^{4}C_{1}$ conformation in this

case. This thermodynamic preference may be rationalized by stereoelectronic influences, namely the contribution of the anomeric effect given the low dielectric constant of the media. Furthermore, considering the structural flexibility of **9**, a plausible driving force towards the lower energy calculated for the $^4C_1$ conformer is intramolecular hydrogen bonding involving the 3-hydroxy group and the exocyclic oxygen, as shown in figure S2. This weak non-covalent interaction (O···O distance of 2.8 Å and O–H···O angle of 143º) may be exacerbated in chloroform which features poor hydrogen bonding capability. In turn, a very negligible energy difference was obtained for the two conformations of **9** in methanol, although experimental data provides unambiguous evidence that only the $^1C_4$ conformer is populated. Accounting for the great ability of the protic solvent to establish competitive intermolecular hydrogen bonds and further decrease the anomeric effect, we conclude that this result arises from an overestimation of the intramolecular hydrogen bond in methanol, resulting from a limited description of solvation effects by the implicit model used in the calculations.

Our results expose pentopyranoside anomeric chemistry as particularly challenging regarding endo and exo-anomeric effects, resulting in unpredictable inversion of conformation and reaction outcomes when compared to the hexopyranoside analogs, in line with findings reported on other systems, where conformation inversion of xylopyranosides and sulfur exo-anomeric effect played an important role in reaction outcome.[63]

Nature and kinetics of antibacterial activity

The studies on bacteriostatic/bactericide activity and bioactivity kinetics were performed with the easily available glycoside **1**, and the bacterial strain *B. cereus* ATCC 14579 with the broth microdilution method following CLSI guidelines. The resulting MIC values are twice those described for the agar dilution method, but this methodology permits simultaneous data assessment by varying multiple experimental conditions.

The kinetic study was performed with a temporal resolution of 10 min, the minimal time required for sampling, at the concentrations of 4 – 32 μg mL^{-1} (figure S4, table S2). Although the resolution used in this study is far superior to the traditional one collecting results hourly, the kinetics of bacterial cell death could not be followed at concentrations of 32 μg mL^{-1} and of 16 μg mL^{-1}, the latter at 10^6 starting cell concentration, because complete cell death was observed at the first temporal point. However, 1000-fold reduction of initial inoculum ($T_{99.9}$) was reached within 60 min with starting cell concentrations of 10^7 or 10^8, while at 4 and 8 μg mL^{-1} bacterial growth was similar to that of the control. In all performed assays MIC and MBC values were the same, indicating that bioactivity is bactericidal in nature. The extremely fast bactericide action suggests that no metabolic cascade plays a determinant role in bacterial death.

Bilayer thickness and glycoside-phospholipid interactions

The average bilayer thickness increases when the glycoside molar fraction is increased (figure S12), similarly to the results obtained for the order parameter. The distribution of glycoside headgroups along the bilayer normal (figure S13) is also dependent on glycoside molar fraction. In fact, at higher molar fractions, glycoside headgroups populate outer regions of the bilayer, particularly in the case of more polar headgroups, indicating that the loading capacity of the bilayer is limited. Independently of this effect, glycoside molecules are typically inserted below phospholipid phosphates, interacting with neighboring phospholipids by establishing hydrogen bonds with different acceptors (figure S14).

3 | Supplementary Figures

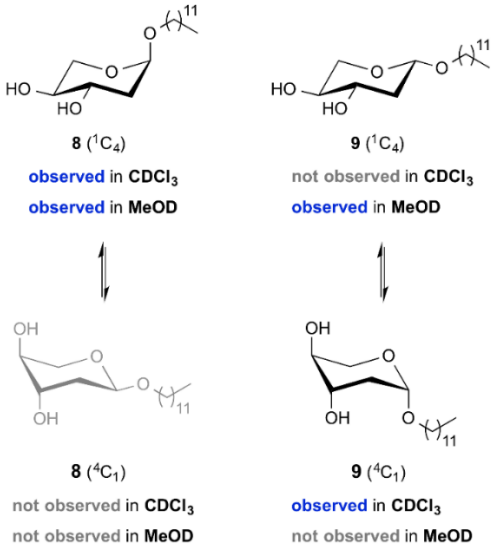

Figure S1 Conformational preferences detected by NMR in chloroform-*d* and methanol-d_4 for dodecyl 2-deoxy-α-L-*threo*-pentopyranoside **8** (left) and dodecyl 2-deoxy-β-L-*threo*-pentopyranoside **9** (right).

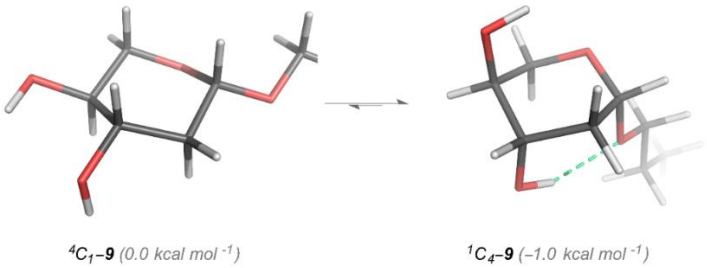

Figure S2. DFT-optimized geometry for the two chair conformers of dodecyl 2-deoxy-β-L-*threo*-pentopyranoside **9** in chloroform. The intramolecular hydrogen bond observed in the lower energy conformation is highlighted as light green dashes.

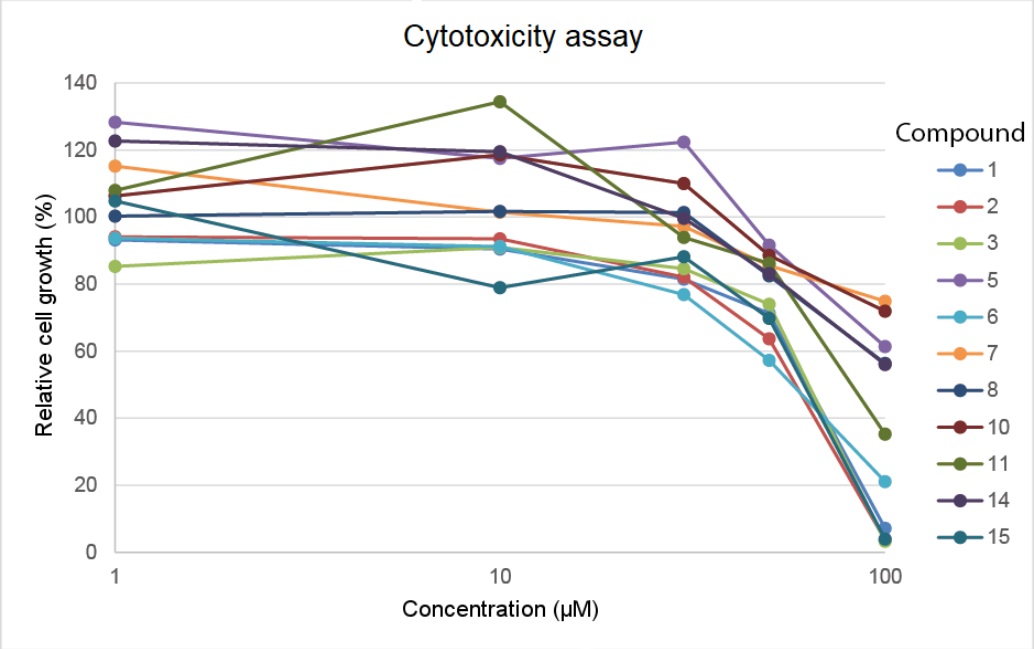

Figure S3: Graphical representation of the vitality variation of Caco-2 cells with different concentrations of dodecyl O-/S- and C-glycosides.

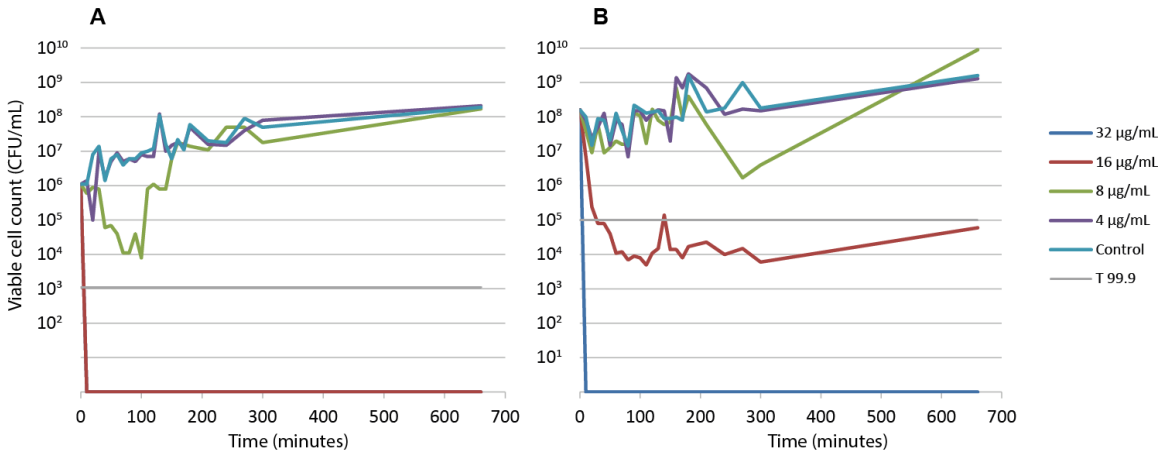

Figure S4. Time-killing curve for *B. cereus* ATCC 14579 strain in the presence of compound **1** at a starting inoculum of A) 10^6 CFU/mL B) 10^8 CF.

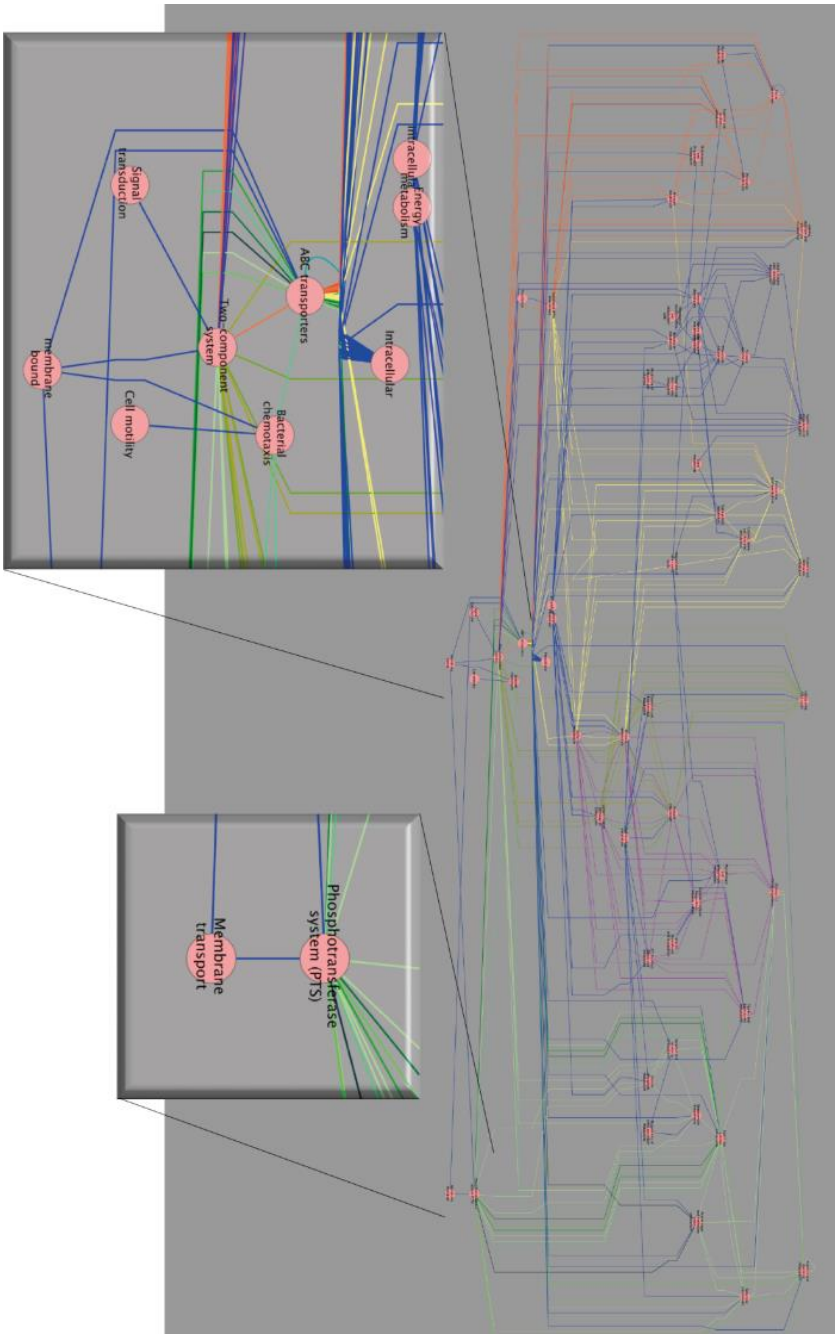

Figure S5. Detail of the metabolic reconstruction of the model strain *B. cereus* ATCC-14579 affected by compound **1**.

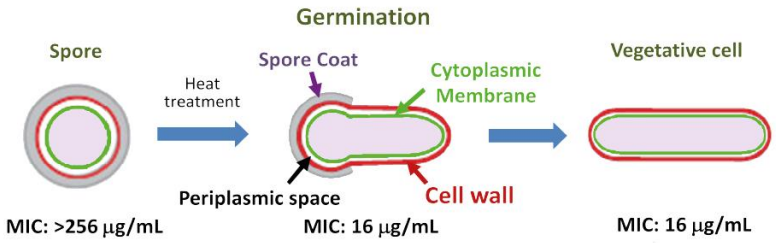

Figure S6. Depiction of compound **1** activity after spore germination.

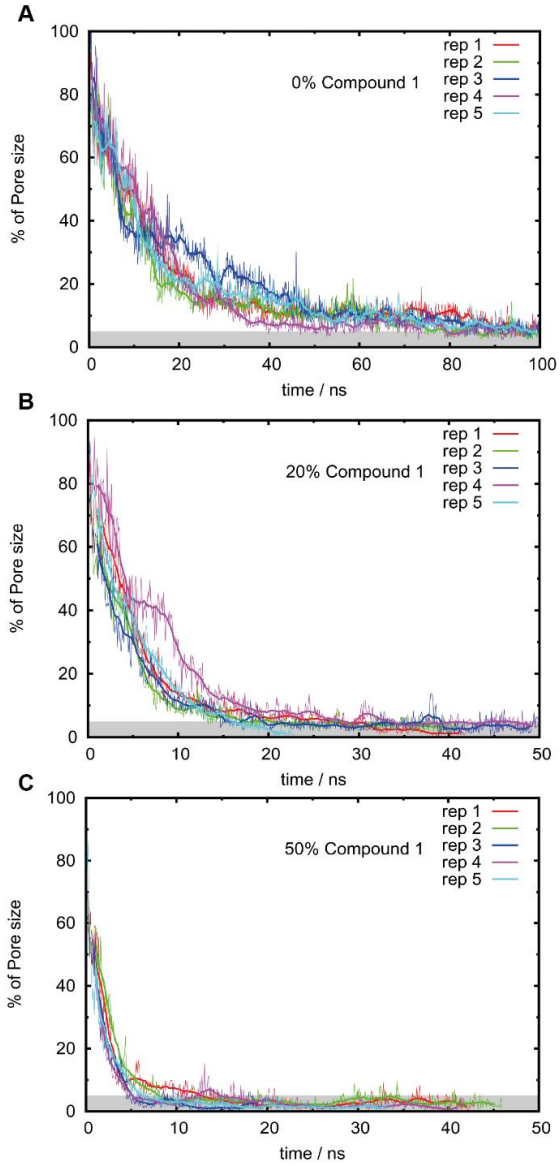

Figure S7. Estimated size of several pre-formed membrane pores over simulation time. **A.** pure DMPC (control); **B.** a mixture containing compound **1** (20%); **C.** a mixture containing compound **1** (50%). The graphic shows the results of five replicates for each system. Pore size was estimated using the number of water molecules in the interior of the transmembrane cavity. A full pore corresponds to a region with ~1800 water molecules between leaflets. The gray region represents very small pore sizes and, in most cases, complete closure of the pore.

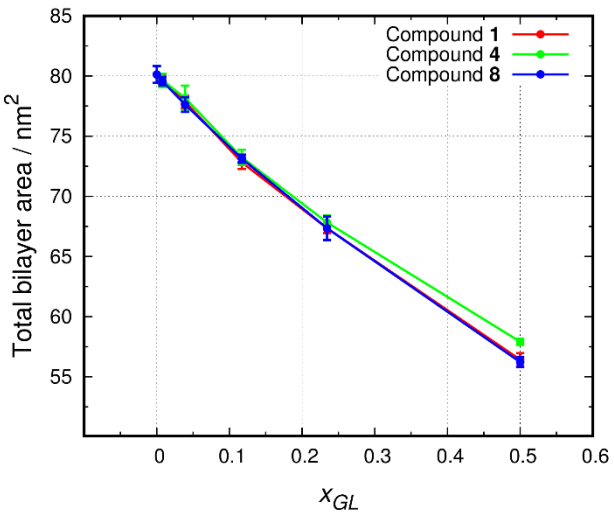

Figure S8. Total cross-sectional area of the bilayer as a function of the glycoside molar fraction for the simulated binary mixture systems.

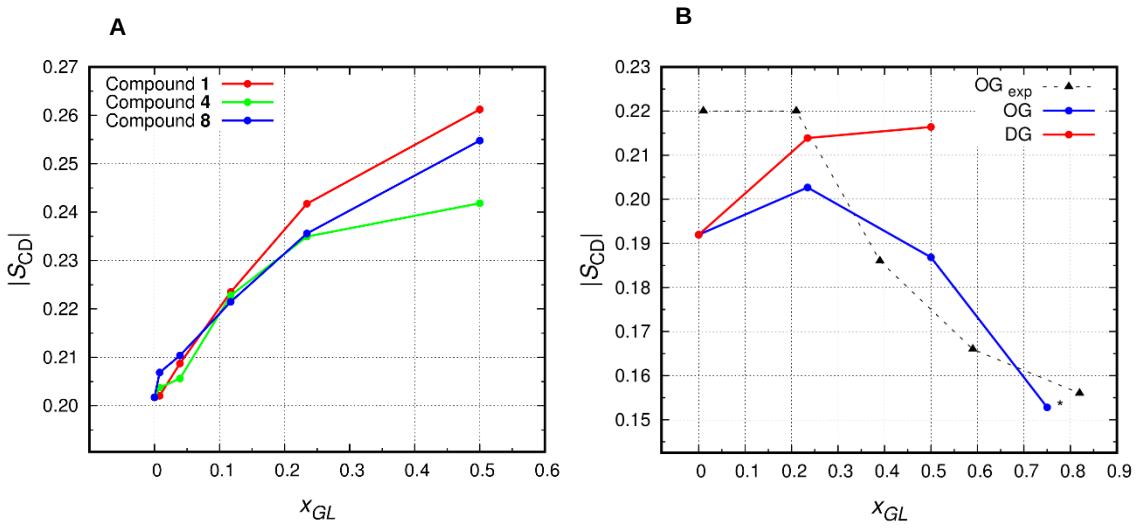

Figure S9. Deuterium order parameters at the 6th methylene group of DMPC (**A**), averaged over both *sn*-1 and *sn*-2 chains, as a function of the respective glycoside molar fraction; and control deuterium order parameters at the 7th methylene group of DMPC (**B**) in the presence of octyl β-D-glucopyranoside (OG) or dodecyl β-D-glucopyranoside (DG). Experimental data shown has been determined for multilamellar bilayer dispersions containing DPPC and OG at 45 ºC.[24] *For x_{OG} = 0.75, the bilayer structure distorts significantly by the end of the simulation.

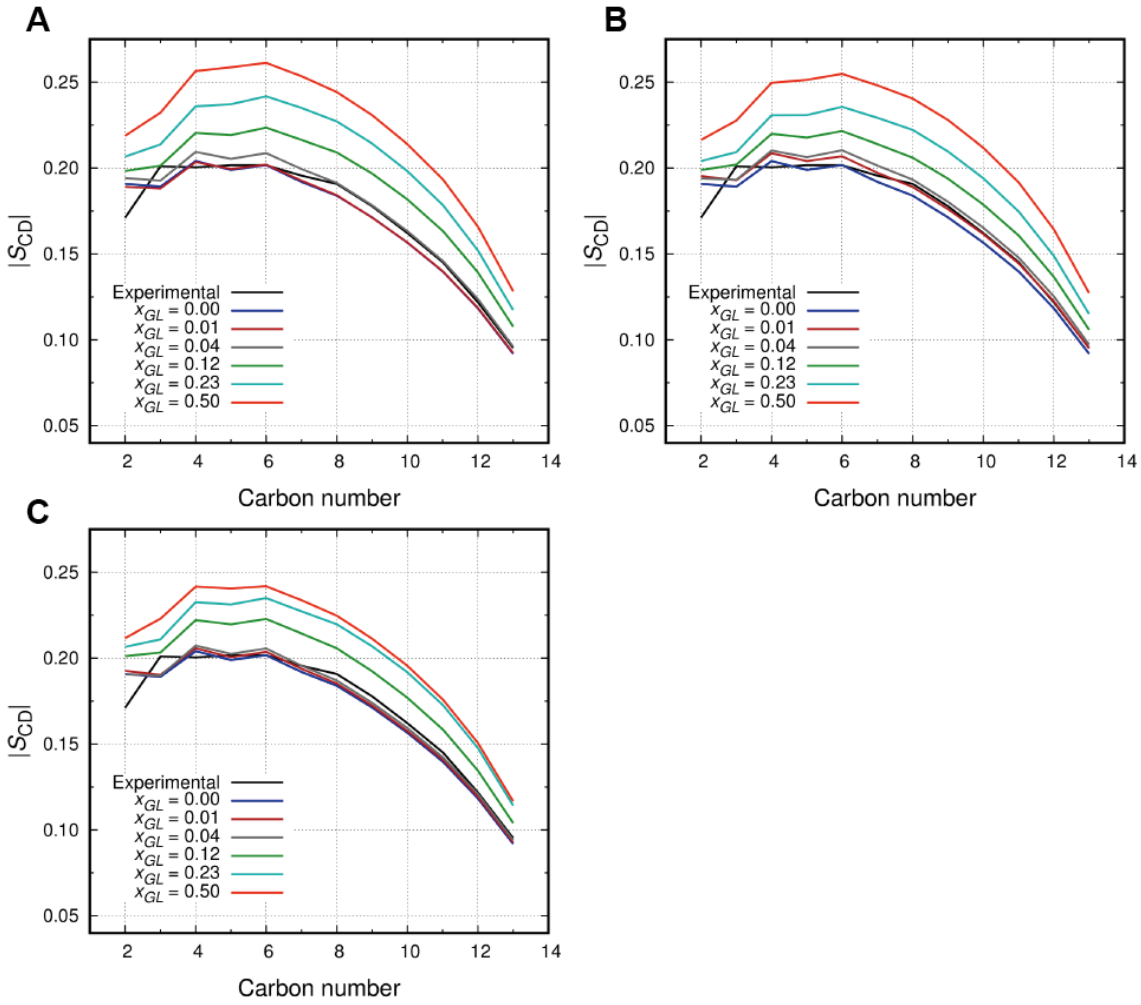

Figure S10. Deuterium order parameter profiles averaged over both *sn*-1 and *sn*-2 acyl chains of DMPC for the simulated binary mixtures at different glycoside molar fractions. **A)** GL = compound **1**; **B)** GL = compound **8**; **C)** GL = compound **4**. Note that the $|S_{CD}|$ values computed for the control simulation (x_{GL} = 0) greatly reproduce experimental results reported in the literature for pure DMPC (when linearly interpolated for T=310K).[64]

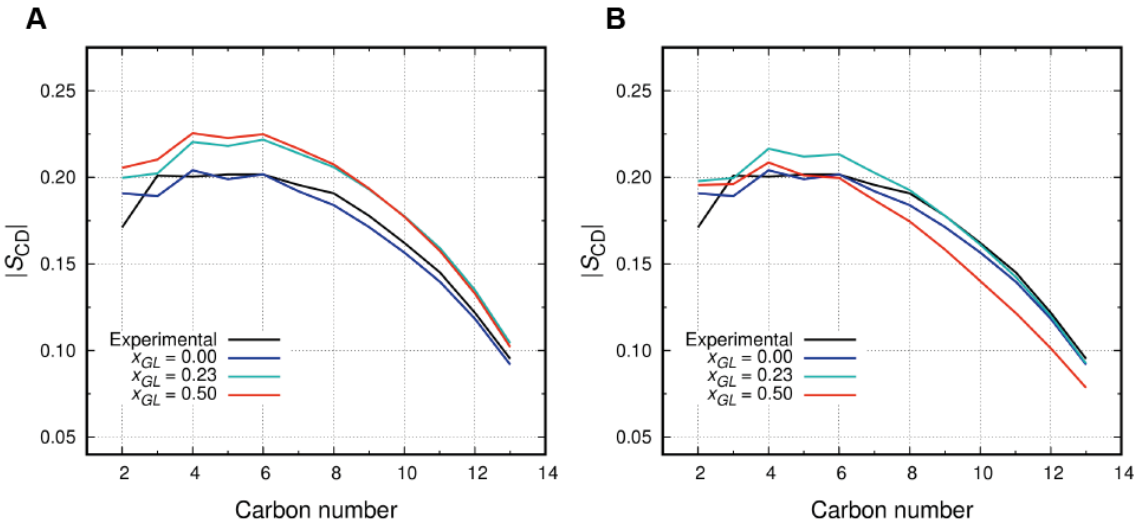

Figure S11. Deuterium order parameter profiles averaged over both *sn*-1 and *sn*-2 acyl chains of DMPC for the simulated binary mixtures at different glycoside molar fractions. **A)** GL = dodecyl β-D-glucopyranoside (DG); **B)** GL = octyl β-D-glucopyranoside (OG). Note that the $|S_{CD}|$ values computed for the control simulation (x_{GL} = 0) greatly reproduce experimental results reported in the literature for pure DMPC (when linearly interpolated for T=310K).[64]

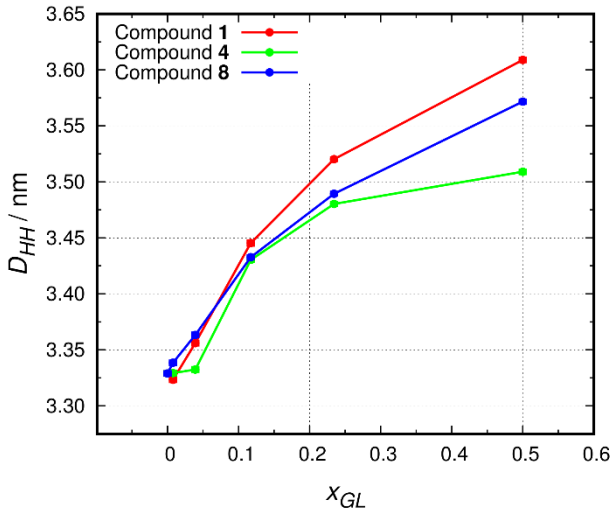

Figure S12. Bilayer thickness, D_{HH}, defined as the average distance between headgroup phosphorus atoms in the *z*-component, both as a function of the glycoside molar fraction. A value of 3.329 ± 0.002 nm was obtained for pure DMPC bilayer simulation which is also in excellent agreement with experimental data (3.49 ± 0.07 nm at 30 ºC and 3.22 ± 0.07 nm at 50 ºC).[65]

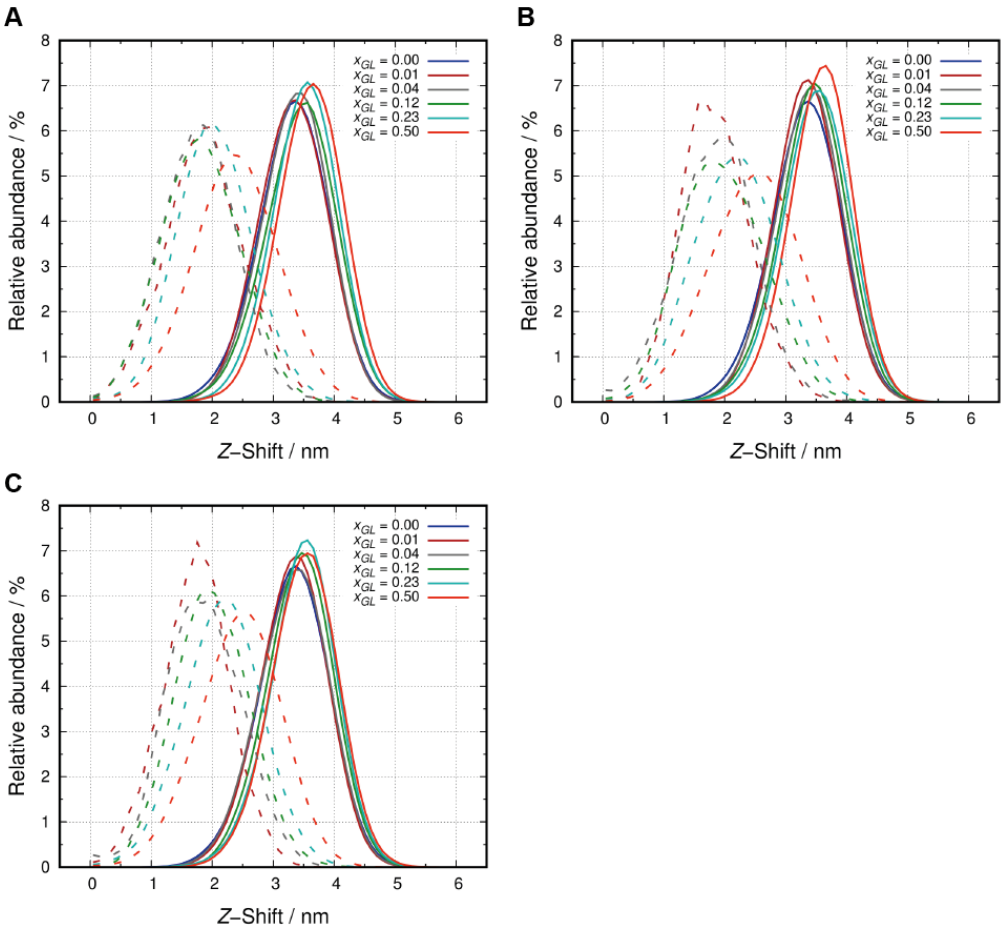

Figure S13. Histograms of twice the distance to the bilayer center. For DMPC, all phospholipid phosphorus atoms were used (solid lines) and these distances correspond to D_{HH}, while for glycosides, endocyclic oxygen atoms were used (dashed lines), and it corresponds to their preferred regions. **A)** GL = compound **1**; **B)** GL = compound **8**; **C)** GL = compound **4**.

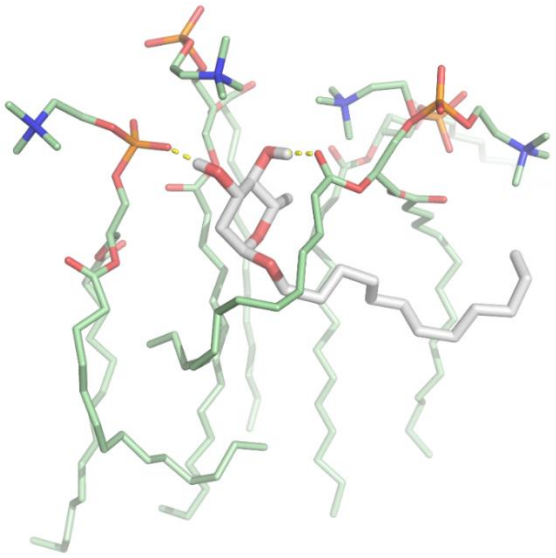

Figure S14. Representative snapshot of compound **1** surrounded by neighboring DMPC molecules in a bilayer environment taken from one of the simulations (x_{GL} = 0.23). The glycoside molecule is show in light gray sticks (carbon atoms), red sticks (oxygen atoms) and white sticks (hydroxyl group hydrogens), while phospholipid molecules are represented as light green sticks (carbon atoms), red sticks (oxygen atoms), orange sticks (phosphorus) and blue sticks (nitrogen). Hydrogen bond interactions are highlighted in dashed lines. Non-polar hydrogen atoms, water molecules and the remaining lipids have been omitted for clarity.

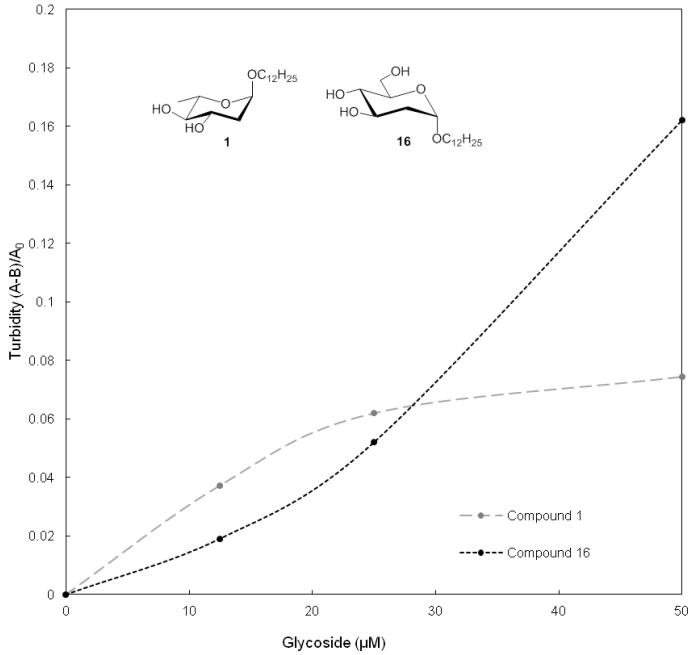

Figure S15. Turbidity increase upon addition of compounds **1** and **16** to LUVs of POPE at 35 ºC. Results are given as a quotient between the absorbance of LUVs in the presence of glycoside minus its intrinsic absorbance (A-B), and the absorbance of LUVs in the presence of ethanol (A_0), thus expressing exclusively the changes in turbidity of LUVs caused by their interaction with glycosides. This assay compliments the fluorescence anisotropy assay, since turbidity changes reflect the behavior of liposomes upon increasing glycoside concentration, while in the fluorescence anisotropy test the glycoside was previously incorporated in the liposomes, at the highest concentration tested.

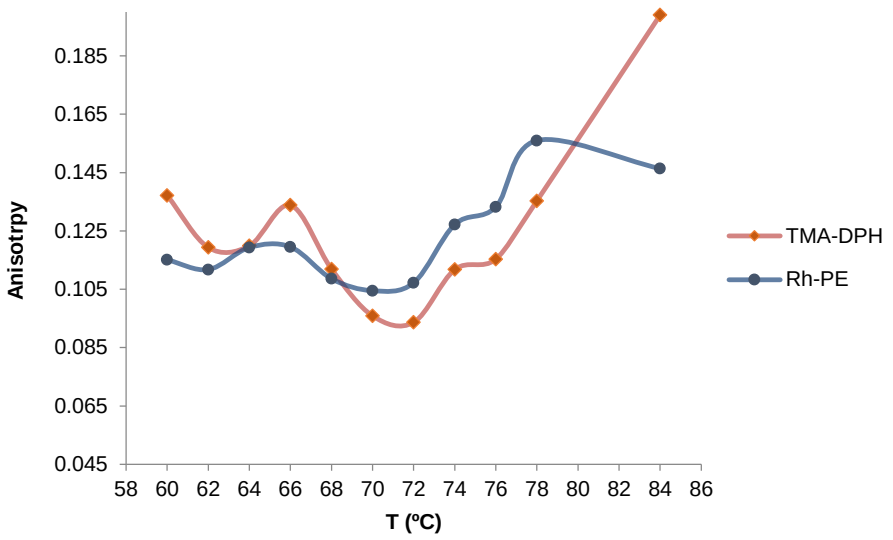

Figure S16. Thermotropic phase behavior of POPE, determined by steady-state fluorescence anisotropy of TMA-DPH and Rh-PE.

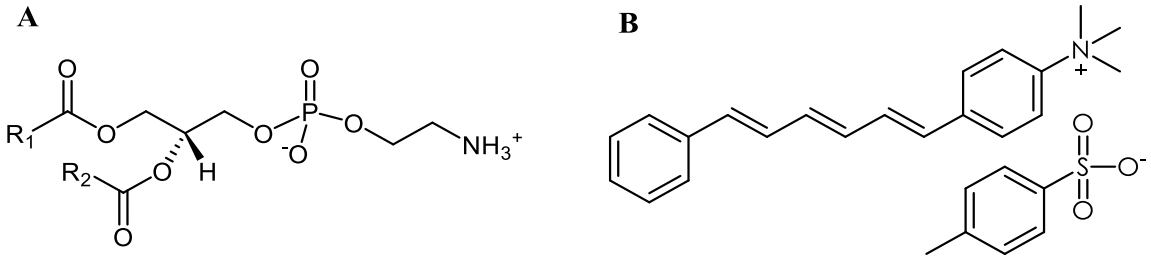

Figure S17. **A)** General structure of phosphatidylethanolamine (PE) lipids; **B)** probe used for fluorescence anisotropy measurements, 1-(4-trimethylammoniumphenyl)-6-phenyl-1,3,5-hexatriene *p*-toluenesulfonate (TMA-DPH).

4 Supplementary tables

Table S1. Relative Gibbs free energies between the two chair conformations of dodecyl 2-deoxy-α-L-*threo*-pentopyranoside (**8**) and dodecyl 2-deoxy-β-L-*threo*-pentopyranoside (**9**) obtained by DFT calculations.

Solvent	**ΔG ($^4C_1 \rightarrow {}^1C_4$) (kcal/mol)**	
	α-anomer **(8)**	β-anomer **(9)**
Chloroform	-4.2	1.0
Methanol	-3.2	0.2

Table S2: Cell death kinetics study at MIC and 2 times MIC concentration values of compound **1.**

[CFU/mL]^{ini}	**[1] (µg/mL)**	**T99.9 (min)**	**ΔLog CFU/h**	**ΔLog CFU/24h**	**MBC (µg/mL)**
10^8	16	40	4	4	32
10^8	32	10	8	8	32
10^6	16	<10	6	6	16
10^6	32	<10	6	6	16

Table S3. Susceptibility of *B. cereus* ATCC 14579 to compounds presented.

Compound number	MIC (µg/mL)	MBC (µg/mL)	**Compound number**	MIC (µg/mL)	MBC (µg/mL)
1	**16**	**16**	**12**	**32**	**32**
4	32	32	**17**	32	32
7	32	32	**19**	128	128
8	16	16	**55**	32	32
10	16	16			

Table S4. Susceptibility of resistant strains.

		Compound 1 (mg/L)	
Antibiotic	**MIC**	MIC	MBC
Erythromycin	**20 mg/L**	**16**	**16**
Penicillin	**20 mg/L**	16	16
Vancomycin	**5 mg/L**	16	16
Ciprofloxacin	**50 mg/L**	16	16
Tetracycline	**50 mg/L**	16	16

Table S5: Obtained mutants and susceptibility to compound **1.**

Strain	**Description**	**MIC (µg/mL)**	**MBC (µg/mL)**
Bacillus cereus ATCC 14579	Control strain	16	32
Bacillus subtilis 168	Parental isogenic strain	16	32
Bacillus subtilis ΔygaD	Putative ABC transporter (ATP-binding protein)	16	16
Bacillus subtilis ΔyjdD	PTS mannose-specific enzyme IIBCA component	16	16
Bacillus subtilis ΔyhcJ	Putative ABC transporter (binding lipoprotein)	16	16

Bacillus subtilis ΔyhaQ	Na+-efflux ABC transporter (ATP-bindingprotein)	16	16
Bacillus subtilis ΔykfD	Putative cell wall oligopeptide ABC transporter(ATP binding protein)	16	16
Bacillus subtilis ΔykoD	Thiamine-related ABC transport system ATP-binding protein, thi-box regilon	16	16
Bacillus subtilis ΔywhQ	ABC transport system ATP-binding protein, subtilosin production	16	32
Bacillus subtilis ΔyknU	Putative ABC transporter (ATP-binding protein)	16	32
Bacillus subtilis ΔykpA	Fructose-1-phosphate kinase(similar to ABC transport system ATP-binding protein)	16	32
Bacillus subtilis ΔyheH	Multidrug ABC transporter (ATP-binding protein), involved in the signalling pathway that activates KinA during sporulation initiation	16	32
Bacillus subtilis ΔyvcC	Multidrug ABC transporter	16	32
Bacillus subtilis ΔywbA	Putative phosphotransferase system enzyme IIC permease component	16	32
Bacillus subtilis ΔyxdM	ABC transporter (permease); efflux of cationicpeptides	16	32
Bacillus subtilis ΔyybL	Putative integral inner membrane protein	16	32
Bacillus subtilis ΔybbF	Putative sugar phosphotransferase enzyme II	16	16
Bacillus subtilis ΔmtlA	Phosphotransferase system (PTS) mannitol-specific enzyme IICB component	16	32
Bacillus subtilis ΔexpZ	ABC transport system ATP-binding protein, export of virginiamycin M and lincomycin	16	32
Bacillus subtilis ΔydhO	PTS oligo-beta-mannoside-specific enzyme IIC component	16	32
Bacillus subtilis ΔyfmR	Putative ABC protein involved in RecA-independent precise excision of transposons	16	16
Bacillus subtilis ΔtreP	Phosphotransferase system (PTS) trehalose-specific enzyme IIBC component	16	16
Bacillus subtilis ΔyfiB	ABC transporter ATP-binding protein	32	32
Bacillus subtilis ΔyfiM	Putative ABC transporter (permease)	16	16

Bacillus subtilis ΔyflF	PTS N-acetylglucosamine-specific enzyme IICB component	16	32
Bacillus subtilis ΔyfiC	Putative ABC transporter (ATP-binding protein)	16	16
Bacillus subtilis ΔyfiN	putative ABC transporter (permease)	16	32
Bacillus subtilis ΔybdB	Exporter of cell killing factor, ABC transport system permease protein, the mutation exhibited highly oligosporogenous phenotypes	16	32
Bacillus subtilis ΔybdA	Exporter of cell killing factor, ABC transport system ATP-binding protein, the mutation exhibited highly oligosporogenous phenotypes	16	32

Table S6. Activity of compound **1** on *E.coli*, *B.cereus*, *S. aureus*, and corresponding spheroplasts, protoplasts, expressed in MIC, compared with the activity of the standard antibiotic polymyxin B.

Strain	**MIC (μg/mL)**	**Polymyxin B**
E. coli K12	256	8
E. coli K12 spheroplasts	4	>1
B. cereus ATCC 14579	16	128
B. cereus ATCC 14579 protoplasts	16	16
S. aureus ATCC 29213	256	128
S. aureus ATCC 29213 protoplasts	256	>1

Table S7. Susceptibility to compound **1** of diverse cellular forms of *B. cereus* ATCC 14579

***B. cereus* ATCC 14579**	**MBC (mg/L)**
Vegetative cells	32
Spores	> 256
Vegetative cells suspended in 1 mM PBS and 0.01 % Tween 20	16
Spores suspended in 1 mM PBS and 0.01 % Tween 20	>256
Vegetative cells after heat treatment at 70 ºC for 30 min	8
Spores after heat treatment at 70 ºC for 30 min	16
Vegetative cells in AGFK buffer at 37 ºC for 20 min	8
Spores after germination, achieved in AGFK buffer at 37 ºC for 20 min	16

*AGFK buffer (30 mM L-asparagine, 5,6 mM D-Glucose, 5,6 mM D-Fructose, 20 mM KCl and 50 mM Tris-HCl, pH 8,4)

REFERENCES

[1] A. K. Goel, Anthrax: A disease of biowarfare and public health importance. *World Journal of Clinical Cases* **2015,** *3* (1), 20-33.

[2] D. A. Sweeney; C. W. Hicks; X. Cui; Y. Li; P. Q. Eichacker, Anthrax infection. *American Journal of Respiratory and Critical Care Medicine* **2011,** *184* (12), 1333-41.

[3] A. Tripathi; M. M. Schofield; G. E. Chlipala; P. J. Schultz; I. Yim; S. A. Newmister; T. D. Nusca; J. B. Scaglione; P. C. Hanna; G. Tamayo-Castillo; D. H. Sherman, Baulamycins A and B, Broad-Spectrum Antibiotics Identified as Inhibitors of Siderophore Biosynthesis in Staphylococcus aureus and Bacillus anthracis. *Journal of the American Chemical Society* **2014,** *136* (4), 1579-1586.

[4] K. H. Jang; S. J. Nam; J. B. Locke; C. A. Kauffman; D. S. Beatty; L. A. Paul; W. Fenical, Anthracimycin, a potent anthrax antibiotic from a marine-derived actinomycete. *Angewandte Chemie (International ed. in English)* **2013,** *52* (30), 7822-4.

[5] B. Nammalwar; R. A. Bunce; K. D. Berlin; C. R. Bourne; P. C. Bourne; E. W. Barrow; W. W. Barrow, Synthesis and biological activity of substituted 2,4-diaminopyrimidines that inhibit Bacillus anthracis. *European Journal of Medicinal Chemistry* **2012,** *54*, 387-96.

[6] A. Martins; M. S. Santos; C. Dias; P. Serra; V. Cachatra; J. Pais; J. Caio; V. H. Teixeira; M. Machuqueiro; M. S. Silva; A. Pelerito; J. Justino; M. Goulart; F. V. Silva; A. P. Rauter, Tuning the Bioactivity of Tensioactive Deoxy Glycosides to Structure: Antibacterial Activity Versus Selective Cholinesterase Inhibition Rationalized by Molecular Docking. *European Journal of Organic Chemistry* **2013,** *2013* (8), 1448-1459.

[7] S. Matsumura; K. Imai; S. Yoshikawa; K. Kawada; T. Uchibor, Surface activities, biodegradability and antimicrobial properties of n-alkyl glucosides, mannosides and galactosides. *Journal of the American Oil Chemists' Society* **1990,** *67* (12), 996-1001.

[8] J. G. Eley; P. Triumalashetty, In vitro assessment of alkylglycosides as permeability enhancers. *AAPS PharmSciTech* **2001,** *2* (3), 81-87.

[9] E. Helgason; O. A. Okstad; D. A. Caugant; H. A. Johansen; A. Fouet; M. Mock; I. Hegna; A. B. Kolsto, Bacillus anthracis, Bacillus cereus, and Bacillus thuringiensis--one species on the basis of genetic evidence. *Applied and Environmental Microbiology* **2000,** *66* (6), 2627-30.

[10] C. Dias; A. Martins; M. S. Santos; A. P. Rauter; M. Malik, Glycal transformation into 2-deoxy glycosides. In *Carbohydrate chemistry: proven synthetic methods*, R. Roy; S. Vidal, Eds. CRC Press: Boca Raton, 2015; Vol. 3, pp 57-72.

[11] M. D. Lewis; J. K. Cha; Y. Kishi, Highly stereoselective approaches to .alpha.- and .beta.-C-glycopyranosides. *Journal of the American Chemical Society* **1982,** *104* (18), 4976-4978.

[12] M. K. Singh; D. Swain; T. N. Guru Row; N. Jayaraman, Crystal structures and thermal analyses of alkyl 2-deoxy-alpha-D-arabino-hexopyranosides. *Carbohydrate Research* **2009,** *344* (15), 1993-8.

[13] M. K. Singh; N. Jayaraman; D. S. Rao; S. K. Prasad, Role of hydroxyl group on the mesomorphism of alkyl glycosides: synthesis and thermal behavior of alkyl 6-deoxy-beta-D-glucopyranosides. *Chemistry and physics of lipids* **2010,** *163* (6), 580-5.

[14] C. a. L. S. Institute, NCCLS document M7-A4. In *Methods for Dilution Antimicrobial Susceptibility Tests for Bacteria that Grow Aerobically*, 2015.

[15] R. F. Epand; J. E. Pollard; J. O. Wright; P. B. Savage; R. M. Epand, Depolarization, Bacterial Membrane Composition, and the Antimicrobial Action of Ceragenins. *Antimicrobial Agents and Chemotherapy* **2010,** *54* (9), 3708-3713.

[16] A. Botan; F. Favela-Rosales; P. F. J. Fuchs; M. Javanainen; M. Kanduč; W. Kulig; A. Lamberg; C. Loison; A. Lyubartsev; M. S. Miettinen; L. Monticelli; J. Määttä; O. H. S. Ollila; M. Retegan; T. Róg; H. Santuz; J. Tynkkynen, Toward Atomistic Resolution Structure of Phosphatidylcholine Headgroup and Glycerol Backbone at Different Ambient Conditions. *The Journal of Physical Chemistry B* **2015,** *119* (49), 15075-15088.

[17] K. A. Brogden, Antimicrobial peptides: pore formers or metabolic inhibitors in bacteria? *Nature reviews. Microbiology* **2005,** *3* (3), 238-50.

[18] W. F. D. Bennett; D. P. Tieleman, The Importance of Membrane Defects—Lessons from Simulations. *Accounts of Chemical Research* **2014,** *47* (8), 2244-2251.

[19] W. F. D. Bennett; C. K. Hong; Y. Wang; D. P. Tieleman, Antimicrobial Peptide Simulations and the Influence of Force Field on the Free Energy for Pore Formation in Lipid Bilayers. *Journal of Chemical Theory and Computation* **2016,** *12* (9), 4524-4533.

[20] M. Fuhrmans; G. Marelli; Y. G. Smirnova; M. Müller, Mechanics of membrane fusion/pore formation. *Chemistry and physics of lipids* **2015,** *185*, 109-128.

[21] N. Awasthi; J. S. Hub, Simulations of Pore Formation in Lipid Membranes: Reaction Coordinates, Convergence, Hysteresis, and Finite-Size Effects. *Journal of Chemical Theory and Computation* **2016,** *12* (7), 3261-3269.

[22] M. le Maire; P. Champeil; J. V. Moller, Interaction of membrane proteins and lipids with solubilizing detergents. *Biochimica et Biophysica Acta* **2000,** *1508* (1-2), 86-111.

[23] A. Capalbi; G. Gente; C. L. Mesa, Solution properties of alkyl glucosides, alkyl thioglucosides and alkyl maltosides. *Colloids and Surfaces A: Physicochemical and Engineering Aspects* **2004,** *246* (1), 99-108.

[24] M. Meier; J. Seelig, Lipid and Peptide Dynamics in Membranes upon Insertion of n-alkyl-β-D-Glucopyranosides. *Biophysical Journal* **2010,** *98* (8), 1529-1538.

[25] G. van Meer; D. R. Voelker; G. W. Feigenson, Membrane lipids: where they are and how they behave. *Nature reviews. Molecular Cell Biology* **2008,** *9* (2), 112-24.

[26] J. L. Nieva; J. Castresana; A. Alonso, The lamellar to hexagonal phase transition in phosphatidylethanolamine liposomes: a fluorescence anisotropy study. *Biochemical and Biophysical Research Communications* **1990,** *168* (3), 987-92.

[27] G. Basanez; J. L. Nieva; E. Rivas; A. Alonso; F. M. Goni, Diacylglycerol and the promotion of lamellar-hexagonal and lamellar-isotropic phase transitions in lipids: implications for membrane fusion. *Biophysical Journal* **1996,** *70* (5), 2299-306.

[28] R. M. Epand; B. T. Leon, Hexagonal phase forming propensity detected in phospholipid bilayers with fluorescent probes. *Biochemistry* **1992,** *31* (5), 1550-4.

[29] X. Han; R. W. Gross, Nonmonotonic alterations in the fluorescence anisotropy of polar head group labeled fluorophores during the lamellar to hexagonal phase transition of phospholipids. *Biophysical Journal* **1992,** *63* (2), 309-16.

[30] D. Marsh, *CRC Handbook of Lipid Bilayers*. 2nd ed.; CRC Press: Boca Raton, 1990.

[31] M. Rappolt; A. Hickel; F. Bringezu; K. Lohner, Mechanism of the Lamellar/Inverse Hexagonal Phase Transition Examined by High Resolution X-Ray Diffraction. *Biophysical Journal* **2003,** *84* (5), 3111-3122.

[32] R. F. Epand; P. B. Savage; R. M. Epand, Bacterial lipid composition and the antimicrobial efficacy of cationic steroid compounds (Ceragenins). *Biochimica et Biophysica Acta* **2007,** *1768* (10), 2500-9.

[33] F. Guilhelmelli; N. Vilela; P. Albuquerque; S. Derengowski Lda; I. Silva-Pereira; C. M. Kyaw, Antibiotic development challenges: the various mechanisms of action of antimicrobial peptides and of bacterial resistance. *Frontiers in Microbiology* **2013,** *4*, 353.

[34] J. G. Hurdle; A. J. O'Neill; I. Chopra; R. E. Lee, Targeting bacterial membrane function: an underexploited mechanism for treating persistent infections. *Nature Reviews. Microbiology* **2011,** *9* (1), 62-75.

[35] D. E. Hunt; H. J. Sandham, Improved agar gradient-plate technique. *Applied Microbiology* **1969,** *17* (2), 329-330.

[36] G. Nesi; N. A. Colabufo; M. Contino; M. G. Perrone; M. Digiacomo; R. Perrone; A. Lapucci; M. Macchia; S. Rapposelli, SAR study on arylmethyloxyphenyl scaffold: looking for a P-gp nanomolar affinity. *European Journal of Medicinal Chemistry* **2014,** *76*, 558-66.

[37] G. S. Stewart; K. Johnstone; E. Hagelberg; D. J. Ellar, Commitment of bacterial spores to germinate. A measure of the trigger reaction. *Biochemical Journal* **1981,** *198* (1), 101-106.

[38] M. J. Frisch; G. W. Trucks; H. B Schlegel; G. E Scuseria; M. Robb; J. Cheeseman; G. Scalmani; V. Barone; B. Mennucci; G. A. H. Petersson; H. Nakatsuji; M. Caricato; X. Li; H. P Hratchian; A. F Izmaylov; J. Bloino; G. Zheng; J. L Sonnenberg; M. Hada; D. Fox *Gaussian 09 (Revision A01)*, Gaussian, Inc.: Wallingford CT, 2009.

[39] C. Adamo; V. Barone, *Toward reliable density functional methods without adjustable parameters: The PBE0 model*. 1999; Vol. 110.

[40] R. J. Krishnan; J. S. Binkley; R. Seeger; J. A. J. Pople, *Self-Consistent Molecular Orbital Methods. XX. A Basis Set for Correlated Wave Functions*. 1980; Vol. 72.

[41] G. Scalmani; M. J. Frisch, Continuous surface charge polarizable continuum models of solvation. I. General formalism. *The Journal of Chemical Physics* **2010,** *132* (11), 114110.

[42] A. V. Marenich; C. J. Cramer; D. G. Truhlar, Universal solvation model based on solute electron density and on a continuum model of the solvent defined by the bulk dielectric constant and atomic surface tensions. *The Journal of Physical Chemistry. B* **2009,** *113* (18), 6378-96.

[43] D. Van Der Spoel; E. Lindahl; B. Hess; G. Groenhof; A. E. Mark; H. J. Berendsen, GROMACS: fast, flexible, and free. *Journal of Computational Chemistry* **2005,** *26* (16), 1701-18.

[44] B. Hess; C. Kutzner; D. van der Spoel; E. Lindahl, GROMACS 4: Algorithms for Highly Efficient, Load-Balanced, and Scalable Molecular Simulation. *Journal of Chemical Theory and Compution* **2008,** *4* (3), 435-47.

[45] N. Schmid; A. P. Eichenberger; A. Choutko; S. Riniker; M. Winger; A. E. Mark; W. F. van Gunsteren, Definition and testing of the GROMOS force-field versions 54A7 and 54B7. *European Biophysics Journal* **2011,** *40* (7), 843-56.

[46] D. Poger; W. F. Van Gunsteren; A. E. Mark, A new force field for simulating phosphatidylcholine bilayers. *Journal of Computational Chemistry* **2010,** *31* (6), 1117-25.

[47] H. S. Hansen; P. H. Hunenberger, A reoptimized GROMOS force field for hexopyranose-based carbohydrates accounting for the relative free energies of ring conformers, anomers, epimers, hydroxymethyl rotamers, and glycosidic linkage conformers. *Journal of Computational Chemistry* **2011,** *32* (6), 998-1032.

[48] J. Hermans; H. J. C. Berendsen; W. F. Van Gunsteren; J. P. M. Postma, A consistent empirical potential for water–protein interactions. *Biopolymers* **1984,** *23* (8), 1513-1518.

[49] M. P. Allen; D. J. Tildesley, *Computer simulation of liquids*. Clarendon Press: 1989; p 385.

[50] H. Chen; T. Xian; W. Zhang; W. Si; X. Luo; B. Zhang; M. Zhang; Z. Wang; J. Zhang, An efficient method for the synthesis of pyranoid glycals. *Carbohydrate Research* **2016,** *431*, 42-46.

[51] Y. Xu; W. Wang; Y. Cai; X. Yang; P. G. Wang; W. Zhao, A convenient and efficient synthesis of glycals by zinc nanoparticles. *RSC Advances* **2014,** *4* (87), 46662-46665.

[52] J. Zhao; S. Wei; X. Ma; H. Shao, A simple and convenient method for the synthesis of pyranoid glycals. *Carbohydrate Research* **2010,** *345* (1), 168-171.

[53] A. M. P. van Steijn; J. P. Kamerling; J. F. G. Vliegenthart, Synthesis of a spacer-containing repeating unit of the capsular polysaccharide of Streptococcus pneumoniae type 23F. *Carbohydrate Research* **1991,** *211* (2), 261-277.

[54] KEGG (Kyoto Encyclopedia of Genes and Genomes) database - http://www.genome.jp/kegg/

[55] V. Mantynen; K. Lindstrom, A rapid PCR-based DNA test for enterotoxic Bacillus cereus. *Applied and Environmental Microbiology* **1998,** *64* (5), 1634-9.

[56] W. L. DeLano, *The PyMol Molecular Graphics System*. 2002; Vol. 30, p 442-454.

[57] P. E. Smith; W. F. van Gunsteren, Consistent dielectric properties of the simple point charge and extended simple point charge water models at 277 and 300 K. *The Journal of Chemical Physics* **1994,** *100* (4), 3169-3174.

[58] G. Bussi; D. Donadio; M. Parrinello, Canonical sampling through velocity rescaling. *The Journal of Chemical Physics* **2007,** *126* (1), 014101.

[59] H. J. C. Berendsen; J. P. M. Postma; W. F. van Gunsteren; A. DiNola; J. R. Haak, Molecular dynamics with coupling to an external bath. *The Journal of Chemical Physics* **1984,** *81* (8), 3684-3690.

[60] B. Hess, P-LINCS: A Parallel Linear Constraint Solver for Molecular Simulation. *Journal of Chemical Theory and Computation* **2008,** *4* (1), 116-22.

[61] S. Miyamoto; P. A. Kollman, Settle: An analytical version of the SHAKE and RATTLE algorithm for rigid water models. *Journal of Computational Chemistry* **1992,** *13* (8), 952-962.

[62] L. S. Vermeer; B. L. de Groot; V. Reat; A. Milon; J. Czaplicki, Acyl chain order parameter profiles in phospholipid bilayers: computation from molecular dynamics simulations and comparison with 2H NMR experiments. *European Biophysics Journal* **2007,** *36* (8), 919-31.

[63] D. Crich; J. Mataka; L. N. Zakharov; A. L. Rheingold; D. J. Wink, Stereoselective formation of glycosyl sulfoxides and their subsequent equilibration: ring inversion of an alpha-xylopyranosyl sulfoxide dependent on the configuration at sulfur. *Journal of the American Chemical Society* **2002,** *124* (21), 6028-36.

[64] H. I. Petrache; S. W. Dodd; M. F. Brown, Area per lipid and acyl length distributions in fluid phosphatidylcholines determined by (2)H NMR spectroscopy. *Biophysical Journal* **2000,** *79* (6), 3172-3192.

[65] N. Kučerka; M.-P. Nieh; J. Katsaras, Fluid phase lipid areas and bilayer thicknesses of commonly used phosphatidylcholines as a function of temperature. *Biochimica et Biophysica Acta - Biomembranes* **2011,** *1808* (11), 2761-2771.

Chapter 4

Reaching hydrophilicity and lipophilicity balance: Assessing the optimal deoxygenation pattern of dodecyl glycosides for antimicrobial activity

The emergence of antibiotic-resistant bacterial strains is becoming a significant public health issue, and there is also increasing concern regarding their use in bioterrorism. This apprehension led to a renovated interest in the search for antibiotics exhibiting structures prone to different mechanisms of action. *Bacillus* genus comprises a variety of pathogenic species, namely *B. anthracis* and *B. cereus*, which despite the genetic similarity, rise diverse concerns. The first is the cause of anthrax, an infectious disease affecting livestock and humans, and a serious bioterrorism threat.[1-2] The latter is responsible for food poisoning and has been reported to form biofilms in medical materials.[3] This feature is particularly worrisome since biofilm forming bacteria have increase capacity to survive hospital environments and implanted medical devices, thriving chronic wounds, persistent infections and creating a barrier to the immune system and to antibiotics,[3] particurlaly in elderly populations. In this context, research in carbohydrate-based antibiotics provides structural diversity and unique physico-chemical properties. In the last decade, our research group has introduced a new family of alkyl deoxy glycosides, some of which exhibiting a potent activity against *Bacillus* spp., particularly *Bacillus anthracis*. Dodecyl 2,6-dideoxy-α-L-*arabino*-hexopyranoside (**1**) exhibits a potent activity against *Bacillus* spp., in particular *B. cereus* and *B. anthracis* (MIC 25 μM).[4-5] These preliminary studies covered also the enantiomer of **1** (compound **2**, Figure 1), also active (MIC 50 μM). Surprisingly, the analogue dodecyl 2-deoxy-α-D-*arabino*-hexopyranoside (**3**) was not active, although it exhibited surface activity parameters such as critical micelle concentration, adsorption and aggregation data of the same order of magnitude as those of compound **1.** These results suggest that compound structural features are determinant for the observed antimicrobial activity, giving insights into a mechanism of action that does not rely only on surface activity properties.

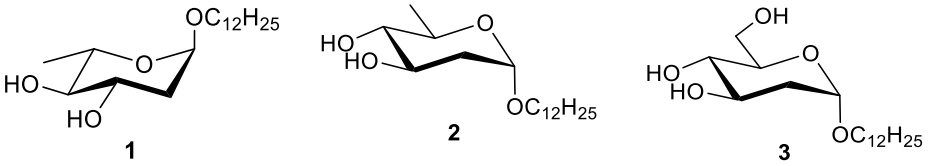

MIC= 25 µM	MIC= 50 µM	Inactive[a]
CMC=1.21x10^5 mol kg^{-1}	CMC=0.86x10^5 mol kg^{-1}	CMC=2.54x10^5 mol kg^{-1}

Figure 1 Antimicrobial activity (MIC) against *B. anthracis* and critical micellar concentration of dodecyl 2,6-dideoxy-α-L-*arabino*-hexopyranoside (**1**), dodecyl 2,6-dideoxy-α-D-*arabino*-hexopyranoside (**2**) and dodecyl 2-deoxy-α-D-*arabino*-hexopyranoside (**3**). [a]Inactive over *B. cereus*.

Interestingly, while surface activity is necessary for the bioactivity, it is not sufficient. This enigmatic feature has been extensively studied in chapter 3, where compound **1** was shown to act via an unprecedented mechanism of action underlying membrane disruption, that results from membrane permeabilization by local induction of phosphatidylethanolamine reorganization from lamellar to inverted hexagonal phases.

Deoxygenation in the sugar moiety plays an important role tuning the bioactivity of such molecules. Thus, aiming at recognizing the optimal deoxygenation pattern for antimicrobial activity, this chapter describes a series of compound **2** analogues, to fully explore the potential of deoxy glycosides as new antibiotics.

Synthetic methodologies towards new dodecyl 2-, 3-, 4-deoxy, and 2,3-, 3,4-, and 4,6-dideoxy glycosides were investigated. Their antimicrobial activity against *Bacillus* species and *Enterococcus faecalis* was assayed and confronted with their cytotoxicy in intestinal and liver cells.

RESULTS AND DISCUSSION

Chemistry. Synthesis of 4-deoxygenated analogues start with protection of positions 4 and 6 of methyl α-D-glucopyranoside, followed by benzylation of the remaining positions. Selective

benzylidene ring opening leaves position 4 free for further manipulation, which is then converted into a triflate and reduced with tetrabutylammonium borohydride (Scheme 1). The resulting 4-deoxyglycosyl precursor **7** reacted with dodecan-1-ol, in the presence of amberlyst A15, an efficient and clean methodology, followed by benzyl deprotection to give the anomeric mixture **8a**,**b** in good yield. Triflation and reduction led to 6-deoxygenation and, but the resulting anomers could only be separated after acetylation to give **9** and **10**, isolated by CC. Deacetylation afforded the target 4,6-dideoxy glycosides **11** and **12** in high yield.

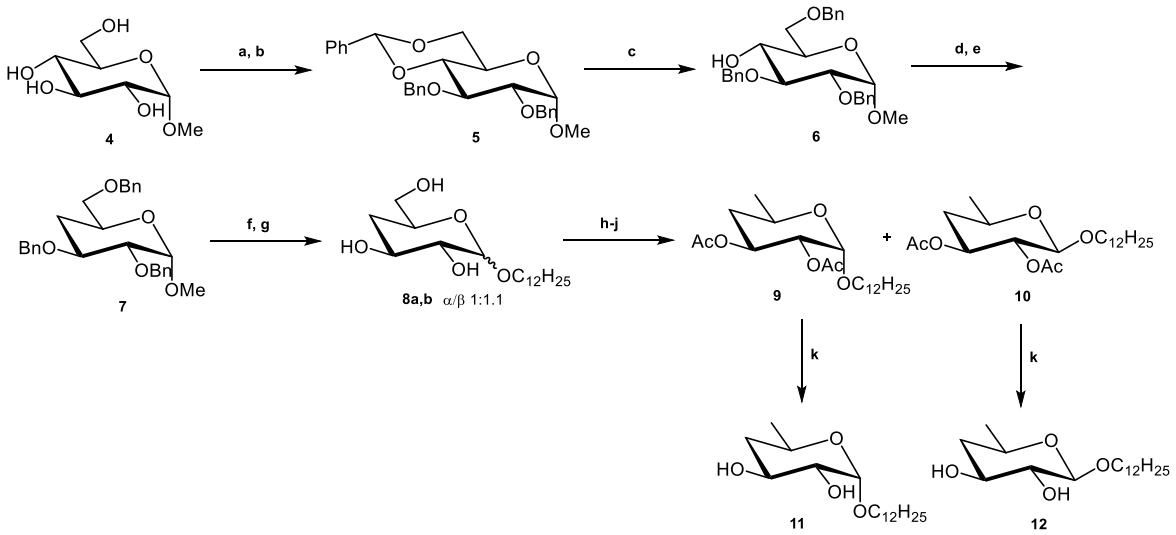

Scheme 1. Synthesis of dodecyl 4-deoxy and 4,6-dideoxy-D-*xylo*-hexopyranosides. a) $PhCH(OMe)_2$, *p*-TsOH, DMF, 60 ºC, 240 mbar, 94%; b) BnBr, NaH, DMF, 82%; c) $NaBH_3CN$, I_2, MeCN, 77%; d) Tf_2O, pyr, DCM, -10ºC; e) n-Bu_4NBH_4, THF, 83% (over two steps); f) $C_{12}H_{25}OH$, A-15; g) Et_3SiH, 10% Pd/C, EtOAc, 80% (over two-steps); h) Tf_2O, pyr, DCM, -10 ºC; i) $LiAlH_4$, THF; j) Ac_2O, pyr, DMAP; (41% over 3 steps); k) NaOMe, MeOH (94-96%).

Deoxygenation of carbon 3 was also investigated (Schemes 2). In the first approach, the 3-deoxy sugar **14** was assessed via desoxygenation of diacetoneglucose (DAG) followed by isopropylidene hydrolysis. It was then used directly as a glycosyl donor in Fisher glycosylation of dodecan-1-ol. Several acidic agents were tested, such as resins A15, IR-120 and dowex-50R, and the clay montmorillonite, but A15 gave the best yield. In all cases, the major product embodied a furanose ring, while pyranoside **17** was isolated only up to 10%. This result prompt us to develop

a second approach, starting with the conversion of 3,4,6-tri-*O*-acetyl-1,5-anhydro-2-deoxy-D-*arabino*-hex-1-enitol in the 2,3-unsaturated dodecyl glycoside **19a** (scheme 2B). This Ferrier product was selectively oxidized with *m*-CPBA into epoxide **13**, which reduction with $LiAlH_4$ gave 3- and 2-deoxy glycosides **17** and **21**, in 20% and 33% yield, respectively. The configuration of the epoxide **20** was first proposed due to a strong correlation of H-3 with H-4 observed in the NOESY spectrum, together with the coupling constants $J_{3,4}$ and $J_{2,3}$. Its final confirmation was deduced from NMR data of the resulting reduction products, in particular the axial H-3 NMR signal of **17**, exhibiting $J_{3ax,4ax}=J_{2ax,3ax}=J_{3ax,3eq}=11$ Hz.

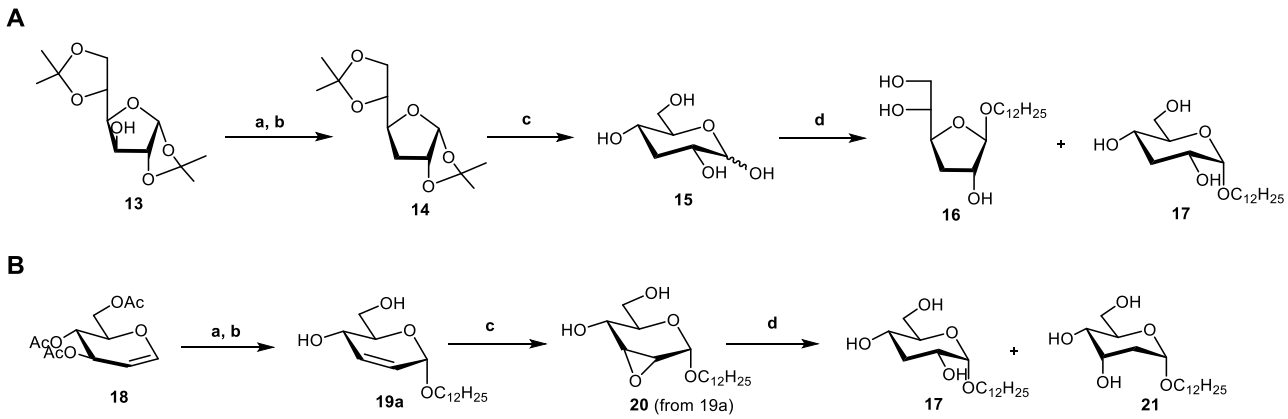

Scheme 2. **A.** Synthesis of dodecyl 3-deoxy-α-D-ribo-hexopyranoside and hexofuranoside, via Fisher glycosylation. a) Tf_2O, pyr, DCM, -10 ºC; b) n-Bu_4NBH_4, THF, 72% (over two steps); c) 80% TFA, 90%; d) $C_{12}H_{25}OH$, A15, reflux (**16**, 28%; **17**, 8%). **B.** Synthesis of dodecyl 3-deoxy-α-D-*ribo*-hexopyranoside via epoxide. a) $C_{12}H_{25}OH$, $BF_3.Et_2O$; b) NaOMe, MeOH, 62% (over two steps); c) m-CPBA, $NaHCO_3$, DCM, 74%; d) $LiAlH_4$, THF (**17**, 20%; **21**, 33%).

Dodecyl glycoside deoxygenated at both positions 2 and 3 (**24**, Scheme 3) could be easily assessed by hydrogenation of benzyl protected Ferrier product (**23a**), which was prepared by a regioselective reaction with zeolyte HY, previously described by us.[6]

Finally, deoxygenation of positions 3 and 4 (**28** and **29**, Scheme 4) was effectively achieved by selectively protecting positions 2 and 6 with the pivaloyl group, followed by triflation of the remaining free hydroxy groups and triflate reduction to give 3,4-dideoxy compound **26** in 29%

isolated yield, with the concomitant formation of the 4-deoxy derivative **27** in 33% yield. **26** was reacted with dodecan-1-ol in the presence of A-15 to give dodecyl glycosides, that, after deacylation, gave the target molecules **28** and **29**.

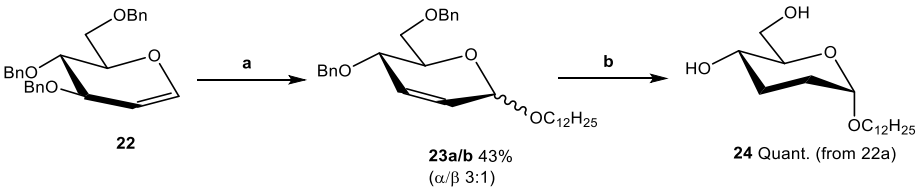

Scheme 3. Synthesis of dodecyl 2,3-dideoxy-D-*erythro*-hexopyranoside (**24**). a) $C_{12}H_{25}OH$, HY, DCE, 43%; b) Et_3SiH 10% Pd/C, quantitative yield.

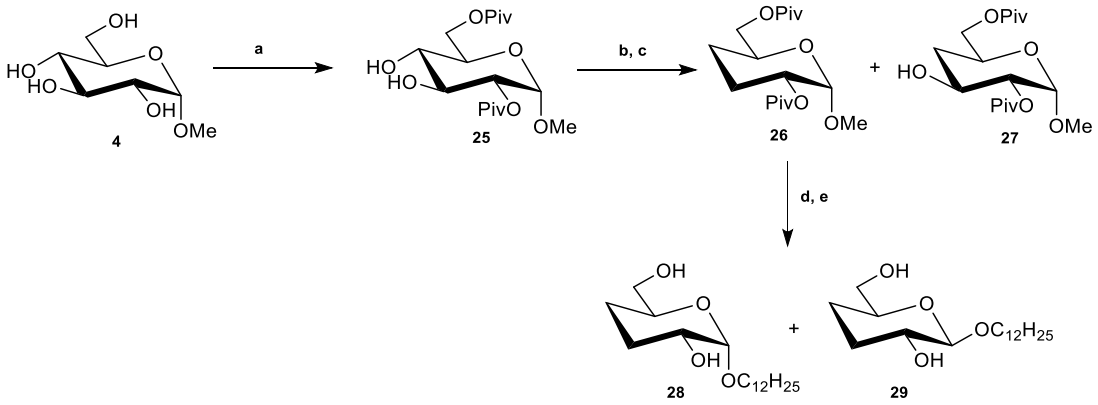

Scheme 4. Synthesis of dodecyl 3,4-dideoxy-D-*erythro*-hexopyranosides. a) PivCl, pyr, DCM, 65%; b) Tf_2O, pyr, DCM, -10 ºC; c) *n*-Bu_4NBH_4, THF, 29% (over two steps); d) $C_{12}H_{25}OH$, A-15; e) KOH, H_2O:MeOH (**28**, 36%; **29**, 15%).

Antimicrobial activity and cytotoxicity

Antimicrobial activity over three *B. anthracis* strains, *B. cereus* and *E. faecalis* was evaluated by the Müller-Hinton agar dilution method, in concentrations raging from 25 to 101 µM (Table 1). Compound **11**, deoxygenated in positions 4 and 6, was the most active one, presenting antimicrobial activity in all tested concentrations. The lack of activity of its beta-anomer (**12**) confirmed, once again, the tendency already reported by us for beta-hexopyranosides.[4,5,7]

Interestingly, when only position 4 is deoxygenated (compound **8a**), a two fold decrease in

activity was found, which is also in line with previous findings (chapter 3). This result can be rationalized as the hydroxy group at 6 position is more readily solvated by water molecules, making this glycoside less lipophilic, with a negative impact on their interaction with phospholipid membranes. Apart from these observations, there is no clear tendency regarding the effect of the deoxygenated position or the number of deoxygenated positions in the antimicrobial activity of alfa-hexopyranosides. For instance, mono-deoxygenated compounds **8a**, **17** and **21**, and bis-deoxygenated compound **24** present virtually the same antimicrobial activity against *B. antracis* strains, while the 3,4-deoxy compound **28** is the least active of the group. It is also interesting to note that pyranoside **17** is active at 48 µM while its furanose analogue (**16**) is twice less active. The difficult structure-activity relationship underlying these results is indeed a characteristic of membrane-targeting antimicrobial compounds, as explained in chapter 1.1.

Table 1. Antibacterial activity expressed in MIC values and cytotoxicity (IC_{50}).

Compound	**MIC in µM**					**Cytotoxicity (IC_{50}) in µM**	
	B. anthracis			*E. faecalis*	*B. cereus*	*Caco-2*	*HepG2*
	sterne	*pathogenic*	*ovine*				
8a (4-deoxy)	48	48	48	48	48	n.d.	n.d.
11 (4,6-dideoxy, α)	≤25	≤25	≤25	≤25	≤25	50	>100
12 (4,6-dideoxy, β)	>101	>101	>101	>101	>101	50	n.d.
16 (3-deoxy, Fur)	96	96	96	96	96	100	n.d.
17 (3-deoxy, Pyr)	48	48	48	48	48	50	100
21 (2-deoxy)	48	48	48	96	96	82	n.d.
24 (2,3-dideoxy)	50	50	50	50	50	100	100
28 (3,4-dideoxy)	101	101	101	101	101	71	n.d.
Ciprofloxacin	≤6	≤6	≤6	≤6	≤6	n.d.	n.d.

The cell viability of intestinal (Caco-2) and hepatic (HepG2) cells was assessed by the MTT assay, after 48 h of incubation time. While most compounds were tested in Caco-2 cells, only compounds **9**, **17** and **24** were selected to be tested in HepG2 cells, as they presented some of the

most interesting antimicrobial results. The IC_{50} of all tested compounds is 50 μM or above, with compounds **16** and **24** being the least toxic ones for intestinal cells. Compound **9** presented an IC_{50} twice its MIC value for Caco-2 cells, and four times the MIC value for HepG2 cells, making it the most promising lead for further development.

CONCLUSIONS

Aiming at recognizing the role of deoxygenation pattern for optimization of dodecyl glycoside antimicrobial activity, mono- and dideoxy dodecyl glycosides were successfully synthesized in moderate to good yields. Dodecyl 2-, 3-, 4-deoxy, and 2,3-, 3,4-, and 4,6-dideoxy glycosides were tested for their antimicrobial activity and cytotoxicity. As it is appanage of membrane-targeting antimicrobial compounds, the structure-activity relationship underlying the antimicrobial results was not clear, as the impact of the deoxygenation position or the number of deoxygenated positions was not linear. Nevertheless, amongst this set of compounds, dodecyl 4,6-dideoxy-α-D-*xylo*-hexopyranoside (**11**) rises as the most promising lead for further development, presenting an IC_{50} twice/four times its MIC value for Caco-2 cells, HepG2 cells, respectively. In future work, it will be paramount to confirm if compound **11** also acts by promoting lamellar-to-hexagonal phase transitions, and how deoxygenation influences this action.

EXPERIMENTAL

Chemistry. Starting materials and reagents were purchased from Sigma–Aldrich, Fluka and Acros. The solvents were dried prior to use with 4 or 3 Å (methanol) molecular sieves. The spectroscopic and physical data of these compounds are in agreement with those previously reported. TLC was carried out on aluminium sheets (20 cm x 20 cm) coated with 0.2 mm silica gel 60 F-254 (Merck) and detection was accomplished by spraying the plates with a solution of

H_2SO_4 in ethanol (10%) followed by heating at 120 °C. The compounds were purified by column chromatography (CC) using silica gel 60G (0.040–0.063 mm, Merck) or silica gel 60G (0.015–0.040 mm, Merck). Melting points were first obtained with a SMP3 Melting Point Apparatus, Stuart Scientific, Bibby. Optical rotations were measured with a Perkin–Elmer 343 polarimeter. NMR spectra were recorded with a Bruker Avance 400 spectrometer at 298 K operating at 100.62 MHz for ^{13}C NMR and at 400.13 MHz for ^{1}H NMR. The solvents used were $CDCl_3$ with 0.03% TMS and CD_3OD (Sigma–Aldrich). The chemical shifts are reported as δ (ppm) and the coupling constants (*J*) are given in Hz. High resolution ESI positive mode mass spectra were obtained on a QqTOF Impact II™ mass spectrometer (Bruker Daltonics) operating in the high-resolution mode. Samples were analyzed by flow injection analysis (FIA) using a isocratic gradient 50 A:50 B of 0.1% formic acid in water (A) and 0.1% of formic acid in acetonitrile (B), at a flow rate of 5 $\mu L min^{-1}$ over 15 min. Calibration of the TOF analyzer was performed with a calibrant solution of sodium formate 10 mM. The full scan mass spectra were acquired over a mass range of 50-1000 *m/z* at a spectra rate of 0.2 Hz. Data was processed using Data Analysis 4.2 software.

Methyl 2,3-Di-*O*-benzyl-4,6-*O*-benzylidene-α-D-glucopyranoside (5). To a solution of methyl 4,6-*O*-benzylidene-α-D-glucopyranoside[8] (3 g, 10.6 mmol) in DMF (200 mL), NaH (60% oil suspension, 2.84 g, 42.4 mmol, 4 equiv.) was carefully added at 0 ºC and the reaction was stirred for 15 min. Then, benzyl bromide (5.1 mL, 42.4 mmol, 4 equiv.) was added and the reaction was stirred at room temperature overnight. The reaction was quenched by pouring it into cooled water (200 mL) and extracted with DCM (3×100 mL). Organic phases were combined, washed with saturated aqueous sodium hydrogen carbonate and dried with $MgSO_4$. After filtration and concentration under reduced pressure, the residue was purified by CC (hex→hex/EtOAc 5:1), affording compound **5** as a white solid, in 82% yield. R_f (hex/EtOAc 2:1) = 0.63; $[\alpha]_D^{20}$ = -30 º (*c*1, $CHCl_3$); **^{1}H NMR** ($CDCl_3$) δ 7.55-7.27 (m, 15H, -Ph), 5.55 (s, 1H, C<u>H</u>-Ph), 4.92 (part A, AB system, 1H, -C<u>H</u>$_2$Ph), 4.85 (AB system, 2H, -C<u>H</u>$_2$Ph), 4.70 (part B, AB system, 1H, -C<u>H</u>$_2$Ph), 4.60

(d, 1H, $J_{1,2}$ = 2.9 Hz, H-1), 4.27 (dd, 1H, $J_{5,6a}$ = 4.0 Hz, $J_{6a,6b}$ = 10.0 Hz, H-6a), 4.05 (t, 1H, $J_{2,3}$=$J_{3,4}$=9.0 Hz, H-3), 3.83 (br td, 1H, $J_{4,5}$= 9.8 Hz, $J_{5,6b}$= 10.0 Hz, H-5), 3.71 (t, 1H, H-6b), 3.63-3.54 (m, 2H, H-2 e H-4), 3.40 (s, 3H, -OMe). **^{13}C NMR** ($CDCl_3$) δ 138.7, 138.1, 137.4 (Cq, Ph), 128.9, 128.4, 128.3, 128.2, 128.1, 128.0, 127.9, 126.0 (-CH, Ph), 101.2 (-CH Benzylidene), 99.2 (C-1), 82.1 (C-4), 79.1 (C-2), 78.6 (C-3), 75.3 (-CH_2Ph), 73.8 (-CH_2Ph), 69.0 (C-6), 62.3 (C-5), 55.3 (-OCH_3). **HRMS**: Calcd. [$C_{28}H_{30}NaO_6$] 485.1935; Found 485.1928 (error 1.4 ppm).

Methyl 2,3,6-tri-*O*-benzyl-α-D-glucopyranoside (6). To a solution of compound **5** (3.00 g, 6.49 mmol) in acetonitrile (60 mL) containing 4Å molecular sieves (ca. 200 mg), sodium cyanoborohydride (2.037 g, 32.4 mmol, 5 equiv.) was added. Then, molecular iodine (3,781 g, 14.9 mmol, 2.3 equiv.) was added portion wise over 1 h (each time iodine was added the solution became orange and only when the solution became white more iodine was added).

After completion of the starting material (3 h), the reaction mixture was diluted with DCM (100 mL) and filtered over celite. The filtered solution was washed with saturated aqueous sodium hydrogen carbonate and then water. Organic phases were combined and dried with $MgSO_4$, filtered, and concentrated under reduced pressure to give a syrup purified by CC eluted with CyHex-EtOAc 4:1, affording compound **6** as a colourless oil in 46% yield. R_f (Hex/EtOAc 3:1) = 0.43; $[\alpha]_D^{20}$= +13 º (*c*1, $CHCl_3$); **^{1}H NMR** ($CDCl_3$) δ 7.35-7.27 (m, 15H, -Ph), 4.99 (d, $J_{A,B}$=11.0 Hz, 1H, -CH_2Ph), 4.78-4.70 (m, 2H, -CH_2Ph), 4.67-4.60 (m, 2H, -CH_2Ph e H-1), 4.55 (d, $J_{A,B}$=12.0 Hz, 2H, -CH_2Ph), 3.79 (t, 1H, $J_{2,3}$ = $J_{3,4}$= 9.2 Hz, H-3), 3.73-3.64 (m, 3H, H-5, H-6a e H-6b), 3.59 (t, 1H, $J_{3,4}$ = $J_{4,5}$= 9.2 Hz, H-4), 3.52 (dd, 1H, $J_{1,2}$ = 4.0 Hz, $J_{2,3}$ = 9 Hz, H-2), 2.46 (d, 1H, OH-4).**^{13}C NMR** ($CDCl_3$) δ 138.7, 137.9, 137.9 (Cq, -Ph), 128.4, 128.3, 128.2, 128.0, 127.9, 127.8, 127.7, 127,5 (-Ph), 98.0 (C-1), 81.3 (C-3), 79.5 (C-2), 75.3 (-CH_2Ph), 73.4 (-CH_2Ph), 73.0 (-CH_2Ph), 70.5 (C-4), 69.8 (C-5), 69.3 (C-6) 55.1 (-OCH_3).

Methyl 2,3,6-tri-*O*-benzyl-4-deoxy-α-D-*xylo*-hexopyranoside (7). Compound **6** (2.28 g, 4.95 mmol) was dissolved in DCM (70 mL) and pyridine (0.9 mL, 11.39 mmol, 2.3 equiv.), and cooled to -10 ºC, under N_2. Trifluoromethanesulfonic anhydride (1.92 mL, 11.39 mmol, 2.3 equiv.) was then added dropwise to the stirred solution, which was then warmed to 0 ºC and stirred for 2 h 30 min. The reaction was quenched by addition of cool distilled water (100 mL), followed by extraction with DCM (2 x 100 mL). Organic phase was dried with $MgSO_4$, filtered and evaporated under reduced pressure, affording highly labile off-white powder composed by methyl 2,3,6-tri-*O*-benzyl-4-deoxy-4-trifluoromethanesulfonyl-α-D-glucopyranoside. The solid was dissolved in toluene (74 mL), and tetra-*n*-butylammonium borohydride (3.76 g, 14.85 mmol, 3 equiv.) was added. The reaction mixture was stirred at 85 ºC for 2 h, cooled to room temperature and then poured into ice cold water (100 mL). After extraction with DCM (2x50 mL), the organic phase was washed with saturated aqueous sodium hydrogen carbonate (2x50 mL) and water (50 mL). Organic phases were combined and dried with $MgSO_4$, filtered, and concentrated under reduced pressure. The residue was purified by CC eluted with hex/EtOAc 10:1 to afford compound **7** as a colourless oil in 83% yield. R_f (hex/EtOAc 3:1) = 0.67; $[\alpha]_D^{20}$= +26 º (*c*1, $CHCl_3$); **^{1}H NMR** ($CDCl_3$) δ 7.42-7.24 (m, 15H, -Ph), 4.86-4.65 (m, 5H, -CH_2Ph, H-1), 4.54 (br s, 2H, -CH_2Ph), 3.97-3.90 (m, 2H, H-3, H-5), 3.50-3.44 (m, 3H, H-6a, H6b, H-2) 3.37 (s, 3H, -OMe), 2.15 (s, 1H, OH-4), 2.05 (dd, 1H, $J_{4ax,4eq}$= 12.0 Hz, $J_{4eq,5}$=$J_{3,4eq}$=3 Hz, H-4eq), 1.50 (q, $J_{4ax,5}$=$J_{3,4ax}$=12 Hz, H-4ax). **^{13}C NMR** ($CDCl_3$) δ 138.8, 138.5, 138.1 (Cq, -Ph), 128.4, 128.0, 127.8, 127.6, 127.5, (-Ph), 99.2 (C-1), 80.4 (C-2), 75.3 (C-3), 75.4 (-CH_2Ph), 73.3 (-CH_2Ph), 72.5 (-CH_2Ph), 72.4 (C-6), 66.7 (C-5), 55.2 (-OCH_3), 33.9 (C-4). **HRMS**: Calcd. [$C_{28}H_{32}NaO_5$] 471.2142; Found 471.2144 (error 0.4 ppm).

Dodecyl 4-deoxy-D-*xylo*-hexopyranoside (8a,b). A solution of compound **7** (1.498 g, 3.34 mmol) in dodecan-1-ol (11.2 mL, 50 mmol, 15 equiv.), containing Amberlyt A15 beads (0.250 g) was

stirred at 100 ºC for 4.5 h. The solution was diluted with DCM, the resin beads were filtered off, and the solution was concentrated under reduced pressure. The residue was taken up in methanol (15 mL) and, after addition of Pd/C 10% (50 mg) and inertization of the vessel with N_2, triethylsilane (1.8 mL, 5.63 mmol, 3.2 equiv.) was added dropwise. After 24 h, the catalyst was filtered off using celite, the solvent was evaporated under reduced pressure and the residue was purified by CC (Petrol. ether/EtOAC 1:1 → EtOAc). The anomeric mixture **8a**,**b** (1.1:1 α/β) was obtained as a white solid, in 80% yield. R_f (EtOAc/Tol 3:1) = 0.20; **^{1}H NMR** (MeOD) δ 4.81 (d, 1H, $J_{1,2}$=3.6 Hz, H-1α), 4.19 (d, 1H, $J_{1,2}$=7.9 Hz, H-1β), 3.91-3.80 (m, 3H, H-3α, H-5α, H1'aβ), 3.72 (td, 1H, $J_{1'a,1'b}$= 9 Hz, $J_{1'a,2'}$=7 Hz, H-1'aα), 3.65-3.48 (m, 7H, H-3β, H-5β, H-6α, H-6β, H1'bβ), 3.42 (td, 1H, H-1'bα), 3.32 (m, 1H, H-2α)*, 3.08 (t, 1H, $J_{1,2}$= $J_{2,3}$=7.9 Hz, H-2β), 1.93 (br dd, 2H, $J_{4ax,4eq}$= 13.1 Hz, $J_{4eq,5}$= $J_{3,4eq}$= 3.1 Hz, H-4_{eq} α, H-4_{eq} β), 1.69-1.67 (m, 4H, H-2' α, H-2'β), 1.42-1.25 (m, 38H, H-3' to H-11'α and β, H-4_{ax}α, H-4_{ax}β), 0.92-0.88 (m, 6H, H-12'α, H-12'β). **^{13}C NMR** (MeOD) δ 104.7 (C-1 β), 100.7 (C-1 α), 76.9 (C-2 β), 75.6 (C-2 α), 73.9, 72.3, 70.9, 70.0 (C-3 e C-4, α and β), 69.1 (C-1' α), 68.9 (C-1' β), 65.7 (C-6 α), 65.6 (C-6 β), 36.6 (C-4α, C-4β), 33.2, 30.9, 30.9, 30.7, 30.6, 27.4, 27.2, 23.8 (C-2' to C-11' α and β), 14.6 (C-12' α and β). *Signal under MeOH signal. **HRMS**: Calcd. [$C_{18}H_{36}NaO_5$] 335.2455; Found 335.2451 (error 1.0 ppm).

Dodecyl 4-deoxy-*α*-D-*xylo*-hexopyranoside (8a). An aliquote of the anomeric mixture **8a**,**b** was further purified by CC with $CHCl_3$:EtOH 95:5, to afford the pure alfa-anomer (**8a**) for biological evaluation. R_f ($CHCl_3$:EtOH 9:1) = 0.3; m.p.=79.6-80.7°C; $[\alpha]_D^{20}$= 71º (*c*1, MeOH). **^{1}H NMR** (MeOD) δ 4.80 (d, 1H, $J_{1,2}$=3.6 Hz, H-1), 3.89-3.80 (m, 2H, H-3, H-5), 3.71 (td, 1H, $J_{1'a,1'b}$= 9 Hz, $J_{1'a,2'}$=7 Hz, H-1'a), 3.52 (br d, 2H, $J_{5,6}$=5 Hz, H-6a,b), 3.41 (td, 1H, H1'b), 3.30 (1H, H-2)*, 1.92 (ddd, 1H, $J_{4ax,4eq}$= 12 Hz, $J_{4eq,5}$=2, $J_{3,4eq}$= 5 Hz, H-4_{eq}), 1.71-1.55 (m, 2H, H-2'), 1.48-1.23 (m, 19H, H-3' to H-11', and H-4_{ax}), 0.92 (t, 3H, H-12'). **^{13}C NMR** (MeOD) δ 100.7 (C-1), 75.5 (C-2), 73.8, 69.9 (C-3, C-5), 69.0 (C-1'), 65.7 (C-6), 36.5 (C-4), 33.1, 30.8, 30.7, 30.6, 30.5, 27.4, 23.7 (C-2'

to C-11'), 14.5 (C-12'). *Signal partially under MeOH signal. **HRMS**: Calcd. [$C_{18}H_{36}NaO_5$] 335.2455; Found 335.2444 (error 3.0 ppm).

Dodecyl 2,3-di-*O*-acetyl-4,6-dideoxy-α/β-D-*xylo*-hexopyranoside (9, 10). The anomeric mixture **8** (0.3176 g, 0.955 mmol) was dissolved in DCM (10 mL) and pyridine (0.12 mL, 1.43 mmol, 1.5 equiv.), and cooled to -10 ºC, under N_2. Trifluoromethanesulfonic anhydride (0.24 mL, 1.43 mmol, 1.5 equiv.) was added dropwise to the stirring solution, which was then warmed to 0 ºC and stirred for 1 h. The reaction was quenched by addition of 20 mL of cool distilled water, followed by extraction with DCM (2 x 20 mL). The organic phase was dried with $MgSO_4$, filtered and evaporated under reduced pressure at 25 ºC, affording a syrup. This intermediate triflate was dissolved in THF (8.3 mL), and a 2 M $LiAlH_4$ solution in THF (1.67 mL, 3.34 mmol, 3.5 equiv.) was added dropwise at 0 ºC. After stirring 1 h at room temperature, the reaction was again cooled to 0 ºC and the aluminium salts were removed following Fieser work-up, as follows: slow addition of water (0.3 mL), aqueous NaOH 15% (0.9 mL) and water (0.9 mL) gave a mixture kept under stirring for 15 min at room temperature. $MgSO_4$ was added to the resulting suspension and after filtration of the solids, the solution was concentrated under reduced pressure to give a syrup composed by an inseparable anomeric mixture of dodecyl 4,6-dideoxy-D-*xylo*-hexopyranoside, which was dissolved in pyridine (4 mL), and Ac_2O (2 mL) followed by a spatula tip of DMAP. The reaction was stirred at room temperature overnight. The fully acetylated glycosides α and β could be distinguished in the TLC plate (hex/EtOAc 5:1). After co-evaporation of pyridine with toluene, the anomers were purified by column chromatography (hex/EtOAc 25:1) to afford the dodecyl 2,3-di-*O*-acetyl-4,6-dideoxy-α-D-*xylo*-hexopyranoside (**9**, 116 mg, η = 30%) and dodecyl 2,3-di-*O*-acetyl-4,6-dideoxy-β-D-*xylo*-hexopyranoside (**10**, 42 mg, η = 11% yield.

Dodecyl 2,3-di-*O*-acetyl-4,6-dideoxy-α-D-*xylo*-hexopyranoside (9). Syrup. R_f (hex/EtOAc 5:1) = 0.50; **^{1}H NMR** ($CDCl_3$) δ 5.25 (ddd, 1H, $J_{2,3}$=10 Hz, $J_{3,4ax}$=11 Hz, $J_{3,4eq}$=4.9 Hz, H-3), 4.97 (d,

1H, $J_{1,2}$=3.4 Hz, H-1), 4.80 (dd, 1H, H-2), 4.05-3.95 (m, 1H, H-5), 3.65 (td, 1H, $J_{1'a,1'b}$= 10 Hz, $J_{1'a,2'}$=7 Hz, H-1'a), 3.36 (td, 1H, $J_{1'b,2'}$=7 Hz H-1'b), 2.18 (br dd, 1H, $J_{3,4eq}$=$J_{4eq,5}$= 4.9 Hz, H-4eq), 2.06 (s, 3H, -OAc), 2.02 (s, 3H, -OAc), 1.60-1.52 (m, 2H, H-2'), 1.41 (quart., 1H, $J_{3,4ax}$= $J_{4,5}$= $J_{4eq,4ax}$=11 Hz, H-4ax), 1.35-1.21 (m, 18H, H-3' to H-11'), 1.18 (d, 3H, H-6, $J_{5,6}$=6 Hz), 0.87 (t, 3H, $J_{11',12'}$=6 Hz, H-12'). **^{13}C NMR** ($CDCl_3$) 170.5 (C=O, OAc), 170.3 (C=O, OAc), 96.3 (C-1), 72.2 (C-2), 68.2 (C-3), 68.0 (C-1'), 63.0 (C-5), 38.2 (C-4), 31.9, 29.7, 29.6, 29.4, 29.3, 26.1, 22.7 (C-2' to C-11'), 21.1 (CH_3, OAc), 20.9 (CH_3, OAc), 20.6 (C-6), 14.1 (C-12').

Dodecyl 2,3-di-O-acetyl-4,6-di-deoxy-β-D-*xylo*-hexopyranoside (10). Colourless oil; R_f (hex/EtOAc 5:1) = 0.39; **^{1}H NMR** ($CDCl_3$) δ 4.96 (ddd, 1H, $J_{2,3}$=10 Hz, $J_{3,4ax}$=10 Hz, $J_{3,4eq}$=5.3 Hz, H-3), 4.85 (dd, 1H, $J_{1,2}$=$J_{2,3}$=8 Hz, H-2), 4.35 (d, 1H, $J_{1,2}$=8 Hz, H-1), 3.85 (td, 1H, $J_{1'a,1'b}$= 10 Hz, $J_{1'a,2'}$=7 Hz, H-1'a), 3.68-3.58 (m, 1H, H-5), 3.45 (td, 1H, H-1'b), 2.12-2.06 (m, 1H, H-4eq), 1.71-1.42 (m, 5H, H-2', H-3', H-4ax), 1.41-1.17 (m, 19H, H-4' to H-11' and H-6); 0.86 (t, 3H, H-12', $J_{11',12'}$=7 Hz). **^{13}C NMR** ($CDCl_3$) 170.1 (C=O, OAc), 169.8 (C=O, OAc), 98.8 (C-1), 72.6 (C-2), 71.2 (C-3), 69.8 (C-1'), 67.7 (C-5), 37.9 (C-4), 31.9, 29.7, 29.6, 29.5, 29.4, 25.9, 22.7 (C-2' to C-11'), 21.0 (CH_3, OAc), 20.9 (CH_3, OAc), 20.7 (C-6), 14.1 (C-12').

Deacetylation reaction. The acetylated compound (**9** or **10**) is dissolved in methanol (100mg/mL), and a 1M solution of NaOMe in methanol (0.1 mL per 0.100 mg of substrate) is added. The reaction mixture is stirred for 2 h at room temperature. Neutralization with amberlite IR-120, filtration and evaporation of the solvent, afforded the deacetylated compounds.

Dodecyl 4,6-dideoxy-α-D-*xylo*-hexopyranoside (11). Obtained from compound **9** (0.099g, 0.25 mmol), as a white solid in 96% yield (0.076 g). R_f (tol/EtOAc 2:3)=0.31; M.p.=31.4-36.0 °C; $[\alpha]_D^{20}$= +103 º (*c*1, CH_2Cl_2); **^{1}H NMR** (MeOD) δ 4.70 (d, 1H, $J_{1,2}$=3.4 Hz, H-1), 3.90 (quint. d, 1H, $J_{5,6}$=6 Hz, $J_{4eq,5}$=2 Hz, H-5), 3.77 (ddd, 1H, $J_{2,3}$=10 Hz, $J_{3,4ax}$= 5 Hz, $J_{3,4eq}$=2 Hz, H-3), 3.62 (td, 1H, $J_{1'a,1'b}$= 10 Hz, $J_{1'a,2'}$=7 Hz, H-1'a), 3.40 (td, 1H, $J_{1'b,2'}$=6 Hz, $J_{1'b,2'}$=7 Hz, H-1'b), 3.24 (dd,

1H, $J_{2,3}$=9 Hz, H-2), 1.91 (ddd, 1H, $J_{4ax,4eq}$= 12 Hz, H-4_{eq}), 1.65-1.51 (m, 2H, H-2'), 1.40-1.18 (m, 19H, H-3' to H-11' and H-4ax), 1.13 (d, 3H, $J_{5,6}$=6 Hz H-6), 0.87 (br t, 3H, $J_{11',12'}$=6 Hz, H-12'). **^{13}C NMR** (MeOD) δ 100.8 (C-1), 75.5 (C-2), 69.1, 68.9 (C-1' and C-3), 65.2 (C-5), 42.3 (C-4), 33.1, 30.8, 30.7, 30.6, 30.5, 27.4, 23.8 (C-2' to C-11'), 21.2 (C-6), 14.5 (C-12'). **HRMS**: Calcd. [$C_{18}H_{36}NaO_4$] 339.2506; Found 339.2509 (error -1.1 ppm).

Dodecyl 4,6-dideoxy-β-D-*xylo*-hexopyranoside (12). Obtained from compound **10** (0.030g, 0.075 mmol), as a white solid in 94% yield (0.022 g). R_f (tol/EtOAc 2:3)=0.31; M.p.=48.2-50.7 °C; $[\alpha]_D^{20}$= -30 º (*c*0.6, CH_2Cl_2); **^{1}H NMR** (MeOD) δ 4.12 (d, 1H, $J_{1,2}$=7.9 Hz, H-1), 3.78 (td, 1H, $J_{1'a,1'b}$= 10 Hz, $J_{1'a,2'}$=7 Hz, H-1'a), 3.60-3.44 (m, 3H, H-1'b, H-3 and H-5), 3.01 (t, 1H, $J_{1,2}$=$J_{2,3}$=8 Hz, H-2), 1.89 (dd, 1H, $J_{4ax,4eq}$= 13 Hz, $J_{3,4eq}$=2 Hz, $J_{4eq,5}$=2 Hz, H-4_{eq}), 1.58 (quint, 2H, $J_{1'a,2'}$=$J_{2'a,3'}$=7Hz, H-2'), 1.39-1.21 18 (m, 19H, H-3' to H-11' and H-4ax), 1.13 (d, 3H, $J_{5,6}$=6 Hz, H-6), 0.87 (br t, 3H, H-12', $J_{11',12'}$=6 Hz). **^{13}C NMR** (MeOD) δ 104.6 (C-1), 76.8 (C-2), 72.2 (C-3), 70-9 (C-1'), 69.1 (C-5), 42.1 (C-4), 33.1, 30.9, 30.8, 30.6, 30.5, 27.1, 23.8 (C-2' to C-11'), 21.3 (C-6), 14.5 (C-12'). **HRMS**: Calcd. [$C_{18}H_{36}NaO_4$] 339.2506; Exp. 339.2495 (error 3.3 ppm).

1,2:5,6-Di-*O*-isopropylidene-3-deoxy-α-D-*ribo*-hexofuranose (14). Triflic anhydride (1.3 mL, 7.68 mmol, 2 equiv.) was added dropwise to a stirring solution of 1,2:5,6-di-O-isopropylidene-α-D-glucofuranose (1.00g, 3.84 mmol) in DCM (30 mL) and pyridine (0.62 mL, 7.68 mmol, 2 equiv.), at -10 ºC under N_2. The reaction was stirred for 15 min, after which complete conversion of the starting material into the triflate derivative had occurred. The reaction was poured into 50 mL of ice cold water and the organic phase was separated. The aqueous phase was further extracted with DCM (2x50 mL). Organic phases were combined, dried with $MgSO_4$ and evaporated under reduced pressure, affording 1,2:5,6-di-*O*-isopropylidene-3-*O*-triflyl-α-D-*ribo*-hexofuranose as a colourless oil in 82% yield. R_f (hex/EtOAC 2:1) = 0.78, **^{1}H RMN** ($CDCl_3$) δ 5.98 (d, 1H, $J_{1,2}$=4.6 Hz, H-1), 5.36 (br s, 1H, H-3), 4.76 (d, 1H, H-2), 4.22-4.13 (m, 3H, H-4, H-5, H-6a), 3.97 (dd, 1H, $J_{6a,6b}$=8.5 Hz, $J_{5,6b}$=3.2 Hz, H-6b), 1.52 (s, 3H, -C$\underline{H}_3$ isoprop.), 1.42 (s, 3H,

-C<u>H</u>$_3$ isoprop.), 1.34 (s, 3H, -C<u>H</u>$_3$ isoprop.), 1.33 (s, 3H, -C<u>H</u>$_3$ isoprop.) **^{13}C RMN** ($CDCl_3$) δ 113.1 (Cq isoprop.), 109.8 (Cq isoprop.), 105.0 (C-1), 88.1 (C-2),83.2 (C-3), 79.9 (C-4), 71.7 (C-5), 67.6 (C-6), 26.8, 26.5, 26.2, 24.8 (-<u>C</u>H$_3$ isoprop.).

1,2:5,6-Di-*O*-isopropylidene-3-*O*-triflyl-α-D-*ribo*-hexofuranose (1.85 g, 4.74 mmol) was dissolved in dried toluene (100 mL) and *n*-Bu_4NBH_4 (2.4 g, 9.47 mmol, 2 equiv.) was added in one portion. The reaction mixture was refluxed under N_2 for 4 h and quenched by pouring the solution into ice cold water (40 mL). The organic phase was extracted with DCM (2 x 50 mL) and washed with a saturated sodium bicarbonate (50 mL) and water (50 mL). The organic phase was dried with $MgSO_4$ and evaporated under reduced pressure. The resulting residue was purified by column chromatography, eluted with hex/EtOAc 9:1, affording compound **14** as a colourless oil in 54% yield (0.624 g). R_f (Hex/EtOAC 4:1) = 0.31; $[\alpha]_D^{20}$= -5 º (*c*1, $CHCl_3$); **^{1}H RMN** ($CDCl_3$) δ 5.82 (d, 1H, $J_{1,2}$=3 Hz, H-1), 5.36 (br s, 1H, H-3), 4.76 (br t, 1H, $J_{2,3b}$=4, H-2), 4.19-4.09 (m, 3H, H-4, H-5, H-6a), 3.82 (dd, 1H, $J_{6a,6b}$=7.9 Hz, $J_{5,6b}$=5 Hz, H-6b), 2.19 (dd, 1H, $J_{3a,3b}$=14 Hz, $J_{3a,4}$=3 Hz, H-3a), 1.77 (ddd, 1H, $J_{3b,4}$=5 Hz, H-3b), 1.52 (s, 3H, -C<u>H</u>$_3$ isoprop.), 1.43 (s, 3H, -C<u>H</u>$_3$ isoprop.), 1.36 (s, 3H, -C<u>H</u>$_3$ isoprop.), 1.32 (s, 3H, -C<u>H</u>$_3$ isoprop.) **^{13}C RMN** ($CDCl_3$) δ 111.3 (Cq isoprop.), 109.6 (Cq isoprop.), 105.6 (C-1), 80.4 (C-2), 78.6 (C-4, C-5), 67.2 (C-6), 35.2 (C-2) 26.8, 26.5, 26.2, 24.8 (-<u>C</u>H$_3$ isoprop.). **HRMS**: Calcd. [$C_{12}H_{21}O_5$] 245.1384; Found 245.1392 (error 3.3 ppm).

3-Deoxy-D-*ribo*-hexopyranose (15). Compound **14** (1.00 g, 4.09 mmol), was dissolved in aqueous trifluoroacetic acid 80% (7 mL) and stirred at 40 ºC for 2 h. Co-evaporation of the acid with toluene gave **15** as a colourless oil in quantitative yield (α/β 0.8:1). R_f (DCM/EtOH 9:1) = 0.15; **^{1}H RMN** (MeOD) δ 4.95 (d, 1H, $J_{1,2}$=3.0 Hz, H-1α), 4.33 (d, 1H, $J_{1,2}$=8.0 Hz, H-1β), 3.77-3.66 (m, 1H, H-6aβ), 3.59-3.50 (m, 4H, H-2α, H-6bβ, H-6aα, H-5β), 3.49-3.36 (m, 3H, H-4α, H-6bα, H-4β), 3.27-3.13 (m, 2H, H-5α, H-2β), 2.20 (td, 1H, $J_{2,3e}$=$J_{3e,4}$=4.8 Hz, $J_{3a,3e}$= 12.0 Hz, H-3$_{eq}$β), 1.99-1.92 (m, 1H, H-3$_{eq}$α), 1.72 (q, 1H, $J_{2,3ax}$=$J_{3ax,4}$=$J_{3ax,3e}$=11.6 Hz, H-3$_{ax}$β), 1.39 (q, 1H,

$J_{2,3ax}$=$J_{3ax,4}$=$J_{3ax,3e}$=11.7 Hz, H-3$_{ax}$α). **^{13}C RMN** (MeOD) δ 100.1 (C-1β), 92.6 (C-1α), 81.7 (C-5α), 80.7, 76.8 (C-4α, C-4β), 73.7 (C-5β), 70.4 (C-2β), 66.2 (C-2α), 65.1 (C-6α), 62.8 (C-6β), 40.5 (C-3β), 36.1 (C-3α). **HRMS**: Calcd. [$C_6H_{12}NaO_5$] 187.0577; Found 187.0574 (error -1.6 ppm).

Ficher glycosylation procedure. Compound **15** (0.068g, 0.382 mmol) and amberlyst A15 (50mg/300mg substrate) were dissolved in dodecan-1-ol (1.3 mL, 0.572 mmol, 15 equiv.) and the solution was stirred for 5 h at 100 ºC. Reaction products were isolated by CC eluted with a gradient from dichloromethane to dichlotomethane/ethanol 10:1. Compound **16** was isolated in 8% yield, as a colourless oil, while compound **17** was isolated in 28% yield, as a white solid. Both beta anomers were detected in the TLC as traces and were not isolated.

Dodecyl 3-deoxy-α-D-*ribo*-hexofuranoside (16). R_f (DCM/MeOH 12:1)=0.29; $[\alpha]_D^{20}$= -50 º (*c*0.1, CH_2Cl_2); **^{1}H NMR** (MeOD) δ 4.83 (s, H-1), 4.22 (q, 1H, $J_{3b,4}$=$J_{4,5}$=7 Hz, H-4), 4.13 (d, 1H, $J_{2,3a}$=4 Hz, H-2), 3.73 (dd, 1H, $J_{5,6a}$=3Hz, $J_{6a,6b}$=12 Hz, H-6a), 3.65 (dist. td, 1H, $J_{1'a,1'b}$= 9 Hz, $J_{1'a,2'}$=7 Hz, H-1'a), 3.55 (dd, 1H, $J_{5,6b}$=6 Hz, H-6b), 3.50-3.43 (m, 1H, H-5), 3.36 (td, 1H, $J_{1'b,2'}$=7 Hz, H-1'b), 2.12-2.03 (m, 1H, H-3a), 1.97 (dd, 1H, $J_{3b,4}$= 7 Hz, $J_{3a,3b}$= 13 Hz, H-3b), 1.58-1.49 (m, 2H, H-2'), 1.39-1.22 (m, 18H, H-3' to H-11'), 0.90 (t, 3H, $J_{11',12'}$=6Hz, H-12'). **^{1}C NMR** (MeOD) δ 109.7 (C-1), 80.7 (C-4), 76.9 (C-5), 76.5 (C-2), 68.4 (C-1'), 65.2 (C-6), 36.0 (C-3), 33.1, 30.8, 30.7, 30.6, 30.5, 27.3, 23.7 (C-2' to C-11'), 14.5 (C-12'). **HRMS**: Calcd. [$C_{18}H_{36}NaO_4$] 335.2455; Found 335.2454 (error 0.3 ppm).

Dodecyl 3-deoxy-α-D-*ribo*-hexopyranoside (17). R_f **(**DCM/MeOH 12:1) = 0.31; m.p.=94.0-95.0°C; $[\alpha]_D^{20}$= +83 º (*c*0.3, CH_2Cl_2); **^{1}H NMR** (MeOD) δ 4.64 (d, $J_{1,2}$=3 Hz, H-1), 4.59 (s, 1H, -OH), 3.80-3.68 (m, 2H, H-1'a, H-6a), 3.64-3.54 (m, 2H, H-2, H-6b), 3.50-3.39 (m, 3H, H-1'b, H-4 and H-5), 2.01 (td, 1H, $J_{2,3eq}$=$J_{3eq,4}$=4 Hz, $J_{3e,3ax}$=11 Hz, H-3eq), 1.76 (q, 1H, $J_{2,3ax}$=$J_{3ax,4}$=$J_{3e,3ax}$=11 Hz, H-3ax), 1.67-1.54 (m, 2H, H-2'), 1.45-1.20 (m, 18H, H-3' to H-11'),

0.87 (t, 3H, $J_{11',12'}$=6 Hz, H-12'). **^{1}C NMR** (MeOD) δ 98.9 (C-1), 74.4 (C-4), 68.8 (C-1'), 68.5 (C-2), 66.2 (C-5), 62.7 (C-6), 36.9 (C-3), 33.1, 30.8, 30.7, 30.5, 27.4, 23.8 (C-2' to C-11'), 14.5 (C-12'). **HRMS**: Calcd. [$C_{18}H_{36}NaO_5$] 355.2455; Found 355.2449 (error 1.6 ppm).

Dodecyl 2,3-dideoxy-α,β-D-*erythro*-hex-2-enopyranosides (19a/b). To a solution of 3,4,6-tri-*O*-acetyl-1,5-anhydro-2-deoxy-D-*arabino*-hex-1-enitol (2.0 g, 7.35 mmol) in dichloromethane (60 mL), dodecan-1-ol (1.81 mL, 8.08 mmol, 1.1 equiv.) and $BF_3.Et_2O$ (0.05 mL, 0.37 mmol, 0.05 equiv.) were added. After 2 h at room temperature, the reaction, which had turned blue, was washed with twice with $NaHCO_3$ (2 x 100 mL) and with brine (100 mL). The organic phase was dried with anhydrous $MgSO_4$, which was filtered off, and concentrated under reduced pressure. The resulting residue was dissolved in methanol (25 mL) and, after addition of a 1M solution of NaOMe in MeOH (0.6 mL), the reaction stirred for 1.5h at room temperature. Neutralization with amberlite IR-120, filtration and evaporation of the solvent gave a residue that was purified by CC eluted with hex/EtOAc 2:1, affording compound **19a** as a white solid in 73% yield, along with the beta anomer **19b** as a colourless oil in 11% yield.

Dodecyl 2,3-dideoxy-α-D-*erythro*-hex-2-enopyranoside (19a). R_f (hex/EtOAc 1:1) = 0.45; m.p.=68.6-69.6 °C; $[\alpha]_D^{20}$= +45 º (*c*0.3, CH_2Cl_2); **^{1}H NMR** ($CDCl_3$) δ 5.87 (br d, 1H, $J_{2,3}$=10 Hz, H-3), 5.69 (td, 1H, $J_{1,2}$=2 Hz, H-2), 4.93 (br s, 1H, H-1), 3.99 (dd, 1H, $J_{3,4}$=1 Hz, $J_{4,5}$=9 Hz, H-4), 3.83-3.74 (m, 2H, H-6a and H-1'a), 3.70-3.57 (m, 2H, H-5 and H-6b), 3.44 (td, 1H, $J_{1'a,1'b}$= 10 Hz, $J_{1'b,2'}$=6 Hz, H-1'b),1.60-1.51 (m, 2H, H-2'), 1.39-1.20 (m, 18H, H-3' to H-11'), 0.88 (t, 3H, $J_{11',12'}$=6 Hz, H-12').**^{13}C NMR** ($CDCl_3$) δ 134.6 (C-3), 127.3 (C-2), 95.5 (C-1), 73.6 (C-5), 69.5 (C-1'), 64.2 (C-4), 62.7 (C-6), 33.1, 30.9, 30.8, 30.6, 30.5, 27.4, 23.8 (C-2' to C-11'), 14.5 (C-12'). **HRMS**: Calcd. [$C_{18}H_{34}NaO_4$] 337.2349; Found 337.2348 (error 0.5 ppm).

Dodecyl 2,3-dideoxy-β-D-*erythro*-hex-2-enopyranoside (19b). R_f (hex/EtOAc 1:1) = 0.33; $[\alpha]_D^{20}$= +8 º (*c*1, MeOH); **^{1}H NMR** ($CDCl_3$) δ 6.02 (br d, 1H, $J_{2,3}$=10 Hz, H-3), 5.78 (br d, 1H, H-

2), 5.14 (br s, 1H, H-1), 4.20 (br d, 1H, $J_{4,5}$=5 Hz, H-4), 3.90-3.75 (m, 3H, H-6a, H-6b and H-1'a), 3.68 (ddd, 1H, $J_{5,6a}$=2 Hz, $J_{5,6b}$=6 Hz, H-5), 3.51 (td, 1H, $J_{1'a,1'b}$= 9 Hz, $J_{1'b,2}$= 7 Hz, H-1'b), 2.88 (br s, 2H, OH), 1.64-1.54 (m, 2H, H-2'), 1.38-1.18 (m, 18H, H-3' to H-11'), 0.88 (t, 3H, $J_{11',12'}$=6 Hz, H-12'). **^{13}C NMR** ($CDCl_3$) δ 132.0 (C-3), 128.1 (C-2), 96.3 (C-1), 78.2 (C-5), 68.7 (C-1'), 63.3, 63.2 (C-4 and C6), 31.9, 29.7, 29.6, 29.5, 29.4, 26.0, 22.7 (C-2' to C-11'), 14.1 (C-12'). **HRMS**: Calcd. [$C_{18}H_{34}NaO_4$] 337.2349; Found 337.2353 (error -1.1 ppm).

Dodecyl 2,3-anhydro-α-D-*allo*-hexopyranoside (20). Sodium hydrogen carbonate (0.033g, 0.40 mmol, 2 equiv.) and m-CPBA (0.069g, 0.40 mmol, 2 equiv.) were added to a stirring solution of 2,3-unsaturated compound **19a** (0.063g, 0.20 mmol) in DCM (2 mL). The solution was stirred vigorously at room temperature for 3d. The reaction mixture was diluted with DCM (10 mL). washed with saturated aqueous $NaHCO_3$ (2x25 mL), and saturated aqueous $Na_2S_2O_3$ (2x25 mL). The organic phase was dried with $MgSO_4$, filtered and evaporated, to give a residue which was purified by CC eluted with cyHex/EtOAc 1:1. Compound **20** was isolated in 74% yield, based on reacted starting material, recovered in 12% yield. R_f (hex./EtOAc 1:2)=0.23; m.p.= 91.2-94.0°C; $[\alpha]_D^{20}$= +40 º (*c0*.1, CH_2Cl_2); **^{1}H NMR** (MeOD) δ 4.96 (d, 1H, $J_{1,2}$=2.8 Hz, H-1), 4.60 (br s, 1H, -OH), 3.83-3.68 (m, 3H, H-6a, H-1'a, H-5), 3.63-3.56 (m, 2H, H-6b, H-4), 3.50-3.43 (m, 2H, H-1'b, H-2), 3.35 (br dd, $J_{2,3}$=4.0 Hz, $J_{3,4}$=1.5 Hz, H-3), 1.63-1.54 (m, 2H, H-2'), 1.40-1.22 (m, H-3' to H-11', 18H), 0.87 (t, $J_{11',12'}$=6.5 Hz). The coupling constants are in agreement with those registered for an acetylated analogue in the literature.[9] **^{1}C NMR** (MeOD) δ 94.9 (C-1), 70. 9 (C-4), 69.2 (C-1'), 66.4 (C-5), 62.4 (C-6), 56.2 (C-2), 55.2(C-3), 33.1, 30.8, 30.7, 30.6, 30.5, 27.3, 23.8 (C-2' to C-11'), 14.5 (C-12'). **HRMS**: Calcd. [$C_{18}H_{34}NaO_5$] 353.2298; Found 353.2308 (error -2.7 ppm).

Dodecyl 3-deoxy-α-D-*ribo*-hexopyranoside (17) and **dodecyl 2-deoxy-α-D-*ribo*-hexopyranoside (21).** To a solution of epoxide **20** (0.0762g, 0.242 mmol) in THF (2 mL), a 2M solution of LiAlH4 in THF (0.24 mL, 0.484 mmol, 2 equiv.) was added dropwise, at 0 ºC. After stirring for 24h at room temperature, the reaction was cooled to 0 ºC and the aluminium salts were removed following the Fieser work-up, as follows: after addition of water (0.2 mL), then aqueous NaOH 15 % (0.6 mL), followed by addition of water (0.6 mL), the reaction mixture was stirred for 15 min at room temperature. $MgSO_4$ was added to the resulting suspension and, after filtration of the solids, the solution was concentrated under reduced pressure to give a syrup, purified by CC eluted with hex/EtOAc 1:3, to give both 3-deoxy glycoside and **17** and 2-deoxy glycoside **21** in 20% yield and 33% yield, respectively, both as white solids.

Dodecyl 3-deoxy-α-D-*ribo*-hexopyranoside (17). White solid; R_f (hex./EtOAc 1:4)=0.35; Spectroscopic characterization is in full agreement with the product obtained by Fischer glycosylation (above).

Dodecyl 2-deoxy-α-D-*ribo*-hexopyranoside (21). R_f (hex./EtOAc 1:4)=0.54; m.p.=51.6-52.8°C; $[\alpha]_D^{20}$= +13 º (*c*0.5, CH_2Cl_2); **^{1}H NMR** (MeOD) δ 4.87 (H-1, under MeOH signal), 4.60 (s, 1H, OH), 3.91 (br d, 1H, $J_{2,3}$=3 Hz, H-3), 3.85-3.6 (m, 4H, H-1'a, H-5, H-6), 3.44 (dd, 1H, $J_{3,4}$=2.2Hz, $J_{4,5}$=9.5 Hz, H-4), 3.36 (td, 1H, $J_{1'a,1'b}$= 10 Hz, $J_{1'b,2'}$=6 Hz, H-1'b), 2.02 (ddd, 1H, $J_{1,2eq}$= 1 Hz, $J_{2eq,3}$=3Hz, $J_{2ax,2eq}$=14 Hz, H-2eq), 1.89 (td, 1H, $J_{2ax,3}$=$J_{1,2}$= 3 Hz, H-2ax), 1.66-1.50 (m, 2H, H-2'), 1.40.20 (m, 18H, H-3' to H-11'), 0.87 (t, 3H, $J_{11',12'}$=7 Hz, H-12'). **^{1}C NMR** (MeOD) δ 98.3 (C-1), 70.0 (C-4), 69.0 (C-3), 68-9 (C-1'), 68.5 (C-5), 63.0 (C-6), 36.2 (C-2), 33.1, 30.8, 30.7, 30.6, 30.5, 27.4, 23.8 (C-2' to C-11'), 14.5 (C-12'). **HRMS**: Calcd. [$C_{18}H_{36}NaO_5$] 335.2455; Found 335.2450 (error 1.3 ppm).

Dodecyl 4,6-di-O-benzyl-2,3-dideoxy-D-*erythro*-hex-2-enopyranosides (23a,b). To a solution of 3,4,6-tri-*O*-benzyl-1,5-anhydro-2-deoxy-D-*arabino*-hex-1-enitol (0.500 g, 1.2 mmol) in

dichloroethane (5 mL), dodecan-1-ol (0.559g, 3 mmol, 2.5 equiv.) and zeolyte HY (0.192g, pre-activated to 140 ºC) were added. The reaction was heated to 100ºC under microwave irradiation (200 W) in a closed vessel microwave reactor for 30 min. The solution was then diluted in dichloroethane, filtered and concentrated. The residue was purified by CC eluted with Hex/EtOAc 25:1, affording compounds **23a** and **23b** in 29% and 14% yield, respectively, both as colourless oils.

Dodecyl 4,6-di-O-benzyl-2,3-dideoxy-α-D-*erythro*-hex-2-enopyranoside (23a). R_f (hex/EtOAc 8:1)= 0.5; $[\alpha]_D^{20}$= +58 º (*c*1, CH_2Cl_2); **^{1}H NMR** ($CDCl_3$) δ 7.41-7.24 (m, 10H, $CH_2\underline{Ph}$), 6.09 (d, 1H, H-3, $J_{2,3}$=10 Hz), 5.80 (br d, 1H, H-2), 5.04 (br s, 1H, 1H), 4.72-4.44 (m, 4H, $\underline{CH_2}PH$), 4.20 (d, 1H, $J_{4,5}$=9Hz, H-4), 4.02-3.96 (m, 1H, H-5), 3.83-3.69 (m, 3H, H-6, H-1'a), 3.50 (td, 1H, $J_{1'a,1'b}$= 10 Hz, $J_{1'a,2'}$=7 Hz, H-1'b), 1.68-1.54 (m, 2H, H-2'), 1.40-1.20 (m, 18H, H-3' to H-11'), 0.91 (t, 3H, $J_{11',12'}$=7 Hz, H-12'). **^{13}C NMR** ($CDCl_3$) δ 138.2, 138.1 (Cq, Ph), 130.5 (C-3), 128.4, 128.3, 127.9, 127.8, 127.7, 127.6 (CH, Ph), 126.7 (C-2), 94.6 (C-1), 73.3, 71.0 ($\underline{C}H_2Ph$), 70.3 (C-4), 69.1 (C-5), 68.9 (C-6), 68.7 (C-1'), 31.9, 29.8, 29.7, 29.6, 29.4, 29.3, 26.2, 22.7 (C-2' to C11'), 14.1 (C-12'). **HRMS**: Calcd. [$C_{32}H_{46}NaO_4$] 517.3291; Found 517.3288 (error -0.4 ppm).

Dodecyl 4,6-di-O-benzyl-2,3-dideoxy-β-D-*erythro*-hex-2-enopyranoside (23b). R_f (hex./EtOAc 8:1)=0.49; **^{1}H NMR** ($CDCl_3$) δ 7.39-7.20 (m, 10H, $CH_2\underline{Ph}$), 6.06 (d, 1H, H-3, $J_{2,3}$=10 Hz), 5.77 (br td, 1H, $J_{1,2}$=2 Hz, H-2), 5.01 (br s, 1H, 1H), 4.67-4.42 (m, 4H, $\underline{CH_2}PH$), 4.17 (d, 1H, $J_{4,5}$=9Hz, H-4), 3.98-3.93 (m, 1H, H-5), 3.83-3.66 (m, 3H, H-6, H-1'a), 3.47 (td, 1H, $J_{1'a,1'b}$= 9 Hz, $J_{1'a,2'}$=6 Hz, H-1'b), 1.61-1.54 (m, 2H, H-2'), 1.35-1.20 (m, 18H, H-3' to H-11'), 0.88 (t, 3H, $J_{11',12'}$=7 Hz, H-12'). **^{13}C NMR** ($CDCl_3$) δ 138.3, 137.9 (Cq, Ph), 129.2 (C-3), 128.4, 128.3, 127.7, 127.6 (CH, Ph), 126.7 (C-2), 96.0 (C-1), 73.3, 71.0 ($\underline{C}H_2Ph$), 75.3 (C-4), 69.9 (C-5), 69.6 (C-6), 68.4 (C-1'), 29.8, 29.7, 29.6, 29.5, 29.3, 26.1, 22.7 (C-2' to C11'), 14.1 (C-12') **HRMS**: Calcd. [$C_{32}H_{46}NaO_4$] 517.3291; Found 517.3290 (error -0.2 ppm).

Dodecyl 2,3-dideoxy-α-D-*erythro*-pyranoside (24). To a solution of compound **23a** (0.050g, 0.113 mmol) in MeOH (5 mL) and EtOAc (1 mL), was added a suspension of 10% Pd/C (0.200g, wet) in MeOH (2 mL). Under N_2, triethylsilane was added dropwise (0.7 mL), leading to a visible evolution of H_2, and the solution was stirred overnight. After filtration of the catalyst through celite, and evaporation of the solvent, title compound was obtained as a colourless oil in 46% yield (16.3 mg). R_f (Petrol. ether/EtOAC 1:1)=0.5; $[\alpha]_D^{20}$= +86 º (*c*0.1, CH_2Cl_2); **^{1}H NMR** ($CDCl_3$) δ 4.72 (d, 1H, $J_{1,2}$=3 Hz, H-1), 3.75 (dd, 1H, $J_{5,6a}$=2 Hz, $J_{6a,6b}$=11 Hz, H-6a), 3.67 (td, 1H, $J_{1'a,1'b}$= 10 Hz, $J_{1'a,2'}$=7 Hz, H-1'a), 3.62 (dd, 1H, $J_{5,6b}$=5 Hz, H-6b), 3.47 (ddd, 1H, $J_{4,5}$=9 Hz, H-5), 3.44-3.37 (m, 1H, H-4), 3.34 (td, 1H, H-1'b), 1.83-1.65 (m, 4H, H-2 and H-3), 1.60-1.51 (m, 2H, H-2'), 1.42-1.20 (m, 18H, H-3' to H-11'), 0.87 (t, 3H, $J_{11'12'}$=7 Hz, H-12'). **^{13}C NMR** ($CDCl_3$) δ 95.3 (C-1), 73.3 (C-5), 66 (C-1'), 65.1 (C-4), 61.1 (C-6), 31.1, 28.8, 28.6, 28.5 (C-2' to C-11'), 28.4, 21.8 (C3 and C4), 12.5 (C-12'); **HRMS**: Calcd. [$C_{18}H_{36}NaO_4$] 339.2506; Found 339.2503 (error 0.7 ppm).

Methyl 2,6-di-*O*-pivaloyl-α-D-glucopyranoside (25). To a solution of methyl α-D-glucopyranoside (2 g, 10.4 mmol) in pyridine (20 mL), a solution of pivaloyl chloride (2 equiv., 23 mmol, 2.8 mL) in DCM (4 mL) was added dropwise, at -78 ºC. After stirring at -10 ºC for 2h, the reaction was diluted with DCM (100 mL), washed with a 2M HCl solution until the odour of pyridine was no longer detected. The organic phase then washed with water, dried with $MgSO_4$, filtered and evaporated. The resulting residue was purified by CC eluted with Petrol. ether/ EtOAc 5:1. Compound **25** was obtained as a white solid in 64.6% (2.41g) yield. M.p.=83.0-85.4 °C; $[\boldsymbol{\alpha}]_{\boldsymbol{D}}^{\boldsymbol{20}}$= +89 º (*c*1; $CHCl_3$); R_f (Petrol. ether/EtOAc 2:1)=0.33; **^{1}H NMR** (MeOD) δ 4.88 (d, 1H, $J_{1,2}$ = 3.8 Hz, H-1), 4.60 (dd, 1H, $J_{1,2}$ = 3.8 Hz, $J_{2,3}$ = 10.0 Hz, H-2), 4.49 (dd, 1H, $J_{6a,6b}$ = 12.0 Hz, $J_{6b,5}$ = 4.6 Hz, H-6a), 4.27 (dd, 1H, $J_{6a,6b}$ = 12.0 Hz, $J_{6a,5}$ = 2.0 Hz, H-6b), 3.98 (td, 1H, $J_{2,3}$ = $J_{3,4}$ = 10.0 Hz, $J_{3,OH}$ = 3.0, H-3), 3.79-3.75 (m, 1H, H-5), 3.31 (br d, 1H, $J_{4,OH}$ = 3.0 Hz, OH-4), 3.40-3.33 (m, 4H, H-4, OMe), 2.70 (d, 1H, $J_{3,OH}$ = 3.0 Hz, OH-3), 1.24 (s, 18H, -OPiv); **^{13}C**

NMR (MeOD) δ 179.6 (C=O, Piv), 178.6 (C=O, Piv), 97.2 (C-1), 73.2 (C-2), 71.5 (C-3), 70.7 (C-4), 69.6 (C-5), 63.2 (C-6), 55.5 (-OMe), 39.1 (Cq, Piv), 39.0 (Cq, Piv), 27.4 ($\underline{C}H_3$, Piv) 27.2 ($\underline{C}H_3$, Piv). **HRMS**: Calcd. [$C_{17}H_{30}NaO_8$] 385.1833; Found 385.1826 (error 1.7 ppm).

Methyl 2,6-di-*O*-pivaloyl-3,4-dideoxy-α-D-*erythro*-hexopyranoside (26) and **methyl 4-deoxy-2,6-di-*O*-pivaloyl-α-D-*xylo*-hexopyranoside (27).** Compound **25** (1 g, 2.75 mmol) was dissolved in DCM (30 mL) and pyridine (0.89 mL, 11.0 mmol, 4 equiv.), and cooled to -10 ºC, under N_2. Trifluoromethanesulfonic anhydride (1.86 mL, 11.0 mmol, 4 equiv.) was then added dropwise to the stirring solution, which was then warmed to 0 ºC and stirred for 2h30. The reaction was quenched by addition of 100 mL of cool distilled water, followed by extraction with DCM (2 x 100 mL). Organic phase was dried with $MgSO_4$, filtered and evaporated under reduced pressure, affording highly labile colourless syrup virtually composed of methyl 2,6-di-*O*-pivaloyl-3,4-di-*O*-trifluoromethanesulfonyl-α-D-glucopyranoside. The syrup was dissolved in toluene (32 mL), tetra-*n*-butylammonium borohydride (4.1799 g, 16.5 mmol, 6 equiv.) was added, and the reaction mixture was stirred at 85ºC overnight, cooled to room temperature and poured into ice cold water (100 mL). After extraction with DCM (2x50 mL), the organic phase was washed with saturated aqueous sodium hydrogen carbonate (2x50 mL) and water (50 mL). The organic phase was dried with $MgSO_4$, filtered, and concentrated under reduced pressure to give a syrup, that was purified by CC eluted with Hex/EtOAc 10:1, to afford compound **26** as a colourless oil in 29% yield (0.263 mg) and compound **27** also as a colourless oil in 33% yield (0.223 mg).

Methyl 2,6-di-*O*-pivaloyl-3,4-dideoxy-α-D-*erythro*-hexopyranoside (26). $[\alpha]_D^{20}$= +82 º (*c*1; $CHCl_3$); R_f (hex/EtOAc 3:1)= 0.67; **^{1}H NMR** ($CDCl_3$) δ 4.78 (d, 1H, $J_{1,2}$=3.2 Hz, H-1), 4.72 (ddd, $J_{2,3ax}$=12 Hz, $J_{2,3eq}$=4 Hz, H-2), 4.11-4.00 (m, 2H, H-6), 3.97-3.89 (m, 1H, H-5), 3.39 (s, 3H, -OMe), 1.94 (qd, 1H, $J_{3ax,3eq}$=12 Hz, $J_{3a,4e}$=$J_{3a,4a}$=4 Hz, H-3ax), 1.84-1.77 (m, 1H, H-3eq), 1.72 (ddd, $J_{4a,4e}$=13 Hz, H-4eq), 1.53 (qd, H-4ax), 1.21 (s, 9H, -OPiv), 1.19 (s, 9H, -OPiv). **^{13}C NMR**

($CDCl_3$) δ 178.3, 178.1 (C=O, Piv), 96.9 (C-1), 69.8 (C-2), 66.1 (C-5 and C-6), 55.0 (OMe), 38.8, 38.7 (Cq, -OPiv), 27.2, 27.0 ($\underline{C}H_3$, -OPiv), 26.5 (C-4), 22.8 (C-3). **HRMS**: Calcd. [$C_{17}H_{30}NaO_6$] 353.1935; Found 353.1935 (error 0.0 ppm).

Methyl 4-deoxy-2,6-di-*O*-pivaloyl-α-D-*xylo*-hexopyranoside (27). R_f (hex/EtOAc 3:1)= 0.58; $[\alpha]_D^{20}$= +75 º (*c*1; $CHCl_3$); R_f (hex/EtOAc 3:1)= 0.58; **^{1}H NMR** ($CDCl_3$) δ 4.72 (d, 1H, $J_{1,2}$=4 Hz, H-1), 4.55 (s, 1H, -OH), 4.30-4.22 (m, 2H, H-3 and H-5), 4.15-4.02 (m, 3H, H-6 and H-2), 3.43 (s, 3H, -OMe), 2.02 (td, 1H, $J_{4e,5}$=$J_{3,4e}$=3 Hz, $J_{4e,4a}$=14 Hz, H-4ax), 1.83 (ddd, $J_{4a,5}$=$J_{3,4a}$=11 Hz, H-4ax), 1.21 (s, 9H, -OPiv). **^{13}C NMR** ($CDCl_3$) δ 178.2 (C=O, Piv), 101.0 (C-1), 68.2 (C-2), 67.9, 68.8 (C-5 and C-6), 61.3 (C-3), 55.9 (OMe), 38.8 (Cq, -OPiv), 34.0 (C-4), 27.2 ($\underline{C}H_3$, -OPiv). **HRMS**: Calcd. [$C_{17}H_{30}NaO_7$] 369.1884; Found 369.1883 (error 0.1 ppm).

Dodecyl 3,4-dideoxy-D-*erythro*-hexopyranosides (28/29). Compound **26** (0.260 g, 0.787 mmol) and amberlyst A15 (0.050 g) were suspended in dodecan-1-ol (2.41 mL, 10.76 mmol, 14 equiv.) and stirred at 95 ºC for 20 h. Reaction was then cooled to r.t., diluted with DCM, the A-15 beads were filtered off and DCM was evaporated under reduced pressure. The residue was ressuspended in 3 mL of MeOH:H_2O 50:50, and potassium hydroxide pellets (0.6 g) were added to the stirring solution. After 16 h at room temperature, reaction was diluted with MeOH (3 mL) and neutralized with IR-120. After filtration and evaporation of the solvent, the residue was purified by CC elute with hex/acetone 4:1, affording the alfa anomer **28** as a white solid in 36% yield (0.0896 g), and the beta-anomer **29** as a colourless oil, in 14% yield (0.0338 g).

Dodecyl 3,4-dideoxy-α-D-*arabino*-hexopyranoside (28). R_f (CyHex/EtOAc 1:3)=0.65; M.p. = 52.9.0-53.8°C; $[\alpha]_D^{20}$= +71 º (*c*1, CH_2Cl_2); **^{1}H NMR** ($CDCl_3$) δ 4.66 (d, 1H, $J_{1,2}$= 3 Hz, H-1), 3.75-3.66 (m, 2H, H-5 and H-1'a), 3.55 (ddd, 1H, $J_{2,3ax}$=11 Hz, $J_{2,3eq}$=4 Hz, H-2), 3.46-3.37 (m, 2H, H-6 and H-1'b), 1.80 (qd, 1H, $J_{3ax,3eq}$=12 Hz, $J_{2,3eq}$=4 Hz, H-3eq), 1.75-1.68 (m, 1H, H-3ax), 1.67-

1.54 (m, 3H, H-4eq and H-2'), 1.45-1.34 (m, 3H, H-4ax, H-3'), 1.33-1.21 (m, 16H, H-4' to H-11'), 0.87 (t, 3H, $J_{11',12'}$=7 Hz, H-12'). **^{13}C NMR** ($CDCl_3$) δ 99.8 (C-1), 70.1 (C-5), 69.6 (C-2), 68.8 (C-1'), 65.9 (C-6), 33.1, 30.8, 30.7, 30.5, 23.8 (C-2', C-4' to C-11'), 27.8, 27.4, 27.3 (C-3, C-4 and C-3'), 14.5 (C-12'). **HRMS**: Calcd. [$C_{18}H_{36}NaO_4$] 339.2506; Found 339.2500 (error 1.6 ppm).

Dodecyl 3,4-dideoxy-β-D-*erythro*-hexopyranoside (29). R_f (CyHex/EtOAc 1:3)0.64; $[\alpha]_D^{20}$= -22 º (*c*0.2, CH_2Cl_2); **^{1}H NMR** ($CDCl_3$) δ 4.21 (d, 1H, $J_{1,2}$=8 Hz, H-1), 3.90 (td, 1H, $J_{1'a,1'b}$= 10 Hz, $J_{1'a,2'}$=7 Hz, H-1'a), 3.66-3.56 (m, 3H, H-5 and H-6), 3.51 (td, 1H, H-1'b), 3.43-3.35 (m, 1H, H-2), 2.14-2.08 (m, 1H, H-3ax), 1.97 (br s, 2H, -OH), 1.66-1.54 (m, 3H, H-2' and H-4ax), 1.52-1.42 (m, 2H, H-3eq and H-4eq), 1.35-1.15 (m, 18H, H-3' to H-11'), 0.87 (t, 3H, $J_{11',12'}$= 6.5 Hz, H-12'). **^{13}C NMR** ($CDCl_3$) 105.3 (C-1), 76.4 (C-5), 69.9 (C-1'), 69.8 (C-2), 65.3 (C-6), 31.9, 29.7, 29.6, 29.4, 29.3, 28.9, 26.0, 25.9, 22.7 (C-3, C-4, and C-2' to C11'), 14.1 (C-12'). **HRMS**: Calcd. [$C_{18}H_{36}NaO_4$] 339.2506; Found 339.2507 (error -0.3 ppm).

Antimicrobial assays and bacterial strains. For results presented in table 1, the broth microdilution method on Müller-Hinton medium was employed to determine the MIC values, according to the Clinical and Laboratory Standards Institute (CLSI) guidelines.[10] Three strains of the *B. anthracis* (INSA private collection), *B. cereus* (ATCC 11778) and *E. faecalis* (ATCC 29212) were used. Compounds were incubated with bacteria for 16 h at 37 °C prior to determining the MIC, which is defined as the lowest concentration of the tested compounds at which no bacterial growth was observed.

Cytotoxicity. Caco-2 and HepG2 cell culture and viability assays were performed using a pre-established methodology.[10] Caco-2 and HepG2 cells were grown in DMEM high glucose supplemented with 10% foetal bovine serum, glutamine (2 mM), penicillin (100 U/mL), and streptomycin (100 μg/mL), in a humidified incubator at 37 °C with a 5 % CO_2 atmosphere. The

cells were trypsinized twice a week with trypsin/EDTA (0.05%/0.02%) and the medium was also changed twice a week. Determination of cell growth was performed using the MTT [3-(4,5-dimethylthiazol-2-yl)-2,5-diphenyltetrazolium bromide] assay. On day 1, 20,000 cells/well were seeded into 96-well plates in a volume of 100 μL. On day 2, the different drugs concentration (0.1–100 μM) were added to the plate. In all the experiments, the various drug-solvents (EtOH, DMSO) were added in each control to evaluate a possible solvent cytotoxicity. After the established incubation time with drugs, MTT (0.5 mg/mL) was added to each well, and after 3-4 h incubation at 37 °C, the supernatant was removed. The formazan crystals were solubilized using DMSO/EtOH (1:1) (100 μL) and the absorbance values at 570 nm and 630 nm were determined on the microplate reader Victor3 from Perkin Elmer Life Sciences.

.

REFERENCES

[1] Sweeney, D. A.; Hicks, C. W.; Cui, X.; Li, Y.; Eichacker, P. Q., Anthrax Infection. *American Journal of Respiratory and Critical Care Medicine* **2011,** *184* (12), 1333-1341.

[2] Goel, A. K., Anthrax: A disease of biowarfare and public health importance. *World Journal of Clinical Cases* **2015,** *3* (1), 20-33.

[3] Celandroni, F.; Salvetti, S.; Gueye, S. A.; Mazzantini, D.; Lupetti, A.; Senesi, S.; Ghelardi, E., Identification and Pathogenic Potential of Clinical *Bacillus* and *Paenibacillus* Isolates. *PloS one* **2016,** *11* (3), e0152831.

[4] Silva, F. V.; Goulart, M.; Justino, J.; Neves, A.; Santos, F.; Caio, J.; Lucas, S.; Newton, A.; Sacoto, D.; Barbosa, E.; Santos, M. S.; Rauter, A. P., Alkyl deoxy-arabino-hexopyranosides: synthesis, surface properties, and biological activities. *Bioorganic & Medicinal Chemistry* **2008,** *16* (7), 4083-92.

[5] Martins, A.; Santos, M. S.; Dias, C.; Serra, P.; Cachatra, V.; Pais, J.; Caio, J.; Teixeira, V. H.; Machuqueiro, M.; Silva, M. S.; Pelerito, A.; Justino, J.; Goulart, M.; Silva, F. V.; Rauter, A. P., Tuning the Bioactivity of Tensioactive Deoxy Glycosides to Structure: Antibacterial Activity Versus Selective Cholinesterase Inhibition Rationalized by Molecular Docking. *European Journal of Organic Chemistry* **2013,** *8*, 1448-1459.

[6] Rauter, A.; Almeida, T.; Vicente, A.; Ribeiro, V.; C. Bordado, J.; P. Marques, J.; Ramôa-Ribeiro, F.; Ferreira, C.; Guisnet, M., Reactions of N-, S- and O- Nucleophiles with 3,4,6-Tri-O-benzyl-D-

glucal Mediated by Triphenylphosphane Hydrobromide versus Those with HY Zeolite. *European Journal of Organic Chemistry* **2006,** *10*, 2429-2439.

[7] Rauter, A. P.; Lucas, S.; Almeida, T.; Sacoto, D.; Ribeiro, V.; Justino, J.; Neves, A.; Silva, F. V.; Oliveira, M. C.; Ferreira, M. J.; Santos, M. S.; Barbosa, E., Synthesis, surface active and antimicrobial properties of new alkyl 2,6-dideoxy-L-*arabino*-hexopyranosides. *Carbohydrate Research* **2005,** *340* (2), 191-201.

[8] Cachatra, V.; Almeida, A.; Sardinha, J.; Lucas, S. D.; Gomes, A.; Vaz, P. D.; Florêncio, M. H.; Nunes, R.; Vila-Viçosa, D.; Calhorda, M. J.; Rauter, A. P. Wittig Reaction: Domino Olefination and Stereoselectivity DFT Study. Synthesis of the Miharamycins' Bicyclic Sugar Moiety. *Organic Letters* **2015** *17* (22), 5622-5625.

[9] Ferrier, R. J.; Prasad, N., Unsaturated carbohydrates. Part IX. Synthesis of 2,3-dideoxy-[small alpha]-D-*erythro*-hex-2-enopyranosides from tri-O-acetyl-D-glucal. *Journal of the Chemical Society C: Organic* **1969,** (4), 570-575.

[10] Clinical & Laboratory Standards Institute, NCCLS document M7-A4. In *Methods for Dilution Antimicrobial Susceptibility Tests for Bacteria that Grow Aerobically*, 2015.

[11] G. Nesi; N. A. Colabufo; M. Contino; M. G. Perrone; M. Digiacomo; R. Perrone; A. Lapucci; M. Macchia; S. Rapposelli, SAR study on arylmethyloxyphenyl scaffold: looking for a P-gp nanomolar affinity. *European Journal of Medicinal Chemistry* **2014,** *76*, 558-66.

Chapter 5

2-Deoxy glycosylation towards more effective and bioavailable neuroprotective molecules inspired by nature

Naturally occurring phenolic compounds are known for their beneficial health-promoting effects in chronic and degenerative diseases. Stilbenes, particularly resveratrol, are amongst the most well documented and emblematic neuroprotective natural products. In addition to its antioxidant and anti-inflammatory activities, typical of polyphenols, resveratrol is also able to inhibit Aβ oligomeric cytotoxicity and to reduce neuronal cell death.[1-2] Despite the promising activities of resveratrol, its bioavailability in humans is less than 1%, as a consequence of a quick and extensive metabolism, mainly through glucuronidation and sulfurylation. In addition, the water-insolubility of stilbenes limits their further pharmacological exploitation.[3-4]

Recently, concerns have been raised on the promiscuity and on the lack of therapeutic selectivity of some natural compounds, the so called Pan Assay Interference compounds (PAINs).[5] In the case of resveratrol, its planarity is allegedly guilty to induce membrane intercalation effects and interfere with bioassays.

Coupling sugars to bioactive polyphenols can be a resourceful way to improve the bioavailability and pharmacological activity of such molecular entities,[6] as well as to minimize concerns associated with PAINS, by compromising their planarity. Literature shows a number of efforts to improve resveratrol water solubility and bioavailability via enzymatic glucosylation. Indeed, water solubilitiy of the α-glucosylated derivatives (at 3 or 4-position) were at least 65- and 5-fold higher than those of resveratrol and of the natural β-glucosylated derivative (piceid), respectively.[7] On the other hand, rosmarinic acid, previously identified by our research group as the active principle of the neuroprotective plant *Salvia sclareoides*, prevents amyloid aggregation, and reduces a number of other events underlying AD pathology.[8-10] Interestingly, methyl caffeate itself, a sub structural unit of rosmarinic acid, significantly reduces Aβ oligomeric cytotoxicity by

promoting disaggregation of Aβ aggregates, while having low bioavailability,[10] making it also an interesting candidate for glycosylation.

Coupling sugars to polyphenols can have a deeper impact than physicochemical properties modulation. Carbohydrates have the also the ability to prevent oxidation by masking phenolic groups,[7] favouring drugs' access to the brain via hexose transporters (GLUTs) at the blood–brain barrier.[11] Their effect on retarding amyloid fibril formation by stabilizing the native state through preferential hydration was also reported [12] These findings encouraged us to investigate glycosylation of natural or nature inspired neuroprotective molecules, using glycals as easily accessed glycosyl donors. This robust methodology allowed the generation of a set of new resveratrol and phenolic acid glycosides, envisioning more effective and bioavailable compounds. Two glycosyl moieties were selected, namely 2,6-dideoxy-L-*arabino*-pyranosyl and 2-deoxy-D-*arabino*-pyranosyl and glycosides' synthesis is here fully disclosed. Their ability to protect neuronal cells from oxidative stress was assessed as well as their permeability properties, which will also be discussed.

RESULTS AND DISCUSSION

Chemistry

3'-*O* and 4-*O*-glycosides **4, 5, 8** and **9** were prepared by reaction of resveratrol with the appropriate glycal (**2** and **3**, respectively), in the presence of triphenylphosphane hydrobromide (TPHB). The respective beta anomers were detected only as traces on the TLC plate, and were not isolated. Separation of 3-*O* and 4-*O*' glycosides was only possible after consecutive column chromatography, resulting in low isolated yields of 21% and 6% for **4** and **5**, respectively, and 22% and 8% for **8** and **9**. After purification, Zemplén deprotection afforded glycosides **6, 7, 10** and **11** in quantitative yield.

For the synthesis of the caffeic acid derivative, aromatic hydroxy groups of caffeic acid were protected with *tert*-butyldimethylsilyl group, and the aglycone was prepared by Steglich esterification, prior to sugar coupling. Compound **13** was converted in 2-hydroxyethyl ester by DCC, in an overall yield of 54%. Ester **14** was converted into 2,6-dideoxy *arabino*-pyranoside, following the same procedure described above, as an anomeric mixture (α/β 3:1). The protecting groups of the glycosyl donor **15** were changed accordingly, for a mild final deprotection using TBAF.

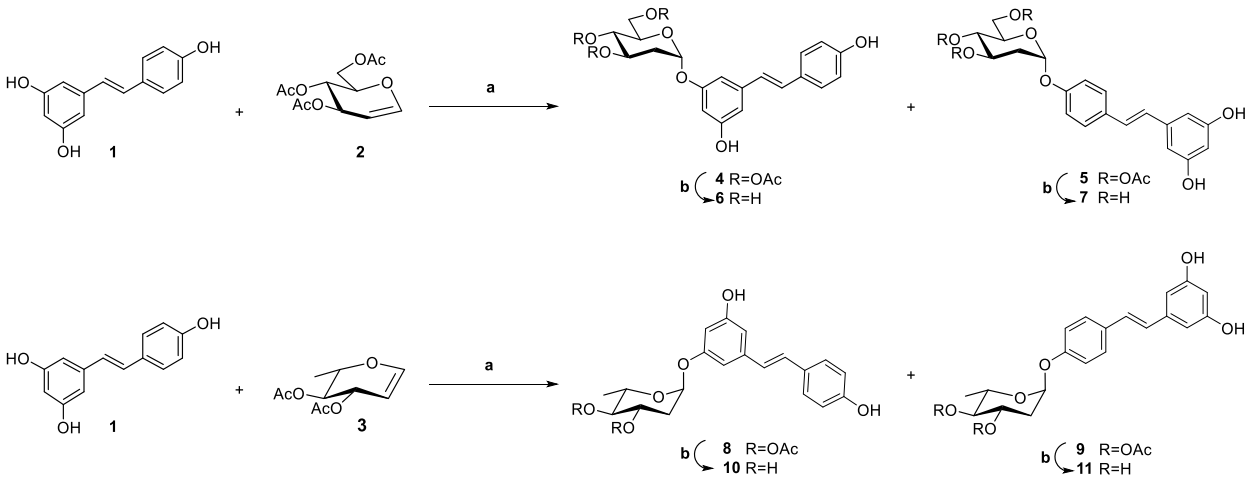

Scheme 1. Synthesis of resveratrol glycosides. a) TPHB, THF, 40 ºC, 48h; b) NaOMe, MeOH.

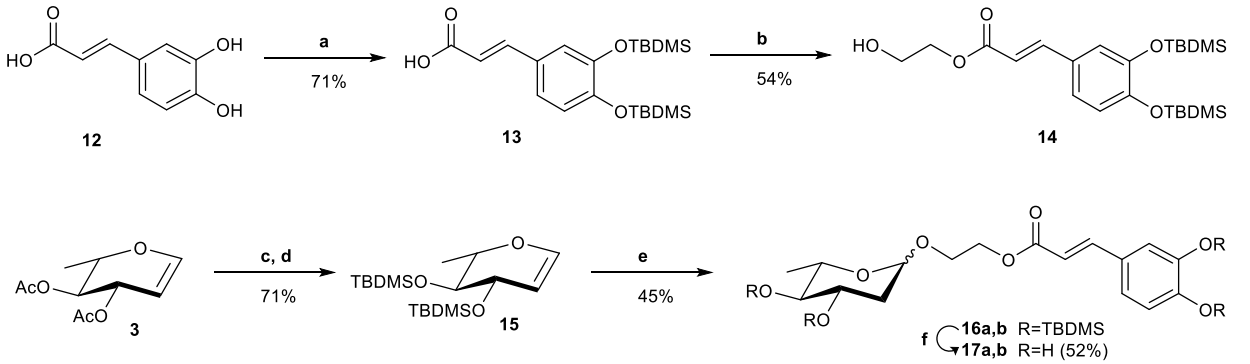

Scheme 2. Synthesis of **17**. a) TBMDSCl, DCM; b) Ethylene glycol, DCC, DMAP, DCM; c) NaOMe, MeOH, d)TBMDSCl, imidazole, DMF; e) TPHB, THF; f) TBAF, THF.

Neuroprotective effects

The link between oxidative stress and the pathogenesis of acute or chronic neurodegenerative processes has been extensively studied. The excessive production of free radicals damages cellular essentials such as lipids, proteins, and DNA,[13-15] leading ultimately to the induction of apoptosis in neuronal cells.[16] In fact, hydrogen peroxide overproduction has been associated with events such as amyloid aggregation,[17-18] dopamine oxidation,[19] and brain ischemia/reperfusion.[20]

In this study, hydrogen peroxide was used to cause oxidative stress in neuroblastoma cells (SH-SY5Y) to assess the neuroprotective effects of the synthesized glycosides. Prior to neuroprotection assay, the eventual cytotoxic effects of compounds **1, 6, 7, 11** and **17** was assessed (Figure 1). Only compounds **7** and **11** led to a statistically different loss of viability at 50 µM, although it remained above 50% in all cases.

Incubating cells with 100 µM of H_2O_2 led to a decrease in cell viability of ca. 60%, as expected. Incubating the cells with both hydrogen peroxide (100 µM) and resveratrol glycosides **6** and **11** resulted in a statistically significant increase in the percentage of cells remaining viable (Figure 1). Surprisingly, resveratrol glycosides **7** and **10** had no statistically significant effect on cell viability.

Our results show that resveratrol glycosides **6** and **11** were more effective at protecting neuronal cells from peroxide-induced cytotoxicity than resveratrol itself, although there is no link between sugar moiety/glycosylation position and neuroprotective activity. Caffeic acid derivative **17** showed good neuroprotection activity, being able to maintain cellular viability similar to that of the control. Although the mechanism of neuroprotection of compounds **6** and **11** remains unknown, resveratrol had been previously shown to protect embryonic neural stem cells, since it decreases oxidative stress by inducing higher activity of antioxidant enzymes, decreasing nitric oxide production and nitric oxide synthase activity, and alleviating both nuclear and mitochondrial

DNA damage in embryonic neural stem cells.[21] We can only speculate whether resveratrol glycosides act through the same mechanism, enhanced by the sugar moiety.

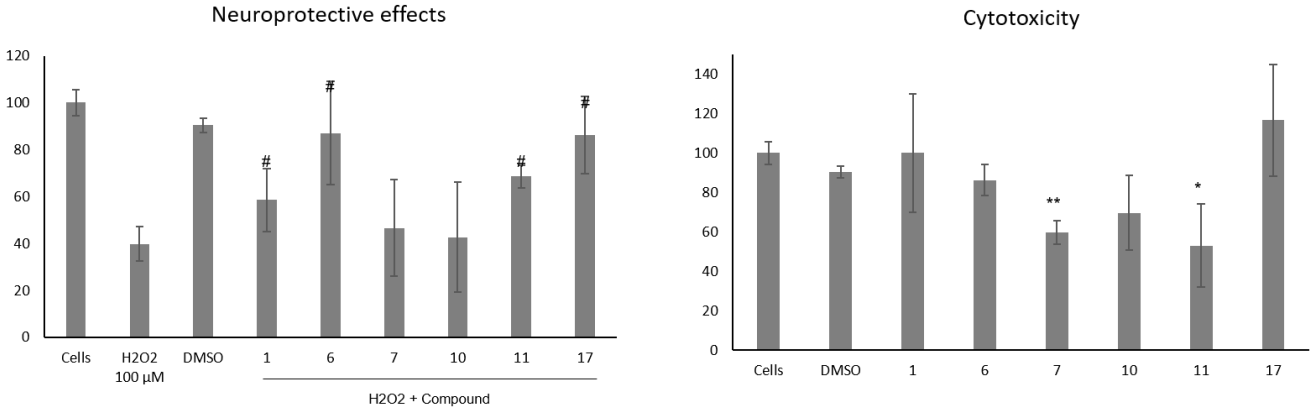

Figure 1. Neuroprotective and cytotoxic effects of synthesized compounds in neuroblastoma (SH-SY5Y) cells. * = significantly different when compared to cells control (p-value < 0.05); # = significantly different when compared to hydrogen peroxide controls (p-value < 0.05). Error bars represent the standard error of the mean.

The toxicity of the two most promising compounds was also assessed in Caco-2 and in HepG2 cell lines, used as models of intestinal and liver toxicity, respectively. There was no decrease in the viability of either HepG2 or Caco-2 cells following 24h and 48h incubation with varying concentrations of compounds **6** and **17**, with concentrations ranging from 0.1 to 100 µM.

Table 1. Caco-2 and HepG2 cell viability (%) pf **6** and **17**.

Compound	**Cytotoxicity IC_{50} (µM)**	
	Caco-2	**HepG2**
6	>100	>100
17	>100	>100

Physicochemical properties and intestinal permeability

To evaluate the druggability of the newly synthesized compounds, lipophilicity and permeability parameters were evaluated, by determining the partition coefficient at physiological pH (Log $D_{7.4}$) and the PAMPA permeability values, respectively (Table 2).

The measured Log $D_{7.4}$ values for resveratrol glycosides indicate a moderate lipophilicity, essential to their bioavailability and blood-brain barrier penetration. Log D values between 0 and 3 are associated with a good balance between solubility and permeability, optimal oral absorption and low metabolic instability. Indeed, LogD values close to 2 have been established as ideal for BBB penetration.[22-23] In fact, the median cLogD for marketed CNS drugs is 1.7.[23] In addition, MWs and numbers of HBA and HBD of all assessed molecules were in the acceptable ranges for drug-likeness, respecting Lipinski rule of 5.

Table 2. Physicochemical properties and permeability of lead candidates.

Compound	HBA	HBD	log $D_{7.4}$	PAMPA (-log *Pe*)/cms^{-1})
1	0	3	n.d.[a]	3.97 ± 0.02
6	2	5	1.748 ± 0.074	10.00 ± 0.00
7	2	5	1.747 ± 0.097	6.73 ± 0.18
10	2	4	2.013 ± 0.061	5.56 ± 0.13
11	2	4	2.813 ± 0.112	4.82 ± 0.02
17	3	4	n.d.[a]	10.00 ± 0.00

[a]Not detected due to poor ionization

From the synthesized compounds, the 2,6-dideoxy *arabino*-pyranosides **10** and **11** (L-series) presented the best permeability results. In addition, glycosylation at position 4 seems to benefit permeation, when compared to 3'-glycosyation. Glycosylation of resveratrol did not improve passive permeation, but it is important to highlight that, although PAMPA assay highly correlates with permeation across a variety of barriers, it only accounts for passive permeation.[24] The conjugation of sugars may improve active permeation via hexose transporters, but confirmation of this effect requires further studies.

CONCLUSIONS

The synthesis of 2-deoxy glycosides embodying natural neuroprotective polyphenols as aglycones was carried out successfully, expecting to improve the bioavailability and neuroprotective activity of such molecular entities. Resveratrol glycosides **6** and **11** were more effective at protecting the neuronal cells from peroxide-induced cytotoxicity than resveratrol itself, and caffeic acid derivative **17** also showed remarkable neuroprotection activity. The two most promising compounds in terms of neuroprotection, **6** and **17** were not toxic to neuroblastoma, intestinal or liver cells at all concentrations tested. Coefficient partition measurements demonstrated the moderate lipophilicity of resveratrol glycosides, which logD values are typical of CNS drug and ideal for BBB penetration while passive permeation assessed by the PAMPA revealed that 2,6-dideoxy L-*arabino*-pyranosides were more effective than 2-deoxy-D-*arabino*-pyranosides to permeate the intestinal barrier.

EXPERIMENTAL SECTION

Chemical synthesis

Starting materials and reagents were purchased from Sigma–Aldrich, Fluka and Acros. The solvents were dried prior to use with 4 Å or 3 Å (methanol) molecular sieves. Reactions were

followed by UPLC-MS and/or TLC. TLC was carried out on aluminum sheets (20 cm x 20 cm) coated with 0.2 mm silica gel 60 F-254 (Merck) and detection was accomplished by spraying the plates with a solution of H_2SO_4 in ethanol (10%) followed by heating at 120 °C.

Glycosylation of resveratrol was followed by UPLC(DAD)-MS, using method A or B (%CP stands for chromatographic purity) for chromatography, and ES-API ionization. Chromatographic methods are as follows:

Method A (high pH)*:* The column used was an XBridge C18 column (2.1 x 50 mm) with a 3.5 μm-particle size. The mobile phase consisted of eluent A: 10mM ammonium bicarbonate; and eluente B: MeCN. The flow rate was maintained at 1.2mL/min at 50 ºC. The gradient as ramped from 10% B to 95 %B over 1.5 min, with additional 0.5 min hold time.

Method B (low pH)*:* The column used was an Gemini NX C18 column (2.1 x 50 mm) with a 3 μm-particle size. The mobile phase consisted of eluent A: 0.1% formic acid in water; and eluent B: 0.1% formic acid in MeCN. The flow rate was maintained at 1.2mL/min at 50 ºC. The gradient as ramped from 5% B to 95 %B over 1.5 min, with additional 0.5 min hold time.
Compounds were purified by flash chromatography using silica gel 60G (0.040–0.063 mm, Merck), or by preparative HPLC.

Melting points were obtained with a SMP3 Melting Point Apparatus, Stuart Scientific, Bibby. Optical rotations were measured with a Perkin–Elmer 343 polarimeter. NMR spectra were recorded with a Bruker Avance 400 spectrometer at 298 K operating at 100.62 MHz for ^{13}C NMR and at 400.13 MHz for ^{1}H NMR. The solvents used were $CDCl_3$ with 0.03% TMS and CD_3OD (Sigma–Aldrich). The chemical shifts are reported as δ (ppm) and the coupling constants (J) are given in Hz.

High resolution mass spectra of new compounds were acquired on a Bruker Daltonics HR QqTOF Impact II mass spectrometer (Billerica, MA, USA). The nebulizer gas (N_2) pressure was

set to 1.4 bar, and the drying gas (N_2) flow rate was set to 4.0 L/minute at a temperature of 200 °C. The capillary voltage was set to 4500 V and the charging voltage was set to 2000 V.

Compound names are given according to IUPAC recommendations. However, for comparison purposes, in the NMR assignment the locants numbering do dot follow IUPAC nomenclature, but are rather numbered as follows:

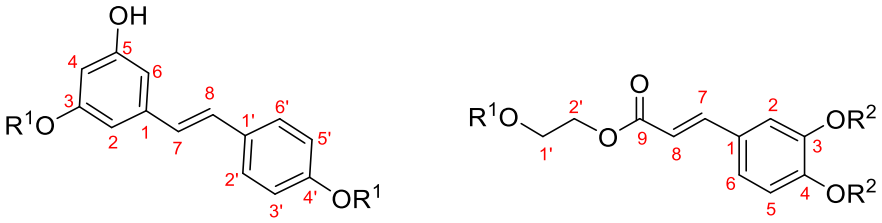

Figure 2. Numbering used for the NMR assignment of stilbenoid and phenylpropenoid glycosides. R^1=H or Sugar. Sugar atoms are numberered from 1" to 6", starting from the anomeric position. R^2=TBDMS or H.

Glycosylation procedure. The appropriate glycal (**2** or **3**, 2.0 mmol) was dissolved in THF (5 mL), and resveratrol (1.5 equiv) was adde. The reaction mixture was stirred overnight at 40 ºC and reaction course followed by LC-MS and TLC. The reaction mixture was diluted with DCM (20 mL), washed with saturated sodium hydrogenocarbonate (30 mL), and then extracted with DCM (2x 20 mL). The organic layers were combined, dried with magnesium sulphate, which was filtered off along with precipitated resveratrol. Solvent was evaporated and, to remove excess resveratrol, it was again suspended in 2 mL of EtOH and 20 mL of $CHCl_3$, filtered again, and the filtrate was evaporated to give a residue which was purified by consecutive flash chromatography with $CHCl_3 \rightarrow$ 95:5 $CHCl_3$/EtOH, to afford the corresponding 3-O- and 4'-resveratrol glycosides.

3-*O*-(3'',4''-di-*O*-acetyl-2-deoxy-α-D-*arabino*-hexopyranosyl) resveratrol (4). Reaction of glycal **2** with resveratrol afforded compound **4**, isolated in 21% yield (0.210 g), as yellowish oil. LC-MS data (low pH): RT: 0.96, [M+H]=501.00 m/z, [M+Na]=523.00 m/z, [M-H]=499.00 m/z. R_f ($CHCl_3$/EtOH 95:5)=0.35; **^{1}H NMR** ($CDCl_3$) δ 7.33 (d, 2H, $J_{2',3'}$= $J_{5',6'}$=8 Hz, H-2' and H-6'),

6.94 (d, 1H, $J_{7,8}$=16 Hz, H-8), 6.82 (d, 2H, H-3' and H-5'), 6.77 (d, 1H, H-7), 6.74 (br s, 1H, H-2), 6.64 (br s, 1H, H-6), 6.49 (br t, 1H, $J_{4,6}$= $J_{2,4}$= 2Hz, H-4), 5.64 (d, 1H, $J_{1'',2''}$=2 Hz, H-1''), 5.52 (ddd, 1H, $J_{2eq'',3''}$=5 Hz, $J_{3'',4''}$=10 Hz, H-3''), 5.09 (t, 1H, $J_{3'',4''}$= $J_{4'',5''}$=10 Hz, H-4''), 4.31 (dd, 1H, $J_{5'',6a''}$=5 Hz, $J_{6''a,b}$=12 Hz, H-6a''), 3.99-4.10 (m, 2H, H-5'' and H-6b''), 2.45 (dd, 1H, $J_{2ax'',2eq''}$=13 Hz, $J_{2eq'',3''}$=5 Hz, H-2eq''), 2.06 (s, 3H, CH_3, -OAc), 2.08-2.05 (m, 7H, H-2ax'' and two -OAc), 2.02 (br s, 3H, -OAc).**^{13}C NMR** ($CDCl_3$) δ 171.4, 170.9 170.3 (C=O, OAc), 157.4 (C-3), 157.2 (C-5), 155.9 (C-4'), 140.1 (C-1), 129.6 (C-1'), 129.1 (C-8), 128.1 (C-2' and C-6'), 125.8 (C-7), 115.7 (C-3' and C-5'), 107.6 (C-6), 106.5 (C-2), 102.8 (C-4), 95.1 (C-1''), 69.2, 69.1 (C-4'' and C-3''), 68.6 (C-5''), 62.2 (C-6'') 35.0 (C-2''), 21.0, 20.7, 20.7 (CH_3, OAc).

4'-*O*-(3'',4''-di-*O*-acetyl-2-deoxy-α-D-*arabino*-hexopyranosyl)resveratrol (5). Reaction of glycal **2** with resveratrol afforded compound **5**, isolated in 3% yield (0.031 mg), as yellowish oil. LC-MS data (low pH): RT: 1.07, [M+H]=501.00 m/z, [M+Na]=523.00 m/z, [M-H]=499.00 m/z. R_f ($CHCl_3$/EtOH 95:5)=0.27. **^{1}H NMR** (MeOD) δ 7.50 (d, 2H, $J_{2',3'}$= $J_{5',6'}$=9 Hz, H-2' and H-6'), 7.11 (d, 2H, H-3' and H-5'), 7.02 (d, 1H, $J_{7,8}$=16 Hz, H-8), 6.90 (d, 1H, H-7), 6.49 (d, 2H, $J_{2,6}$= 2Hz, H-2 and H-6), 6.20 (br t, 1H, $J_{4,6}$= $J_{2,4}$= 2Hz, H-4), 5.79 (d, 1H, $J_{1'',2ax''}$=2 Hz, H-1''), 5.47 (ddd, 1H, $J_{2eq'',3''}$=5 Hz, $J_{3'',4''}$=10 Hz, H-3''), 5.04 (t, 1H, $J_{3'',4''}$= $J_{4'',5''}$=10 Hz, H-4''), 4.25 (dd, 1H, $J_{5'',6a''}$=5 Hz, $J_{6''a,b}$=12 Hz, H-6a''), 4.09-4.00 (m, 2H, H-5'' and H-6b''), 2.47 (dd, 1H, $J_{2ax'',2eq''}$=13 Hz, $J_{2eq'',3''}$=5 Hz, H-2eq''), 2.06 (s, 3H, CH_3, -OAc), 2.05 (s, 3H, CH_3, -OAc), 2.03-1.95 (m, 4H, H-2ax'' and -OAc). **^{13}C NMR** (MeOD) δ 171.0, 170.6, 170.3 (C=O, OAc), 158.3 (C-3 and C-5), 155.7 (C-4'), 139.5 (C-1), 131.9 (C-1'), 127.4, 127.3 (C-7 and C-8), 127.2(7) (C-2' and C-6'), 116.5 (C-3' and C-5'), 104.6 (C-2 and C-6), 101.6 (C-4), 95.2 (C-1''), 69.2 (C-4''), 68.8 (C-3''), 68.5 (C-5''), 62.1 (C-6'') 34.5 (C-2''), 19.4, 19.2, 19.2 (CH_3, OAc).

3-*O*-(3'',4''-di-*O*-acetyl-2,6-dideoxy-α-L-*arabino*-hexopyranosyl)resveratrol (8). Reaction of glycal **3** with resveratrol afforded compound **8**, isolated in 22% yield (0.195g), as a yellowish oil. LC-MS data (high pH): RT: 0.99, [M+H]=443.00 m/z, [M+Na]=465.00 m/z, [M-H]=441.00 m/z; R_f ($CHCl_3$/EtOH 95:5)=0.40. **^{1}H NMR** ($CDCl_3$) δ 7.30 (d, 2H, $J_{2',3'}$= $J_{5',6'}$=8 Hz, H-2' and H-6'), 6.90 (d, 1H, $J_{7,8}$=16 Hz, H-8), 6.81 (d, 2H, H-3' and H-5'), 6.74 (d, 1H, H-7), 6.71 (br s, 1H, H-2), 6.61 (br s, 1H, H-6), 6.48 (br s, 1H, H-4), 5.57 (d, 1H, $J_{1'',2ax''}$=2 Hz, H-1''), 5.47 (ddd, 1H, $J_{2eq'',3''}$=5 Hz, $J_{3'',4''}$=10 Hz, H-3''), 4.83 (t, 1H, $J_{3'',4''}$= $J_{4'',5''}$=10 Hz, H-4''), 3.96 (qd, 1H, $J_{5'',6''}$=6 Hz, H-5''), 2.42 (dd, 1H, $J_{2ax'',2eq''}$=13 Hz, H-2eq''), 2.06 (s, 3H, -CH_3, OAc), 2.05 (s, 3H, -CH_3, OAc), 1.92 (br td, 1H, H-2ax''), 1.14 (d, 3H, H-6''). **^{13}C NMR** ($CDCl_3$) δ 171.3, 170.8 (C=O, OAc), 157.6 (C-3), 157.1 (C-5), 155.8 (C-4'), 140.1 (C-1), 129.6 (C-1'), 129.1 (C-8), 128.1 (C-2' and C-6'), 125.9 (C-7), 115.6 (C-3' and C-5'), 107.3 (C-6), 106.6 (C-2), 102.6 (C-4), 95.0 (C-1''), 74.7 (C-4''), 69.2 (C-3''), 66.6 (C-5''), 35.2 (C-2''), 21.1, 20.9 (CH_3, OAc), 18.2 (C-6''). Calcd. [$C_{24}H_{27}O_8$] 443.1700; Found 443.1695 (error 1.2 ppm).

4'-*O*-(3'',4''-di-*O*-acetyl-2,6-dideoxy-α-L-*arabino*-hexopyranosyl) resveratrol (9). Reaction of glycal **3** with resveratrol afforded compound **8**, isolated in 8% yield (0.071 g), as a yellowish oil. LC-MS data (high pH): RT: 0.99, [M+H]=443.00 m/z, [M+Na]=465.00 m/z, [M-H]=441.00 m/z. R_f ($CHCl_3$/EtOH 95:5)=0.31. **^{1}H NMR** ($CDCl_3$) δ 7.37 (d, 2H, $J_{2',3'}$= $J_{5',6'}$=9 Hz, H-2' and H-6'), 7.01 (d, 2H, H-3' and H-5'), 6.94 (d, 1H, $J_{7,8}$=16 Hz, H-8), 6.79 (d, 1H, H-7), 6.54 (d, 2H, $J_{2,6}$= 2Hz, H-2 and H-6), 6.28 (br t, 1H, $J_{4,6}$= $J_{2,4}$= 2Hz, H-4), 5.59 (d, 1H, $J_{1'',2ax''}$=2 Hz, H-1''), 5.47 (ddd, 1H, $J_{2eq'',3''}$=5 Hz, $J_{3'',4''}$=10 Hz, H-3''), 4.83 (t, 1H, $J_{3'',4''}$= $J_{4'',5''}$=10 Hz, H-4''), 3.94 (qd, 1H, $J_{5'',6''}$=6 Hz, H-5''), 2.42 (dd, 1H, $J_{2ax'',2eq''}$=13 Hz, H-2eq''), 2.06 (s, 3H, -CH_3, OAc), 2.05 (s, 3H, -CH_3, OAc), 1.92 (br td, 1H, $J_{2ax'',3}$=3 Hz, H-2ax''), 1.14 (d, 3H, H-6''). **^{13}C NMR** ($CDCl_3$) δ 171.3, 170.8 (C=O, OAc), 158.3 (C-3 and C-5), 155.7 (C-4'), 139.5 (C-1), 131.9 (C-1'), 127.4, 127.3 (C-7 and C-8), 127.2(7) (C-2' and C-6'), 116.5 (C-3' and C-5'), 104.6 (C-2 and C-6), 101.6 (C-4), 95.0

(C-1"), 74.7 (C-4"), 69.2 (C-3"), 66.6 (C-5"), 35.2 (C-2"), 21.1, 20.9 (CH_3, OAc), 18.2 (C-6"). **HRMS:** Calcd. [$C_{24}H_{27}O_8$] 443.1700; Found 443.1695 (error 1.2 ppm).

Deacetylation procedure: The acetyl protected glycosides (**4**, **5**, **8** or **9**) was dissolved in MeOH (50mg/mL) and a solution of NaOMe in MeOH (5% w/w) was added to a final 1% NaOMe in the reaction. The solution was stirred at room temperature for 1.5 h. Neutralization with Amberlite IR120, filtration and evaporation afforded the crude final compounds in quantitative yield, with chromatographic purity from 72-92%. Purer fractions (>98 %CP) were obtained by purification either with flash chromatography or with preparative HPLC, using an elution method equivalent to the low pH method described above.

3-*O*-(2-deoxy-α-D-*arabino*-hexopyranosyl)resveratrol (6). Deacetylation of compound **4** (0.200 g, 0.4 mmol) afforded compound **6** in quantitative yield, with 92 % CP (0.158 g). LC-MS data (low pH): RT: 0.69, [M+Na]=397.00 m/z, [M-H]=373.00 m/z. $[\alpha]_D^{20}$= +148 (*c*0.5, MeOH); **^{1}H NMR** (MeOD) δ 7.35 (d, 2H, $J_{2',3'}$= $J_{5',6'}$=8 Hz, H-2', H-6'), 6.99 (d, 1H, $J_{7,8}$=16 Hz, H-8), 6.84 (d, 1H, H-7), 6.79-6.75 (m, 3H, H-3', H-5', H-2), 6.61 (br t, 1H, $J_{4,6}$= $J_{2,6}$= 2Hz, H-6), 6.44 (br t, 1H, $J_{2,4}$= $J_{4,6}$= 2Hz, H-4), 5.64 (d, 1H, $J_{1",2ax"}$=3 Hz, H-1"), 4.04 (ddd, 1H, $J_{2eq",3"}$=5 Hz, $J_{2ax",3"}$=13 Hz, $J_{3",4"}$=10 Hz, H-3"), 3.75 (br d, 2H, $J_{5",6"}$=4 Hz, H-6"), 3.63 (td, 1H, $J_{4",5"}$=10 Hz, H-5"), 3.41 (t, 1H, H-4"), 2.26 (dd, 1H, $J_{2ax",2eq"}$=13 Hz, $J_{2eq",3"}$=5 Hz, H-2eq"), 1.78 (td, 1H, $J_{2ax",3"}$= $J_{2ax",2eq"}$=13 Hz, H-2ax"). **^{13}C NMR** (MeOD) δ 159.5 (C-3 and C-5), 158.4 (C-4'), 140.9 (C-1), 130.3 (C-1'), 129.8 (C-8), 128.9 (C-2' and C-6'), 126.7 (C-7), 116.5 (C-3' and C-5'), 107.9 (C-6), 107.1 (C-2), 104.1 (C-4), 97.5 (C-1"), 74.7 (C-5"), 72.9 (C-4"), 69.8 (C-3"), 62.6 (C-6"), 38.9 (C-2"). **HRMS:** Calcd. [$C_{20}H_{22}NaO_7$] 497.1258; Found 497.1258 (error 3.2 ppm).

4'-*O*-(2-deoxy-α-D-*arabino*-hexopyranosyl)resveratrol (7). Deacetylation of compound **5** (0.031 g, 0.06 mmol) afforded compound **7** in quantitative yield, with 72 % CP (0.026 mg). Further purification by flash chromatography eluted with $CHCl_3 \rightarrow CHCl_3$/EtOH 85:15 afforded the title compound with 100 %CP as a colourless oil. LC-MS data (low pH): RT: 0.66, [M+H]=375.00 m/z, [M+Na]=397.00 m/z, [M-H]=373.00 m/z**;** $[\alpha]_D^{20}$= +123 (*c*0.9, MeOH); **^{1}H NMR** (MeOD) δ 7.43 (d, 2H, $J_{2',3'}$= $J_{5',6'}$=8 Hz, H-2' and H-6'), 7.08 (d, 2H, H-3' and H-5'), 6.97 (d, 1H, $J_{7,8}$=16 Hz, H-8), 6.86 (d, 1H, H-7), 6.43, 6.42 (each singlet, 2H, H-2 and H-6), 6.17 (br s, 1H, H-4), 5.67 (d, 1H, $J_{1'',2ax''}$=3 Hz, H-1''), 4.04 (ddd, 1H, $J_{2eq'',3''}$=5 Hz, $J_{2ax'',3''}$=13 Hz, $J_{3'',4''}$=10 Hz, H-3''), 3.73 (br d, 2H, $J_{5'',6''}$=4 Hz, H-6a'' and H-6b''), 3.61 (td, 1H, $J_{4'',5''}$=10 Hz, H-5''), 3.39 (t, 1H, H-4''), 2.28 (dd, 1H, $J_{2ax'',2eq''}$=13 Hz, $J_{2eq'',3''}$=5 Hz, H-2eq''), 1.79 (td, 1H, $J_{2ax'',3''} \approx J_{2ax'',2eq''} \approx$13 Hz, H-2ax''). **^{13}C NMR** (MeOD) δ δ 160.5 (C-3 and C-5), 157.7 (C-4'), 140.8 (C-1), 132.9 (C-1'), 128.7 (C-8), 128.6 (C-7), 128.5 (C-2' and C-6'), 117.9 (C-3' and C-5'), 105.9 (C-2 and C-6), 103.5 (C-4), 97.6 (C-1''), 74.8 (C-5''), 72.9 (C-4''), 69.7 (C-3''), 62.5 (C-6''), 38.9 (C-2''). **HRMS:** Calcd. [$C_{20}H_{22}NaO_7$] 497.1258; Found 497.1239 (error 4.6 ppm).

3-*O*-(2,6-dideoxy-α-L-*arabino*-hexopyranosyl)resveratrol (10). Deacetylation of compound **8** (0.190 g, 0.44 mmol) afforded compound **10** in quantitative yield, with 97 % CP (0.158 g). Further purification by preparative HPLC (low pH method) afforded the title compound with 100 % CP as a colourless oil. LC-MS data (low pH): RT: 0.78, [M+H]=359.00 m/z, [M+Na]=381.00 m/z, [M-H]=357.00 m/z**;** $[\alpha]_D^{20}$= -52 (*c*0.6, MeOH); **^{1}H NMR** (MeOH) δ 7.34 (d, 2H, $J_{2',3'}$= $J_{5',6'}$=8 Hz, H-2' and H-6'), 6.98 (d, 1H, $J_{7,8}$=16 Hz, H-8), 6.81 (d, 1H, H-7), 6.75 (d, 2H, H-3' and H-5'), 6.67 (br s, 1H, H-2), 6.59 (br s, 1H, H-6), 6.40 (br s, 1H, H-4), 5.59 (d, 1H, $J_{1'',2ax''}$=3 Hz, H-1''), 3.97 (ddd, 1H, $J_{3'',4''}$=9 Hz, H-3''), 3.70 (qd, 1H, $J_{4'',5''}$=9 Hz, $J_{5'',6''}$=6 Hz, H-5''), 3.04 (t, 1H, H-4''), 2.27 (dd, 1H, $J_{2ax'',2eq''}$=13 Hz, $J_{2eq'',3''}$=5 Hz, H-2eq''), 1.77 (td, 1H, $J_{2ax'',3''}$= $J_{2ax'',2eq''}$=13 Hz, H-2ax''), 1.23 (d, 3H, H-6''). **^{13}C NMR** δ 159.7 (C-3 and C-5), 157.7 (C-4'), 141.4 (C-1), 129.8 (C-1'), 129.1 (C-

8), 128.8 (C-2' and C-6'), 128.1 (C-7), 116.9 (C-3' and C-5'), 106.6 (C-2), 104.0 (C-4), 97.1 (C-1"), 78.8 (C-4"), 70.1 (C-5"), 69.6 (C-3"), 39.2 (C-2"), 18.2 (C-6"). **HRMS**: Calcd. [$C_{20}H_{22}NaO_6$] 381.1309; Found 381.1300 (error 2.3 ppm).

4'-*O*-(2,6-dideoxy-α-L-*arabino*-hexopyranosyl) resveratrol (11). Deacetylation of compound **9** (0.071 g, 0.016 mmol) afforded compound **11** in quantitative yield, with 75 %CP (0.058 g). Further purification by preparative HPLC (low pH method) afforded the title compound with 100 %CP as a yellowish oil. LC-MS data (low pH): RT: 0.76, [M+H]=359.00 m/z, [M+Na]=381.00 m/z, [M-H]=357.00 m/z; $[\alpha]_D^{20}$= -93 (*c*0.9, MeOH); **^{1}H NMR** (MeOD) δ 7.44 (d, 2H, $J_{2',3'}$= $J_{5',6'}$=9 Hz, H-2' and H-6'), 7.04 (d, 2H, H-3' and H-5'), 6.99 (d, 1H, $J_{7,8}$=16 Hz, H-8), 6.87 (d, 1H, H-7), 6.47, 6.46 (each singlet, 2H, H-2, H-6), 6.17 (t, 1H, $J_{2,4}$=$J_{4,6}$=2 Hz, H-4), 5.52 (d, 1H, $J_{1",2ax"}$=2 Hz, H-1"), 3.98 (ddd, 1H, $J_{2eq",3"}$=5 Hz, $J_{3",4"}$=9 Hz, H-3"), 3.66 (qd, 1H, $J_{4",5"}$=9 Hz, $J_{5",6"}$=6 Hz, H-5"), 3.04 (t, 1H, H-4"), 2.27 (ddd, 1H, $J_{2ax",2eq"}$=13 Hz, $J_{1",2eq"}$=0.7 Hz, H-2eq"), 1.79 (br td, 1H, $J_{2ax",3}$=3 Hz, H-2ax"), 1.21 (d, 3H, H-6"). **^{13}C NMR** (MeOH) δ 159.7 (C-3 and C-5), 157.7 (C-4'), 141.0 (C-1), 132.7 (C-1'), 128.9 (C-8), 128.6 (C-2' and C-6'), 128.3 (C-7), 117.7 (C-3' and C-5'), 105.9 (C-4), 97.1 (C-1"), 78.8 (C-4"), 70.1 (C-5"), 69.5 (C-3"), 39.1 (C-2"), 18.2 (C-6"). **HRMS**: Calcd. [$C_{20}H_{23}O_6$] 359.1489; Found 359.1492 (error -0.9 ppm).

3,4-Di-O-*tert*-butyldimethylsilyl caffeic acid (13). 3-(3,4-Di-*tert*-butyldimethylsilyloxyphenyl)prop-2-enoic acid (13). In a round bottom flask equipped with a magnetic stirrer, TBDMSCl (3.011g, 0.020 mol, 3.6 equiv.) and imidazole (2.834g, 0.042 mol, 7.5 equiv) were added to a solution of caffeic acid (1g, 5.55 mmol) in DMF (5 mL), and the reaction mixture was stirred at room temperature for 4 h. The reaction was quenched by adding purified water (50 mL), and extracted with DCM (4x25 mL). The combined organic phases were dried with anhydrous $MgSO_4$, filtered and evaporated under reduced pressure. The residue was purified

by column chromatography, eluted with hex/EtOAc 5:1 → 3:1, affording the title compound as a colorless oil in 71% yield (1.62g). **Rf**=0.42 (Hex/EtOAc 2:1); m.p. = 154.3-155.5°C; **^{1}H NMR (CDCl$_3$)** δ 7.68 (d, 1H, $J_{7,8}$=16 Hz, H-7), 7.06-7.03 (m, 2H, H-2, H-6), 6.84 (br d, $J_{5,6}$=8 Hz, H-5), 6.25 (d, 1H, H-8), 1.00, 0.99 (two singlets, each 9H, *tert*-butyl), 0.22, 0.22 (two singlets, each 6H, -CH_3). **^{13}C NMR (CDCl$_3$)** δ 171.2 (C-9), 149.9 (C-7), 147.3, 147.0 (C-3, C-4), 127.6 (C-1), 122.7 (C-6), 121.2 (C-5), 120.6 (C-2), 114.6 (C-8), 25.9(0), 25.8(8) (-CH_3, *tert*-butyl), 18.5, 18.4 (Cq, *tert*-butyl) , -4.0, -4.1 (-CH_3,). **HRMS:** Calcd. [$C_{21}H_{36}O_4Si_2$] 409.2225; Found 409.2217 (error 1.9 ppm).

2-Hydroxyethyl 3-(3,4-di-*tert*-butyldimethylsilyloxy)prop-2-enoate (14). In a round bottom flask equipped with a magnetic stirrer, to a solution of compound **13** (0.500g, 1.22 mmol) in DCM (2 mL). DMF (2 mL), DMAP (7.5mg, 0.061 mmol) and ethyleneglycol (0.3 mL, 5.36 mmol, 4.4 equiv) were added and the solution was cooled to 0 ºC. *N*,*N*-dicyclohexylcarbodiimide (DCC, 0.278 g, 1.34 mmol, 1.1 equiv) was added in one portion, stirred for 5 min at 0 ºC and 20 h at room temperature. Formed urea was filtered off, and the filtrate was evaporated under reduced pressure. The resulting residue was purified by column chromatography, eluted with hex/EtOAc 6:1, affording the title compound as a colorless oil in 54% yield (0.300 g). Rf=0.83 (Hex/EtOAc 4:1); **^{1}H NMR (CDCl$_3$)** δ 7.60 (d, 1H, $J_{7,8}$=16 Hz, H-7), 7.02-6.98 (m, 2H, H-2, H-6), 6.80 (br d, $J_{5,6}$=8 Hz, H-5), 6.26 (d, 1H, H-8), 4.35-4.31 (m, 2H, H-1'), 3.91-3.87 (m, 2H, H-2'), 0.99, 0.99 (two singlets, each 9H, *tert*-butyl), 0.20, 0.21 (two singlets, each 6H, -CH_3). **^{13}C NMR (CDCl$_3$)** δ 167.7 (C-9), 149.6, 147.2 (C-3 and C-4), 145.5 (C-7), 127.8 (C-1), 122.5 (C-2), 121.2 (C-5), 120.4 (C-6), 115.1 (C-8), 66.1 (C-1'), 61.3 (C-2'), 25.8, 25.8 (-CH_3, *tert*-butyl), 18.4, 18.3 (Cq, *tert*-butyl) , -4.1, -4.2 (-CH_3,). **HRMS:** Calcd. [$C_{23}H_{41}O_5Si_2$] 453.2487; Found 453.2479 (error 1.8 ppm).

1,5-anhydro-3,4-di-*O*-*tert*-butyldimetylsilyl-2,6-dideoxy-L-*arabino*-hex-1-enitol (15). To a solution of 3,4-di-*O*-acetyl-1,5-anhydro-2,6-dideoxy-D-*arabino*-hex-1-enitol (1.0g, 4.9 mmol) in MeOH (10 mL), NaOMe (0.050g, 0.92 mmol, 0.2 equiv) was added under stirring. After 1 h at room temperature, methanol was evaporated under reduced pressure, and the residue was re-suspended in DMF (40 mL). The solution was cooled to 0 ºC, and imidazole (2.54g, 37.3 mmol, 8 equiv) and *tert*-butyldimetylsilyl chloride (6.6g, 43.8 mmol, 9 equiv.) were added. After 5 min at 0 ºC, the reaction was stirred at room temperature for 42 h. The reaction mixture was poured into purified water (150 mL), and extracted with EtOAc (3x150 mL). The organic layers were combined and washed with a saturated solution of $NaHCO_3$ (150 mL) and water (150 mL), and then dried with anhydrous $MgSO_4$, filtered and evaporated. The residue was purified by column chromatography eluted with Hex →Hex/EtOAc 95:5, affording the title compound in 71% yield (0.329 g) as a colorless liquid. R_f (Hex/EtOAc 9:1)=0.87; $[\alpha]_D^{20}$= +146 (*c*1, CH_2Cl_2). **^{1}H NMR (CDCl$_3$)** δ 6.29 (d, 1H, $J_{1,2}$=6 Hz, 1H), 4.70-4.65 (m, 1 H, H-2), 4.08-4.12 (m, 1H, H-3), 3.95 (br q, 1H, $J_{5,6}$=6 Hz, H-5), 3.58 (br t, 1H, $J_{4,5}$=6 Hz H-4), 1.34 (d, 3H, H-6), 0.92 (br s, 18H, *tert*-butyl), 0.14 (br s, 3H, -Me), 0.12 (br s, 9H, -Me). **^{13}C NMR (CDCl$_3$)** δ 143.4 (C-1), 102.9 (C-2), 75.2 (C-3), 74.7 (C-4), 69.4 (C-5), 26.0, 25.9 (-CH_3, *tert*-butyl), 18.1, 18.0, 17.2 (Cq, *tert*-butyl), -3.6, -3.9, -4.1, -4.2 (brd s, 9H, -CH_3). **HRMS:** Calcd. [$C_{18}H_{30}NaO_3Si_2$] 381.2252; Found 381.2253 (error -0.3 ppm).

(3,4-Di-*O*-*tert*-butyldimethylsilyl-2,6-dideoxy-α/β-L-*arabino*-hexopyranosyloxy)ethyl *(E)*-3-*(*3,4-di-*tert*-butyldimetylsilyloxyphenyl)prop-2-enoate (16a,b). A solution of glycal **15** (0.149g, 0.42 mmol) in DCM (0.5 mL) was added to a solution of **14** (0.255 g, 0.56 mmol, 1.3 equiv.) in THF (2 mL). Then, TPHB (0.0141g, 0.041 mmol, 0.1 equiv) was added and the solution was heated to 35 ºC for 5 h. The reaction mixture was neutralized with a saturated solution of $NaHCO_3$ (2x40 mL), and extracted with DCM (2x40 mL). The organic layers were combined, dried with

anhydrous $MgSO_4$, filtered and evaporated under reduced pressure. The resulting residue was purified by column chromatography eluted with hex→ hex/EtOAc 20:1, affording the title compound as an anomeric mixture (α/β 2.3:1) in 45% yield (0.150g) as a colourless oil. R_f (hex/EtOAc 30:1)=0.3; $[\alpha]_D^{20}$= -21 (*c*1, MeOH); **^{1}H NMR** ($CDCl_3$) δ 7.58 (d, 1H, $J_{7",8"}$=16 Hz, H-7β), 7.57 (d, 1H, $J_{7,8}$=16 Hz, H-7α), 7.03-6.98 (m, 4H, H-2α/β and H-6α/β), 6.81 (d, 1H, $J_{5,6}$=9 Hz, H-5α/β), 6.28 (d, 1H, H-8β), 6.25 (d, 1H, H-8α), 4.83 (d, 1H, $J_{1",2ax"}$=2 Hz H-1"α), 4.50 (dd, 1H, $J_{1",2ax"}$=9 Hz, $J_{1",2eq"}$=2 Hz, H-1"β), 4.44-4.27 (m, 4H, H-1'α/β) 4.08 (ddd, 1H, H-2a'β), 3.92 (ddd, 1H, H-3"α), 3.84 (ddd, 1H, H-2a'α), 3.77 (ddd, 1H, H-2b'β), 3.71-3.59 (m, 3H, H-2b'α, H-5"α and H-3"β), 3.23 (qd,1H, $J_{5",6"}$=6 Hz, $J_{4",5"}$=9 Hz, H-5"β), 3.14 (t, 2H, $J_{3",4"}$=$J_{4",5"}$=9 Hz, H-4"α/β), 2.15 (ddd, 1H, $J_{2ax",3"}$=5 Hz, $J_{2ax",2eq"}$=13 Hz, H-2ax"β), 2.08 (ddd, 1H, $J_{2ax",3"}$=5 Hz, $J_{2ax",2eq"}$=13 Hz, H-2ax"α), 1.69-1.60 (m, 2H, H-2eq" α/β), 1.27 (d, 3H, $J_{5",6"}$=6 Hz, H-6"β), 1.22 (d, 3H, $J_{5",6"}$=6 Hz, H-6"α), 0.99, 0.99, 0.89, 0.87 (four singlets, each 18H, *tert*-butyl, OTBDMS, α/β), 0.22, 0.21, 0.09, 0.07 (four singlets, each 12H, Me, OTBDMS, α/β) .**^{13}C NMR** ($CDCl_3$) δ 169.1 (C-9), 149.6 (C-7), 147.1, 146.8 (C-3 and C-4), 127.7 (C-1), 123.0 (C-6), 116.5 (C-5), 115.1 (C-8), 114.9 (C-2), 101.1 (C-1"α), 98.7 (C-1"β), 78.9 (C-4"α), 78.5 (C-4"β), 73.4 (C-5"β), 72.1 (C-3"β), 69.6 (C-5"α), 69.3 (C-3"α), 68.1 (C-1'α), 66.3 (C-1'β), 64.6 (C-2'α), 61.5 (C-2'β), 40.5 (C-2"β), 39.1 (C-2"α), 18.2 (C-6" α and β). **HRMS:** Calcd. [$C_{41}H_{79}O_8Si_4$] 811.4847; Found 811.4816 (error -3.8 ppm).

(2,6-Dideoxy- α/β-L-*arabino*-hexopyranosyloxy)ethyl (*E*)-3-(3,4-dihydroxyphenyl)prop-2-enoate (17a,b). A 1M solution of TBAF in THF (2.6 mL, 2.6 mmol, 1.6 equiv.) was added to a solution of compound **16** (0.130g, 0.160 mmol) in THF (2 mL). After 14 h at room temperature, the solution was neutralized with saturated ammonium chloride aqueous solution (20 mL), and extracted with EtOAc (4x25 mL). The organic layers were combined, dried with anhydrous $MgSO_4$, filtered and evaporated to dryness. This residue was purified by column chromatography

eluted with EtOAc/CAN 9:1, to give the title compound (anomeric mix α/β 3.8:1) as colourless oil in 52% yield (0.030 g). R_f (EtOAc/ACN 9:1)=0.3; $[\alpha]_D^{20}$= -21 (*c*1, MeOH); **^{1}H NMR** (MeOH) δ 7.56 (d, 1H, $J_{7,8}$=16 Hz, H-7αβ), 7.05 (brd d, 1H, $J_{2,3}$=2Hz, H-2αβ), 6.96 (dd, 1H, $J_{5,6}$=8Hz, H-5αβ), 6.78 (d, 1H, H-6αβ), 6.28 (d, 1H, H-8αβ), 4.88 (d, 1H, H-1"α, under MeOH signal), 4.59 (dd, 1H, $J_{1",2ax"}$=10 Hz, $J_{1",2eq"}$=2 Hz, H-1"β), 4.32 (t, 2H, $J_{1',2'}$=5 Hz, H-1'αβ), 4.02 (m, 1H, H-2'aβ), 3.90-3.75 (m, 3H, H-2a'α, H-2b'β, H-3"α), 3.70-3.62 (m, 2H, H-2b'β, H-5"α), 3.51 (ddd, 1H, H-3"β), 3.25 (qd,1H, $J_{5",6"}$=6 Hz, $J_{4",5"}$=9 Hz, H-5"β), 2.95 (t, 1H, $J_{3",4"}$=$J_{4",5"}$=9 Hz, H-4"α), 2.91 (t, 1H, $J_{3",4"}$=$J_{4",5"}$=9 Hz, H-4"β), 2.18-2.11 (m, 1H, H-2ax"β), 2.08 (ddd, 1H, $J_{2ax",3"}$=5 Hz, $J_{2ax",2eq"}$=12 Hz, $J_{1",2ax"}$=0.7 Hz, H-2ax"α), 1.62 (ddd, 1H, $J_{2ax",3"}$=3 Hz, $J_{1",2eq"}$=1 Hz, H-2eq"α), 1.50 (qd, 1H, $J_{2ax",2eq"}$=12 Hz, H-2eq"β), 1.29 (d, 3H, $J_{5",6"}$=6 Hz, H-6"β), 1.24 (d, 3H, $J_{5",6"}$=6 Hz, H-6"α). **^{13}H NMR** (MeOH) δ 169.1 (C-9), 149.6, 147.1 (C-3, C-4), 146.8 (C-7), 127.7 (C-1), 123.0 (C-5), 116.5 (C-6), 115.1, 114.9 (C-8 and C-2), 101.1 (C-1"β), 98.7 (C-1"α), 78.9 (C-4"α), 78.5 (C-4"β), 73.4 (C-5"β), 72.1 (C-3"β), 69.6 (C-5"α), 69.3 (C-3"α), 68.1 (C-1'α), 66.3 (C-1'β), 64.6 (C-2'β), 61.5 (C-2'α), 40.5 (C-2"β), 39.1 (C-2"α), 18.2 (C-6" α/β). **HRMS:** Calcd. [$C_{17}H_{22}NaO_8$] 377.1207; Found 377.1225 (error -4.7 ppm).

Log* P *determination. The *in-silico* prediction tool ALOGPS[25-26] was used to estimate the octanol-water partition coefficients (log *P*) of the compounds. Depending on these values, the compounds were classified into three categories: hydrophilic compounds (log *P* below zero), moderately lipophilic compounds (log *P* between zero and one) and lipophilic compounds (log *P* above one). For each category, two different ratios (volume of octan-1-ol to volume of buffer) were defined as experimental parameters (Table 3).

Table 3. Compound classification based on estimated log *P* values.

Compound type	log *P*	Ratios (octan1-ol: buffer)
hydrophilic	< 0	30:140, 40:130
moderately lipophilic	0 - 1	70:110, 110:70
lipophilic	> 1	3:180, 4:180

Equal amounts of phosphate buffer (0.1 M, pH 7.4) and octan-1-ol were mixed and shaken vigorously for 5 min to saturate the phases. The mixture was left until separation of the two phases, and the buffer was retrieved. Stock solutions of the test compounds were diluted with buffer to a concentration of 1 μM. For each compound, three determinations per octan-1-ol:buffer ratio were performed in different wells of a 96-well plate. The respective volumes of buffer containing analyte (1 μM) were pipetted to the wells and covered by saturated octan-1-ol according to the chosen volume ratio. The plate was sealed with aluminum foil, shaken (1350 rpm, 25 °C, 2 h) on a Heidolph Titramax 1000 plate-shaker (Heidolph Instruments GmbH & Co. KG, Schwabach, Germany) and centrifuged (2000 rpm, 25 °C, 5 min, 5804 R Eppendorf centrifuge, Hamburg, Germany). The aqueous phase was transferred to a 96-well plate for analysis by liquid chromatography-mass spectrometry (LCMS, see below).

The log *P* coefficients were calculated from the octan-1-ol:buffer ratio (o:b), the initial concentration of the analyte in buffer (1 μM), and the concentration of the analyte in buffer (*cB*) with Equation 1:

$$\log P = \log\left(\frac{1\,\mu M - c_B}{c_B} \times \frac{1}{o{:}b}\right) \quad \text{(eq. 1)}$$

The average of the three log *P* values per octan-1-ol:buffer ratio was calculated. If the two means obtained for a compound did not differ by more than 0.1 units, the results were accepted.

Parallel artificial membrane permeability assay (PAMPA). Effective permeability (log *P*e) was determined in a 96-well format with PAMPA.[24] For each compound, measurements were performed at pH 7.4 in quadruplicate. Four wells of a deep well plate were filled with 650 μL of PRISMA HT universal buffer, adjusted to pH 7.4 by adding the requested amount of NaOH (0.5 M). Samples (150 μL) were withdrawn from each well to determine the blank spectra by UV/Vis-spectroscopy (190 to 500 nm, SpectraMax 190, Molecular Devices, Silicon Valley, CA, USA). Then, analyte dissolved in DMSO (10 mM) was added to the remaining buffer to yield 50 μM solutions. To exclude precipitation, the optical density (OD) was measured at 650 nm, and solutions exceeding OD 0.01 were filtrated. Afterwards, samples (150 μL) were withdrawn to determine the reference spectra. Further 200 μL were transferred to each well of the donor plate of the PAMPA sandwich (pIon, P/N 110 163). The filter membranes at the bottom of the acceptor plate were infused with 5 μL of GIT-0 Lipid Solution and 200 μL of Acceptor Sink Buffer were filled into each acceptor well. The sandwich was assembled, placed in the GutBoxTM, and left undisturbed for 16 h. Then, it was disassembled and samples (150 μL) were transferred from each donor and acceptor well to UV-plates for determination of the UV/Vis spectra. Effective permeability (log *P*e) was calculated from the compound flux deduced from the spectra, the filter area, and the initial sample concentration in the donor well with the aid of the PAMPA Explorer Software (pIon, version 3.5).

LC-MS measurements. Analyses were performed using a 1100/1200 Series HPLC System coupled to a 6410 Triple Quadrupole mass detector (Agilent Technologies, Inc., Santa Clara, CA, USA) equipped with electrospray ionization. The system was controlled with the Agilent MassHunter Workstation Data Acquisition software (version B.01.04). The column used was an AtlantisR T3 C18 column (2.1 x 50 mm) with a 3 μm-particle size (Waters Corp., Milford, MA, USA). The mobile phase consisted of eluent A: 10 mM ammonium acetate, pH 5.0 in 95:5,

H_2O:MeCN; and eluent B: MeCN containing 0.1% formic acid. The flow rate was maintained at 0.6 mL/min. The gradient was ramped from 95% A/5% B to 5% A/95% B over 1 min, and then hold at 5% A/95% B for 0.1 min. The system was then brought back to 95% A/5% B, resulting in a total duration of 4 min. MS parameters such as fragmentor voltage, collision energy, polarity were optimized individually for each drug, and the molecular ion was followed for each compound in the multiple reaction monitoring mode. The concentrations of the analytes were quantified by the Agilent Mass Hunter Quantitative Analysis software (version B.01.04).

Neuroprotective assays in human neuroblastoma (SHSY-5Y) cells. SHSY-5Y cells were grown in Dulbecco's Modified Eagle Medium (DMEM, Gibco, Life Technologies) containing 10% fetal bovine serum (FBS, Biochrom GmbH) and 1% Penicillin-Streptomycin (Gibco, Life Technologies) at 37 ºC, 5% CO_2. For the neuroprotective activity assay, undifferentiated SGSY-5Y cells were plated onto 96-well flat-bottomed microtiter plates at a density of 1 x 10^4 cells/well in DMEM supplemented with 2% FBS and preincubated for 24 h at 37 ºC, 5% CO_2. Compounds (stored as 10 mM solutions in DMSO at -20 ºC) were then added to achieve a final concentration of 50 μM and, after 30 min, cells were incubated in the presence or absence of 100 μM of H_2O_2 (Sigma-Aldrich, dissolved to 10 mM in 0.9% NaCl aqueous solution immediately prior to the assay) overnight at 37 ºC, 5% CO_2. The final DMSO percentage was 0.5%. In the following morning, 20 μL of 3-(4,5-dimethylthiazol-2-yl)-2,5-diphenyltetrazolium bromide (MTT, Sigma-Aldrich) solution in PBS (Gibco, Life Technologies) (5 mg/mL) were added to each well and the plates were further incubated for 4 h at 37 ºC, followed by the addition of DMSO (200 μL) to each well in order to dissolve the resulting insoluble dye crystals. After 2 h incubating at 37 ºC, the optical density (OD) at 540 nm (with a 620 nm reference filter) was measured in an Amersham Biosciences Biotrak II Plate Reader. The percentage of MTT reduction was determined according to eq. (1). All experiments were performed in triplicate and results are presented as means ±

standard error. Differences between experimental conditions were compared for statistical significance by one-way ANOVA followed by a Tukey's post-test – an analysis carried out using GraphPad Prism Software (LA Jolla, CA). Differences were considered significant when $P < 0.05$. In order to exclude direct MTT reduction, compounds were also tested in the absence of cells, using the same experimental conditions above described.

Eq. (1) $$MTT\ Reduction\ (\%\ of\ Control) = \left[\frac{OD_{sample} - OD_{medium}}{OD_{cell\ control} - OD_{medium}}\right] x\ 100$$

REFERENCES

[1] S. D. Rege; T. Geetha; G. D. Griffin; T. L. Broderick; J. R. Babu, Neuroprotective effects of resveratrol in Alzheimer disease pathology. *Frontiers in Aging Neuroscience* **2014,** *6*, 218.

[2] C. Riviere; T. Richard; L. Quentin; S. Krisa; J. M. Merillon; J. P. Monti, Inhibitory activity of stilbenes on Alzheimer's beta-amyloid fibrils in vitro. *Bioorganic & Medicinal Chemistry* **2007,** *15* (2), 1160-7.

[3] T. Walle, Bioavailability of resveratrol. *Annals of the New York Academy of Sciences* **2011,** *1215*, 9-15.

[4] E. Wenzel; V. Somoza, Metabolism and bioavailability of trans-resveratrol. *Molecular Nutrition & Food Research* **2005,** *49* (5), 472-81.

[5] J. B. Baell, Feeling Nature's PAINS: Natural Products, Natural Product Drugs, and Pan Assay Interference Compounds (PAINS). *Journal of Natural Products* **2016,** *79* (3), 616-28.

[6] C. Dias; A. M. Matos; A. P. Rauter, Chemical Approaches Towards Neurodegenerative Disease Prevention: The Role of Coupling Sugars to Phenolic Biomolecular Entities. In *Coupling and Decoupling of Diverse Molecular Units in Glycosciences* Z. J. Witczak; R. Bielski, Eds. Springer International Publishing AG: Cham, Switzerland, 2017; Vol. In press pp 167-194.

[7] P. Torres; A. Poveda; J. Jimenez-Barbero; J. L. Parra; F. Comelles; A. O. Ballesteros; F. J. Plou, Enzymatic Synthesis of α-Glucosides of Resveratrol with Surfactant Activity. *Advanced Synthesis & Catalysis* **2011,** *353* (7), 1077-1086.

[8] F. Marcelo; C. Dias; A. Martins; P. J. Madeira; T. Jorge; M. H. Florêncio; F. J. Cañada; E. J. Cabrita; J. Jiménez-Barbero; A. P. Rauter, Molecular Recognition of Rosmarinic Acid from Salvia sclareoides Extracts by Acetylcholinesterase: A New Binding Site Detected by NMR Spectroscopy. *Chemistry – A European Journal* **2013,** *19* (21), 6641-6649.

[9] T. Alkam; A. Nitta; H. Mizoguchi; A. Itoh; T. Nabeshima, A natural scavenger of peroxynitrites, rosmarinic acid, protects against impairment of memory induced by Abeta(25-35). *Behavioural Brain Research* **2007,** *180* (2), 139-45.

[10] C. Airoldi; E. Sironi; C. Dias; F. Marcelo; A. Martins; A. P. Rauter; F. Nicotra; J. Jimenez-Barbero, Natural compounds against Alzheimer's disease: molecular recognition of Abeta1-42 peptide by Salvia sclareoides extract and its major component, rosmarinic acid, as investigated by NMR. *Chemistry, an Asian Journal* **2013,** *8* (3), 596-602.

[11] A. A. Qutub; C. A. Hunt, Glucose transport to the brain: a systems model. *Brain Research Reviews* **2005,** *49* (3), 595-617.

[12] M. Abe; Y. Abe; T. Ohkuri; T. Mishima; A. Monji; S. Kanba; T. Ueda, Mechanism for retardation of amyloid fibril formation by sugars in Vλ6 protein. *Protein Science* **2013,** *22* (4), 467-474.

[13] R. A. Floyd; J. M. Carney, Free radical damage to protein and DNA: mechanisms involved and relevant observations on brain undergoing oxidative stress. *Annals of Neurology* **1992,** *32 Suppl*, S22-7.

[14] J. M. Gutteridge, Hydroxyl radicals, iron, oxidative stress, and neurodegeneration. *Annals of the New York Academy of Sciences* **1994,** *738*, 201-13.

[15] D. C. Malins; N. L. Polissar; S. J. Gunselman, Progression of human breast cancers to the metastatic state is linked to hydroxyl radical-induced DNA damage. *Proceedings of the National Academy of Sciences* **1996,** *93* (6), 2557-2563.

[16] L. Annunziato; S. Amoroso; A. Pannaccione; M. Cataldi; G. Pignataro; A. D'Alessio; R. Sirabella; A. Secondo; L. Sibaud; G. F. Di Renzo, Apoptosis induced in neuronal cells by oxidative stress: role played by caspases and intracellular calcium ions. *Toxicology Letters* **2003,** *139* (2-3), 125-133.

[17] M. G. Dickens; K. J. Franz, A prochelator activated by hydrogen peroxide prevents metal-induced amyloid Beta aggregation. *ChemBioChem* **2010,** *11* (1), 59-62.

[18] M. Yamato; W. Kudo; T. Shiba; K. I. Yamada; T. Watanabe; H. Utsumi, Determination of reactive oxygen species associated with the degeneration of dopaminergic neurons during dopamine metabolism. *Free Radical Research* **2010,** *44* (3), 249-57.

[19] A. Fernandez-Ferreiro; J. Gil-Longo, Vascular pro-oxidant effects related to the autoxidation of dopamine. *Free Radical Research* **2009,** *43* (3), 295-303.

[20] P. G. Arthur; S. C. C. Lim; B. P. Meloni; S. E. Munns; A. Chan; N. W. Knuckey, The protective effect of hypoxic preconditioning on cortical neuronal cultures is associated with increases in the activity of several antioxidant enzymes. *Brain Research* **2004,** *1017* (1-2), 146-154.

[21] S. Konyalioglu; G. Armagan; A. Yalcin; C. Atalayin; T. Dagci, Effects of resveratrol on hydrogen peroxide-induced oxidative stress in embryonic neural stem cells. *Neural Regeneration Research* **2013,** *8* (6), 485-495.

[22] E. H. Kerns; L. Di, Chapter 5 - Lipophilicity. In *Drug-like Properties: Concepts, Structure Design and Methods*, Academic Press: San Diego, 2008; pp 43-47.

[23] Z. Rankovic, CNS Drug Design: Balancing Physicochemical Properties for Optimal Brain Exposure. *Journal of Medicinal Chemistry* **2015,** *58* (6), 2584-2608.

[24] M. Kansy; F. Senner; K. Gubernator, Physicochemical high throughput screening: parallel artificial membrane permeation assay in the description of passive absorption processes. *Journal of Medicinal Chemistry* **1998,** *41* (7), 1007-10.

[25] I. V. Tetko; J. Gasteiger; R. Todeschini; A. Mauri; D. Livingstone; P. Ertl; V. A. Palyulin; E. V. Radchenko; N. S. Zefirov; A. S. Makarenko; V. Y. Tanchuk; V. V. Prokopenko, Virtual computational chemistry laboratory--design and description. *Journal of Computer-Aided Molecular Design* **2005,** *19* (6), 453-63.

[26] VCCLAB - Virtual Computational Chemistry Laboratory. http://www.vcclab.org (accessed 15-02-2017).

Chapter 6

Overview and Concluding remarks

The 2013 Global Risks Report warned about the growing risks associated to antimicrobial resistance and highlighted the two main causes: the misuse of antibiotics in both human and livestock, and the void in the development of new classes of antibiotics since the 1980s. Until today, new classes of anti-infectious agents have not yet been marketed, and resistance to the existing drugs continues to spread relentlessly.

When it comes to infectious diseases, the work herein described aimed at giving a contribution to the search for new antibiotics, with alternative mechanisms of action. The research herein described focused mainly on alkyl glycosides, previously reported by Rauter *et al*. as powerful antimicrobial agents against *Bacillus* species. Because of the amphiphilic properties of the designed dodecyl glycosides, we preview their potential to interact with bacteria cell membrane. What makes targeting cell membrane so appealing is its essentiality, which does not depend on the metabolic state of the cell, while the well-known differences between eukaryotic and prokaryotic cell membrane composition can be a vehicle for selectivity.

In chapter 2, we illustrate the synthesis of 2-deoxy glycosides via reaction of glycals with long-chain alcohols in the presence of triphenylphosphane hydrobromide (TPHB), a stereoselective and easy to perform reaction, that can be applied to the synthesis of structurally diverse bioactive 2-deoxy glycosides, by changing glycal structure. The acid catalyzed addition of an alcohol to an acetylated glycal occurs usually with concomitant Ferrier allylic rearrangement, giving the 2,3-unsaturated derivative as major reaction product. However, when TPHB is used, as first described by Bolitt and co-workers, formation of the 2,3-unsaturated glycosides is minimal.

This method was used to synthesize a new series of alkyl 2-deoxyglycosides and thio analogues, described in chapter 3. The action of the lead compound on the thermotropic behaviour of phosphatidylethanolamine-enriched membranes was investigated, leading to the proposal of the

mechanism for the antimicrobial action for this family of compounds. The lead compound promotes the reorganization of the lipid matrix into a hexagonal phase, which can ultimately be the cause of bacteria cell lysis. This unprecedented mode of action is the first report of glycosides responsible for specific carbohydrate-phospholipid interactions, triggering innovation on membrane-targeting antibiotics against anthrax and other *Bacillus* species, namely *B. cereus*.

Knowing that deoxygenation in the sugar moiety plays an important role tuning the bioactivity of this family of compounds, alkyl 3-deoxy, 4-deoxy and 6-deoxy glycosides were also prepared, aiming at a better insight of the role of deoxygenation pattern for the antimicrobial activity (chapter 4). Dodecyl 2-, 3-, 4-deoxy, and 2,3-, 3,4-, and 4,6-dideoxy glycosides were synthesized in moderate to good yields using new methodologies, and were tested for their antimicrobial activity and cytotoxicity. As it is appanage of membrane-targeting antimicrobial compounds, the structure-activity relationship underlying the antimicrobial results was not clear, as the impact of the deoxygenation position or the number of deoxygenated positions was not linear. Nevertheless, amongst this set of compounds, dodecyl 4,6-dideoxy-α-D-*xylo*-hexopyranoside was the most promising lead for further development, presenting a MIC value below 25 μM for *Bacillus species* and *E. faecalis*, and low toxicity.

A deep literature investigation showed how carbohydrates may play an important role toward neurodegenerative disease prevention (Chapter 1.2 and 1.3). The synthesis of 2-deoxy glycosides embodying natural neuroprotective polyphenols as aglycones was carried out successfully, expecting to improve the bioavailability and neuroprotective activity of such molecular entities. Two resveratrol glycosides were more effective at protecting the neuronal cells from peroxide-induced cytotoxicity than resveratrol itself, and the caffeic acid derivative also showed remarkable neuroprotection activity. The two most promising compounds in terms of neuroprotection were not toxic to neuroblastoma, intestinal or liver cells at all tested concentrations. Coefficient partition measurements demonstrated the moderate lipophilicity of

resveratrol glycosides, which logD values are typical of CNS drug and ideal for BBB penetration. Passive permeation assessed by the PAMPA revealed that 2,6-dideoxy-L-*arabino*-pyranosides were more effective than 2-deoxy-D-*arabino*-pyranosides.

With the work presented in this thesis, the application of dodecyl glycosides for infectious diseases finds itself in a consolidated and ever more promising stage. Meanwhile, the generation of glycosides embodying phenolic structures for neuroprotective purposes, which has been proposed in the original Ph.D project, gained strength by the interaction with Eli Lilly within the D3i4AD project context (Diagnostic and Drug Discovery Initiative for Alzheimer's Disease, FP7-PEOPLE-2013-IAPP), motivating us to pursue this rather exploratory line of investigation. This work clearly demonstrates the uniqueness and versatility of carbohydrates as exceptional scaffolds for medicinal chemistry applications.

ANNEXES

^{1}H and ^{13}C of final products

Annex 1. ^{1}H and ^{13}C of final products described in chapter 2

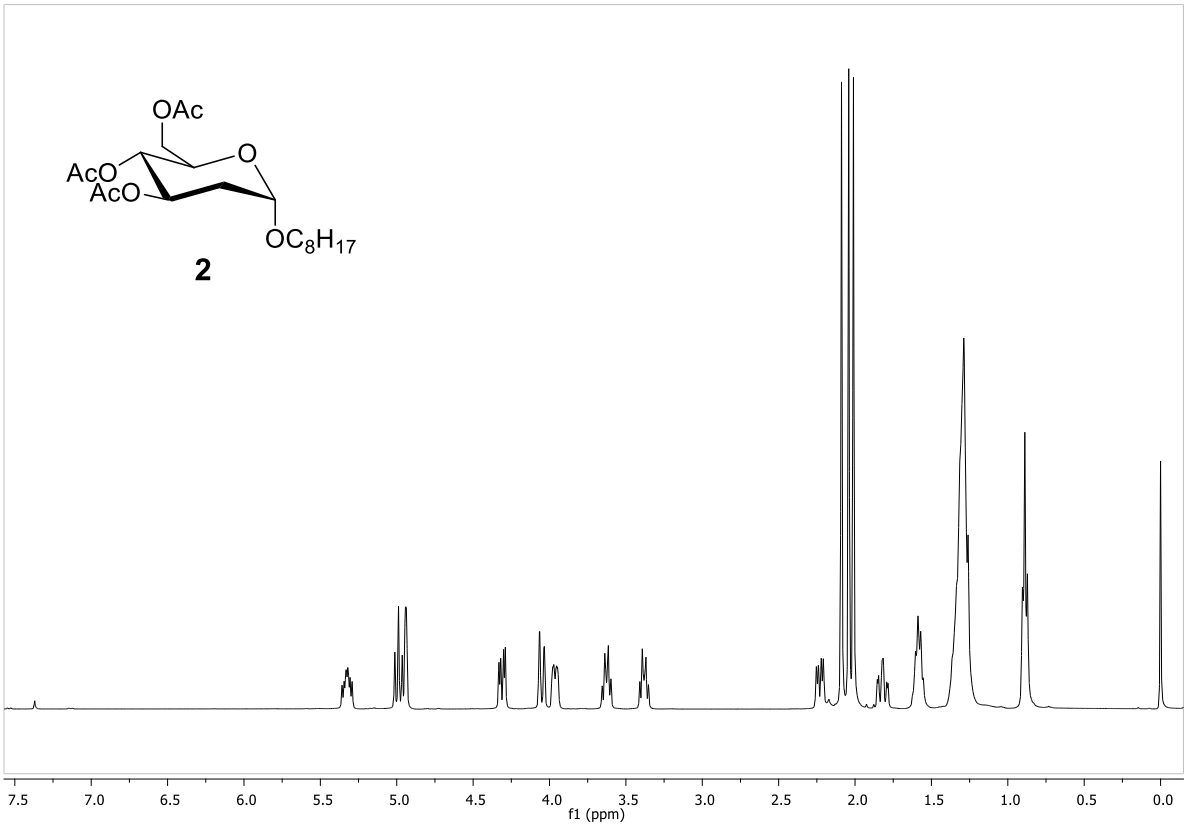

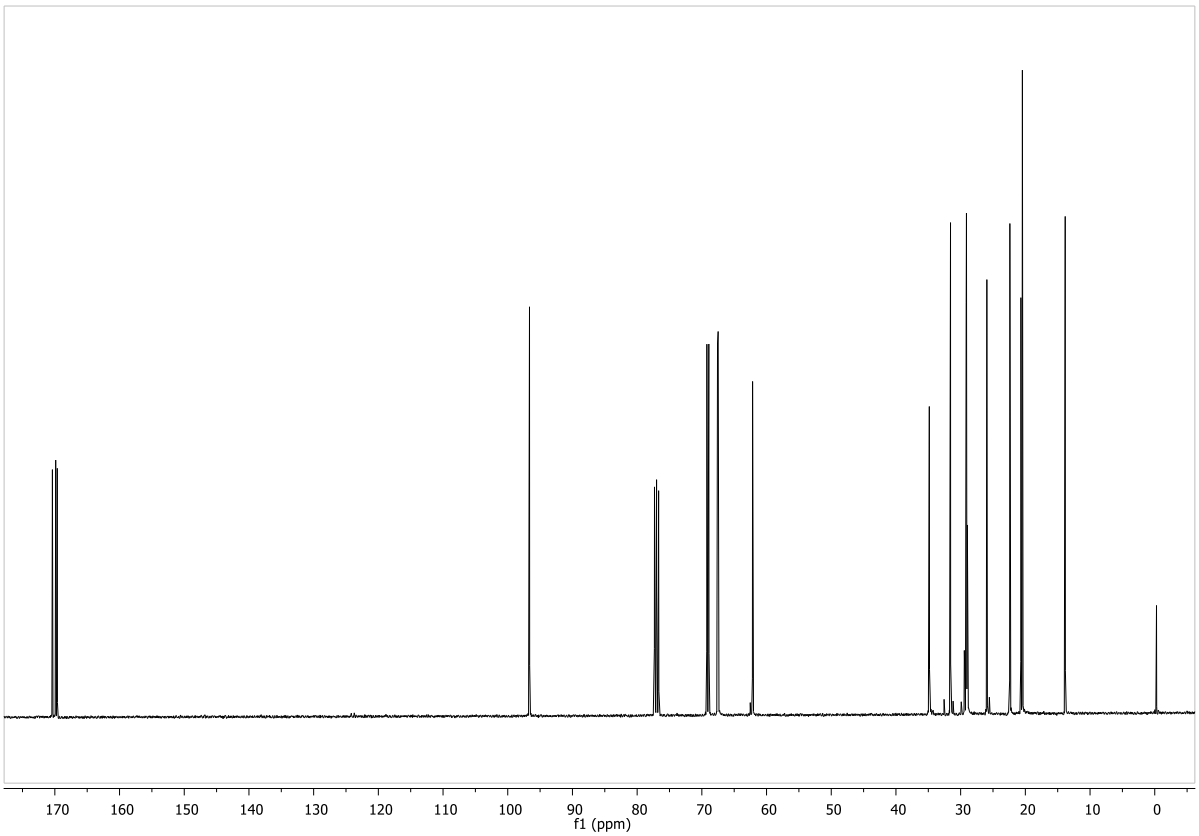

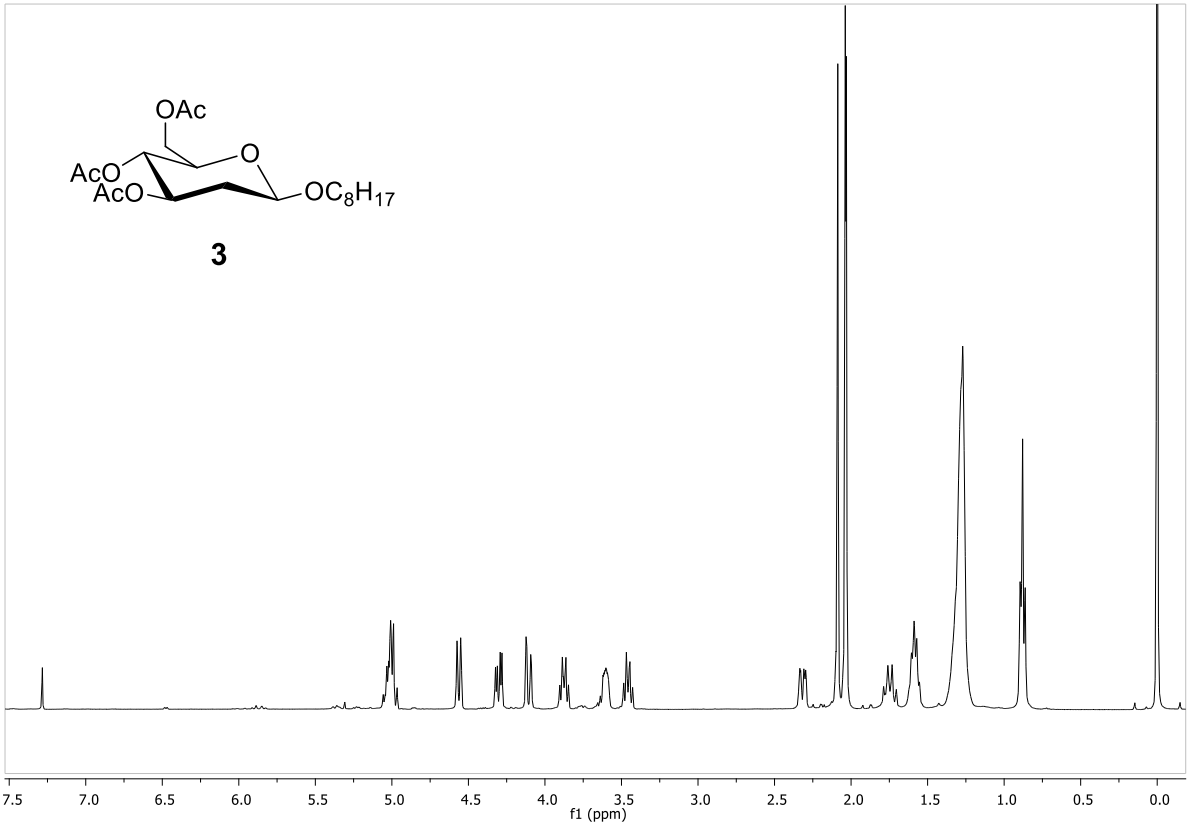
OAc
O
AcO
AcO
OC8H17
3
7.5
7.0
6.5
6.0
5.5
5.0
4.5
4.0
3.5
3.0
2.5
2.0
1.5
1.0
0.5
0.0
f1 (ppm)

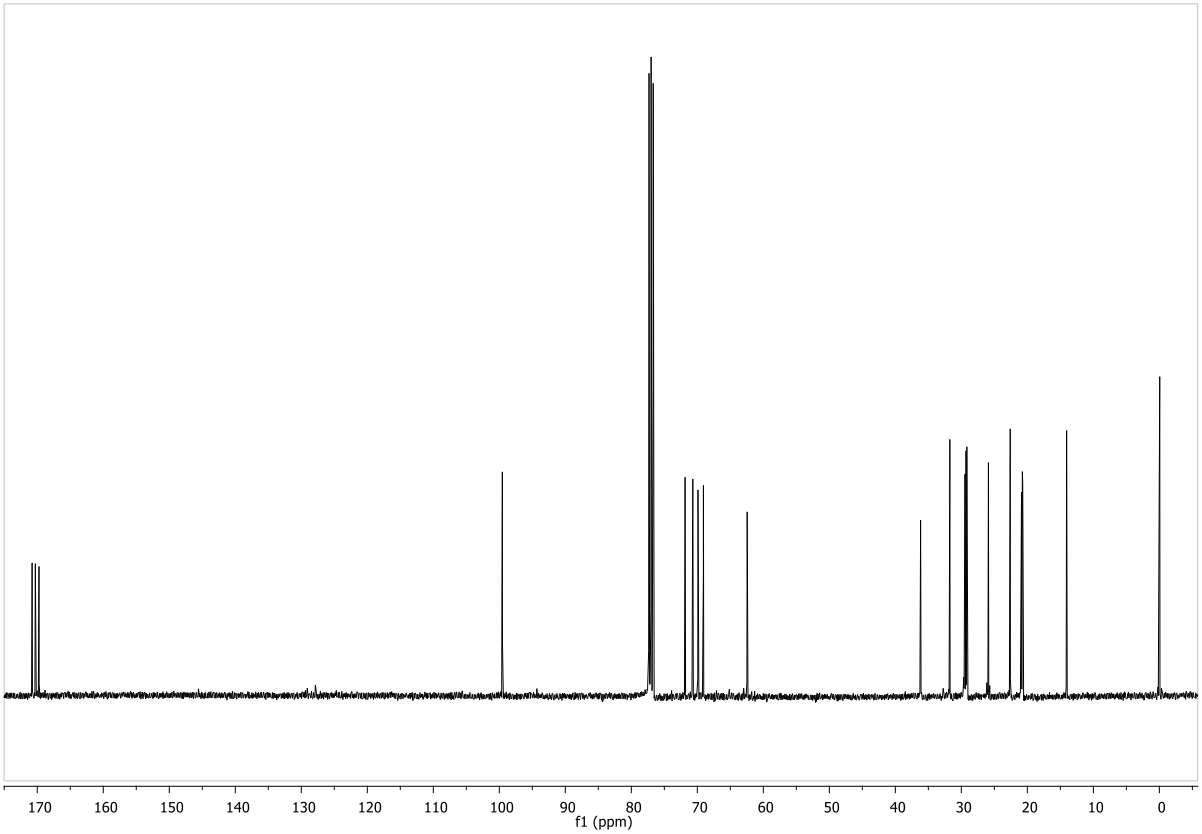
170
160
150
140
130
120
110
100
90
80
70
60
50
40
30
20
10
0
f1 (ppm)

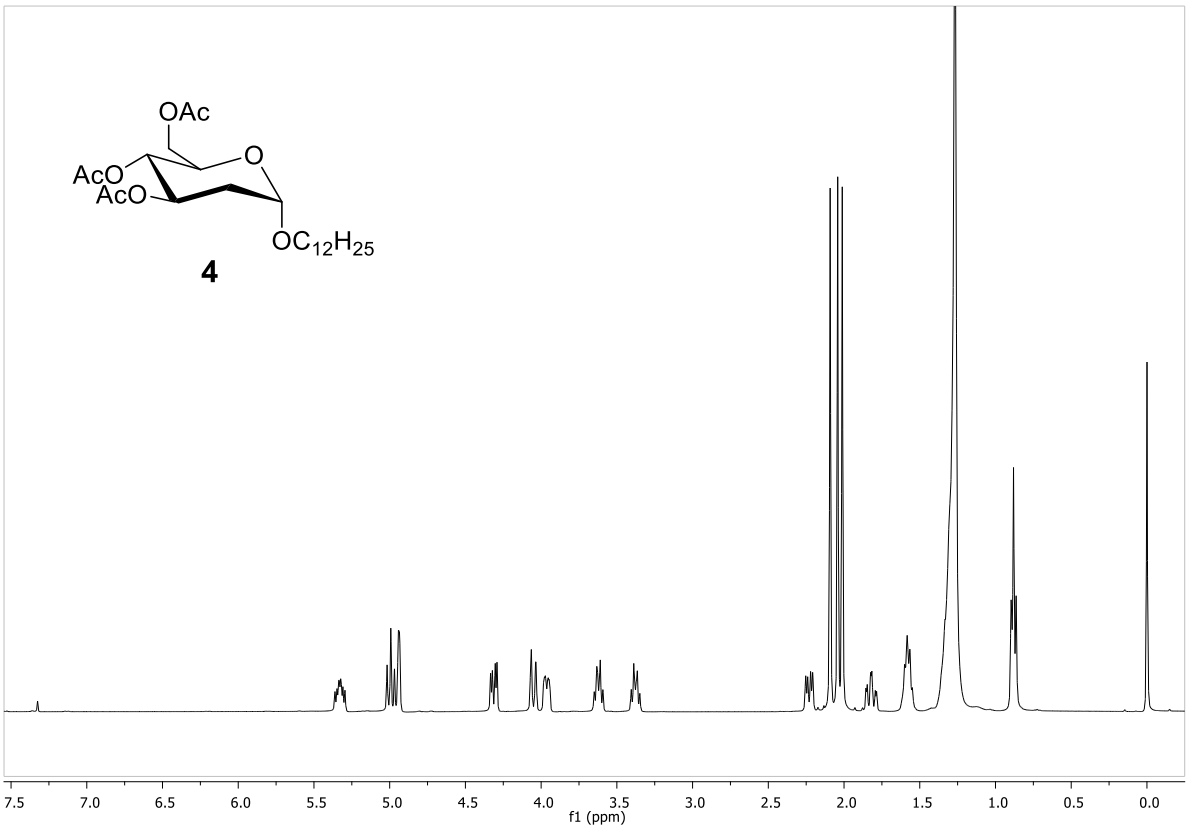
OAc
AcO
AcO
O
OC12H25
4
7.5
7.0
6.5
6.0
5.5
5.0
4.5
4.0
3.5
3.0
2.5
2.0
1.5
1.0
0.5
0.0
f1 (ppm)

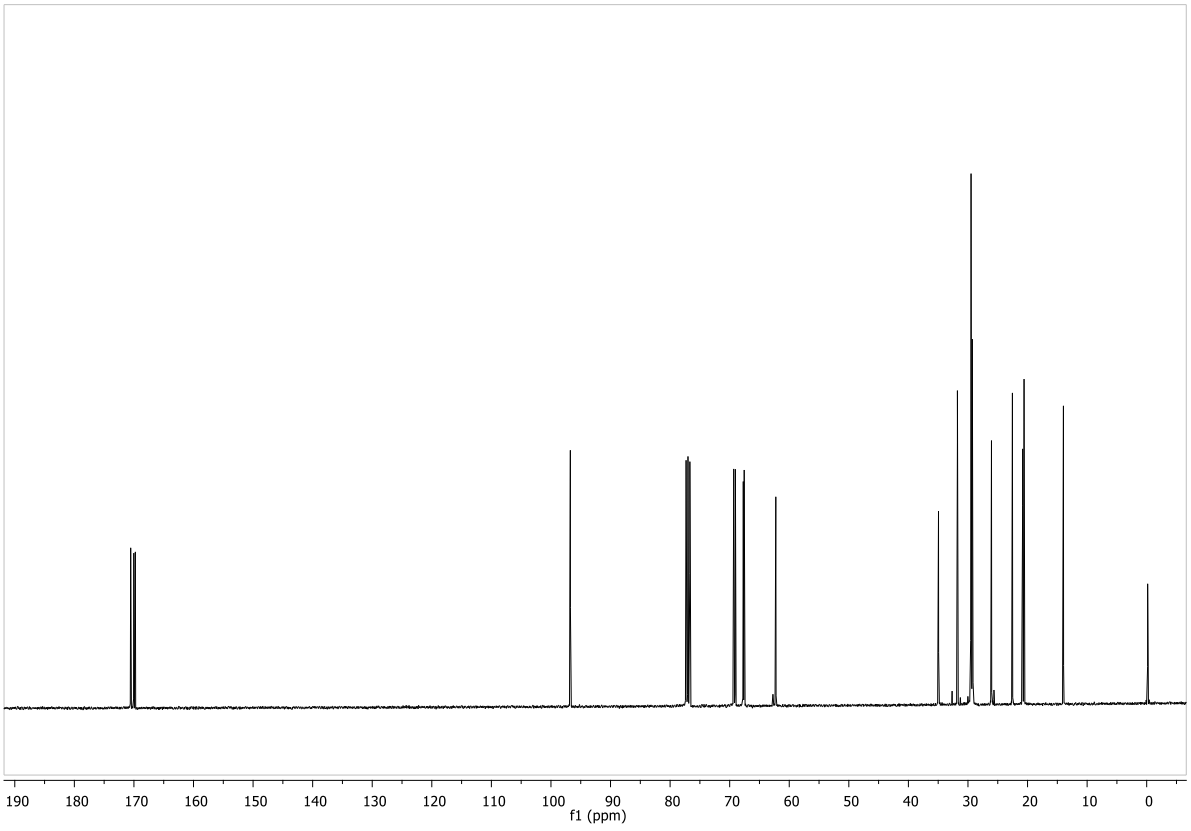
190
180
170
160
150
140
130
120
110
100
90
80
70
60
50
40
30
20
10
0
f1 (ppm)

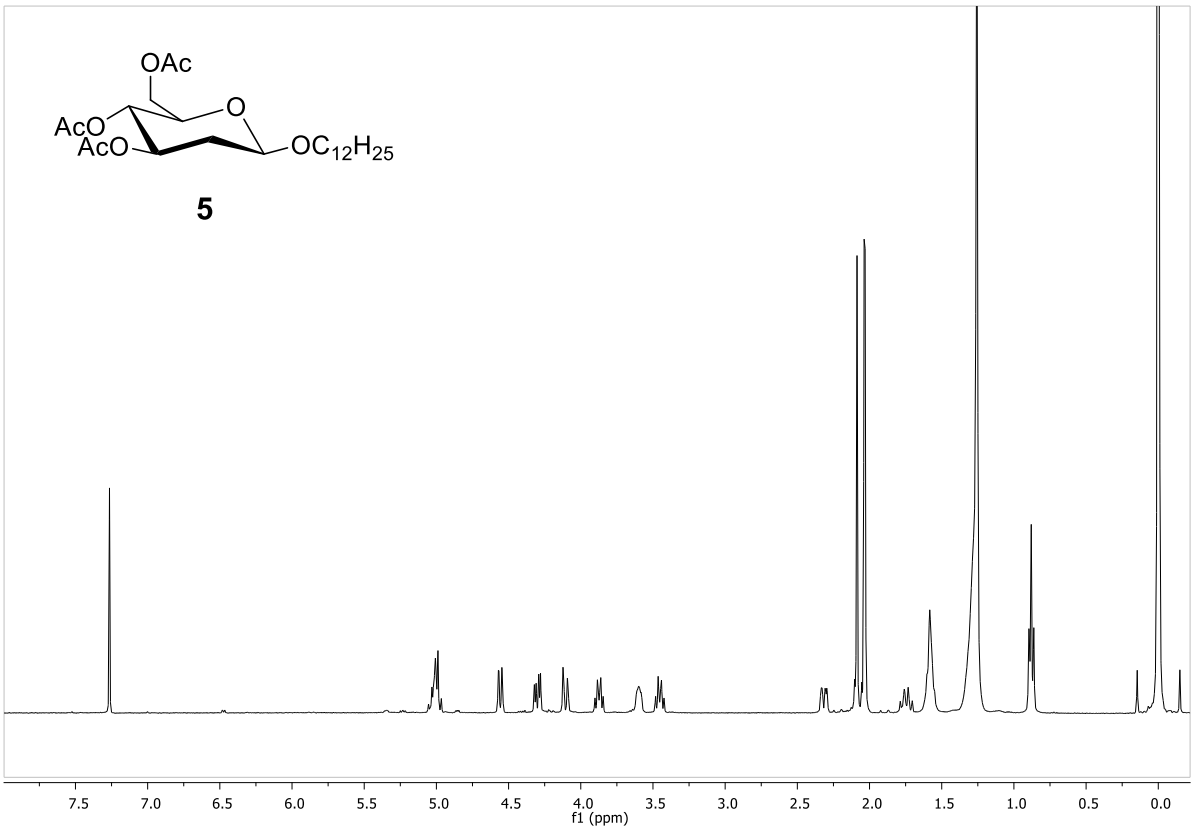
OAc
O
AcO
AcO
$OC_{12}H_{25}$
7.5
7.0
6.5
6.0
5.5
5.0
4.5
4.0
3.5
3.0
2.5
2.0
1.5
1.0
0.5
0.0
f1 (ppm)

5

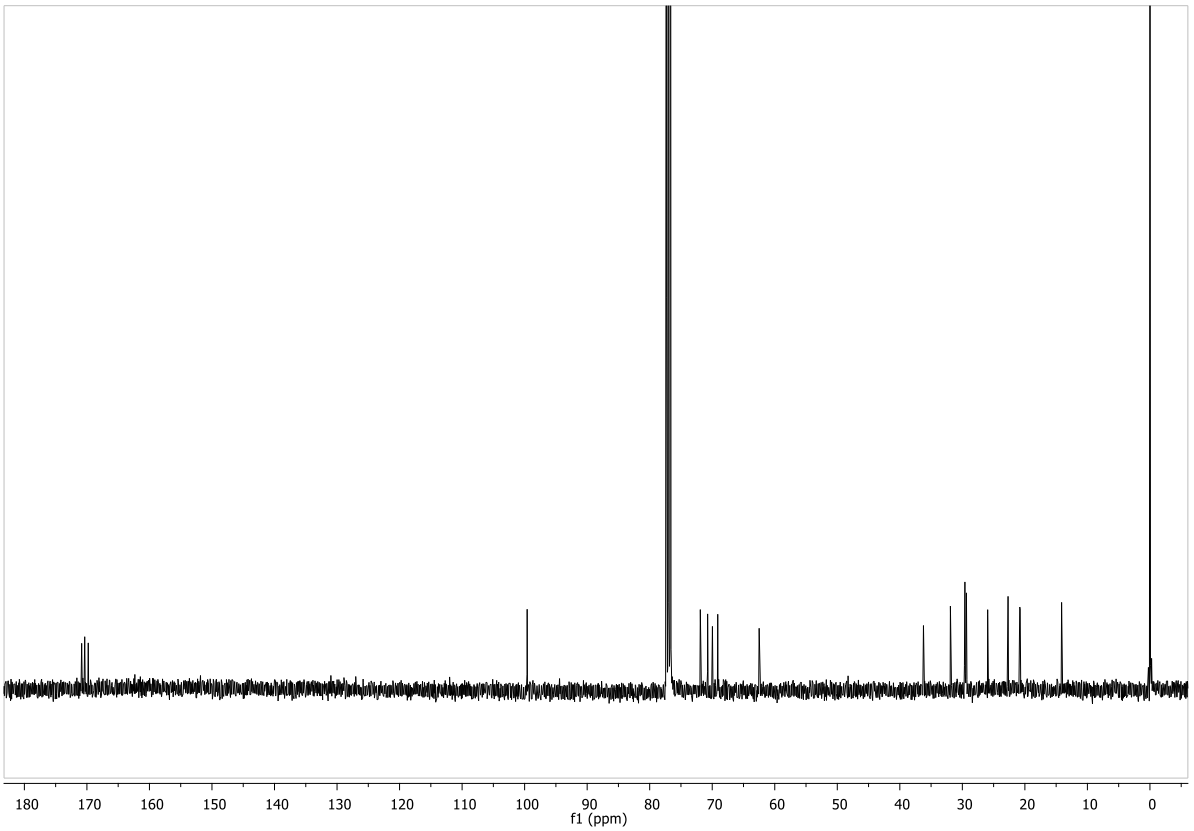
180
170
160
150
140
130
120
110
100
90
80
70
60
50
40
30
20
10
0
f1 (ppm)

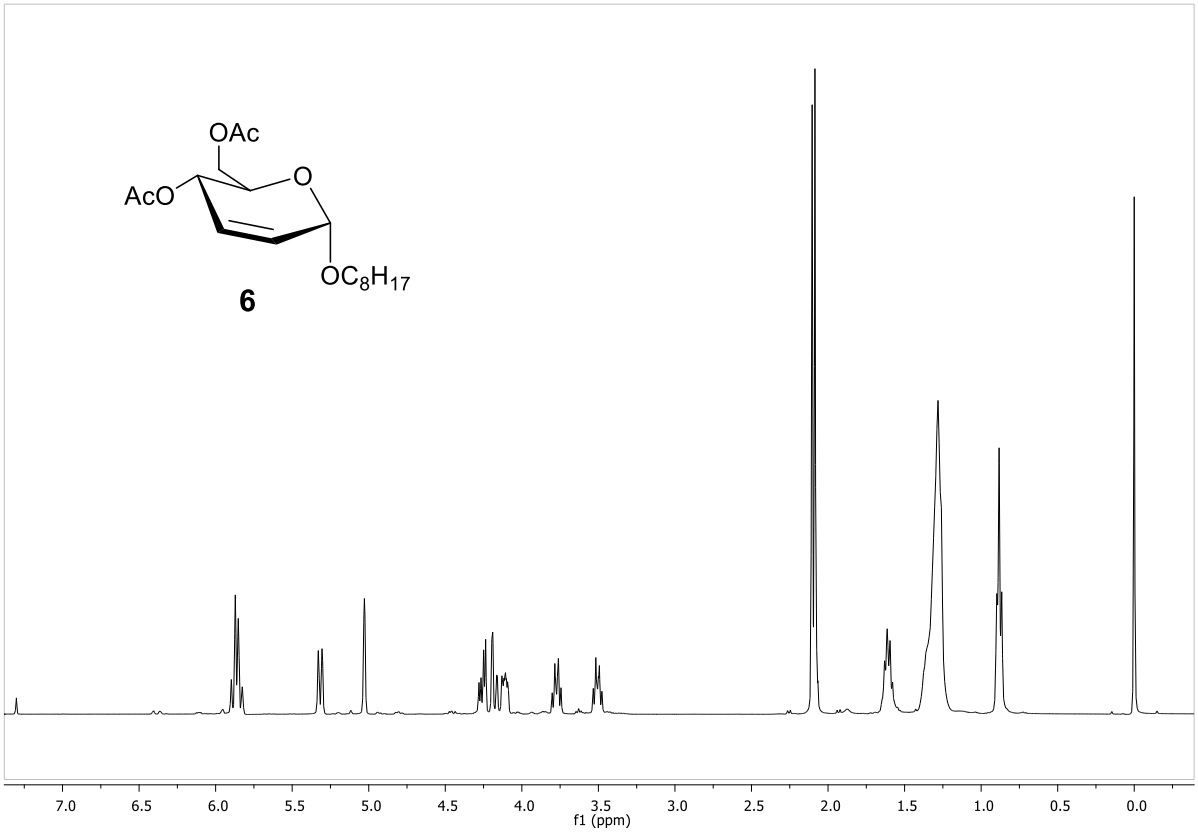
OAc
AcO
O
OC_8H_{17}
6
7.0
6.5
6.0
5.5
5.0
4.5
4.0
3.5
3.0
2.5
2.0
1.5
1.0
0.5
0.0
f1 (ppm)

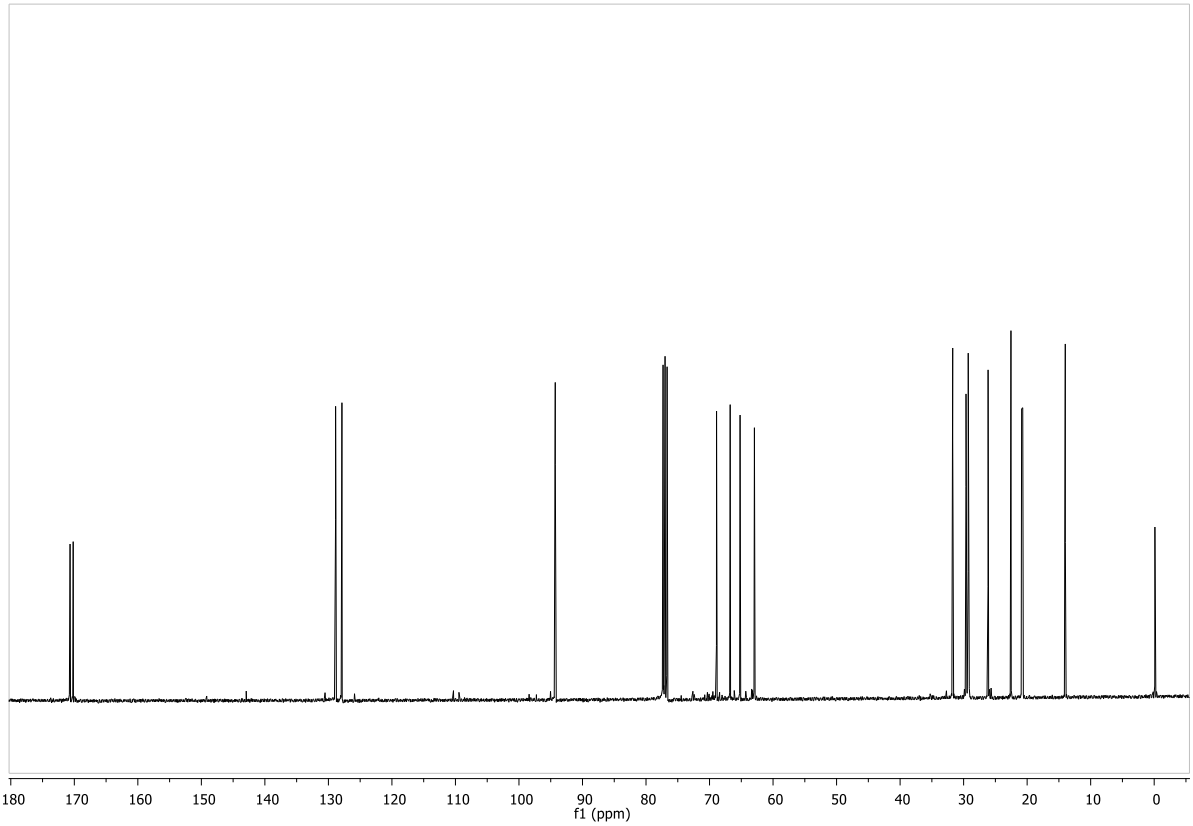
180
170
160
150
140
130
120
110
100
90
80
70
60
50
40
30
20
10
0
f1 (ppm)

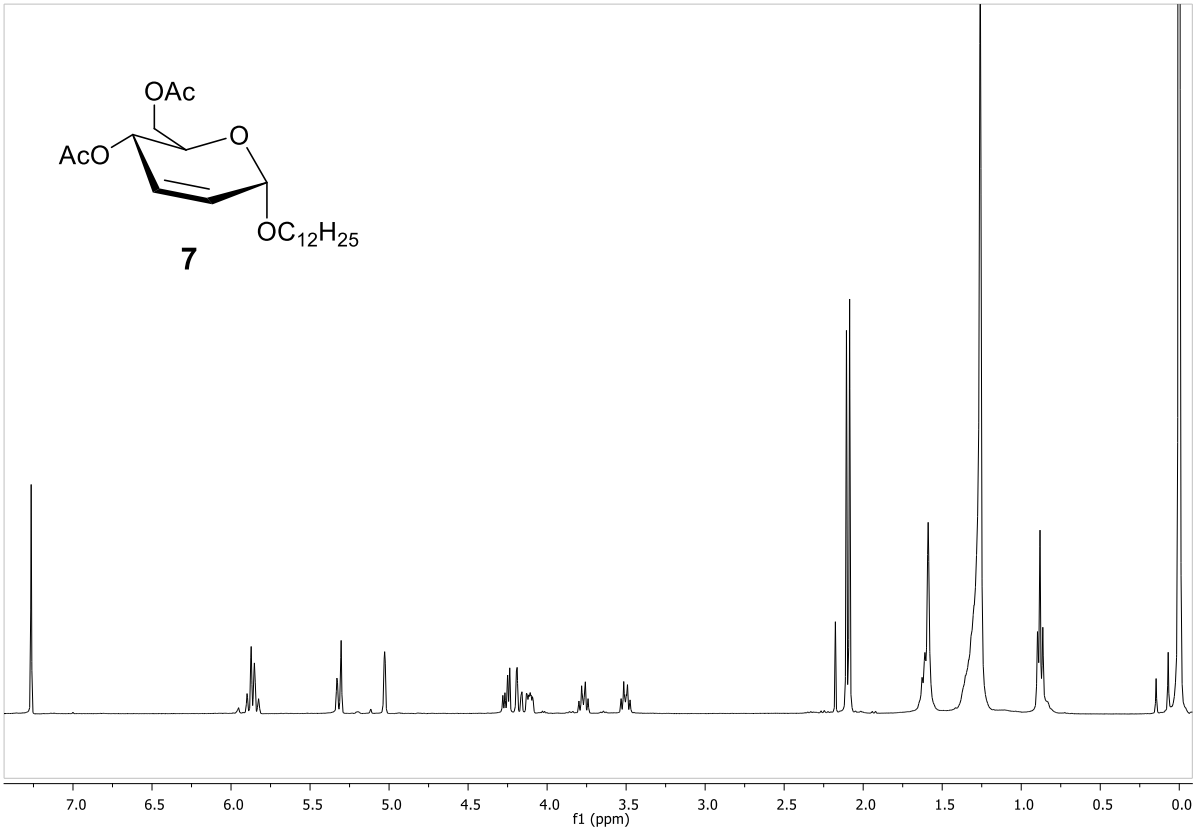
OAc
AcO
O
$OC_{12}H_{25}$
7
7.0
6.5
6.0
5.5
5.0
4.5
4.0
3.5
3.0
2.5
2.0
1.5
1.0
0.5
0.0
f1 (ppm)

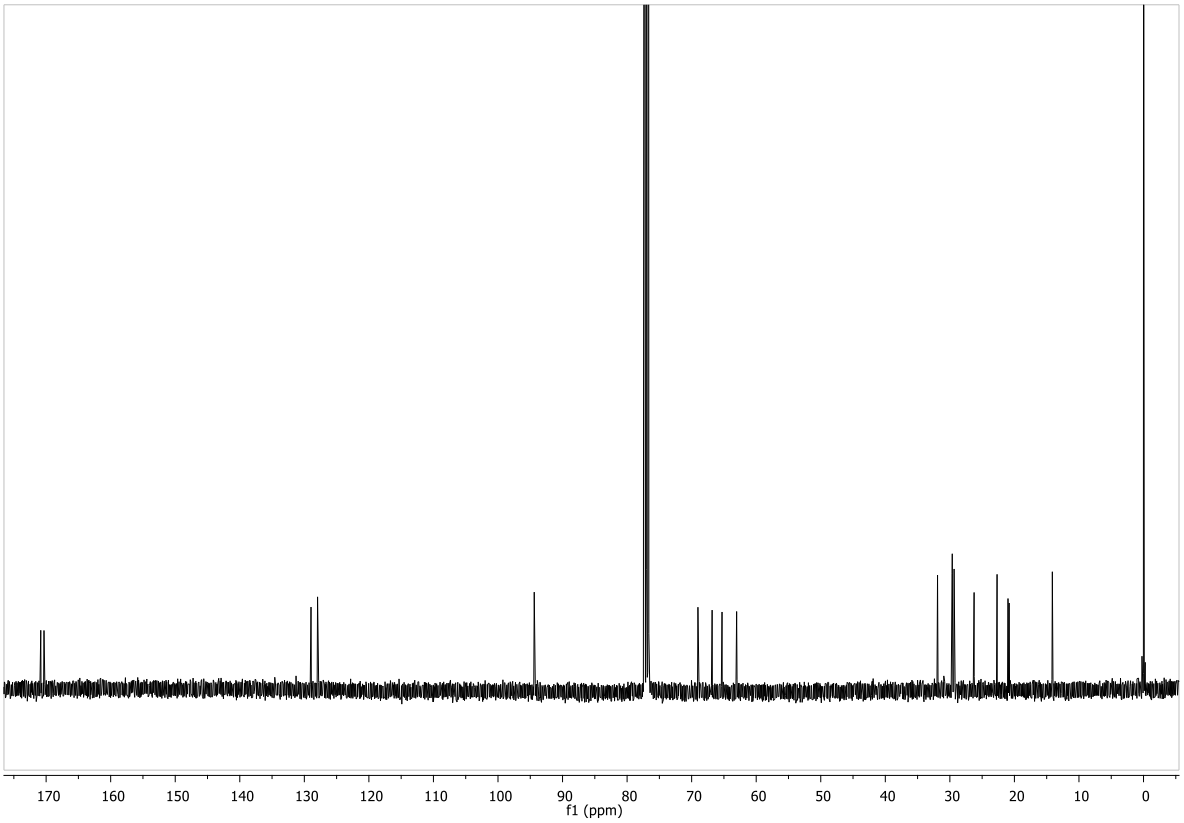
170
160
150
140
130
120
110
100
90
80
70
60
50
40
30
20
10
0
f1 (ppm)

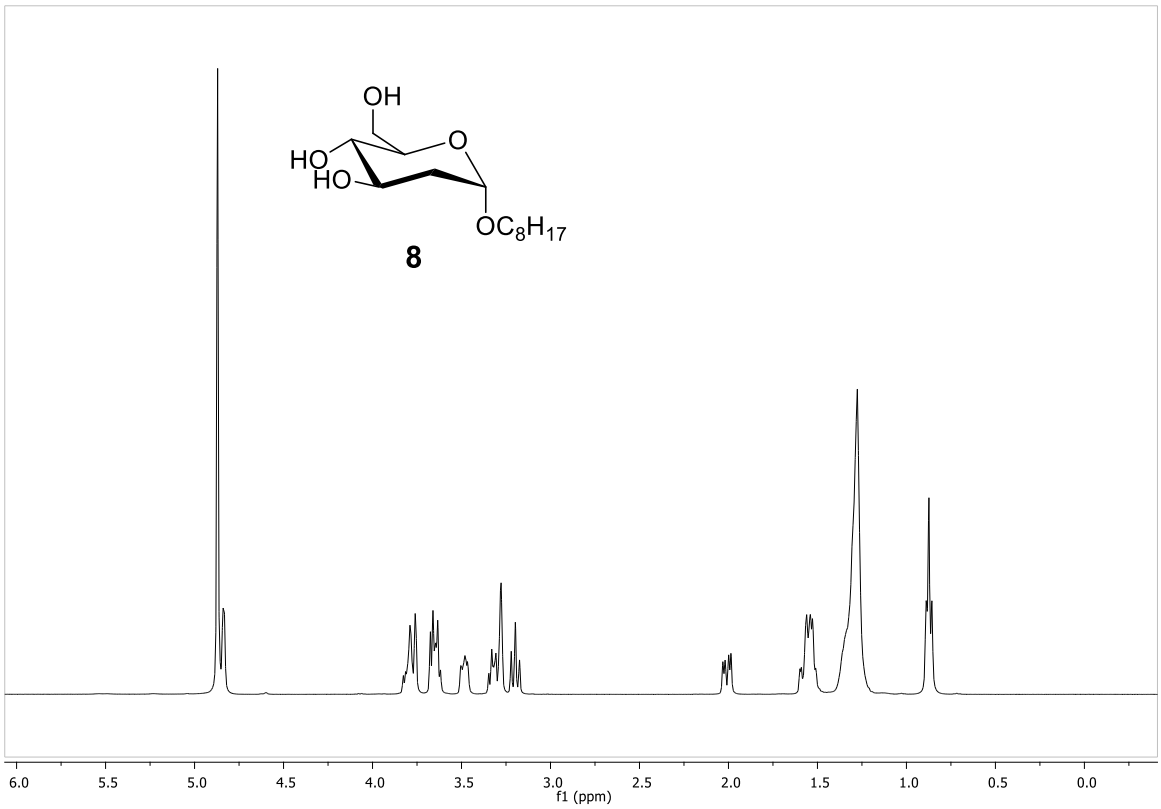
OH
O
HO
HO
OC_8H_{17}
8
6.0
5.5
5.0
4.5
4.0
3.5
3.0
2.5
2.0
1.5
1.0
0.5
0.0
f1 (ppm)

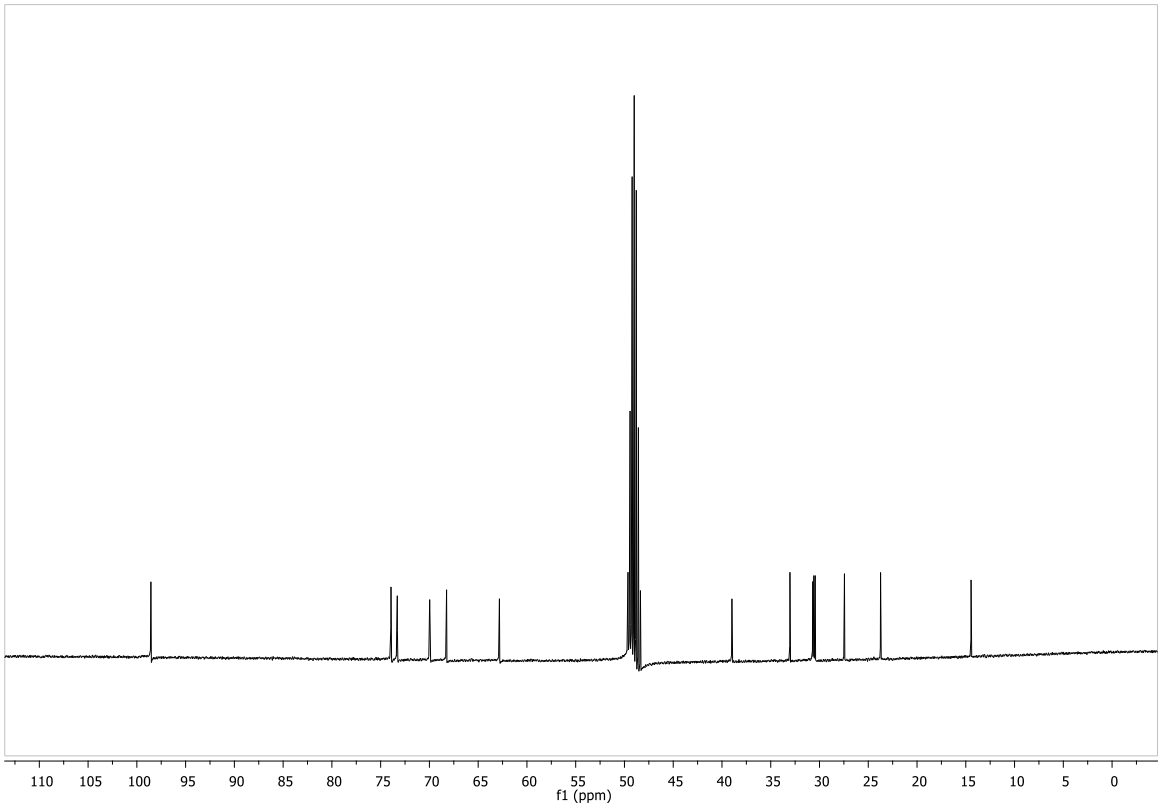
110
105
100
95
90
85
80
75
70
65
60
55
50
45
40
35
30
25
20
15
10
5
0
f1 (ppm)

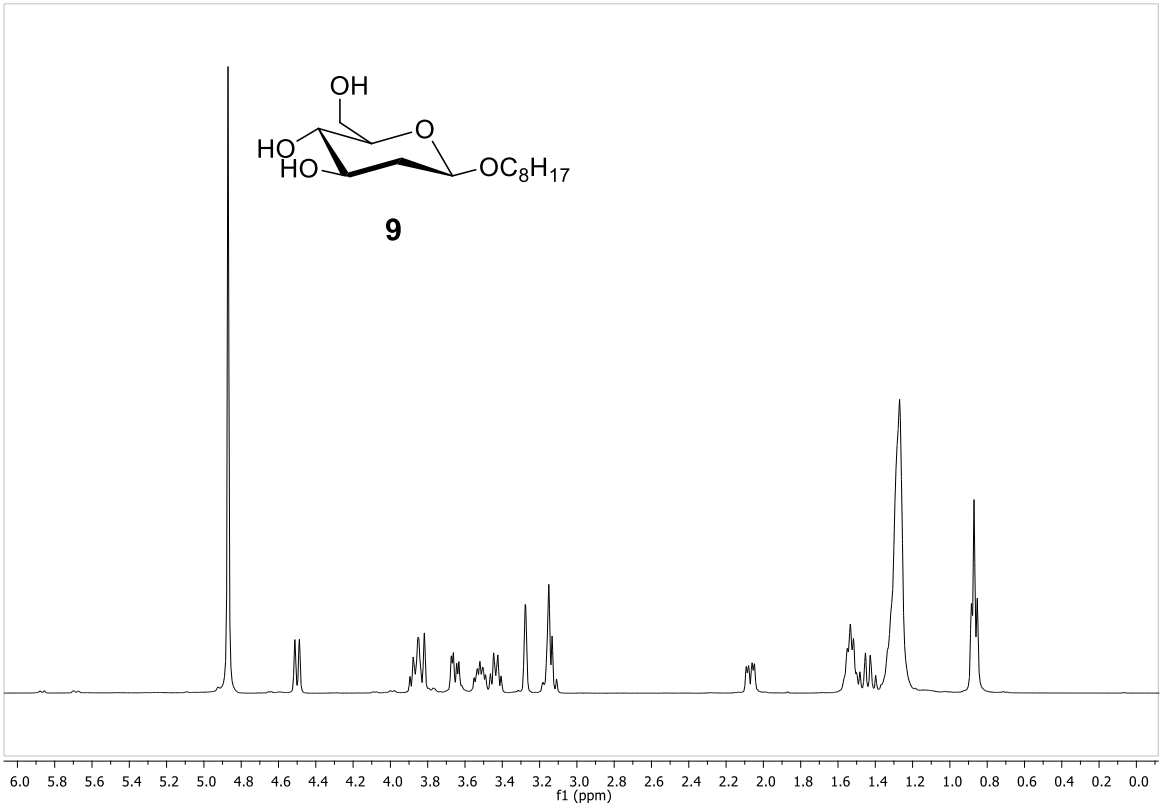
OH
HO
HO
O
OC8H17
9
6.0 5.8 5.6 5.4 5.2 5.0 4.8 4.6 4.4 4.2 4.0 3.8 3.6 3.4 3.2 3.0 2.8 2.6 2.4 2.2 2.0 1.8 1.6 1.4 1.2 1.0 0.8 0.6 0.4 0.2 0.0
f1 (ppm)

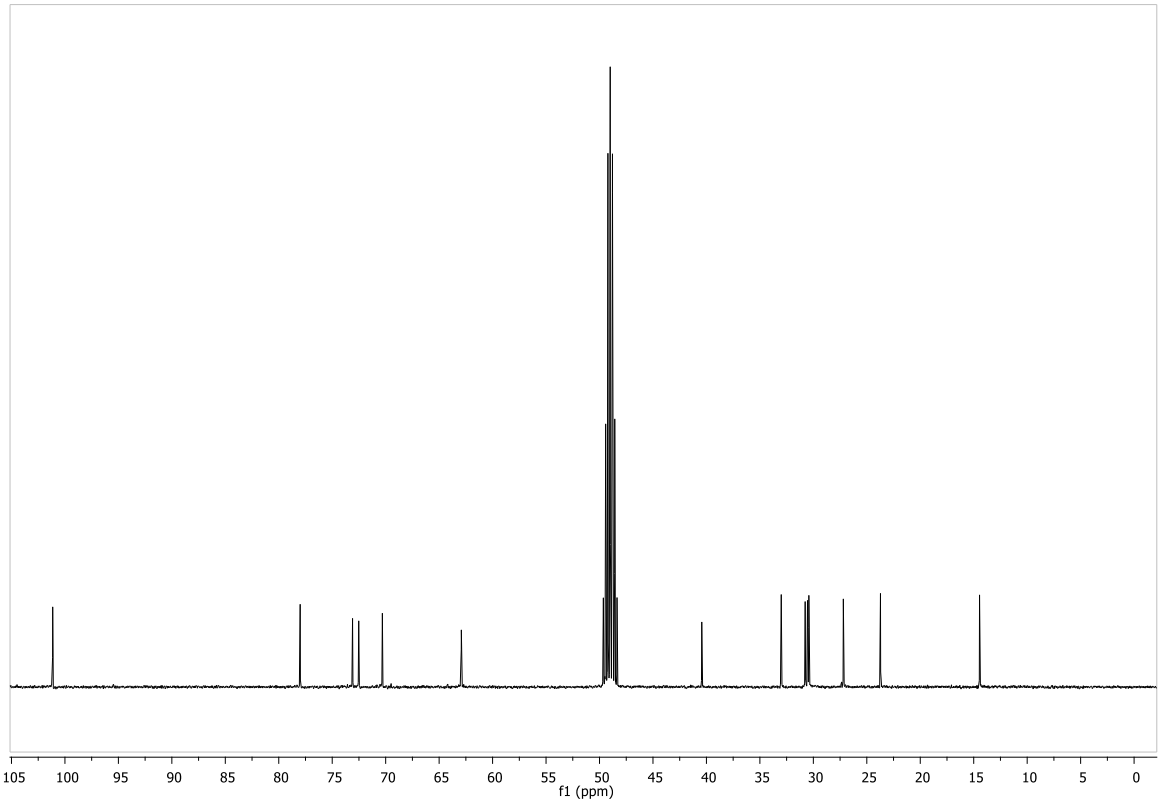
105 100 95 90 85 80 75 70 65 60 55 50 45 40 35 30 25 20 15 10 5 0
f1 (ppm)

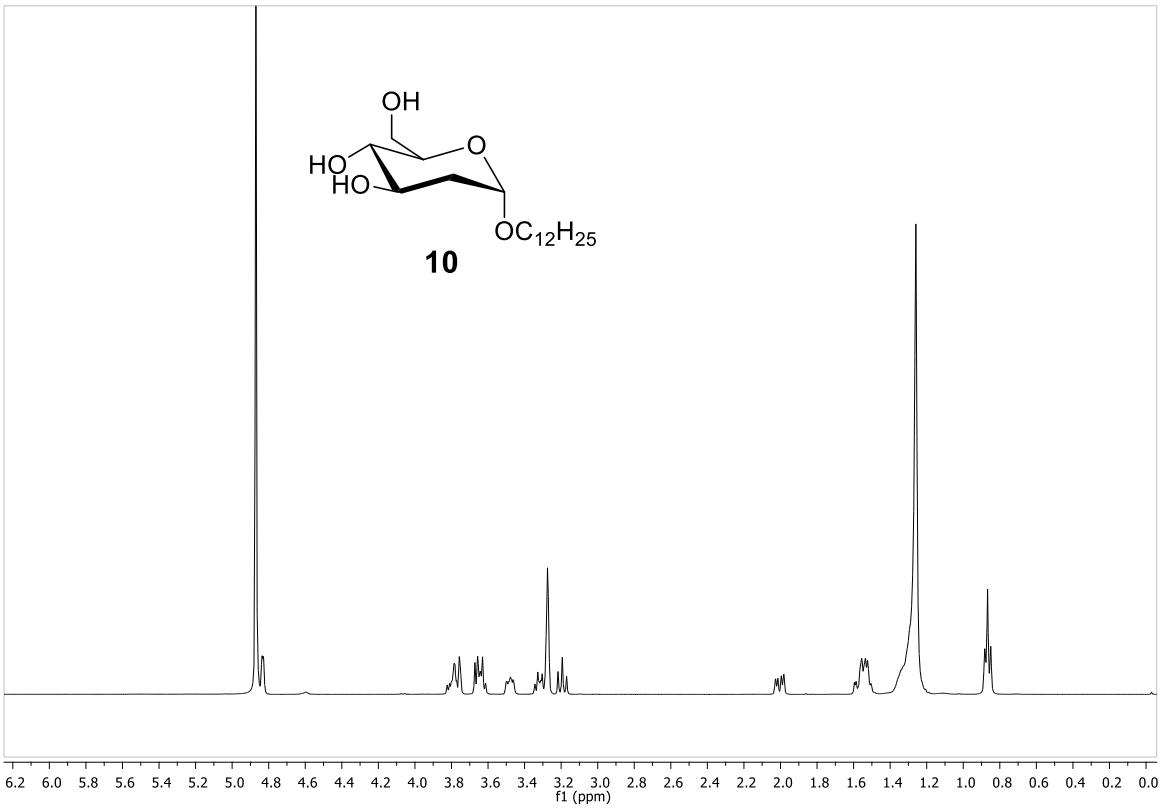
OH
O
HO
HO
$OC_{12}H_{25}$
10
6.2 6.0 5.8 5.6 5.4 5.2 5.0 4.8 4.6 4.4 4.2 4.0 3.8 3.6 3.4 3.2 3.0 2.8 2.6 2.4 2.2 2.0 1.8 1.6 1.4 1.2 1.0 0.8 0.6 0.4 0.2 0.0
f1 (ppm)

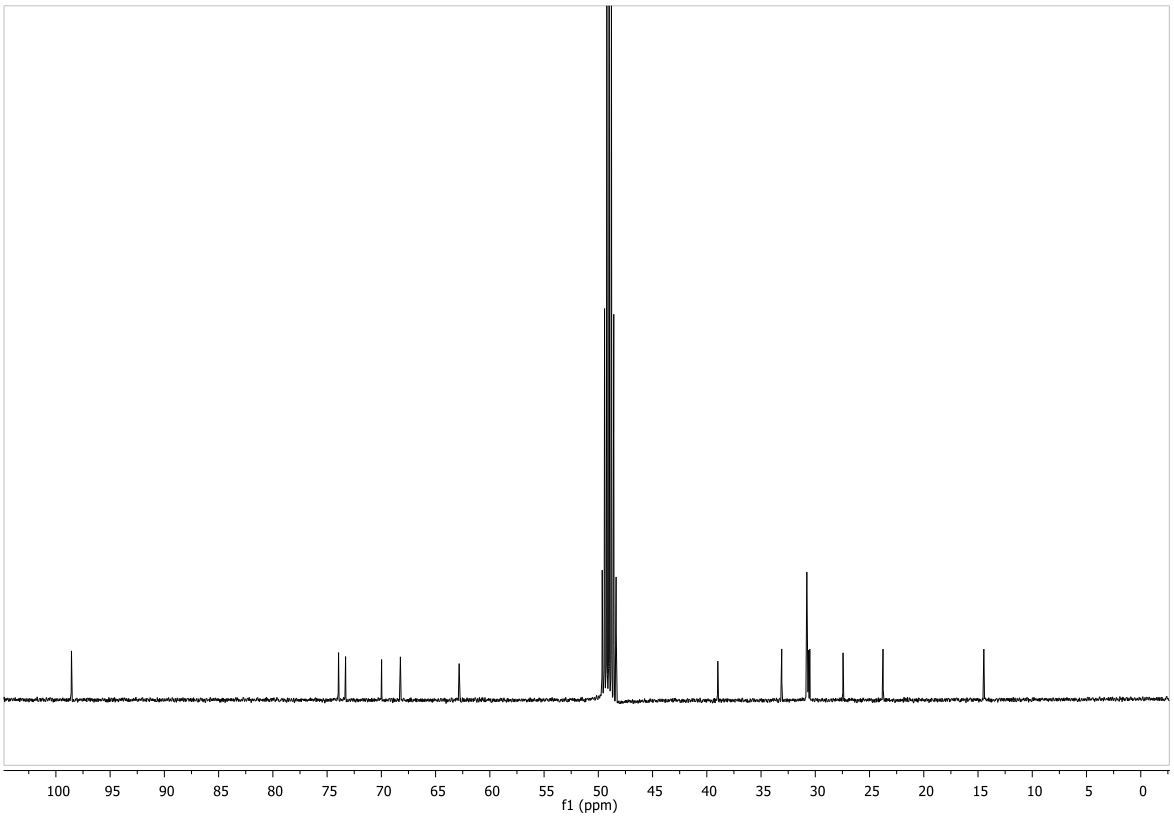
100 95 90 85 80 75 70 65 60 55 50 45 40 35 30 25 20 15 10 5 0
f1 (ppm)

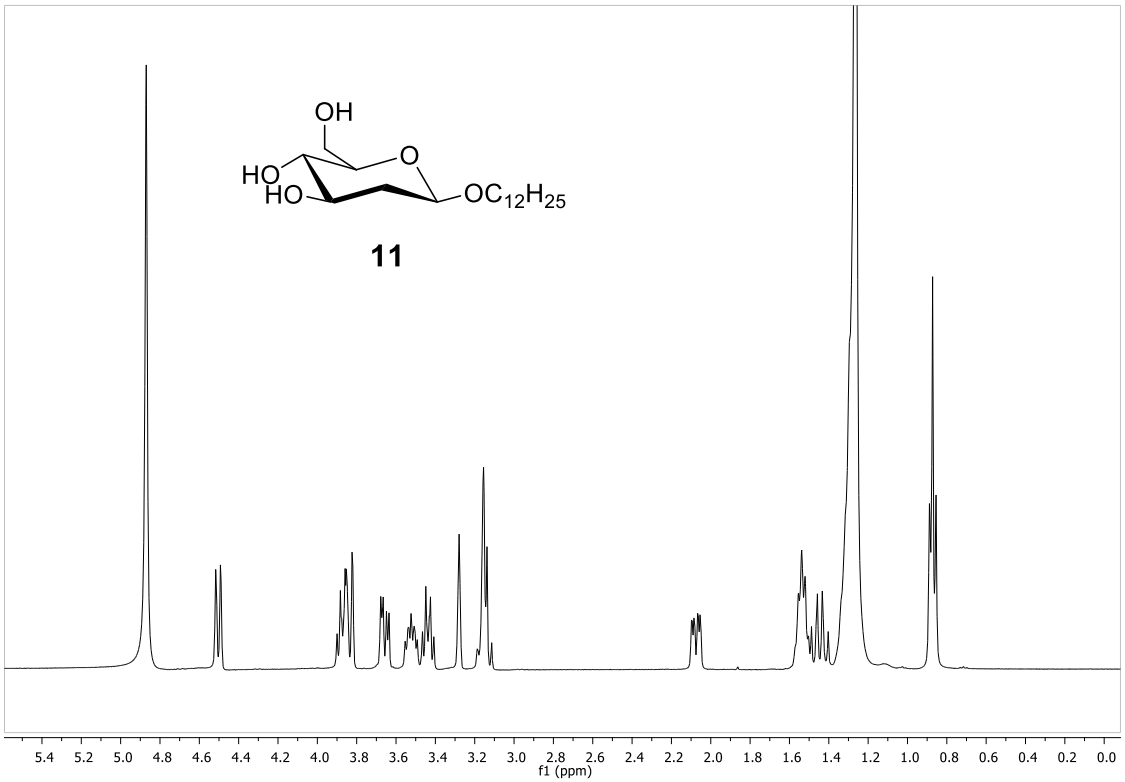
OH
O
HO
HO
OC12H25
11
5.4 5.2 5.0 4.8 4.6 4.4 4.2 4.0 3.8 3.6 3.4 3.2 3.0 2.8 2.6 2.4 2.2 2.0 1.8 1.6 1.4 1.2 1.0 0.8 0.6 0.4 0.2 0.0
f1 (ppm)

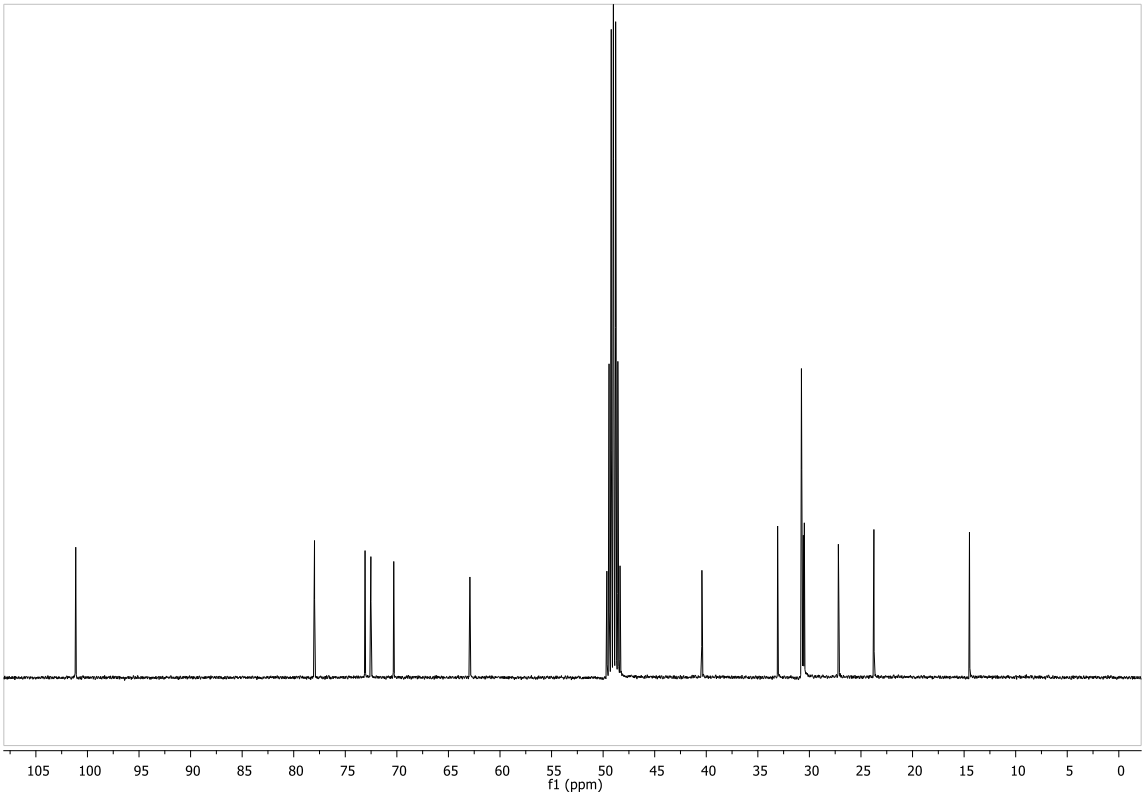
105 100 95 90 85 80 75 70 65 60 55 50 45 40 35 30 25 20 15 10 5 0
f1 (ppm)

Annex 2. *^{1}H and ^{13}C of final products described in chapter 3*

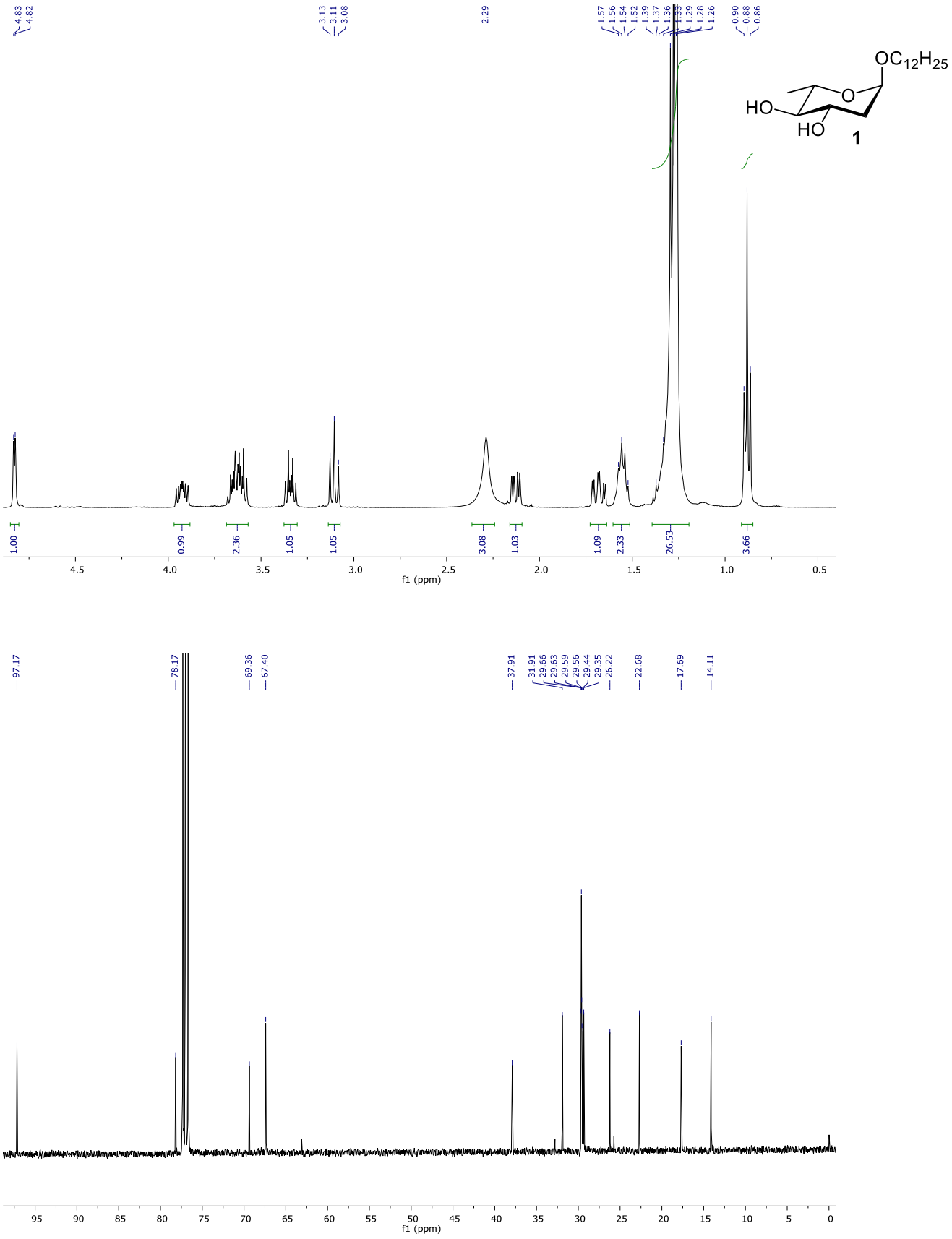

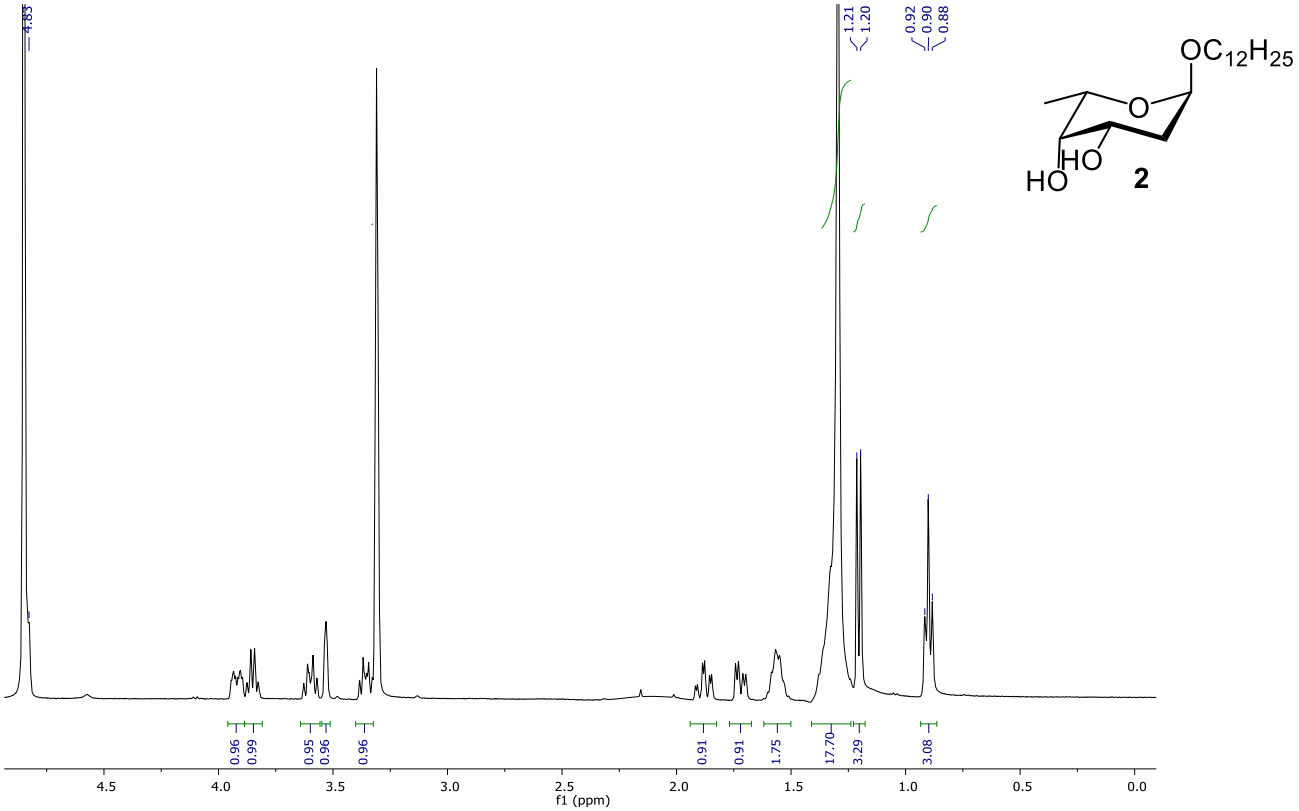
4.83
1.21
1.20
0.92
0.90
0.88
OC12H25
O
HO
HO
2
0.96
0.99
0.95
0.96
0.96
0.91
0.91
1.75
17.70
3.29
3.08
4.5
4.0
3.5
3.0
2.5
2.0
1.5
1.0
0.5
0.0
f1 (ppm)

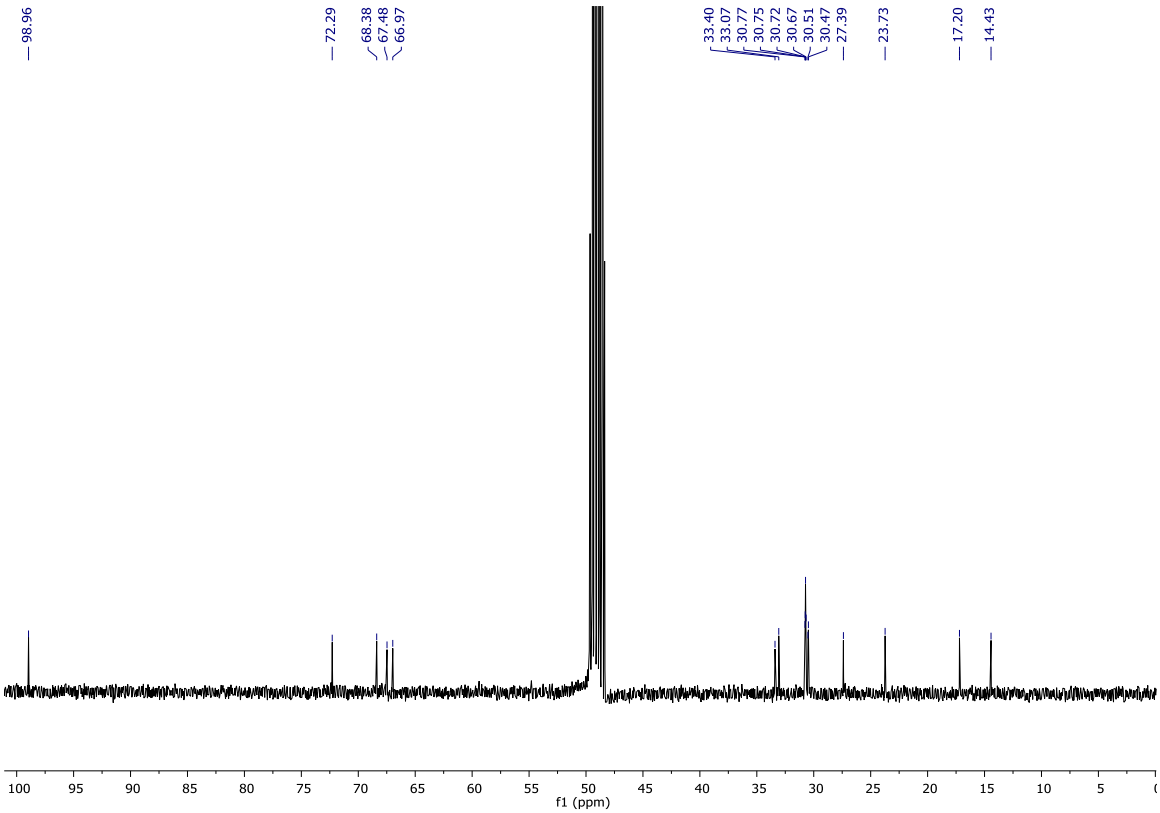
98.96
72.29
68.38
67.48
66.97
33.40
33.07
30.77
30.75
30.72
30.67
30.51
30.47
27.39
23.73
17.20
14.43
100
95
90
85
80
75
70
65
60
55
50
45
40
35
30
25
20
15
10
5
f1 (ppm)

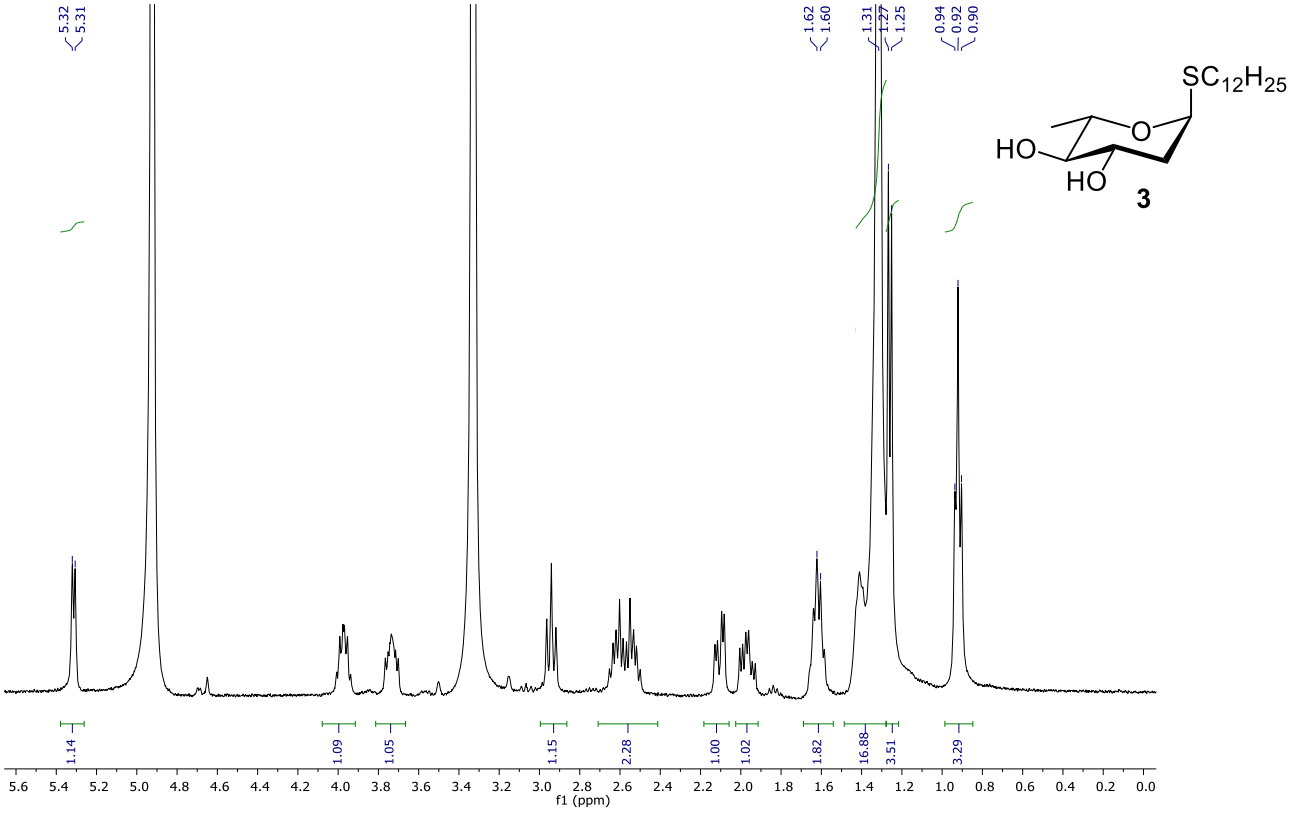
5.32
5.31
1.62
1.60
1.31
1.27
1.25
0.94
0.92
0.90
SC12H25
HO
HO
O
3
1.14
1.09
1.05
1.15
2.28
1.00
1.02
1.82
16.88
3.51
3.29
f1 (ppm)

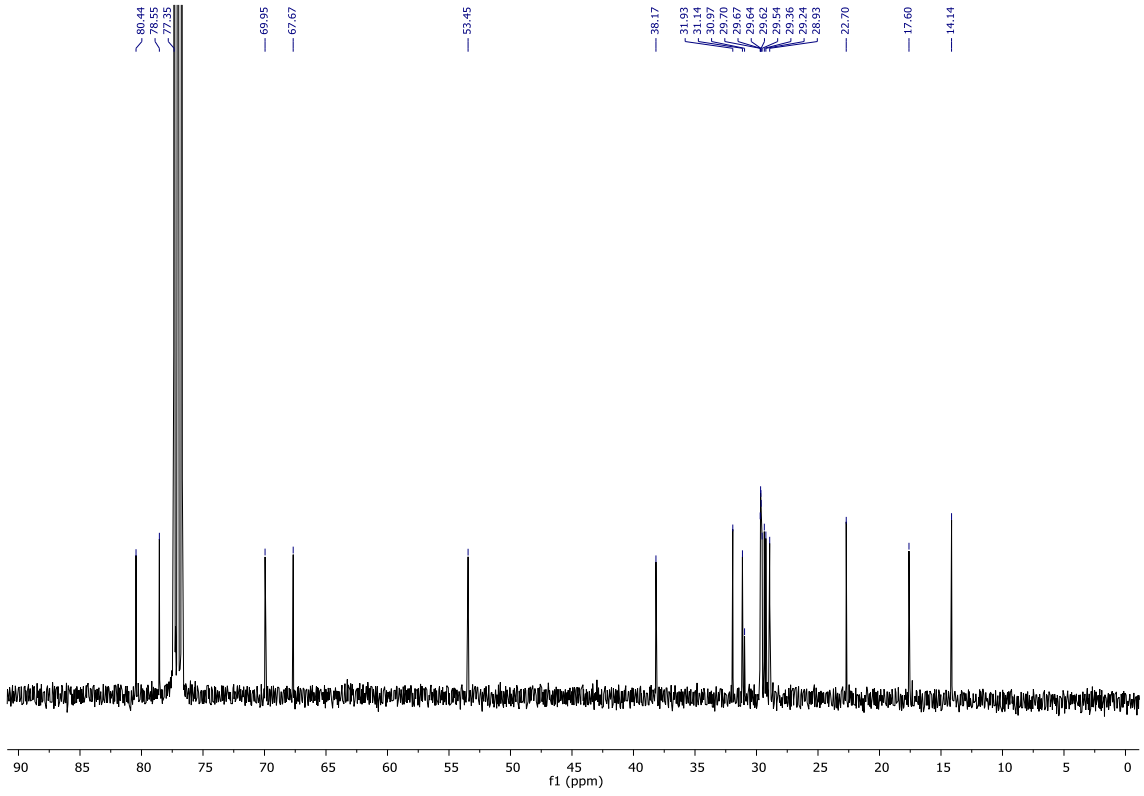
80.44
78.55
77.35
69.95
67.67
53.45
38.17
31.93
31.14
30.97
29.70
29.67
29.64
29.62
29.54
29.36
29.24
28.93
22.70
17.60
14.14
f1 (ppm)

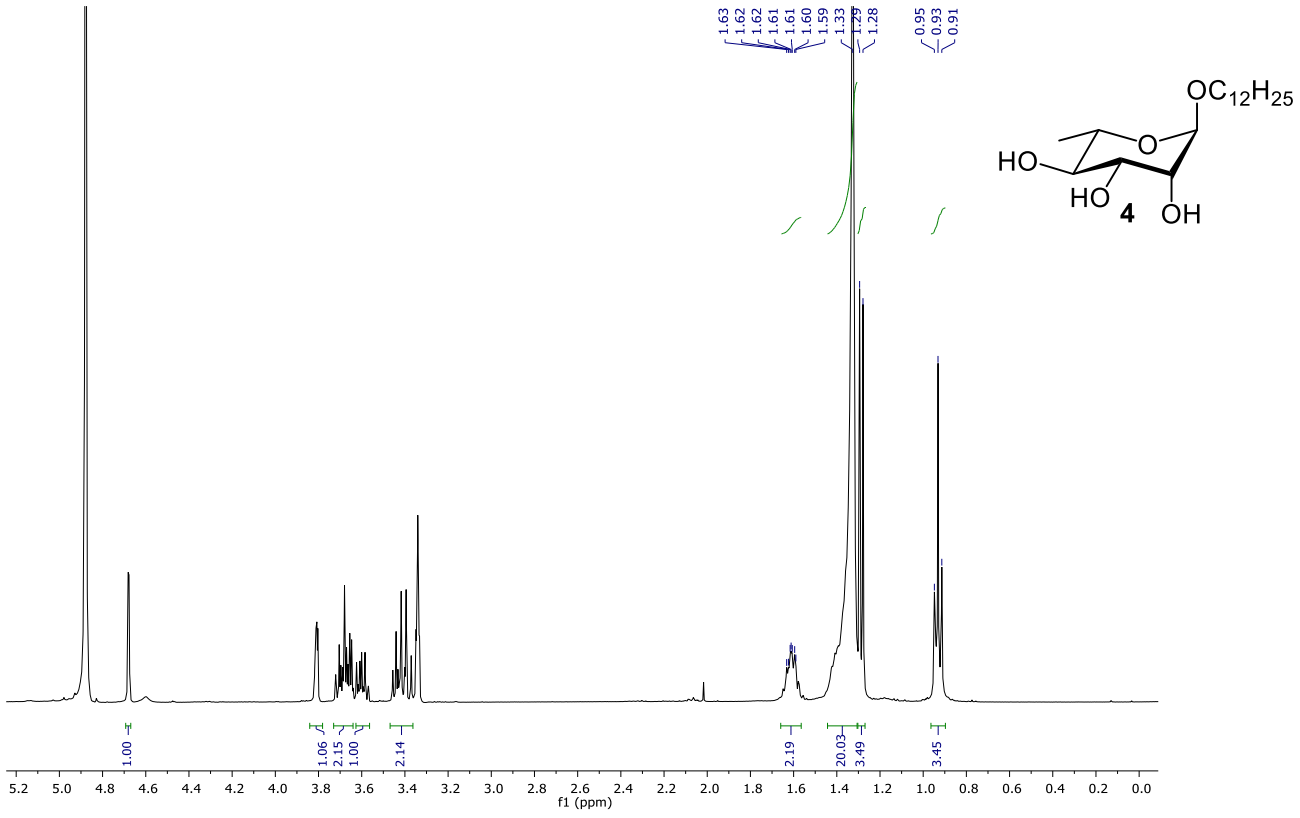
1.63
1.62
1.62
1.61
1.61
1.60
1.59
1.33
1.29
1.28
0.95
0.93
0.91
OC12H25
O
HO
HO
4
OH
1.00
1.06
2.15
1.00
2.14
2.19
20.03
3.49
3.45
f1 (ppm)

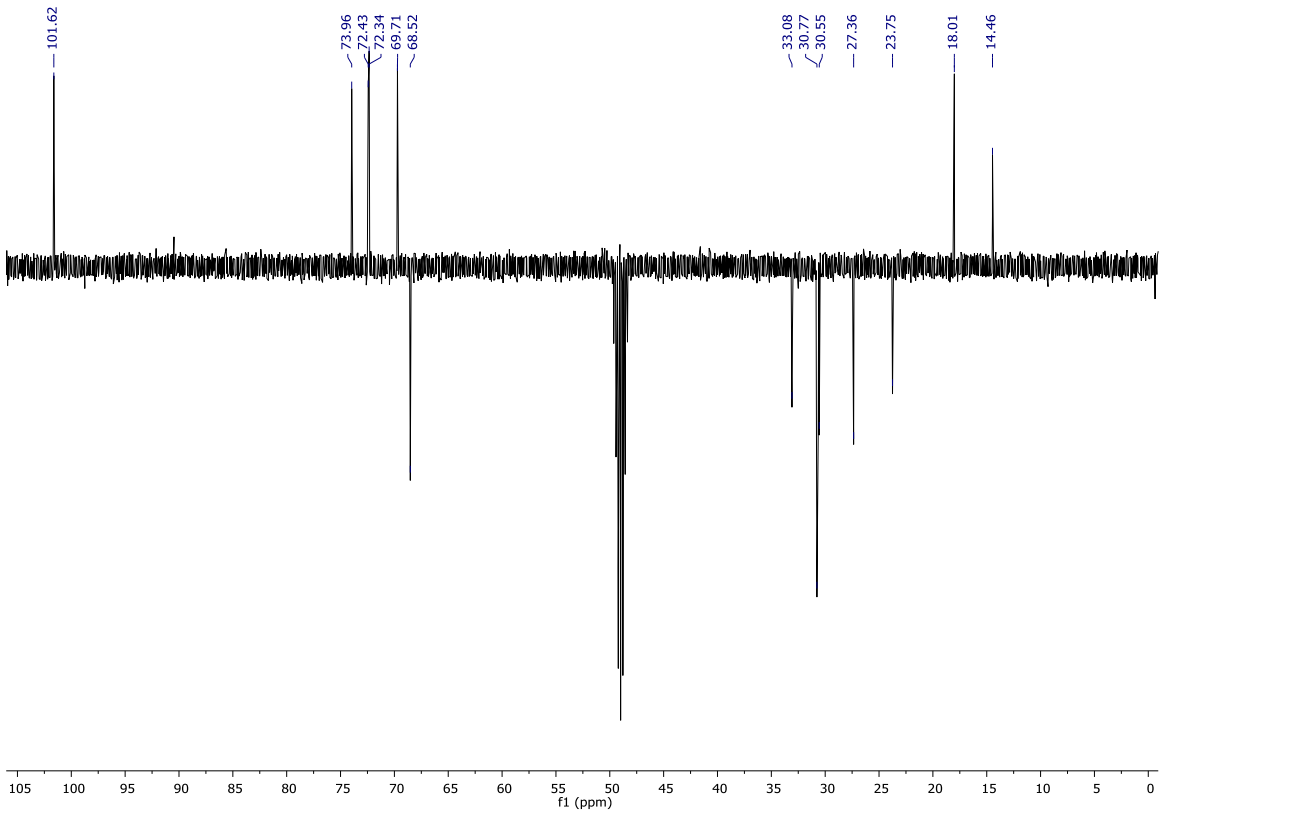
101.62
73.96
72.43
72.34
69.71
68.52
33.08
30.77
30.55
27.36
23.75
18.01
14.46
f1 (ppm)

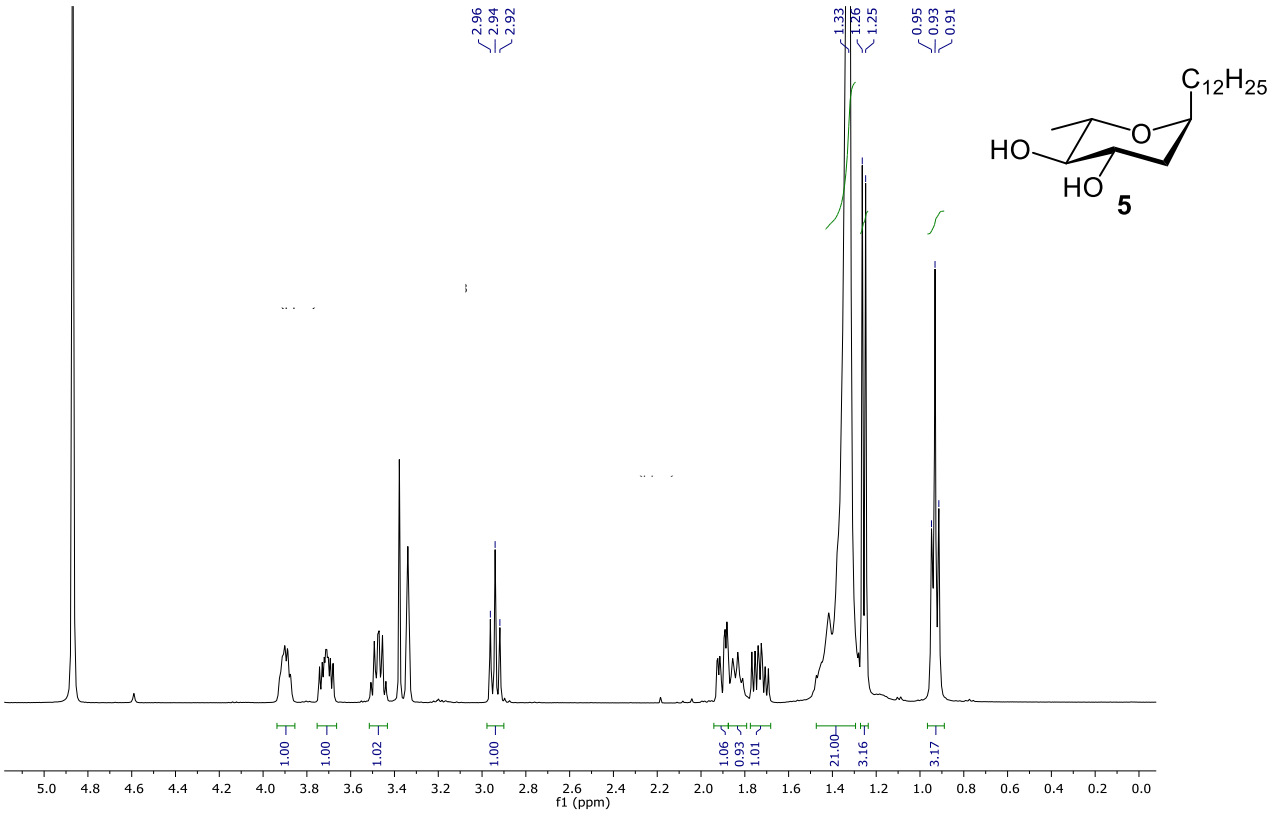
2.96
2.94
2.92
1.33
1.26
1.25
0.95
0.93
0.91
1.00
1.00
1.02
1.00
1.06
0.93
1.01
21.00
3.16
3.17
f1 (ppm)

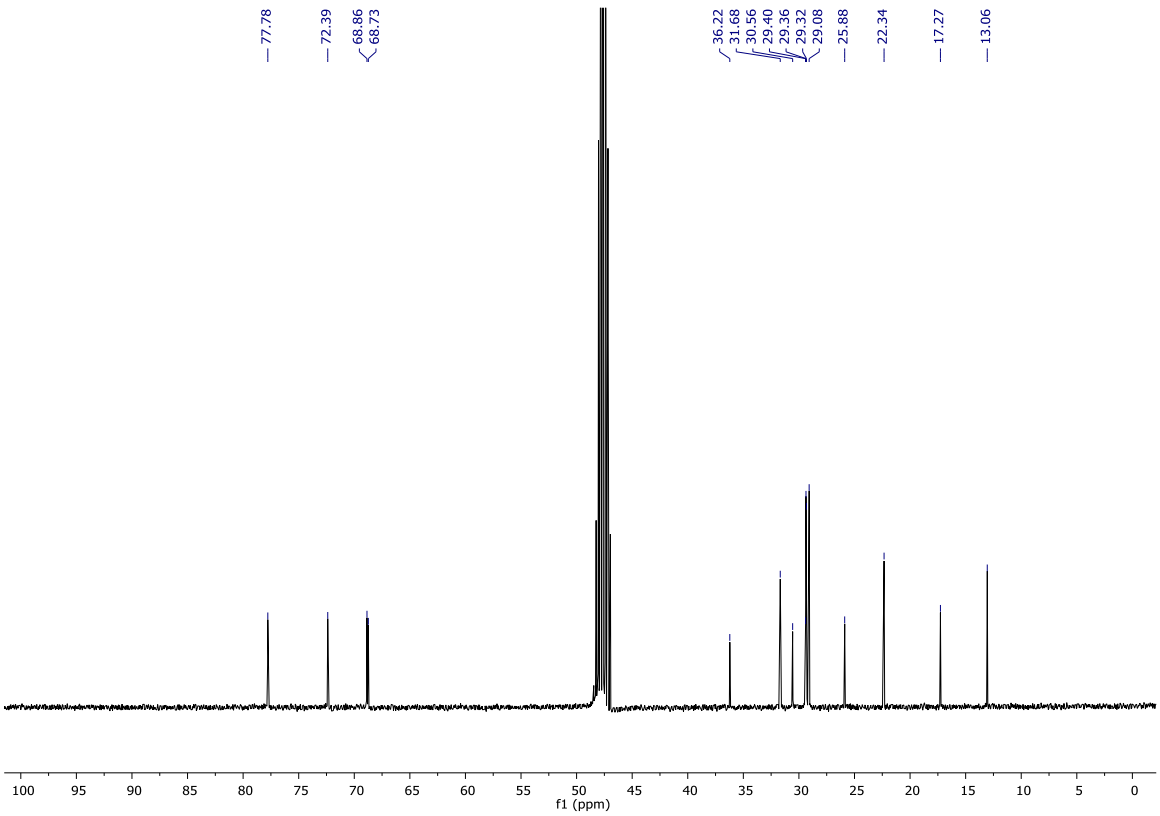
77.78
72.39
68.86
68.73
36.22
31.68
30.56
29.40
29.36
29.32
29.08
25.88
22.34
17.27
13.06
f1 (ppm)

C12H25
O
HO
HO
5

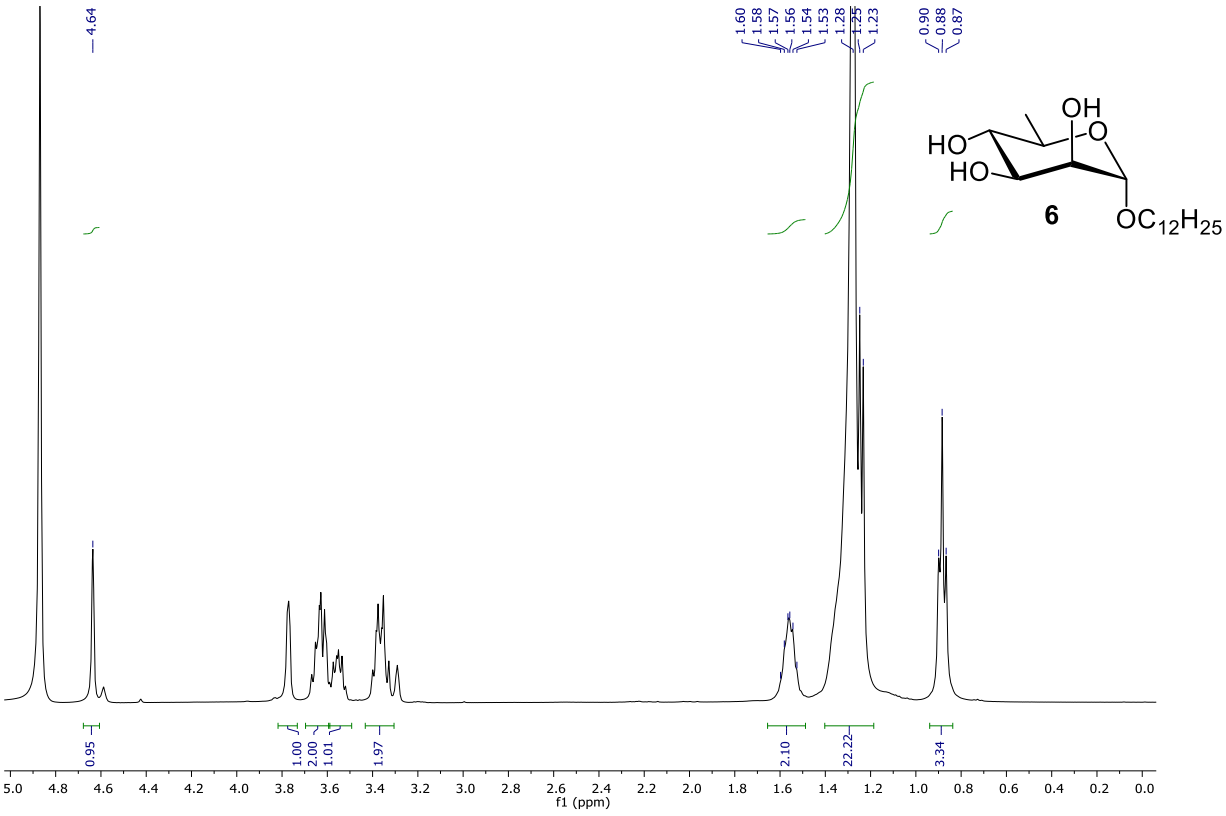
4.64
1.60
1.58
1.57
1.56
1.54
1.53
1.28
1.25
1.23
0.90
0.88
0.87
OH
HO
HO
O
6
$OC_{12}H_{25}$
0.95
1.00
2.00
1.01
1.97
2.10
22.22
3.34
f1 (ppm)

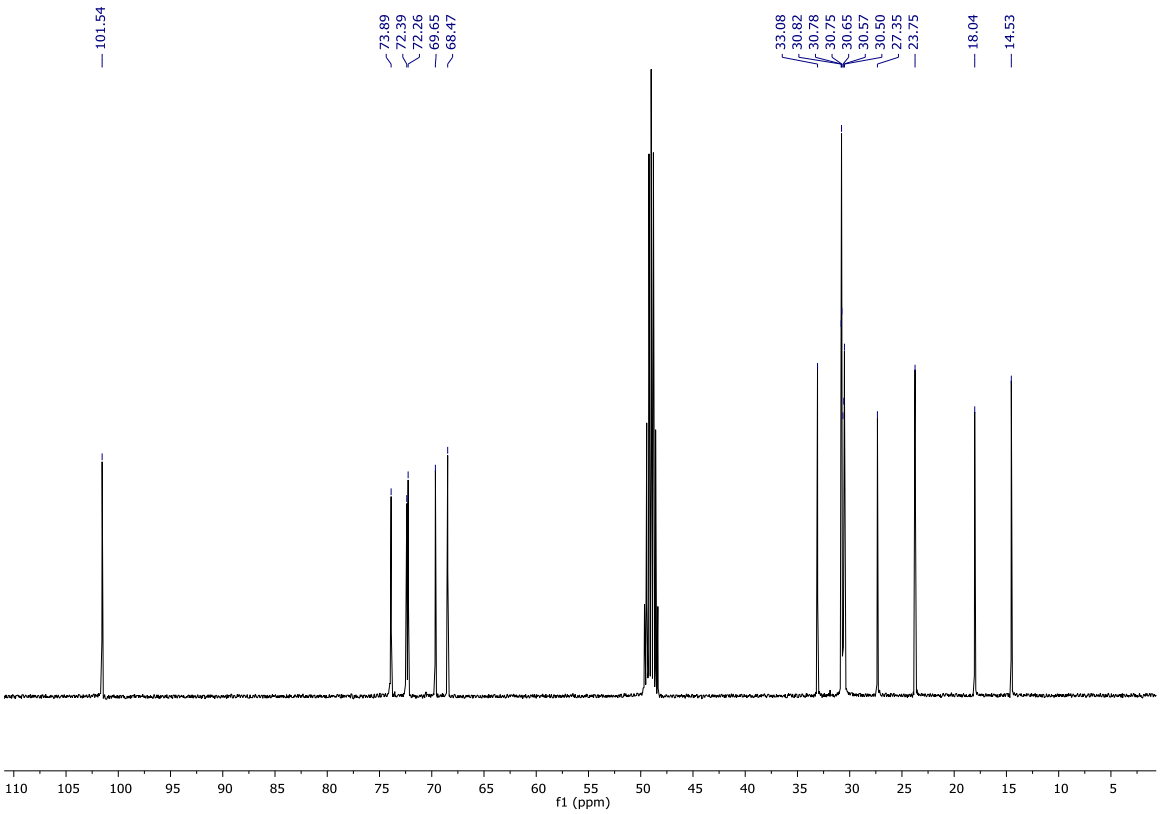
101.54
73.89
72.39
72.26
69.65
68.47
33.08
30.82
30.78
30.75
30.65
30.57
30.50
27.35
23.75
18.04
14.53
f1 (ppm)

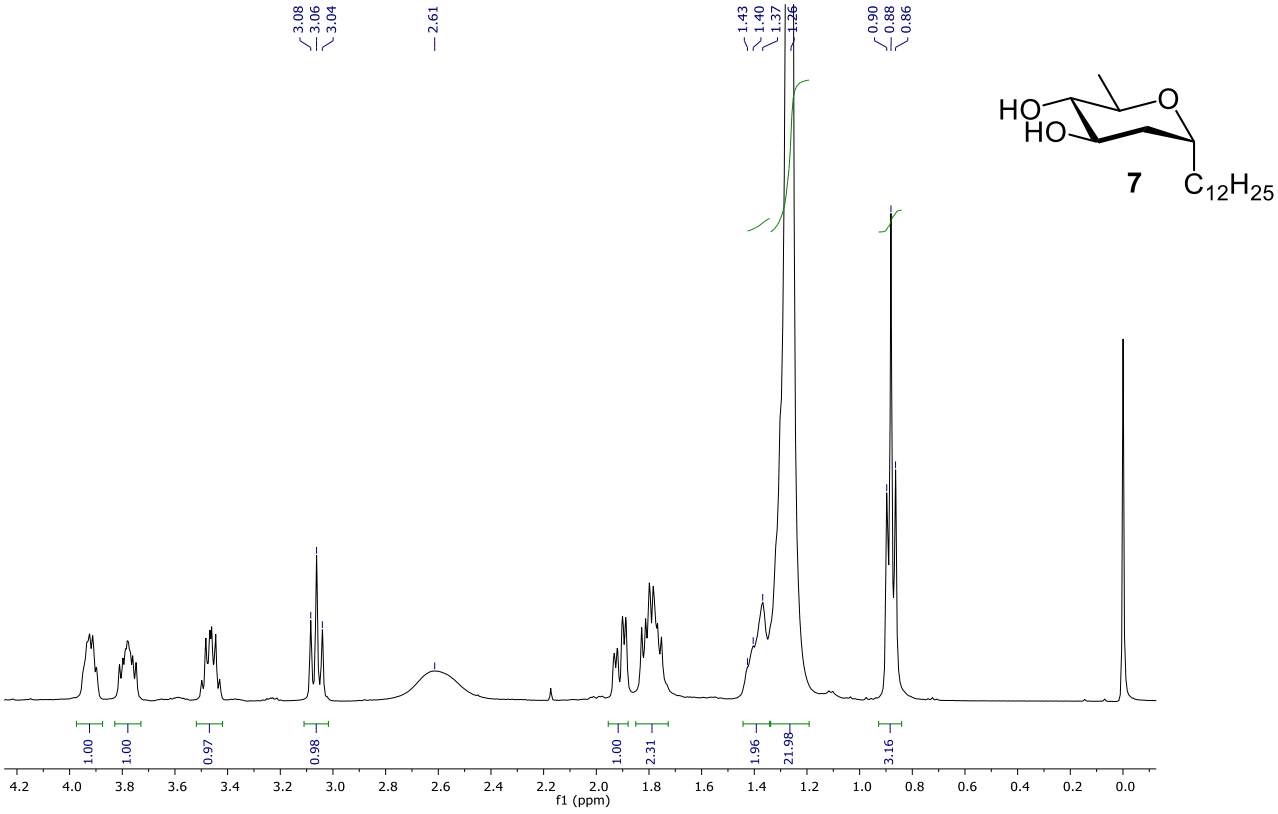
3.08
3.06
3.04
2.61
1.43
1.40
1.37
1.26
0.90
0.88
0.86
HO
HO
O
7
$C_{12}H_{25}$
1.00
1.00
0.97
0.98
1.00
2.31
1.96
21.98
3.16
f1 (ppm)

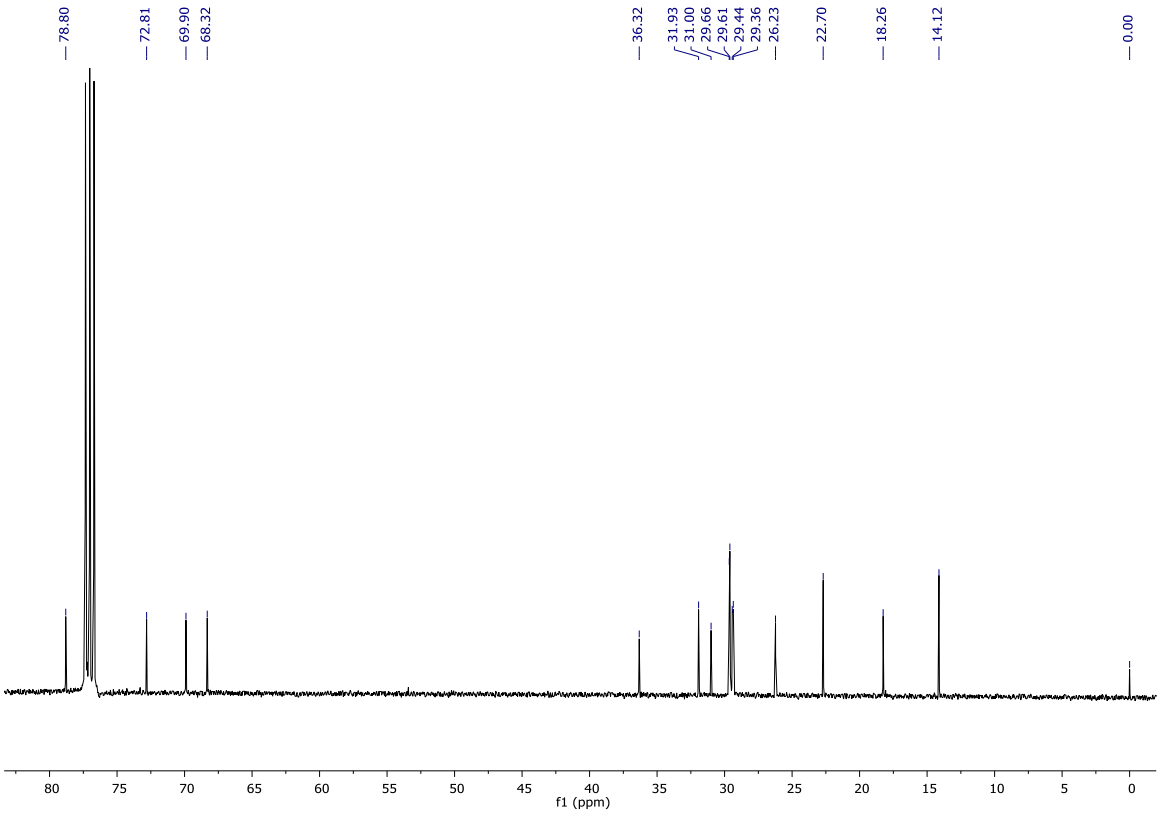
78.80
72.81
69.90
68.32
36.32
31.93
31.00
29.66
29.61
29.44
29.36
26.23
22.70
18.26
14.12
0.00
f1 (ppm)

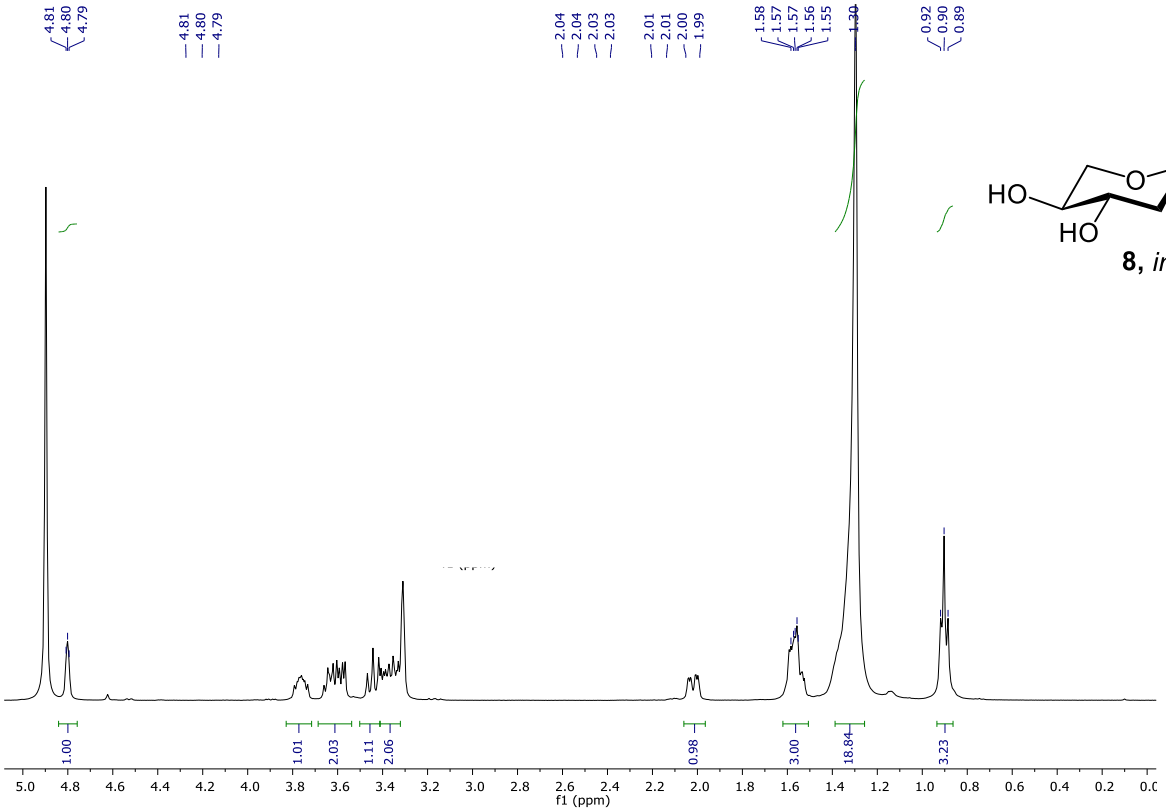
4.81
4.80
4.79
2.04
2.04
2.03
2.03
2.01
2.01
2.00
1.99
1.58
1.57
1.57
1.56
1.55
1.30
0.92
0.90
0.89
1.00
1.01
2.03
1.11
2.06
0.98
3.00
18.84
3.23
f1 (ppm)

OC12H25
HO
O
HO

8, *in MeOD*

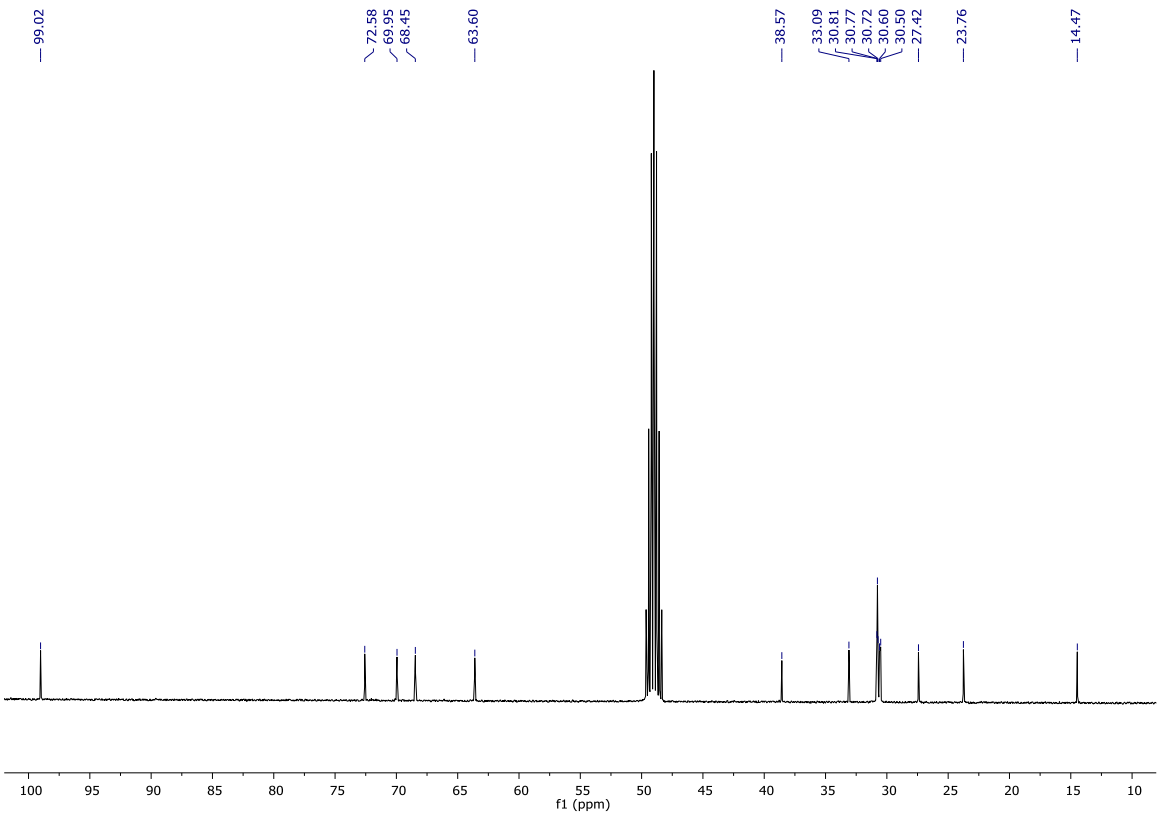
99.02
72.58
69.95
68.45
63.60
38.57
33.09
30.81
30.77
30.72
30.60
30.50
27.42
23.76
14.47
f1 (ppm)

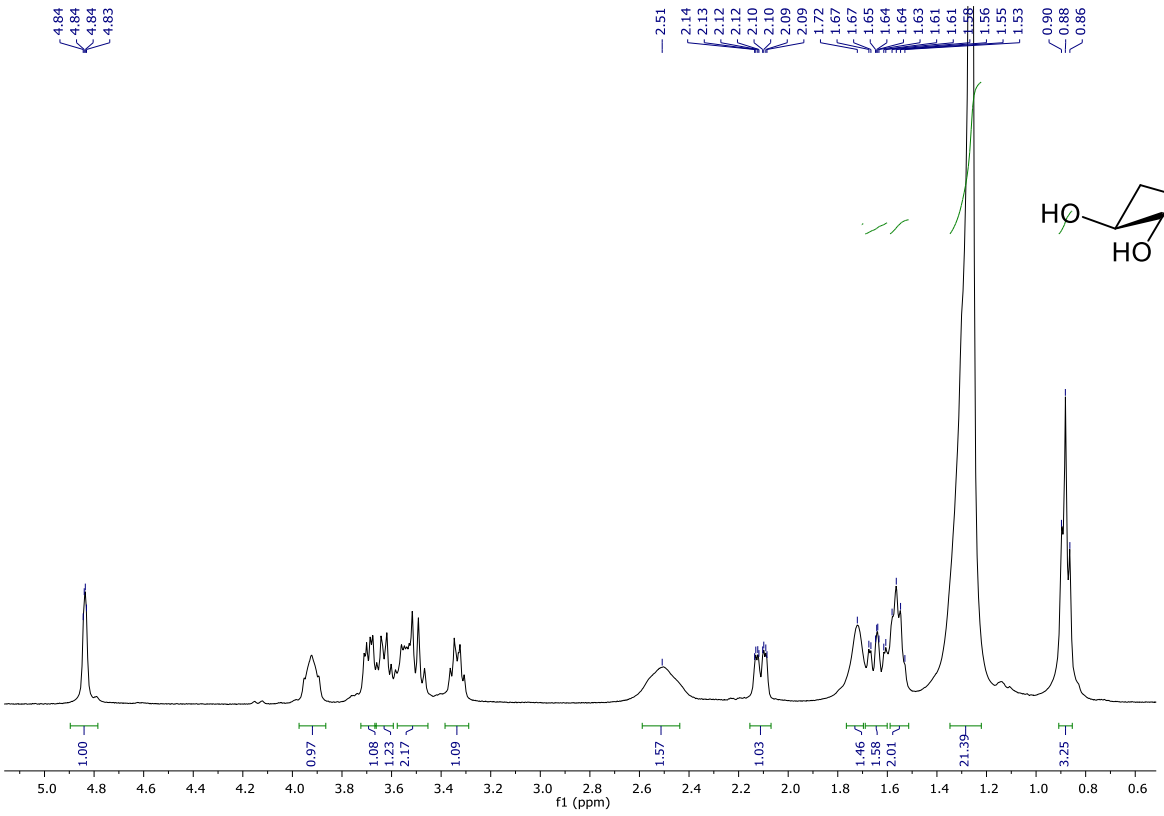
4.84
4.84
4.84
4.83
2.51
2.14
2.13
2.12
2.12
2.10
2.10
2.09
2.09
1.72
1.67
1.67
1.65
1.64
1.64
1.63
1.61
1.61
1.58
1.56
1.55
1.53
0.90
0.88
0.86
1.00
0.97
1.08
1.23
2.17
1.09
1.57
1.03
1.46
1.58
2.01
21.39
3.25
f1 (ppm)

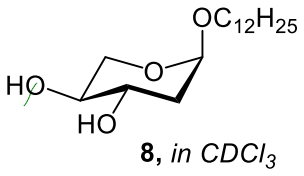
OC12H25
O
HO
HO

8, *in $CDCl_3$*

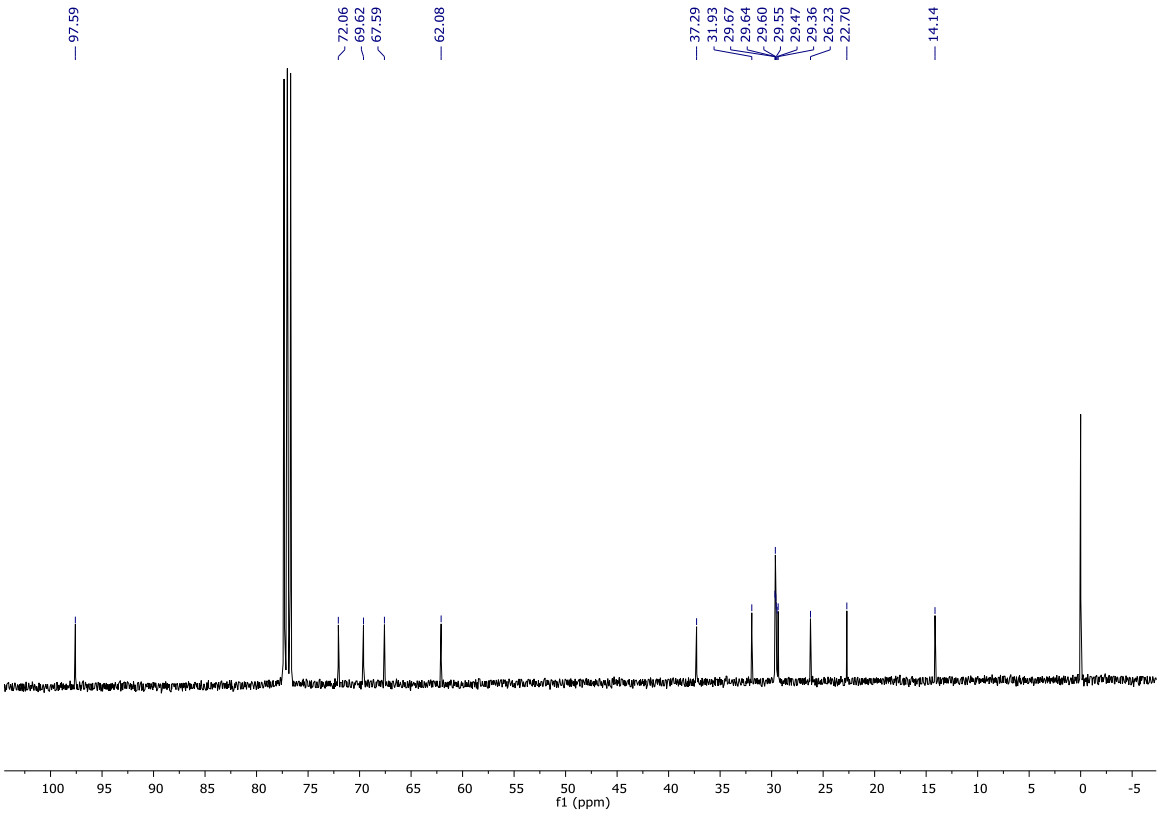
97.59
72.06
69.62
67.59
62.08
37.29
31.93
29.67
29.64
29.60
29.55
29.47
29.36
26.23
22.70
14.14
f1 (ppm)

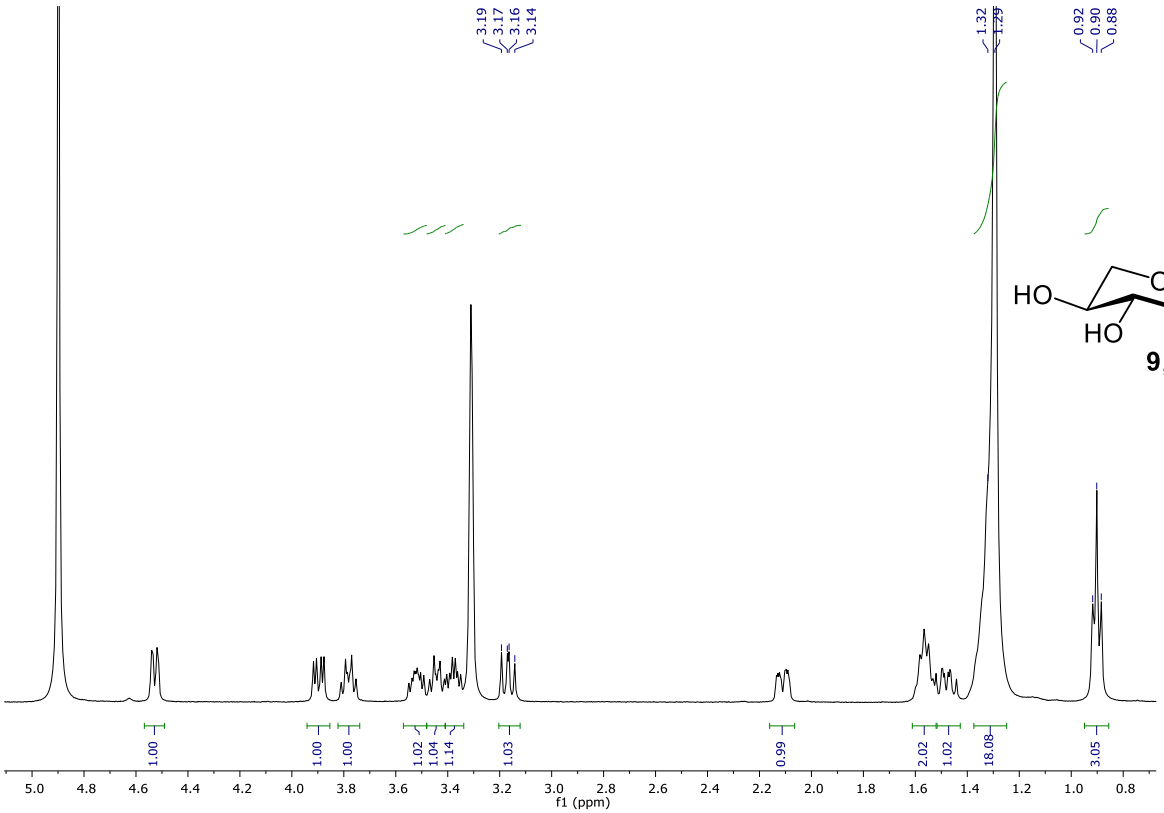
3.19
3.17
3.16
3.14
1.32
1.29
0.92
0.90
0.88
1.00
1.00
1.00
1.02
1.04
1.14
1.03
0.99
2.02
1.02
18.08
3.05
f1 (ppm)

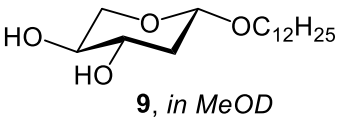
HO
O
OC12H25
HO

9, *in MeOD*

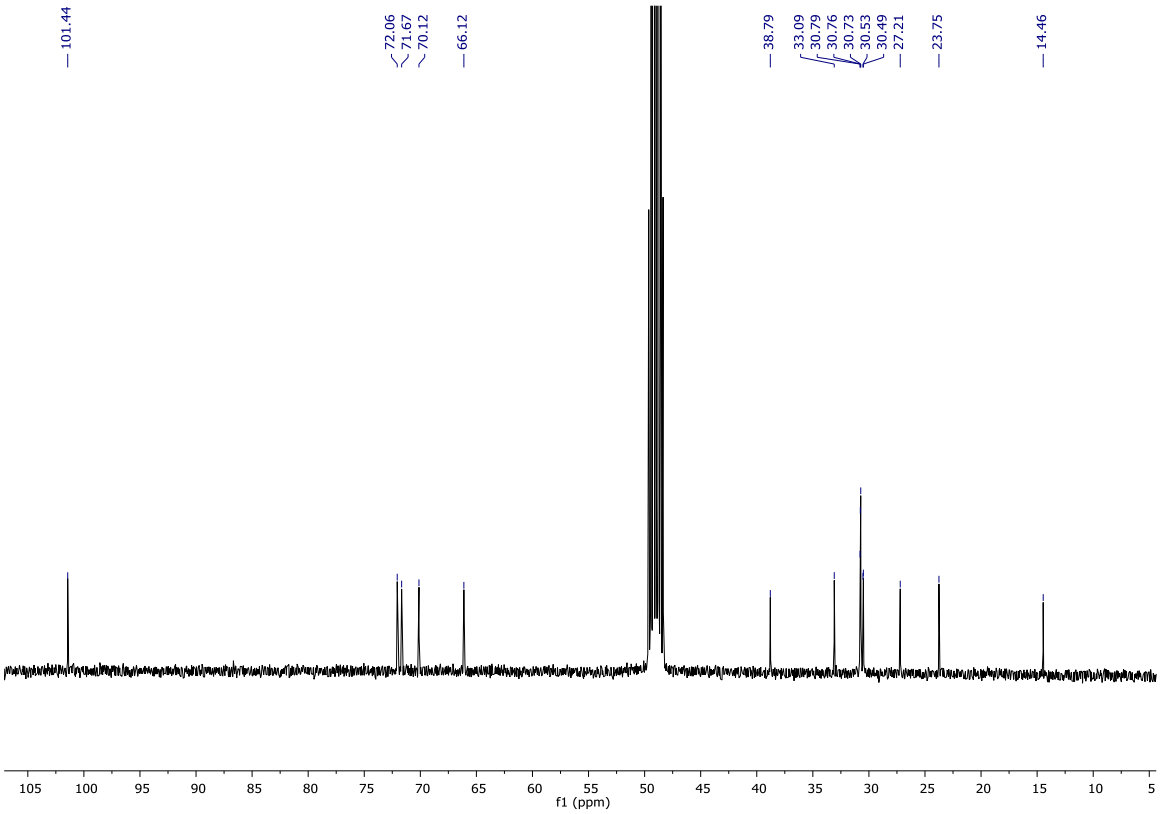
101.44
72.06
71.67
70.12
66.12
38.79
33.09
30.79
30.76
30.73
30.53
30.49
27.21
23.75
14.46
f1 (ppm)

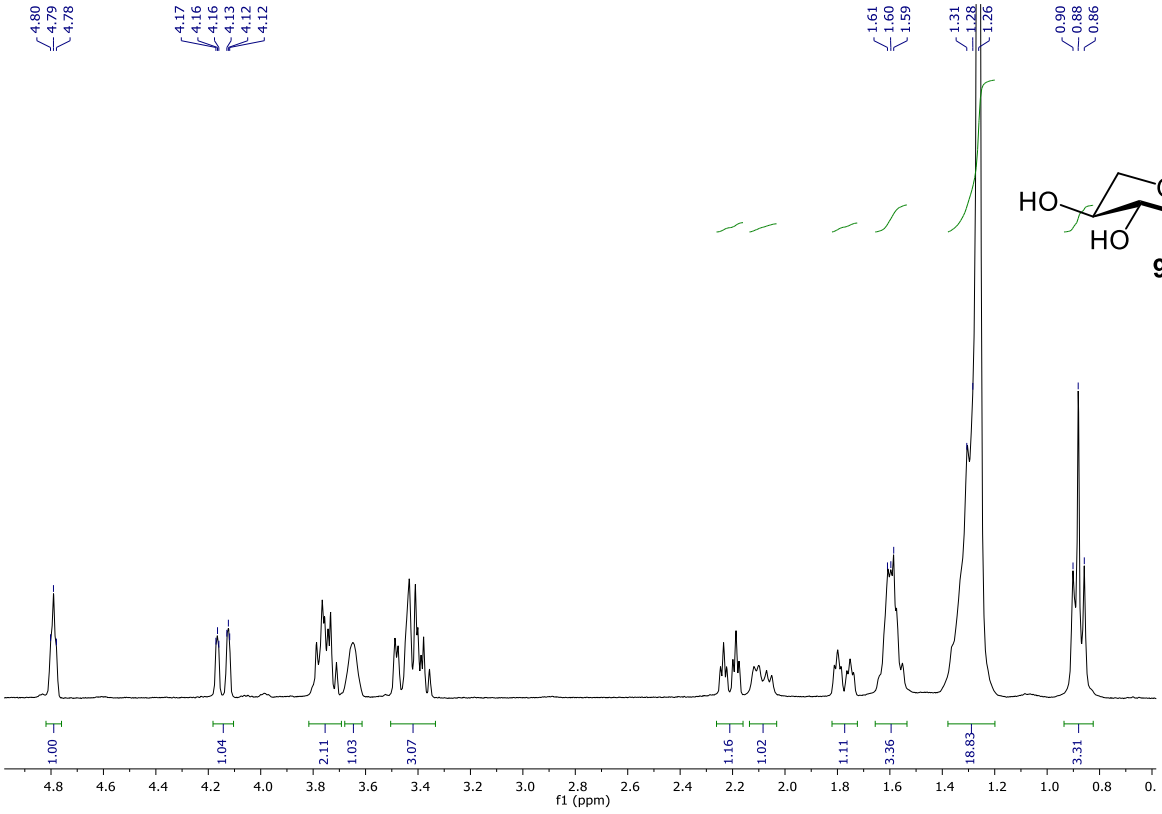
4.80
4.79
4.78
4.17
4.16
4.16
4.13
4.12
4.12
1.61
1.60
1.59
1.31
1.28
1.26
0.90
0.88
0.86
HO
O
OC12H25
HO
9, in CDCl3
1.00
1.04
2.11
1.03
3.07
1.16
1.02
1.11
3.36
18.83
3.31
f1 (ppm)

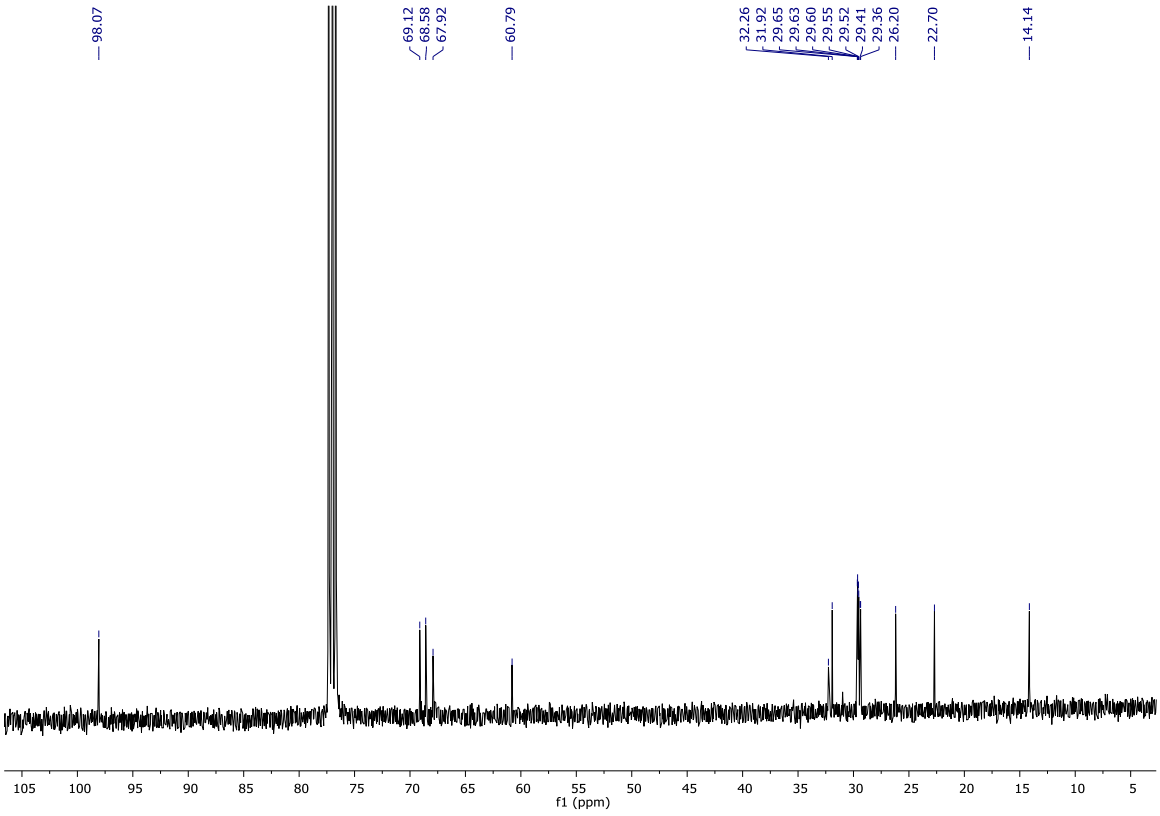
98.07
69.12
68.58
67.92
60.79
32.26
31.92
29.65
29.63
29.60
29.55
29.52
29.41
29.36
26.20
22.70
14.14
f1 (ppm)

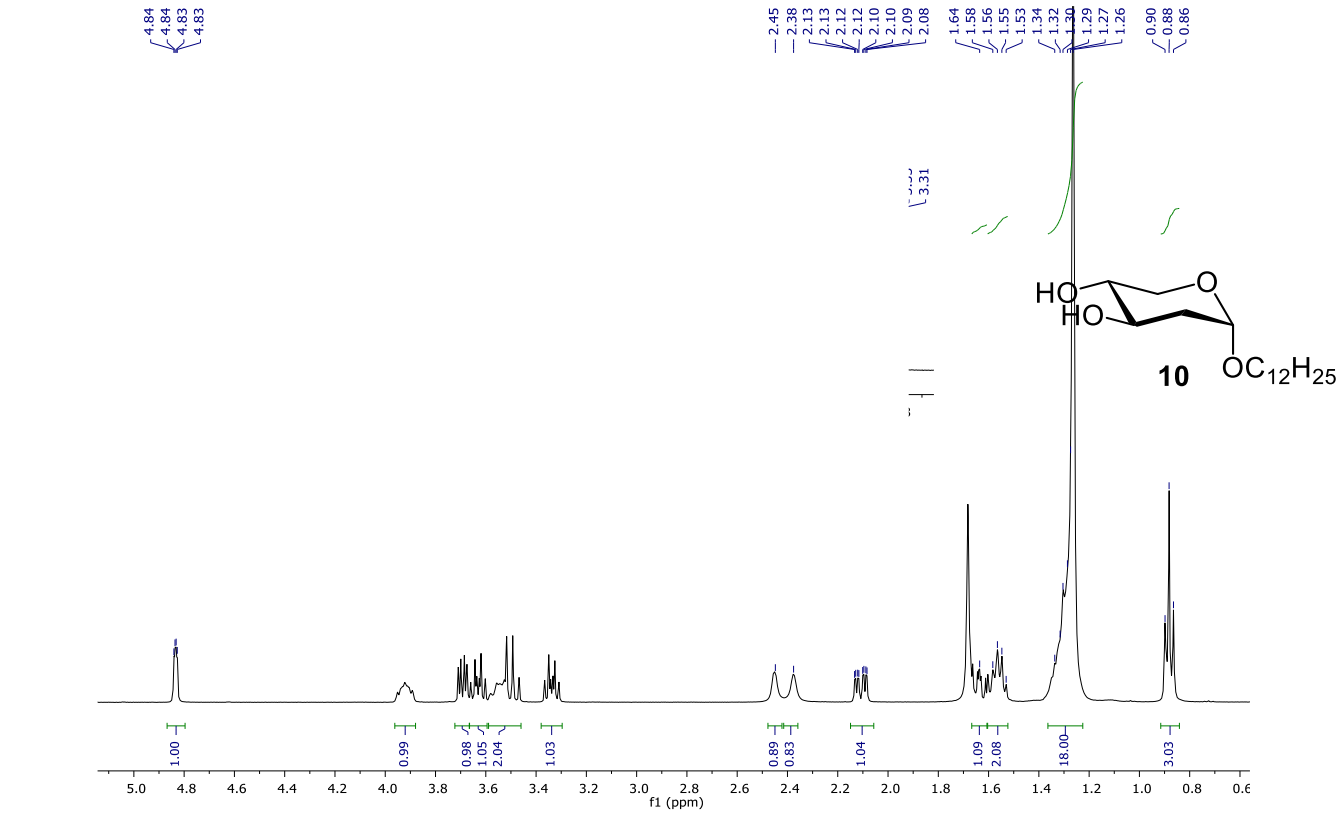
4.84
4.84
4.83
4.83
2.45
2.38
2.13
2.13
2.12
2.12
2.10
2.10
2.09
2.08
1.64
1.58
1.56
1.55
1.53
1.34
1.32
1.30
1.29
1.27
1.26
0.90
0.88
0.86
3.31
HO
HO
O
10
OC12H25
1.00
0.99
0.98
1.05
2.04
1.03
0.89
0.83
1.04
1.09
2.08
18.00
3.03
f1 (ppm)

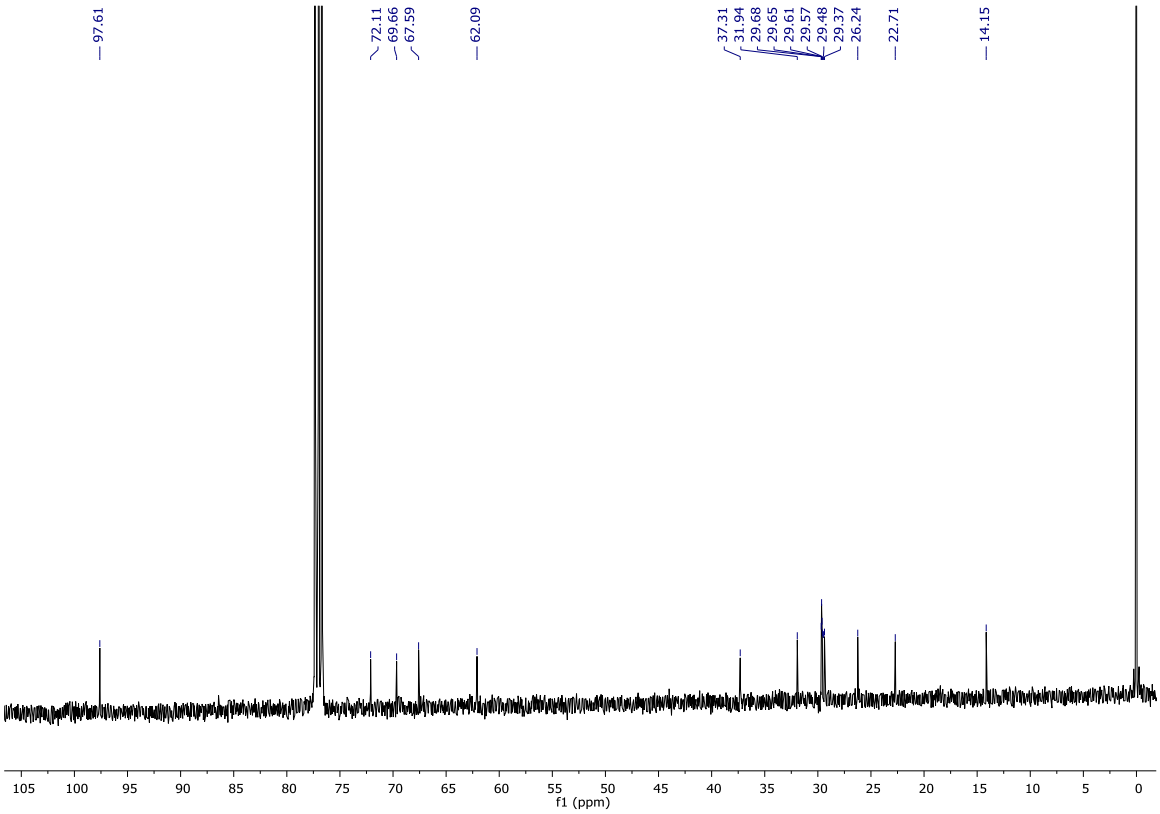
97.61
72.11
69.66
67.59
62.09
37.31
31.94
29.68
29.65
29.61
29.57
29.48
29.37
26.24
22.71
14.15
f1 (ppm)

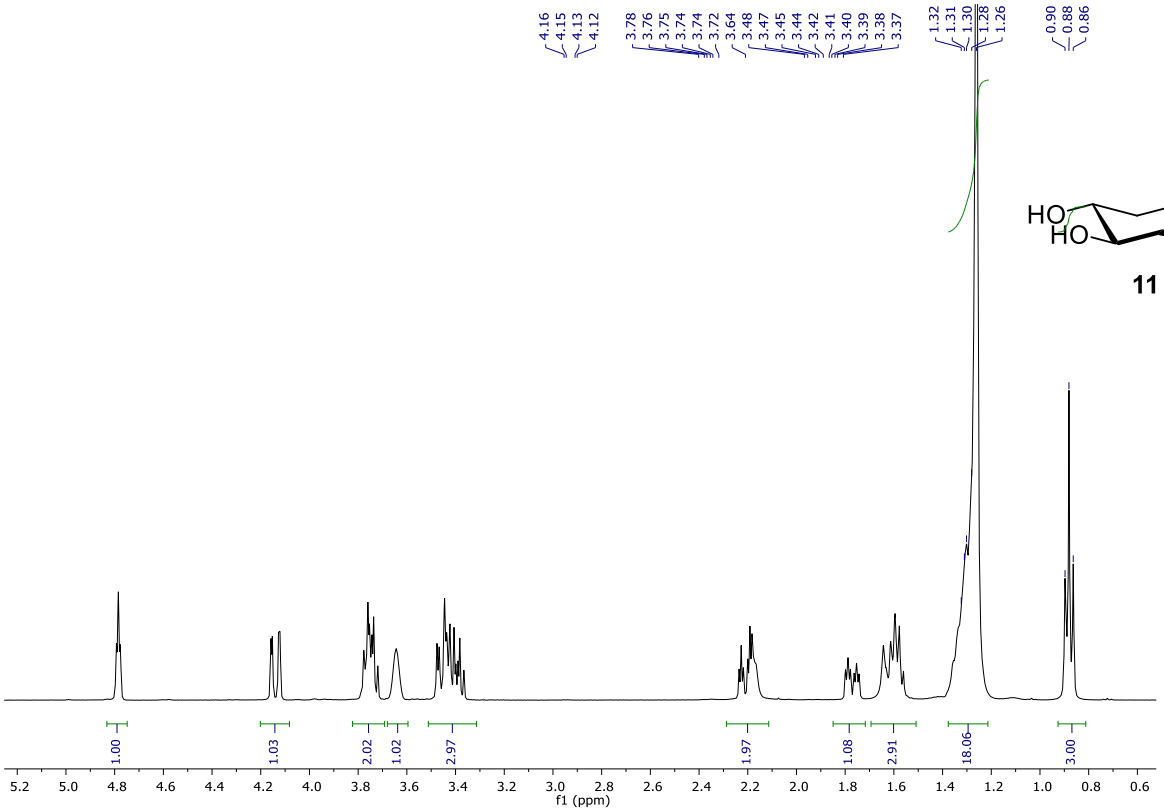
4.16
4.15
4.13
4.12
3.78
3.76
3.75
3.74
3.74
3.72
3.64
3.48
3.47
3.45
3.44
3.42
3.41
3.40
3.39
3.38
3.37
1.32
1.31
1.30
1.28
1.26
0.90
0.88
0.86
HO
HO
O
OC12H25
11
1.00
1.03
2.02
1.02
2.97
1.97
1.08
2.91
18.06
3.00
f1 (ppm)

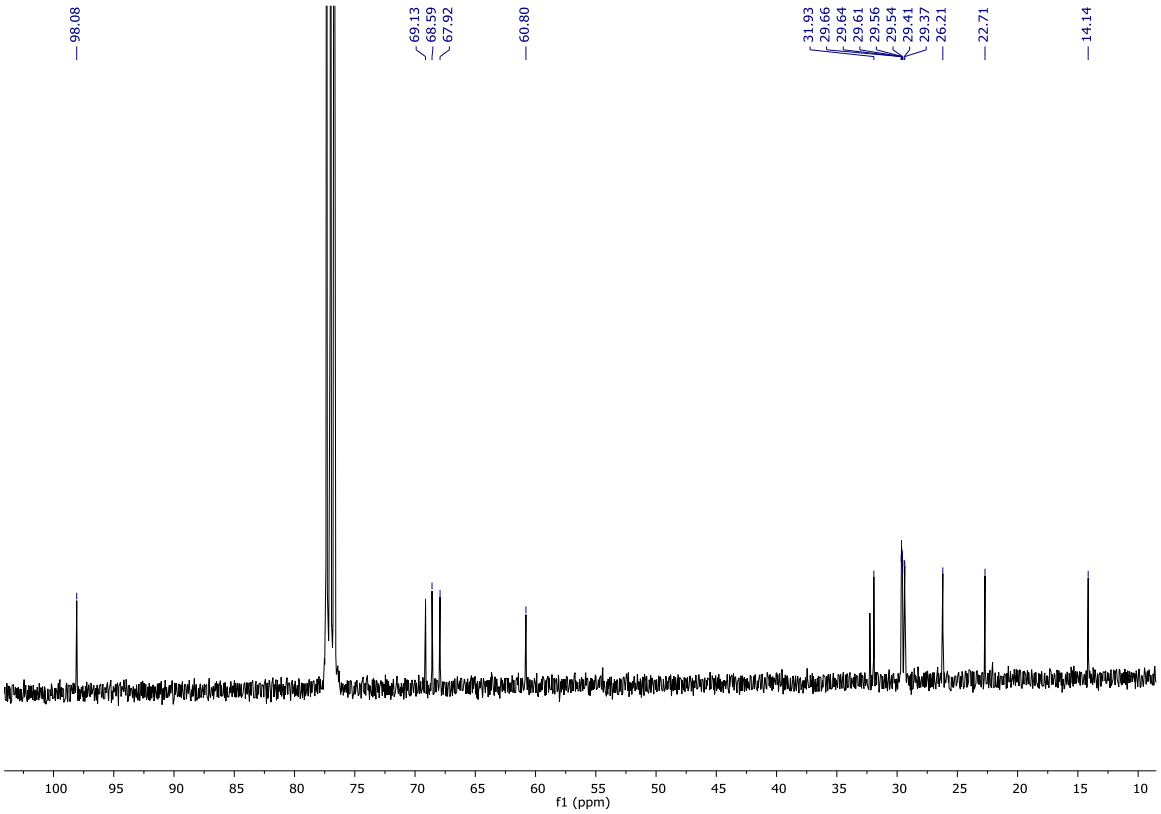
98.08
69.13
68.59
67.92
60.80
31.93
29.66
29.64
29.61
29.56
29.54
29.41
29.37
26.21
22.71
14.14
f1 (ppm)

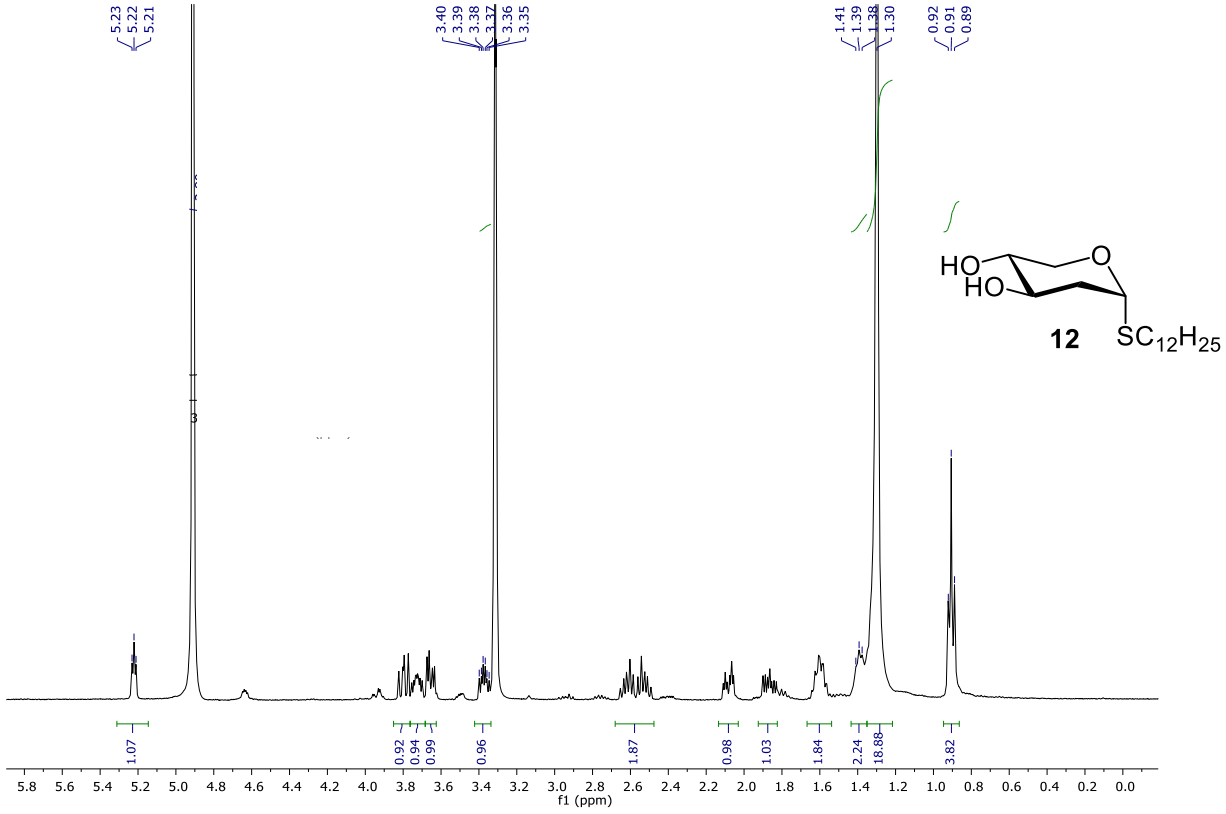
5.23
5.22
5.21
3.40
3.39
3.38
3.37
3.36
3.35
1.41
1.39
1.38
1.30
0.92
0.91
0.89
HO
HO
O
12
SC12H25
1.07
0.92
0.94
0.99
0.96
1.87
0.98
1.03
1.84
2.24
18.88
3.82
f1 (ppm)

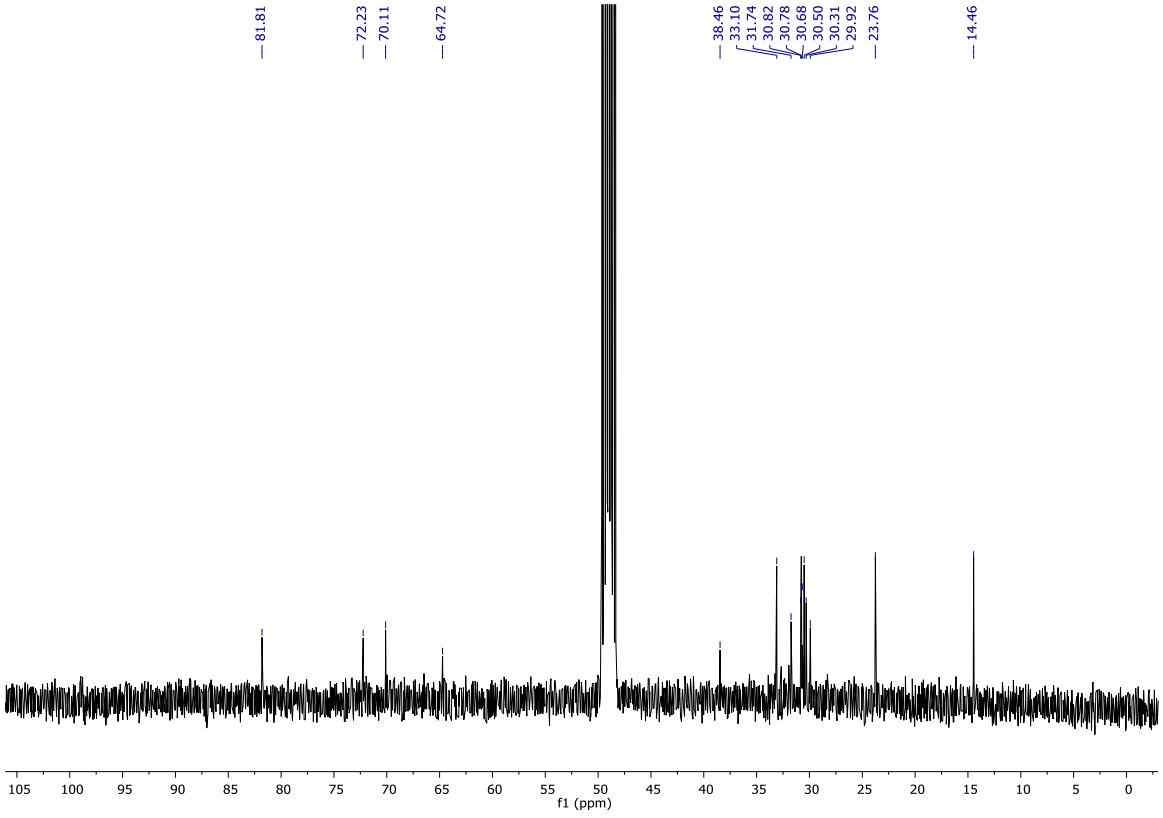
81.81
72.23
70.11
64.72
38.46
33.10
31.74
30.82
30.78
30.68
30.50
30.31
29.92
23.76
14.46
f1 (ppm)

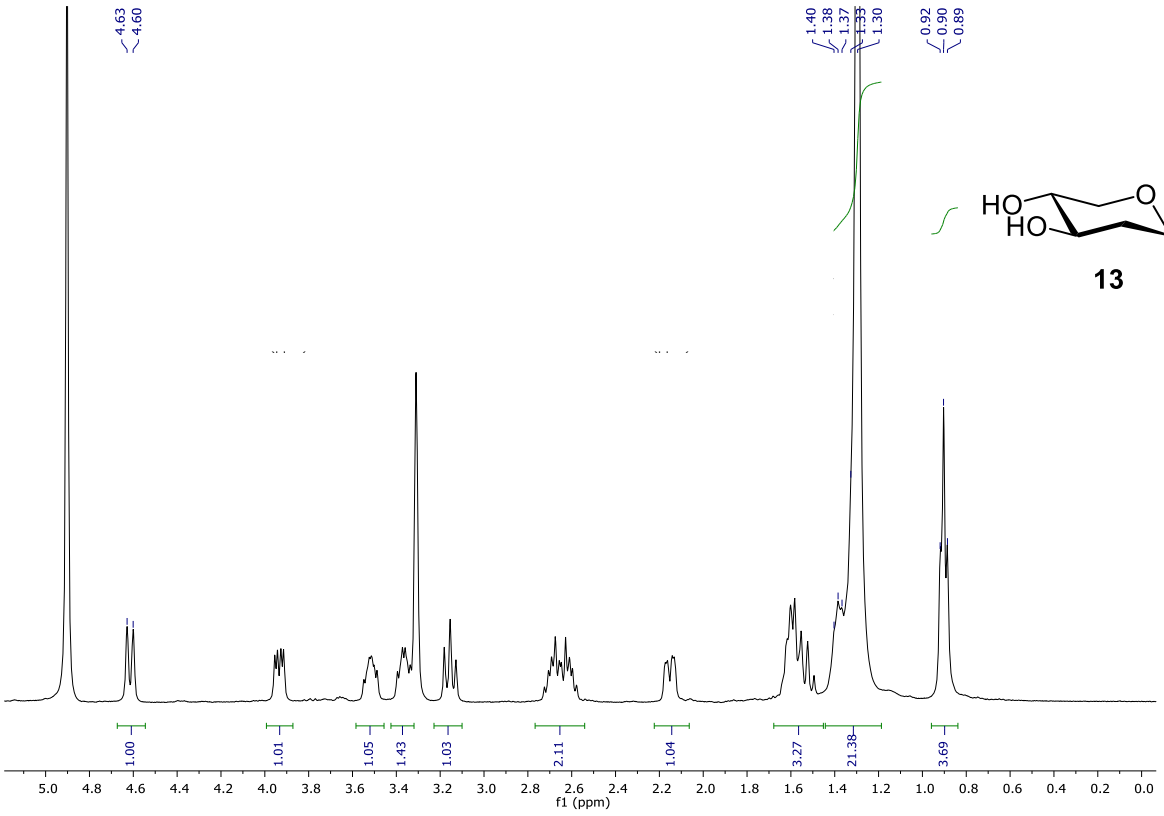
4.63
4.60
1.40
1.38
1.37
1.35
1.30
0.92
0.90
0.89
1.00
1.01
1.05
1.43
1.03
2.11
1.04
3.27
21.38
3.69
f1 (ppm)

HO
HO
O
SC12H25

13

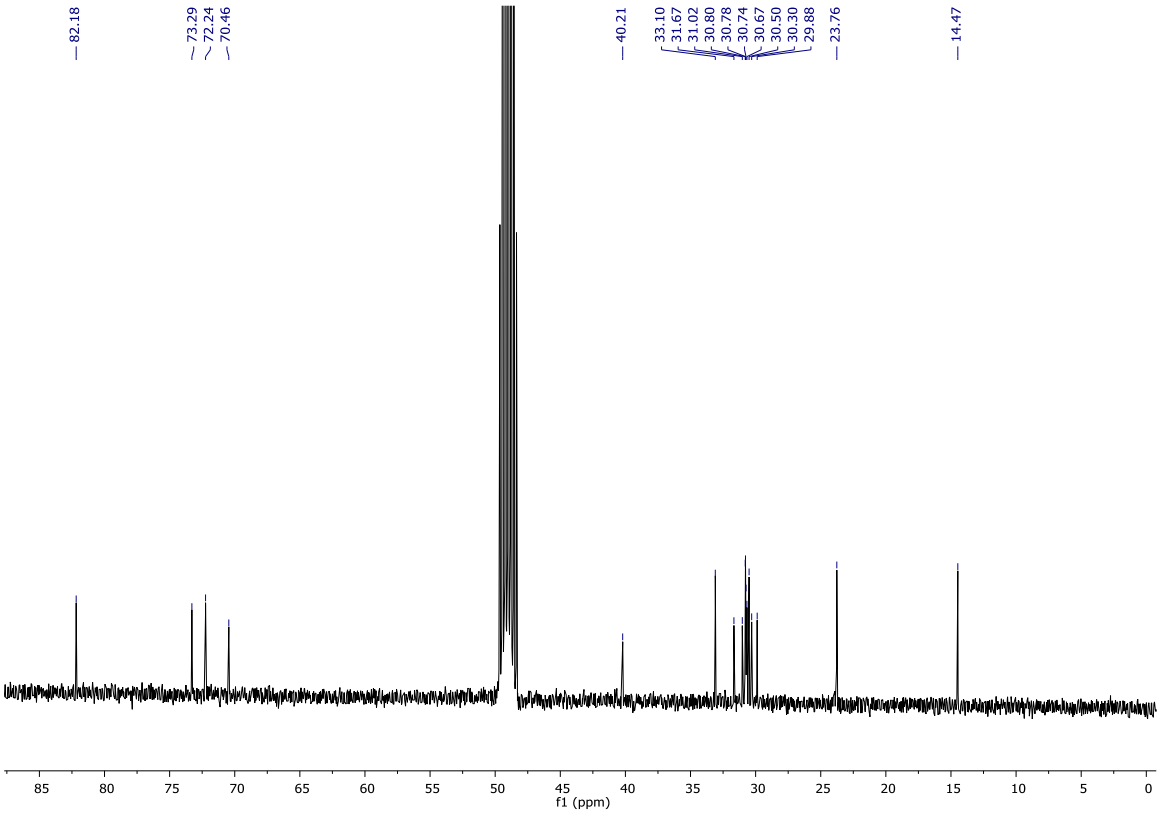
82.18
73.29
72.24
70.46
40.21
33.10
31.67
31.02
30.80
30.78
30.74
30.67
30.50
30.30
29.88
23.76
14.47
f1 (ppm)

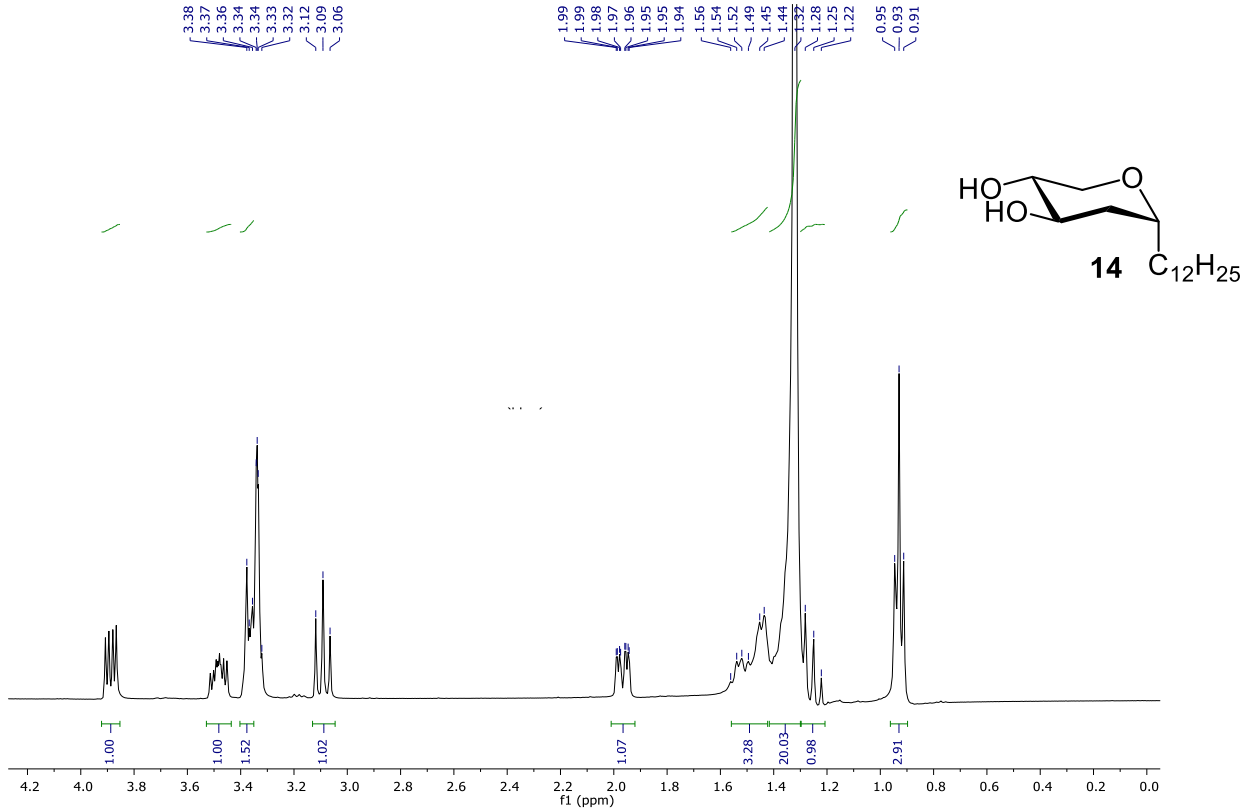
3.38
3.37
3.36
3.34
3.34
3.33
3.32
3.12
3.09
3.06
1.99
1.99
1.98
1.97
1.96
1.95
1.95
1.94
1.56
1.54
1.52
1.49
1.45
1.44
1.32
1.28
1.25
1.22
0.95
0.93
0.91
HO
HO
O
14
$C_{12}H_{25}$
1.00
1.00
1.52
1.02
1.07
3.28
20.03
0.98
2.91
f1 (ppm)

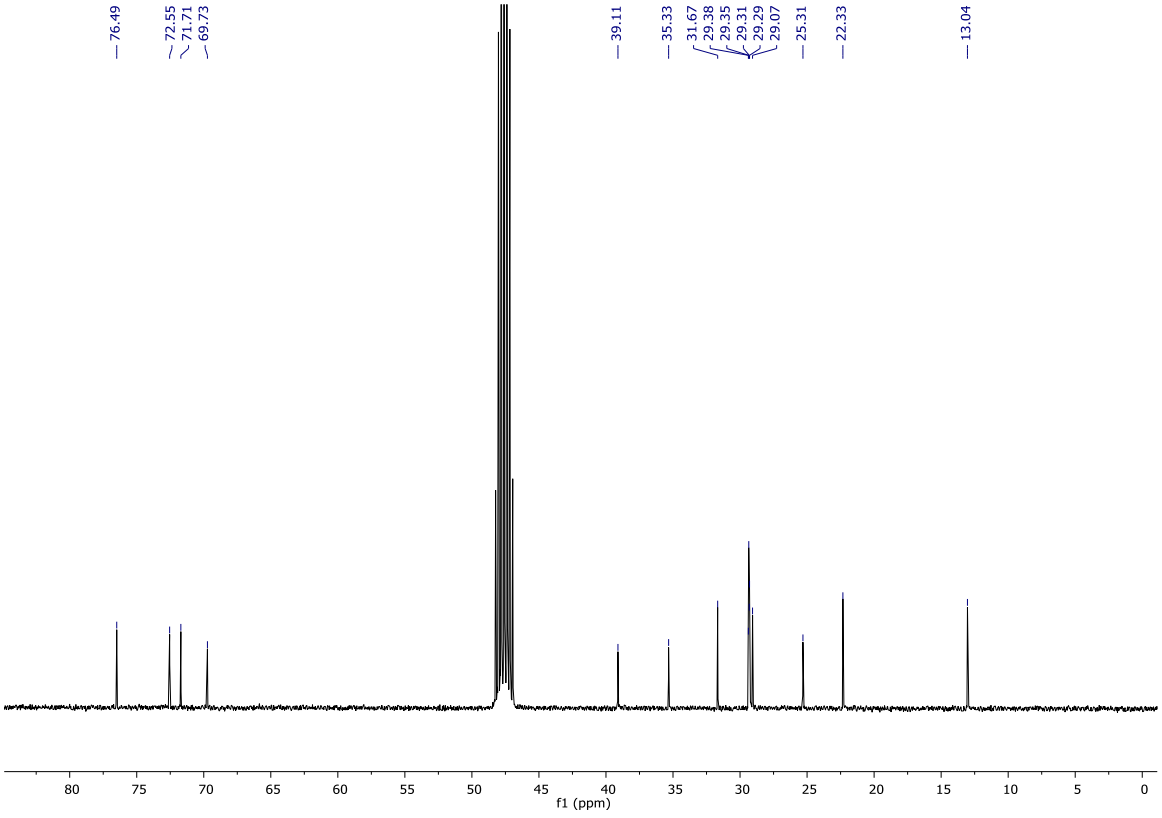
76.49
72.55
71.71
69.73
39.11
35.33
31.67
29.38
29.35
29.31
29.29
29.07
25.31
22.33
13.04
f1 (ppm)

Annex 3. *^{1}H and ^{13}C of final products described in chapter 4*

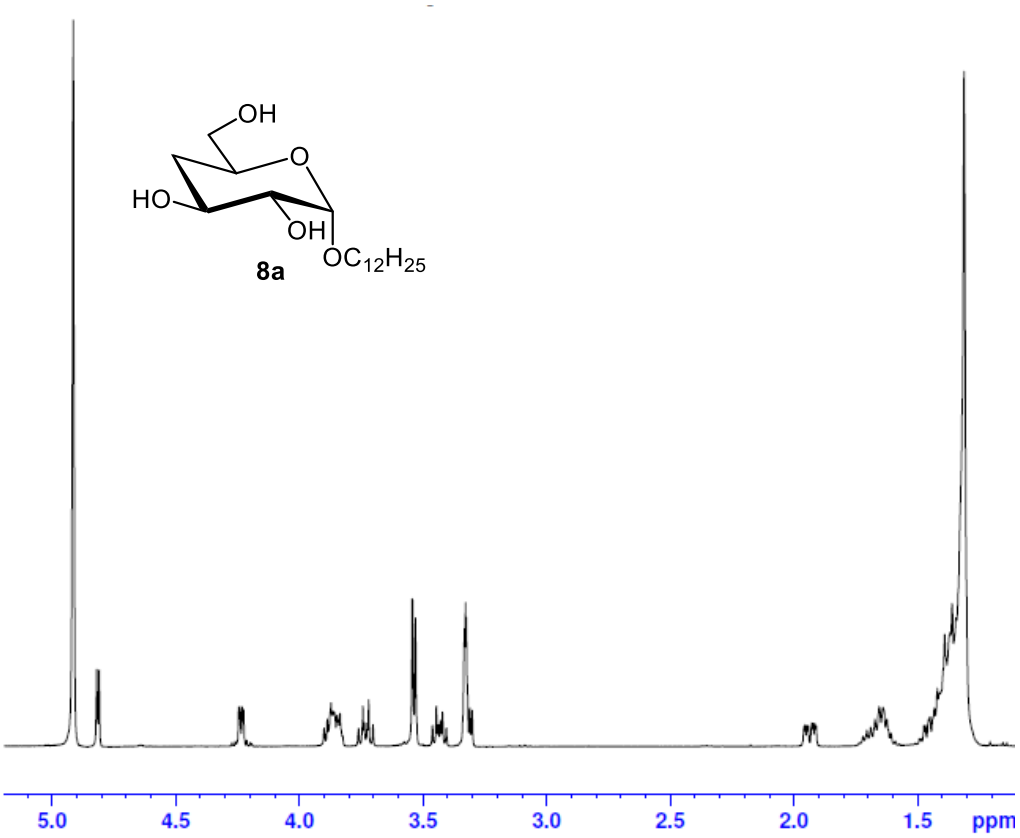

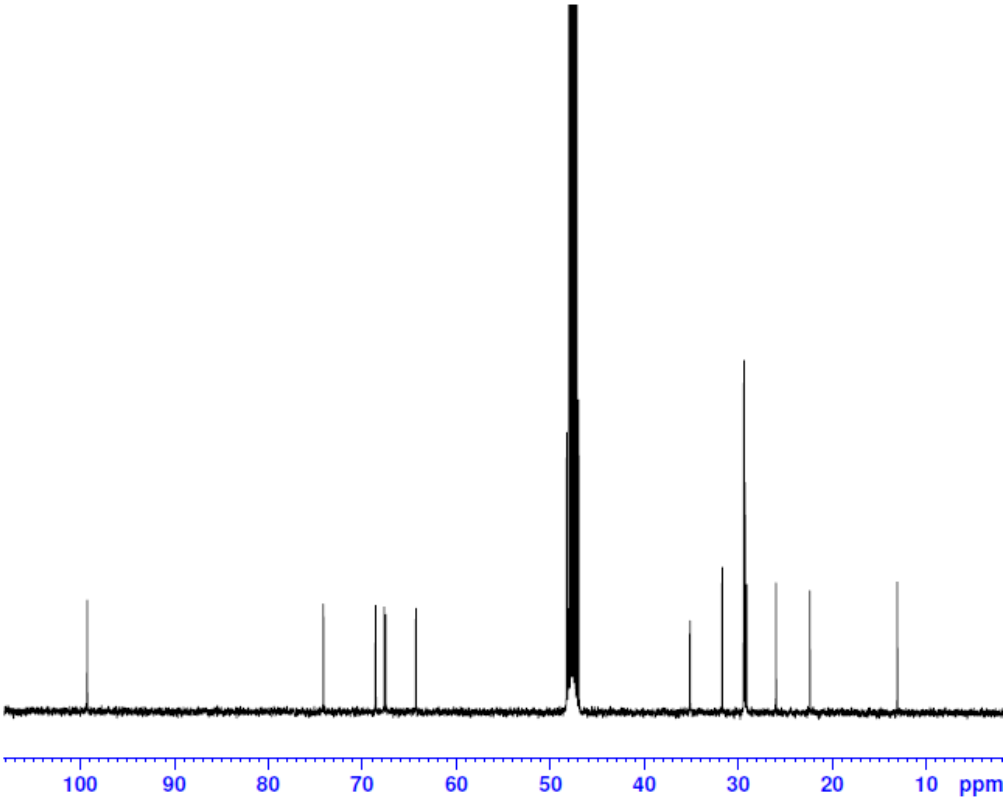

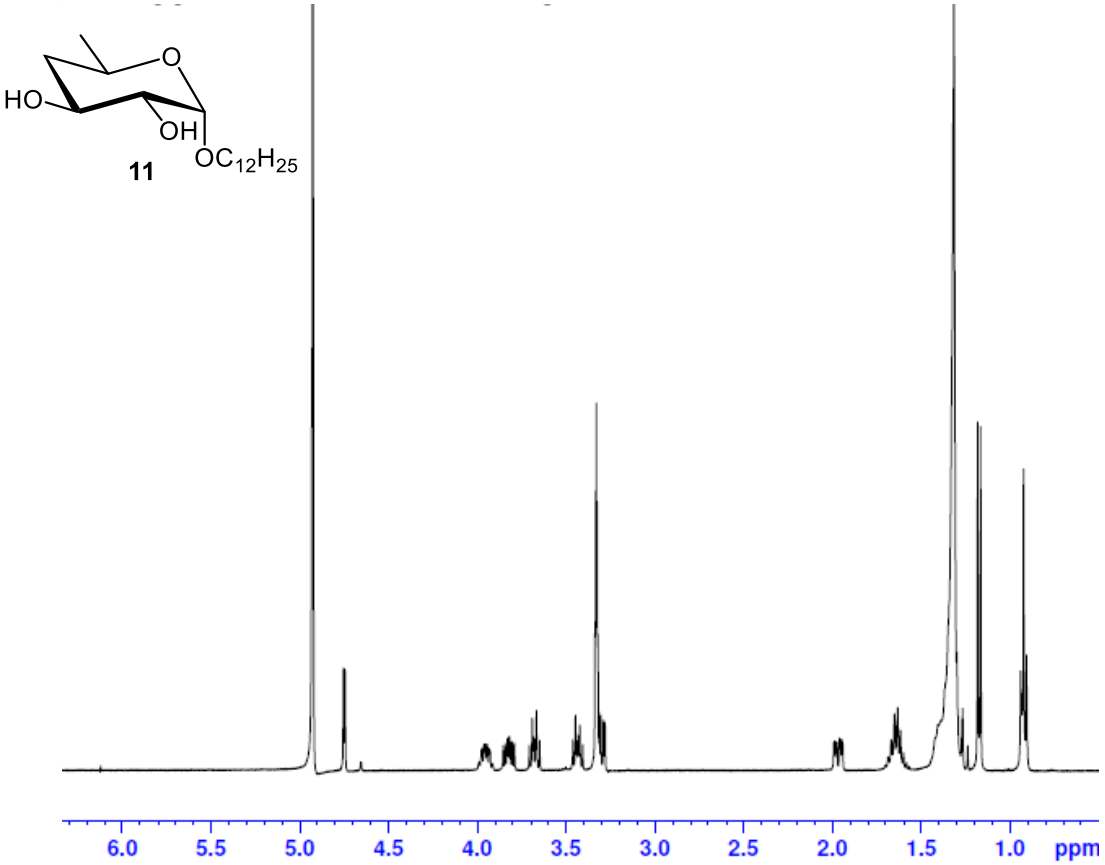
HO
O
OH
OC12H25
11
6.0
5.5
5.0
4.5
4.0
3.5
3.0
2.5
2.0
1.5
1.0
ppm

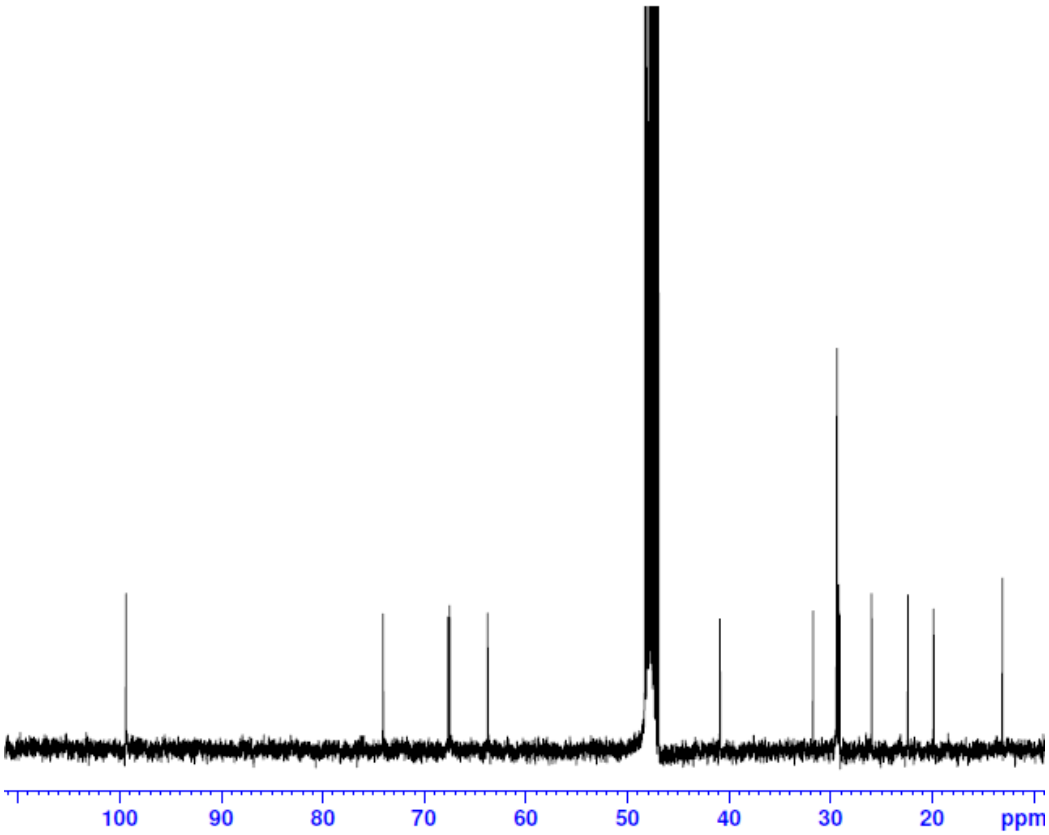
100
90
80
70
60
50
40
30
20
ppm

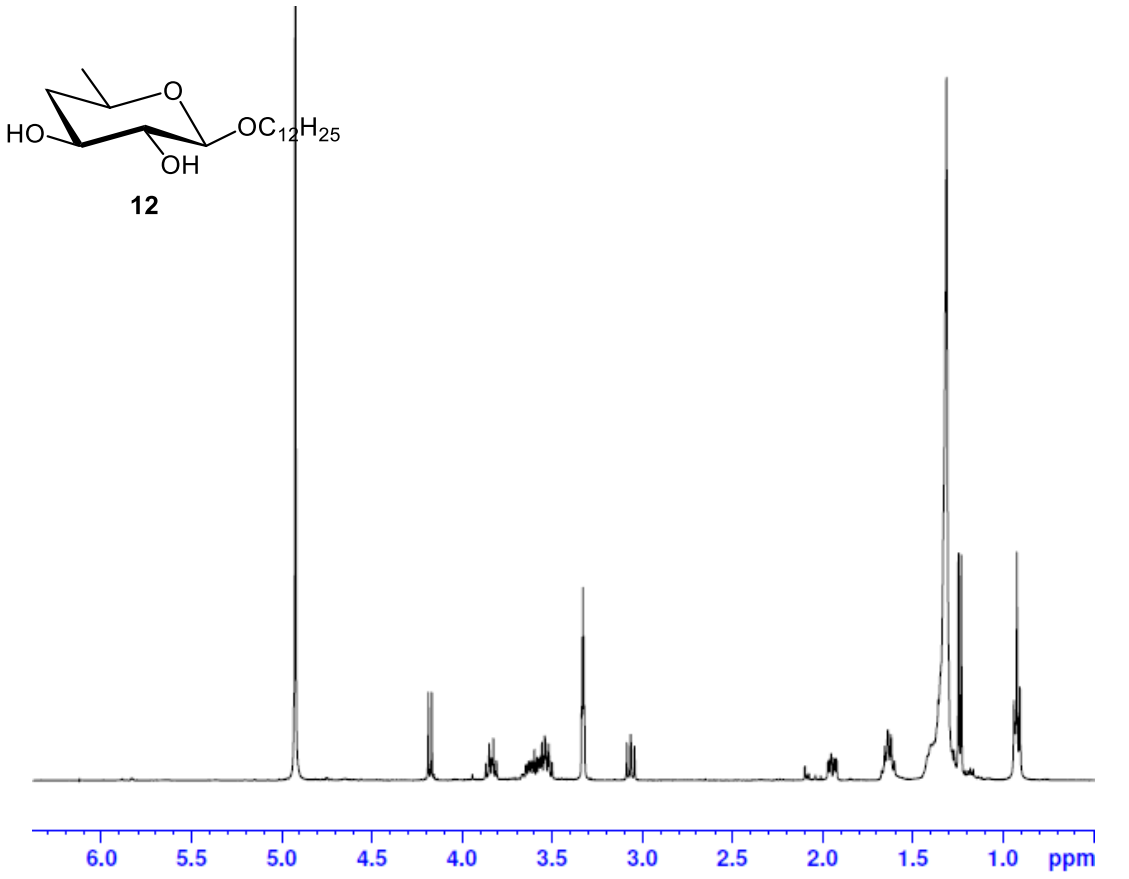
HO
O
OC12H25
OH
6.0
5.5
5.0
4.5
4.0
3.5
3.0
2.5
2.0
1.5
1.0
ppm

12

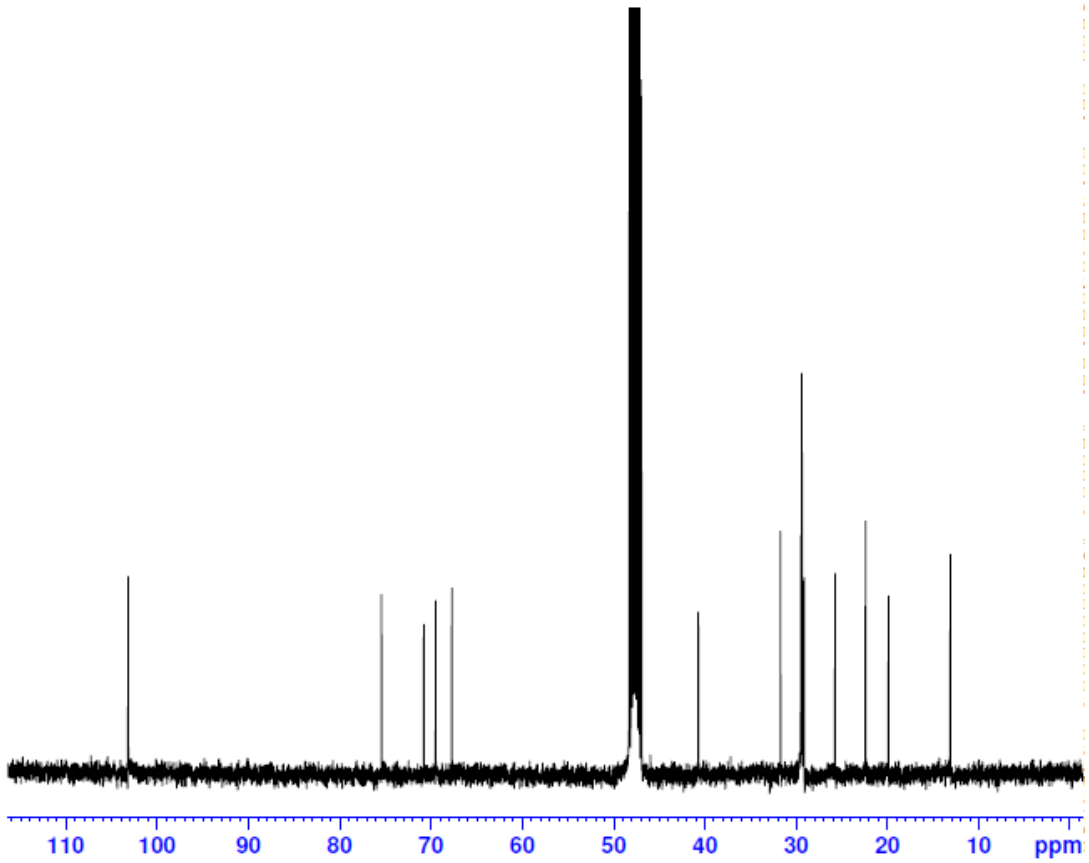
110
100
90
80
70
60
50
40
30
20
10
ppm

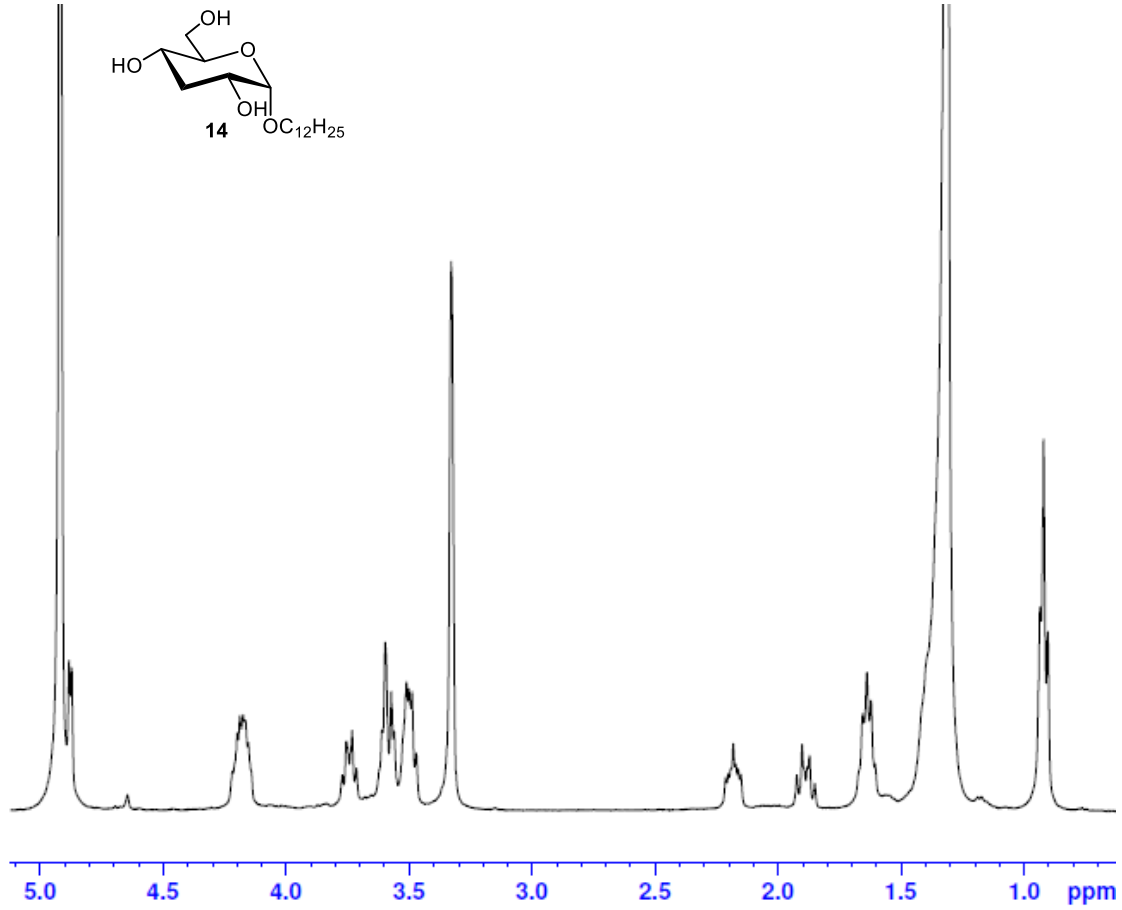
OH
HO
O
OH
OC12H25
14
5.0
4.5
4.0
3.5
3.0
2.5
2.0
1.5
1.0
ppm

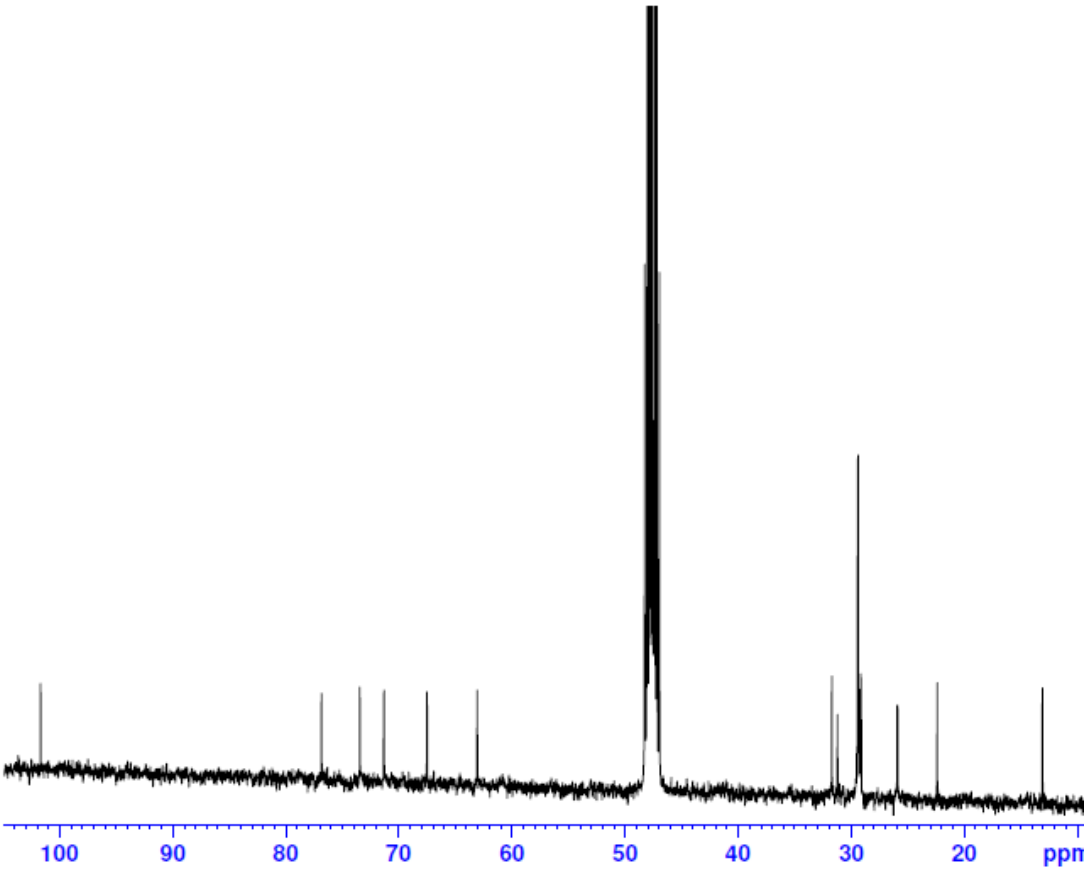
100
90
80
70
60
50
40
30
20
ppm

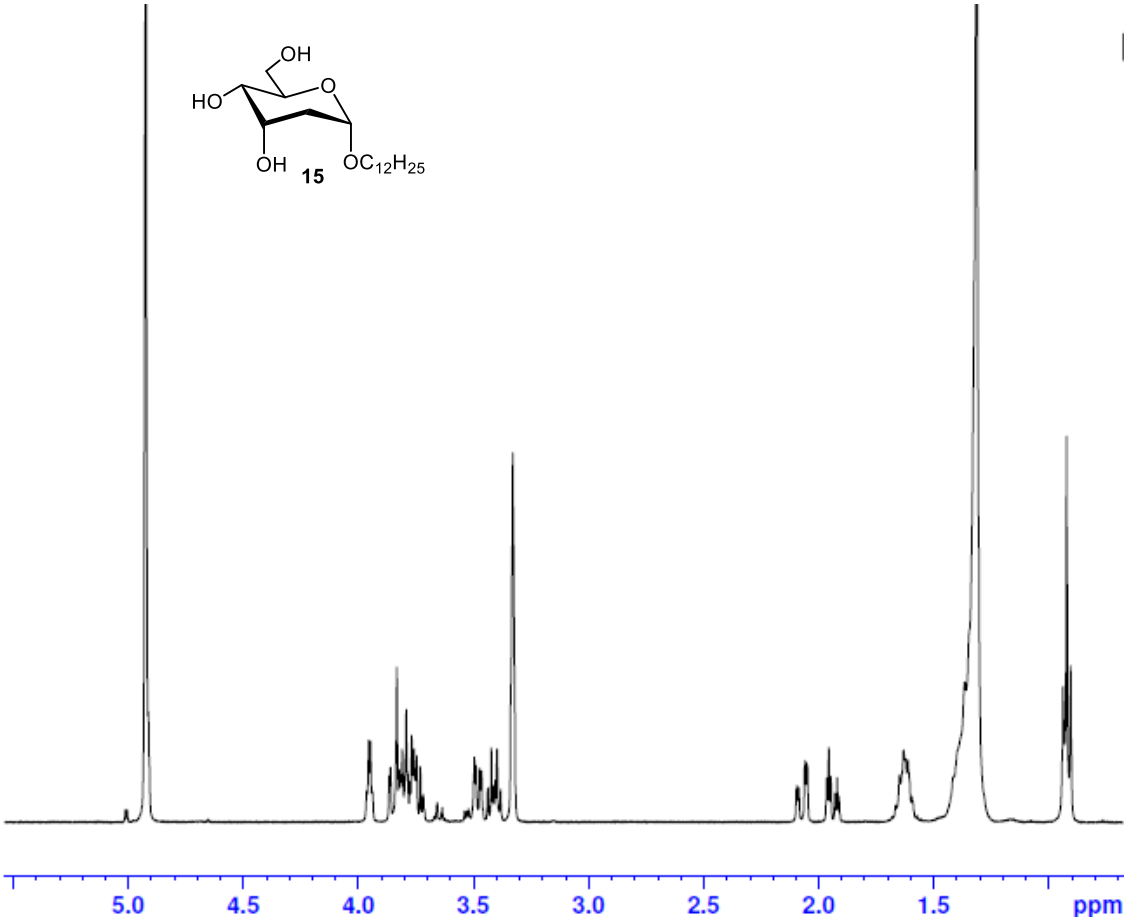
OH
HO
O
OH
OC12H25
15
5.0
4.5
4.0
3.5
3.0
2.5
2.0
1.5
ppm

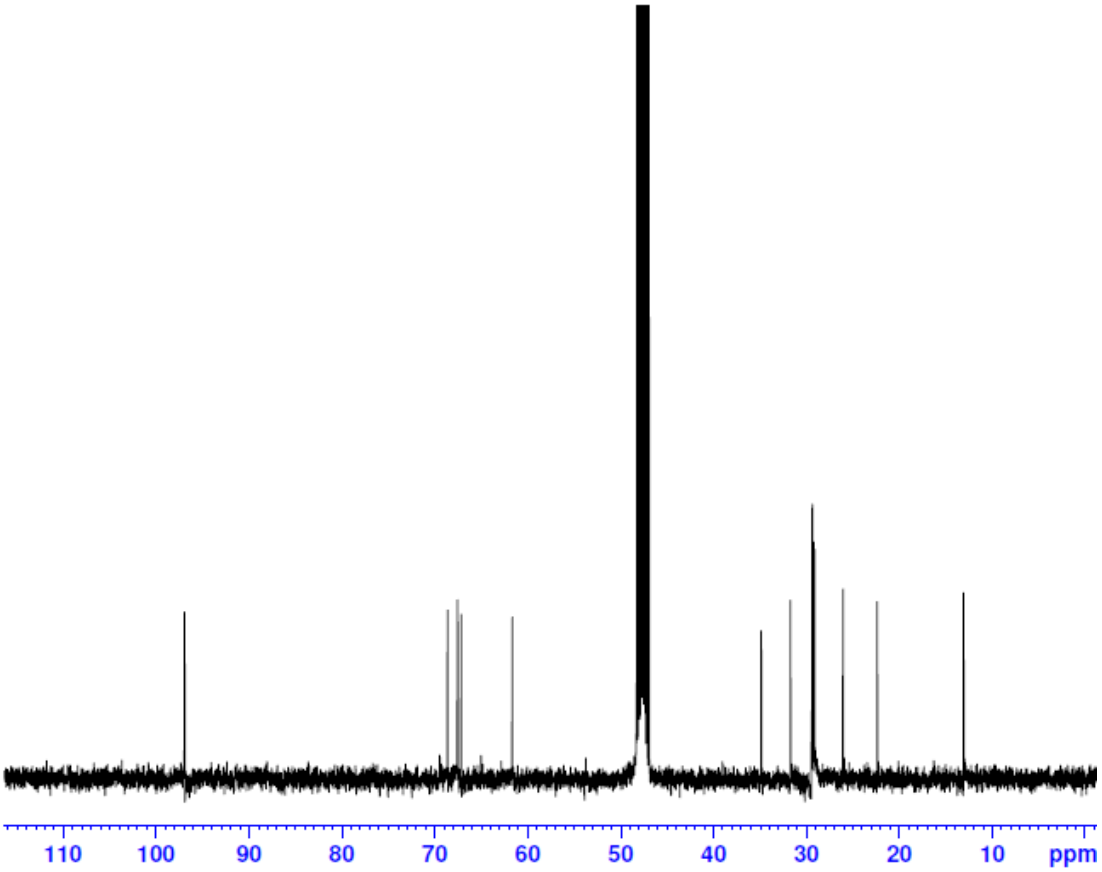
110
100
90
80
70
60
50
40
30
20
10
ppm

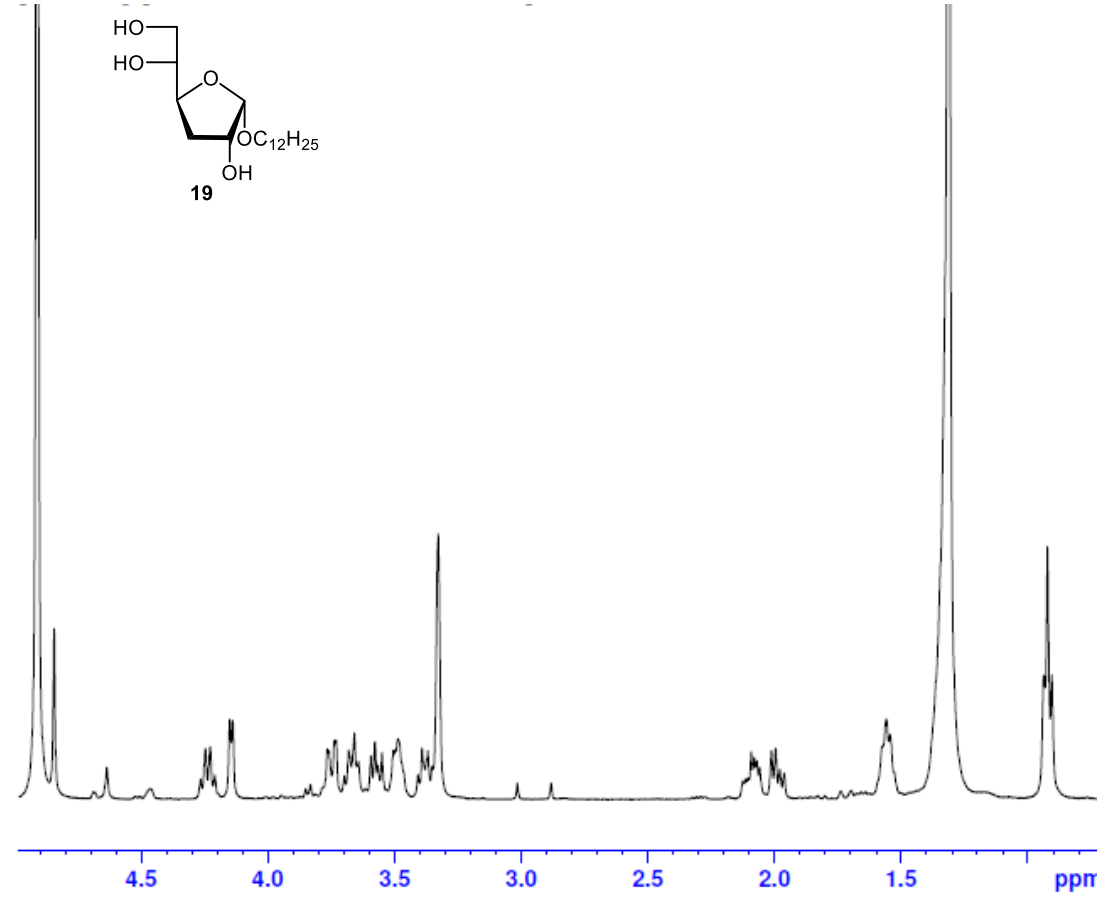
HO
HO
O
OC12H25
OH
19
4.5
4.0
3.5
3.0
2.5
2.0
1.5
ppm

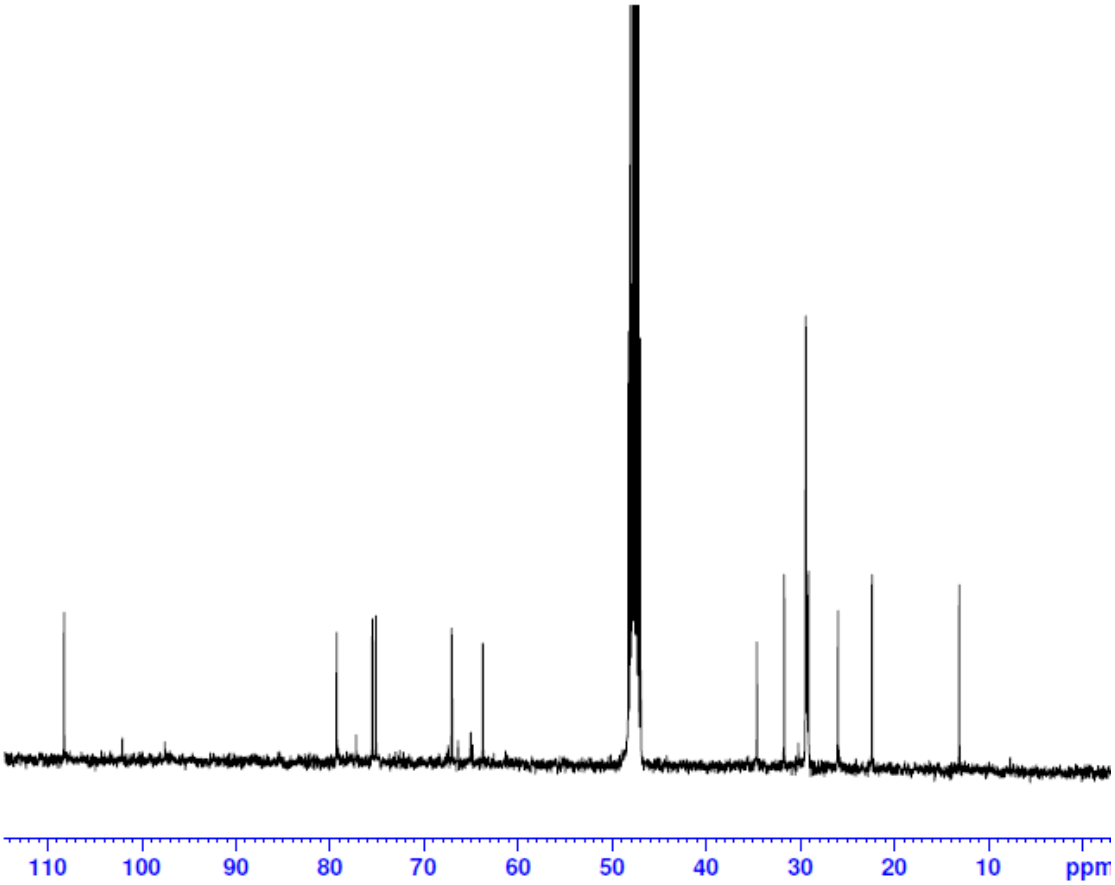
110
100
90
80
70
60
50
40
30
20
10
ppm

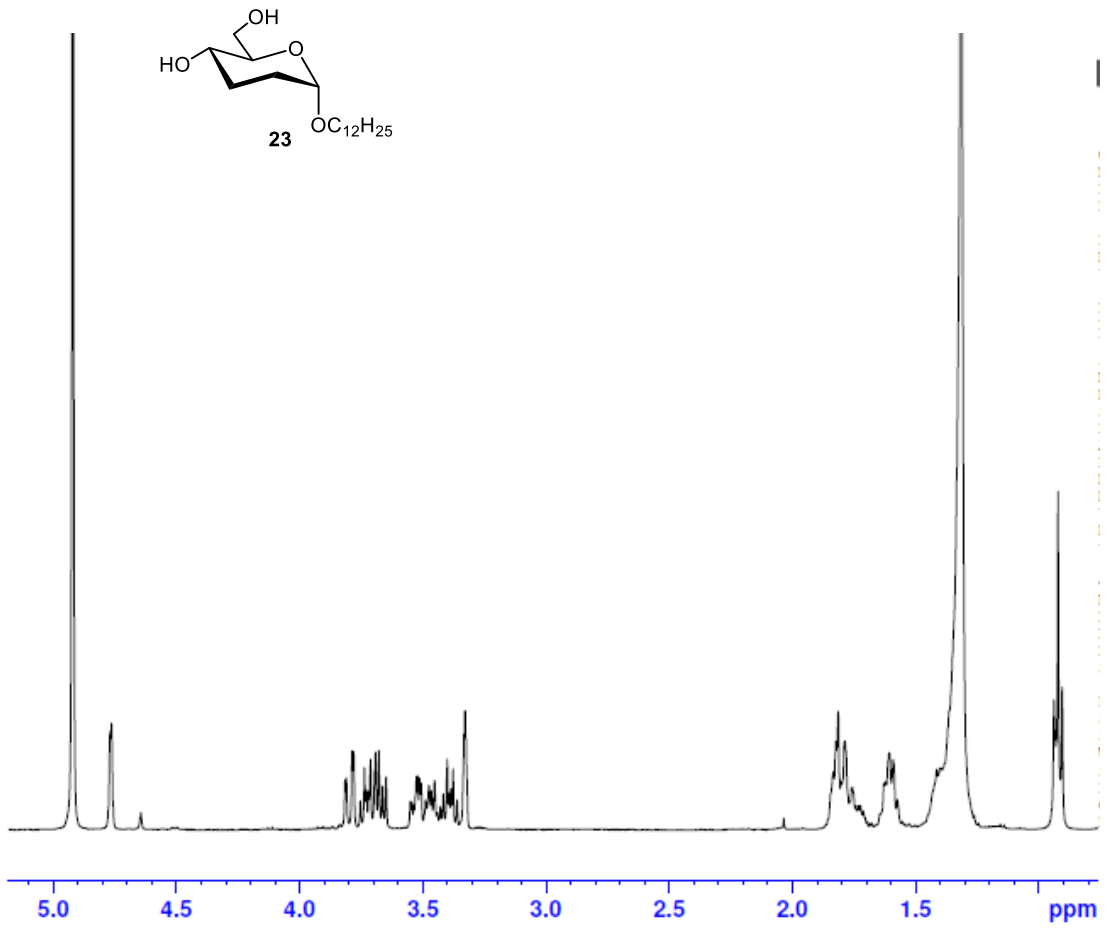
OH
HO
O
OC12H25
23
5.0
4.5
4.0
3.5
3.0
2.5
2.0
1.5
ppm

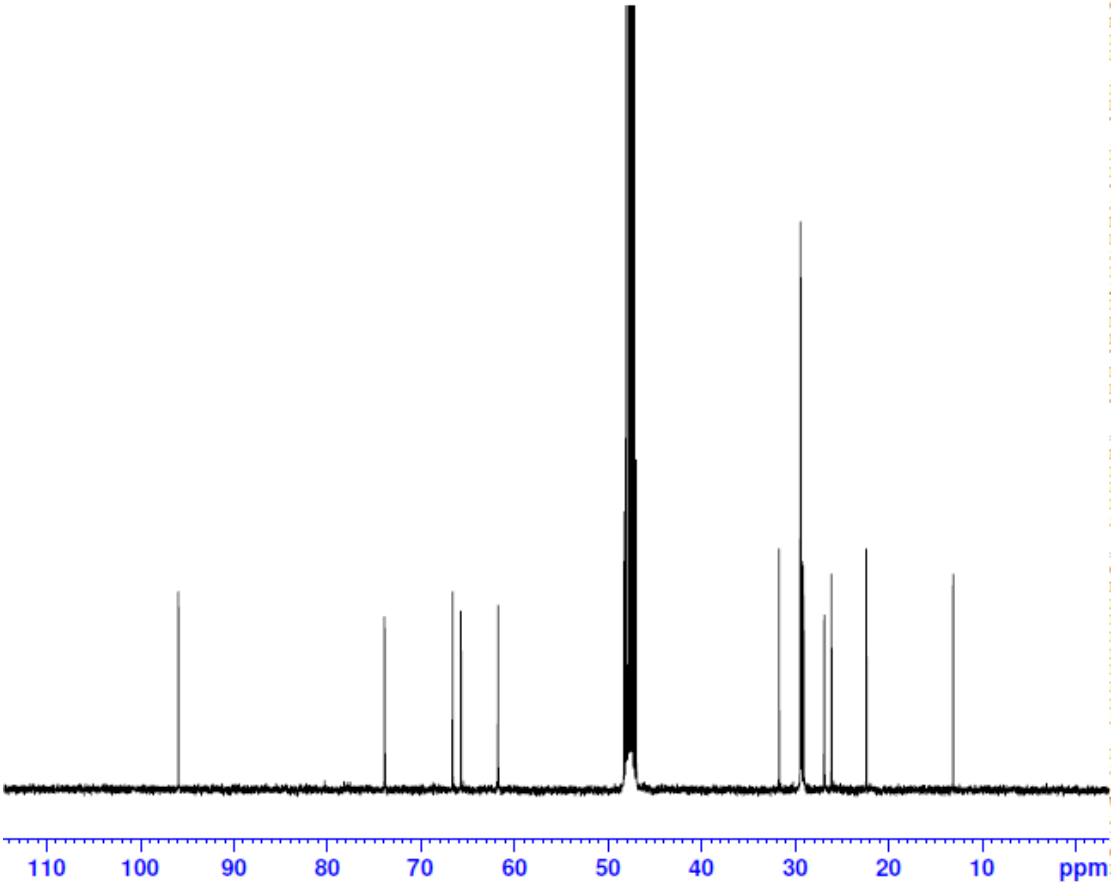
110
100
90
80
70
60
50
40
30
20
10
ppm

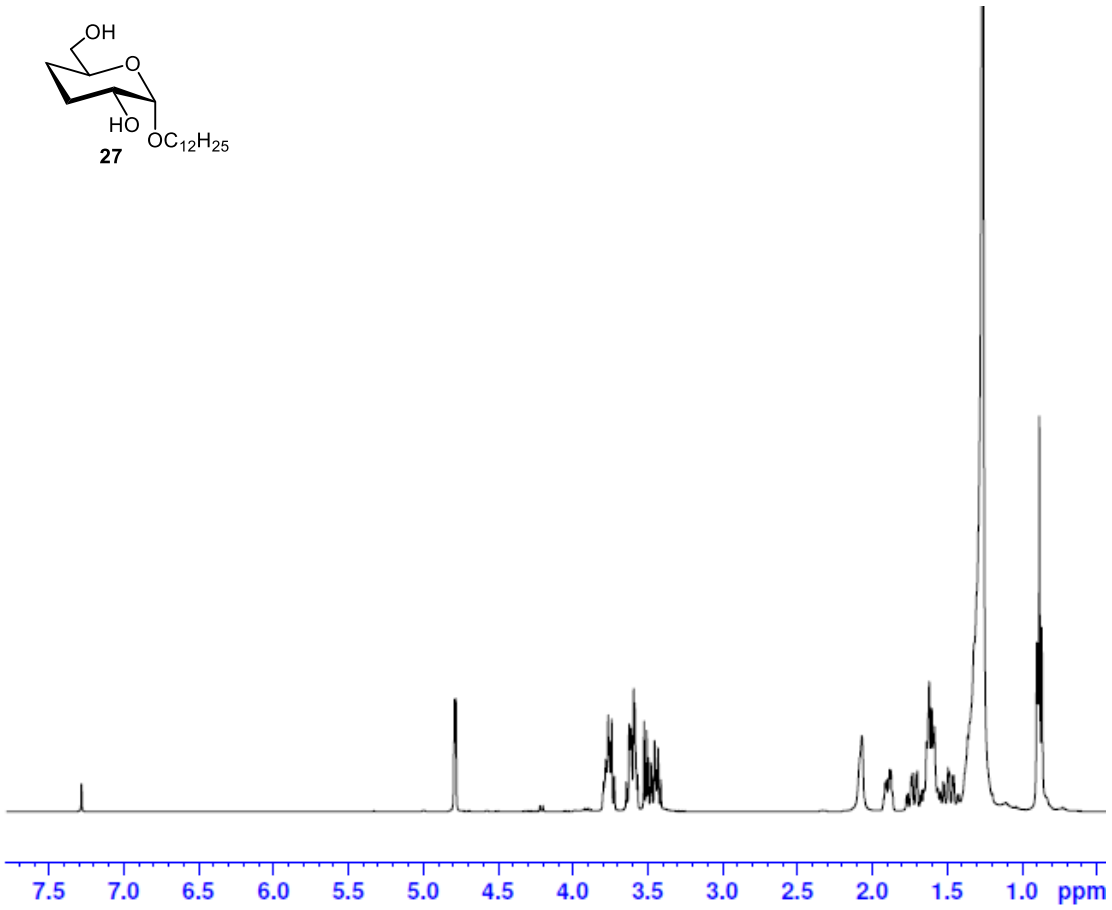
OH
O
HO
OC12H25
27
7.5
7.0
6.5
6.0
5.5
5.0
4.5
4.0
3.5
3.0
2.5
2.0
1.5
1.0
ppm

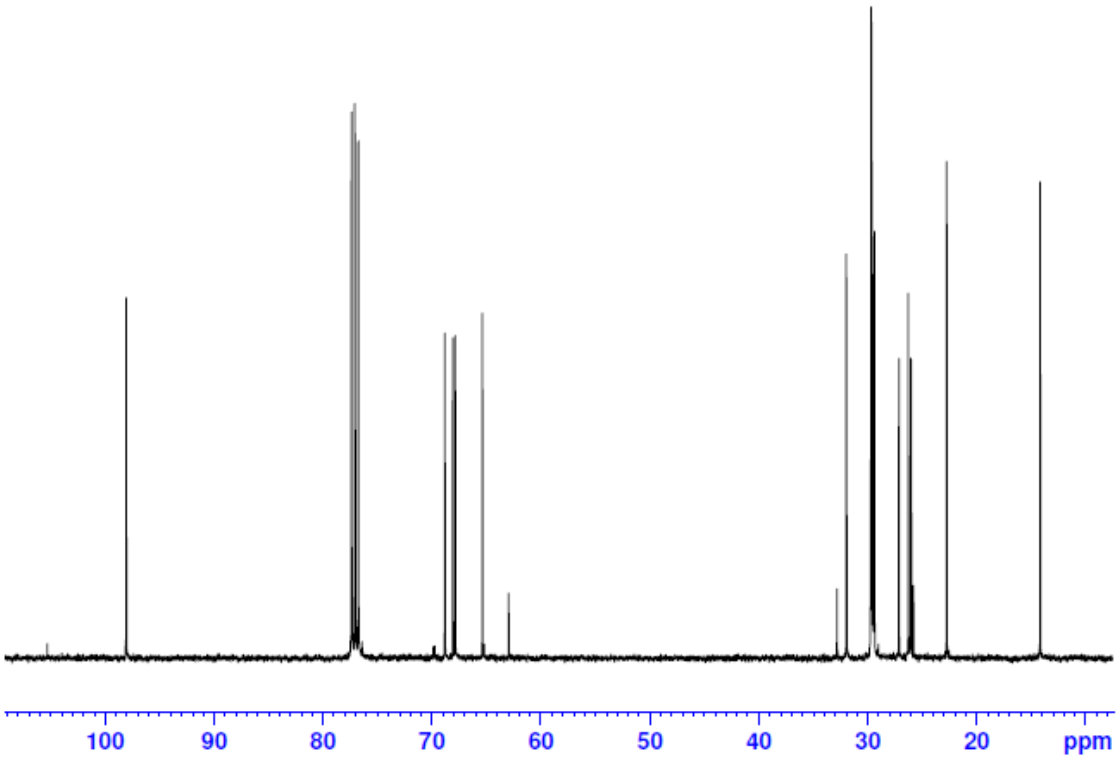
100
90
80
70
60
50
40
30
20
ppm

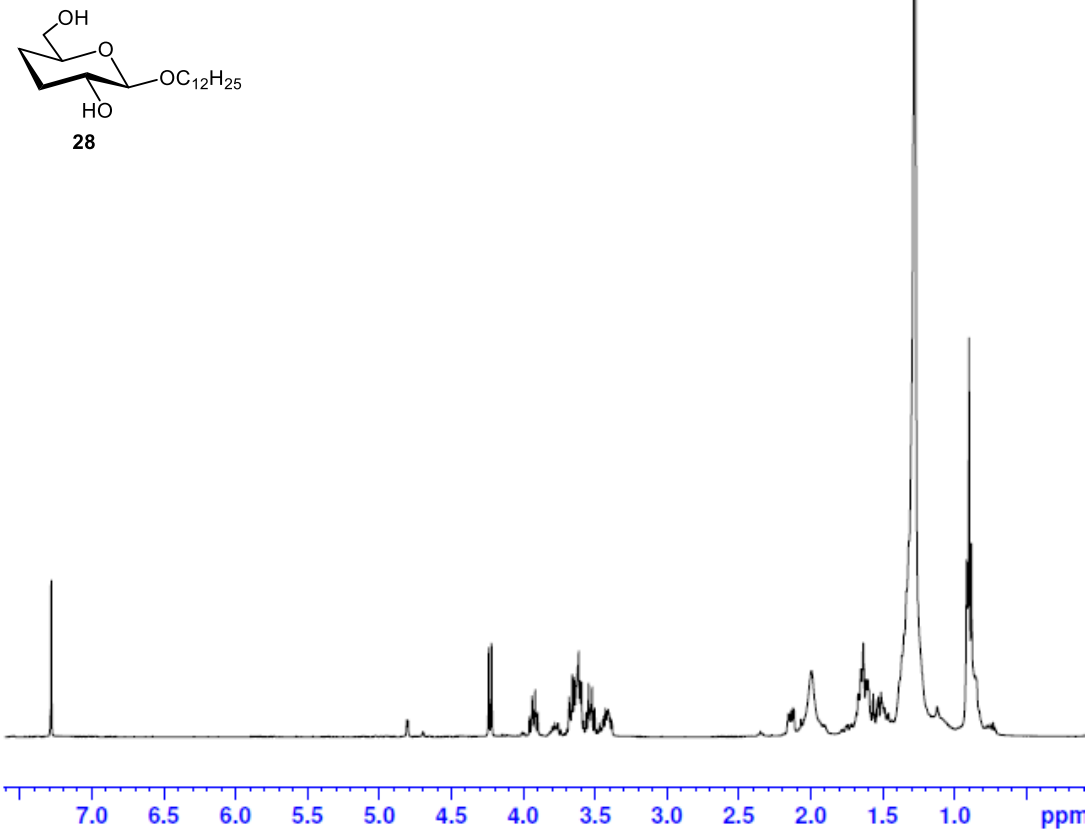
OH
O
OC12H25
HO
28
7.0
6.5
6.0
5.5
5.0
4.5
4.0
3.5
3.0
2.5
2.0
1.5
1.0
ppm

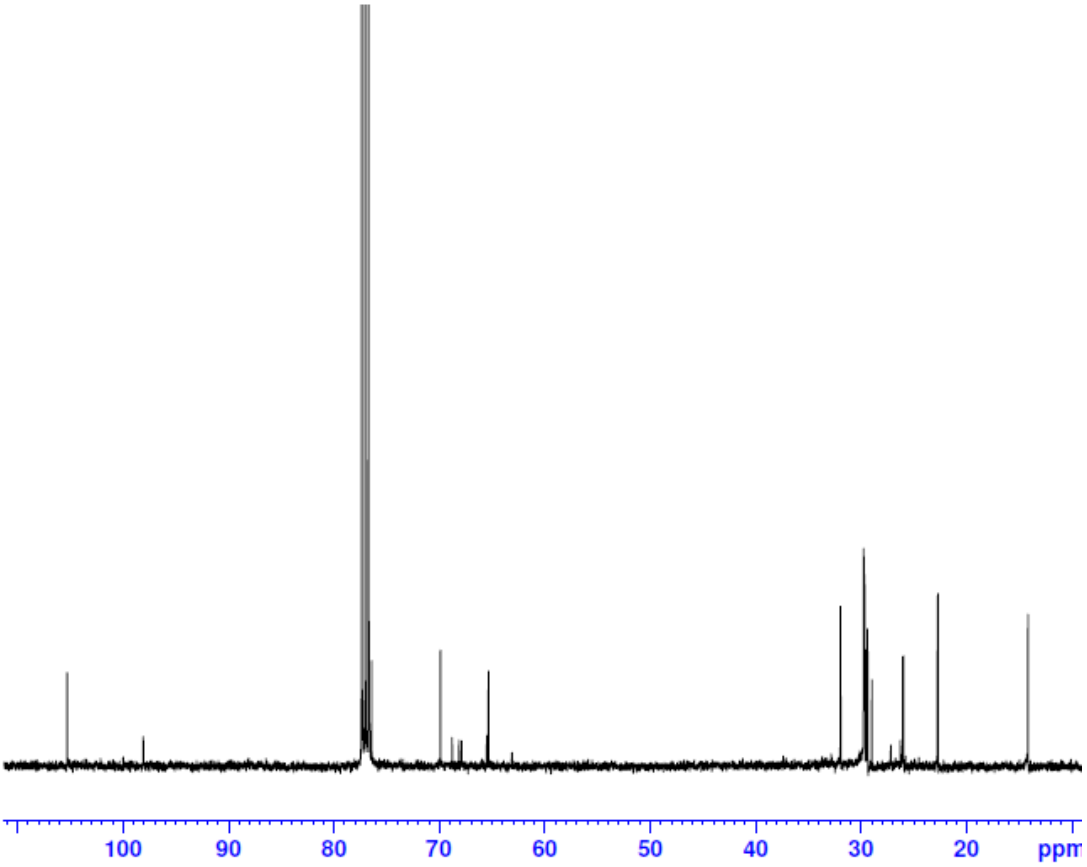
100
90
80
70
60
50
40
30
20
ppm

Annex 4. *^{1}H and ^{13}C of final products described in chapter 5*

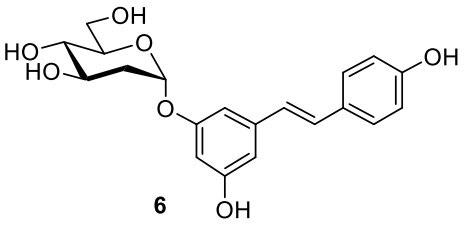

6

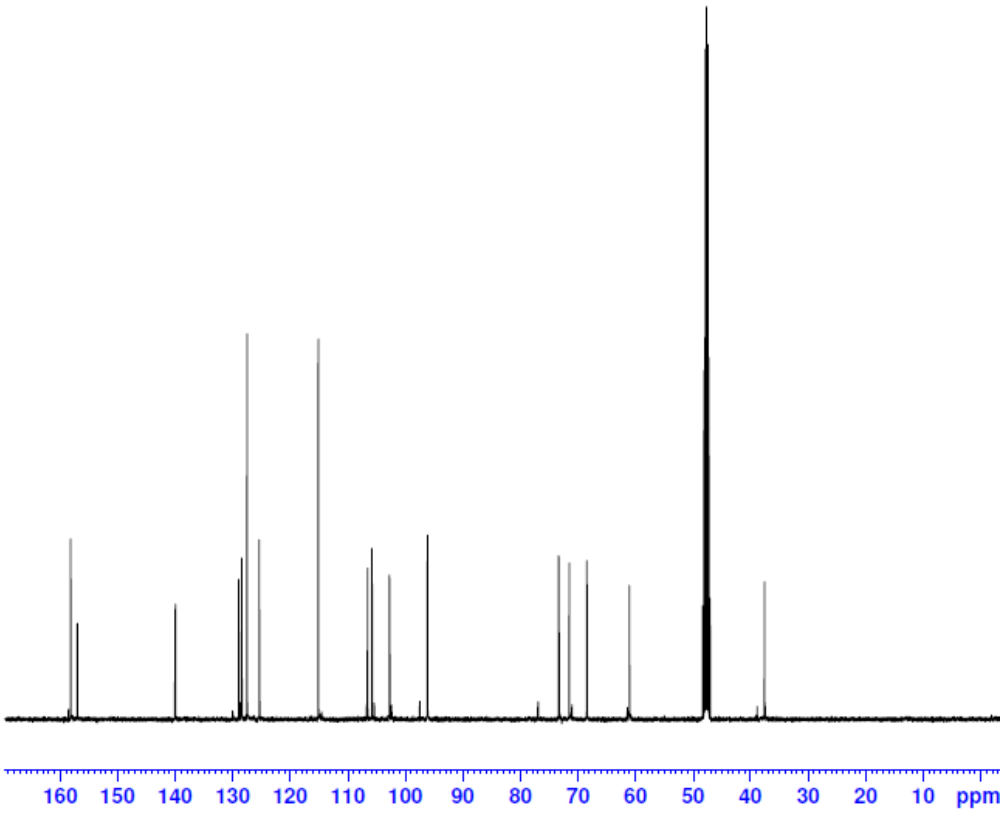

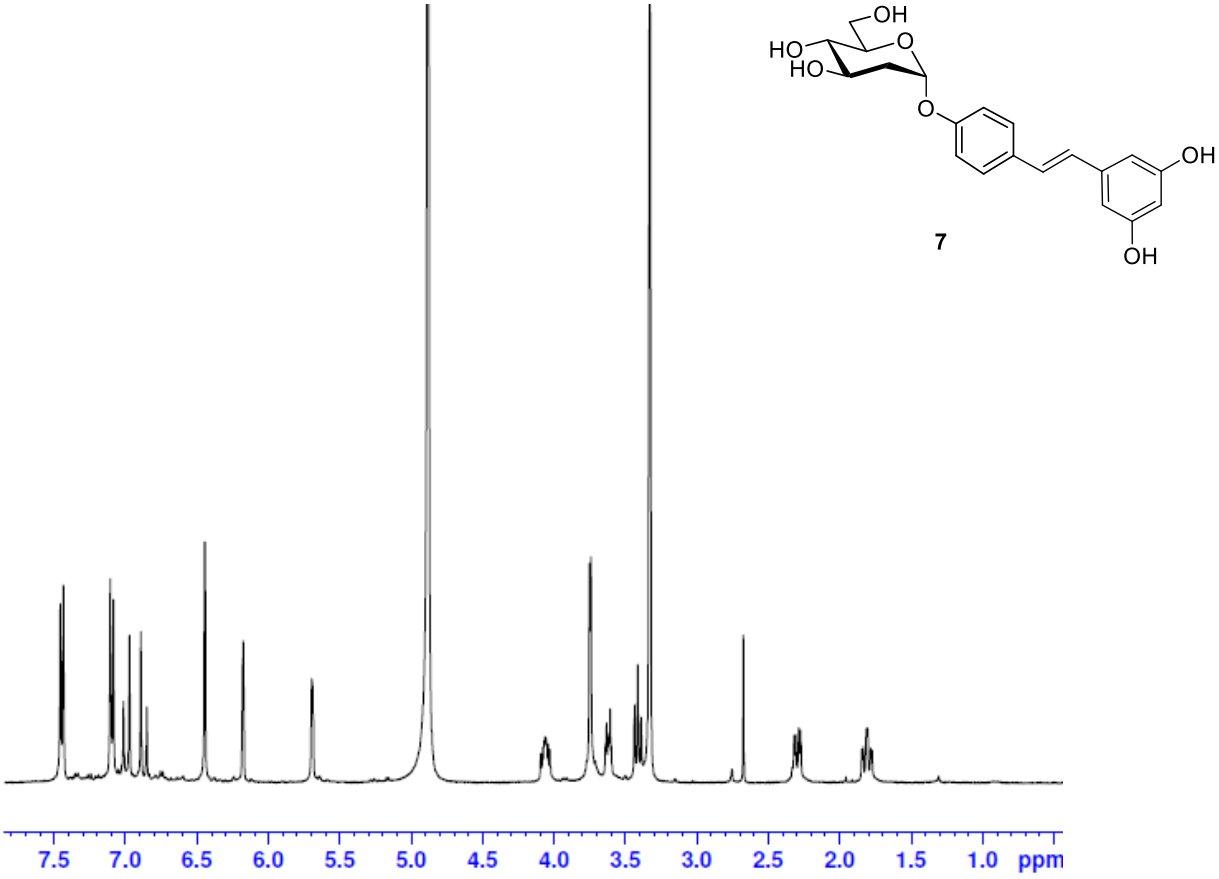
OH
HO
HO
O
O
OH
OH
7
7.5 7.0 6.5 6.0 5.5 5.0 4.5 4.0 3.5 3.0 2.5 2.0 1.5 1.0 ppm

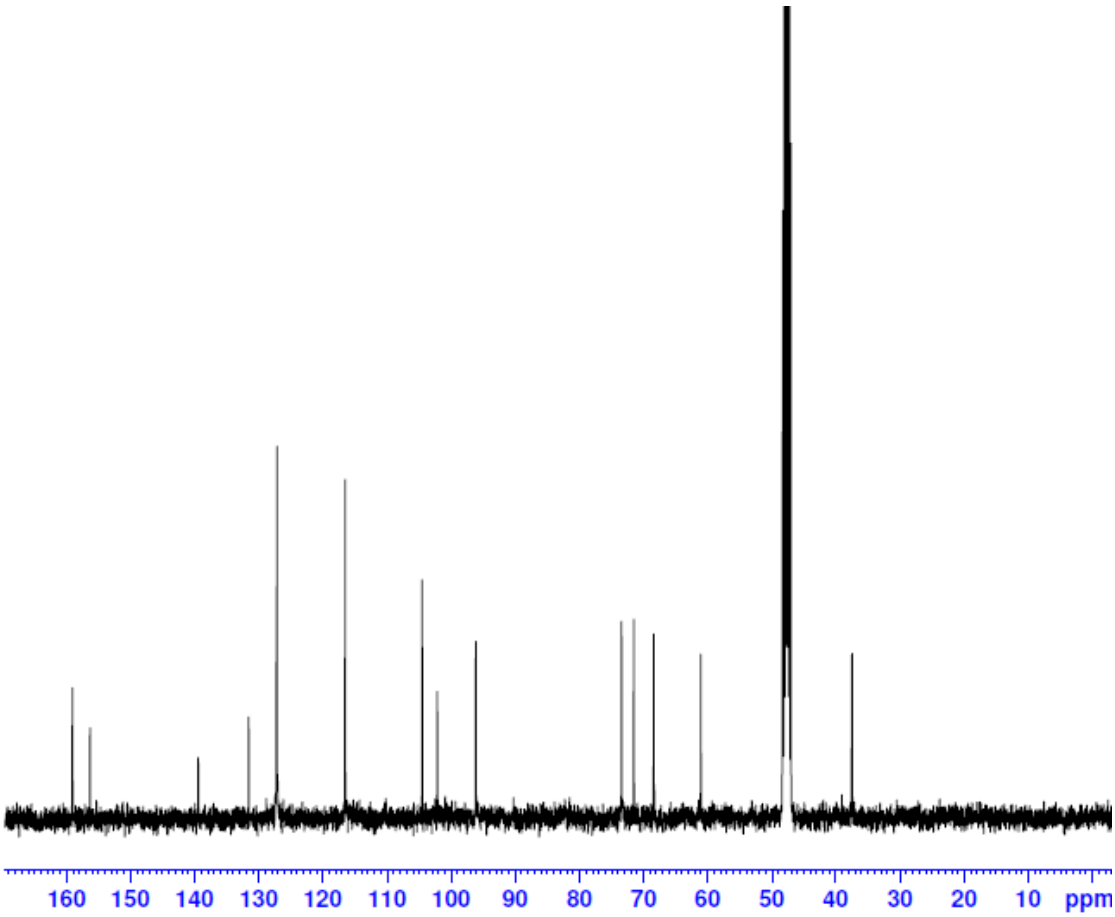
160 150 140 130 120 110 100 90 80 70 60 50 40 30 20 10 ppm

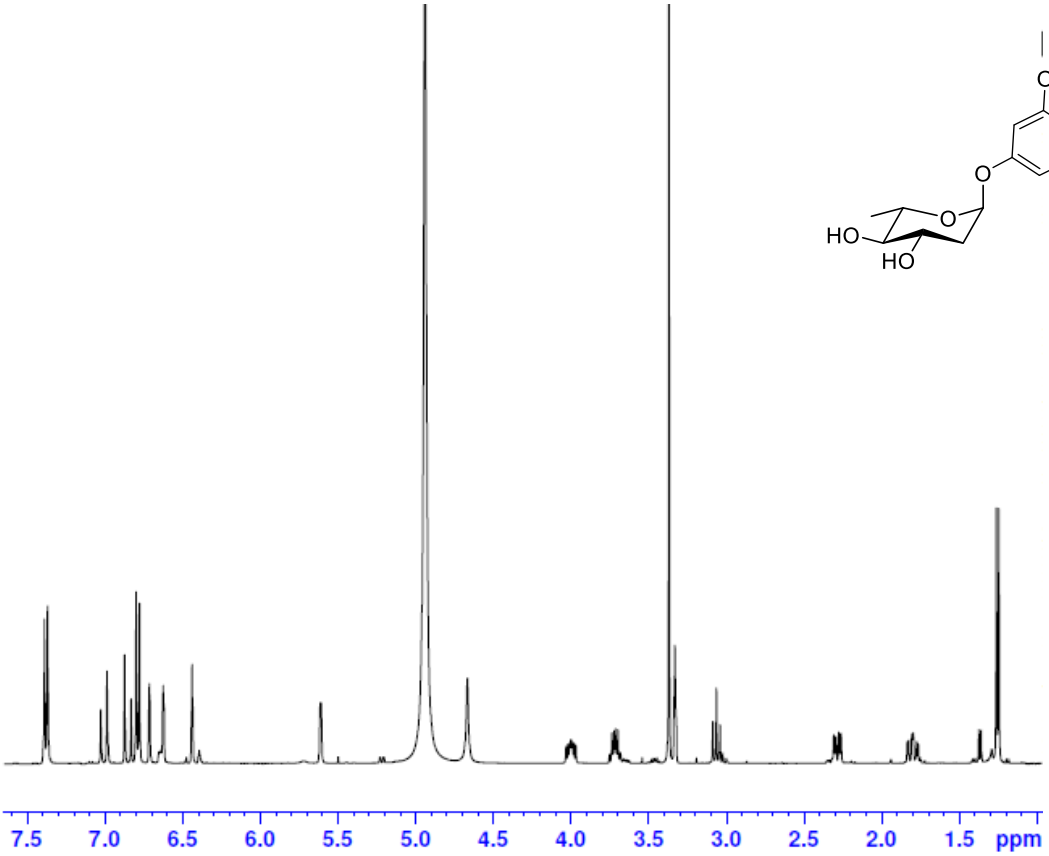
OH
O
O
HO
HO
OH
10
7.5
7.0
6.5
6.0
5.5
5.0
4.5
4.0
3.5
3.0
2.5
2.0
1.5
ppm

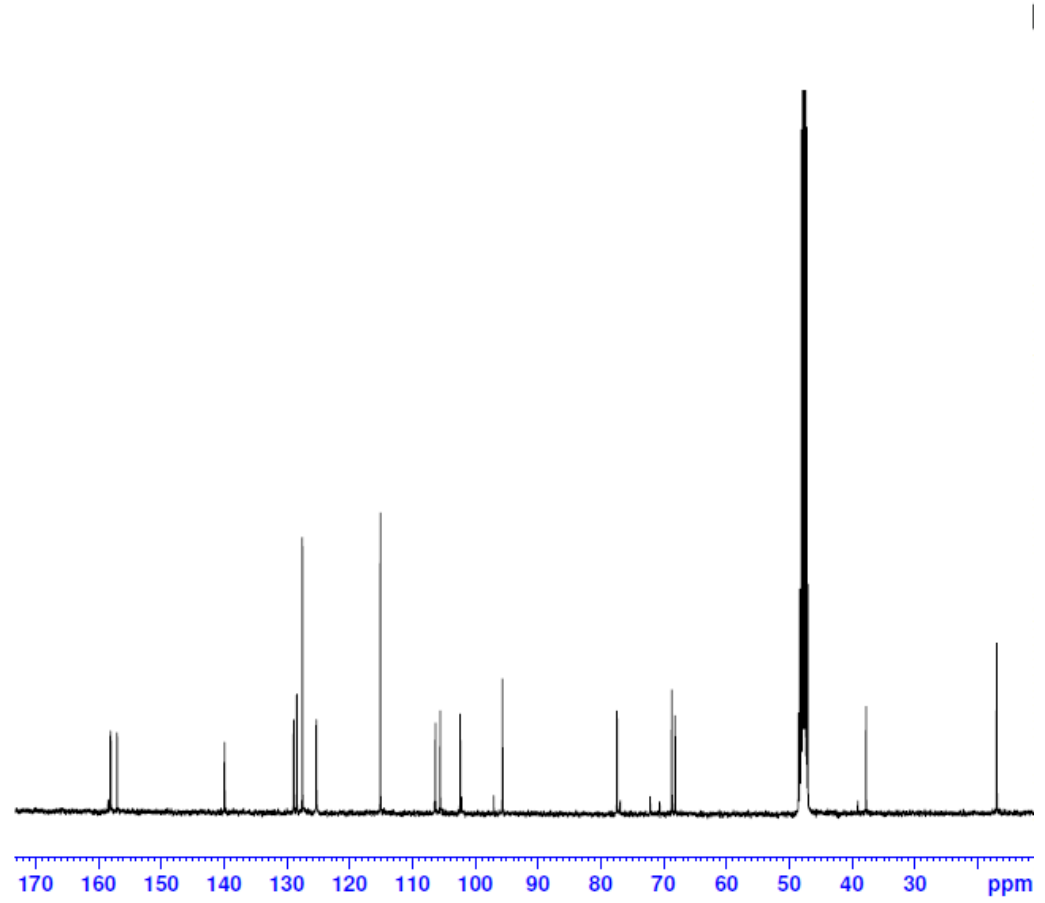
170
160
150
140
130
120
110
100
90
80
70
60
50
40
30
ppm

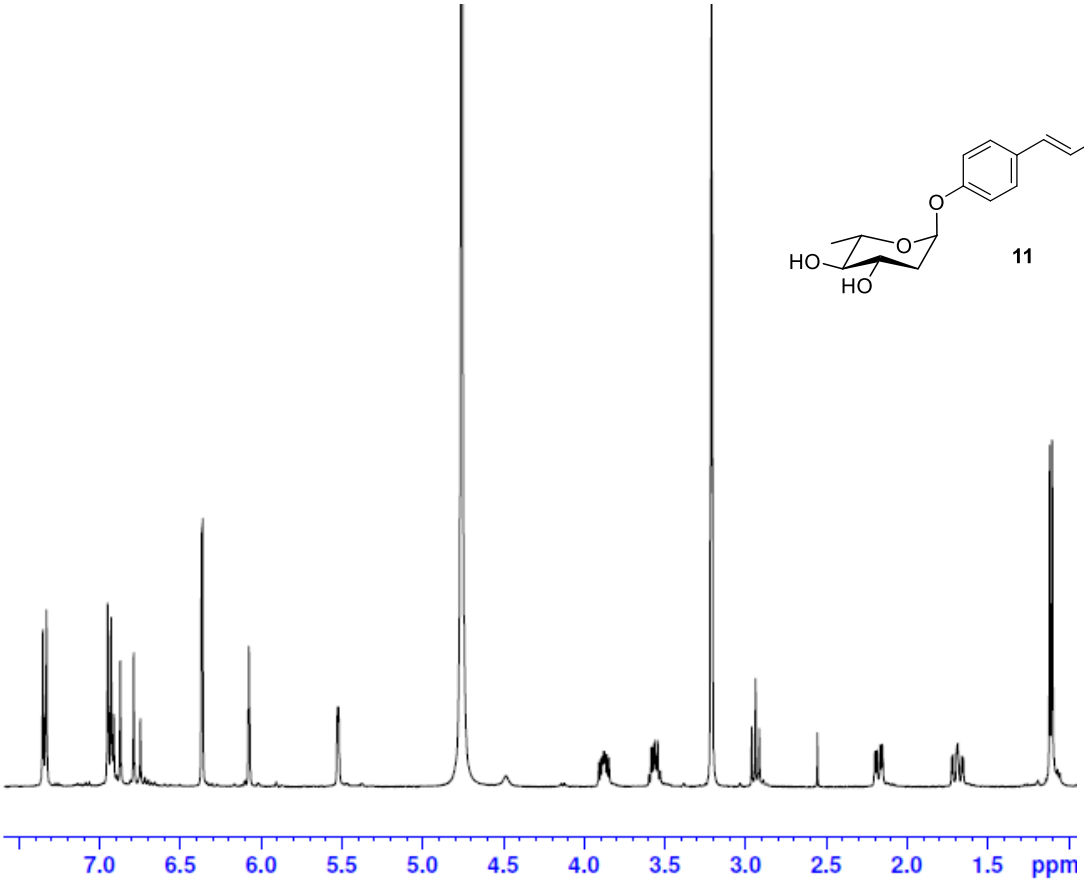
OH
OH
O
O
HO
HO
11
7.0
6.5
6.0
5.5
5.0
4.5
4.0
3.5
3.0
2.5
2.0
1.5
ppm

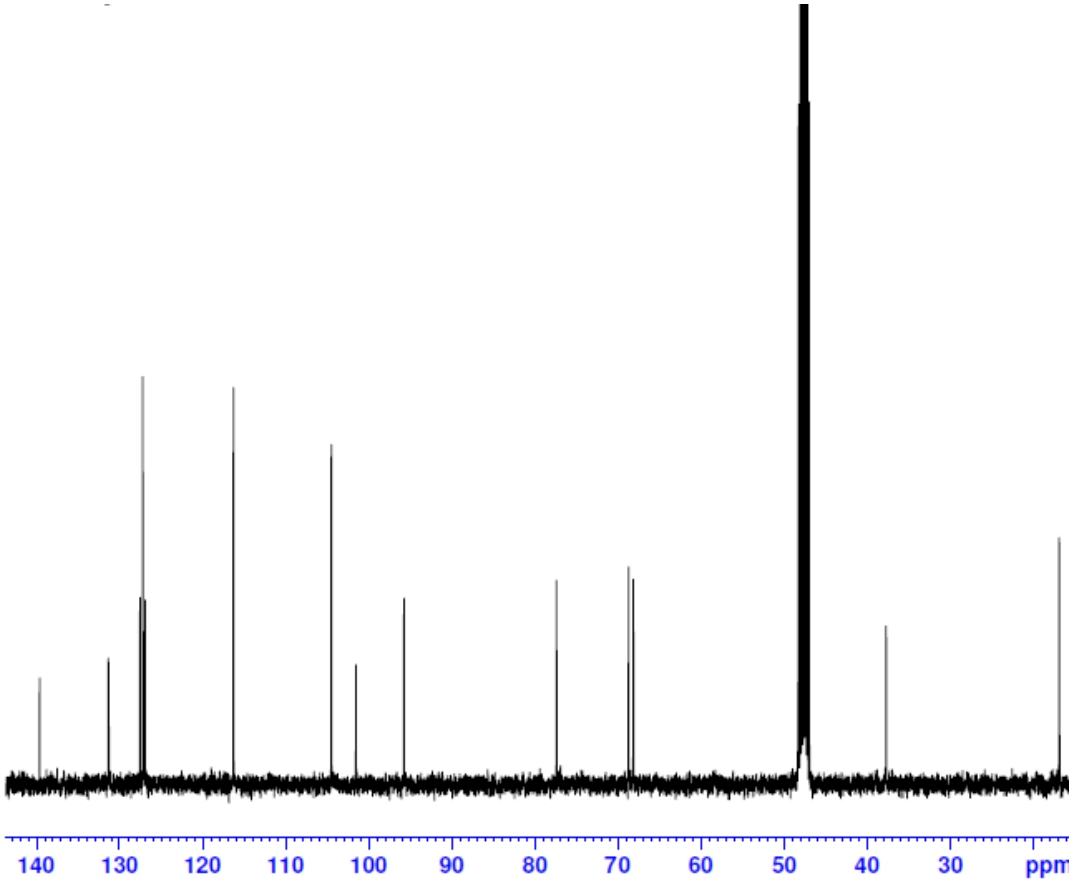
140
130
120
110
100
90
80
70
60
50
40
30
ppm

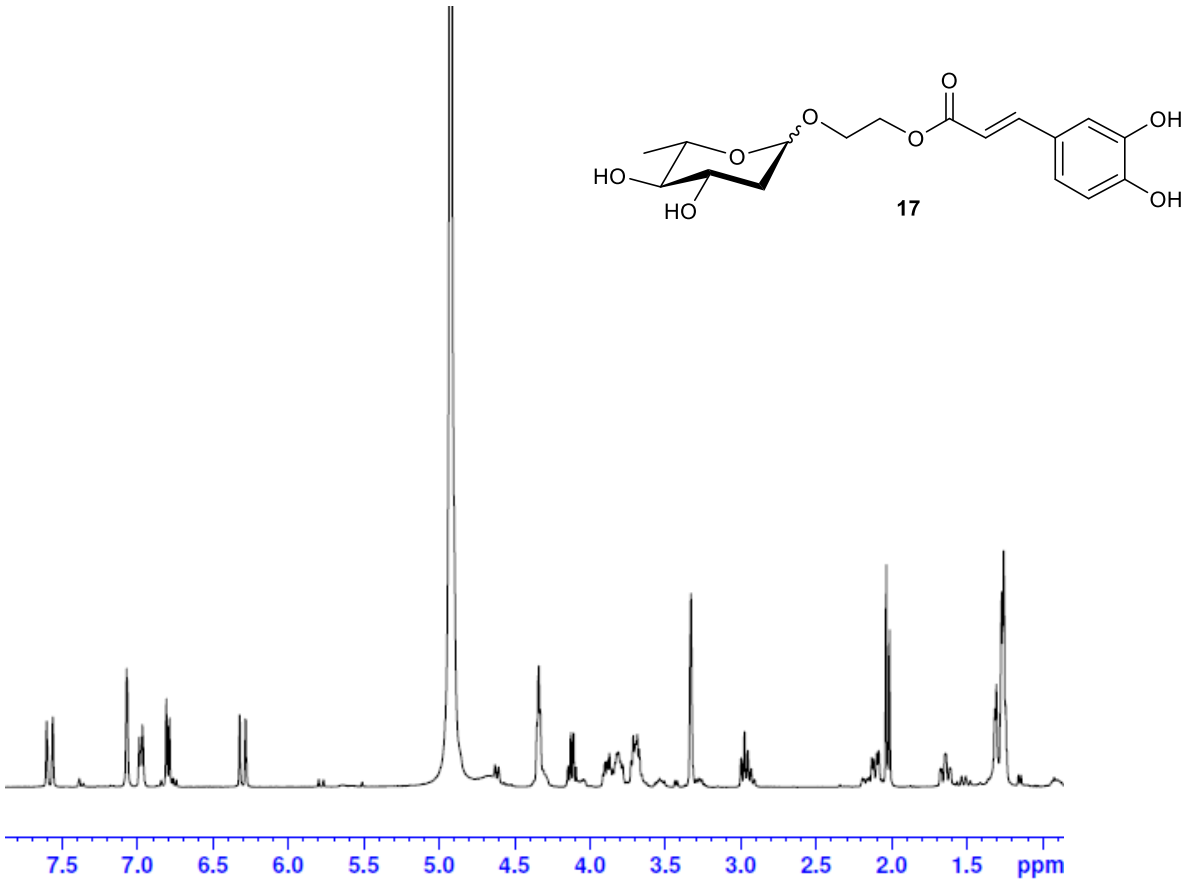
HO
HO
O
O
O
O
OH
OH
17
7.5
7.0
6.5
6.0
5.5
5.0
4.5
4.0
3.5
3.0
2.5
2.0
1.5
ppm

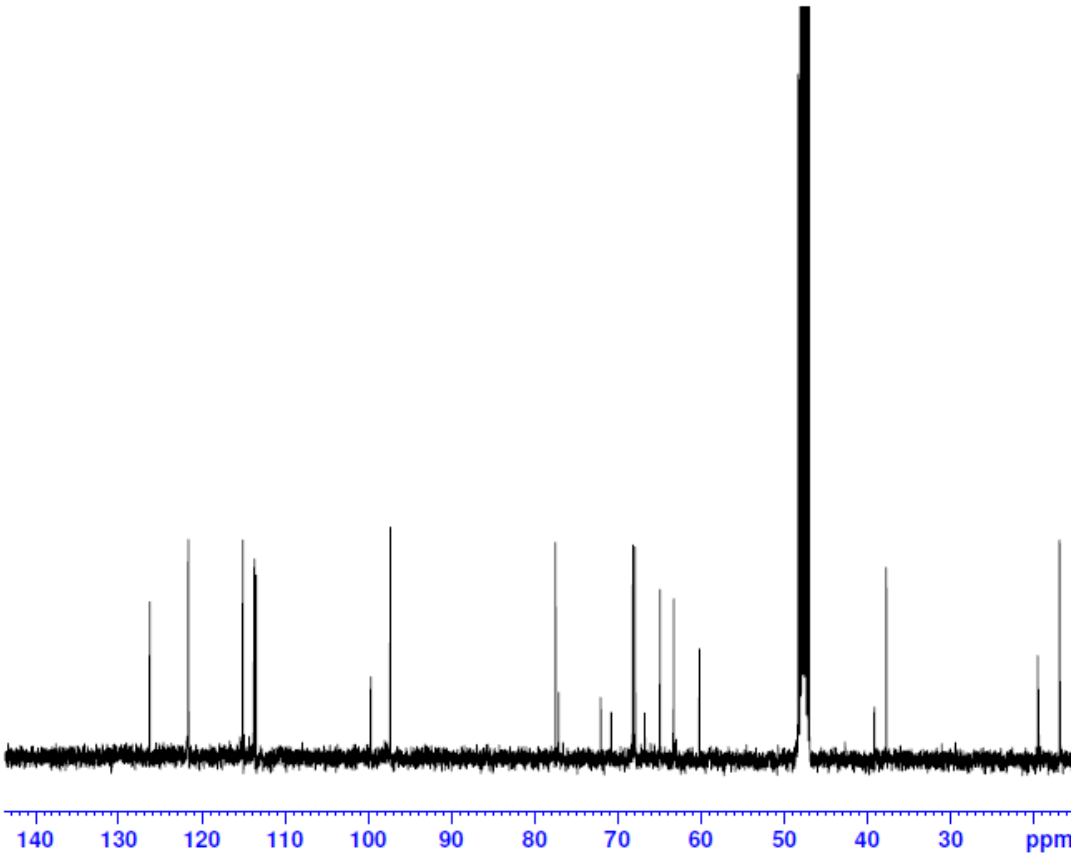
140
130
120
110
100
90
80
70
60
50
40
30
ppm